

AD-A084 740

DAVID W TAYLOR NAVAL SHIP RESEARCH AND DEVELOPMENT CE--ETC P/6 13/10
AIR CUSHION CRAFT DEVELOPMENT. FIRST REVISION. (U)

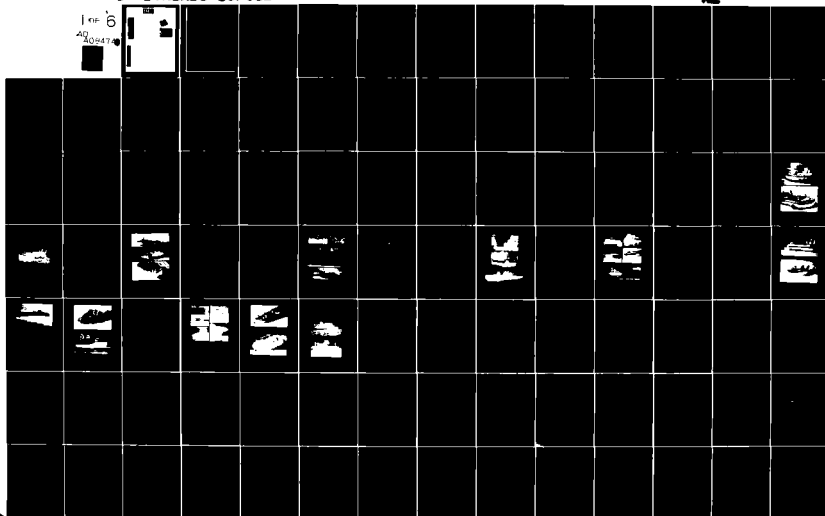
JAN 80 P J HANTLE

UNCLASSIFIED

DTNRDC-80/012

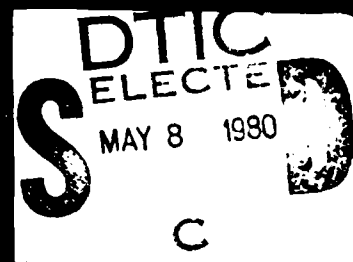
NL

1 of 6
AQ 20247



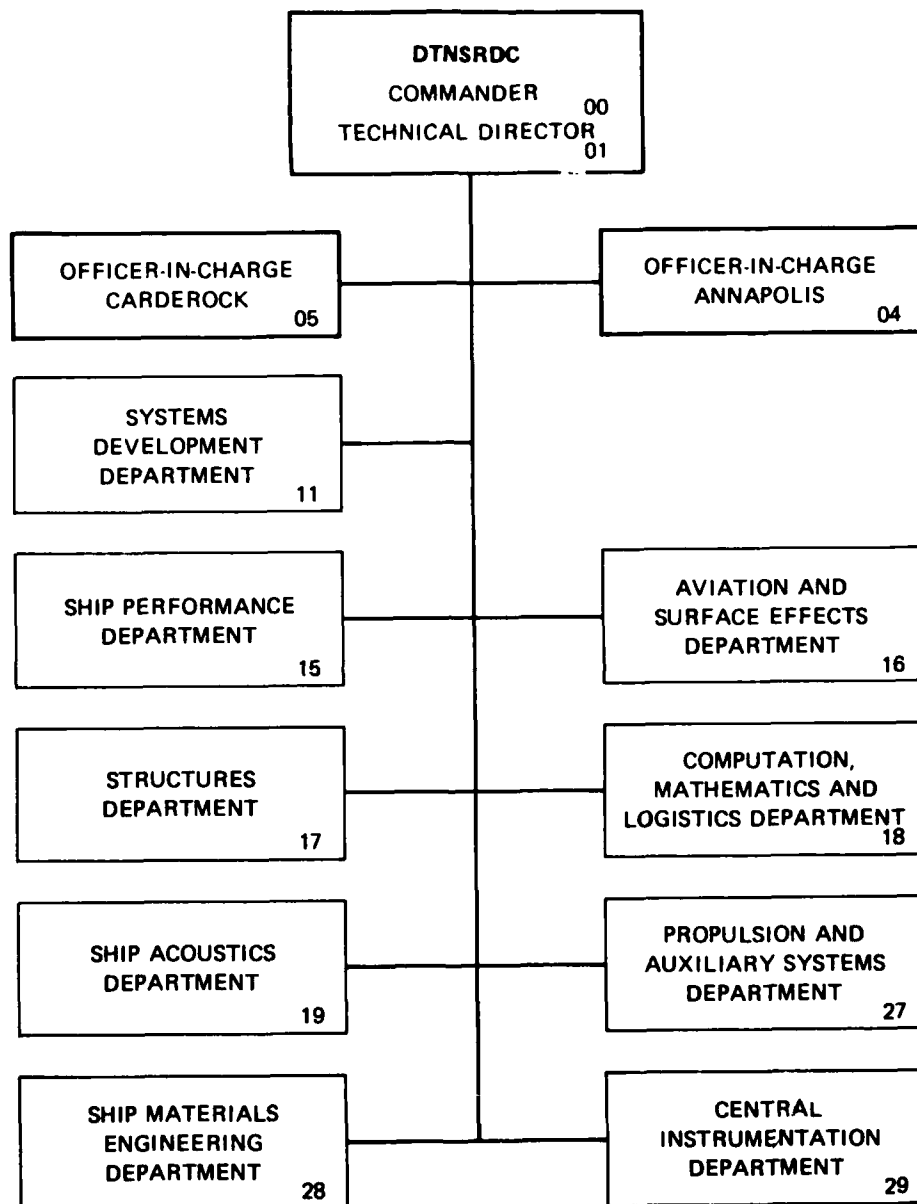
LEVEL 

ADA 084740



DDC FILE COPY

MAJOR DTNSRDC ORGANIZATIONAL COMPONENTS



80 5 8 028

UNCLASSIFIED

SECURITY CLASSIFICATION OF THIS PAGE (When Data Entered)

REPORT DOCUMENTATION PAGE		READ INSTRUCTIONS BEFORE COMPLETING FORM													
1. REPORT NUMBER DTNSRDC-80/012 (4727 REVISED)	2. GOVT ACCESSION NO. AD 40847404	3. RECIPIENT'S CATALOG NUMBER ②													
4. TITLE (and Subtitle) AIR CUSHION CRAFT DEVELOPMENT, (FIRST REVISION)	5. TYPE OF REPORT & PERIOD COVERED Final														
7. AUTHOR(s) Peter J. Mantle	6. PERFORMING ORG. REPORT NUMBER														
9. PERFORMING ORGANIZATION NAME AND ADDRESS Mantle Engineering Company, Inc. Alexandria, Virginia 22304	8. CONTRACT OR GRANT NUMBER(s) 135541														
11. CONTROLLING OFFICE NAME AND ADDRESS David W. Taylor Naval Ship Research and Development Center Bethesda, Maryland 20084	10. PROGRAM ELEMENT, PROJECT, TASK AREA & WORK UNIT NUMBERS Program Element 63566N Task Area S0241-AW001 Work Unit 1180-710														
14. MONITORING AGENCY NAME & ADDRESS (if different from Controlling Office)	12. REPORT DATE January 1980														
	13. NUMBER OF PAGES 525														
	15. SECURITY CLASS. (of this report) UNCLASSIFIED														
16. DISTRIBUTION STATEMENT (of this Report) APPROVED FOR PUBLIC RELEASE: DISTRIBUTION UNLIMITED															
17. DISTRIBUTION STATEMENT (of the abstract entered in Block 20, if different from Report) 1.1802-1180-710															
18. SUPPLEMENTARY NOTES															
19. KEY WORDS (Continue on reverse side if necessary and identify by block number)															
<table border="0"> <tr> <td>Air Cushion Craft</td> <td>Wing-In-Ground Effect</td> <td>Captured-Air</td> </tr> <tr> <td>Surface Effect Ships</td> <td>Ride Quality</td> <td>Bubble</td> </tr> <tr> <td>Air Cushion Vehicles</td> <td>Lift Fans</td> <td>Ground Effect</td> </tr> <tr> <td>Hovercraft</td> <td></td> <td>Machine</td> </tr> </table>				Air Cushion Craft	Wing-In-Ground Effect	Captured-Air	Surface Effect Ships	Ride Quality	Bubble	Air Cushion Vehicles	Lift Fans	Ground Effect	Hovercraft		Machine
Air Cushion Craft	Wing-In-Ground Effect	Captured-Air													
Surface Effect Ships	Ride Quality	Bubble													
Air Cushion Vehicles	Lift Fans	Ground Effect													
Hovercraft		Machine													
20. ABSTRACT (Continue on reverse side if necessary and identify by block number)															
<p>A technical summary is given of the development of air cushion craft from their inception to the present day. The designation "air cushion craft" encompasses any craft that relies on a cushion of air for a significant part of its support and operates in close proximity to the surface. The technical summary covers both aerostatic craft known as air cushion vehicles (ACV) and surface effect ships (SES) as well as aerodynamic craft -</p> <p style="text-align: center;">387682</p> <p style="text-align: right;">(Continued on reverse side)</p>															

DD FORM 1473
1 JAN 73EDITION OF 1 NOV 65 IS OBSOLETE
S/N 0102-014-6601UNCLASSIFIED
SECURITY CLASSIFICATION OF THIS PAGE (When Data Entered)

UNCLASSIFIED

SECURITY CLASSIFICATION OF THIS PAGE (When Data Entered)

(Block 20 continued)

such as wing-in-ground effect vehicles (WIG). Other variants are included in the review.

Where possible, the various available theories, empirical laws, and experimental data have been brought together and expressed in unified form. Emphasis has been given to reducing the data and analysis to their simplest forms for easy understanding and isolation of fundamental parameters. In the interest of historical accuracy, care has been taken to cite the original work on any particular theory or piece of data. To make this report readily available, in some instances it has been necessary to avoid the use of classified or proprietary data but this has not hampered the citing of original work. Currently operational craft, those still in their construction jigs, or in some cases those still on the drawing board are assessed and compared to the basic theories to give a measure of the state-of-the-art.

This technical summary is an updated and expanded version of a similar review conducted in 1975 and published as DTNSRDC Report 4727. The additions include a new chapter on Control and appendices on performance, weight data, and seakeeping. Much expanded material in the main text includes such topics as performance, propulsion, ride quality, and high speed aerodynamic craft.

Accession For	
NIS	X
DOI	
Univ	
Other	
Price	\$13.00
Dist.	GPO
Author	
Dist.	special
A	24

Stock # 008-047-00291-2

For Cushion Craft Development

Price \$13.00

UNCLASSIFIED

SECURITY CLASSIFICATION OF THIS PAGE (When Data Entered)

TABLE OF CONTENTS

	Page
LIST OF FIGURES	vii
LIST OF TABLES.	xix
NOTATION.	xxi
ABSTRACT.	1
ADMINISTRATIVE INFORMATION.	1
ACKNOWLEDGMENTS	2
CHAPTER I - INTRODUCTION	3
WHAT'S IN A NAME	5
THE AIR CUSHION CRAFT.	6
CHAPTER II - BACKGROUND DEVELOPMENT	9
DESCRIPTION OF AIR CUSHION CRAFT	10
Aerostatic Class.	11
Waterborne Class.	13
Aerodynamic Class	16
MAIN DEVELOPMENT EFFORTS	19
Low Speed Development	19
Intermediate Speed Development.	22
High Speed Development.	33
CONCLUDING REMARKS	33
CHAPTER III - PERFORMANCE ASPECTS	35
THE BASIC PERFORMANCE EQUATIONS.	35
The Economic Equation	36
The Range Equation.	37
SOME OVERALL SIZING RELATIONSHIPS.	43
Cushion Pressure.	47
Cushion Flow.	49
Power	52
Transport Efficiency.	55
Payload Capability.	58
PERFORMANCE CHARACTERISTICS.	61
Basic Relationships	61
Dynamic Similitude	61
Power Coefficient.	64
Speed Coefficient and Pressure Number.	64
Pressure and Flow.	66
Lift Power Requirements.	75
Calm Water Lift Power.	76
Wave Pumping Requirements in Rough Water	79

For sale by the Superintendent of Documents, U.S. Government Printing Office
Washington, D.C. 20402

Stock Number 008-047-00291-2

	Page
Momentum Drag	83
Cushion Wave Drag.	85
Seal or Skirt Drag	95
Calm Water Skirt Drag.	97
Rough Water Skirt Drag	100
Drag while Traversing Ice.	105
Sidehull Drag.	106
Aerodynamic Drag	112
Total Drag Estimation	115
Drag Polar.	117
Lift-to-Drag Ratio.	120
CHAPTER IV – STABILITY AND RIDE QUALITY	125
STATIC STABILITY IN HEAVE.	127
EFFECT OF FAN CHARACTERISTICS AND SCALING ON HEAVE RESPONSE	131
HEAVE STABILITY CRITERIA	138
PITCH AND ROLL STABILITY	140
PLOW-IN.	145
RIDE QUALITY	151
Some Fundamental Relationships.	153
Some Basic Ride Quality Results	155
THE SEA SPECTRA.	159
TRANSFER FUNCTION.	164
HEAVE RESPONSE AND RIDE QUALITY.	165
RIDE QUALITY CRITERIA.	175
MOTION SICKNESS CRITERIA	176
WORKING EFFICIENCY CRITERIA.	177
CHAPTER V – CONTROL	181
TYPES OF CONTROL SYSTEMS	181
Aerodynamic Control Surfaces.	182
Thrust Producing Devices.	182
Lift Vectoring Devices.	182
AERODYNAMIC CONTROL SURFACES	182
THRUST PRODUCING DEVICES	184
MULTIPLE PROPELLER CONTROL	189
Tandem Operation.	189
Yaw Performance	190
Reverse Thrust.	193
PUFF PORTS AND BOW THRUSTERS	195

	Page
LIFT VECTORING DEVICES	197
AERODYNAMIC AND HYDRODYNAMIC FORCE VARIATIONS.	200
GIMBAL FAN CONTROL	206
CHAPTER VI – SEALS AND SKIRT DEVELOPMENT	209
PERFORMANCE CHARACTERISTICS.	209
Bag-Finger Skirt.	211
Bounce	213
Finger Oscillation	216
Bag Shape and Size	221
Loop-Segment Skirt.	225
Jupe Skirt System	226
Pericell Skirt System	230
SES Hinge and Flexible Seals.	231
SKIRT MATERIAL	235
Skirt Material Failure Modes.	240
Skirt Material Weight and Life.	245
SKIRT SYSTEM WEIGHT.	250
CHAPTER VII – STRUCTURAL DESIGN	253
DESIGN CRITERIA.	257
Factors of Safety	266
Structural Weight Fraction.	267
CURRENT CONSTRUCTION	274
CHAPTER VIII – LIFT FAN SYSTEM	295
AERODYNAMIC DESIGN ASPECTS	298
Lift System Efficiency.	298
Fan Selection and Categorization.	302
Pressure-Flow Characteristics	310
Passive Fan Systems.	312
Active Fan Systems	318
MECHANICAL DESIGN ASPECTS.	326
Fan Weight.	327
Fan Noise	328
CHAPTER IX – PROPULSION	331
PROPULSION SYSTEM WEIGHT CONSIDERATIONS.	332
Temperature Effect.	339
Air Flow Problems	339
Foreign Object Damage	339
Engine Noise.	339
Filtration.	340

	Page
PROPULSORS	345
Air Propulsion.	345
Air Propellers	346
Propulsive Efficiency	350
Propeller Construction Development.	356
Air Propeller Weight.	368
Air Jet Propulsion	369
Air Jet Propulsion Efficiency	372
Water Propulsion.	378
Waterscrew Propulsion.	378
Subcavitating Propellers.	380
Supercavitating Propellers.	384
Propeller Weight.	394
Waterjet Propulsion.	394
CHAPTER X – HIGH AND LOW SPEED DEVELOPMENTS	407
HIGH SPEED DEVELOPMENT	407
Some Basic Data	408
Possible End Plate Solutions.	414
Stability and Control Considerations.	419
CONCLUDING REMARKS ON AERODYNAMIC (HIGH SPEED) AIR CUSHION CRAFT.	423
LOW SPEED DEVELOPMENT.	425
CHAPTER XI – CONCLUSIONS	429
PERFORMANCE ASPECTS (CHAPTER III).	430
STABILITY AND RIDE QUALITY (CHAPTER IV).	430
CONTROL (CHAPTER V).	431
SEALS AND SKIRT DEVELOPMENT (CHAPTER VI)	431
STRUCTURAL DESIGN (CHAPTER VII).	432
LIFT FAN SYSTEM (CHAPTER VIII)	432
PROPULSION (CHAPTER IX).	433
HIGH AND LOW SPEED DEVELOPMENTS (CHAPTER X).	433
APPENDIX A – DERIVATION OF RANGE AND PRODUCTIVITY EQUATIONS.	435
APPENDIX B – AIR CUSHION CRAFT WEIGHT BREAKDOWN	441
APPENDIX C – HUMP THRUST MARGIN	465
APPENDIX D – SOME SEAKEEPING FORMULAE	481
REFERENCES.	491

LIST OF FIGURES

	Page
1 - Air Cushion Craft	7
2 - Air Cushion Craft Family Tree	10
3 - Plenum and Peripheral Jet Basic Forms	11
4 - Air Cushion Craft SR.N1 and SR.N4	12
5 - Stretched SR.N4 (Super 4)	13
6 - Hydrostatic and Hydrodynamic Basic Forms	14
7 - Waterborne Air Cushion Craft	15
8 - Aerodynamic Cushion Craft Basic Forms	16
9 - Aerodynamic Cushion Craft	18
10 - Caspian Sea Monster	19
11 - Main Development of Air Cushion Craft	20
12 - Low Speed Applications of Air Cushion Principle	21
13 - British Air Cushion Craft	23
14 - Japanese (Top) and French Air Cushion Craft	26
15 - SEDAM N.500 (Ingenieur Jean Bertin)	27
16 - SKMR-1 with and without Skirts.	28
17 - U.S. Navy High Density Air Cushion Craft	30
18 - JEFF(A) Underway in Florida	31
19 - JEFF(B) Underway in Florida	31
20 - Bell-Canada Voyageur and Viking	32
21 - Generalized Breguet Range Chart	40
22 - Cushion Density Trends	45
23 - Size of Air Cushion Craft	46
24 - Cushion Pressure of Air Cushion Craft	48

	Page
25 - Nominal Air Gap	49
26 - Trace of SR.N4 Hemline Movement	50
27 - Effect of Air Gap on Power	51
28 - Total Installed Power for Air Cushion Craft	52
29 - Power, Weight, and Speed.	54
30 - Transport Efficiency of Several Craft	56
31 - Transport Efficiency of Air Cushion Craft	57
32 - Effect of Size on Transport Efficiency	58
33 - Light Ship Weight of Air Cushion Craft	59
34 - Disposable Load of Transport Craft	60
35 - Speed Characterization of Air Cushion Craft	66
36 - Nozzle Geometry of Peripheral Jet Craft	67
37 - Pressure and Velocity Distribution Across Jet	69
38 - Saunders-Roe Theory and Test for Peripheral Jet	70
39 - Pressure and Flow for Peripheral Jet	71
40 - Geometry of Plenum Craft	72
41 - Nondimensional Flow for Plenum and Peripheral Jet	74
42 - Plenum and Peripheral Jet Hover Power	78
43 - Wave Pumping Power	82
44 - Air Cushion Craft Lift Power	83
45 - Momentum Drag Power (Peripheral Jet and Plenum)	84
46 - Early Wave Drag Results	86
47 - Deep and Shallow Water Wave Drag	88

	Page
48 - Wave Drag for Unshaped and Shaped Pressure Distributions	84
49 - SES-100B Shallow Water Performance	91
50 - Deep Water Hump Drag	92
51 - High L/B Craft XR-5	94
52 - Effect of L/B on SES Drag	95
53 - Theory and Model Drag for High L/B SES	96
54 - Drag Breakdown of Typical Large Air Cushion Craft	98
55 - Calm Water Skirt Drag Components	99
56 - Rough Water Skirt Drag	102
57 - Rough Water Performance of SR.N4	103
58 - Speed in Rough Seas	104
59 - Skirt Drag Over Simulated Ice	105
60 - Sidehull Drag of SES-100A	107
61 - Hovermarine HM.2	110
62 - Low Cavitation Number Sidehull	110
63 - Hydrodynamic Lift-to-Drag Ratio of SES-100A and SES-100B	112
64 - Typical Aerodynamic Drag Coefficients	114
65 - Drag Polar for Amphibious Air Cushion Craft	118
66 - Drag Polar for SES-100B	119
67 - Typical Effective Lift-to-Drag Ratio	122
68 - Cruise Speed of Air Cushion Craft	123
69 - Typical Simulation Comparison with Test Data	126

	Page
70 - Effective Wave Amplitude Function	128
71 - Normalized Heave Response Over Waves	130
72 - Heave Response Amplitude Operator	132
73 - Plenum Heaving Over Water	133
74 - Effect of Scaling on Model Response	139
75 - Basic Methods of Cushion Stability	141
76 - Typical Roll Stability Curves	144
77 - Skirt Height of Air Cushion Craft	145
78 - Early Results on Plow-In Solution	147
79 - SR.N5 Speed-Yaw Boundary	148
80 - SES-100A Plow-In with Early Planing Bow Seal	149
81 - SES-100A Plow-In Solution	151
82 - Modified SES-100A with Planing Seal and Thick Sidehulls	152
83 - Motion Response to a Seaway	154
84 - Some Current Treatments of Motion	156
85 - Ride Quality of Cushions and Foils	157
86 - Air Cushion Craft Ride Quality with Active Lift System	159
87 - Wave Period and Wavelength	160
88 - Pierson-Moskowitz Sea Spectra	163
89 - Transfer Function of Selected Craft	165
90 - Typical Traces of Air Cushion Craft	167
91 - Typical Trace of Planing Craft	168
92 - SES-100A Ride Control System	169

	Page
93 - Power Spectral Density of SES-100B	172
94 - SES-100B Acceleration (RMS g) (Ride Control 0	173
95 - SES-100B Acceleration (RMS g) (Ride Control On).	174
96 - Ride Quality Criteria	176
97 - SES-100B Broadband Response and Narrow Band Criteria	179
98 - VRC-1 With Dorsal Fin Control	183
99 - VRC-1 Initiating Turn to Starboard	184
100 - VA-3 and SR.N3 Thrust Vectoring	185
101 - Control of the SR.N4	186
102 - Free Propeller and Ducted Fan Configurations	187
103 - JEFF Craft Propeller Installations	187
104 - Swiveling Control Ports	188
105 - Efficiency of Tandem Propellers	191
106 - Typical Propeller Forces in Yaw	192
107 - Thrust and Normal Force on Free Propeller	193
108 - Thrust and Normal Force on Shrouded Propeller	194
109 - Reverse Thrust of Free Propeller	195
110 - Bow Thruster	196
111 - Cushion Valves and Ports	198
112 - Skirt Lift	199
113 - Cushion Shift	199
114 - BH.7 Yawing Moment Coefficient	201

	Page
115 - BH.7 Yawing Moment at 50 Knots	201
116 - BH.7 Model Hydrodynamic Sideforce	203
117 - Variation of Wave Drag with Froude Number and Yaw Angle	204
118 - Wave Drag of Rectangular Air Cushion Craft in Yaw	205
119 - Gimbal Fan Aeromobile 14	207
120 - Gimbal Fan Aeromobile 16	208
121 - Basic Skirt Systems	210
122 - BH.7 Mk 2 Bag-Finger Skirt System	212
123 - Development of Bag-Finger Skirt through 1966	213
124 - Developments in Finger Length.	214
125 - Skirt Bounce	215
126 - Antiplow and Antibounce Webs (SR.N4)	216
127 - Typical Finger and Attachment	217
128 - Wave Following Vertical Acceleration	219
129 - Compartmentation Development	221
130 - Keel and Rear Skirt Sections	222
131 - Two-Dimensional Bag Section	224
132 - Schematic and Details of VT 1 Skirt	227
133 - Segments in VT 1 Loop-Segment Skirt	228
134 - Some Jupe Skirt Characteristics	229
135 - Pericell Skirt Forms	232
136 - JEFF(A) Pericell Skirt System	233
137 - Deep Pericell Roll Stiffness	234

	Page
138 - SES-100B Stern Seal	236
139 - Tensile and Tear Strength of Skirt Materials	237
140 - Typical Skirt Fabric Weave Patterns	239
141 - Skirt Material Testing	242
142 - Delamination and Wear of Skirt Material	244
143 - Tensile Fatigue Tests on Skirt Material	245
144 - Skirt Material Specific Weight	246
145 - Skirt Finger Life	249
146 - Finger Life Improvement	251
147 - Skirt System Weight	251
148 - Structural Weight of Various Craft	254
149 - Air Cushion Craft and Hydrofoil Costs	256
150 - Load and Pressure Wave Impact Factors	260
151 - Hull Impact Design Limit Pressures (U.S. Craft)	261
152 - Slam Pressure on SES Bow	262
153 - Bow Impact Pressure Design Criteria	264
154 - Typical Structural Models	268
155 - Idealized Structural Model	269
156 - Structural Weight Fraction	271
157 - Effect of Density on Structural Weight	273
158 - SES-100A Construction	277
159 - SES-100B Construction	279
160 - Typical Structural Index Comparison	281

	Page
161 - JEFF(A) Hull Construction	283
162 - Finished Structure of JEFF(A)	284
163 - JEFF(B) Hull Construction	285
164 - Finished Structure of JEFF(B)	286
165 - Bell-Halter 110	287
166 - B-H 110 Midship Section	288
167 - B-H 110 Under Construction	289
168 - VT 1 and BH.7 Construction	291
169 - Construction of Stretched SR.N4	292
170 - Plating Weights	293
171 - Typical Lift Fan System	296
172 - Types of Lift Fans	297
173 - Typical Pressure Distribution Through Lift System	299
174 - Some Actual Lift System Arrangements	303
175 - XR-1D Lift System Arrangement	303
176 - Generalized Fan Sizing	306
177 - SR.N4 Model Fan (SR.85) Characteristics	309
178 - Typical Pressure-Flow and Efficiency Curves	311
179 - Dowty-Rotol Fan Data	313
180 - SR.N4 Fan	315
181 - Some Centrifugal Fans	316
182 - Typical HEBA-B Fan Performance	317
183 - SES-100A Venting System	320
184 - Hamilton-Standard Active Axial Fan Scheme	321

	Page
185 - Aerojet Active Centrifugal Fan Scheme	322
186 - Variable Geometry Lift Fan	323
187 - Fan Pressure-Flow Characteristics Under Dynamic Conditions	325
188 - Centrifugal Rotating Fan Weight	329
189 - Air Cushion Craft Propulsion System Weight	332
190 - Specific Propulsion System Weight	333
191 - Specific Weight of Engines	335
192 - Specific Fuel Consumption of Marine Gas Turbines	337
193 - Specific Fuel Consumption of Diesel Engines	337
194 - SR.N Engine Air Filtration Schemes	342
195 - Spray Suppressant Skirt.	344
196 - JEFF(B) Operating in Spray	345
197 - Typical Thrust and Drag Curves	346
198 - Static Thrust of Air Propellers	348
199 - Free Propeller Thrust Efficiency	353
200 - Shrouded Propeller Thrust Efficiency	354
201 - VT 2 with Shrouded Propellers	355
202 - Bow Thrusters in Cruise Condition	356
203 - Bow Thrusters in Reverse Thrust Position	357
204 - Dowty-Rotol Air Cushion Craft Propellers	358
205 - Carbon Fiber Reinforced Plastic SR.N6 Propeller	360
206 - SR.N6 Mk 6 Twin Propeller Installation	361

	Page
207 - Hawker-Siddeley Dynamics Composite Blade	361
208 - JEFF(A) Propeller and Shroud	363
209 - VT 2 Model and Propeller Blade	364
210 - VT 2 Propeller	365
211 - VT 2 Propeller and Shroud	366
212 - Hamilton-Standard Q-Fan	367
213 - Free and Shrouded Propeller Weight	368
214 - Air Jet Propelled Air Cushion Craft	371
215 - Air Jet Propulsion Elements	372
216 - Fan Air Jet Propulsion Thrust Efficiency	375
217 - Jet Velocity Ratio and Fan Parameters	376
218 - HEBA-B Fan Performance Characteristics	377
219 - Hovermarine HM.2 Subcavitating Propeller	381
220 - Some Supercavitating Propellers	382
221 - Subcavitating Waterscrew Efficiency	383
222 - Supercavitating Foil and Propeller Sections	385
223 - Typical Supercavitating Propeller Thrust Curve	386
224 - Variable-Geometry Marine Propulsor	387
225 - Operating Regions for Subcavitating and Supercavitating Propellers	388
226 - Supercavitating Waterscrew Efficiency	389
227 - Preliminary Design Chart for Waterscrews	391
228 - Preliminary Design Chart Example	393
229 - Subcavitating and Supercavitating Propeller Weight	394

	Page
230 - Waterjet Schematic	397
231 - Waterjet Efficiency	399
232 - Waterjet Inlet Cavitation	400
233 - Nondimensional Waterjet Pump Performance	403
234 - SES-100A Thrust Curve (Pod Inlet)	404
235 - Waterjet Pumps	405
236 - Aerodynamic Lift and Drag in Surface Effect	409
237 - U.S. Navy PAR-WIG Model in Tow Tank	411
238 - Geometry of PAR-WIG	412
239 - PAR-WIG Static Lift and Drag	413
240 - End Plate Immersion	414
241 - Kawasaki KAG-3 and Lippisch X-113	416
242 - Aerofoilcraft RFB-114	417
243 - Channel Flow Craft Lift and Drag	418
244 - Variable Geometry Skirted WIG Concept	419
245 - Jet Flap Effect on Aerodynamic Center in Ground Effect	421
246 - VRC-1 Jet Flap	422
247 - Efficiency of Variable Geometry Craft	424
248 - Some Low Speed Applications of Air Cushion Principle	427
249 - Air Cushion Icebreaking Attachment	428
250 - Identification of Weight Items	448
251 - Structural Weight Fraction	449
252 - Propulsion System Weight	451

	Page
253 - Specific Propulsion System Weight	452
254 - Electrical System Weight	453
255 - Specific Electrical System Weight	454
256 - Command and Surveillance System Weight	455
257 - Auxiliary Less Lift System Weight	456
258 - Lift System and Skirt System Weight	458
259 - Manning Aboard Ship	459
260 - Outfit and Furnishings Systems Weight	460
261 - Armament System Weight	462
262 - Empty Weight Fraction	463
263 - Typical Supercavitating Propeller Thrust Curve	466
264 - Typical Thrust and Drag Curves	467
265 - TUCUMCARI Thrust and Drag	468
266 - PCH-1 (MOD 0) Thrust and Drag	469
267 - 200 Tonne ACV Thrust and Drag	470
268 - 1264 Tonne ACV Thrust and Drag	470
269 - 3000 Tonne ACV Thrust and Drag (Water Propelled)	471
270 - 3000 Tonne ACV Thrust and Drag (Air Propelled)	472
271 - Thrust Margin and Hump Time	473
272 - Hump Time and Displacement	474
273 - Hump Drag in Rough Water	476
274 - Wave Pattern Combining Four Regular Waves	483

	Page
275 - Energy Spectrum of Random Sea	484
276 - Spectral Density for Hypothetical Craft	489

LIST OF TABLES

1 - Leading Particulars of Representative Air Cushion Craft	34
2 - Air Cushion Craft Drag Components	116
3 - Air Cushion Craft Power Requirements	121
4 - Effect of Cushion Compressibility	138
5 - Crest Factors for Air Cushion Craft	178
6 - Bag Parameters of Existing Craft	222
7 - Finger Parameters of Existing Craft	223
8 - Typical Factors of Safety	266
9 - SR.N4 Power Distribution	301
10 - Air Cushion Craft Lift Fans	308
11 - Engine Specific Weights	336
12 - Air Cushion Craft Air Propellers	347
13 - Subcavitating and Supercavitating Waterscrews	379
14 - Waterjet Pumps	402
15 - Low Speed Air Cushion Platforms	426
16 - Air Cushion Craft Weight Breakdown	442
17 - Light Ship Weight Groups	443
18 - Loads Groups	445
19 - Changes from 1973 SWBS to 1977 SWBS	446
20 - Acceleration and Time to Hump Speed	475

	Page
21 - Computation of Hump Thrust Margin	479
22 - Random Sea Wave Heights	486
23 - Pierson-Moskowitz Wind and Sea Scale	488
24 - Frequency Interval Factors	490

NOTATION

The following is a list of the most used symbols in the report, together, where appropriate, with the equation number in parentheses or figure number where its definition may be found. Where convenient or not defined in the text, the definition is also included here. Less used symbols and self-explanatory subscripts are not listed. Occasionally, the same symbol is used for different quantities, e.g., λ both for wavelength and for scale factor. This is in deference to common practice and should not cause confusion. All uses of a symbol are included in this list.

A	Wave amplitude, maximum height of fan volute disk area
A.F.	Activity factor
AR	Aspect ratio (B^2/S)
B	Cushion beam, width of fan volute
b	Width of sidehull, fan outlet depth column width
C	Peripheral length of cushion;
C_c	Cushion capacitance (125)
C_D	Drag coefficient (92)
C.G.	Center of gravity
C_L	Lift coefficient (12) (227)
C_{L_1}	Integrated design lift coefficient (169)
C_N	Yawing moment (151)
C.P.	Center of pressure
C_P	Power coefficient (27)
C_Q	Flow coefficient (26)
C_T	Thrust coefficient (210)
C_μ	Jet blowing coefficient (233)
c	Chord

D	Drag, diameter, bending material depth
DOC	Direct operating cost (1)
D_c	Discharge coefficient
D_s	Specific diameter (179), (184), (225)
d	Water depth
E	Energy of response (147) (see also Appendix D)
e	Exponential
F. No.; F_N	Froude number (23)
$F(x)$	Function of jet thickness (49)
$G(\omega)$	Transfer function (138) (see also Appendix D)
$G(x)$	Function of jet thickness (42)
g	Gravitational constant (32.2 ft/sec ²)
H_f	Total head across fan (171)
H_j	Total head (34)
h	Nominal leakage air gap or height (19)
h_c	Cushion depth (height)
h_f	Finger height
h_s	Skirt depth or height (137), (Figure 77)
h_w	Wave height (101) (see also Appendix D)
IVR	Inlet velocity ratio (222)
J	Advance ratio (V/nD)
K	Waterjet loss factor (223)
K_ϕ	Roll stiffness (136)
k	Pressure number (29)

L	Cushion length (14), lift, column length
L_e	Effective cushion length (152)
M	Magnification ratio (112)
M_ϕ	Rolling moment (134)
m	Mass, bending moment
N	rpm, cycles to failure
N_s	Specific speed (178)
n	Vertical acceleration (153), rotational speed
n_w	Wave impact load factor (161)
P	Power
P_i	Ideal propulsive power (190)
p	Pressure (gage)
P_A	Absolute pressure of air
P_b	Bag pressure
P_c	Cushion pressure (17)
P_v	Vapor pressure of water
Q	Cushion flow (38), (40)
q	Dynamic head in air
q_w	Dynamic head in water
R	Range (239)
RAO	Response Amplitude Operator (114)
R. No.	Reynolds number

$R(\omega)$	Response spectral density (138)
r	Radius
S	Cushion area, applied load
S_F	Frontal area of craft
$S(\omega)$	Seaway spectral density (141), (143) (see also Appendix D)
s	Laplace operator
sfc	Specific fuel consumption
T	Thrust, bag tension (154)
TAC	Trapped air cushion
TOC	Total operating cost (2)
t	Thickness of jet, time, plate thickness
U	Enclosed volume of fan volute
U_j	Peripheral jet velocity
$u(r)$	Velocity in jet (31)
V	Craft speed
V_b	Block speed
V_c	Cushion volume
V_j	Exhaust jet velocity (211)
V_s	Sink velocity, structural enclosed volume
V_v	Vertical velocity (162)
V_w	Wind speed (142)
W	Craft displacement (13)
$W_i (i=1,2,\dots)$	Subsystem weights (see Appendix B)

W_c	Column weight
W_F	Fuel weight
W_p	Payload (see Appendix B)
W_s	Craft structural weight (170)
w	Specific weight
x	Nondimensional jet thickness (33), nondimensional distance
Z	Vertical displacement
α	Angle of attack
β	Hull deadrise, propeller pitch, half cone angle
γ	Ratio of specific heats
Δ	Sidehull displacement (85)
ϵ	Intake recovery factor
ζ	Damping ratio (113)
η	Efficiency
η_p	Propulsive efficiency (198), (199)
η_s	Fan static efficiency (173)
η_t	Fan total efficiency (172), (185)
θ	Jet inclination, pitch trim
λ	Wavelength, scale factor
μ	Viscosity
ρ	Mass density of air (slugs/ft ³)
ρ_w	Mass density of water (slugs/ft ³)

σ	Cavitation number (24), average stress
τ	Trim angle of hull
ϕ	Flow coefficient (177), roll angle, phase angle
ψ	Pressure coefficient (175)
ω	Wave frequency (101)
ω_e	Encounter frequency (139)
ω_m	Wave frequency for maximum energy (144)
ω_n	Natural frequency (107)

ABSTRACT

A technical summary is given of the development of air cushion craft from their inception to the present day. The designation "air cushion craft" encompasses any craft that relies on a cushion of air for a significant part of its support and operates in close proximity to the surface. The technical summary covers both arostatic craft known as air cushion vehicles (ACV) and surface effect ships (SES) as well as aerodynamic craft such as wing-in-ground effect vehicles (WIG). Other variants are included in the review.

Where possible, the various available theories, empirical laws, and experimental data have been brought together and expressed in unified form. Emphasis has been given to reducing the data and analysis to their simplest forms for easy understanding and isolation of fundamental parameters. In the interest of historical accuracy, care has been taken to cite the original work on any particular theory or piece of data. To make this report readily available, in some instances it has been necessary to avoid the use of classified or proprietary data but this has not hampered the citing of original work. Currently operational craft, those still in their construction jigs, or in some cases those still on the drawing board are assessed and compared to the basic theories to give a measure of the state-of-the-art.

This technical summary is an updated and expanded version of a similar review conducted in 1975 and published as DTNSRDC Report 4727. The additions include a new chapter on Control and appendixes on performance, weight data, and seakeeping. Much expanded material in the main text includes such topics as performance, propulsion, ride quality, and high speed aerodynamic craft.

ADMINISTRATIVE INFORMATION

The preparation of this summary was undertaken by the Systems Development Department in order to fill the need for an all-inclusive document giving the technical status of the state-of-the-art in air cushion craft.

This work was performed under the Amphibious Assault Landing Craft Program and was funded by the Naval Sea Systems Command (SEA 0325) under Program Element 63566N, Task Area S0241-AW001, and Work Unit 1180-710.

The Center cannot assume responsibility for the universal availability of all references mentioned in a technical document. Both the age of the document and sensitivity caused by imminent implementation of a system may impose originator's limits on availability.

ACKNOWLEDGMENTS

The author would like to take this opportunity to acknowledge the work of his coworkers, both past and present in the exciting field of the advanced marine vehicle and specifically the air cushion craft. Many of them have aided its development and their work is referred to in this report.

In addition, specific acknowledgment is given to the following organizations who readily have made available data and photographs of their products:

- Aerojet Liquid Rocket Company
- Bell Aerospace Company
- Bell-Halter Marine
- Bertelsen Incorporated
- Bertin et Cie
- Blandford Press
- British Hovercraft Corporation
- Dowty-Rotol Division of Dowty Exports Limited
- Hamilton-Standard Division of United Aircraft Limited
- Hawker-Siddeley Dynamics Limited
- Hovercraft Systems, Incorporated
- Hovermarine Transport Limited
- Jane's Surface Skimmers
- U.S. Navy Program and Technical Officers (various)
- Vosper-Thornycroft Limited

Especial thanks are extended to Mr. William Ellsworth, Associate Technical Director for Systems Development of the David W. Taylor Naval Ship Research and Development Center for the opportunity to prepare this summary.

CHAPTER I

INTRODUCTION

The air cushion craft* is one member of a class of advanced marine vehicles that offers superior performance or some other unique advantage over conventional craft. Along with the hydrofoil, it offers the high speed and improved rough sea performance over displacement craft of the same tonnage and payload. In contradistinction to other advanced marine vehicles, it offers, in its amphibious form, the unique capability of independence of the surface within certain limitations, and thus can operate over water, land, ice, or other terrain.

Attempting to write a summary of the state-of-the-art of air cushion craft after 20 years of exciting hardware development could be considered presumptuous in the light of the international proportions to which the development has expanded. Time well spent reading through Jane's Surface Skimmers^{1**} will convince the reader of the rapidly developing international interest. Since Sir Christopher Cockerell's ideas evolved into the first modern developmental hardware, the SR.N1 in 1959, developments have expanded in its birthplace, England, and in other corners of Europe, in the United States, and in the U.S.S.R.

Upon reflection on these last 20 years, it can be reported that an impressive record of development has been realized in both technical understanding and in operational exploitation. As might be expected along with the record of achievement, there still remain many fundamental questions where the designer must rely on empirical relationships in the absence of physical descriptions. Here, we have a dilemma; because, while the technical state-of-the-art is improving rapidly the cost of the vehicle is also increasing at a rate that threatens further development. Sophistication of design rather than simplicity of design unfortunately has become common practice in some recent craft such that the accompanying high cost has masked the true value of the concept. Accordingly, in consonance with the theme established in the first issue of this technical summary,² emphasis will continue to be maintained in this volume to present analyses and results in a simple yet physically correct form for rapid use by a designer seeking an answer to a reasonable and practical level of accuracy.

The air cushion craft, in all its forms, is still a little tender in its development as it seeks its true place in the commercial field of transportation or as a fighting vehicle in the Navies of the world. Its characteristics (and cost!) change significantly as its speed, size, and seakeeping requirements change. Variations in these requirements have ramifications in the various technologies that need to be developed. For example, if speed is increased for some military or economic advantage the state-of-the-art of performance, seakeeping, and materials becomes less defined inviting protracted development periods.

*This name is used as a general descriptive; see section on names, page 5.

**A complete listing of references is given on page 491.

It should not be assumed, however, that an advanced marine vehicle shall always be faster than an existing means of transporting payload. Perhaps it is more important to be better in terms of fuel economy or to minimize turnaround time among other important economic and tactical factors.

Therefore, the intent here is to examine the air cushion craft in its various forms and to accumulate the results of those who have helped in its development, in order to determine the present state-of-the-art. Naturally, on a subject as broad as this and containing many important details, the study frequently must be selective and sometimes qualitative. There are many excellent papers covering either detailed technical aspects or operational considerations and related subjects. Where these occur, the reader is referred for more detailed treatment.

In those chapters dealing with the theoretical aspects, those key results and theories found most useful in craft design have been assembled and expressed in a unifying theory for completeness. For reasons of space, if the subject is well known or can be treated by standard methods known to the naval architect or aircraft designer, only a brief description is necessary. The aerodynamic drag of mound flow bodies would be one such example. Attention is given to those technical aspects that are peculiar to the art and require more development for their complete understanding. Some minor changes in trends have appeared since the earlier summary was published. By and large, the trends have continued and this summary adds to rather than changes the expanding data base.

Similarly, in chapters dealing with hardware systems such as fans, propulsion, and structure, it is considered that the basic engineering follows well-understood principles. Attention is therefore given to describing how those principles resulted in different hardware according to different design philosophies.

With the above approach, it is hoped to determine, in some quantitative manner, the technical status of air cushion craft development as it looks today. It is left to other papers to describe the operational status in terms of economics and mission application. Since the conclusions in the earlier summary contained a specific list of key problem areas that existed at that time, their absence from this summary can be taken as some small measure of the improvement in the state-of-the-art over the last three to four years. In those cases where the key problem has been removed, the reader will find an expanded section in the main body of the report reflecting the work done in that particular area.

Before proceeding, it should be noted that not all of those involved in the development of this craft have agreed on its name over the years. It is important to clarify this, because confusion has arisen in the literature over the use of the same name for craft of different basic principles of operation. Accordingly, with the reader's indulgence, this is tackled first.

WHAT'S IN A NAME?

The various types of craft that are the subject of this report have been described in the literature and by those involved in their design and development by many names, such as:

- Hovercraft
- Air Cushion Craft
- Cushion Craft
- Ground Effect Machine (GEM)
- Interface Craft
- Skimmer
- Air Cushion Vehicle
- Surface Effect Ship
- Surface Effect Vehicle (SEV)
- Aeroglisseur

In addition to these generic names, individual craft names have been used to describe specific forms; these include:

- Wing-in-Ground Effect (WIG)
- Ram Wing
- Channel Flow Wing
- Captured Air Bubble (CAB)
- Plenum Machine

Unfortunately, but not unnaturally, proponents of particular forms have tended to use the names of particular types to reflect a generic form, and confusion has arisen when attempting to describe the nature of the particular craft. Further, national origin has also influenced the name.

Sir Christopher Cockerell, the recognized inventor of the craft in its modern-day form, christened his invention the hovercraft, which is the generic name still used in England to describe all forms of the craft whether amphibious or nonamphibious. It is only proper and fitting that this name appears first on any list.

In France, the late Monsieur Jean Bertin, the French pioneer of the art, named his craft Aeroglisseur, which certainly conveys the idea of sliding along on air.

In the United States, a profusion of names have appeared. Probably one of the earliest names is the ground effect machine or GEM. The name appeared naturally as a result of work with helicopters and vertical and short takeoff and landing (V/STOL) aircraft, where it was noticed that, as the craft approached the ground in its hovering mode, an increase in lift occurred due to the ground effect.

The name surface effect ship originated in the offices of the Maritime Administration when it was decided that the words ground and machine did not fit the nautical world, although it was agreed that the effect was still there. Accordingly, the acronym GEM was changed to SES. This change occurred on an ongoing project in 1961, the MaRad Columbia Project, and, had it proceeded under the old name it would have been "Columbia, the GEM of the Ocean."

The phrase, air cushion vehicles was coined as a generic name for all craft operating on a cushion of air in England in early 1961, and a magazine supplement to "Flight International" entitled "Air Cushion Vehicles" was devoted to the promulgation of the embryonic industry.

Small craft in England using the air cushion principle in early 1962 adopted the name skimmer in close parallel designation to the French word aeroglisser, but these names usually became specific craft names rather than descriptions of the generic form. An example in the United States was the Bell SKMR-I, the first and largest skimmer or air cushion vehicle at that time in 1963.

The term surface effect vehicles took on a more encompassing definition in 1962 in England by including any advanced marine vehicle that operated close to the surface. In July 1962, in the London General Ship Owners Society annual report, there appeared plans for the regulations of operating "Surface Effect Vehicles: Hydrofoil and Hovercraft." On the other hand, in the U.S.S.R.,³ the term surface effect vehicle exclusively applies to a specific form of air cushion craft that would be called the high speed aerodynamic form in this country and would include only wing-in-ground effect and channel flow forms.

This profusion of names on both sides of the Atlantic and the constant redefinition by different groups has made it somewhat difficult to communicate basic principles and differences in performance among the different forms of craft that have appeared over the last 20 years.

It has now become common practice to use the name air cushion vehicle when discussing amphibious craft supported on a cushion of air, and surface effect ship when discussing large displacement, nonamphibious ships supported on a cushion of air.

Accordingly, for this report, the generic name air cushion craft will be used to describe all forms of craft, amphibious and nonamphibious, that use air pressure as an essential part of providing lift.

THE AIR CUSHION CRAFT

To aid discussion, Figure 1 illustrates the basic definition of the air cushion craft in its most general form.

In other words, the air cushion craft is defined as:

"Any craft designed to operate for significant periods of time in the proximity of the surface over which it operates and to generate a significant part of its lift through pressurized air flow."

It is felt that this definition captures the two essential elements: the proximity of the surface and the cushion air pressure support. Such a definition applies to the static and moving hovercraft that generates all

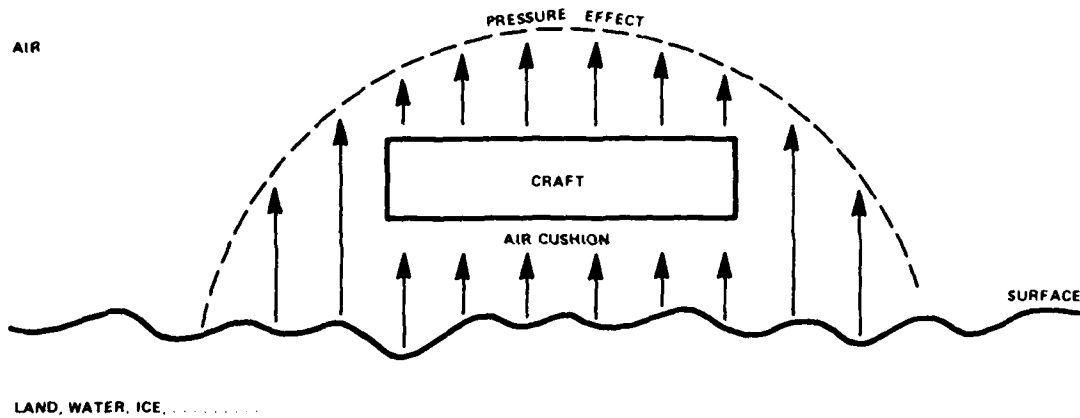


Figure 1 - Air Cushion Craft

of its lift through air cushion support. It also applies to the non-amphibious ship that supports itself partly by hydrodynamic lift. The definition also applies to the ram wing, WIG, and channel flow craft that must remain close to the surface to generate dynamic air pressure lift, but the definition excludes the conventional aircraft that may fly occasionally in ground effect.

From such a description of the air cushion craft, one can see the common, but not too rigorous, usage of its two main forms today: the ACV applying more to small vehicles for amphibious operation and the SES applying more to large ships for commercial and naval applications.

CHAPTER II

BACKGROUND DEVELOPMENT

Several texts are available describing the history of air cushion craft development. Two recent and complete reports are given as References 4 and 5.

In light of this published literature, it is not intended to present a similar chronological listing of historical development but rather to give a categorization of the main themes of development, which hopefully will focus on how the development is unfolding in some of the more dominant directions.

Hayward⁶ provides an excellent search into the past to uncover such devices as Emmanuel Swedenborg's man powered air cushion platform in 1716. Other historical research of note includes the first patent for air lubrication issued in England to another Swedish engineer Gustav Laval, in 1882. Laval's experiments were not successful, however; it was not until after 1916, when Von Tomamhul built a torpedo boat for the Austrian Navy using fans to pump air beneath the hull to form a small air cushion, that various types of air cushion principles began to evolve. In 1925, a patent was issued to V.F. Casey for the use of the energy saving recirculation principle, a principle that has been revived periodically over the last 10 years but has been overshadowed by the development of skirts.

In 1927, K.E. Tsiolkovski a noted Russian scientist, developed what today might be called the hovertrain. This idea proposed to run trains supported by a thin air cushion layer along a track.

In 1929, D.K. Warner won the boat races on Lake Compounce, Connecticut, by the use of the trapped air cushion or captured air bubble principle on his sidehull craft with planing bow and stern seals. Then, in 1935, Toivio Kaario a Finnish engineer, developed both a plenum principle craft and the first ram-wing-principle craft.

While a research of the literature will find many such examples of scientists and engineers around the world who had uncovered the various principles of the air cushion, it was not until 1955 that the modern development began.

In 1955, Christopher Cockerell (now knighted for his achievements) was awarded a patent⁷ for his annular or peripheral jet principle which, because of its power-saving features, offered the most promise for the air cushion craft. Cockerell then proceeded to develop the first annular jet craft in 1959. This craft was built by Saunders-Roe Ltd. (now British Hovercraft Corporation (BHC)) by a team of engineers headed by R. Stanton-Jones, and it was designated the SR.N1. The trials and tribulations of such a development are best described by Cockerell and Stanton-Jones themselves.^{8,9}

In this same period, research was being conducted in the United States along similar lines. Melvin Beardsley narrowly missed being first with his work on annular jets in 1955. Dr. Harvey R. Chaplin¹⁰ was responsible for most of the basic research of air cushion craft that had its beginnings in May 1957 with V/STOL research at the David Taylor Model Basin (presently the David W. Taylor Naval Ship Research and Development Center).

With the above admittedly sketchy background, the air cushion craft will now be described.

DESCRIPTION OF AIR CUSHION CRAFT

In the body of the report, reference is made to the different forms of air cushion craft that are illustrated here. Attention is restricted to those forms that have received serious development; for example, early research into water-sealed curtains is not covered.

There are four basic forces of importance to a craft that operates in the interface between water and air; they are aerostatic, aerodynamic, hydrostatic, and hydrodynamic forces, and it is convenient to use these to classify the air cushion craft.

Figure 2 has been prepared as a family tree that shows where the various craft fit. It has been left incomplete in terms of showing a large range of craft for the sake of clarity.

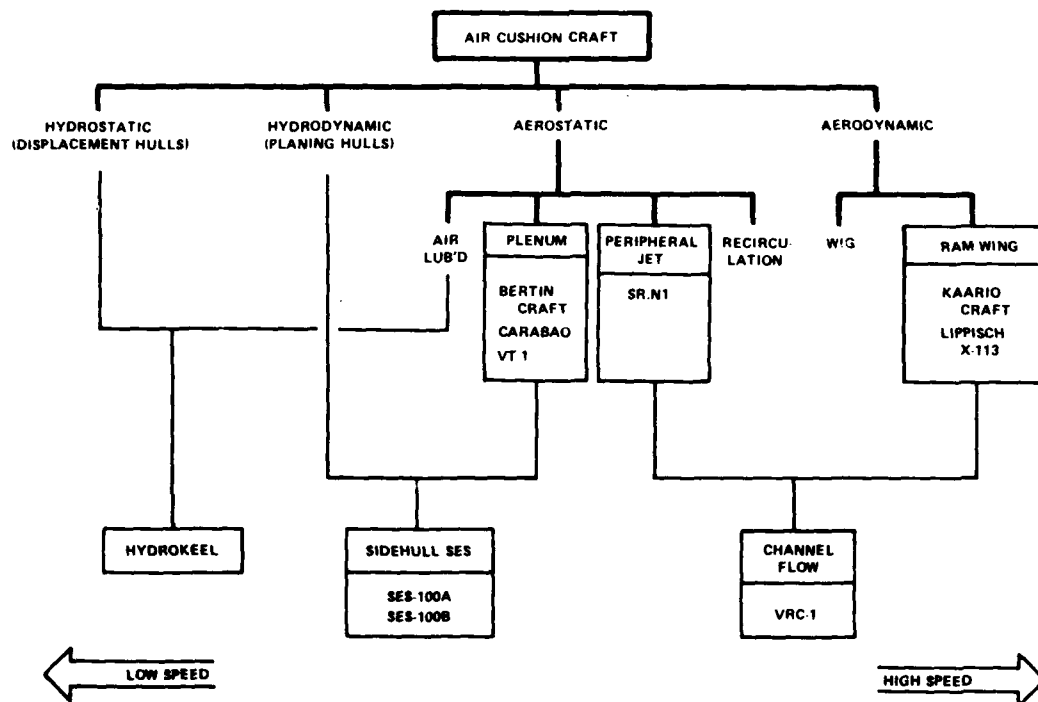


Figure 2 - Air Cushion Craft Family Tree

Aerostatic Class

The first class, and by far the largest, is that designated "aerostatic" and encompassing the plenum and peripheral jet forms pioneered by Cockerell as discussed above. Figure 3 illustrates the basic form of this type of air cushion craft. Two other forms of aerostatic craft would be

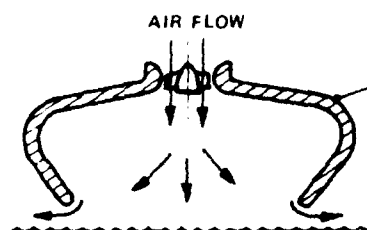


Figure 3a - Simple Plenum

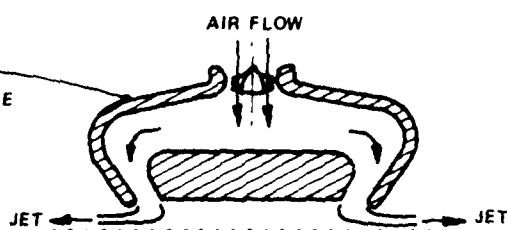


Figure 3b - Simple Peripheral Jet

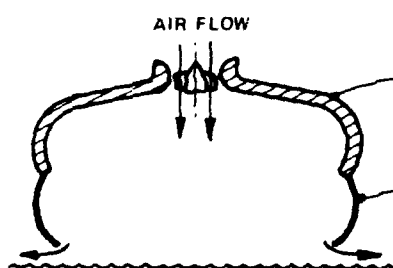


Figure 3c - Skirted Plenum

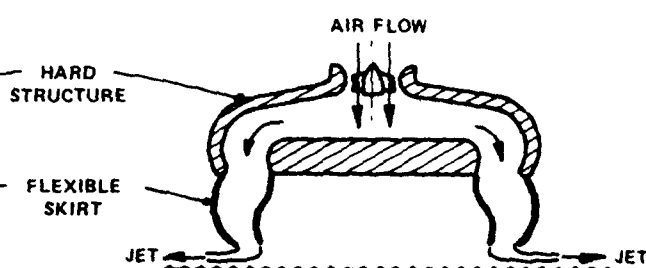


Figure 3d - Skirted Peripheral Jet

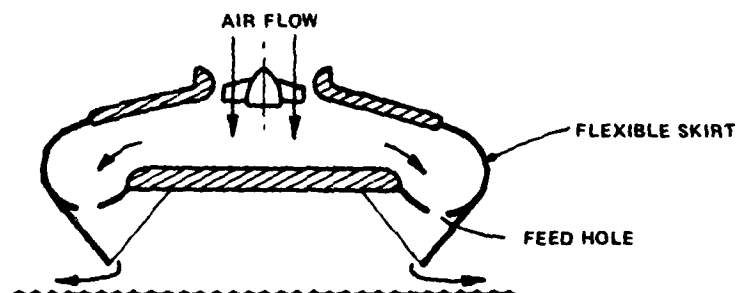


Figure 3e - Modified Plenum (Skirted)

Figure 3 - Plenum and Peripheral Jet Basic Forms

the air-lubricated and recirculation types. These were developed in the late 1950's and early 1960's by such groups as Ford Motor Company, Martin Company, and Canadair Ltd., but have not been pursued since. They are excluded here for brevity. Figure 3a shows the simple inverted bathtub plenum, where fan air is blown into the plenum or cushion, pressurizing it to generate the desired aerostatic lift. Figure 3b shows the simple peripheral jet, where the centrifugal forces generated by the turning jets

reates the desired pressure rise in the cushion. This fundamental principle resulted in the SR.N1 shown in its skirted version in Figure 4.



Figure 4 - Air Cushion Craft SR.N1 and SR.N4

Skirted versions, where flexible extensions are added to increase obstacle (wave) clearance for the same power (see Chapter VI), are shown in diagrammatic form in Figures 3c and 3d. As skirt development progressed, the pure peripheral jet gave way to a modified plenum skirt design similar to Figure 3e. Most operational amphibious air cushion craft today are of this type, and the 170-ton SR.N4, also shown in Figure 4, is one of the most noted examples. The BHC craft SR.N5, SR.N6, SR.N4, and BH.7 would have been listed in Figure 2 as belonging to both the plenum and the peripheral jet craft because of the evolution of their skirt designs.

Since the first technical summary was published, a significant milestone in air cushion craft development occurred when, on 6 April 1978, the Super 4 (a stretched version of the SR.N4) was launched and eight days later entered trials on the Solent, a body of water between the South Coast of England and the Isle of Wight. This 300-ton craft, shown in Figure 5 is, in reality, the SR.N4 Princess Anne with a 55 ft section

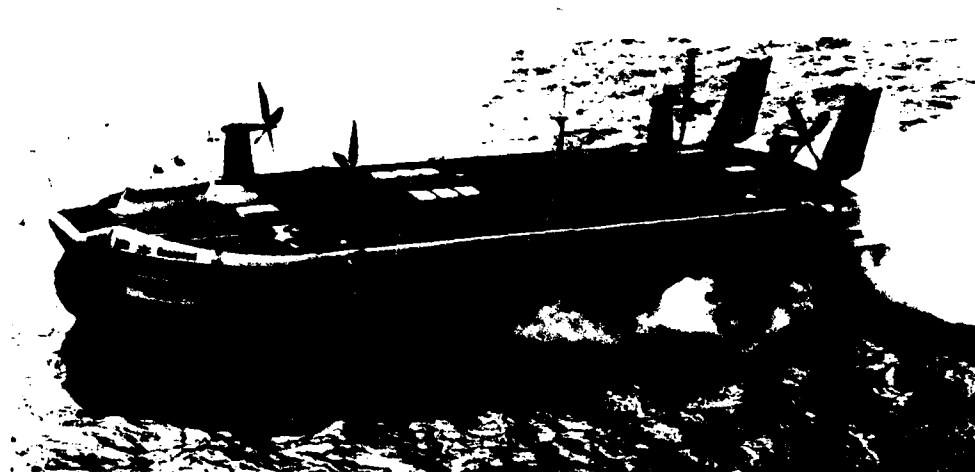


Figure 5 - Stretched SR.N4 (Super 4)

added midship. Other changes include a more bulbous bow skirt for improved wave impact avoidance and raised pylons to accommodate the larger 21-ft diameter propellers (see Chapter IX). This stretched SR.N4, the largest hovercraft in the world today, can now carry 416 passengers and 60 cars over distances up to 150 miles.

Waterborne Class

The second class of craft involves some form of hydrostatic or hydrodynamic surfaces. Figure 6 illustrates the basic forms considered. These include the hydrokeel (Figure 6a), which is essentially an air-lubricated hull with low buoyancy sidehulls sealing along the sides. There is some hydrodynamic lift from the trailing rear seal at speed.

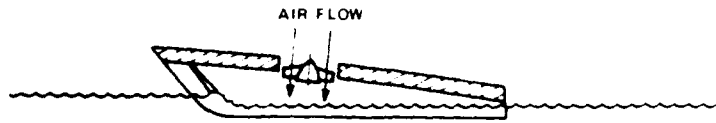


Figure 6a - Hydrokeel



Figure 6b - Captured Air Bubble

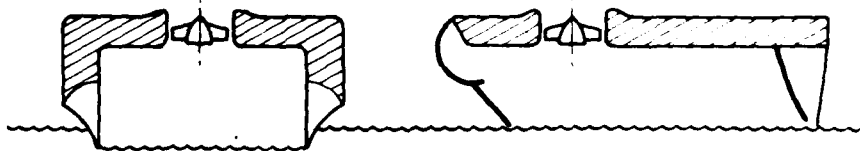


Figure 6 - Hydrostatic and Hydrodynamic Basic Forms

The modern day CAB craft pioneered by Al Ford,¹¹ following some of D.K. Warner's efforts in 1929, of which the basic form is shown in Figure 6b, essentially sought to capture the pressurized air with planing ski-like seals at the bow and stern and nonplaning knife-edge-like sidehulls fore and aft. Longitudinal and lateral stability was provided by the hydrodynamic forces on the planing seals.

The sidehull SES is a result of the development of the CAB and plenum or peripheral jet craft. Its basic form is shown in Figure 6c and includes shaping to the sidehull* to provide stability and ease of control. The seals at the bow and stern can be either planing surfaces or flexible skirts.

Examples of these nonamphibious forms of air cushion craft can be seen in Figure 7, which shows the SES-100A, the XR-3, and the SES-100B. The adjustable planing stern seal on the XR-3 and the flexible skirt-type seal on the SES-100B can be seen in Figure 7.

*Early craft used the term sidewall. Now that stability and performance benefits are found possible by shaping, it is felt that sidehull is a more descriptive term.

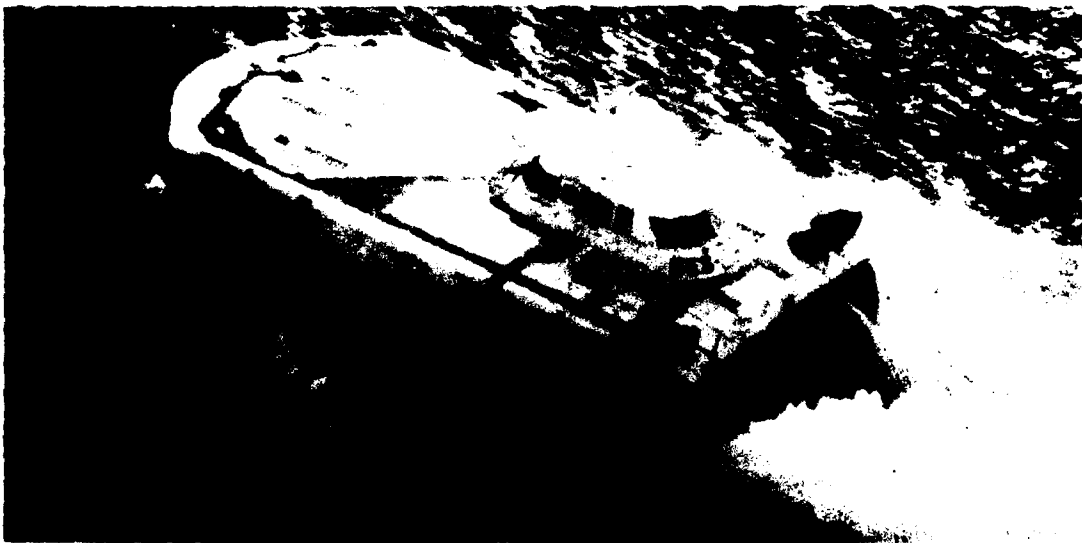
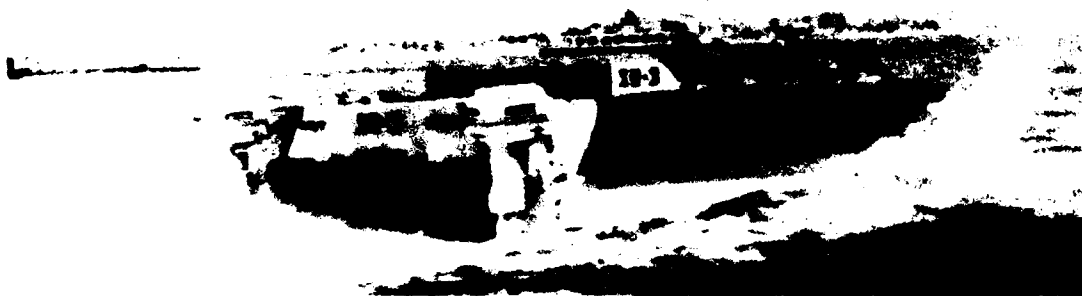
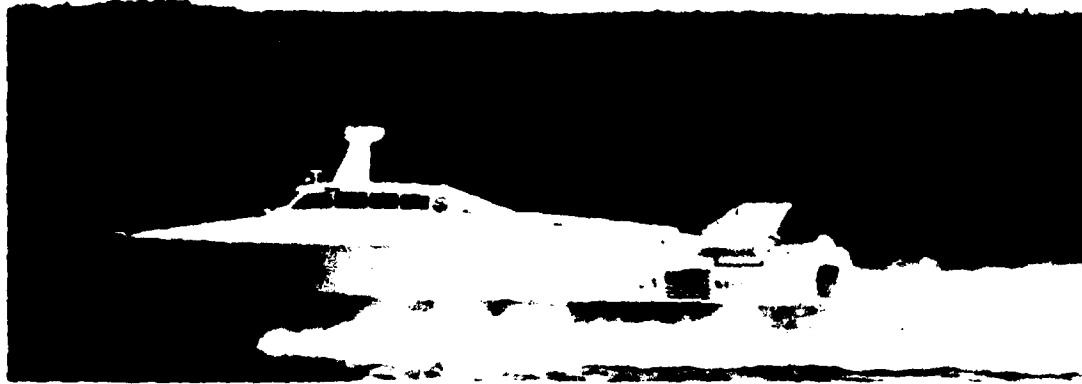


Figure 7 - Waterborne Air Cushion Craft

Aerodynamic Class

The third class of air cushion craft includes those craft that derive a significant amount of lift by aerodynamic means. Figure 8 shows the longitudinal and transverse cross section views of the basic forms of aerodynamic cushion craft.

The WIG effect shown in Figure 8a is simply the application of a conventional (high aspect ratio) wing flying in ground effect. The most cited example of this is the crossing of the Atlantic in 1929 by the Dornier Dox flying boat, which flew close to the sea surface to take advantage of ground effect. There are two important gains in performance by flying in ground effect that are pertinent to the aerodynamic cushion craft.

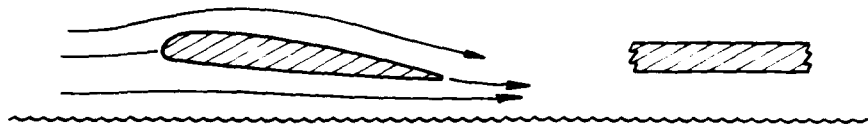


Figure 8a - Wing In Ground Effect



Figure 8b - Ram Wing

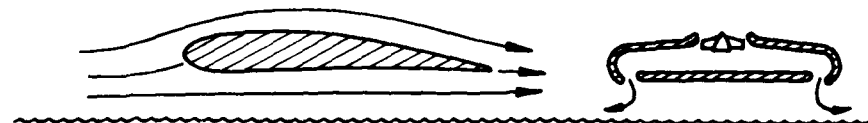


Figure 8c - Channel Flow Wing

Figure 8 - Aerodynamic Cushion Craft Basic Forms

The first gain in performance is that due to the increase in the bound circulation as the wing approaches the surface and distorts the streamlines. The stagnation point moves aft on the under surface and the increased curvature of the streamlines gives increased circulation and lift. The second gain in performance is that due to the partial destruction of the tip vortices. Again, as the wing approaches the surface, the

spanwise flow to the tip is diminished and the tip vortices weaken with the attendant reduction in aerodynamic-induced drag. It was mainly this reduction in drag that allowed the Dornier flying boat to improve its fuel consumption and gave it sufficient range to cross the Atlantic. Karl Weiland, the Swiss engineer, built a prototype of such a craft in 1963.

While gains in performance are realizable with the WIG, it still requires the wing aspect ratio to be of such proportions as to negate its fit to existing harbors, docks, and ways, and thereby, its application to marine use.

The ram wing is a craft that removes the problem of span. It is shown diagrammatically in Figure 8b and is essentially a low aspect ratio wing, with its trailing edge virtually touching the surfaces and with end plates at the wing tips to prevent the spanwise flow and to seal the pressurized ram air underneath. Since the entire lifting mechanism is provided by aerodynamic means, the ram wing has no hovering ability. As mentioned earlier, the first such application of this principle was Kaario's ram wing in 1935. More recent developments include those of A.K. Lippisch,¹² who perfected two prototypes, the X-112 in 1963 and the X-113 in 1971. A more recent version, the X-114, first flew in 1977 and will be shown and discussed in more detail in Chapter X. These craft were of low aspect ratio form and operated both in and out of ground effect. Figure 9 shows both the X-113 flying in ground effect (upper left) and Lippisch's design for a 300-ton transport aerofoil boat (upper right). In the latter case, it can be seen that the (passenger-carrying) sidehulls provide the necessary end-plate effect for the ram wing.

The channel flow wing (Figure 8c) is a development that combines the hovering capability of the peripheral jet principle with the high-speed dynamic lift of the ram wing. The end plate effect is now provided by the sealing of the air jets that run fore and aft at the craft's side edges. The bow and stern jets (not shown in Figure 8c) retract into the main body at high speed, where sufficient lift to support the craft is generated by aerodynamic means. The side jets remain operating to provide the vortex drag reduction. This concept was conceived by Scott Rethorst¹³ for the Columbia project. Figure 9 (middle and lower photographs) shows a prototype, the VRC-1, designed and built by the author in 1964, under test at Edwards Air Force Base, California.

The latest entry into the aerodynamic air cushion craft world is the U.S.S.R. development of a large craft observed on the Caspian Sea in early 1974 (Figure 10). While there is some conjecture as to its function and sea state capability, it is generally agreed that the jet exhausts from the canard mounted engines are tilted to flow beneath the main wing to augment its ground effect lift, reminiscent of the technique used by Kaario in 1935.

It can be seen from the three main classes of air cushion craft that, all else being equal, the designer can optimize the form of craft to meet the speed region required. Generally speaking, it can be inferred from Figure 2 that a progression to the right when combining the different principles results in craft designed for optimization at higher speeds. The specific details, tradeoffs, and limiting factors in a real-world design process are discussed in the succeeding chapters.

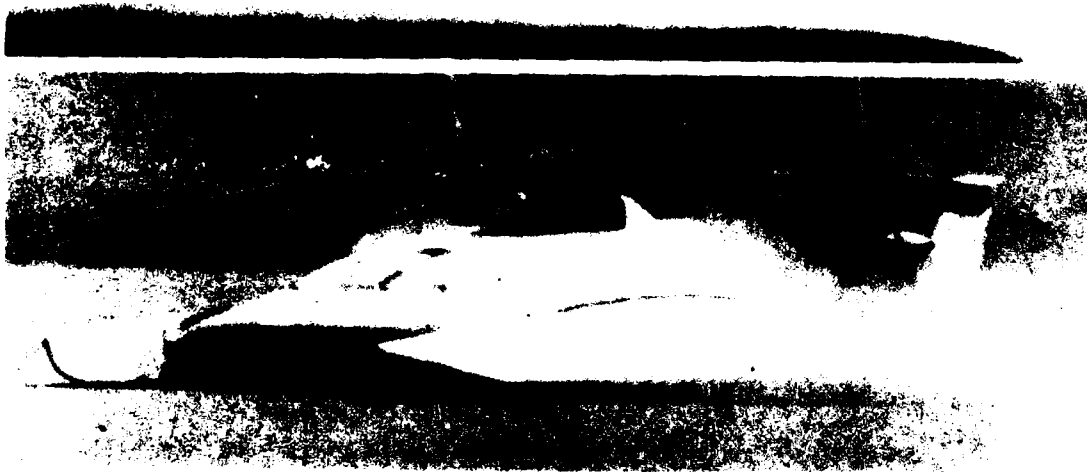
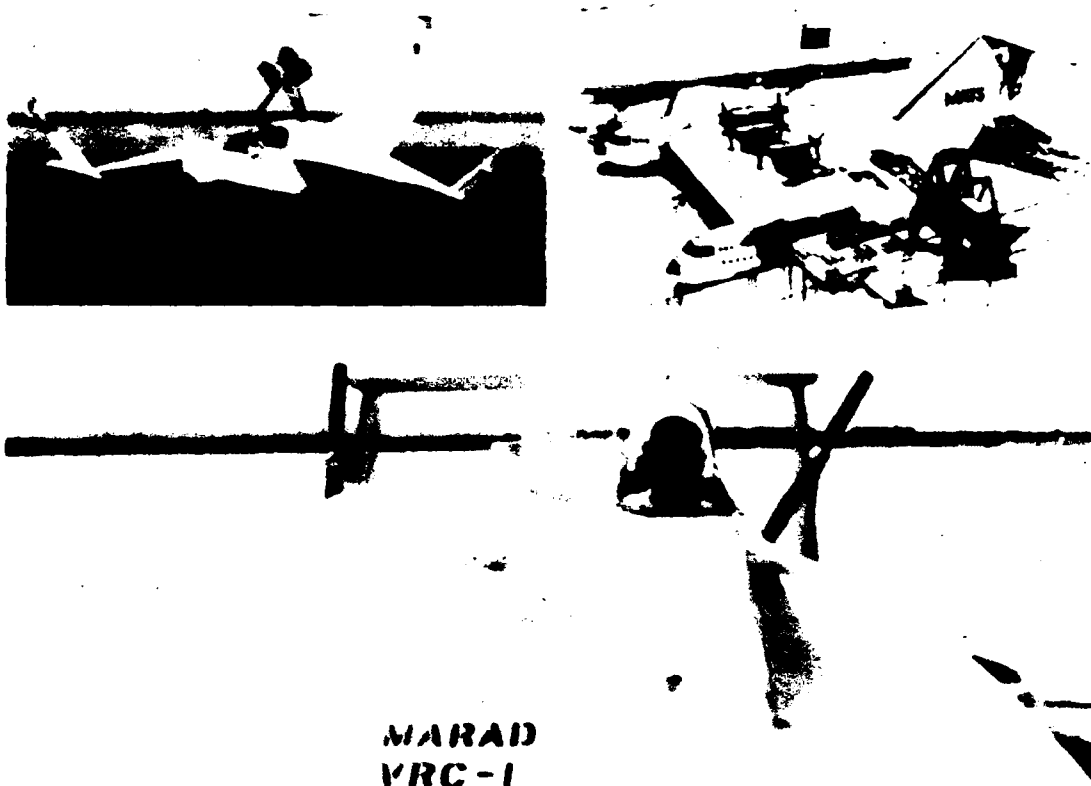


Figure 9 - Aerodynamic Cushion Craft

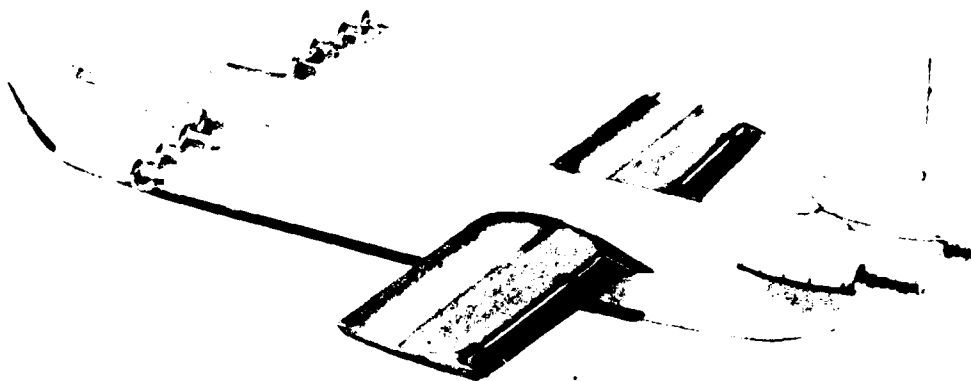


Figure 10 - Caspian Sea Monster

MAIN DEVELOPMENT EFFORTS

With such a wide range of types and many different operating principles, it is sometimes difficult to categorize where a particular development should proceed. It is suggested that there are three main groups of development; the boundaries of each group are necessarily somewhat fluid and overlapping, but at least they provide a means for discussion. These are:

- Low speed development 0 - 30 mph
- Intermediate speed development 30 - 100 mph
- High speed development 100 - 300 mph

Figure 11 summarizes the most visible or the most active developments in the air cushion craft field as grouped by the above rather arbitrary categorization. A few comments on each are felt pertinent.

Low Speed Development

Until relatively recently, the bulk of the development has been in the intermediate speed group spurred on by expectation of ambitious low cost operation. It is encouraging now to see, in addition, the emerging development of a class of vehicles that are designed to meet a need for low cost workhorses that use the air cushion where its uniqueness gives it an advantage over other forms of transport. These range from the industrial application for heavy load movement that started several years ago to the hovertrailers designed to transport heavy equipment into previously unreachable territory. Figure 12 illustrates three typical uses

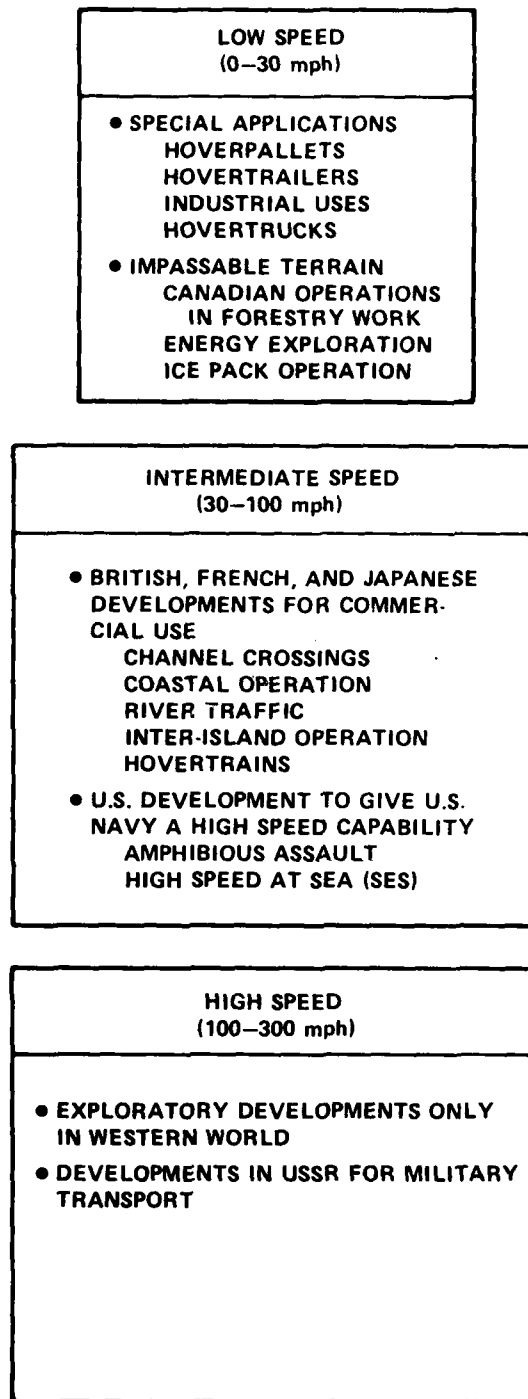


Figure 11 - Main Development of Air Cushion Craft



Figure 12 - Low Speed Applications of Air Cushion Principle

that are indicative of the application of the air cushion principle for low speed use. The top photograph shows the movement of a large storage tank by the use of a wraparound skirt system. The middle photograph shows the Bertin Terraplane, which can operate on the road as a conventional truck and which, by inflating the skirts or jupes, can lower the footprint pressure of the vehicle for traveling over mud or water. Propulsion in this mode is through the use of paddle type appendages to the wheels. The lower photograph typifies the latest area of development, which is currently being used in the development of the outlying territories of Canada. The need to explore new forms of energy and new locations for existing energy sources has hastened the need to move about in areas not presently suitable for conventional transportation. Most of the attention and interest at the present time is focused on Canada, where the oil discoveries at Prudhoe Bay, to cite one example, has prompted the need to move equipment over soft or environmentally sensitive terrain. Reference 14 provides a pertinent discussion on this emerging use of the air cushion principle, where emphasis must be on simplicity and payload capability.

Intermediate Speed Development

By far, the major development work to date has been in this category. There are many excellent papers describing the historical developments in this area which will not be repeated here, other than to note the main themes in encapsulated form.

While it is certainly true that the British have developed craft designed purely for military missions, such as the British Hovercraft Corporation BH.7, and have conducted military operations in such places as Borneo and Aden, it is without doubt that today they are the leaders in the commercial development of the air cushion craft. The largest majority of these craft are designed and built by British Hovercraft Corporation and operate on coastal routes ranging from 5 to 25 miles in length. The record is impressive, as may be seen from the English Channel crossing statistics where, since 1968 when operations began, the BHC SR.N4 craft (shown in Figure 4) have absorbed over one-third of the total cross-channel traffic. On August 16, 1974, Hoverlloyd, one of two air cushion craft operators across the English Channel, carried their 500,000th vehicle on an SR.N4. In 1977 hovercraft carried 27 percent of the cross channel passenger traffic and 23 percent of the vehicular traffic, a slight decline since the last report. To date, the two Seaspeed SR.N4 MK 1 craft have carried over 4,500,000 passengers and 700,000 vehicles and typically make 5,000 channel crossings carrying some 700,000 passengers and 100,000 vehicles each year. Figure 13 shows some of the British craft that are being used or have been used on commercial routes. The upper left photograph in Figure 13 shows the SR.N5, which was the first commercially successful air cushion craft and has operated on commercial routes around the world. It was constructed in 1963, has a nominal gross weight of 7 tons, and carries 20 passengers. Its maximum calm water speed is 66 knots. It has been manufactured under license in the United States by Bell Aerospace and designated the SK-5, and in Japan, by Mitsubishi and

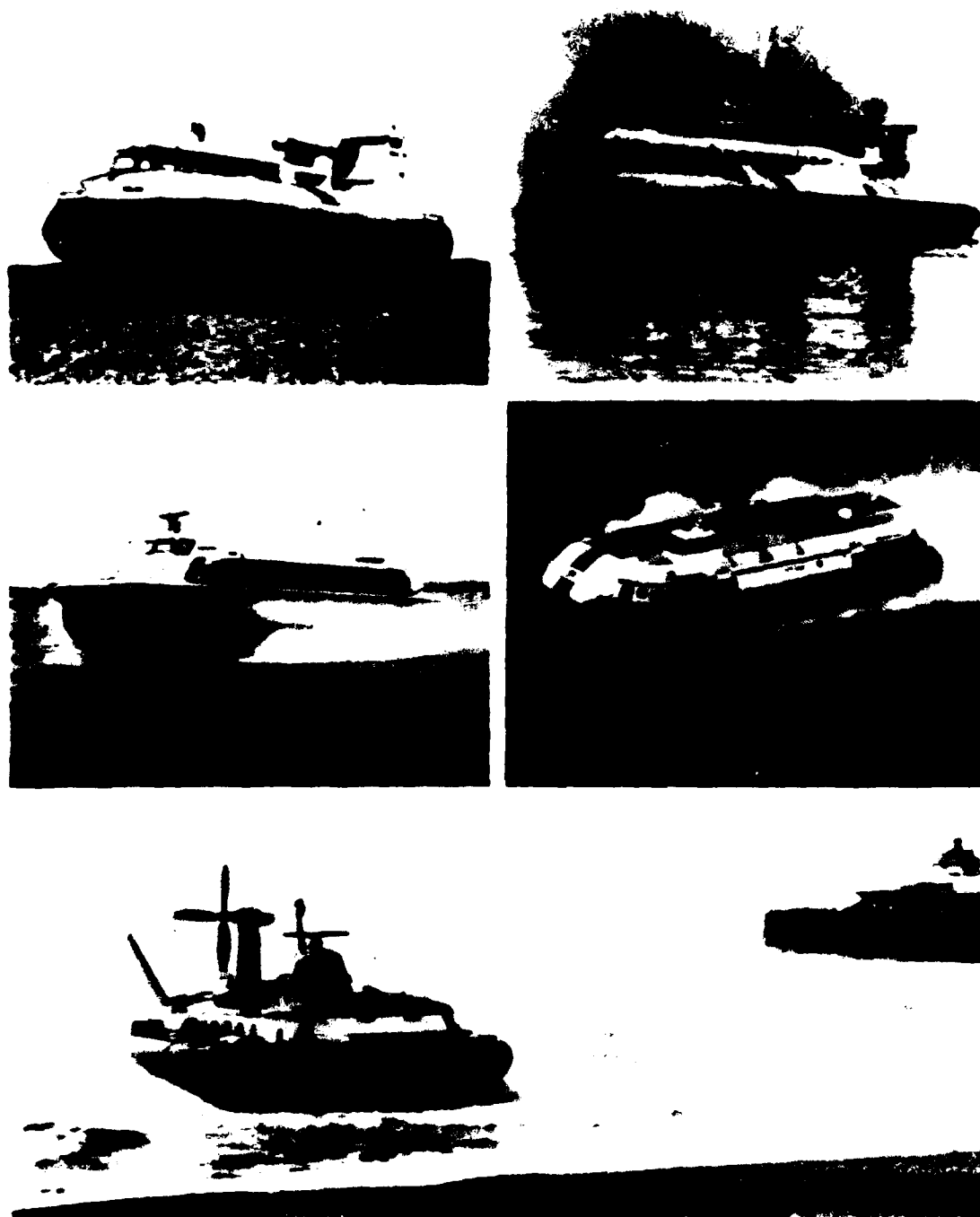


Figure 13 - British Air Cushion Craft

designated the SR.N5(M). In the case of the Bell construction, significant changes were made to the craft to make it suitable for military missions in Vietnam. The SR.N5 is now out of production and has been replaced by the SR.N6 (upper right photograph), which is a 9-ton craft carrying 38 passengers. It has a maximum calm water speed of 60 knots. The SR.N6 is currently in successful commercial operation in England and in other parts of the world. In 1973, BHC developed a twin propeller version for improved control and lower noise. BHC is developing this craft with different "Mark" versions to continue its improvements. Such improvements include a stretched variant to increase its payload capability, a deeper skirt to improve rough water performance, and other variants to make it suitable for cargo missions and for military use.

Three other craft that illustrate the type of intermediate speed craft developed in England are also shown in Figure 13. The middle left photograph shows the HM.2 built by Hovermarine Transport Ltd. This company began in the early 1960's with the Denny sidewall craft and gradually developed the more successful craft. The company is now a subsidiary of Hovermarine Corporation (U.S.A.). Since the last summary report the U.S. manufacturing operations of Hovermarine in Titusville, Florida have closed down due to a lack of a U.S. market. Hovermarine Corporation maintains corporate headquarters in Pittsburgh but manufacturing has been returned to Hovermarine Transport Ltd. in Southampton, England. The HM.2 is a sidehull craft of which again there are several Mark versions. In its standard version, it has a gross weight of 21 tons and carries 65 passengers at a calm water speed of 35 knots. It has seen successful commercial operation on short naval routes in Europe and South America with plans for operation in Australia, Canada, and other countries.

The middle right photograph in Figure 13 shows the Vosper-Thornycroft VT 1. Three such craft were built, two of which were operated commercially between Sweden and Denmark. While the craft operated successfully, the service was eventually discontinued. The reason for the operation's demise can be attributed to non-technical reasons and directly related to stiff price competition from state owned and operated ferries and hydrofoils. The VT 1 was unique in that its cushion system was a fully skirted plenum (modified) as described in Figure 3 but it used marine propulsion. It was argued that, for its intermediate speed region of operation (30 to 40 knots), the quietness and high efficiency of the marine propeller gave it an economic advantage. The demise of these interesting craft is now complete in that in November 1977 Vosper-Thornycroft made the decision to scrap two of the three craft. The third (and original) craft, the VT 1-001 was converted to an air propelled, fully amphibious craft and re-designated VT 2-001. The first "flight" was on 2 September 1975.¹⁵ The craft was modified as a speculative venture to be competitive for the military role in amphibious warfare. More details on the propulsion arrangement may be found in Chapter IX.

The lower photograph in Figure 13 shows the BH.7 on a demonstration run up the beach at Brighton at the 1974 International Hovercraft and

Hydrofoil Conference and Exhibition. The BH.7, built by British Hovercraft Corporation, is specifically designed for military missions. The first of three craft was launched on 31 October 1969. It has a nominal gross weight of 45 tons and has accommodations for 70 fully equipped troops. Its maximum calm water speed is 65 knots.

Two other craft that are representative of commercial operation are the Japanese craft, the Mitsui MV-PP15, and the French SEDAM N.300. These are shown in Figure 14. In the upper photograph can be seen the MV-PP15, which is a 55-ton craft carrying 155 passengers. This craft, with a calm water speed of 65 knots modeled after the British BHC series, operates regularly among the islands in Japan. A unique feature of the Japanese craft is the use of "water rods" or, in the case of MV-PP15, retractable wheels that give precise control in water by alternately dragging them in the water to generate the desired turning moment.

In the lower photograph, the N.300 represents the French success with its unique skirt system (see Chapter V) and is the result of the development of the air cushion principle in France by the Bertin Company. It is currently operating on routes in southern France and has a gross weight of 28 tons and carries 80 passengers. An interesting account of the history of the development of the N.300 and of French air cushion craft in general was given by Monsieur Bertin to the Isle of Wight branch of the Royal Aeronautical Society in 1970.¹⁶

On 26 November 1977 the second of SEDAM's N.500 hovercraft (the first having been destroyed by fire during construction earlier in the year) headed down the Gironde River from the factory in Pauillac, France toward Boulogne-sur-Mer. It arrived on 30 November 1977. It is a 236 ton craft capable of carrying 200 passengers and 60 cars. During trials the craft (christened Ingenieur Jean Bertin) reached a speed of 69 knots in calm seas and operated satisfactorily in seas of up to 10 ft high. It is currently entering commercial service on the Boulogne-Dover route. Figure 15 shows this unique craft operating on the ramp at Pauillac.

Referring to Figure 11, where the main groupings of worldwide developments have been categorized, it is felt that the above brief description summarizes the significant examples of the British, French, and Japanese achievements. These craft all represent a class of vehicles designed to be economically efficient in the 30- to 60-knot speed range and can be categorized as low density craft (30 to 50 lb/ft²).

In the United States, almost the entire development, with some notable exceptions, have been geared to developing high speed, high density craft. Historically, it can be said that, in the early 1960's, several companies were exploring a range of forms of air cushion craft including plenum, sidehull, recirculation, labyrinth seal, and others. The interest in both commercial and military circles waxed and waned depending upon the successes and failures of the various projects. Some of these projects were privately financed, while others were the result of U.S. Government studies to determine the feasibility of air cushion craft.

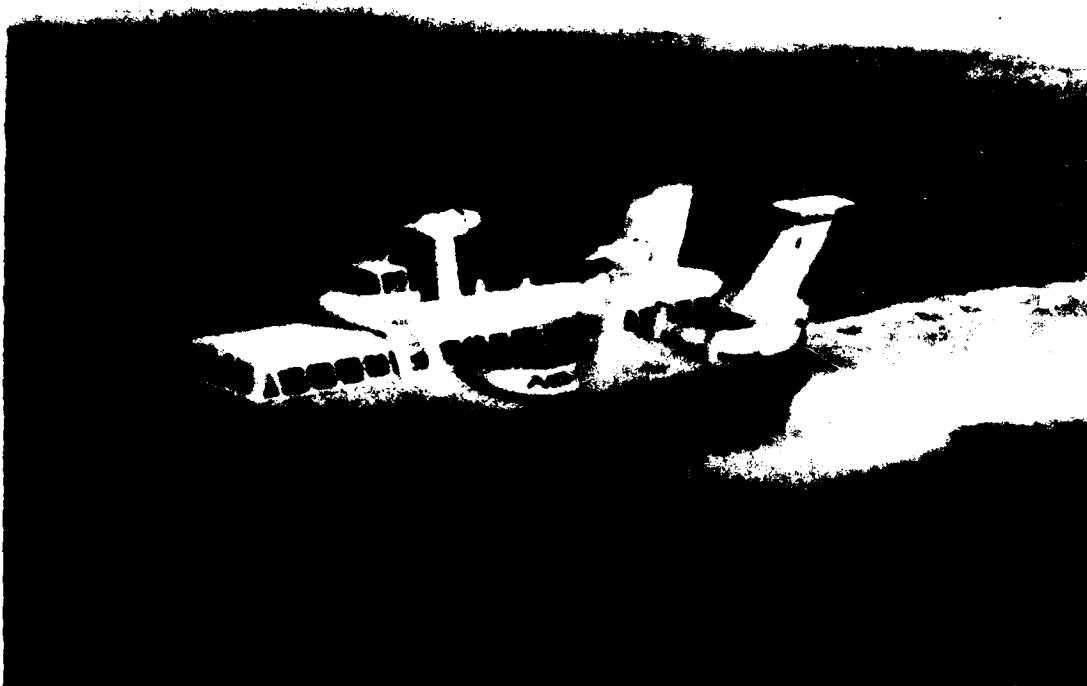
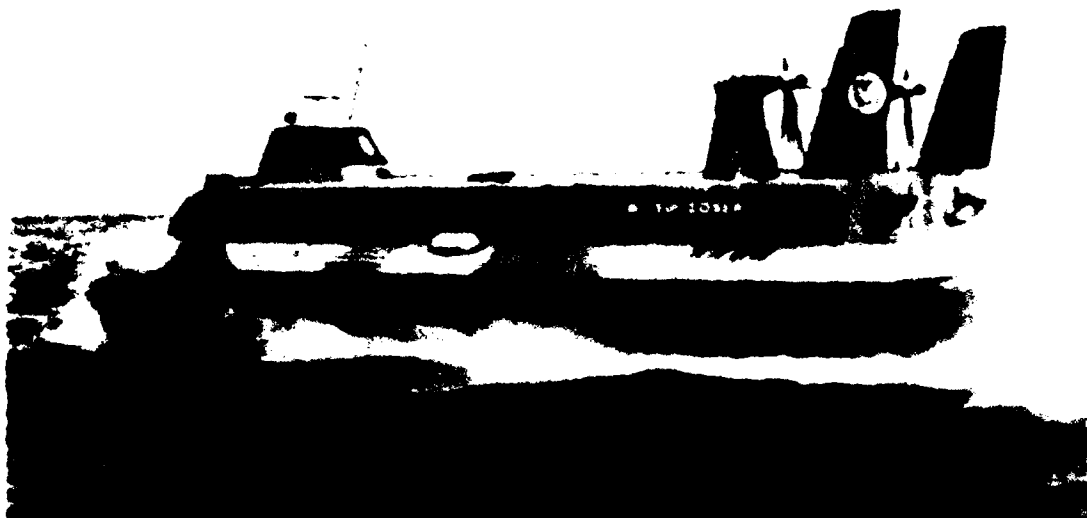


Figure 14 - Japanese (Top) and French Air Cushion Craft

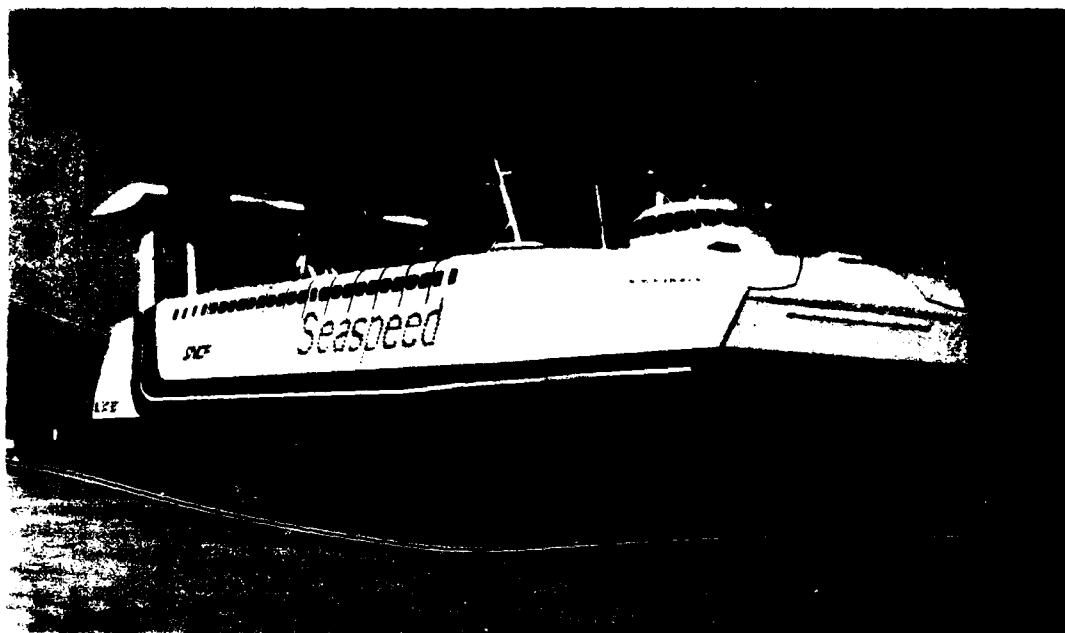


Figure 15 - SEDAM N.500 (Ingenieur Jean Bertin)

Both the Office of Naval Research (ONR) and the (then) Bureau of Ships began studies for military applications. The most successful venture during this early period was the BUSHIPS-sponsored SKMR-1, designed and built by Bell Aerospace Textron (then Bell Aerosystems Company), which saw its debut in 1963. At that time, it was the largest craft in the United States, with a gross weight of 22 to 28 tons, depending on payload, and a calm water speed of 70 knots. Figure 16 shows the SKMR-1 in both its original unskirted form (upper photograph) and in its later configuration when fitted with 4-foot skirts. The SKMR-1 provided considerable basic information on both the technical aspects of aerostatic air cushion craft design as well as its use in military operations (see, for example, Reference 17). Much of the original military interest stemmed from this program.

The commercial interest by the U.S. Government began with the Maritime Administration, which followed on with the original ONR studies and, in 1961, began the Columbia project.¹⁸

A key event in the development of the air cushion craft in the United States occurred in 1965, when the work being done by both industry and Government were brought together to discuss and review the different forms and basic principles and to recommend on which form to continue development.

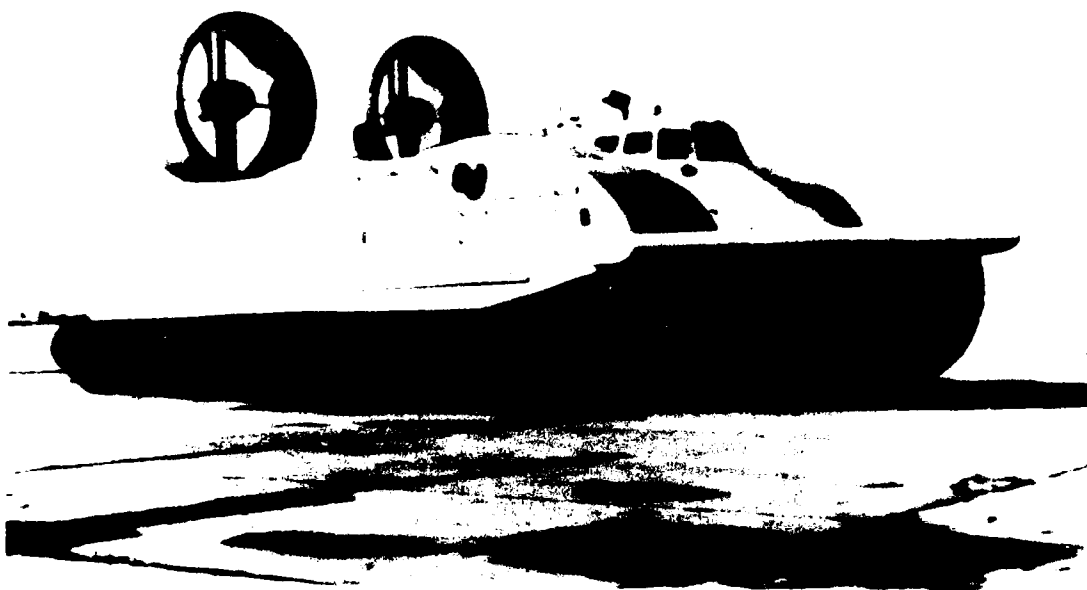


Figure 16 - SKMR-1 with and without Skirts

The Surface Effect Ships for Ocean Commerce (SESOC) Committee met with industry and Government representatives at King's Point, October through December 1965. The result of these reviews was the formation of a joint program between the U.S. Navy and the Department of Commerce and, as a result, the Joint Surface Effect Ship Program Office (JSEPO) was set up in 1966 to develop the high-speed sidehull SES form of air cushion craft. The ultimate goal was to develop a 4000-ton-class, high speed air cushion ship capable of cruising at 80 knots and crossing the Atlantic nonstop. Further discussion relative to this development may be found in Reference 19. By 1970, it became clear to the Maritime Administration that significant development would be required to achieve this size of craft, while it was equally clear that definite military advantage existed in the smaller sizes. Accordingly, at that time, the program became a fully U.S. Navy program administered by what then became SESPO and later PM-17 under the Chief of Naval Material. In mid-1974 this became PMS-304 as part of the new Naval Sea Systems Command. The main activity of PMS-304 at present is the development of the intermediate size ship, the 80-knot, 3000-ton SES. The two most visible products of this program are the Aerojet SES-100A and the Bell Aerospace SES-100B; both are high cushion pressure (100 lb/ft^2), high speed (80 knots) test craft of the sidehull SES form discussed earlier. Since the earlier summary was prepared both test craft have completed their test programs. The semisubmerged propeller driven SES-100B achieved a world speed record of 90.3 knots on April 2, 1977 on St. Andrews Bay near Panama City, Florida. The SES-100A entered a new test phase using retrofitted flush waterjet inlets and a new bow planing seal as a test-bed for the planned 3000-ton SES due to be launched in the early 1980's.

A second key development, based on U.S. Navy and Marine Corps studies in the 1965-70 period, involves the application of the air cushion principle to improve landing craft. More detailed discussion of this development may be found in References 20 and 21. Two such craft are the Aerojet JEFF(A) and the Bell Aerospace JEFF(B), again both high pressure craft (approximately 100 lb/ft^2) capable of high speed. In the case of the JEFF craft, performance is stated as 20 knots in a State 2 sea on a hot day. These four craft are shown in Figure 17 and represent the significant developments underway by the U.S. Navy on the high density form of air cushion craft. The particular knowledge gained in the design and construction of these craft will be described in the following chapters.

The two JEFF craft have since completed their construction phase and are now in the early trials stage. Figure 18 shows the Aerojet JEFF(A) during its first underway run near the U.S. Naval Coastal Systems Laboratory in Panama City, Florida on 17 October 1978.

The Bell JEFF(B) was launched and made its first run (at 42 knots) on 16 December 1977. Figure 19 shows this first run near the U.S. Naval test facility in Panama City, Florida. A progress report describing this first mission is given in Reference 22.

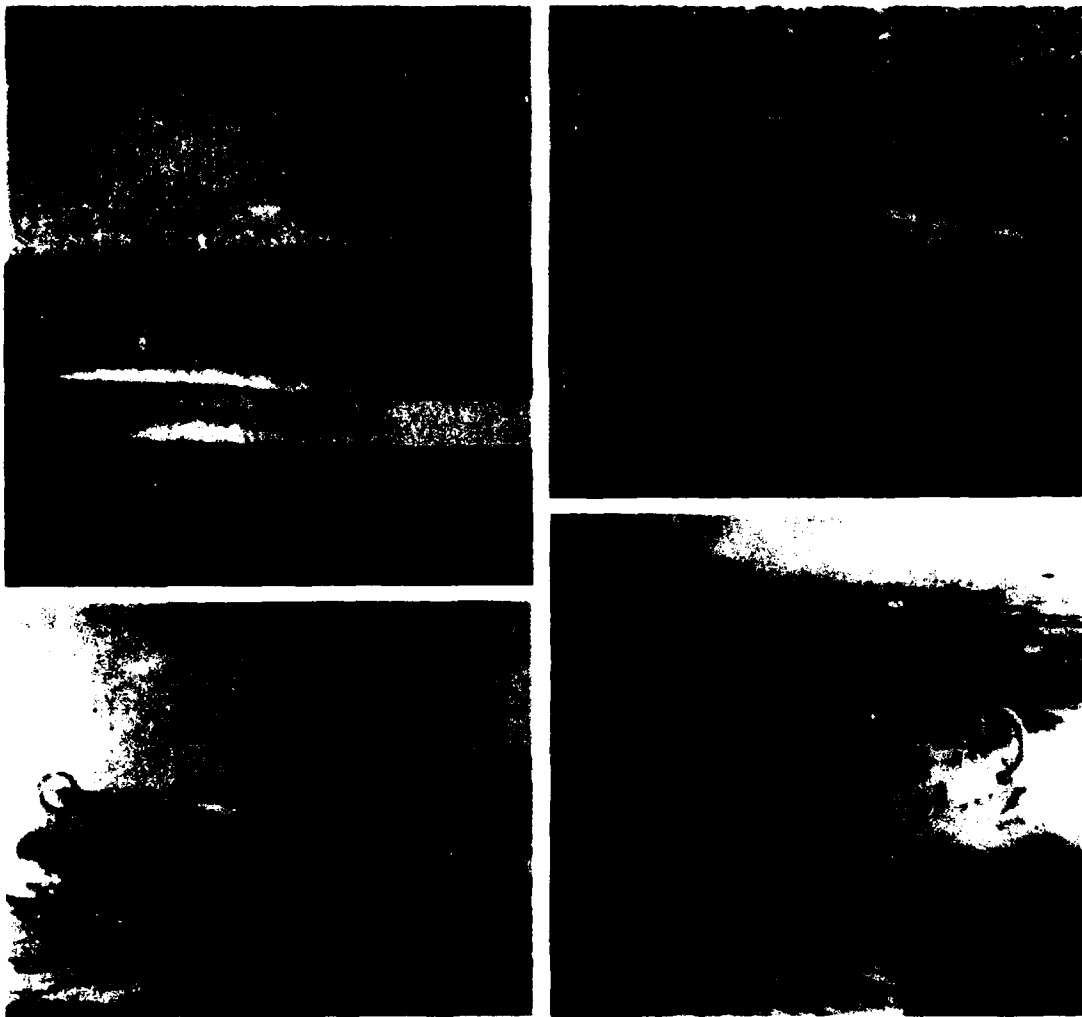


Figure 17 - U.S. Navy High Density Air Cushion Craft

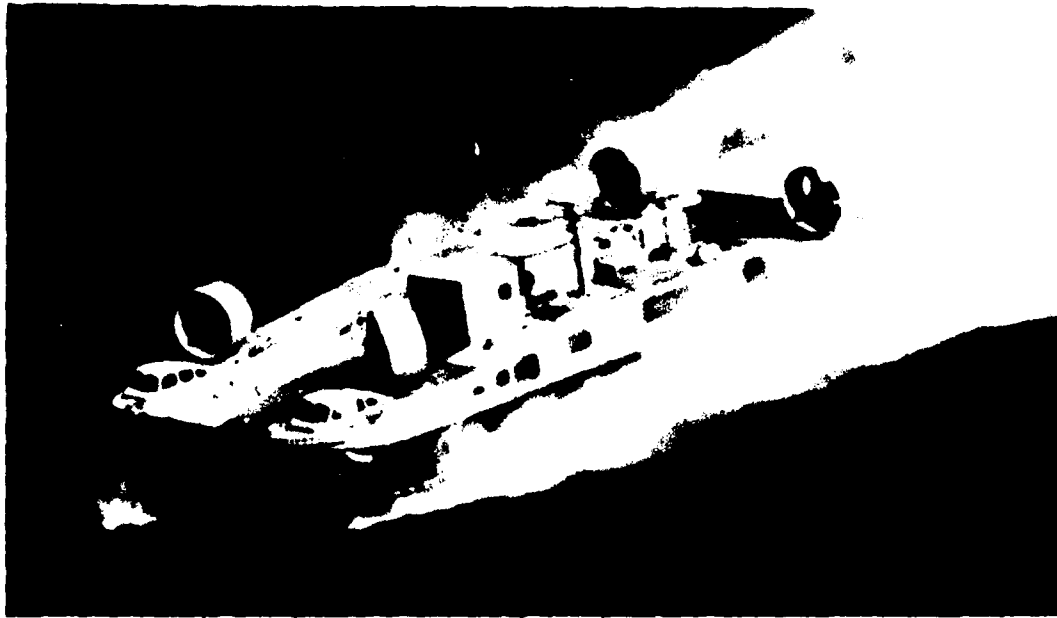


Figure 18 - JEFF(A) Underway in Florida



Figure 19 - JEFF(B) Underway in Florida

In addition to these military developments; the commercial craft, the Voyager and Viking, built by Bell Aerospace Canada in association with the Department of Industry, Trade, and Commerce of the Government of Canada, are indicative of potential development in the commercial field. These craft (Figure 20) are derivatives of the Bell SK-5 craft and the original British Hovercraft Corporation designs. Since a major problem of the intermediate speed craft developed so far is one of high cost, the attempts at low cost through the use of modular construction and standard components (note the conventional truck cabs for operators in both craft) can be seen in these latest developments.

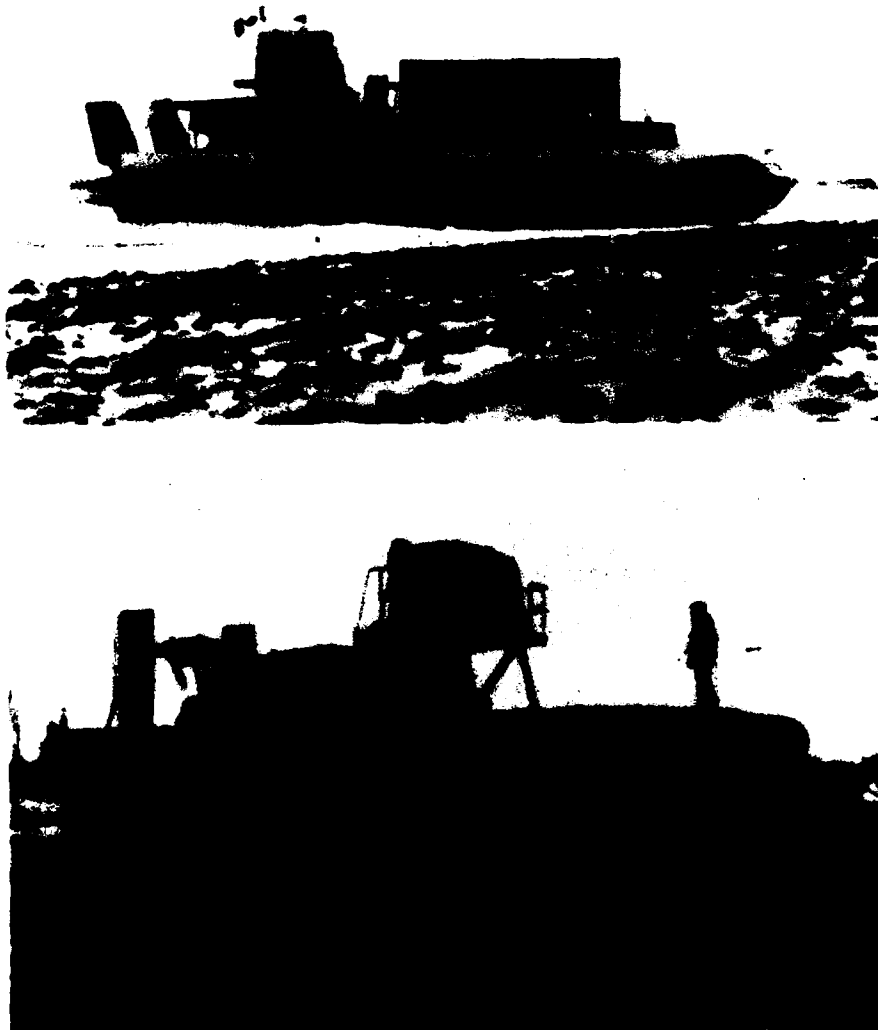


Figure 20 - Bell-Canada Voyager and Viking

High Speed Development

There have been sporadic developments around the world on the development of air cushion craft designed to be efficient at speeds in excess of 100 knots. The early work by Kaario in 1935 has been mentioned. Other developments include the Japanese Kawasaki KAG-3 ram wing, the Lockheed winged hull, the MaRad/Vehicle Research Corporation VRC-1, and Lippisch's aerofoil boat. It is reported¹ that the U.S.S.R. is developing a 300-mph troop transport that operates in ground effect. Some discussion of the technical aspects of such craft are given in Chapter X.

CONCLUDING REMARKS

From the above brief summary it is seen that, by and large, the development of the air cushion craft has concentrated on providing short-haul craft based on the amphibious form, with an increasing amount of development in the U.S. Navy for the large, long-haul, nonamphibious craft. As the development, interest, and funds expand, important offshoots are beginning to form to explore other uses and forms of the air cushion craft. It is important to note in this context that the U.S.S.R. is currently the producer of the largest number of military air cushion craft with indications of increasing production rates from those known today.

For completeness and ease of reference the principal characteristics of representative air cushion craft that either are (or were) operational or in fairly advanced program status are provided here in Table 1. The last column in Table 1 shows the type of air cushion craft shown in accordance with the groupings discussed earlier. The annotation of passive or active refers to the type of lift fan system which is described in Chapter VIII.

In the following chapters, some of the basic results and lessons learned in the design, construction, and test of air cushion craft are summarized and brought together to provide a measure of the technical state-of-the-art.

TABLE 1 - LEADING PARTICULARS OF REPRESENTATIVE AIR CUSHION CRAFT

Air Cushion Craft	Displ. (Short Tons)	No. of Passengers or Payload (T)	Range (n.m.)	Length (ft)	Beam (ft)	Cushion Depth (ft)	Power (hp)	Max. Speed (knots)	Max. Wave Ht. (Sig. ft)	Type
CANADA BELL LACY-30 Viking VOYAGEUR	57.5 16.25 45	30T 6-7T 25T	680 300	76.25 44.5 64.8	36.33 26.0 36.7	4.0 4.0 4.0	2x1400 1x1300 2x1300	66 49.56 46.95	6 6	Passive, Amphibious Passive, Amphibious Passive, Amphibious
FRANCE NAVIFLAME N.300 N.500	29.75 237	120 400 & 41 cars	180	78.75 177.16	34.5 78.75	6.6	2x1500	62 76	13	Passive, Amphibious Passive, Amphibious
GERMAN FEDERAL REP LIPPISCH X-113 X-114	0.38 1.49	1 6	620	27.68 41.98	19.34 22.96		1x48 1x200	115	2	Aerodynamic Aerodynamic
JAPAN MITSUI MV-PP05 MV-PP15	13.45 56	6.16T 155	160 250	52.5 80.1	28.16 41.66	4 5	1x1050 2x1950	55 60		Passive, Amphibious Passive, Amphibious
UNITED KINGDOM BHC BH.7 SR.N4 SR.N6 SUPER 4 CUSHION CRAFT CC-7 HOVERMARINE HM.2 HM.5 VOSPER-THORNY- CROFT VT 1 VT 2	56 212 11.2 336 3.38 21.25 84.9 97.44 70	15.68T 282 & 37 cars 38 416 & 60 cars 10 65 177 146 35.85T	400 250 150 150 150 140 210 340 300	78.34 130.16 48.4 185 25.8 51.0 89.25 95.5 99	45.5 78 23 92 15.2 20 33.5 43.5 43.5	5.5 8 4 9 2 3 5.75 5.5 5.5	1x4250 4x3400 1x900 4x3800 1x510 2x320 2x1200 2x350 2x1675 2x3800	60 70 52 65 36 38 40 38 60	10-12 11-13 10-12	Passive, Amphibious Passive, Amphibious Passive, Amphibious Passive, Amphibious Passive, Amphibious Passive, Sidehull Passive, Sidehull Passive, Semi-amphibious Passive, Amphibious
USA USN 3KSES XR-1 XR-5 AEROJET JEFF (A) SES-100A BELL JEFF (B) SES-100B SKMR1	3360 21.5 4.0 166.5 123ST 162.5 105 32.48	1T 60T 10T 60T 10T	200 Class. 200 Class. 240	266.25 50 46.75 96.1 81.9 86.75 77.67 65.5	108 19 8.25 48.0 41.9 47.0 35.0 27	18 3 3 5 6 5 6 4	4x22500 2x22500 2x 2x55 1x25 6x2800 4x3500 6x2800 3x500 3x3260 4x1080	80+ 43 25 50+ 80 50+ 80+ 70	20 3 3 8 6 8 6 5	Active, Sidehull Active, Sidehull Active, Sidehull Passive, Amphibious Active, Sidehull Passive, Amphibious Active, Sidehull Passive, Amphibious
USSR AIST CASPIAN SH SKATE SORMOVICH ZARNITSA	298 300 29.76 40.24 16.54	100T 50 50 48	230	150 67.6 96 72.25	60 24 3.8 12.67		3x780 1x2300 1x265	70 50 65 10.13		Passive, Amphibious Aerodynamic Passive, Amphibious Passive, Amphibious Passive, Amphibious

CHAPTER III

PERFORMANCE ASPECTS

The performance of a vehicle is an all-encompassing term meaning different things to different people. In a general sense, when one asks how does a particular vehicle perform one thinks of the handling characteristics, and in the case of a seagoing vehicle, the question implies sea-keeping ability as well as the more fundamental questions of how much power, what speed, and can it carry sufficient payload to make it all worthwhile. To make the analysis more manageable it is convenient to discuss the vehicle's characteristics under such separate headings as done in this book. Nevertheless, when making final judgments one must consider all aspects in an integrated manner. To this end, the first section of this chapter is devoted to describing some overall sizing of air cushion craft before tackling the basic powering and other performance aspects. The subjects of seakeeping, lift, and propulsion system characteristics are appropriately left to other chapters.

THE BASIC PERFORMANCE EQUATIONS

It must be recognized that the design process for any vehicle involves a combination of many factors, many of which are in conflict with each other, necessitating compromise. Some are tangible, others intangible. These factors include among many others; performance considerations, stability, seakeeping and safety requirements, economic considerations, manufacturability, material availability, customer needs, and in the case of commercial vehicles, passenger acceptance. It would be impossible in a book such as this to identify and describe the entire design process in detail encompassing the above factors as it applies to the air cushion craft. As a cautionary note, in the commercial world it is sometimes found that what might be a commercial success may well not be amenable to analysis! Likewise in the military arena, a specific vehicle may not be either particularly economical or have good performance efficiency but it serves a unique purpose and is, therefore, used. Such craft are usually short lived, however, until a more economical and efficient vehicle is developed.

Despite this apparent complexity, there are certain basic requirements that must be met (unless consciously departed from for specific reasons) in the craft design. For the purposes of illustration and at the risk of over-simplification these can be discussed from the starting point of two analytical considerations: the economic equation and the range equation; other requirements are usually evolved in support of these two considerations to ensure a workable craft.

Whether the air cushion craft is to be designed for commercial or military use, some element of these equations becomes a driving factor in the design process to produce a vehicle capable of carrying some defined payload over a certain route or for some mission.

The Economic Equation

An indication of the basic design parameters influence on the operating economics of an air cushion craft may be seen from examination of the economic equation that can be derived by methods similar to that known as the Air Transport Association (ATA) method for commercial, gas turbine powered aircraft.²³ While the ATA method of computing operating costs was derived for aircraft use, it can be applied successfully in modified form to the air cushion craft. It is noted here that the author compared this method with other methods that are being developed within the U.S. Navy for determining the cost of military vehicles and found the methods to be of similar functional form. Presentation of more detailed costing methodology for U.S. naval vehicles is excluded at this time for proprietary reasons.

An evaluation of the detailed ATA formulation for operating costs will show that they can be grouped as the sum of three terms to form what the author chooses to call the economic equation for operating costs, viz:

$$DOC = C_1 + C_2 \frac{W_F}{R} + \frac{C_3}{V_b} \quad (1)$$

where DOC = direct operating cost in dollars per mile

C_1 = fixed crew costs, and public liability and property damage insurance in dollars per mile

C_2 = fuel and oil cost in dollars per gallon

C_3 = variable cost factor in dollars per hour (see below)

W_F = fuel consumed in gallons

R = range (or stage length) in miles

V_b = block speed (including terminal time and maneuver time) in miles per hour

The variable cost factor (C_3) is further broken down to:

$$C_3 = K_c + K_m + \frac{K_a}{U}$$

where K_c = operating crew cost in dollars per block hour

K_m = maintenance cost (including burden) in dollars per block hour

K_a = amortization and craft insurance in dollars per annum

U = annual utilization in block hours per annum

Normally, the second and third terms in Equation (1) are by far the largest contributors to the direct operating costs. The total operating costs (TOC) including terminal employees, facilities, and G&A costs is then:

$$TOC = DOC(1 + K_i) \quad (2)$$

where K_i is the indirect to direct cost ratio.

If W_p is the maximum allowable payload (e.g., in tons) carried for a given range then the TOC per available revenue earning capacity is given by TOC/W_p or,

$$\text{dollars per ton mile} = \frac{(1+K_i)}{W_p} \left[C_1 + C_2 \frac{W_F}{R} + \frac{C_3}{V_b} \right] \quad (3)$$

Equation (3) or Equation (1) provides a useful comparative formula embodying the essential ingredients of operating costs yet may not accurately compute the actual cost in any particular case due to the intricate combination of factors for specific operations. More detailed discussions pertaining to the economics and operating costs of air cushion craft is deferred at this time to some future writing.

Key design parameters that appear in the economic Equations (1) and (3) are the range (R), the fuel load (W_F), and the speed (V_b) of the craft. The relationship between these parameters from a design viewpoint can be obtained from the range equation.

The Range Equation

Classical texts on craft performance provide complete derivations of the range equation originally developed by Breguet for aircraft. An abbreviated derivation especially applicable to the air cushion craft is given in Appendix A.

From Appendix A it is shown that the range of an air cushion craft is given by

$$R = 325 \frac{\eta_p}{sfc} \left(\frac{L}{D} \right)_{EFF} \ln \frac{W_i}{W} \text{ (in nautical miles)} \quad (4)$$

where η_p is the propulsive system efficiency, sfc is the net specific fuel consumption of the lift and propulsion engines, and W_i and W are the initial and end cruise weights, respectively, of the craft. The effective lift-to-drag ratio is given as,

$$\left(\frac{L}{D}\right)_{\text{EFF}} = \frac{W}{D + \frac{\eta_p}{\eta_L} \frac{p_c Q}{V}} \quad (5)$$

which may be recognized as the conventional lift-to-drag ratio (W/D) modified by the effect of the lift system power (see Appendix A). In Equation (5), η_L and η_p are the lift and propulsion system efficiencies respectively, p_c is the cushion pressure, Q is the cushion flow, and V is the cruise speed of the craft. In some texts the effective lift-to-drag ratio is defined as given in Equation (5) except that the propulsive and lift system efficiencies are set equal to one another. This is an unnecessary simplification and is difficult to interpret physically. Hence, in this analysis, the effective lift-to-drag ratio will be as defined by Equation (5).

If P is the total power ($= P_L + P_p$), used to both lift and propel the craft, then it can be shown (Appendix A) that

$$\eta_p \left(\frac{L}{D}\right)_{\text{EFF}} = \frac{WV}{P} \quad (6)$$

where WV/P is called the transport efficiency of the craft, i.e., the ratio of the work done by the craft in moving a vehicle weight (W) at a speed (V) divided by the total power required (P) to do the work.

Comparisons are frequently made between vehicles designed for economic application on the basis of the transport efficiency WV/P . Sometimes these comparisons are made on the basis of effective lift-to-drag ratio $\eta(L/D)_{\text{EFF}}$ and sometimes on the basic aerodynamic (or hydrodynamic) lift-to-drag ratio (L/D). Care must be exercised when making such comparisons that they are made on an equal basis.

EXAMPLE PROBLEM

An air cushion craft weighs 175 short tons and cruises at 50 knots with a total power on board of 13,600 horsepower. Its propulsion system efficiency is 60 percent and its lift system efficiency is 40 percent. The

cushion pressure is 100 lb/ft^2 and the total cushion flow is $15,000 \text{ ft}^3 \text{ sec}$. At these conditions what is: (a) the craft's transport efficiency, (b) its effective lift-to-drag ratio, and (c) its aerodynamic lift-to-drag ratio?

SOLUTION

The transport efficiency WV/P is calculated from,

$$\frac{WV}{P} = \frac{175 \times 2000 \times 50 \times 1.689}{550 \times 13,600} = 3.95$$

$$\text{New } P = \frac{1}{\eta_p} \left[DV + \frac{\eta_p}{\eta_L} \right] P_c Q$$

$$\therefore 550 \times 0.60 \times 13,600 = \left[D \times 50 \times 1.689 + \frac{0.60}{0.40} \right] (100 \times 15,000)$$

$$\therefore D = 26,500 \text{ lb}$$

$$\text{Effective } L/D = \frac{W}{D + \frac{\eta_p}{\eta_L} \frac{P_c Q}{V}} = \frac{175 \times 2000}{26,500 + \frac{0.60}{0.40} \frac{100 \times 15,000}{50 \times 1.689}} = 6.59$$

$$\text{Aerodynamic } L/D = W/D = \frac{175 \times 2000}{26,500} = 13.21$$

Hence, solutions are (a) $\frac{WV}{P} = 3.95$; (b) $(L/D)_{\text{EFF}} = 6.59$; and (c) $L/D = 13.21$

An indication of the relative importance of the terms (design factors) in Equation (4) to achieve a given range capability is given in Figure 21. This is an important chart as it sets the basic design requirements on the vehicle to meet a specified range. For example (from Figure 21), an empty weight fraction of 50 percent and an effective lift-to-drag ratio of 10 would be required to achieve an effective Breguet range of 2500 nautical miles. Now, on specific vehicles where there is a wide weight variation from the start of cruise to the end of cruise, then, as discussed in Appendix A, the range is computed in increments as the lift-to-drag ratio and transport efficiency change with displacement. Such calculations are

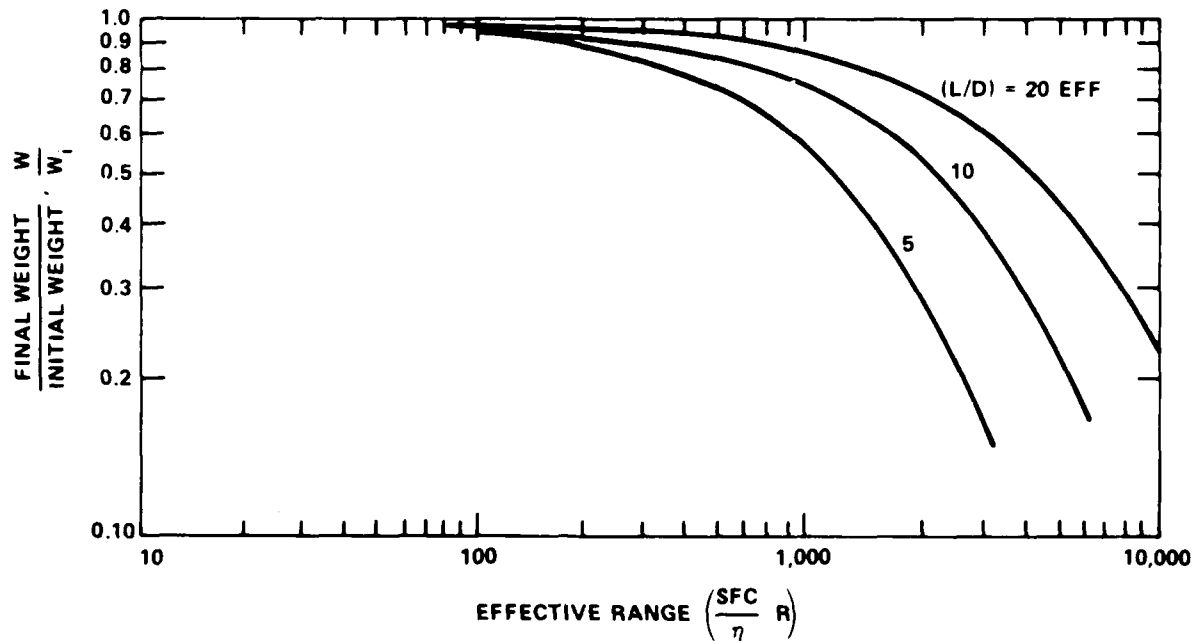


Figure 21 - Generalized Breguet Range Chart

best done by computer to obtain more accurate results but the essential elements of the process are as given in Figure 21.

It is not sufficient in the design process to design a craft with the highest value of transport efficiency, however. Account must be taken of the ability to carry a payload at the same time as designing for high performance. This is expressed in the economic Equation (3) that expressed the total operating cost per ton mile in terms of the craft design parameters of payload, fuel load, range, and speed.

Again, while it is emphasized that more exact calculations are to be followed in specific applications for calculating the range, the simplified, approximate treatment given in Appendix A is shown here for the purposes of illustration. From Appendix A the approximate expression (for small fuel fractions) for the range was found to be:

$$R = 325 \frac{1}{\text{sfc}} \cdot \frac{WV}{P} \cdot \frac{W_F}{W} \quad (7)$$

or

$$R = 325 \frac{\eta}{\text{sfc}} \cdot \left(\frac{L}{D} \right) \text{EFF} \cdot \frac{W_F}{W} \quad (8)$$

If this is substituted into the economic Equation (3) it is found that the total cost per ton mile is given by,

$$\text{dollars per ton mile} = (1+K_i) \left[\frac{C_1}{W_p} + \frac{C_2}{325 \frac{1}{\text{sfc}} \frac{WV}{P} \frac{W}{W_p}} + \frac{C_3}{W_p V_t} \right] \quad (9)$$

where the denominator in the second term is recognized as being proportional to the payload ton miles per pound of fuel. From numerical calculations it can be shown that the second and third terms in Equation (9) are the dominant terms in controlling the operating costs and therefore are key factors in the design process of a well-balanced economical craft. For this reason, craft are sometimes compared on a basis of the product:

$$\left(\frac{WV}{P} \right) \times \left(\frac{W_p}{W} \right)$$

which must be maximized in order to minimize the operating cost. This product can be considered as a product of the aerodynamic or performance efficiency through WV/P and, for want of a better term, design efficiency through W_p/W . This latter efficiency tests the ability of the designer to design efficient structures and lightweight craft subsystems to maximize the space and weight for payload capability. The design challenge is to do this without increasing the craft and subsystem costs (constants C_1 , C_2 , and C_3).

As an illustration of the design process one can consider evaluation of two potential designs of craft with different engine systems, payload capability, fuel consumption rates, power, and weight. Which is the better design? If subscripts (1) and (2) denote the two designs then the comparison in ton miles per pound of fuel becomes:

$$\frac{(\text{ton miles per pound of fuel})_1}{(\text{ton miles per pound of fuel})_2} = \frac{(\text{sfc})_2}{(\text{sfc})_1} \cdot \frac{\left(\frac{WV}{P} \right)_1}{\left(\frac{WV}{P} \right)_2} \cdot \frac{\left(\frac{W_p}{W} \right)_1}{\left(\frac{W_p}{W} \right)_2} \quad (10)$$

It is possible that one craft may have a higher transport efficiency than another but still produce a lower ton miles per pound of fuel value through the effect of the specific fuel consumption and the payload fraction. That the choice is not always an obvious one is best illustrated by an example.

EXAMPLE PROBLEM

Two conceptual designs are proposed for a particular commercial operation. Design A is diesel powered with separate lift and propulsion systems while Design B is gas turbine powered with integrated lift and propulsion systems. How do the craft compare in terms of transport efficiency, payload capability, and ton miles per pound of fuel?

The design study produced the following pertinent characteristics of Design A and Design B.

	<u>Design A</u>	<u>Design B</u>
Weight Empty (less machinery)	35 tons	35 tons
Type of Engines	Diesel	Gas Turbine
Propulsion	(2) CRM 18D/S 1250 hp	(2) TF20 1850 hp
Lift	(2) CRM 12D/S 700 hp	integrated
sfc	0.35 lb/hp/hr	0.65 lb/hp/hr
Machinery Weight	23 tons	16 tons
Fuel Weight	3 tons	6 tons
Payload	17 tons	20 tons
All Up Weight	78 tons	77 tons
Speed	40 knots	41 knots

SOLUTION

As can be seen from the preliminary design estimates the choice of diesels increased the machinery weight for Design A which reduced the available fuel load. The slight difference in power levels from available engines and the weight differences will be reflected in the transport efficiency, viz

$$\text{Design A: } \frac{WV}{P} = \frac{78 \times 2000 \times 40 \times 1.689}{550 \times 3900} = 4.91$$

$$\text{Design B: } \frac{WV}{P} = \frac{77 \times 2000 \times 41 \times 1.689}{550 \times 3700} = 5.24$$

That is, Design B has approximately 7 percent improvement in transport efficiency over Design A. Also, due to the lighter weight of the gas

therefore the Design B payload is increased from 17 tons (22 percent) to 20 tons (26 percent). The ton miles per pound of fuel comparison is given by,

$$\frac{(\text{ton miles per pound of fuel})_A}{(\text{ton miles per pound of fuel})_B} = \frac{0.65 \times 4.91 \times 0.22}{0.35 \times 5.24 \times 0.26} = 1.47$$

Hence, from this example, Design A has a greater ton miles per pound of fuel (by some 47 percent) even though it had a lower transport efficiency and, therefore, would tend to give a lower operating cost.

The above example is for illustrative purposes only as, in an actual case, a complete analysis would be required. For example, these designs had from 4 1/2 to 5 hours endurance. For shorter ranges (endurances) the comparisons would change. Also, as the weight varies the cushion pressure and flow requirements also change thus affecting the total power (P) and the choice of lift fan systems. In the complete design process, the cost factors change with each design, for example, the initial cost of gas turbines is considerably higher than diesel engines but in some models the maintenance costs are lower. Therefore, no general rules can be established although the basic ingredients to the design process remain as outlined above.

Now that some of the basic equations have been identified and the design parameters expressed in their relative positions within the equations, the trends in these parameters for today's air cushion craft will be given and discussed.

SOME OVERALL SIZING RELATIONSHIPS

In presenting a technical summary of this kind, it is well to recognize certain trends or overall sizing of craft to indicate representative values of the craft considered. These trends are not fundamental laws in all cases but frequently represent the results of design compromise, which is so familiar to the practitioner of the art but so often frustrating to the purist.

These overall sizing relationships in terms of size of craft, cushion pressure variation with craft size, and total power requirements among others are, when viewed in their proper context, indicators of the state-of-the-art of air cushion craft. Wherever possible, the effect of the different forms of air cushion craft (ACV, SES, ram wing, and so on) on these overall sizing relationships is given together with pertinent discussion.

Size

For the air cushion craft supported completely by an underneath air cushion, the weight is given by

$$W = p_c S \quad (11)$$

For those air cushion craft that take advantage of aerodynamic lift,

$$W = p_c S + C_L \frac{1}{2} \rho V^2 S \quad (12)$$

but in the hover mode, such aerodynamic air cushion craft must still satisfy Equation (11). Again, on current craft such as the SES, where some degree of buoyant support in hover is available in the side hulls (usually about 5 percent), for all practical purposes Equation (11) still applies, in which case, for air cushion craft

$$W = \left(\frac{p_c/L}{L/B} \right) L^3 \quad (13)$$

Provided the cushion density (p_c/L) and the cushion length-to-beam ratio (L/B) remain constant, weight is seen to vary with cushion length cubed. Note, in this simple relationship that the cushion area is rectangular such that $S = L \times B$. Corrections to this relationship to compute non-rectangular areas, such as adding on semicircular bow sections for example, are easily accomplished but obscure the essential elements under discussion. It is far easier to use an effective cushion length ($L = \frac{S}{B}$) to account for such areas.

The parameters of cushion density and length-to-beam ratio have varied over the years as different considerations were built into the craft. For example, as the first series of air cushion craft evolved, emphasis was given to low density craft, since the wave drag of the cushion was known to increase rapidly with increase in cushion pressure. Today, emphasis is being given to compactness, especially as the craft increase in size to improve the payload-carrying capability and to improve the structural weight fraction. Again, the choice of low density or high density craft is a matter of design philosophy as reflected by Figure 22 which shows the trends over the years for some of the most current craft. The British craft, of which the British Hovercraft Corporation series is most prominent, reflect the low density ($p_c/L < 1.0 \text{ lb/ft}^3$) design philosophy. The American craft, however, reflect the high density ($p_c/L > 1.0 \text{ lb/ft}^3$) design philosophy. Whether a high or low density design is to be pursued is determined from performance, stability, and structural considerations (both weight and volume), which are discussed in this and subsequent

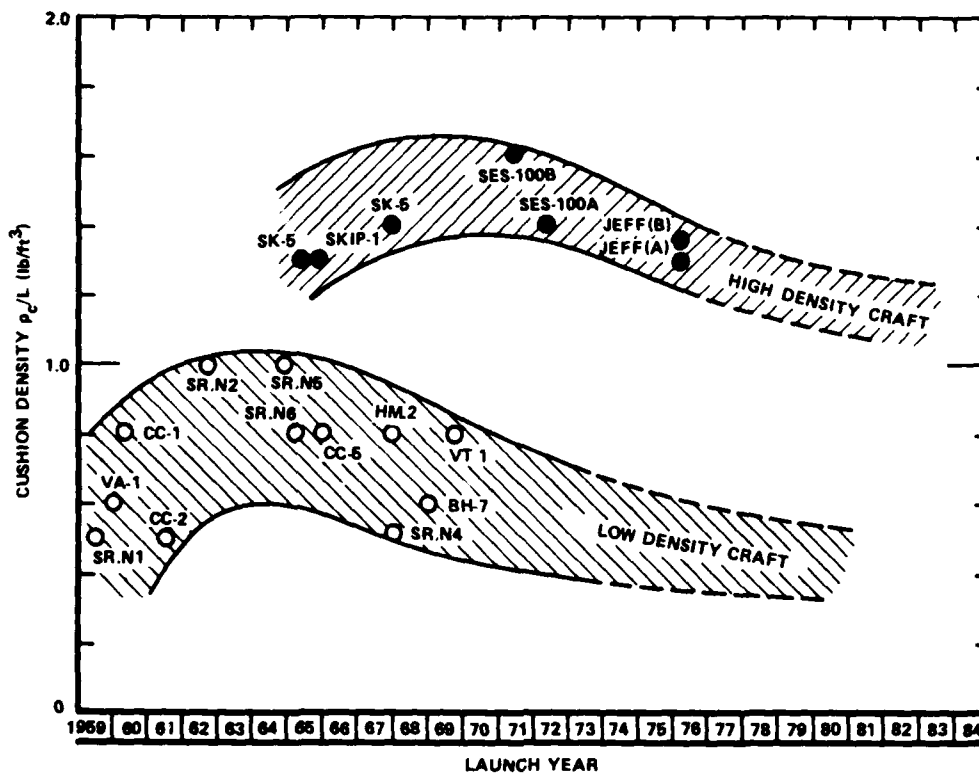


Figure 22 - Cushion Density Trends

chapters. Of course, craft can be designed, built, and operated at intermediary values of cushion density. Voyageur, launched in November 1971 with a value of $p_c/L = 1.1 \text{ lb/ft}^3$, is one such example. Values given in this and other examples (e.g., Figure 22) are for "design" values of p_c . The actual value varies with craft weight, payload, and fuel.

It should be pointed out that these data and conclusions are based on aerostatic craft, where relative freedom is available for choice of cushion density (p_c/L). Aerodynamic forms of air cushion craft tend to optimize at lower cushion densities than the aerostatic form of craft. The length-to-beam ratio of the aerostatic form of air cushion craft has also tended to vary as the newer craft evolve and more knowledge is gained on stability characteristics and performance in state of seas. Except for some developmental work by the U.S. Navy on craft with L/B greater than 5, practically all air cushion craft have steadfastly maintained a length-to-beam ratio of $1.0 < L/B < 2.0$ for reasons of performance and stability that will be discussed in this and subsequent chapters.

Over the years there has been an increasing awareness of the advantages of increasing the L/B of the craft. The Super 4 (see Figure 5) now has grown from an original L/B = 1.40 to a value of L/B = 2.0, with a much improved payload capability for a relatively small change in the propulsion system. In the U.S. Navy, several designs are on the drawing boards reflecting an increase in this basic parameter for performance reasons that will be referred to several times throughout the various chapters.

These considerations, however, for both p_c/L and L/B, influenced the constant of proportionality in Equation (13) and can be seen from the trend in air cushion craft size as shown in Figure 23.

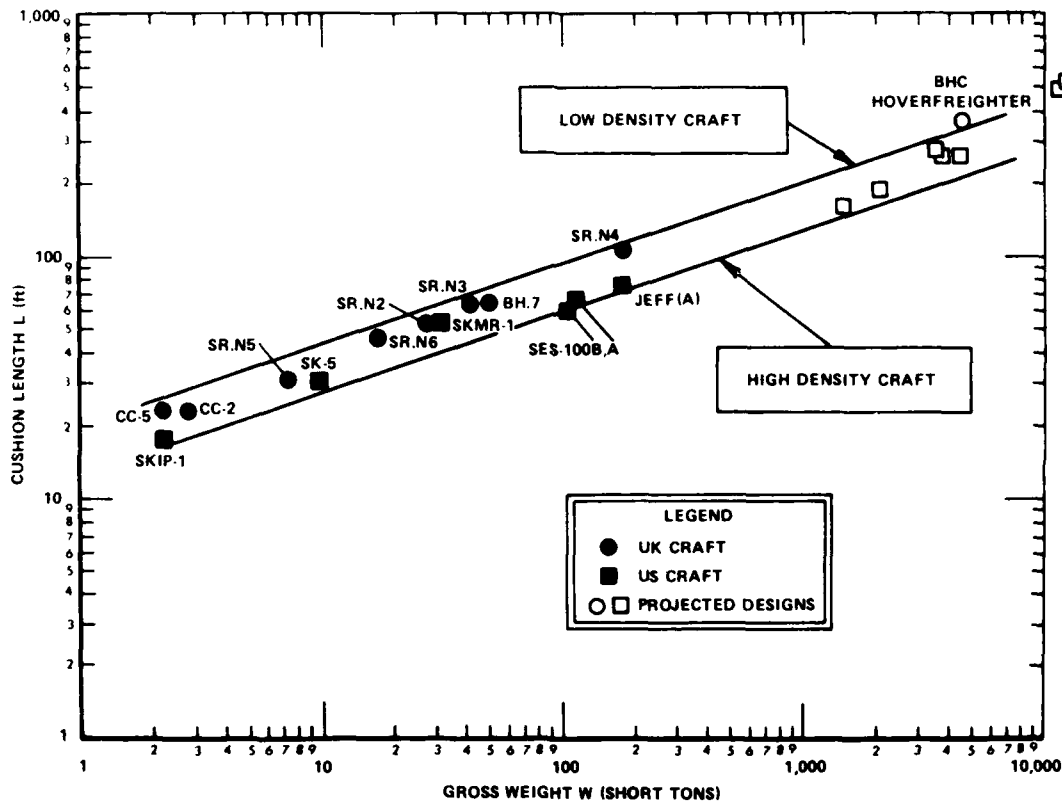


Figure 23 - Size of Air Cushion Craft

From Figure 23 two distinct trends occur in air cushion craft size, depending upon whether high or low density designs are being pursued. The size of such craft can be represented by

$$L = K_1 W^{1/3} \quad (14)$$

where the constant of proportionality (K_1) takes on the values

$$\begin{aligned} K_1 &= 20 \text{ ft/ton}^{1/3} \quad (\text{low density craft}) \\ &= 12.5 \text{ ft/ton}^{1/3} \quad (\text{high density craft}) \end{aligned} \tag{15}$$

when the cushion length (L) is in feet and the gross weight or displacement (W) is in short tons. Since the original summary was issued new craft have been constructed and new designs have been projected. Some of these craft have been added to Figure 23 and it is evident that the trend lines and Equation (14) are still applicable.

Cushion Pressure

Since all air cushion craft have either all or a significant portion of their lift generated by the air pressure in the cushion, it is necessary to know how the basic parameter of cushion pressure varies with the size of the craft.

By expressing the simple relations, Equations (11) and (13), in another way, one can write for the cushion pressure,

$$P_c = \frac{(P_c/L)^{2/3} W^{1/3}}{(L/B)^{1/3}} \tag{16}$$

Figure 24, taken from Reference 24 and updated to include current craft, indicates the values of air cushion pressure of interest to air cushion craft existing now and in the foreseeable future. The remarks pertaining to high and low density and wide and slender craft discussed previously apply equally to these data. Provided that care is taken in accounting for the L/B effect shown in Equation (16), one can write for the trend in cushion pressure,

$$P_c = K_2 W^{1/3} \tag{17}$$

where the constant of proportionality (K_2) has the values,

$$\begin{aligned}
 K_2 &= 10 \text{ lb/ft}^2 \text{ ton}^{1/3} \text{ (low density craft)} \\
 &= 19 \text{ lb/ft}^2 \text{ ton}^{1/3} \text{ (high density craft)}
 \end{aligned}
 \quad \left. \vphantom{\begin{aligned} K_2 &= 10 \text{ lb/ft}^2 \text{ ton}^{1/3} \text{ (low density craft)} \\ &= 19 \text{ lb/ft}^2 \text{ ton}^{1/3} \text{ (high density craft)} \end{aligned}} \right\} (18)$$

when the cushion pressure (p_c) is in pounds per square foot and the gross weight or displacement (W) is in short tons. Again, since the original summary was issued new craft have been designed and constructed. Some of these craft have been added to Figure 24 and the trends are found to be still applicable.

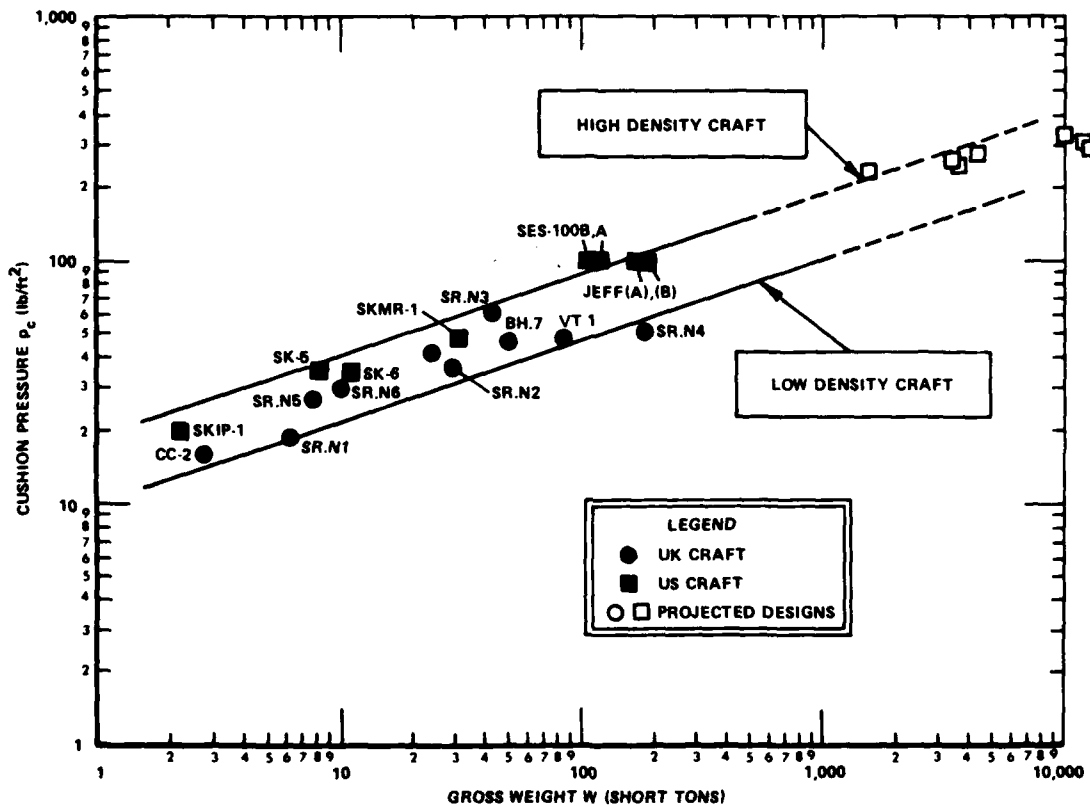


Figure 24 - Cushion Pressure of Air Cushion Craft

Since this parameter of cushion pressure coupled with the air flow requirements have a direct influence on the sizing of the lift fan system, further discussion will be deferred to Chapter VIII: Lift Fan Systems.

Cushion Flow

Determining the proper amount of air flow beneath the skirt hemline of air cushion craft has proven to be a most elusive design feature. Intuitively, it is felt that too much flow will cost too much in lift power and that too little flow will cost too much in propulsion power through increased skirt (or sidehull) resistance in the water. In the "early days" of the 1960's, the sidehull enthusiasts discussed the captured air bubble (CAB) mode of operation¹¹ and the amphibious enthusiasts discussed the trapped air cushion (TAC) mode of operation.²⁵ Both the CAB and the TAC modes of operation recognized the basic premise that zero or minimal flow and air gap would minimize the power requirements. Such a condition would only apply, of course, in calm water operation, which is, in reality, a theoretical operating condition for the practical air cushion craft.

Two factors hampered a more realistic treatment of the more likely rough water operation: (a) the problem of measuring the true leakage area beneath skirts and (b) no valid theoretical treatment of the effect of air flow leakage on the performance and stability of an air cushion craft. The problems of designing for optimum flow are developed and discussed in the succeeding sections and chapters on performance and stability. To provide some indication, as a reference point, for the calm water air gap of current air cushion craft, Figure 25 has been prepared from the scant

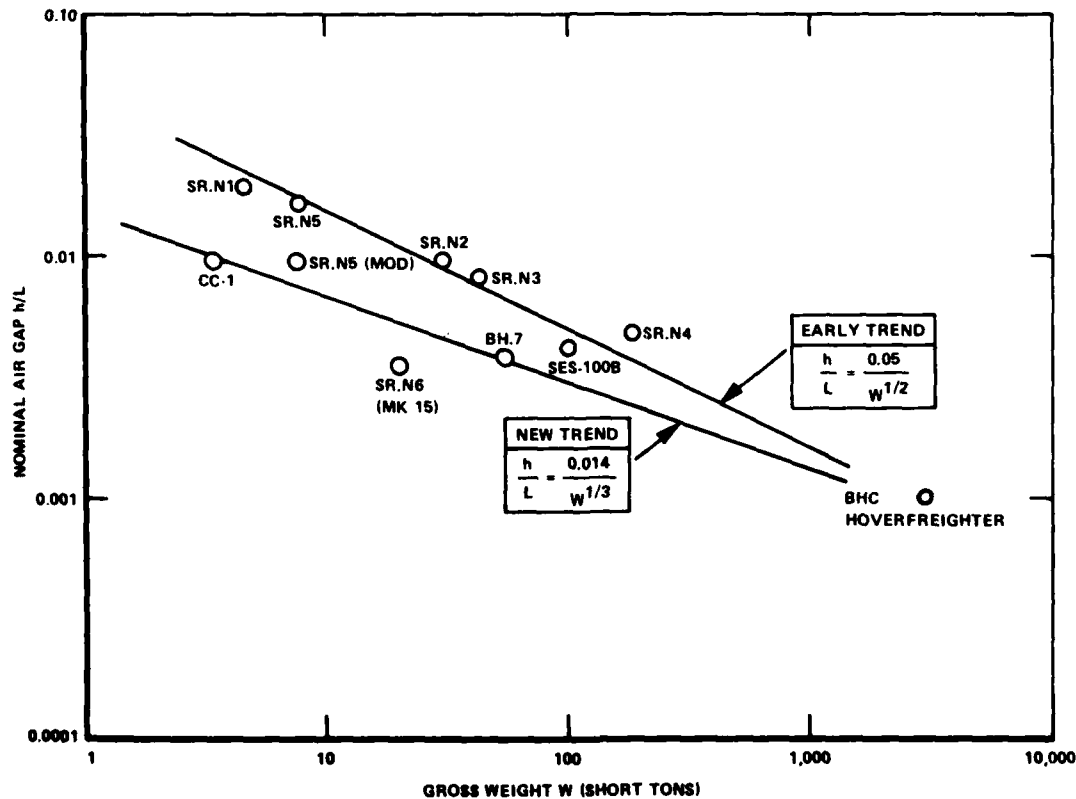


Figure 25 - Nominal Air Gap

information available. The data in Figure 25 has been revised since Reference 2 was published based on more data being made available to the author.* The revised approximation to this elusive parameter is now written, to be more representative of the state-of-the-art as;

$$h/L = \frac{K_3}{W^{1/3}} \quad (19)$$

where the constant of proportionality (K_3) to fit the state-of-the-art is given by $K_3 = 0.014 \text{ tons}^{1/3}$ when the displacement (W) is expressed in short tons.

To indicate the difficulty in determining this parameter, the following notes are provided relative to the geometry of the skirt hemline. The lower edges of the skirt on actual air cushion craft move up and down as a result of wave action and air pressure forces causing constantly varying air gaps. Indeed, this movement or finger oscillation can reach high frequencies and does not always occur in phase with the wave motion. Figure 26, taken from Reference 26, is a trace from a movie record taken inside the cushion of an SR.N4 during operation in waves. This shows the complex motion of the hemline and therefore the resultant local air gap (even ignoring the leakage through other parts of the craft such as through skirt hinge attachments, scalloped fingers, and worn fingers).

Despite the complexities of skirt motion, however, the concept of a nominal or equivalent air gap clearance is useful in performance calculations.

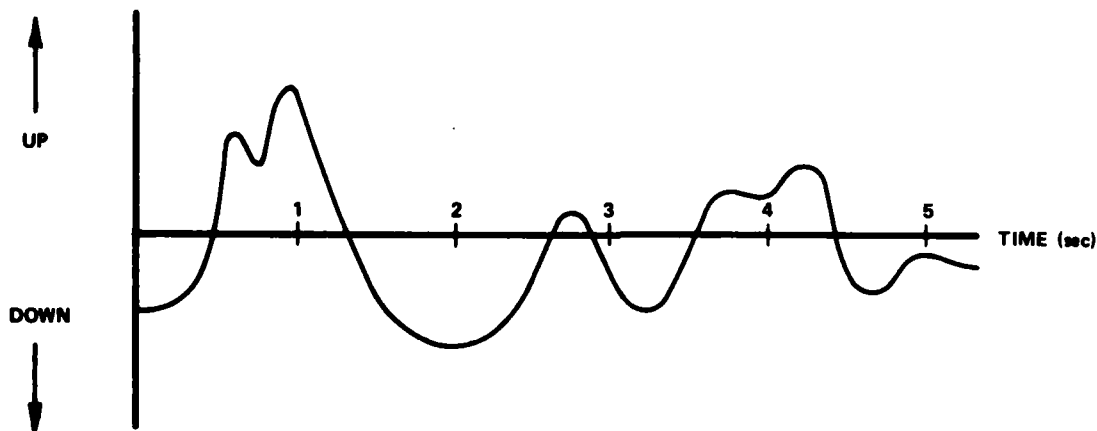


Figure 26 - Trace of SR.N4 Hemline Movement

*Private communication with Peter Crewe (BHC) in June 1975.

Figure 27, taken from Reference 26, shows the effect of the air gap on the power requirements for a craft the size of an SR.N6 (about 17,500 lb). This comparison is for calm water operation at a speed some four times hump speed. The comparison is for both a skirted and an unskirted craft. The thrust power required for the unskirted craft is less than for the skirted craft at the minimum air gap parameter (h/L) shown for the former, but it is to be supposed that, at normal cushion pressure (30 lb/ft^2 for SR.N6), its required power would rise far more rapidly with further decrease in the air gap than if shown for the skirted craft. Extensive bottom contact due to cushion wave-making formation and heavy spray would account for a very rapid drag rise.

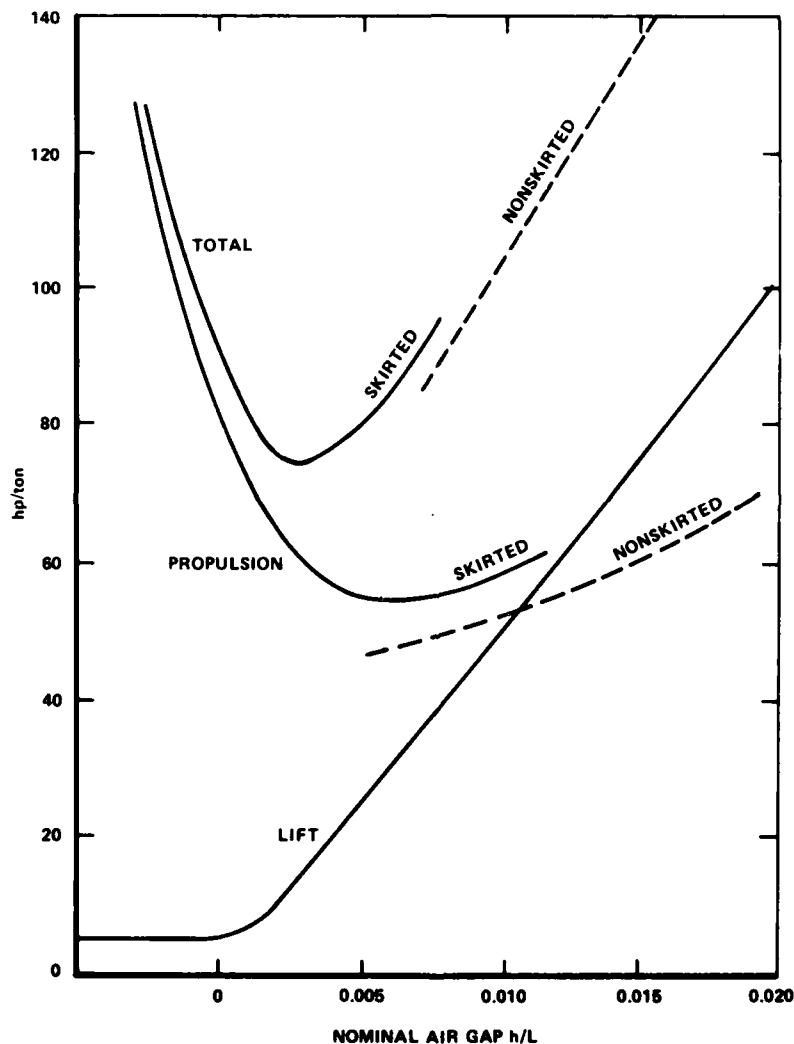


Figure 27 - Effect of Air Gap on Power

Power

The power requirement to both propel and lift an air cushion craft is obviously dependent on many parameters such as craft size, speed, and design sea state among other important considerations. It also depends, of course, on the type of craft, whether it is aerostatic, aerodynamic, or another type. Each of these considerations will be discussed in succeeding sections, but it is frequently helpful to compare the overall power requirement, once all design aspects are complete, in terms of horsepower per ton for comparisons with other air cushion craft and also with other forms of transportation.

Figure 28 shows the total installed horsepower for existing air cushion craft together with those projected in the next 10 years. This figure was first prepared²⁷ in 1967, and it was found then that, with few

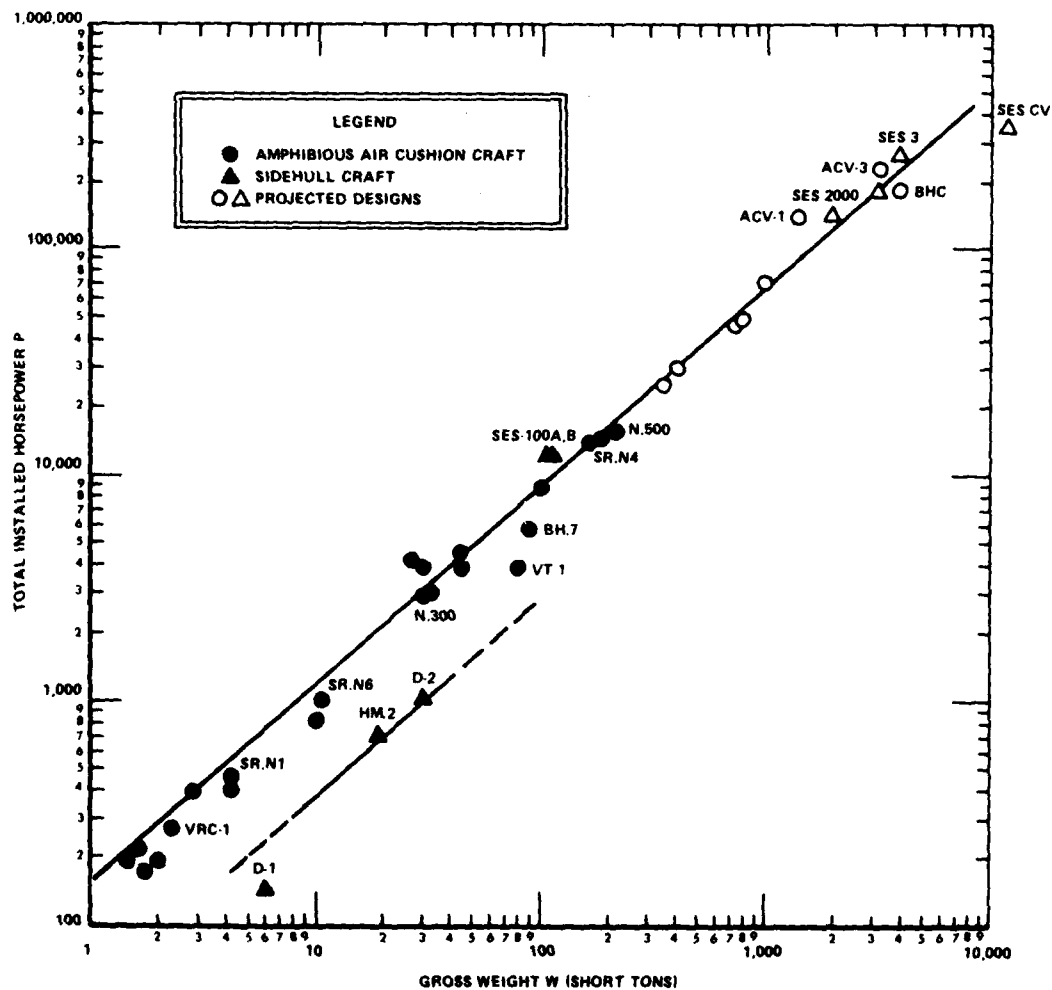


Figure 28 - Total Installed Power for Air Cushion Craft

exceptions, all air cushion craft followed a surprisingly consistent trend, with the total installed power given by

$$P_{TOTAL} = K_4 W^{7/8} \quad (20)$$

where the constant of proportionality (K_4) is given by $K_4 = 165 \text{ hp/tons}^{7/8}$ when the total installed power (P_{TOTAL}) is expressed in horsepower and the gross weight (W) in short tons. The few exceptions that do not follow this trend are discussed below.

Since 1967, new craft have appeared either at the dock or on the drawing board, but all follow the power relationship given by Equation (20). Notable exceptions are lower speed water-propelled craft, for example, VT 1 and HM.2. This result is considered somewhat surprising in that it applies to both amphibious ACV and nonamphibious SES with different missions, design speeds, and operational envelopes. Of course, in using this result, care must be exercised to ensure that all compensating factors have been taken into account. For example, the Hovermarine HM.2 falls below this line (see Figure 28) because of the lower power requirements of sidehull craft compared to the fully skirted craft, provided it is operated at or near the speed for maximum transport efficiency (see next section). The U.S. Navy SES designs and operational craft, however, are required to operate at speeds far in excess of the speed for maximum efficiency with the resultant increased power requirements. As an example, both the SES-100A and SES-100B were designed to gather data at high speeds in super-cavitating flow conditions (around 80 knots), whereas their best transport efficiency speed is closer to 40 knots (see, for example, Figure 63). These compensating factors resulted in both ACV and SES forms of air cushion craft, exhibiting similar power requirements as evidenced by Figure 28.

Projected designs for the amphibious air cushion craft prepared for the Defense Advanced Research Projects Agency (DARPA) for use in the Arctic²⁸ also follow this trend. Similarly, projected SES designs for the U.S. Navy SES-3000 (or 3KSES or LSES) surface effect ship follow this trend as does a BHC Hoverfreighter amphibious air cushion craft design.²⁹ Additional designs of both the amphibious and sidehull SES type of craft also were added from the recent U.S. Navy evaluation of advanced vehicles.³⁰ It will be noticed that the trend has remained the same even with the addition of the new craft and projected designs.

As an insight into this trend line, the effect of size and speed has been separated and shown on Figure 29. A considerable amount of data of other advanced concepts has been left off Figure 29 for purposes of clarity; the important point is to notice the various trends. The cubic function through the displacement ships of roughly 3000-ton displacement is shown to

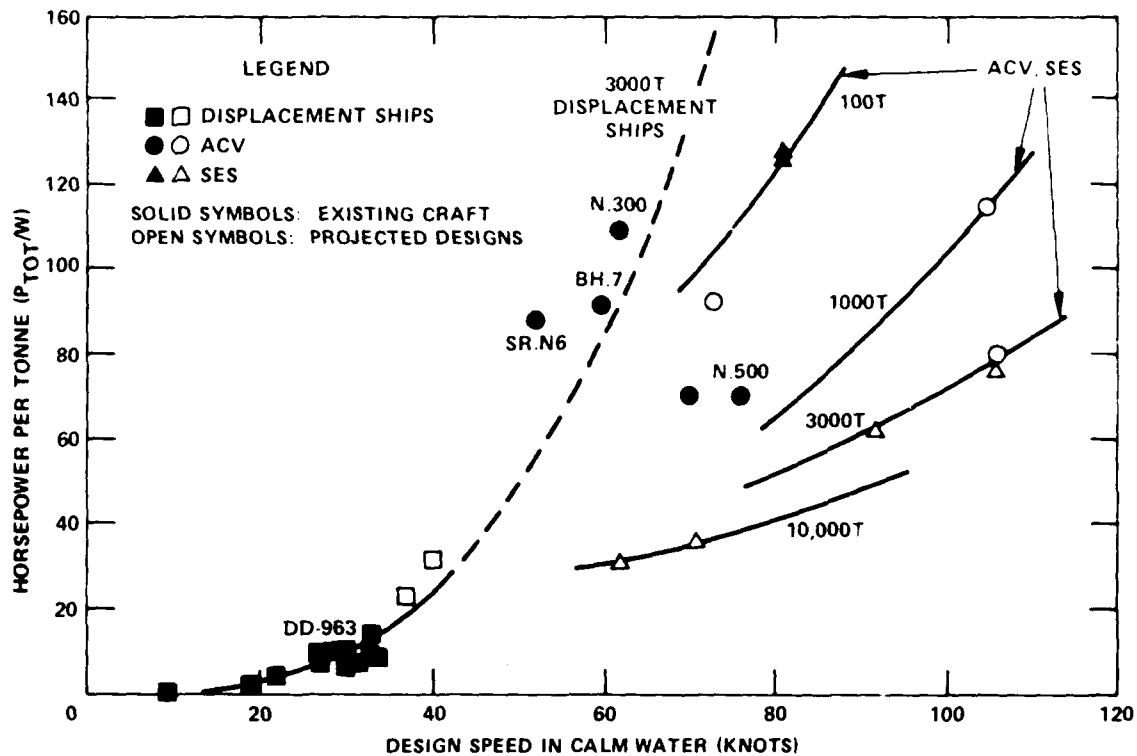


Figure 29 - Power, Weight, and Speed

demonstrate the problems of attempting to push conventional displacement ships much faster than about 30 to 40 knots. The 3000-ton class air cushion craft are seen to have significantly less total power required per ton of displacement even at the much higher speeds. Within the air cushion craft class it is seen by the series of four curves to the right of the dotted displacement ship curve, that as displacement is increased the improvements in power requirements per ton reach a point of diminishing returns for the large displacements (3000-10,000 tons). The compensating effects of weight, power, and speed that result in a common trend line in Figure 28 can now be seen from Figure 29. For example, the 100-ton SES was designed for 80 knots with a power density of about 125 hp/ton such that the power installed would be about 12,500 hp which is as shown on Figure 28. As size is increased, the specific power requirements improve through normal scaling relationships and for a 3000-ton displacement air cushion craft the

power density drops to about 70 hp/ton even for an increased speed of 100 knots. This would give about 210,000 hp installed which again matched Figure 28. Hence, it is seen that the weight and speed selected for the designs have had compensating effects to give a common trend line of power and weight. When the craft falls above or below the trend line in Figure 28 it can usually be traced to a nonscaling of the speed. For example, while there is a tendency to Froude scale the speeds as size is increased to maintain aerodynamic and hydrodynamic efficiency (see later), this is not always done. As a case in point, the 10,000-ton displacement air cushion craft shown in Figure 28 falls below the trend line somewhat. This is because instead of Froude scaling the speed beyond the 100 knots for the 3000-ton craft, the speed was dropped to about 60 knots, such that the power density was around 30 hp/ton (see Figure 29) and the total power became "only" 300,000 hp instead of about 500,000 hp from the trend line in Figure 28. While the interest here has been on discussing trends it is noted that the various designs used have received detailed treatment and are indeed representative of the state-of-the-art. Specific details on the projected designs used may be found in Reference 31.

The power relationship given by Equation (20) is an after-the-fact result and cannot be used in specific design analyses for a specific mission; more fundamental treatment of the power requirements must be undertaken. As seen, the design speed is an important consideration, and each form of air cushion craft must achieve maximum efficiency, that is, the least power to transport a given weight or displacement, at different speeds as discussed earlier in connection with the economic and range equations. These considerations thus prompted evaluation of the transport efficiency WV/P .

Transport Efficiency

It was seen from the basic performance equations given at the beginning of this chapter that the transport efficiency (WV/P) plays an important part in the design of a vehicle. In recognition of this, in 1950, von Karman and Gabrielli³² prepared a succinct method of comparing the transport efficiency of all forms of transport.*

Figure 30, reproduced from Reference 32, is a mosaic of most forms of transport except for the air cushion craft, which did not appear on the modern transportation scene until a decade after von Karman and Gabrielli's researches. Envelopes of tankers, jet aircraft, hydrofoils, and planing craft taken from Reference 27 have been added for comparison with air cushion craft.

Unfortunately, like many simple yet correct expressions, von Karman and Gabrielli's transport efficiency has often been misapplied and treated

* In the original reference, the term "specific power" was used, which is a measure of transport efficiency as used here for direct use in lift-to-drag ratio comparisons.

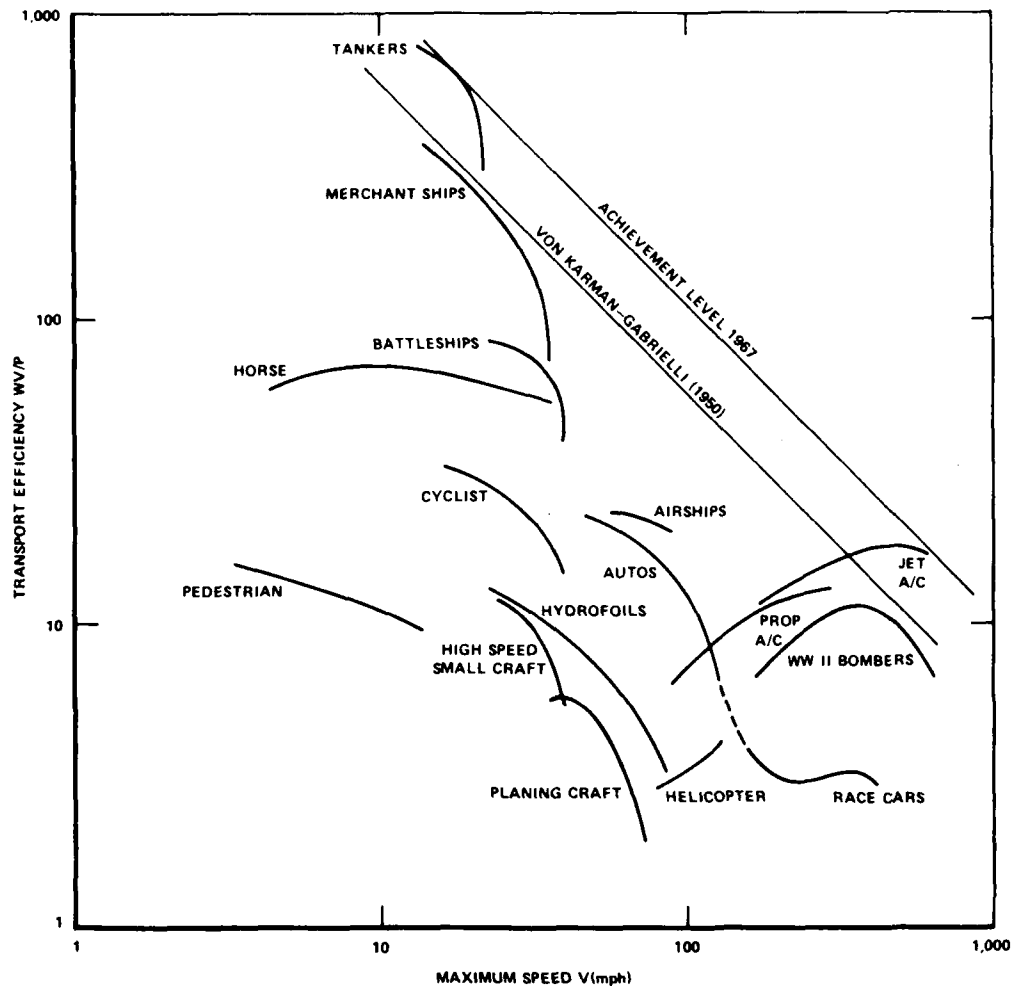


Figure 30 - Transport Efficiency of Several Craft

as an absolute that any vehicle must achieve. In the real world, of course, such is not the case. The usefulness of a vehicle is not always determined by its efficiency alone, as may be seen in the case of the helicopter. The helicopter must expend power to stay motionless in its operating medium (air) while the ship expends no power to stay motionless in its medium (water), but there is no denying the usefulness of the helicopter in the military inventory or in the commercial transportation world. Similarly, the air cushion craft in its amphibious or ACV form offers a unique capability of transporting payload over practically any surface while, like the helicopter, it too must expend power to sustain itself above the surface. Such power is to be included in any computation of its transport efficiency (WV/P). Without the effect of the air cushion lift power, the effective lift-to-drag ratio reduces to the aerodynamic or hydrodynamic lift-to-drag ratio W/D.

In 1967, Reference 27 showed how well air cushion craft fared in achieving high values of transport efficiency and how this efficiency increased as craft size increased. Figures 31 and 32, taken from Reference 27, have been included together with the achievements of craft that have appeared since that time. Additional craft and design studies have been added since Reference 2 was issued and no major change is foreseen other than that associated with the benefits of size.

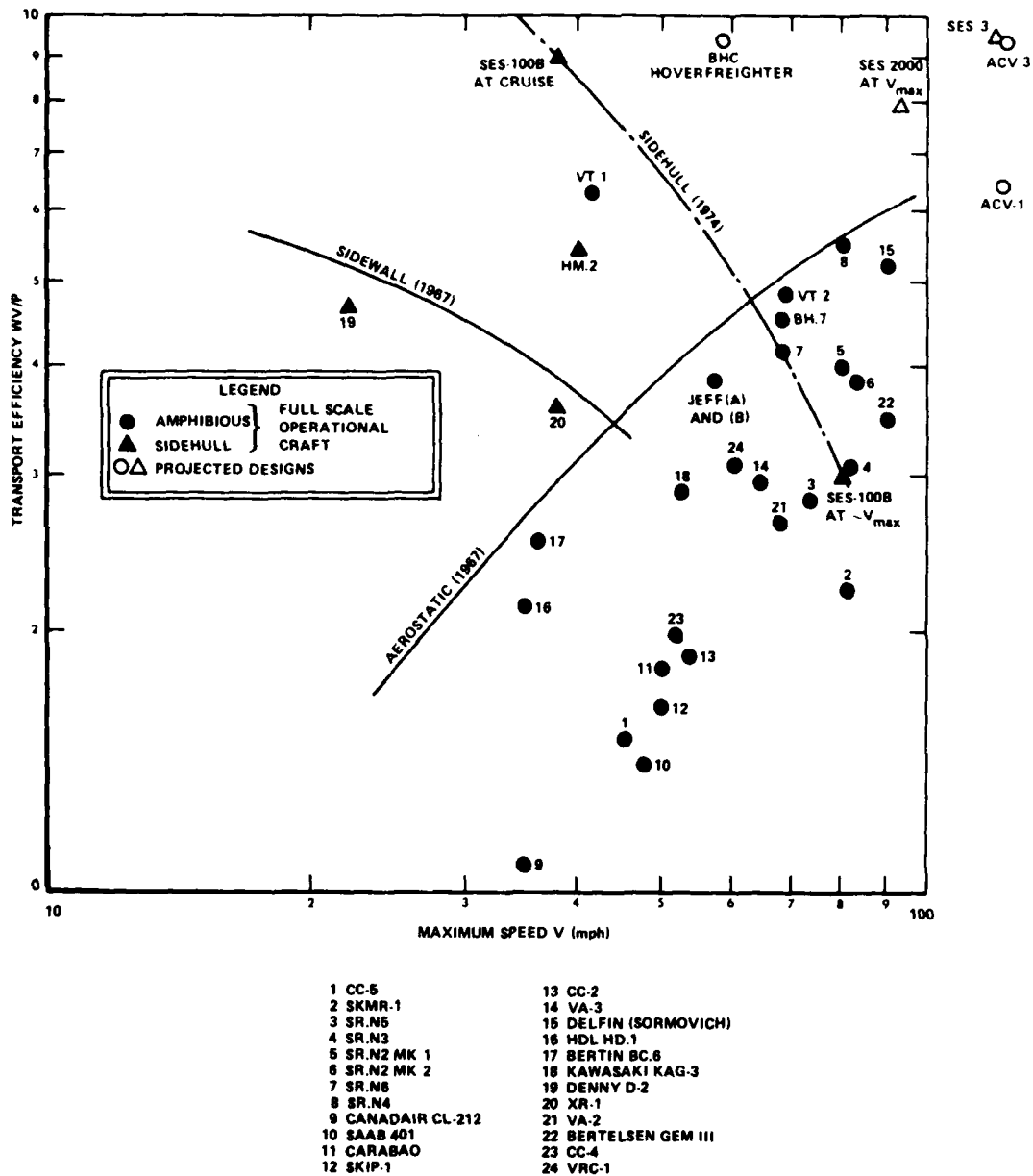


Figure 31 - Transport Efficiency of Air Cushion Craft

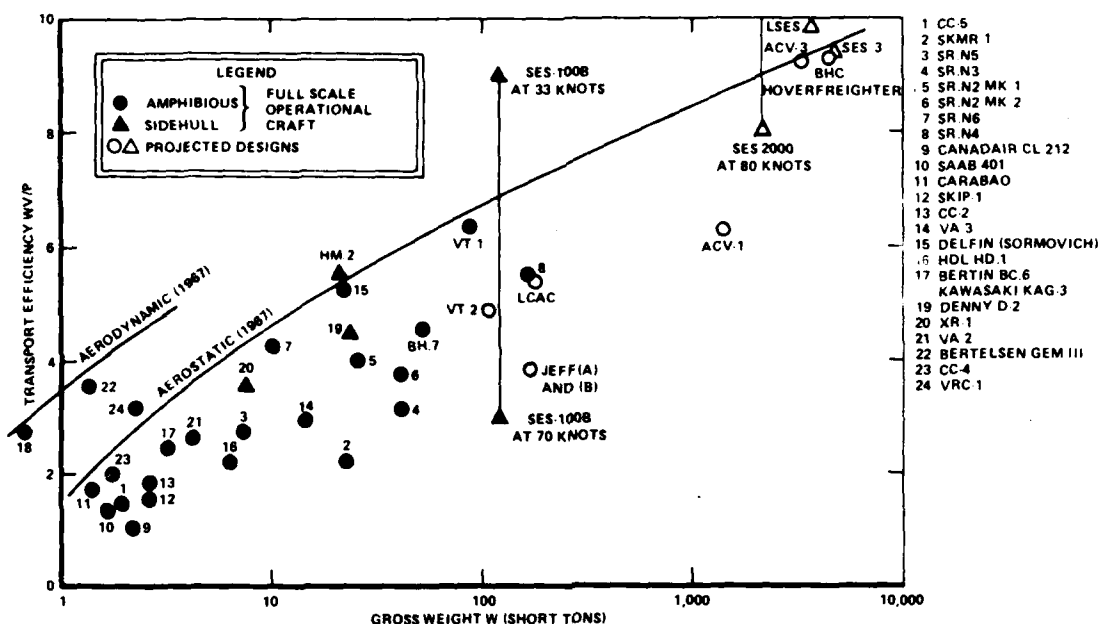


Figure 32 - Effect of Size on Transport Efficiency

As seen from Figures 31 and 32 it has proven difficult to increase transport efficiencies to much above 5 at the craft maximum speed, despite optimism in the early 1960's when values in excess of 20 were predicted. The transport efficiency of the SES-100B has been included at both its minimum drag speed (approximately 33 knots) and at a value at 70 knots to indicate the pronounced effect of speed. Note that von Karman and

Gabrielli's work³² and the data given in Figures 31 and 32 are at the maximum speed and not the most efficient speed. The difficulties of maximizing the transport efficiency or minimizing the total power requirements have been caused, in general, by the need to operate in rough seas and to provide a comfortable ride to crew and passengers. This will be discussed in more detail as the power components and ride requirements are examined.

Payload Capability

To complete the overall sizing parameters it will be recalled from the beginning of the chapter that the second major term in the basic performance equation discussion was the payload capability of the craft. In a similar vein to the comparison of transport efficiency of various craft, it is useful to compare how well the air cushion craft fared with other forms of transportation in this regard.

The gross weight of the craft can be written,

$$W = W_F + (W_F + W_P) \quad (21)$$

where W_E is the empty weight of the craft. The terms in the parentheses in Equation (21) are the fuel load (W_F) and the payload (W_p) which together comprise the disposable load (W_d). While Equation (21) appears simple there has been great difficulty in making comparisons among vehicles because of the wide variations in the definition of each of the items in the vehicles among the various design communities around the world. At the present time, it is felt that the recent U.S. Navy ship work breakdown structure (SWBS) is the most consistent method³³ and has been used by this author, converting other system data to this format wherever possible. Although it should be noted that it too has complications as will be discussed later, errors are bound to occur at the subsystem level because weight information (and their definition) are not readily available for many reasons. Appendix B is a compilation of data by weight groups felt to be the most reliable. While there is cause for concern at the subsystem level there is less concern at the aggregate level for the empty weight and light ship weight. Based on analyses of data compiled in Appendix B, it is felt that Figure 33, upgraded from Reference 34, is a fair representation of how the light ship weight fraction (W_{LS}/W) varies as a function of vehicle size.

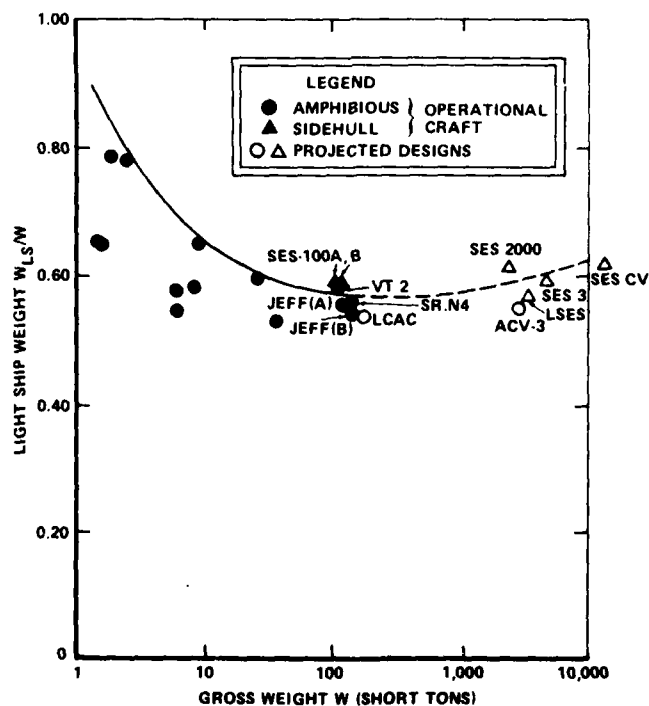


Figure 33 - Light Ship Weight of Air Cushion Craft

Since Figure 33 was originally prepared several new craft have appeared on the scene and new design projections have been made. It will be noticed that as projected designs have turned into hardware the weight has invariably increased--or to misquote Murphy's Law "Anything that can get heavier, will get heavier!"

The complementary term to empty weight is, from Equation (21), the disposable load.* Envelopes of the disposable load for several types of craft have been compiled and are shown in Figure 34. Disposable load functions of 40 percent are seen to be relatively easy to achieve for air cushion craft, but stringent weight control is required to achieve 50 percent disposable load fractions.

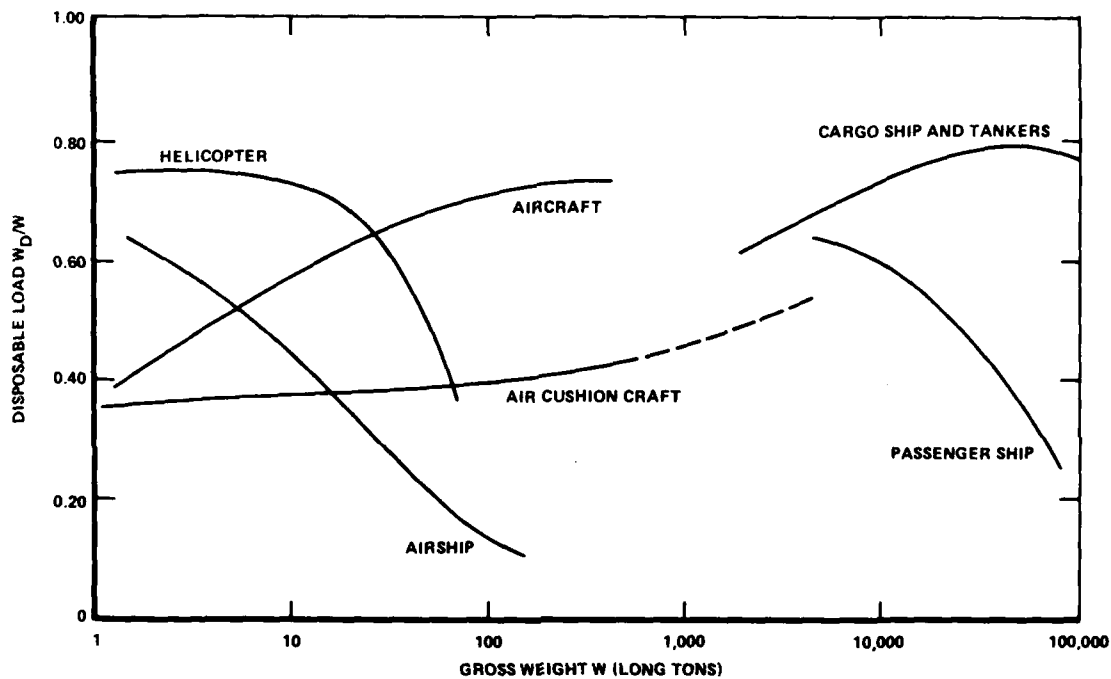


Figure 34 - Disposable Load of Transport Craft

*Definitions of all weight terms such as "empty weight," "light ship weight," and "disposable load" are given in Appendix B.

PERFORMANCE CHARACTERISTICS

Having expressed some of the overall sizing considerations of the air cushion craft and where it sits in relation to other competitive forms, attention is now given to the development of the detailed performance parameters for use by the designer. Wherever possible emphasis is given to expressing these parameters in terms of easily measurable quantities that can be obtained "in the field." This is considered important in that it improves the likelihood of feedback from operational craft to verify the design rules that produced the craft in the first place.

While some of the basic theories of the performance of air cushion craft were developed in the early period of 1959 to 1965, there are still several unknown characteristics and, as a result, many empirical formulas are still being used. Some of the more reliable formulas and those found most useful by the author in the design of air cushion craft are presented here and discussed.

The majority of the development applies to the amphibious air cushion craft with appropriate treatment given wherever applicable to the non-amphibious or SES form of craft. The performance considerations of high speed aerodynamic craft are given in Chapter X.

Much of the basic work is done with models, and it is important to understand the theory of models and dynamic similitude if proper interpretation is to be placed on the results. For the air cushion craft, this is particularly difficult because of the flow phenomena associated with the proximity and effect of the surface over which it moves.

Basic Relationships

There are several basic relationships that govern scaling laws and relationships of pressure, flow, power and speed that need to be discussed. They are outlined here.

Dynamic Similitude. Systems are said to be dynamically similar if (a) they are geometrically similar and (b) if the forces acting in one system are in the same ratio to each other as similar forces in the second system.

The forces acting on an air cushion craft are a complex function of both aerodynamic and hydrodynamic forces for the typical case of amphibious craft. The forces acting on the craft can be assumed to be a function of several key parameters; namely,

$$F = f(L, V, \mu, \rho, g, p_c, Q, h_w, p_{amb}, \dots) \quad (22)$$

where L = characteristic length, taken as length of cushion
 V = craft speed
 μ = viscosity
 ρ = density
 g = gravitational constant
 p_c = cushion air pressure
 Q = flow through cushion
 h_w = wave height of sea
 p_{amb} = ambient pressure

From the Buckingham π theorem of dimensional analysis independent dimensionless groups can be derived to describe the forces acting on the craft as given by Equation (22). Such an analysis would show that the forces become a function of the following major dimensionless groups:

Reynolds number	$(R. No.) = \frac{\rho V L}{\mu}$	} (23)
Froude number	$(F. No.) = \frac{V}{\sqrt{gL}}$	
Cavitation number	$\sigma = \frac{p_{amb}}{1/2 \rho V^2}$	
Sea roughness parameter	$= h_w / L$	
Cushion density	$= \frac{p_c}{\rho g L}$	
Flow coefficient	$C_Q = \frac{Q}{V L^2}$	

Both the Reynolds number, which is the ratio of inertia forces to viscous forces, and the Froude number, which is the ratio of the inertia forces

generated by the oncoming water stream to the gravity forces in the surface waves, are well known to the ship designer and need no further discussion. The cavitation number, more usually defined as

$$\sigma = \frac{P_c - P_v}{1/2 \rho V^2} \quad (24)$$

where p_v , the vapor pressure, is of particular significance in high speed water flow problems and will be discussed later.

The two parameters of particular significance to the air cushion craft are the so-called cushion density $p_c/\rho gL$, or as commonly used, p_c/L (see earlier), and the flow coefficient Q/VL^2 . Both these parameters characterize the pressure and flow in the air cushion and are of fundamental importance in the performance of the craft as already discussed. As will be shown in Chapter VII, the cushion density p_c/L is also important as a structural index reflecting how dense a structure is for the craft.

Some researchers find that a more general form of the cushion density is useful where the geometrical proportions of the craft are removed and the reference cushion area S is used, such that

$$\text{Cushion density} = \frac{P_c}{S^{1/2}} = (L/B)^{1/2} \cdot \frac{P_c}{L} \quad (25)$$

Both the length form and the area form of cushion density will be used here to describe its effect on different aspects of the air cushion craft as used by the different groups. Note that the cushion density in Equation (25) is not nondimensional but has the units of density (usually pounds per cubic foot).

Similarly, it is usually assumed that the flow coefficient is referred to the cushion area, such that

$$\text{Flow coefficient} = C_Q = \frac{Q}{VS} \quad (26)$$

Other dimensionless parameters are important to the air cushion craft, depending upon the domain of operation (high or low speed), the relative importance of hydrodynamic and aerodynamic forces acting on the craft, and other influences that will be described in succeeding sections.

Two other important coefficients complete this basic definition of terms; they are the nondimensional forms of power and speed.

Power Coefficient. There are two fundamental power components of concern to the air cushion craft: the lift power to sustain the craft above the surface and the propulsion power to propel the craft along its path. Both of these power components depend on the pressure and flow in the air cushion, and it is convenient to define a nondimensional power coefficient,*

$$C_P = \left(\frac{\rho}{2}\right)^{1/2} \cdot \frac{550 \eta P/W}{\frac{Ch}{S} \left(\frac{W}{S}\right)^{1/2}} \quad (27)$$

where ρ is the density of air (slugs per cubic foot) and η is the total lift and propulsion system efficiency. The power P is expressed in units of horsepower.

This power coefficient can be viewed as the horsepower per pound of the craft, nondimensionalized by the pressure and flow parameters, W/S and Ch/S , where Ch/S expresses the ratio of the net leakage area to the cushion area. For the rectangular cushion,

$$\frac{Ch}{S} = 2 (1+L/B) \frac{h}{L} \quad (28)$$

where L/B is the length-to-beam ratio of the cushion.

The air gap h in its simplest or purest sense is the leakage gap between the bottom of the (skirted) craft and the surface. In practice, however, there is considerable leakage throughout the craft and at the lower edges of the skirt as already discussed. The air gap is usually taken as an equivalent air gap determined for particular configurations. Further discussion on this is deferred until the discussion on calm water lift power requirements and wave pumping air flow requirements in rough seas.

The nondimensional power coefficient C_P is a complex function of several craft parameters but can be expressed as a function of an independent variable related to the speed of the craft.

Speed Coefficient and Pressure Number. For conventional marine craft, it is known that movement through waves is characterized by Froude number. The air cushion craft, however, that spends a majority of its operating

*Note that the numerical value of these coefficients assumes the use of English units as used throughout this report.

time over water is characterized not only by the Froude number but also by the speed-dependent dynamic air pressure. A pressure number k is defined, which combines these two effects as follows:

$$k = \frac{1/2 \rho V^2}{p_c} \quad (29)$$

This pressure number expresses the ratio of the dynamic forces generated by the oncoming air stream to the static forces generated by the air cushion pressure. It may be seen from the results of dimensional analysis in Equations (22) and (23) that the pressure number is a combination of two of the dimensionless groups; the Froude number V/\sqrt{gL} and the cushion density p_c/L , such that

$$k = \frac{\rho g}{2} \frac{(F. No.)^2}{p_c/L} \quad (30)$$

Fortunately, in conducting experiments and scaling model test data to full-scale craft, there is no incompatibility between Froude number and pressure number, provided cushion density is also scaled.

The pressure number aides in the classification of the air cushion craft as the aerodynamic flow field is strongly dependent on this parameter. For low values of pressure number ($k < 0.1$), the aerodynamic effects are minimal, the hydrodynamic effects dominate, and the craft form is appropriately shaped. At high values of the pressure number ($k \geq 1$), the aerodynamic effects dominate and the craft takes on a significantly different geometric form. The carpet plot in Figure 34 illustrates the range of values of the pressure number, Froude number, and cushion density that are pertinent to the air cushion craft and are derived from Equation (30). Several operational air cushion craft are displayed in Figure 35 to indicate today's design point operation. Note that most air cushion craft are designed to operate in a region of $0.20 < k < 0.60$ and at a cruise speed some two to three times hump speed. Hump speed is where self-induced wave resistance is a maximum.

Some indication of the influence of the pressure number on the flow field around an air cushion craft can be seen from the results of some experiments done in 1961 by N.K. Walker.³⁵ These experiments were conducted on the peripheral jet form of air cushion craft but are indicative of the flow field distortion on all such craft.

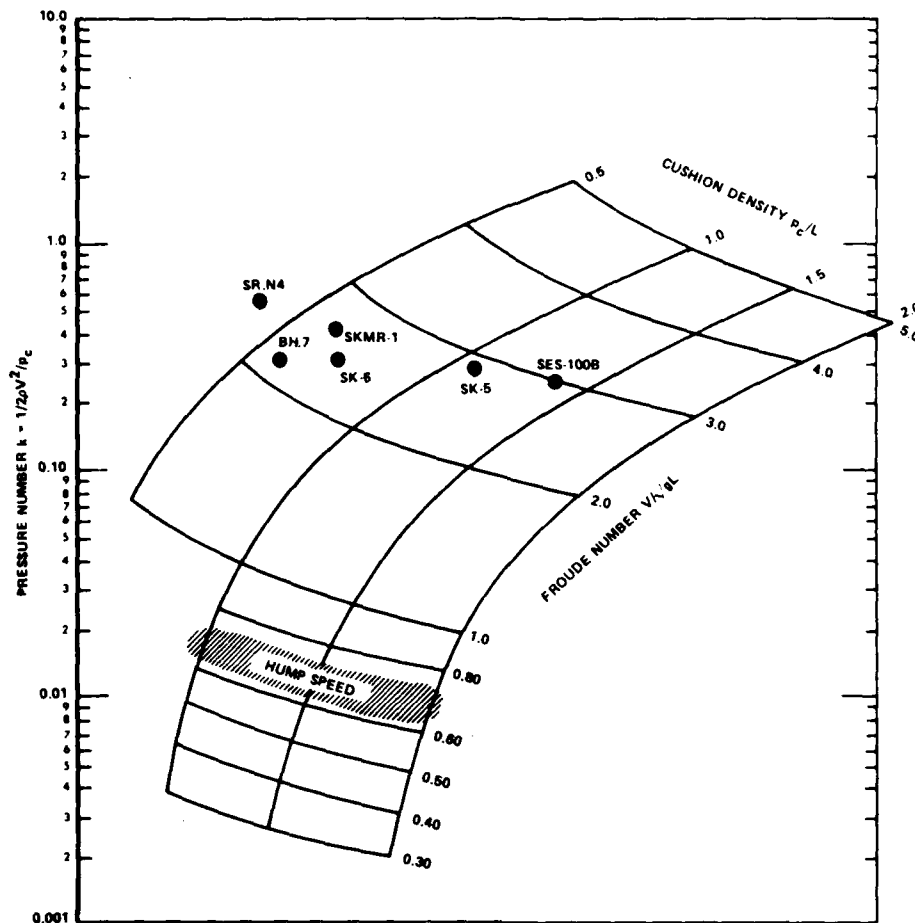


Figure 35 - Speed Characterization of Air Cushion Craft

Pressure and Flow. There are two basic forms of air cushion of interest: the peripheral jet and the plenum. Both have been used in craft design. The peripheral jet is basically more efficient than the plenum and was applied to the first series of air cushion craft. Later craft have tended to operate more in the fashion of plenum craft as the hardware complexities of jets have given way to the simpler plenum. Both forms, however, are still of importance and are given here. The peripheral jet form of air cushion is considered first. Figure 36 shows the pertinent geometry.

The theory of peripheral jet flows received exhaustive treatment in the late 1950's and early 1960's. Some of this work was directly related to air cushion craft and some was a result of V/STOL work. The V/STOL interest arose out of a need to understand the pressure and flow field beneath a helicopter and a jet nozzle as each approached the ground.

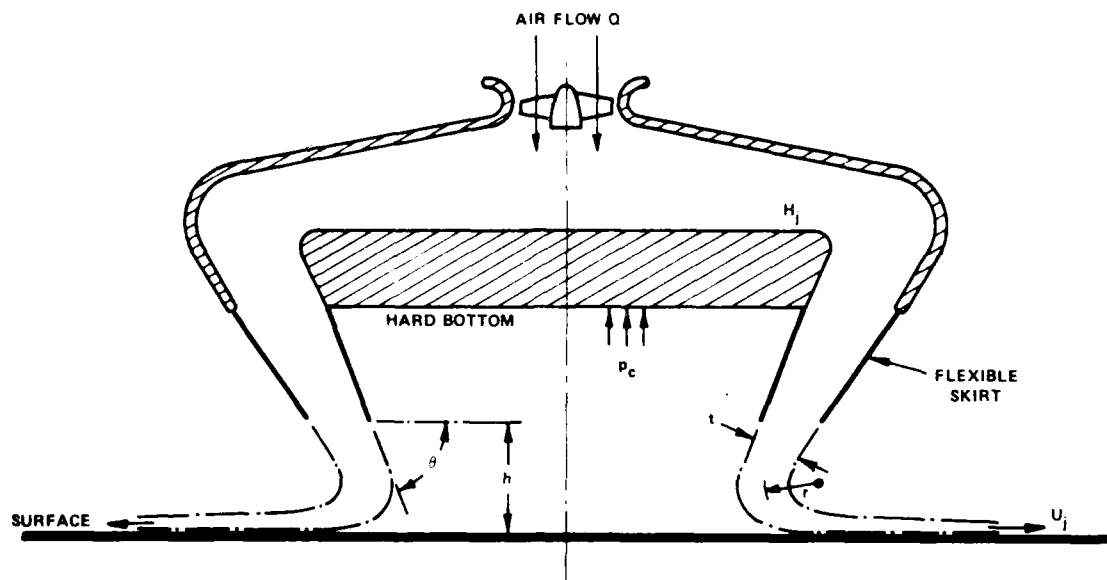


Figure 36 - Nozzle Geometry of Peripheral Jet Craft

Sir Christopher Cockerell³⁶ made his early calculations of jet flows in 1955 directly related to his hovercraft, while von Glahn³⁷ reported on ground proximity effects on the thrust of annular nozzles in 1957.

Since these early formulations, there have been many calculations and experiments on peripheral jet flows for air cushion craft. Some of these theories are based on inviscid flow, some are empirical, and some exact. It would be cumbersome to report on each of these theories, and the reader is referred to the work of Elsley and Devereux³⁸ for a synopsis of the various theories and to Payne³⁹ for a similar synopsis and experiments on curved jet flows applicable to air cushion craft.

Of all the theories, the one found the most useful is the so-called exponential theory developed by British Hovercraft Corporation. The exact authorship is a little unclear. It was developed to aid performance calculations for the SR.N1 by Elsley⁴⁰ and presented by Stanton-Jones⁹ at the Princeton Symposium in 1959 as an appendix to his paper, although copies of the appendix were not reproduced. Stanton-Jones⁴¹ developed the theory again together with a simplified momentum theory in 1961.

This theory and comparison with experiment are given here as follows: In the peripheral jet craft, the jets emanating from the hard structure or the bottom of the skirts create an increase in pressure beneath the craft

by virtue of the centrifugal forces generated by the curvature of the jets as they turn away from the craft at the surface (see Figure 36). Stanton-Jones⁴¹ reasoned that the pressure gradient across the jet must balance these centrifugal forces, such that

$$\frac{\partial p}{\partial r} = \frac{\rho u^2}{r} \quad (31)$$

where r is the local jet radius of curvature and u is the local jet velocity. Then it can be shown,³⁸ upon integration, that the cushion pressure becomes

$$p_c - p_o = (H_j - H_o) (1 - e^{-2x}) \quad (32)$$

where p_o is the ambient static pressure, H_j is the pressure source total head, and H_o is the total head of the free stream. The nondimensional jet thickness is

$$x = \frac{t}{h} (1 + \cos \theta) \quad (33)$$

where t is the actual thickness of the jet, which is inclined at an angle θ relative to the surface. Note that h is the actual clearance beneath the jet nozzle and not the clearance of the hard bottom of the craft.

The total head in the jet, which is assumed equal to the total head in the plenum source, is

$$H_j = \frac{1}{t} \int_0^t p(r) dr + \frac{1}{2} \rho u_j^2 \quad (34)$$

The variation of the static pressure $p(r)$ and the velocity distribution $u(r)$ across the jet are functions of the jet geometry. Figure 37 shows a typical variation of pressure and velocity across a thick jet taken from the experimental results of Payne.³⁹ The particular results shown are for jet parameters $t/h = 1$, $h = 2.0$ in. and $\theta = 30$ deg.

AD-A084 740

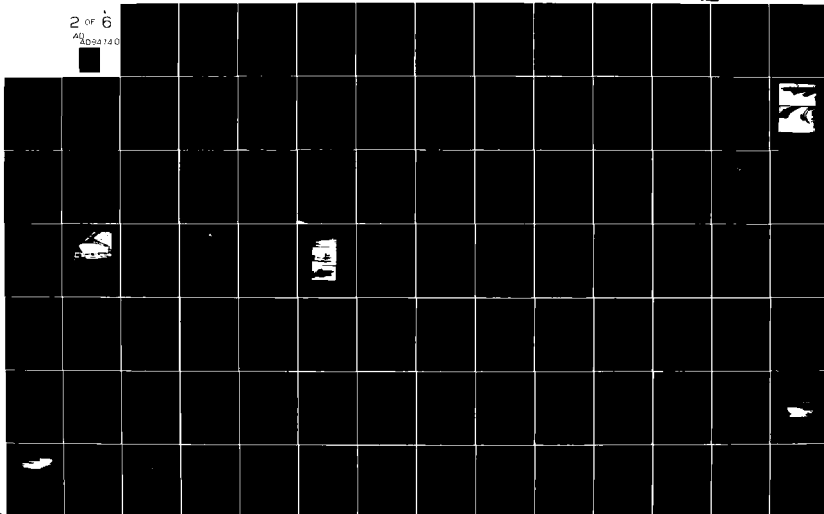
DAVID W TAYLOR NAVAL SHIP RESEARCH AND DEVELOPMENT CE—ETC F/G 13/10
AIR CUSHION CRAFT DEVELOPMENT. FIRST REVISION.(U)
JAN 80 P J HANTLE
DTNRDC-80/012

UNCLASSIFIED

NL

2 of 6

AD-A084 740



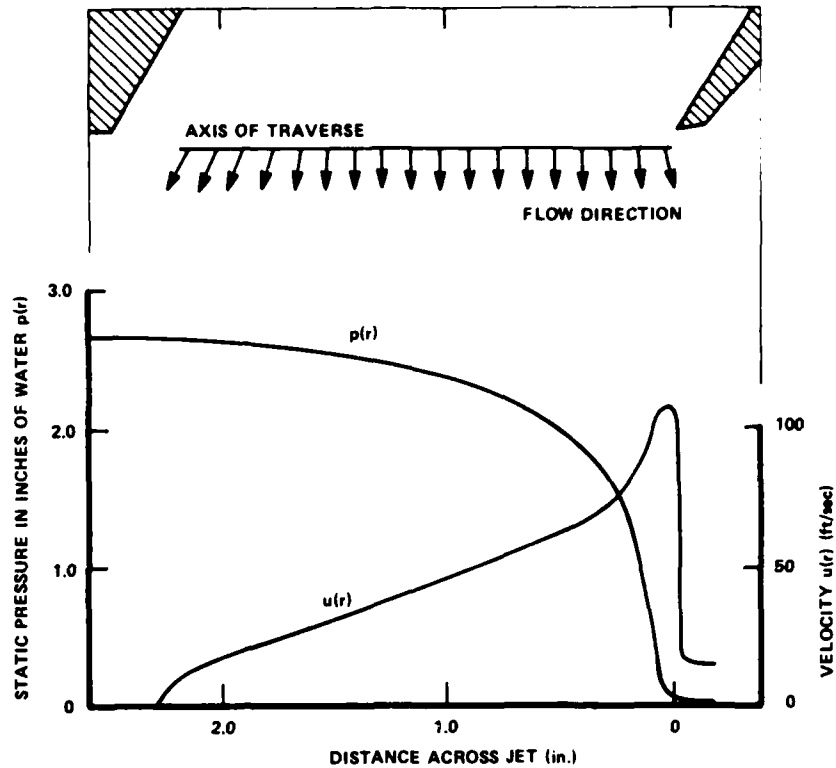


Figure 37 - Pressure and Velocity Distribution Across Jet

From such pressure variations, the mean pressure in the jet can be quite different from the average of the cushion pressure and the ambient pressure. If such an assumption is made, however, then the result called simple theory by Elsley⁴⁰ and Stanton-Jones⁹ is obtained, and

$$\frac{p_c - p_o}{H_j - H_o} = \frac{2x}{1 + x} \quad (35)$$

If, on the other hand, the variation of static pressure across the jet similar to that shown in Figure 37 is considered, then the result known as the exponential theory is obtained, such that

$$\frac{p_c - p_o}{H_j - H_o} = 1 - e^{-2x} \quad (36)$$

Stanton-Jones⁴¹ shows the comparison of these two theories with model test results. Figure 38 shows this comparison for a range of jet thicknesses.

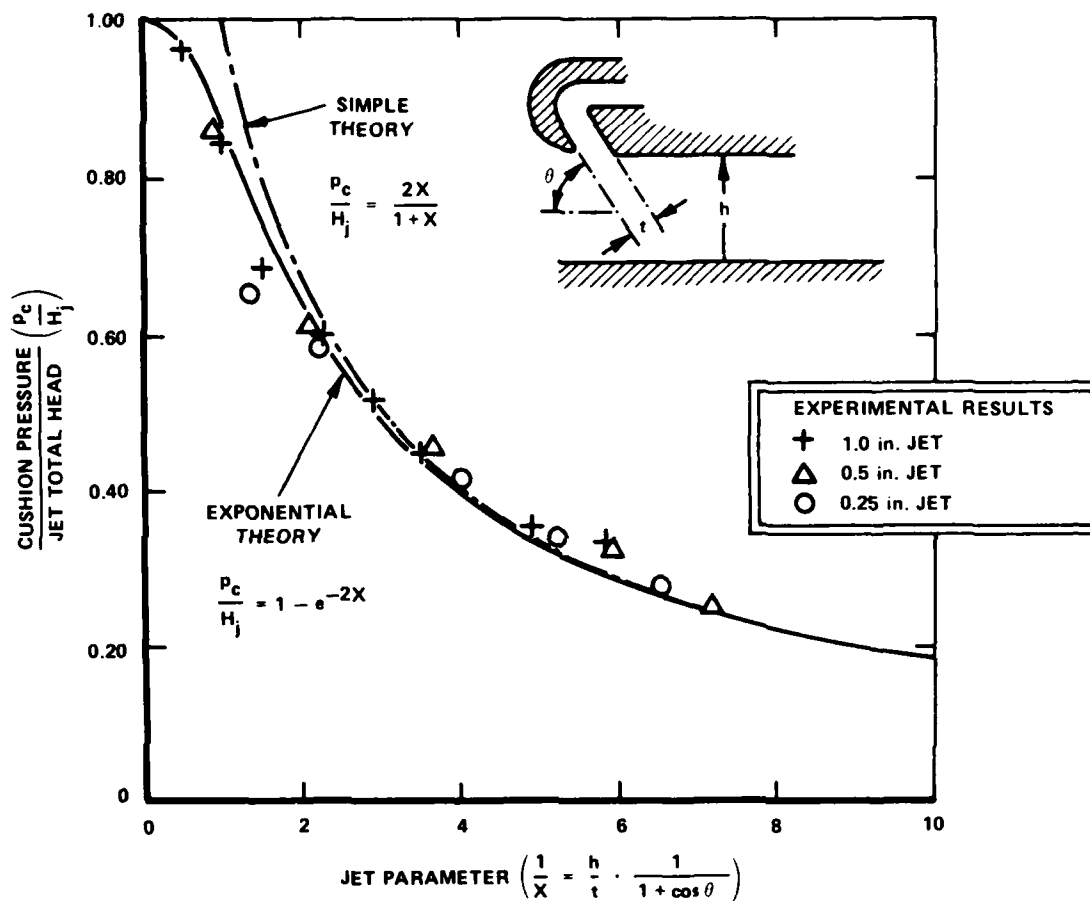


Figure 38 - Saunders-Roe Theory and Test for Peripheral Jet

The flow for the peripheral jet can then be calculated from

$$Q = C \int_0^t u(r) \cdot dr \quad (37)$$

where C is the total peripheral length of the jet. After appropriate substitution from the pressure relation,

$$Q = \left(\frac{2}{\rho}\right)^{1/2} (H_j - H_o)^{1/2} \cdot \frac{Ch}{1 + \cos \theta} (1 - e^{-x}) \quad (38)$$

Experiments by Carmichael and Southcote⁴² conducted over a range of non-dimensional jet thicknesses show excellent agreement with both the pressure and flow as predicted by the exponential theory. Figure 39 shows this comparison.

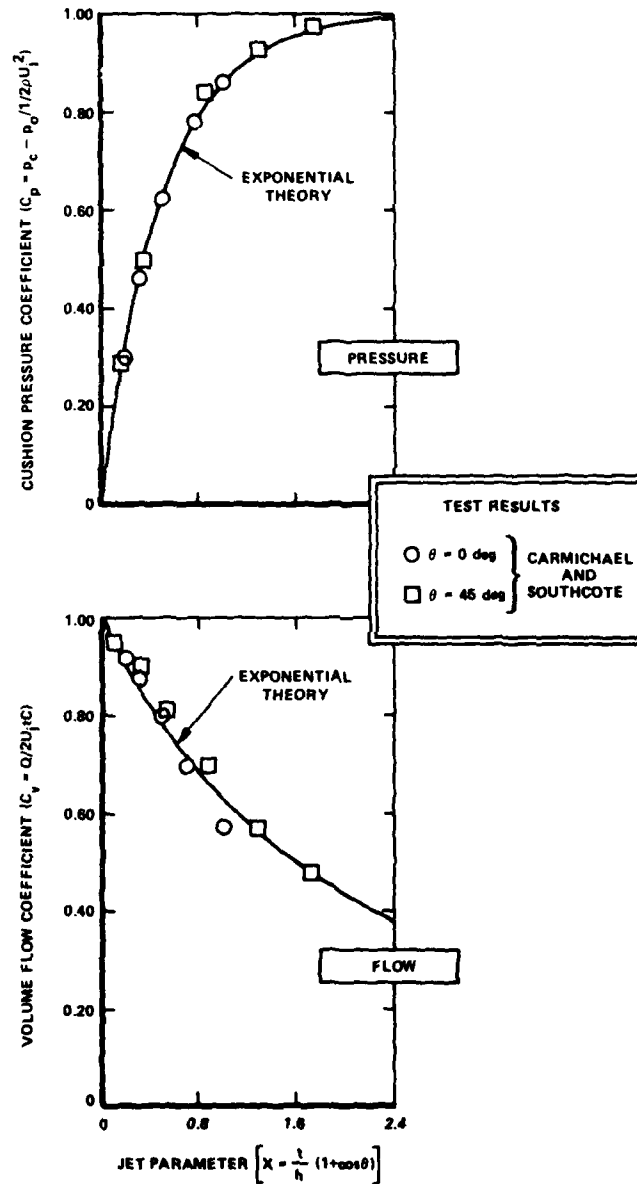


Figure 39 - Pressure and Flow for Peripheral Jet

The agreement of the exponential theory with test results, while not completely rigorous in its boundary conditions or treatment of viscous effects, led to its wide use in performance calculations for air cushion craft.

For the plenum type of air cushion craft, the results are much simpler. Figure 40 shows the basic geometry of a plenum air cushion craft.

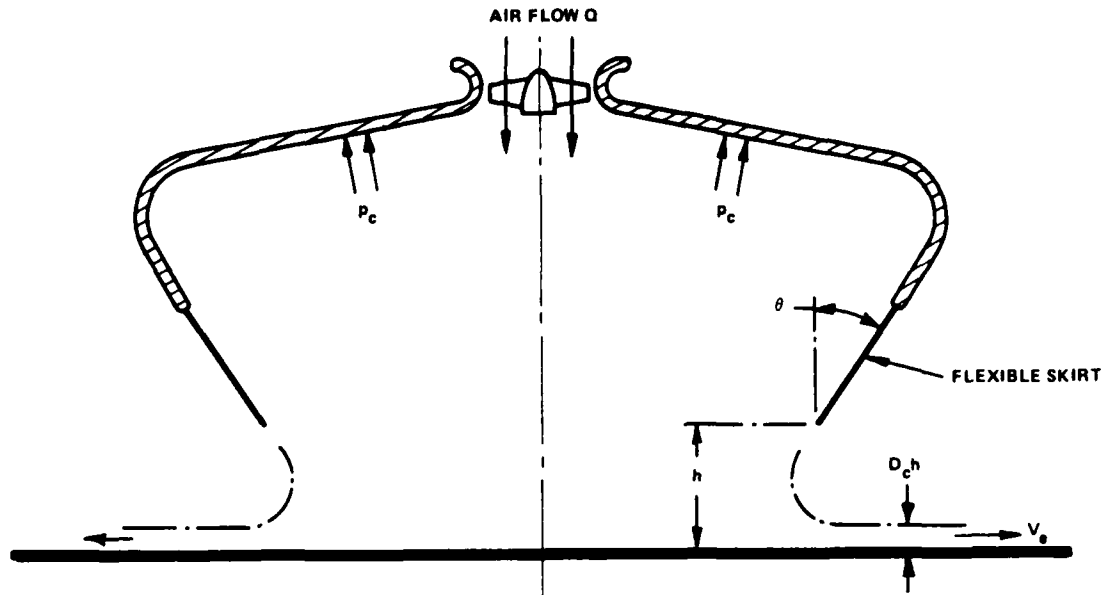


Figure 40 - Geometry of Plenum Craft

For the plenum craft, the pressure is simply

$$p_c = \frac{W}{S} \quad (39)$$

Note: It is assumed here and throughout, that the cushion pressure quoted is gage pressure. The flow for the plenum craft is given by,

$$Q = \sqrt{\frac{2p_c}{\rho}} \cdot Ch \cdot D_c \quad (40)$$

where D_c is the coefficient of discharge of the exiting flow beneath the skirt.

It is sometimes useful to determine the flow per unit cushion area for air cushion craft, and simple relationships exist for both peripheral jet and plenum craft. If, in a similar vein to the normalization of the power coefficients (see Equation (27)), the flow per unit area is normalized by the basic parameters W/S and Ch/S , then it can be shown that

$$\text{Peripheral jet: } \frac{Q/S}{\frac{Ch}{S} \left(\frac{W}{S}\right)^{1/2}} = \left(\frac{2}{\rho}\right)^{1/2} \frac{G(x)}{1 + \cos \theta} \quad (41)$$

$$\text{Plenum: } \frac{Q/S}{\frac{Ch}{S} \left(\frac{W}{S}\right)^{1/2}} = \left(\frac{2}{\rho}\right)^{1/2} D_c \quad (42)$$

where the peripheral jet function, $G(x) = (1-e^{-x})(1-e^{-2x})^{-1/2}$

The flow has been expressed in various coefficient forms in the literature and the different forms should be recognized. From dimensional analysis, a flow coefficient based on craft velocity was determined, viz:

$C_{Q_1} = \frac{Q}{VS}$. The above formulation reflects a flow coefficient based on jet velocity ensuing from the bottom of the skirt, viz $C_{Q_2} = \frac{Q}{V_j S}$. The relationship between these two forms is clearly through the jet velocity ratio V_j/V . Equation (42) can then be written,

$$C_{Q_2} = \frac{Q}{S \left(\frac{2}{\rho}\right)^{1/2} p_c^{1/2}} = D_c \cdot \frac{Ch}{S} \quad (43)$$

In this form, it is seen that the flow coefficient C_Q is then directly proportional to the equivalent air gap with the constant of proportionality being the discharge coefficient. From Reference 43 typical values of C_{Q_2} are

0.015 - 0.03 for amphibious craft

0.005 - 0.01 for sidehull craft

Figure 41 compares the normalized flow from Equations (41) and (42) for both plenum and peripheral jet craft. This figure shows that the plenum craft is basically less efficient, in that it takes more air flow to support a craft for a given air gap and weight. Despite this greater flow requirement, the majority of today's operational craft operate on the plenum principle because of its relative simplicity and its more practical application to operation in rough water, as may be seen from the chapter on skirts (Chapter VI).

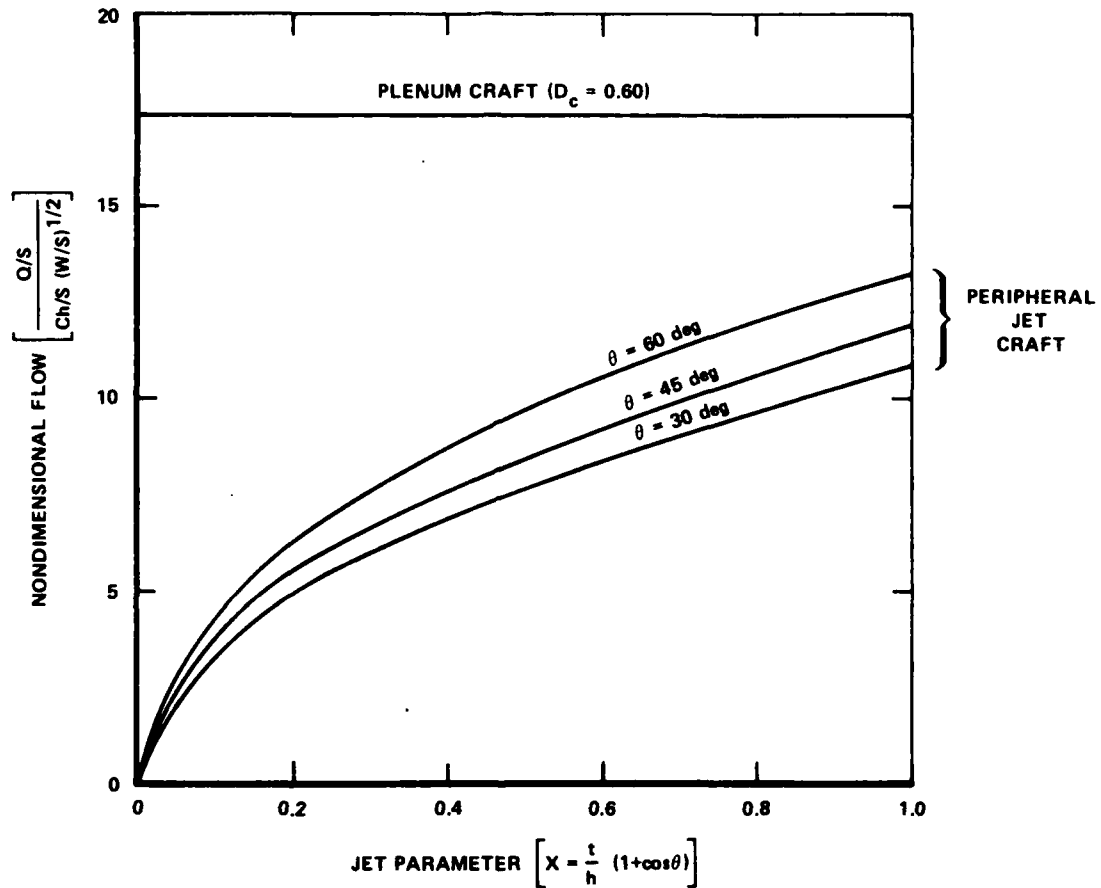


Figure 41 - Nondimensional Flow for Plenum and Peripheral Jet

When working from such basic parameters as those described above, it becomes possible to develop expressions for the various power components of air cushion craft. In a report such as this, space does not permit room for a rigorous development of each of the theories, and emphasis will be placed on presenting both new developments and the results of various researchers, designers, and operators in a common light.

Each of the power components will now be given in turn, concentrating on the basic peripheral jet and plenum forms of craft but including those data that can be released on the SES form of craft.

These power and drag components may be listed as follows:

- Lift power (in hover and in forward motion)
- Wave pumping power
- Momentum drag
- Cushion wave drag
- Seal or skirt drag (over water and ice)
- Sidehull drag
- Aerodynamic drag

Depending on the form of craft and the nature of the operating conditions, not all of these components are additive, as will be discussed. The following sections develop the various theories and empirical laws based on experimental data for both power and drag components. Where applicable, current research and development into different craft types as a result of the data is identified.

Lift Power Requirements. The amount of lift power required by an air cushion craft is still, surprisingly enough, not a completely resolved entity. In the early craft it was thought that power sufficient to lift the craft some prescribed height was the amount of lift power to install in the craft. Later, it was realized that the actual height chosen was closely interrelated with the amount of lift fan flow, and the manner in which the flow is supplied to the cushion strongly affects the ride quality of the craft in rough water. The net result of these various effects is that the designer must frequently make a compromise to satisfy the requirements over the operating envelope (sea state and speed) of the craft.

There are certain basic requirements, however, and these can be stated simply for the plenum and peripheral jet forms.

A lift power coefficient (C_{P_L}) is defined in agreement with the previous dimensional analysis discussion, where η_L is the total lift system efficiency and P_L is the installed power required for lift.

$$C_{P_L} = \left(\frac{\rho}{2}\right)^{1/2} \cdot \frac{550 \eta_L \frac{P_L}{W}}{\frac{Ch}{S} \left(\frac{W}{S}\right)^{1/2}} \quad (44)$$

The actual calculation of lift power for the air cushion craft (restricting attention to the aerostatic forms) is done for both calm water and in rough water to accommodate wave pumping needs and then sizing the lift system by the larger of the two needs.

Calm Water Lift Power. The lift system efficiency η_L is discussed more fully in Chapter VIII but here is defined as the ratio of the air horsepower to the installed lift engine power.* For the case of the peripheral jet, the lift power is given by

$$550 \eta_L P_L = Q (H_j - \epsilon \eta_D q) \quad (45)$$

where the intake recovery factor (ϵ) and the diffuser efficiency (η_D) are usually known parameters from the specific design in work. The free stream dynamic head is $q = 1/2 \rho V^2$. In terms of the nondimensional power coefficient, Mantle²⁷ showed (for calm water operation) that

$$C_{P_L} = (1 - C_{L_u} k)^{3/2} \frac{F(x)}{1 + \cos \theta} \left[1 - \epsilon \eta_D \frac{k (1 - e^{-2x})}{1 - C_{L_u} k} \right] \quad (46)$$

This expression has assumed some alleviation in lift power due to upper surface lift generation, that is,

$$p_c = \frac{W}{S} \sim C_{L_u} \frac{1}{2} \rho V^2 \quad (47)$$

or

$$p_c = \frac{W}{S} [1 - C_{L_u} k] \quad (48)$$

*This definition applies equally to integrated lift and propulsion designs despite the difficulty during test of determining such powers.

For today's air cushion craft, typical values of this lift coefficient are 0.30 to 0.40. In the expression for the lift power coefficient, the main effect of the nozzle geometry reduces to

$$F(x) = \frac{1 - e^{-x}}{(1 - e^{-2x})^{3/2}} \quad (49)$$

At zero forward speed ($k=0$), the lift power coefficient (C_{P_L}) for the peripheral jet reduces to the hover power coefficient

$$C_{P_{L_0}} = \frac{F(x)}{1 + \cos \theta} \quad (50)$$

For the plenum form of air cushion craft, the lift power is simply

$$550 \eta_L P_L = p_c Q \quad (51)$$

and the lift power coefficient becomes, again for calm water,

$$C_{P_L} = (1 - C_{L_u} k)^{3/2} D_c \quad (52)$$

Where referring to Figure 39, the discharge coefficient due to the vena contracta of the issuing flow is D_c . Elsley and Devereux³⁸ show, from hovercraft model experiments, how this discharge coefficient varies with skirt angle θ . Typical values for D_c are 0.50 to 0.60.

At zero forward speed ($k=0$), the lift power coefficient for the plenum craft reduces to the hover power coefficient

$$C_{P_{L_0}} = D_c \quad (53)$$

Figure 42 compares the hover power in coefficient form for the peripheral jet and plenum forms of air cushion craft. It can be seen from this plot why the emphasis was placed on peripheral jet craft in the initial development period (1960-65). Today's craft more closely approximate plenum craft, although there is still a tortuous path in getting the air from the fans to the cushion, and it is not simply a matter of straight conversion of fan dynamic head to static energy in the cushion. Some of the air is dumped into the cushion directly and some through the skirt system. Nevertheless, the tortuous path only increases the losses and reduces overall system efficiency while the power requirements in the cushion remain as given above. A discussion of the lift system efficiency is given in Chapter VIII on fans.

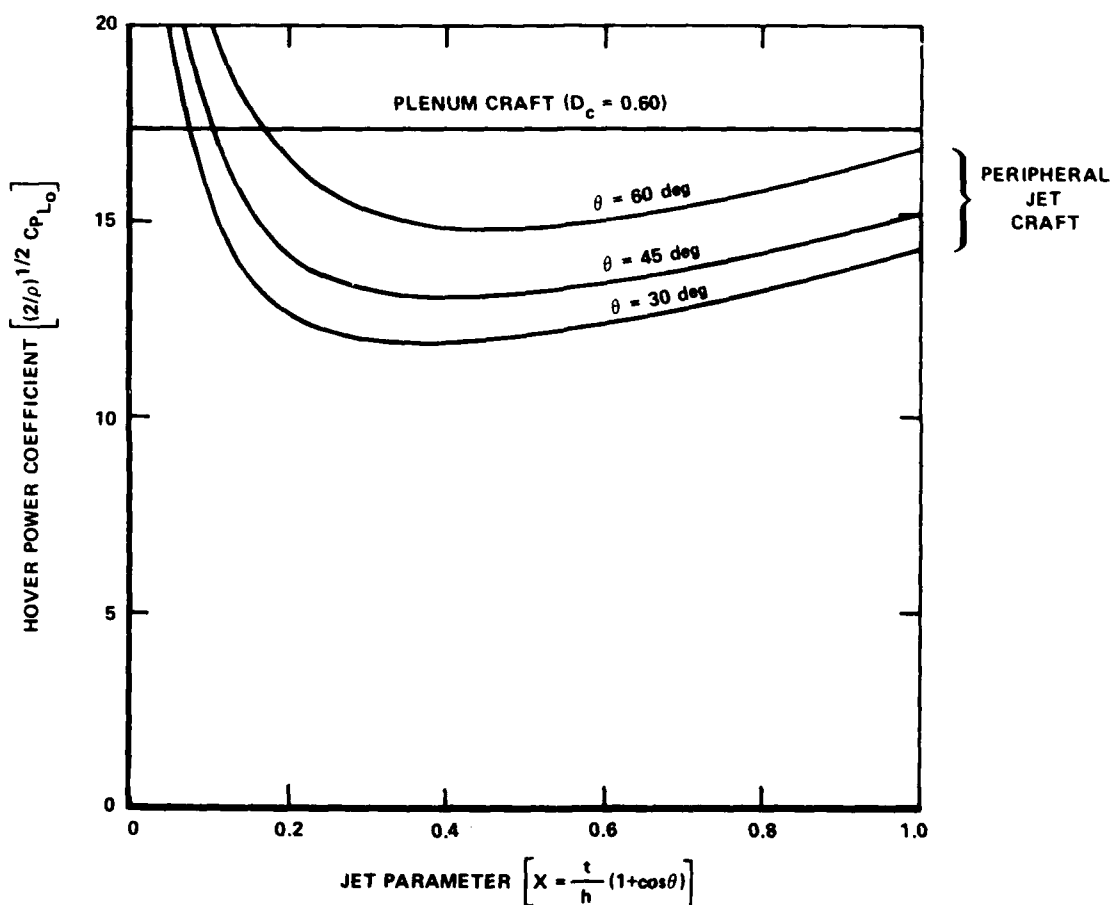


Figure 42 - Plenum and Peripheral Jet Hover Power

Wave Pumping Requirements in Rough Water. In rough water operation, the problem of power estimation becomes much more complex. The lift fan system power must now be sufficient to provide the desired air gap; it must provide sufficient air flow for the desired ride quality; and it must provide sufficient air flow to instantaneously replenish the cushion swept away by wave action. This latter requirement is significant in that if, after the waves have "pumped" out the cushion, there is insufficient lift power to replenish the cushion, the craft will rapidly lose altitude and pitch into the waves. Wave pumping then, is, a general problem associated with the replenishment of the cushion air during rough water operation over the complete operational range of speed and sea states for the particular craft in question. The particularly troublesome case where the craft responds to the waves at encounter frequency is included in this general condition of wave pumping.

The complexities of the craft dynamics and the irregular or random nature of sea wave motion have made the prediction of such phenomena difficult. Also, the power to provide a desired air gap, adequate ride quality, and wave pumping are not additive but interrelated in a manner that depends on the craft conditions, seal or skirt compliance, and operator technique.

It is usual practice to calculate the power requirements in each case and then select a power based on experience. Trillo⁴⁴ suggests the use of an effective flow coefficient that, in effect, compares the flow required for calm water operation (see previous section) to that required for wave pumping. The larger of the two is then used for design.

Beardsley⁴⁵ prepared an analysis specifically for the SES type of air cushion craft but the result provides a measure of the wave pumping power for any air cushion craft. Although the analysis contains several simplifying assumptions, such as incompressible flow, sinusoidal wave form, and no side leakage, it has been applied successfully in several operational craft to date.

Beardsley considers two extreme cases: the case of maximum wave pumping flow requirement for zero deck motion and the case of constant cushion volume (zero wave pumping). In both cases, it is assumed that there is no hard bottom contact by the waves, which is a reasonably realistic operational condition by today's commercial hovercraft in England.

For the case of maximum wave pumping (and zero vertical acceleration)

$$Q = B h_w V \sin \frac{\pi L}{\lambda} \quad (54)$$

where h_w is the wave height trough to crest and λ is the wavelength of the oncoming sea.

For the case of zero wave pumping (and maximum vertical acceleration)

$$\frac{d^2 z}{dt^2} = -\frac{v^2}{10} \cdot \frac{v^2}{L} \quad (55)$$

The practical amount of lift flow is somewhere between the extreme case of maximum flow, to remove all vertical acceleration, and zero flow (other than the calm water hover power), to result in maximum acceleration levels.

Considering the case of maximum wave pumping, the instantaneous power requirement would be

$$550 \eta_L \frac{P_{wp}}{W} = \pi \frac{h_w}{\lambda} \cdot v \cdot \frac{\sin \frac{\pi L}{\lambda}}{\frac{\pi L}{\lambda}} \quad (56)$$

where P_{wp} is the wave pumping power.

In terms of the nondimensional power coefficient, this becomes

$$C_{P_{wp}} = \pi \frac{h_w/\lambda}{Ch/S} \cdot F(L/\lambda) \cdot k^{1/2} \quad (57)$$

where the relationship of craft size to wavelength is given by

$$F(L/\lambda) = \left| \frac{\sin \pi L/\lambda}{\pi L/\lambda} \right| \quad (58)$$

The sign of $F(L/\lambda)$ has been removed, since whether the flow is into or out of the cushion is of no consequence because the numerical value of the power is the same.

The designer must now make the comparison between the calm water power and the wave pumping power, i.e., answer the question:

$$\text{Is } C_{P_{wp}} \lesseqgtr C_{P_{L_0}} ? \quad (59)$$

or in terms of the simple plenum, is

$$\pi \frac{h_w/\lambda}{Ch/S} \cdot F(L/\lambda) k^{1/2} \leq D_c \quad ? \quad (60)$$

This inequality illustrates the fact that the greater power (flow) requirement depends on sea state, craft size, speed, and air gap.

Beardsley⁴⁵ computes the wave pumping power for the SR.N5 by Equation (56) to be 235 hp for the 15,000-lb craft operating at 70 mph in 2.5-ft waves. It was assumed that the worst wave pumping condition would occur in such waves when $L/\lambda = 1/2$ and $L = 28$ ft. For the same SR.N5 craft operating with a 4-in. air gap ($h/L = 0.019$) and a 50-percent lift system efficiency, Equation (52) predicts a lift power of 280 hp.

For the SR.N5, it is seen* that sufficient lift fan power is available to compensate for any wave pumping that might be experienced within its operating envelope and that the air gap method of computing lift power was adequate in this case. For larger craft operating at lower values of h/L or Ch/S and in higher states of sea this is not the case, however, and wave pumping power dominates.

While it is recognized that the power for wave pumping, as computed by Equation (57), is a maximum value in a sinusoidal sea, it is a useful design tool if the limitations are recognized. Accordingly, Figure 43 has been prepared to aid such performance estimation. Lines of constant air gap power can be added from Equation (53) to indicate which particular combination of craft parameters yields the greater power for any given design.

It is seen that there are many considerations and various geometric and operational features that influence the final choice of lift power. While the rudiments of the many considerations have been provided in what has gone before, it is informative to see how the lift power varies with craft size as used in actual craft as well as in design studies. Figure 44 shows this data covering a wide range of vehicles sizes, speeds, and configurations. The craft in Figure 44 cover a size range from less than 10-ton displacement to greater than 200-ton displacement for actual operational craft and to greater than 10,000-ton displacement for design studies. Two main trends are seen: that trend associated with the low speed group (0-30 mph) and that trend associated with the intermediate speed group (30-100 mph) where the groups are as discussed in Chapter I (see Figure 11).

*The SR.N5 is an integrated lift and propulsion design with a 1000-hp GE LM-100 engine and approximately one-third of total power is devoted to lift.

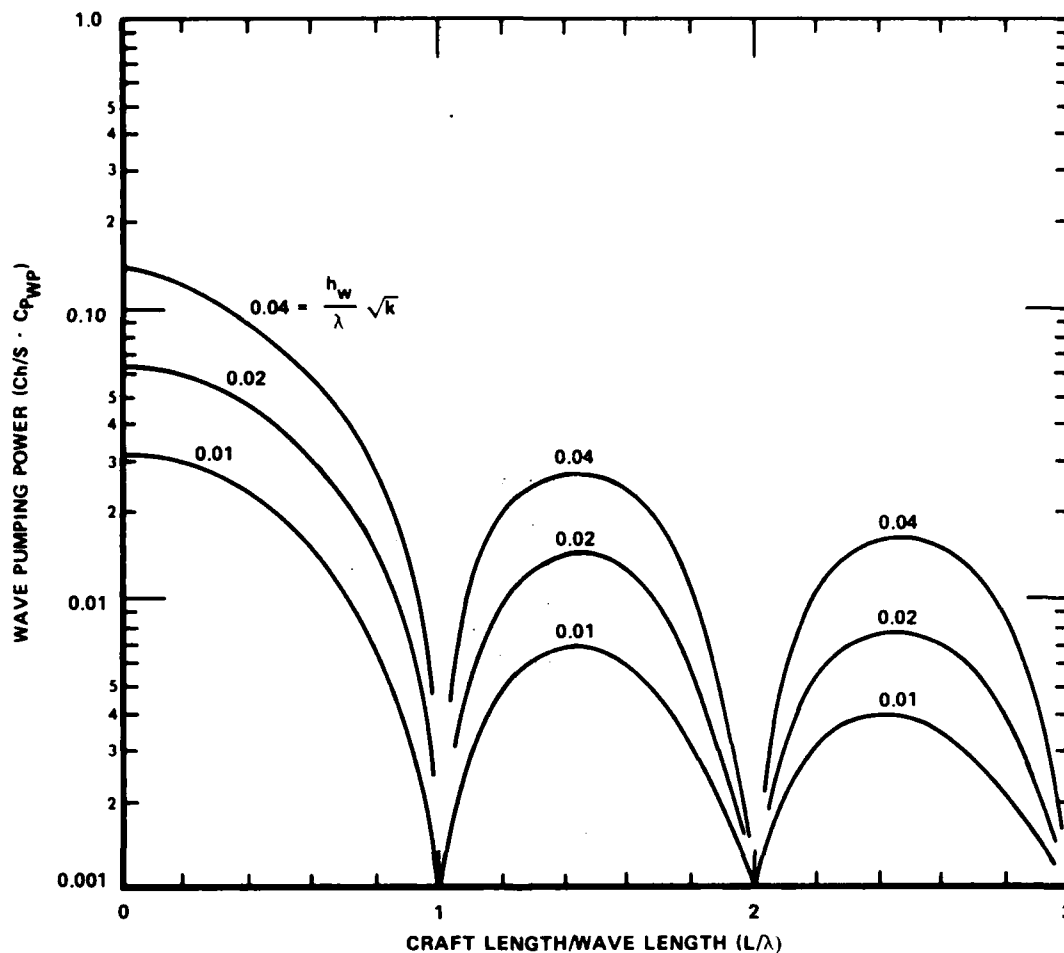


Figure 43 - Wave Pumping Power

Even though there are a multitude of variables it is seen that within the groups there is a surprisingly consistent trend where for the low speed group the lift power can be represented by

$$P_{\text{LIFT}} = K_s W^{2/3} \quad (61)$$

where the constant of proportionality is given by $K_s = 31 \text{ hp/ton}^{2/3}$.

For the intermediate speed group, which covers the majority of the data and carries the major emphasis in this book, the lift power can be represented by

$$P_{\text{LIFT}} = K_6 W^{7/8} \quad (62)$$

where the constant of proportionality is given by $K_6 = 45 \text{ hp/ton}^{7/8}$.

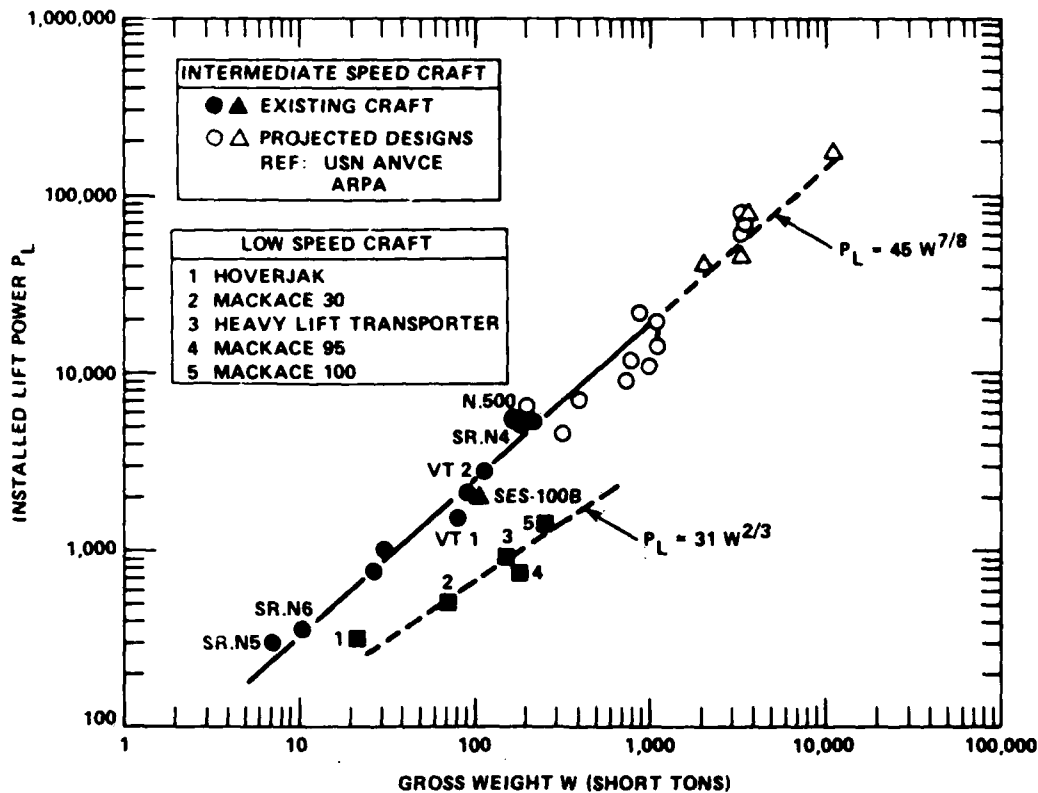


Figure 44 - Air Cushion Craft Lift Power

Since, for the intermediate speed group the total power, given by Equation (20) was also seen to vary with craft size by a similar functional form ($P_{TOTAL} \sim W^{7/8}$) then it is seen that a consistent relationship between lift and total power has existed over the range of air cushion craft considered. Specifically, from Equation (62) and Equation (20) it is seen that the lift power is approximately 27 percent of the total power which may be compared to the approximately 'one-third total power' statements given earlier for such craft as the SR.N5.

Momentum Drag

The momentum drag or ram drag is that force due to the rate of change of momentum of accelerating the cushion air and engine air to craft velocity. For all practical purposes and in good craft design, the engine air is (after passing through the engine) exhausted rearward with a relative velocity at least equal to the craft velocity and virtually no net drag results. In that case, the momentum drag is directly associated with the cushion air and one can write

$$D_{MOM} = \rho Q V \quad (63)$$

For the case of the peripheral jet craft, Mantle²⁸ showed that, in power coefficient form, this power loss can be written

$$C_{P_M} = \frac{2 G(x)}{1 + \cos \theta} \cdot k (1 - C_{L_u} k)^{1/2} \quad (64)$$

For the plenum craft, the momentum or ram power coefficient can be written

$$C_{P_M} = 2 D_c k (1 - C_{L_u} k)^{1/2} \quad (65)$$

These power components are given in Figure 45 for the optimum peripheral jet ($x = 0.40$) at $\theta = 45$ deg and for the typical plenum $D_c = 0.60$.

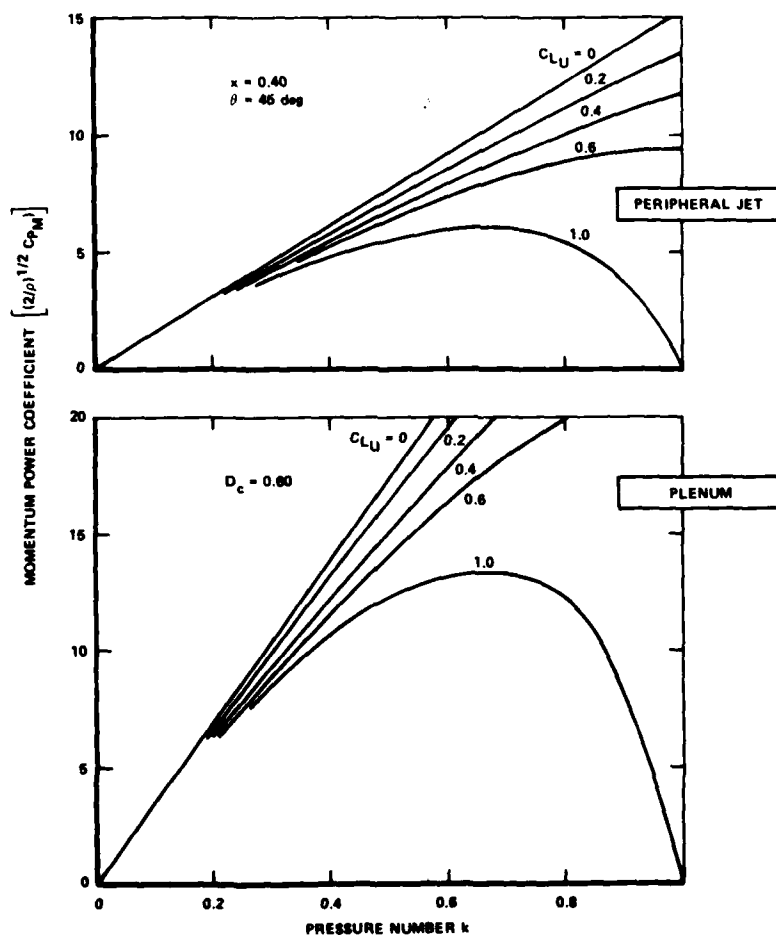


Figure 45 - Momentum Drag Power (Peripheral Jet and Plenum)

It has been found in some air cushion craft that not all of this momentum is lost. If, for example, more air escapes in the direction of the relative wind than escapes forward, then the effective momentum drag is less than that given by Equation (63). In those cases where it occurs, it is said that a cushion thrust is being experienced. Practical applications of this are the SR.N5 and SR.N6 cushion craft where cushion air is exhausted to the rear to provide slipstream for the rudders at low speed, thereby improving rudder control.

Attempts to utilize cushion thrust as an aid to propulsion have not had too much success. If the rear skirt is raised to generate cushion thrust, the craft pitches slightly nose down and the increased bow skirt drag normally nullifies the cushion thrust. It can be done, however, and a particular example of interest is the SES-100B that underwent hover tests in July 1971 when it was tethered to a center buoy in Michoud Slip, New Orleans, Louisiana. By raising the stern seal, the craft moved steadily in a circle at 4 knots, and by raising the bow seal, it moved rearward at 2 knots.

Other means of ejecting cushion air for thrust or control are the "puff-ports" pioneered by British Hovercraft Corporation⁴⁶ and the lift fan propulsion introduced by Britten-Norman in their CC-4 hovercraft. Further discussion of momentum thrust is deferred to Chapter IX.

Cushion Wave Drag. The wave drag of the pressurized air cushion as it moves through the water has received various theoretical treatments since the first analyses of Sir Havelock⁴⁷ and Sir Horace Lamb.⁴⁸ Sir Havelock gave the solution for a point source pressure distribution while Lamb developed an approximate two-dimensional theory for the wave drag of a moving depression generated by a pressure (p_c) and a length (L). Working from Lamb's approximate theory, Crewe and Eggington⁴⁹ developed the result specifically for use on hovercraft as

$$\frac{D_w}{W} = \frac{2 p_c}{\rho_w g L} \left[1 - \cos \frac{1}{F^2} \right] \quad (66)$$

where D_w is the wave drag of the cushion traveling at a Froude number of

$$F = \frac{V}{\sqrt{gL}}$$

In terms of some of the basic parameters discussed earlier, this can be written

$$\frac{D_w}{(\rho_c/L)^2 L^3} = \frac{2}{\rho_w g} \frac{L/B}{\left[1 - \cos \frac{1}{F^2}\right]} \quad (67)$$

Crewe and Eggington,⁴⁹ in connection with the basic analyses associated with the SR.N1, conducted model tests at two L/B ratios as part of the initial design work on the SR.N1 and compared the results with Equation (66). Figure 46 shows this comparison.

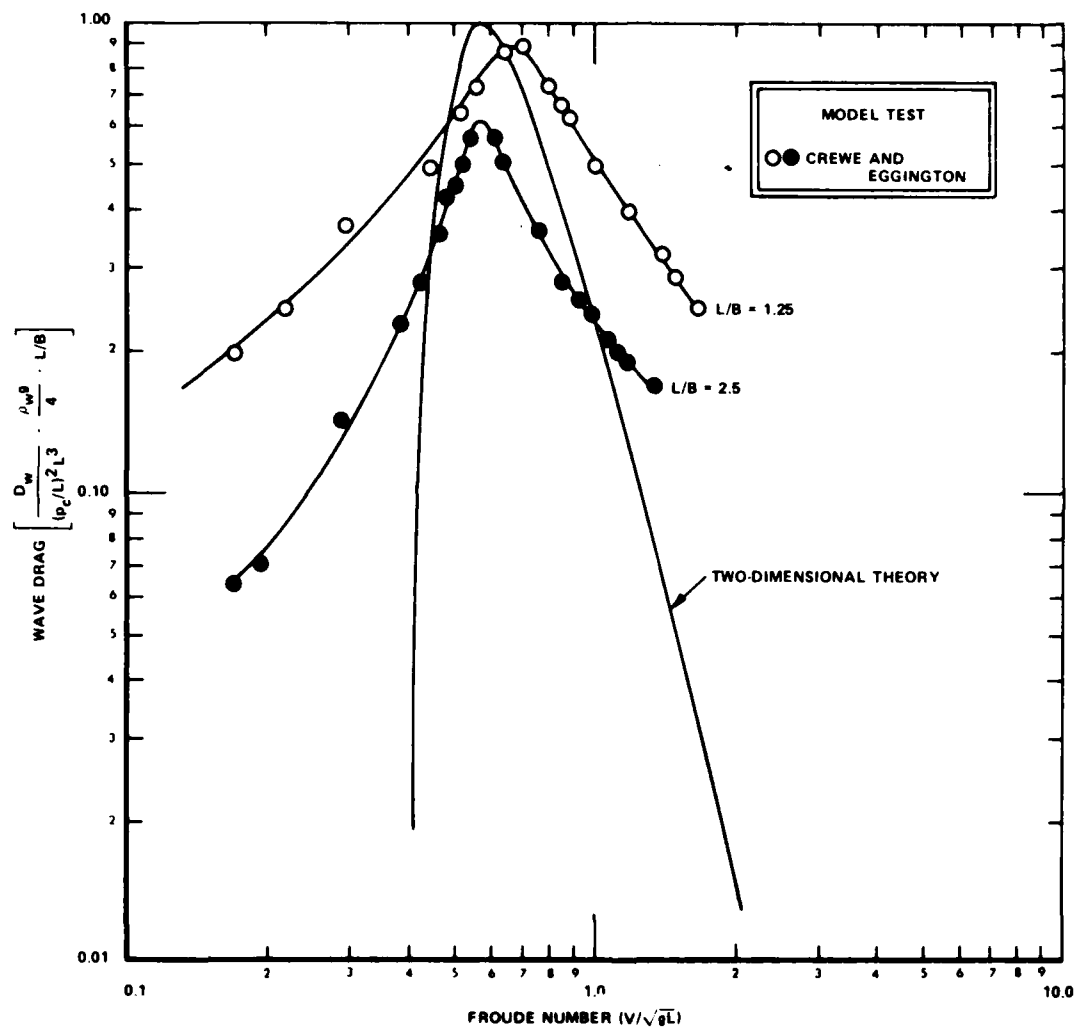


Figure 46 - Early Wave Drag Results

While the shape of the drag curve around hump is not in complete agreement with the two-dimensional theory, the model data maximum hump drag value does agree with the theoretical maximum value

$$\left[\frac{D_w}{(p_c/L)^2 L^3} \right]_{\max} = \frac{4}{\rho_w g L/B} \quad (68)$$

that occurs at a speed given by the Froude number

$$(F. No.)_{D_w \max} = \frac{1}{\sqrt{\pi}} \quad (69)$$

More complete treatments for the wave drag of air cushion craft then followed by Newman and Poole⁵⁰ in 1962, Barratt⁵¹ in 1965, and Doctors⁵² in 1970. These more complete treatments include three-dimensional effects such as the effect of cushion planform, water depth, and edge effects. The two-dimensional model results by Crewe and Eggington apply only to deep water.

Everest and Hogben⁵³ conducted extensive model tests in both deep and shallow water and compared the results with the theoretical predictions (References 50 and 51). Figure 47 is a comparison of the Everest and Hogben experiments with the Barratt theory for both shallow and deep water. A similar comparison would be seen if compared to the Newman and Poole theory. Fairly good agreement is seen in deep water, especially in the region of primary hump. Progressively poorer agreement occurs in the secondary and tertiary humps. Indeed, the character and even existence of these secondary and tertiary humps resulted in much discussion among researchers. The edge factor or shape of the cushion pressure distribution at the edge of the depression is known to have a strong effect on these secondary humps. Figure 48 taken from Reference 54 illustrates this by comparing the Newman and Poole theory (for sharp edged pressure distributions) with the Doctors theory (for pressure distributions with pressure falloff at the edges).

Doctors' predictions⁵² shown on the lower set of curves of Figure 48 have pressure falloff or edge effect parameters affecting the pressure region on the four sides. By varying these parameters (α , β), the shape of the wave drag curve with Froude number varies and most predominantly so in the subhump region or in that region where the secondary and tertiary humps occur. Wilson⁵⁴ reports that choosing the edge effect parameters $\alpha = 5$ and $\beta = \infty$ gives the best match with SES model test data and the curves

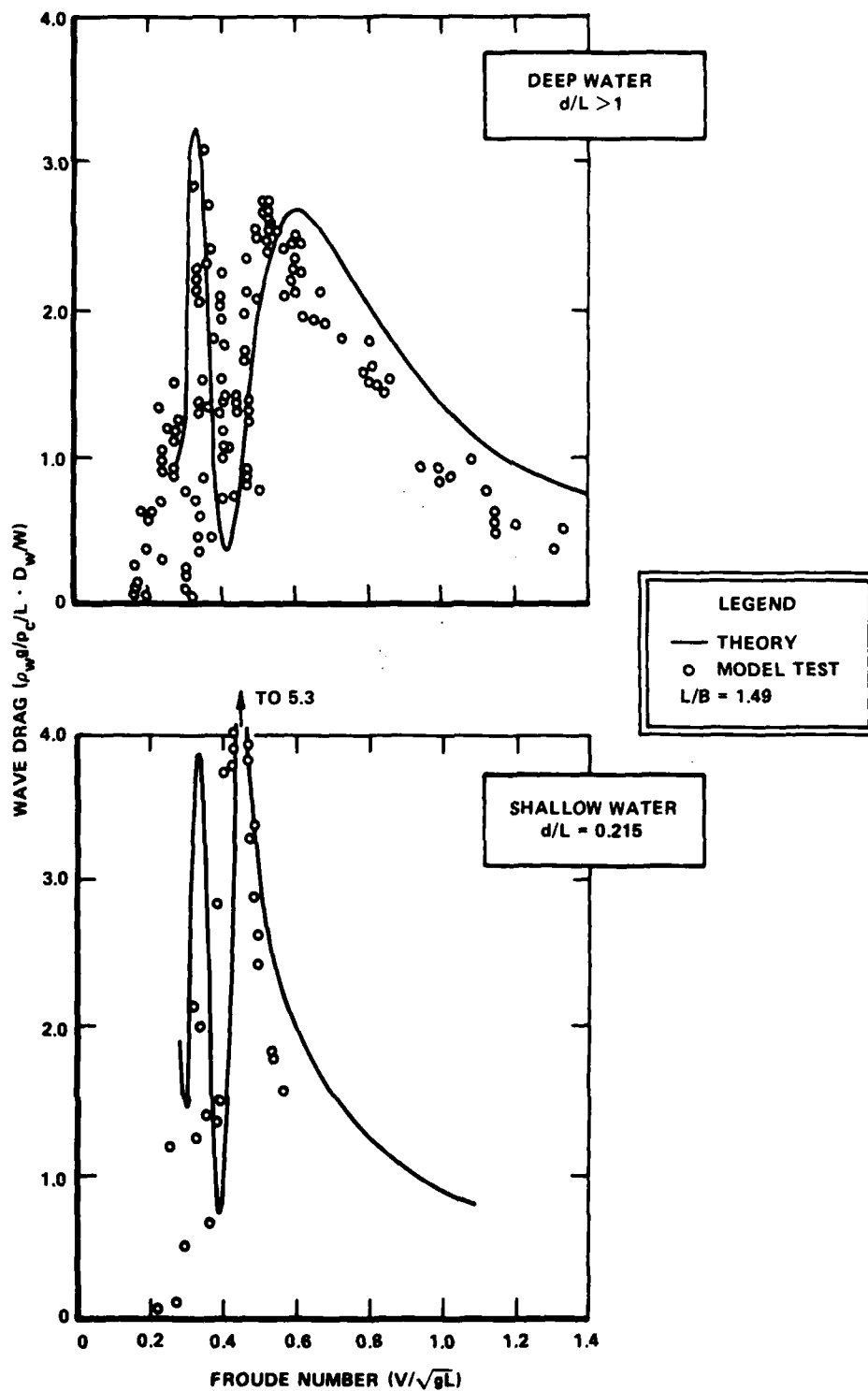


Figure 47 - Deep and Shallow Water Wave Drag

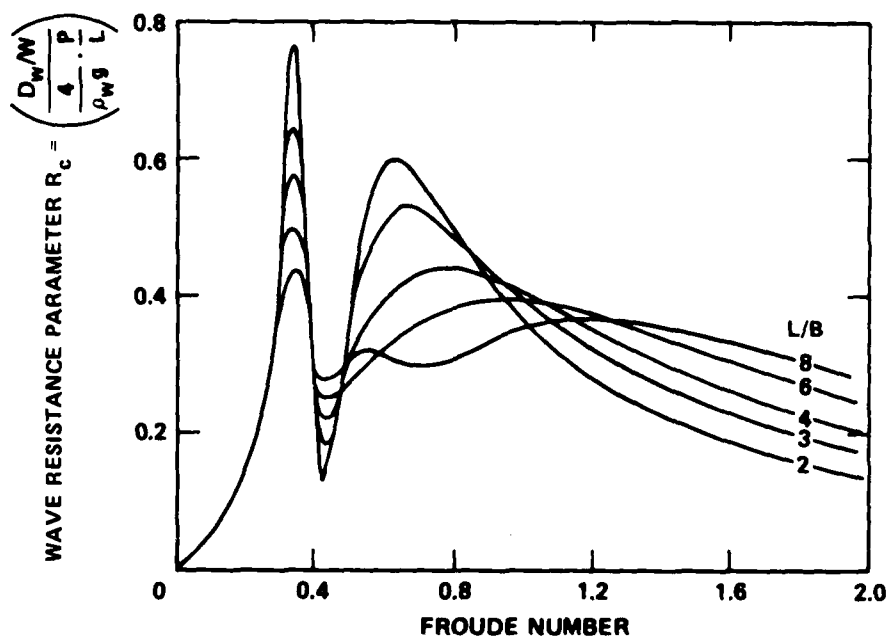


Figure 48a - Newman and Poole Theory (Unshaped)

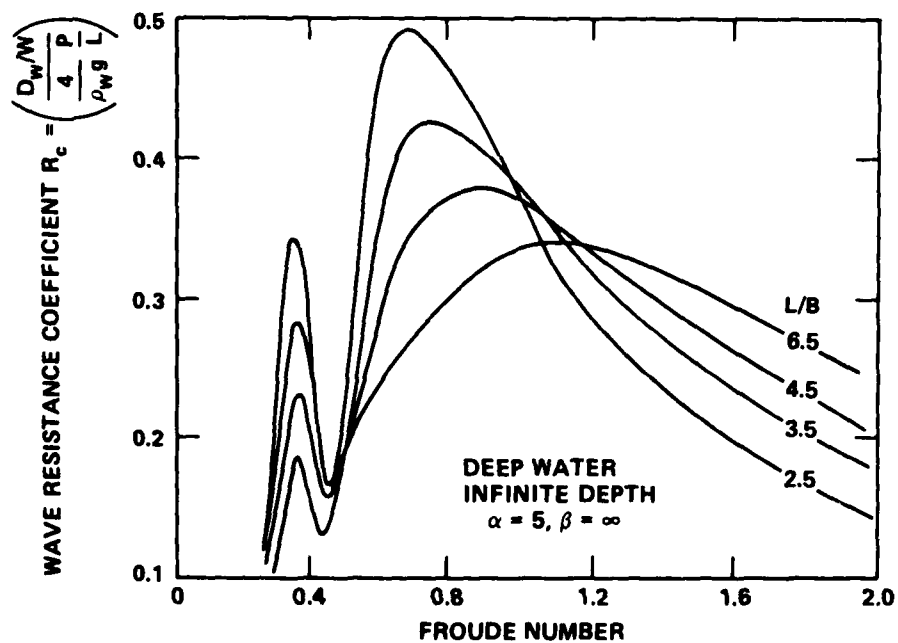


Figure 48b - Doctors Theory (Shaped)

Figure 48 - Wave Drag for Unshaped and Shaped Pressure Distributions

shown in Figure 48 are for these particular values of edge parameter. The marked change in the secondary hump is evident from Figure 48 by comparing the upper set of curves (unshaped pressure distribution) with the lower set of curves (shaped pressure distribution).

Shallow water wave drag does not show such good agreement in the magnitude of the hump drags both at primary and secondary hump speeds.

Everest and Hogben⁵³ suggest that the application of the linearized wave theory to low speeds and shallow water becomes progressively more hazardous as cushion pressures are increased from the level of small disturbances toward realistic scale pressures and that this would tend to explain the absence of secondary humps in shallow water.

Very little evidence is available on full-scale air cushion craft to add to the model test results cited above. Some data were collected on the sidehull air cushion craft, the U.S. Navy SES-100B, in both deep and shallow water that provides some full-scale evidence on wave drag. Mantle³⁴ showed that, during trials in shallow water in 1972, the SES-100B did not experience the hump drag predicted. Figure 49 shows these results. In particular, the data for the shallow water case were taken in Lake Pontchartrain, Louisiana, where the water depth is approximately 15 ft, which would give a depth parameter of $d/L = 0.25$; approximately that given in Figure 47. While the results are not conclusive, the full-scale test results of the SES-100B agree with the model test results of Everest and Hogben, because the theoretical peaks predicted are not realized in practice.

It is often reasoned that, because the rate of change of wave drag with speed is greater for shallow water than for deep water, accelerated motion might reduce the hump drag. Everest and Hogben showed by model test that this could occur, provided there was no water contact. Such a result has been developed theoretically by Doctors⁵⁵ and, depending on craft parameters and water depth, drag reductions of 10 to 15 percent might be expected. The full-scale data for the SES-100B shown in Figure 49, however, cannot be explained by consideration of acceleration alone. It could be that the water depth was not the critical depth, or it could be that the wave reflections off the muddy bottom of Lake Pontchartrain were attenuated or it could be that the edge effects of the cushion pressure distribution were sufficient to attenuate the wave drag hump in a manner similar to that shown in Figure 48. Crewe* reports that any comparison between wave drag experiment and theory must take account of the limiting steepness at which waves break, and by precise experimentation using a one-twelfth scale SR.N4 model in a 6 ft deep tank did find verification of primary, secondary, and even tertiary hump drag. For practical purposes, the bulk of design work on air cushion craft will be for operation in deep water and most performance analyses are based on the computerized application of Newman and Poole or Barratt or Doctors theories invariably modified by the designer in the subhump region according to some experience that the researcher might have. Frequently, all that is required is an estimate of the maximum value

*Reported in a private communication.

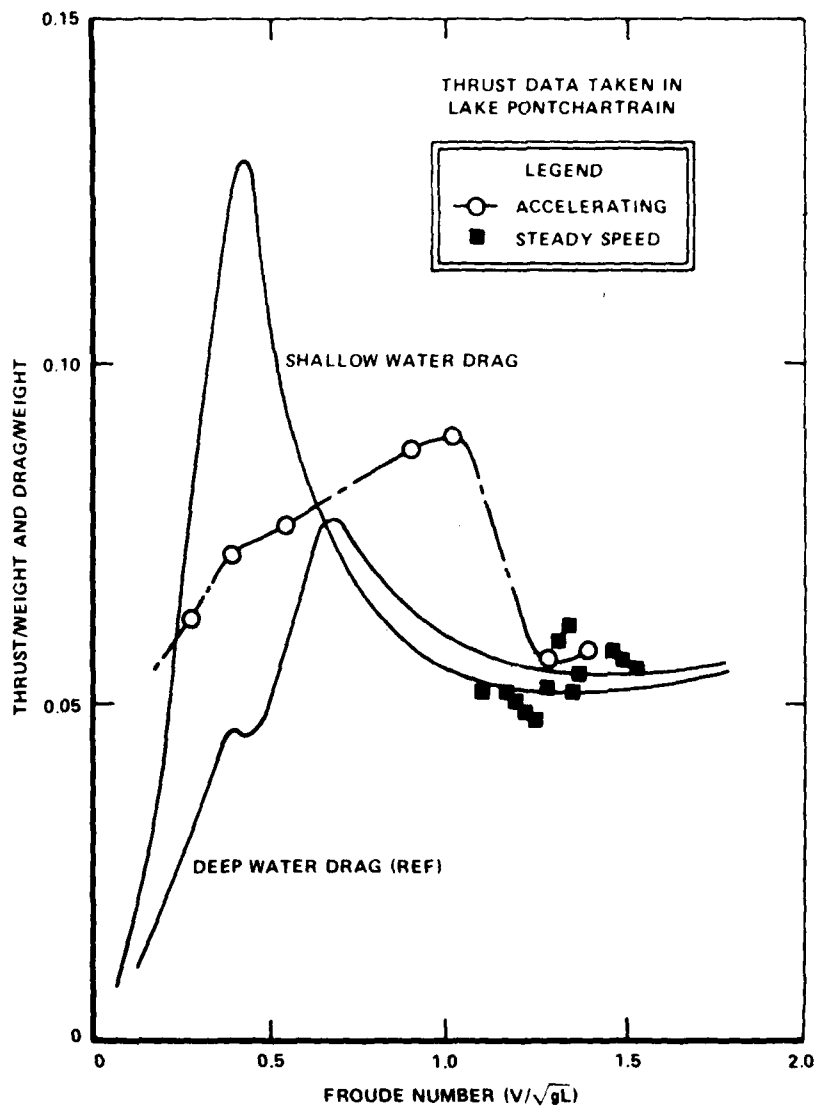


Figure 49 - SES-100B Shallow Water Performance

at primary hump since this sets (in most cases) the propulsive thrust level at low speed. If the craft is to accelerate to any speed past hump speed, clearly it must have a positive thrust margin over the drag at that speed. The actual value of thrust margin to be used in design is a question not satisfactorily resolved and to-date has been largely based on an experience factor. Because the value used can result in a craft that is either under

powered or over powered, this is an important consideration. A suggested treatment of the hump thrust margin which involves knowledge of both the propulsive thrust and the drag characteristics of the craft is provided in Appendix C.

Returning to the wave drag component at primary hump speed, Barratt⁵¹ showed this situation, which, when expressed in craft parameters, can be written

$$\frac{D_{WH}(L/B)^{1/2}}{(p_c/L)^2 L^3} = f(L/B; F_H) \quad (70)$$

where D_{WH} is the value of the wave drag at hump speed F_H , which itself is a function of the cushion L/B values. Figure 50 shows this hump drag value compared to the model test results of Crewe and Eggington and of Everest and Hogben.

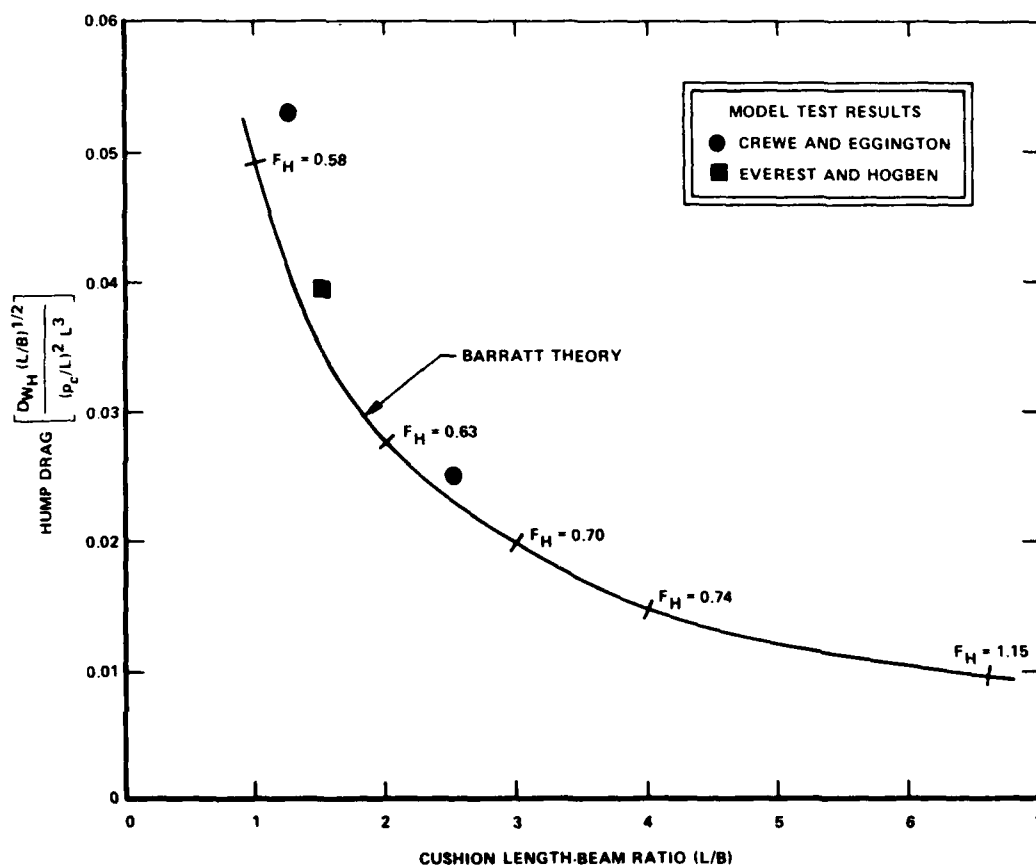


Figure 50 - Deep Water Hump Drag

In terms of the power coefficient defined earlier, the power to overcome hump drag in deep water can be written

$$\frac{Ch}{S} C_{P_{w_H}} = \sqrt{\frac{\rho g}{2}} \cdot C_{D_{w_H}} \cdot F_H \cdot (p_c/L)^{1/2} (L/B) \quad (71)$$

where the wave drag coefficient at hump $C_{D_{w_H}}$ is determined from the drag given by Equation (70), and is related to the parameter R_c in Figure 48.

Figure 50 shows two significant points besides the rough agreement of theory and data. The first is that the hump drag reduces significantly with cushion length-to-beam ratio and the second, that the speed at which the hump drag is a maximum also increases as length-to-beam ratio is increased. This has been verified experimentally by many researchers.

The large values of hump drag are particularly troublesome from both a power viewpoint and the incurred complexities in the design of a suitable propulsor (see Chapter IX). Hence, the prospect of eliminating (or at least suppressing to a large degree) the hump drag stimulated research in several quarters. Data such as that shown in Figure 50 indicate that substantial savings are possible by designing to a high L/B ratio. The U.S. Navy is conducting research into such configurations, and Figure 51 shows the model and test craft XR-5 used during such research. The XR-5, designed by A.G. Ford and his team at DTNSRDC has an L/B = 6.5 and is currently undergoing trials at the U.S. Navy Test Facility at Patuxent River. By designing to such high values of L/B, the hump drag essentially disappears (and moves to higher Froude numbers), and much lower propulsion power requirements appear possible. It should be pointed out, however, based on the theories of Barratt and Newman and Poole, that once over hump, the drag for high L/B is greater than for low L/B craft. Hence, the intent is to optimize such craft to operate subhump.

Since the first summary (Reference 2) was published, the XR-5 has continued on its trials and the U.S. Navy (Reference 30) has sponsored more model testing in this promising area. Figure 52, taken from Reference 56, illustrates the effect of designing a ship of high L/B to suppress the primary hump wave drag or at least move it to beyond the operating range of the ship. This selected example case of an 8000-ton displacement SES has a cushion density (based on area) of $p_c/S^{1/2} = 2$, which, from Figure 22 and Equation (25) might be called a low-to-medium density depending on the L/B ratio.

The design choices that come available can be seen from Figure 52. If the need is for very high speed (e.g., 80-100 knots) then clearly the air cushion craft whether it be of the amphibious or sidehull type should



Figure 51 - High L/B Craft XR-5

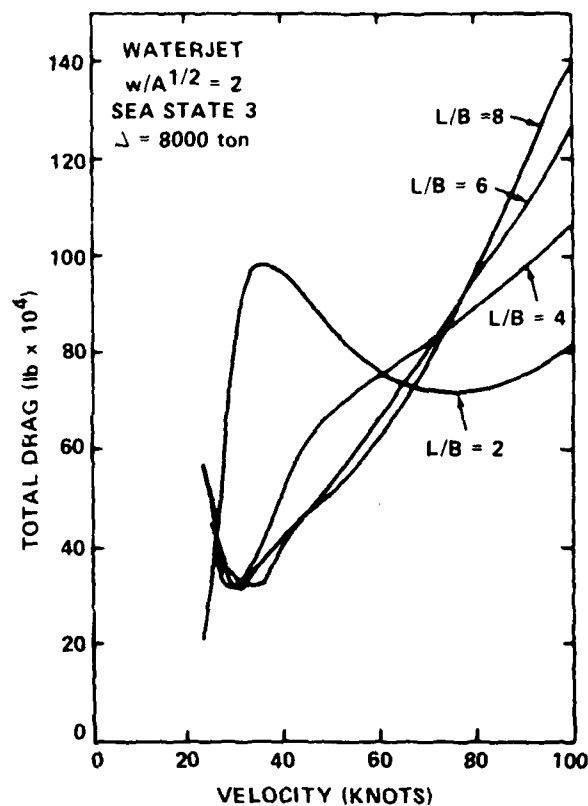


Figure 52 - Effect of L/B on SES Drag

be designed with low L/B. If speeds of 40-60 knots are sufficient then, from Figure 52, more slender ships with L/B values of 4 to 8 would consume less power. Using the theories discussed earlier for wave drag together with other drag components, encouraging agreement is found with the experimental results. Figure 53 shows such correlation⁵⁶ for various values of cushion density and length-to-beam ratio.

Seal or Skirt Drag. A terminology has grown with the practitioners of the art to where seals and skirts are used almost interchangeably. There is a slight bias in that skirts are usually referred to when discussing the cushion sealing mechanism of the amphibious form, and seals are referred to when discussing the nonamphibious form of air cushion craft. Frequently, the hardware design is, in concept, practically identical in each case. Seals are also exclusively used when referring to nonflexible sealing mechanisms such as hinged seals. Chapter VI discusses the basic types and, when drag is discussed in this report, it will be exclusively confined to the flexible or skirt type of seal.

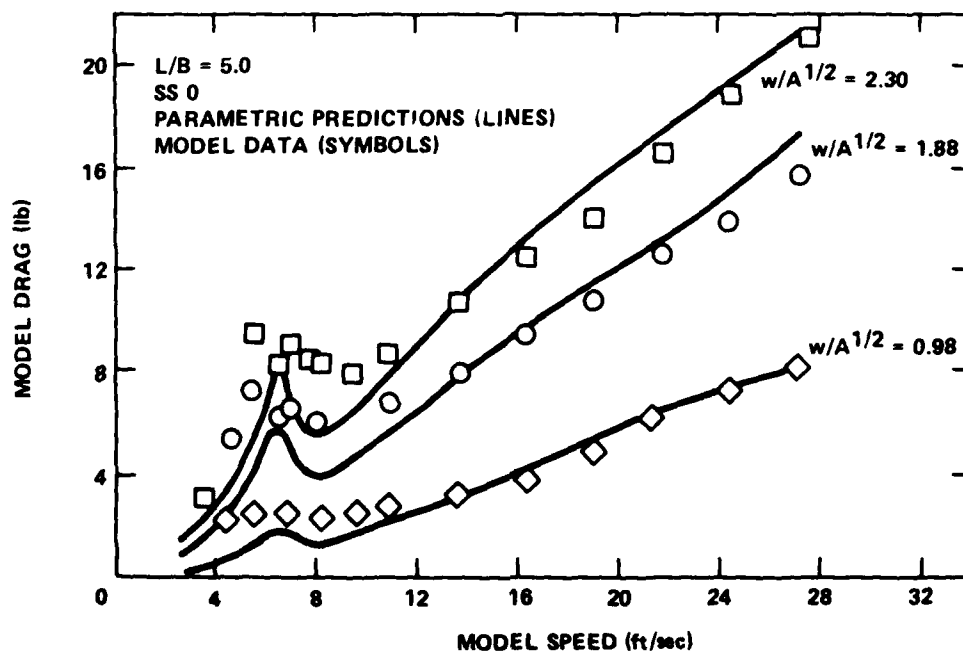
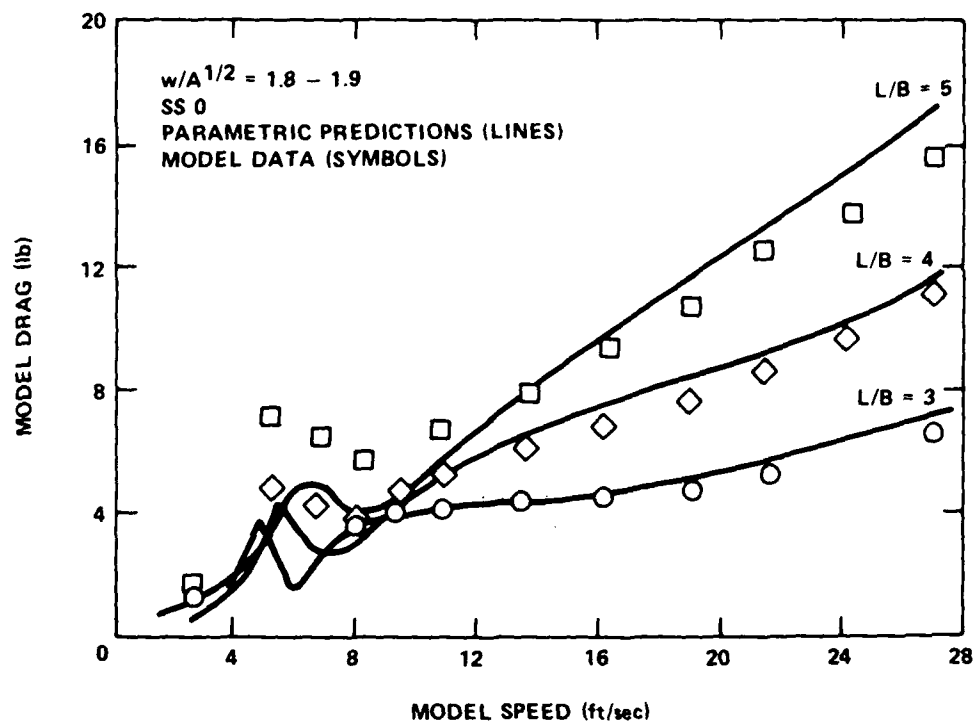


Figure 53 - Theory and Model Drag for High L/B SES

To date, there is no adequate completely theoretical treatment for the drag of skirts in both calm and rough water. Because practically all the rough water resistance of an air cushion craft is attributable to the skirts, it means that there is still no adequate theoretical method of predicting the rough water performance of air cushion craft. There are, however, some empirical methods for a restricted number of skirt designs, and these are used in all performance analyses. Considerable reliance is placed on model data for this drag component. The skirt drag is considered to be made up of two components, viz:

1. Calm Water Skirt Drag is incurred through skin friction, cushion pressure related wavemaking and spray drag.
2. Rough Water Skirt Drag is incurred through wave contact from the naturally developed waves of the sea.

The state-of-the-art of predicting skirt drag is still not at a completely satisfactory stage but some insights and formulations can be given for each drag component.

Calm Water Skirt Drag. It has long been recognized³⁸ that the drag of skirts in calm water is the result of many contributing factors such as air gap clearance, craft size, shape, and skirt design. It is also suspected that cushion pressure is important in that this affects skirt stiffness, shape, and spray generation. Wheeler⁵⁷ discusses the implications of the air gap on this calm water drag component, which can approach 30 percent of the craft drag for an air cushion craft the size of the SR.N4. Wheeler does point out, however, that this drag component becomes progressively less important as craft size increases.

Since the last summary, work is continuing to reduce the spray since this has ramifications on both drag and engine life (see Chapter IX). Hovercraft Systems Ltd., a Canadian company involved in supplying air cushion equipment for use in the Canadian Arctic developed a spray skirt, that purports to reduce spray by 50 to 75 percent. A more detailed description, which is in the form of an addition to the existing skirt, is provided in Chapter VI. It is sufficient here to note that promising developments are underway to reduce this drag component (and the spray's other deleterious effects). While the addition of an antispray skirt minimizes spray problems, there is no evidence that it results in any reduction of this (drag) component. In fact, the converse may prove to be true; i.e., spray drag may be even higher.

For large air cushion craft of 1000-ton displacement, it is expected that small air gaps ($h/L = 0.001$) (see Figure 25) will be satisfactory and not give rise to excessive wetting drags. Figure 54, taken from Reference 57, illustrates the drag breakdown in both calm and rough water (6- to 8-ft waves) for a typical large air cushion craft of the SR.N4 type and, in particular, illustrates the need to understand skirt drag in both calm and rough water.

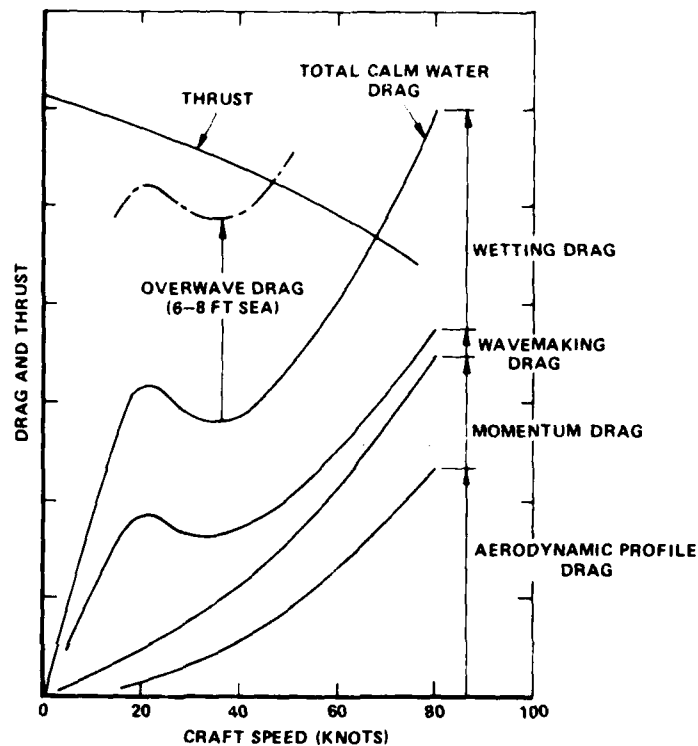


Figure 54 - Drag Breakdown of Typical Large Air Cushion Craft

Bell and British Hovercraft Corporation (BHC) researchers⁵⁸ showed, in the DARPA studies on the application of air cushion craft for use in the Arctic, that good agreement with model tests could be achieved if the calm water skirt drag was considered to be made up of two components, as follows:

1. Wetting Drag (D_{SK_w}) - a drag component related to craft speed, hemline length, and volume flow on air gap.
2. Wavemaking Related Drag ($D_{SK_{wm}}$) - a drag component related to the cushion wavemaking generated by the cushion pressure or density of the craft.

Examining these components of the calm water skirt drag in order, it has been found that there is good correlation between the model data and the equation for the skirt wetting drag, as:

$$D_{SK_w} = K_7 \left(\frac{h}{c} \right)^{-0.34} \cdot C\sqrt{S} \cdot q_w \quad (72)$$

The constant K_7 is strongly dependent on the geometry and cushion density of the particular craft and skirt. Variations in K_7 range from 2.13×10^{-6} for the low cushion density SR.N4 to 3.71×10^{-6} for the high cushion density JEFF(B). An average value of $K_7 = 3.46 \times 10^{-6}$ gives a reasonable fit over a wide range of cushion densities. Note that the air gap function is related to the peripheral hemline length c . The cushion area S and the dynamic pressure of the water q_w are self evident terms.

Expressing Equation (72) in nondimensional forms gives,

$$\frac{D_{SK_w}}{W} = 0.0058 \left(\frac{h}{c} \right)^{-0.34} \cdot \frac{1 + L/B}{(L/B)^{1/2}} \cdot k \quad (73)$$

where k is the pressure number defined by Equation (29). Figure 55 (upper curves) illustrates the magnitude of this drag component for the particular case $L/B = 2.0$. The effect of L/B is fairly small with the dominant geometric effect being given by h/c .

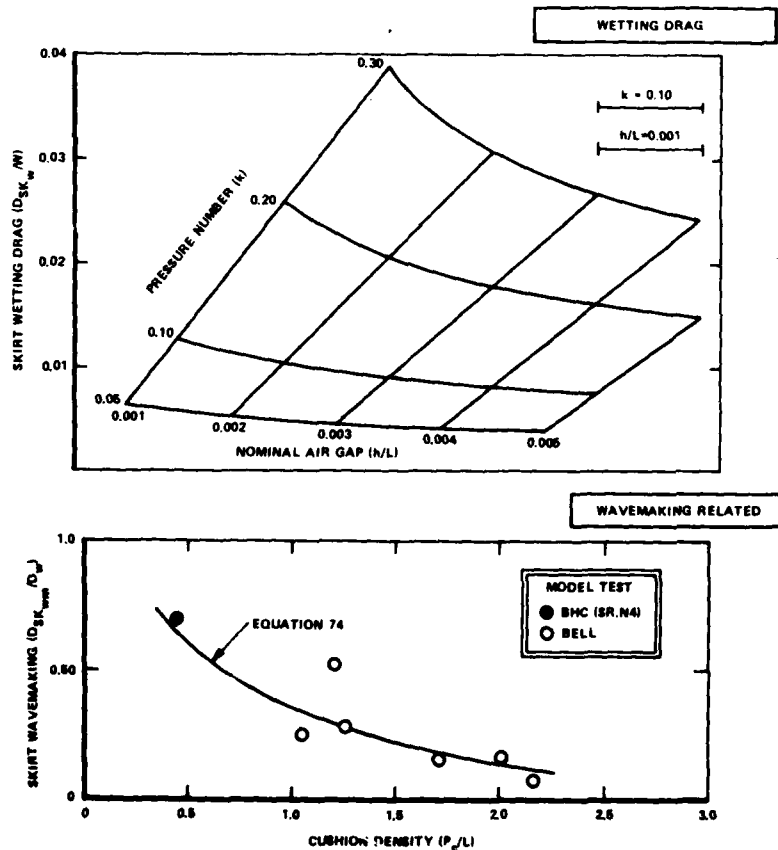


Figure 55 - Calm Water Skirt Drag Components

The second component of calm water skirt drag ($D_{SK_{wm}}$) was found to be⁵⁸ strongly dependent on the cushion density as shown in Figure 55 (lower curve). An empirical relation is given here that is based on both the Bell and BHC model tests as:

$$\frac{D_{SK_{wm}}}{D_w} = 1.374 \left(\frac{P_c}{L} \right)^{-0.259} - 1 \quad (74)$$

which, if used in conjunction with Figures 47, 48, and 50 for the basic cushion wavemaking drag (D_w), will provide an estimate for the calm water wavemaking drag of the skirt. Typically, this component can amount to some 25 to 30 percent of the basic cushion wavemaking drag at higher P_c/L .

Rough Water Skirt Drag. For the drag of skirts in rough water, experimental evidence has been more easily obtained, but predictive methods based on theoretical analysis have so far eluded the air cushion craft designer. It is also accepted that any methods used are only generally applicable for sea conditions where the wave height is no more than about 80 percent of the cushion height. Above this value there is almost certain to be hard bottom contact and the drag of the craft (and skirts) is more dependent on craft response than on skirt geometries.

The method still used, as described by Elsley and Devereux,³⁸ involves predicting the craft drag components by methods described in the early part of this chapter and attributing to the rough water skirt drag, the difference between the prediction and the measured total drag. The method of normalizing the data has, naturally, varied between the engineering groups conducting the tests. Elsley and Devereux³⁸ shows the functional relationship as

$$\frac{D_{rough}}{W} = f(p_c/h_c, h_w/h_c, V/V_H) \quad (75)$$

where h_c is the cushion height.

Republic Aviation^{59,60} shows the rough water drag, based on the early VA-3 air cushion craft tests, as

$$\frac{D_{\text{rough}}}{qS} = f\left(\frac{h_w - 2h_c}{L}\right) \quad (76)$$

Bell,⁶¹ using Bell model data and full scale data from BHC on the SR.N4 and SR.N6 tests, show that the rough water skirt drag follows the functional form,

$$\frac{D_{\text{rough}}}{q_w C\sqrt{S}} = f\left(\frac{2h_w}{h_c + h_f}\right) \quad (77)$$

where h_c is the total cushion depth, as before, made up of bag and finger depth, and h_f is the finger depth alone.

The author used different skirt systems information to determine an analytical representation of the functional form of Equation (77). This additional data has been added to the data base as shown in Figure 56. Although there is some large scatter seen in Figure 56 on this important drag component, it is found that the following equation gives a good fit to the data

$$\frac{D_{\text{rough}}}{q_w C\sqrt{S}} = 20 \times 10^{-5} \left[\frac{2h_w}{h_c + h_f} \right]^{5/3} \quad (78)$$

which in terms of the craft parameters used in this report is expressed as,

$$\frac{D_{\text{rough}}}{W} = 0.34 \cdot \frac{1 + L/B}{(L/B)^{1/2}} \cdot \left[\frac{2h_w}{h_c + h_f} \right]^{5/3} \cdot k \quad (79)$$

Because the bulk of the air cushion craft shown in Figure 56 have "fingers" (see Chapter VI) that have a height (h_f) for some 50 percent of the cushion depth (h_c) the skirt-wave parameter in brackets in Equation (79) is very nearly the roughness parameter h_w/h_c and, in any event is related to it by a constant.

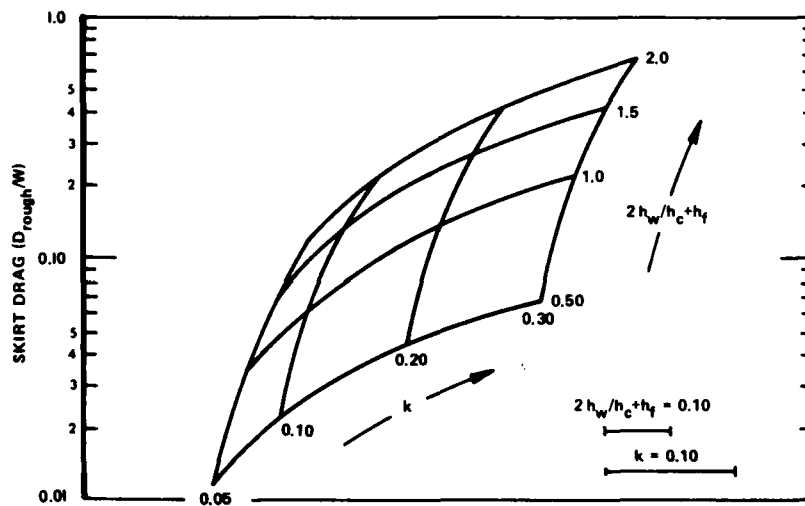
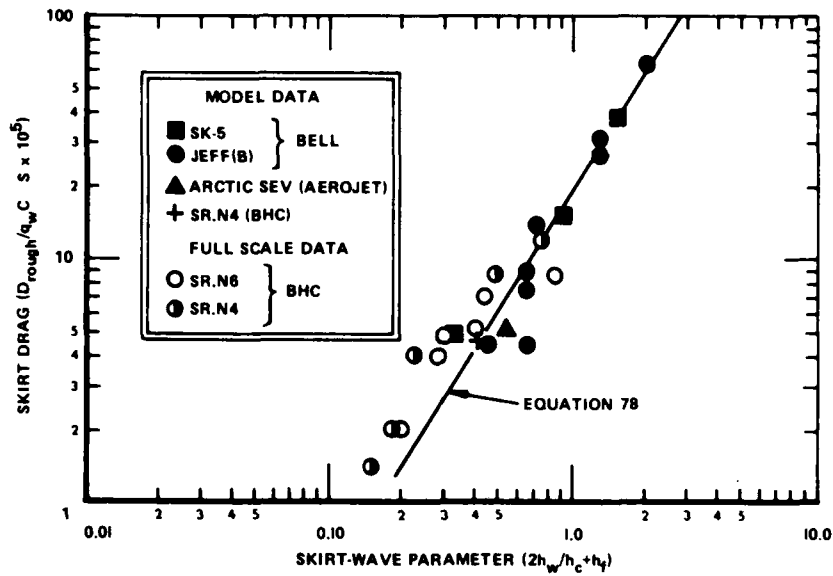


Figure 56 - Rough Water Skirt Drag

The lower set of curves in Figure 56 are computed from the upper curve using Equation (79) for $L/B = 2.0$.

The bulk of the data included in Figure 56 result from the "bag and finger" type of skirt (see Chapter VI) where stability dividers are present

with expected influences on drag. The data from the AALC JEFF(A) air cushion craft have been included. This type of skirt, termed the "pericell" type, has no such cushion dividers but has a tendency to scoop, giving rise to drag. In plotting such a skirt system it was assumed that the finger height and the pericell were synonymous. Although not plotted in Figure 56, Vosper and Thornycroft report that their "loop-segment" skirt, again discussed in Chapter VI follows a similar relationship. Equation (79), generally predicting a little high for the "loop-segment" skirt at the craft's design operating speed, is most likely due to the absence of any cushion skirt dividers. At low speeds, however, model tests would indicate that Equation (79) underpredicts the rough water drag of the "loop-segment" skirt. This underprediction could be the result of complex wave formation and interaction with the skirts.

Thus, while the empirical treatment of the rough water skirt drag is not completely rigorous and must be used with caution with any new skirt designs, it does represent the present state-of-the-art of drag prediction for the main types of skirt in use on air cushion craft today.

From Figure 56 and Equation (79) it is seen that the drag of skirts in rough seas can constitute a significant portion of the craft drag, and other than the effect of craft response is the main contributor to the drop off of speed of the craft in rough water. The problem of predicting skirt drag in rough water is further complicated by the wearing of the skirt lower edges (edges in the form of fingers, cells, or segments). Figure 57, taken from Reference 62, shows the performance in rough water of the SR.N4

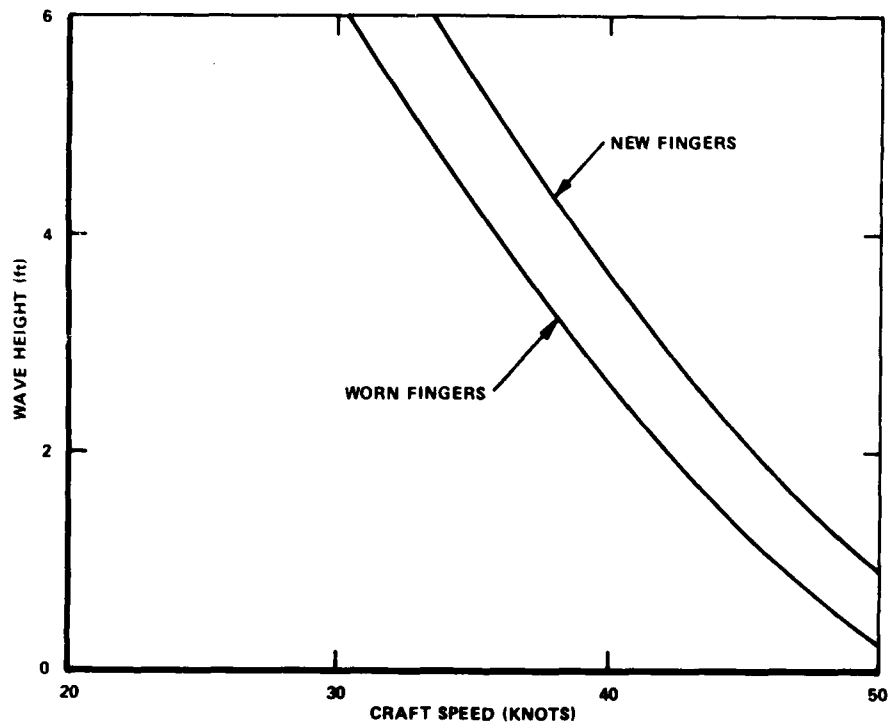


Figure 57 - Rough Water Performance of SR.N4

with the fingers in both new and worn condition. It is usual to discuss rough water performance in broad bands of speed because, besides its depending on wave height, it depends on such variables as wavelength, wind-speed and direction. For example, the BH.7 is quoted as having a rough water speed of 20 to 35 knots in seas of significant wave height of 4 ft depending on the heading, wavelength of the waves, and wind speed.

An attempt has been made to remove some of the variations by normalizing the performance in rough seas by expressing the speed (in rough seas) as a fraction of the calm water speed; the size effect is further normalized by the ratio of significant wave height (h_w) to the cushion depth (h_c). Figure 58 shows such a normalization for a wide selection of air cushion craft using full-scale operational data, model data, and design

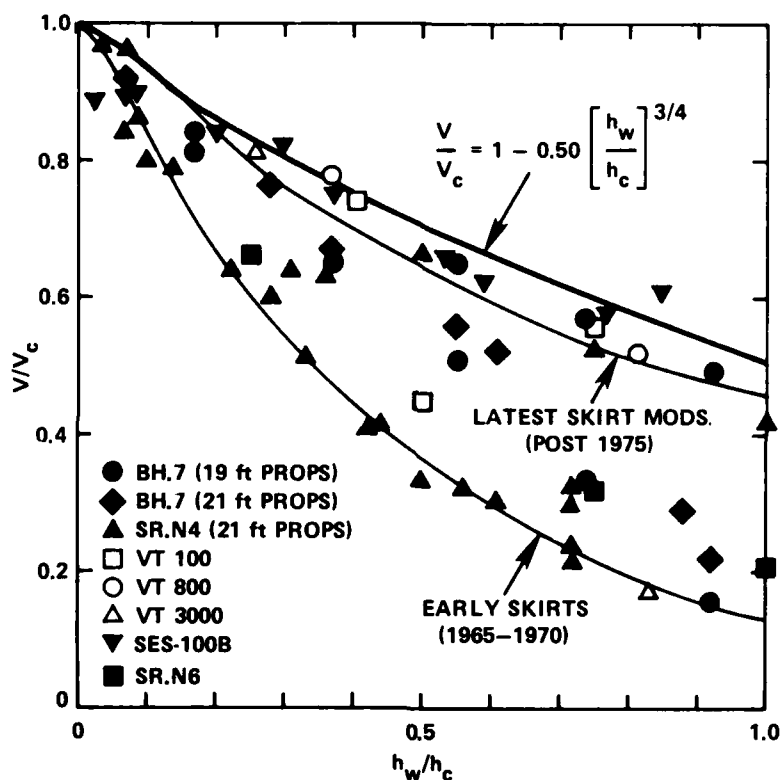


Figure 58 - Speed in Rough Seas

study results. It is seen from Figure 58 that there is a wide variation in speed for a given sea condition for all the craft considered. Much of

this variation is due to the effect of wind speed and the nature and steepness of the waves. It also depends on whether the craft is heading into or is running with the waves. It further depends on whether the craft is being designed to platform or contour the waves for seakeeping considerations. Another key factor that is buried in the data in Figure 58 is the operator's natural tendency to lower the speed to meet ride quality limits (see Chapter IV). In anticipation that the designer will strive to attain the highest possible speed, especially in a military craft, it can be assured that the upper range of data is an achievable speed. A reasonable fit to the data is given by the equation

$$\frac{V}{V_c} = 1 - 0.50 \left[\frac{h_w}{h_c} \right]^{3/4} \quad (80)$$

where V = the speed in seas of significant wave height (h_w)

V_c = the speed attainable in calm water at the same power setting

h_c = the average cushion depth

Attempts to normalize out the effects of wavelength and windspeed (strong influences) were not successful due to the lack of consistent data among the various craft analyzed.

Drag while Traversing Ice. A particular advantage of the amphibious air cushion craft, or ACV type, is its ability to traverse surfaces not readily passable by more conventional means of transport, that must depend on rolling friction for traction. The need to operate in the Arctic prompted DARPA to evaluate the air cushion craft as a possible means of year round transport over the tundra, sea, and ice for such industrial uses as oil exploration and mining. Extensive studies were accomplished²⁸ as part of the DARPA program and a much improved state-of-the-art of such vehicles was the result. While space does not permit a complete summary of the findings, it is thought appropriate to include the results of analysis and model tests on the drag component related to traversing ice. Figure 59

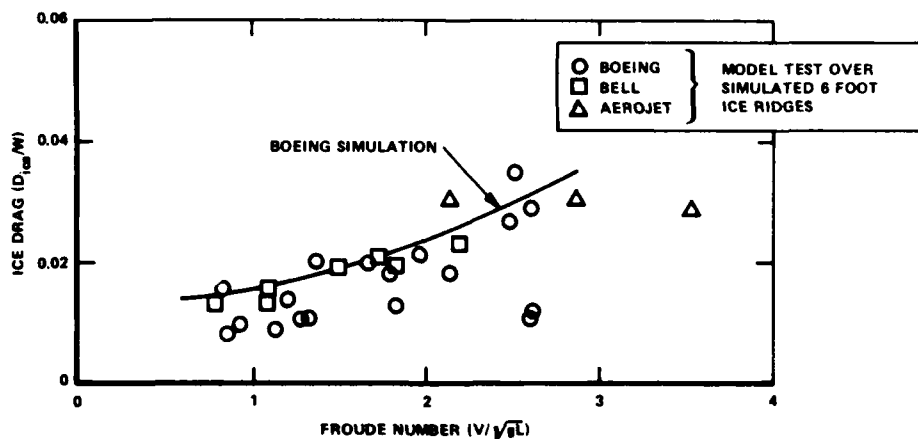


Figure 59 - Skirt Drag Over Simulated Ice

shows the various model test results^{58,63,64} for operation over 6-ft ice ridges with craft fitted with 9-ft deep skirts, i.e., $h_c = 9$.

Although each set of data applies to different skirt concepts (as was done for the rough water drag correlation shown earlier), all craft employ flexible material in the skirts that come into contact with the ice ridges. Although there is scatter, there is a trend which follows a theoretical treatment⁶⁴ that predicts the functional relationship

$$D_{ice} \sim V^{2/3} \quad (81)$$

By way of example, rough ice skirt drag values of $D/W = 0.02$ appear likely for a Froude number of 1.76, which corresponds to a 170-ton air cushion craft travelling at 60 knots. Comparing this result with the rough water drag on Figure 56, it is seen that the time-averaged skirt drag over 6-ft (simulated) ice ridges is considerably less than skirt drag over 6-ft waves, but it should be noted that the frequency of encounter was greatly reduced for the former.

Sidehull Drag. For those air cushion craft that are nonamphibious, the hydrodynamic resistance of the sidehulls and their appendages (rudders, fins, propulsor pods, and so on) forms a major portion of the total resistance.

All operating sidehull air cushion craft today (HM.2, SES-100A, SES-100B) are designed to be hydrodynamically efficient at high speed, specifically, at superhump speeds of $F. No. > 2.0$.

Figure 60 illustrates the relative magnitude of the sidehull drag and that of its appendages of the SES-100A in its pod inlet configuration prior to its modification in 1975 to a flush inlet. The large drag of pod inlets was sufficient cause to initiate the retrofit to a flush inlet. The counter considerations are the relatively lower efficiency of the flush inlet and the increased likelihood of air ingestion from the cushion or atmosphere in off-design operating conditions. It is often found, as was the case for the SES-100A, that some form of fence must be added to a flush inlet to prevent air ingestion. Such fences have drag associated with them and much of the advantage is lost in departing from the positive pressure ram inlet to the pressure gradient sensitive flush inlet. More discussion on the various types of inlet is given in Chapter IX on propulsion.

The sidehull type of craft or SES has been tested to very high speeds that strain the state-of-the-art of hydrodynamic hull forms and border on speed regimes where the aerostatic or ACV form is more efficient. The high speed requirement has brought an additional factor to the sidehull hydrodynamic design. This factor is the cavitation number σ , which relates the static pressure (p_{st}) on the surface of the sidehull to the vapor pressure of water (p_v) and the dynamic pressure of the oncoming water stream; that is,

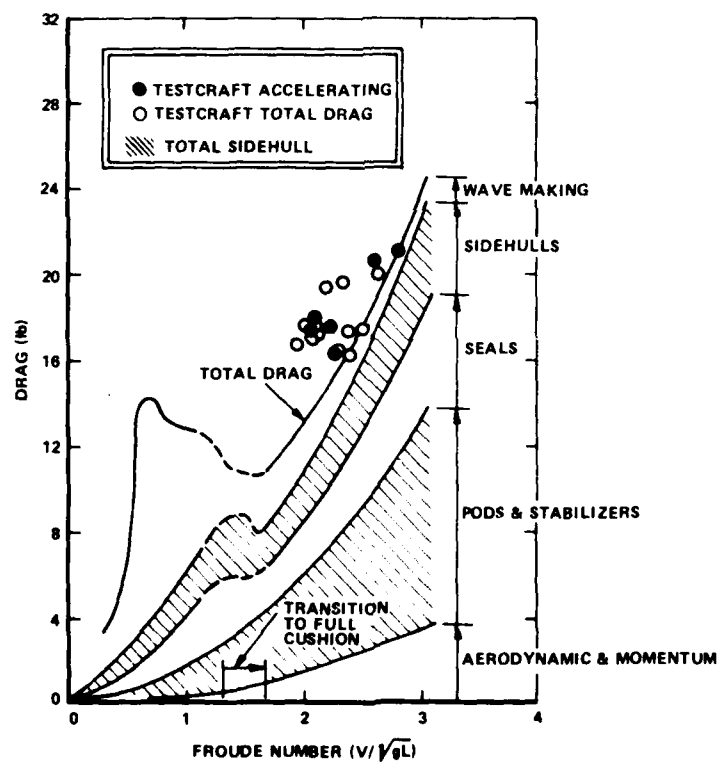
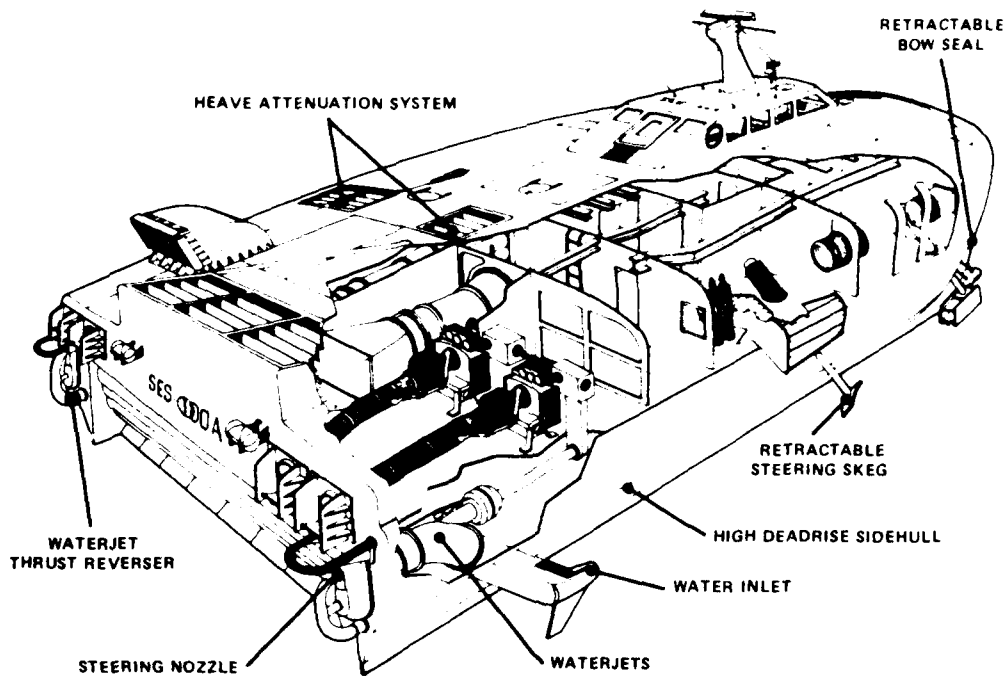


Figure 60 - Sidehull Drag of SES-100A

$$\tau = \frac{P_{st} - P_v}{1/2 \rho_w V^2} \quad (82)$$

The hydrodynamic design of hulls, and, in particular, air cushion craft sidehulls, is strongly influenced by both Froude number and Cavitation number. Some early designs used high speed displacement hull forms where the resistance followed the conventional formulas available to the naval architect. Such hull forms are the Series 60 and Series 64 which are most efficient in the nondimensional speed range of $0.30 < F. No. < 0.80$.

The hull form most applicable to air cushion craft is the Series 62 or planing hull form, which is most efficient at high speeds ($F. No. > 1.0$) where a considerable amount of hydrodynamic lift is required. Several important differences occur, however, between the conventional planing hull application and the air cushion craft.

The sidehull air cushion craft uses very slender planforms such that b/L_H , where b is the span or width of the sidehull of length L_H , may typically have values of 1:10 to 1:20. Again, in the air cushion craft, one side (the inboard side) of the sidehull operates with a depressed waterline from the air cushion pressure with the attendant crossflow. This crossflow component especially at high Froude numbers and low Cavitation numbers complicates the flow field and contributes to the difficulty in making accurate predictions of sidehull forces and moments. Most methods even today, still rely very strongly on model tests and scaling techniques for full-scale drag prediction.

The sidehull drag is still treated as principally the sum of two components: the sidehull wave drag and the skin friction incurred through the sidehull wetted area. While there are many variations on the theme in the various reports on drag prediction, the sidehull drag equation can be written,

$$D_{SH} = \Delta \tan \tau + \frac{C_f 1/2 \rho_w V^2 S_{SH}}{\cos \tau} \quad (83)$$

where the (single) sidehull drag D_{SH} is a sum of the wave drag determined by a vertical force Δ which is selected by design to be approximately 5 to 10 percent of the total craft displacement W , and the skin friction force. The frictional force acts on the wetted area of the sidehull S_{SH} and the sidehull is assumed to plane at an angle τ , which may or may not be equal to the cushion wave drag angle implied by Equation (66).

The difficulty arises, in design, of determining the vertical force Δ and the wetted area S_{SH} , especially in the presence of crossflow, disturbed

water surface, and spray. The problem is further complicated in rough water where extreme variations in wetted area occur and cushion air escapes beneath the keel.

Locke⁶⁵ originally showed the nonlinear nature of the lift coefficient of long slender hulls; namely,

$$C_{L_{SH}} = \eta K \tau^n \quad (84)$$

where η is a factor depending on operating conditions. The factors K and n were found experimentally, and both vary with the slenderness ratio of the sidehull. A further complication is the effect of the angle of deadrise β of the sidehull. The normal force acting on the hull is

$$\Delta = C_{L_{SH}} (A; \tau, \beta) \frac{1}{2} \rho_w V^2 S_{SH} \quad (85)$$

Due to the complex flow patterns near the sidehull, the local values of aspect ratio $A (=b/L_{SH})$, the trim angle (τ), and the deadrise (β) vary down the length of the hull. Because of this, digital computational techniques are used to integrate the local forces where the actual geometry of the sidehull cross section is determined empirically.

The actual geometry of the sidehulls has been the subject of considerable research by both Government agencies and private industry; much of it classified. Some specific examples, however, illustrate the type of hulls used in current craft. Figure 61 shows the simple clean lines of the Hovermarine HM.2 which is designed to operate in the Froude number range of 1.5 to 2.0 and with Cavitation numbers from 0.60 to 2.0. Structural and fabrication considerations over and above those of performance strongly influenced the HM.2 shape which are possible in the particular ranges of F. No. and σ quoted.

Figure 62, on the other hand, shows an extreme example of a research craft designed to be hydrodynamically efficient at low cavitation numbers. This research craft, the XR-3, was designed specifically for high Froude number (F. No. > 3) and low cavitation number ($\sigma < 0.15$). The above waterlines are a modified parabolic shape while those near and below the normal on-cushion waterline have been further modified by thickening in the after sections to provide increased space necessary for installation of waterjet inlets. The parabolic-like lines were to reduce the likelihood of cavitation, and the thick after-lines operated in ventilated (and low drag) conditions. Given reasonably simple shapes, the drag can be computed from Equations (83), (84), and (85) and any model data scaled to full-scale using classical scaling laws. The main variables are the wave drag

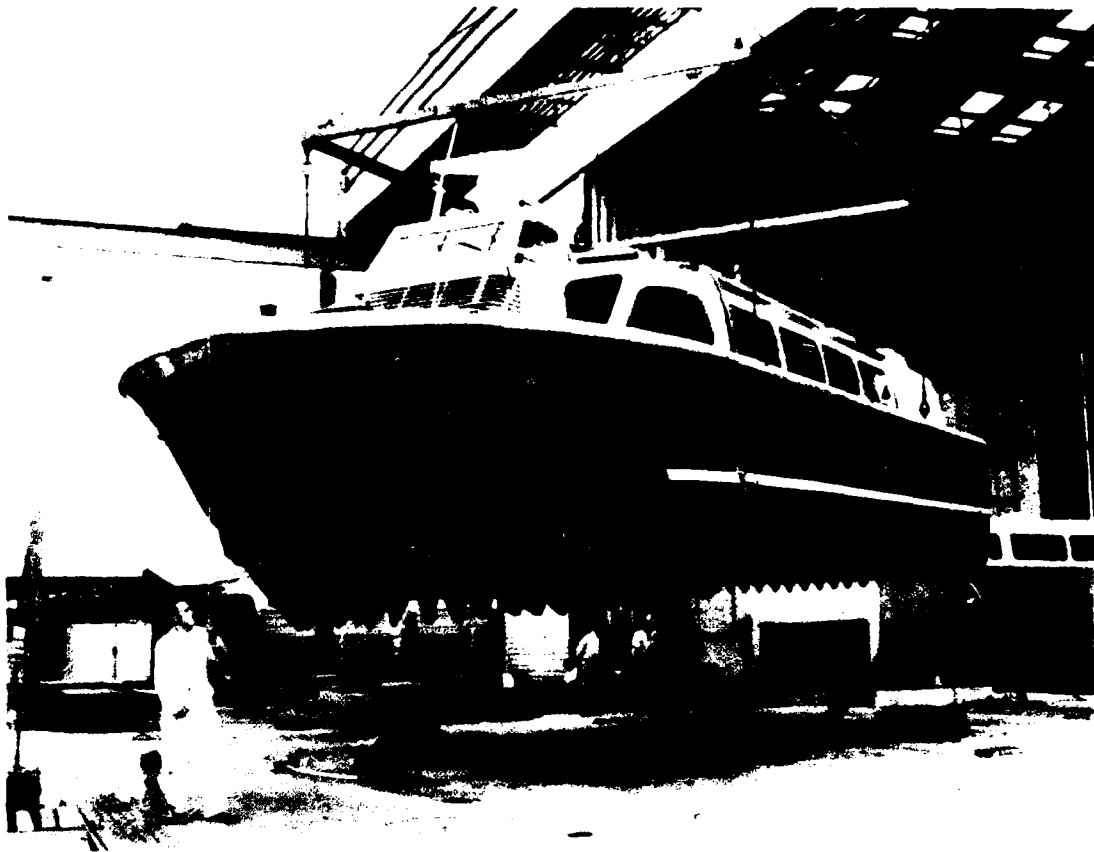


Figure 61 - Hovermarine HM.2

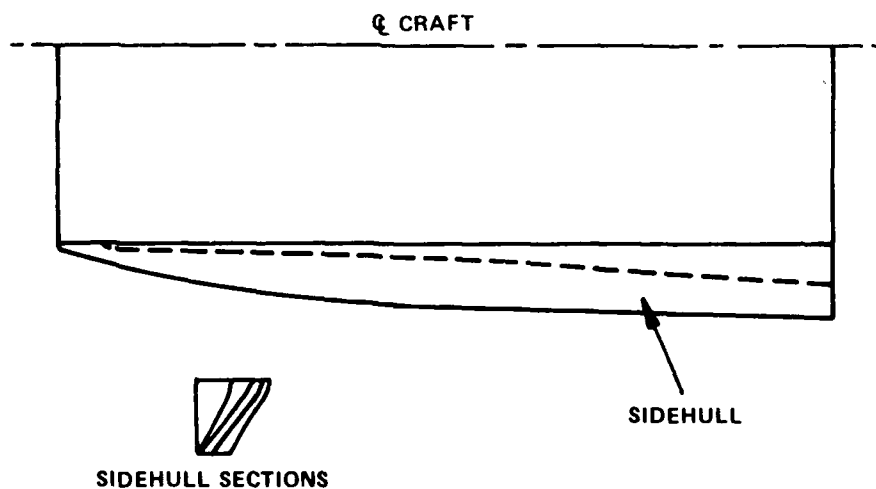


Figure 62 - Low Cavitation Number Sidehull

component ($\Delta \tan \tau$) which, if the scale factor from full scale to model is λ , scales as λ^3 (Froude scaling). The skin frictional coefficient (C_f) varies with Reynolds number and the wetted area scales as λ^2 . Wilson⁵⁴ describes a typical method of scaling from model sidehull drag values to full-scale. Detailed various approximations are made in computing the wetted area on both the outside of the sidehull and on the inside that has a depressed waterline due to the cushion pressure. It is important to note, however, that improper testing for the Cavitation number can change the flow field and thus the waterline. Use of an improperly scaled cushion pressure can also reduce confidence in the results. The particular problem of scaling cushion pressure will be referred to again in Chapter IV in the discussion of heave motion and cushion compressibility.

While simple shapes lend themselves to simple scaling techniques, in actual operational craft, other practical requirements apply that further complicate the hull lines and make theoretical sidehull drag prediction difficult. The technology is still too young to have data banks of drag values of component sidehull shapes--similar to data banks which exist in the aircraft industry on wing, body, and junction drag values. For the sidehull craft, these practical considerations include provision for rudder and fin mounting, propulsion pod for waterscrew or waterjet installation, thickness of keel for grounding, high speed impact, and stability devices. The SES-100A and the SES-100B represent the most current operational hardware specifically designed for high Froude number and low Cavitation number operation, and both have basically different hull forms to meet the same performance criteria. Although the actual hull lines are classified, it can be stated that the SES-100A has a thin high deadrise hull form ($\beta = 60$ deg) with auxiliary devices added for stability. The SES-100B has a low deadrise hull ($\beta = 30$ deg) with sufficient thickness in the sidehulls to provide the needed stability.

Mantle⁶⁶ showed that the two hull forms produced marked differences in the drag of the craft. Figure 63 shows the hydrodynamic lift-drag ratio of each craft as determined from their full-scale test programs recently completed for the U.S. Navy Surface Effect Ship Program Office.

Data were obtained in controlled tests in calm water for both craft at optimum trim setting. The thicker hull form and lower deadrise angle of the SES-100B proved to be most efficient in a Froude number range of from 1.2 to 1.5 and has developed the predicted high hydrodynamic lift-to-drag ratio of $L/D = 20$. At higher Froude number (> 2.5), however, the sidehull drag becomes very large and the efficiency falls to values of $L/D < 7$. The steeper deadrise angle and narrower sidehull beam of the SES-100A shows generally a lower drag and higher lift-to-drag ratio ($L/D > 10$) at Froude number = 2.50 although the single SES-100B data point at high Froude number suggests this is not always the case.

Both the SES-100A and the SES-100B were designed to provide basic technical information for the design of much larger surface effect ships and specifically, for the next generation SES, the 3000-ton class displacement craft currently in the design stage. From dynamic similarity

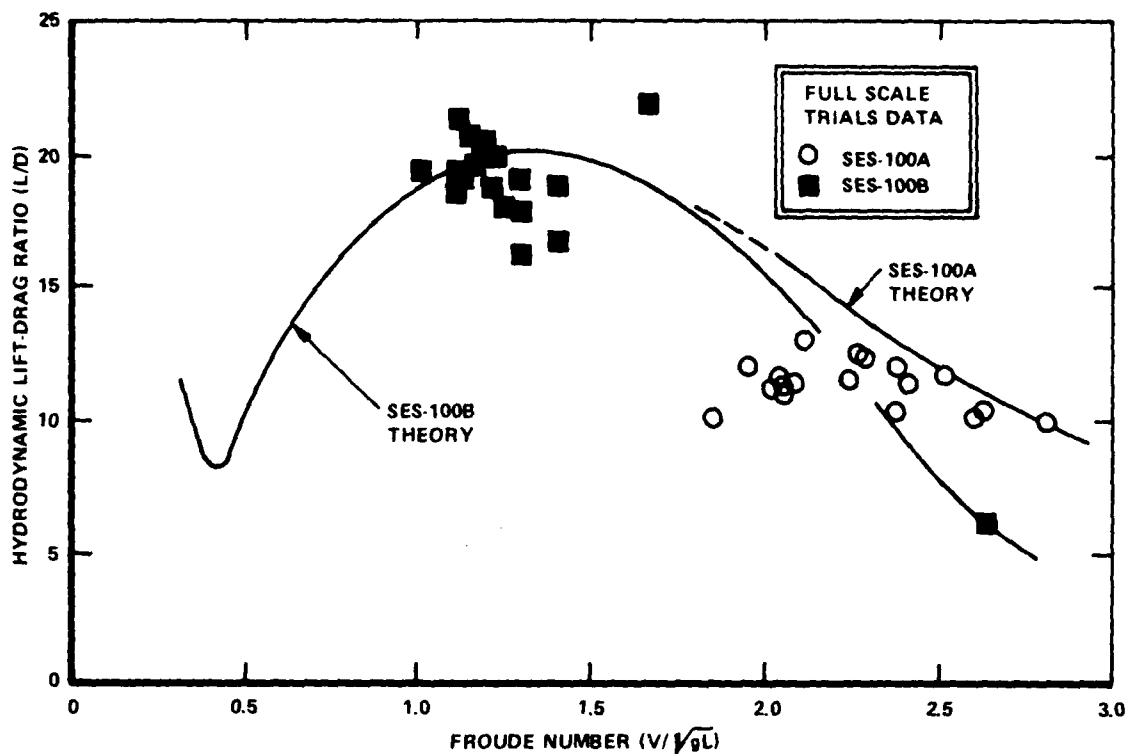


Figure 63 - Hydrodynamic Lift-to-Drag Ratio of SES-100A and SES-100B

laws, the high lift-to-drag ratio of the SES-100B at a Froude number of 1.5 corresponds to a 3000-ton SES traveling with the same lift-to-drag ratio* at 70 to 80 knots. Proper interpretation of the data from both the SES-100A and SES-100B can then yield the needed information on Froude scaling and cavitation scaling.

From the above brief discussion, it can be seen that the shaping of the sidehull for the air cushion craft designed to operate at Froude numbers much greater than from 2.0 to 3.0 and at cavitation numbers less than 0.15 is a subject still being pursued. It is to be expected that the future hull form will be much different from the hull forms seen today.

Aerodynamic Drag. The aerodynamic drag of air cushion craft is mainly the profile drag for today's craft designed to operate at speeds where $k < 0.50$. At higher values of k , which is the domain of the aerodynamic form

*Actually, the value of L/D would be even higher due to the scaling of viscous and inertial forces.

of air cushion craft (see Figure 8), consideration must be given to the aerodynamic induced drag. This is discussed in Chapter X where aerodynamic air cushion craft are discussed in more detail. The discussion here will be confined to the intermediate speed form. The estimation of the profile drag is well established either by using basic data available in the literature⁶⁷ or by wind tunnel testing the particular configuration under study. Various techniques, in use since the early days of air cushion craft, are still valid. These include testing of models with and without fan intake air flowing, and testing over fixed and moving ground boards. In the case of sidehull air cushion craft, it is common practice to suspend the entire model clear of the water but with keels almost touching the water and to take runs to determine the aerodynamic profile drag.

The profile drag coefficients vary from the streamlined SR.N2 with a C_{D_o} based on frontal area of 0.25 to the nonstreamlined SR.N5 with a C_{D_o} of 0.38. Figure 64 shows the shape of both craft to give an indication of the effect of streamlining. It has usually been found that the cost of streamlining, both in fabrication and loss of space, far outweighs the advantage of lower drag. The SES-100B, also shown in Figure 64, was designed for ease of fabrication having either flat surfaces or minimal single curvature contours. From wind tunnel tests, the SES-100B has a profile drag coefficient of $C_{D_o} = 0.32$ based on frontal area.

Of more significance is the side area of the air cushion craft, especially that of the amphibious form. In this case, large yaw angles are frequently experienced and the forces incurred due to the large side area can be significant. Hence, shaping is directed more to maintaining adequate yaw stability.

The profile drag of air cushion craft can be written as

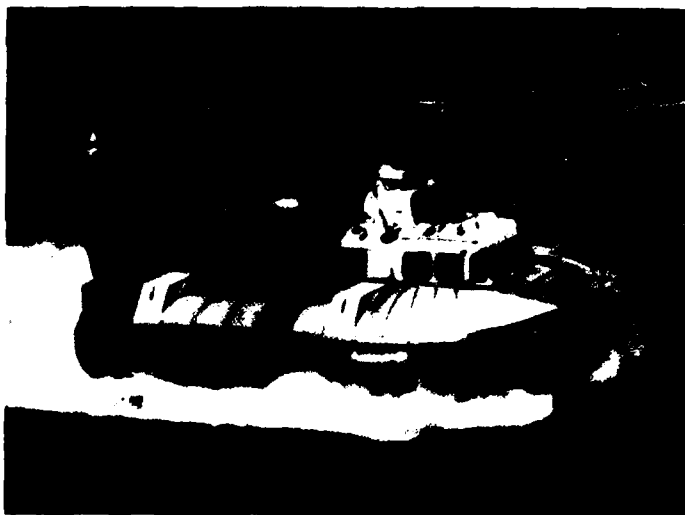
$$D_{aero} = C_{D_o} \frac{1}{2} \rho v^2 \left(\frac{S_F}{S} \right) S \quad (86)$$

where C_{D_o} is the profile drag coefficient referred to above, based on frontal area S_F . The power required to overcome this drag, in coefficient form, is then simply

$$\frac{Ch}{S} C_{P_{aero}} = C_{D_o} k^{3/2} \left(\frac{S_F}{S} \right) \quad (87)$$



$$C_{D_o} = 0.25$$



$$C_{D_o} = 0.38$$



$$C_{D_o} = 0.32$$

Figure 64 - Typical Aerodynamic Drag Coefficients

Total Drag Estimation

The foregoing sections have attempted to encapsulate the essential elements of the power-consuming components for air cushion craft. Obviously, each design must be carefully analyzed and subjected to model test to determine its particular drag characteristics. It would be presumptuous to imply that the extensive work done by various groups to refine drag estimation and drag reduction could be adequately covered in such a summary as this. However, it is believed that the essential elements are included and attention given to stating those areas that are well known and, therefore, within the state-of-the-art, and those that are still giving us a few challenges. The total drag (D) of an (intermediate speed) air cushion craft is given by,

$$D = D_{\text{aero}} + D_{\text{mom}} + D_{\text{wave}} + D_{\text{sk}} \quad (88)$$

where the aerodynamic drag (D_{aero}) is given as the profile drag of the craft. Induced aerodynamic drag has been ignored and is only significant in high speed air cushion craft (see Chapter X). The momentum drag (D_{mom}) is a function of the air flow through the cushion and the cushion wave drag (D_{wave}) is a strong function of cushion pressure and length-to-beam ratio of the craft. The skirt drag (D_{sk}), a strong component in influencing the speed of the craft in rough water, is broken into other components and the most current empirical methods for estimating its magnitude are provided in the analysis. Spray drag was ignored because experience has shown that it is a small component for most well-designed air cushion craft. Also, no adequate prediction method for its computation is available.

The dimensional analysis at the beginning of the chapter and the subsequent derivations for the drag components showed that the drag of the air cushion craft was a function of such nondimensional numbers as Froude number F . No., cushion density ($\rho/S^{1/2}$), flow coefficient (C_Q) and Pressure number (k). While not explicitly developed here, the components can be scaled reasonably well from model experiments following the classical laws of scaling that may be found in any aerodynamic or naval architectural textbook. The requirements for dynamic similitude between model experiment and full-scale were also provided in the appropriate sections early in this chapter.

For convenience, the main equations given for the various drag components are summarized in Table 2. A perusal of Table 2 leaves the impression that the drag of an air cushion craft is at best, described by a collection of empirical relationships, especially in some of the major components. This is still true even at this stage of development, although well conducted model experiments give a high degree of confidence

TABLE 2 - AIR CUSHION CRAFT DRAG COMPONENTS

Component	Drag Equation	Relevant Figure
Momentum	$D_M = \rho QV$	-----
Wave Drag	$\frac{D_w (L/B)^{1/2}}{(P_c/L)^2 L^3} = f(L/B; F)$	Figure 47 and Figure 48
Skirt Drag (calm water)	<p><u>Wavemaking Component</u></p> $\frac{D_{Sk_w}}{W} = 0.0058 \left(\frac{h}{c}\right)^{-0.34} \cdot \frac{1 + L/B}{(L/B)^{1/2}} \cdot k$ <p><u>Wavemaking Component</u></p> $\frac{D_{Sk_{wm}}}{W} = 1.374 \left(\frac{P_c}{L}\right)^{-0.259} - 1$	Figure 55
Skirt Drag (rough water)	$\frac{D_{rough}}{W} = 0.34 \frac{1 + L/B}{(L/B)^{1/2}} \left(\frac{2h_w}{h_c + h_f}\right)^{5/3} k$	Figure 56
Skirt Drag (over ice)	$\frac{D_{ice}}{W} \sim V^{2/3}$	Figure 59
Sidehull Drag	-----	Figure 60
Aerodynamic Drag	$\frac{D_{aero}}{W} = C_{D_o} \left(\frac{S_F}{S}\right) k$	Figure 64

in predicting the drag of any specific craft. The problem is due to the physics of the mixed flow of air and water at the interface and to the randomness of the wave action during rough water operation.

Drag Polar

While there is still a large amount of empiricism in the prediction techniques there is some order that can be seen if one collapses all the drag components in coefficient form in the form of a drag polar akin to that used with success in the design of airplanes. The method works well in the cruise mode where the nondimensional speed is high, i.e., specifically for $F. No. > 1$. At these speeds the cushion wave drag given by the curves shown in Figure 48 can be approximated by the simple expression

$$\frac{D_w}{(\rho_c/L)^2 L^3} = \frac{2.40}{(L/B)^{3/2} \cdot \rho_w g \cdot F^2} ; \quad F > 1 \quad (89)$$

Then after some algebraic manipulation this can be expressed in coefficient form as,

$$C_{D_w} = \kappa C_L^2 \quad (90)$$

The analogy of the wave drag coefficient to the induced drag coefficient familiar to the airplane designer is now apparent from Equation (90). The wave drag factor κ is simply,

$$\kappa = \frac{1.2}{(L/B)^{1/2}} \cdot \frac{\rho}{\rho_w} \quad (91)$$

With these expressions, together with the flow coefficient given by Equation (26), the drag polar equation becomes,

$$C_D = C_{D_o} + \kappa C_L^2 + 2 C_Q \quad (92)$$

The intercept on the polar, which is the profile drag coefficient in the case of an aircraft, becomes a combination of profile drag and skirt drag for the air cushion craft; namely,

$$C'_{D_o} = C_{D_o} + 0.34 \frac{1 + L/B}{(L/B)^{1/2}} \left(\frac{2hw}{h_c + h_f} \right)^{5/3} \quad (93)$$

where the second term is recognized as the constant in the rough water skirt drag equation, Equation (79). The general form of the drag polar is shown in Figure 65.

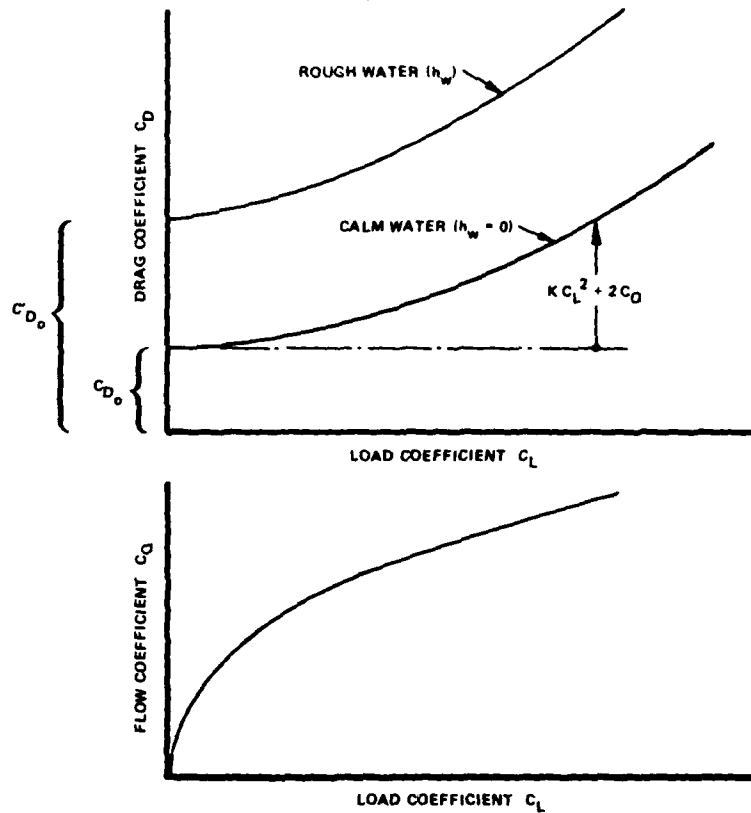


Figure 65 - Drag Polar for Amphibious Air Cushion Craft

The flow coefficient C_Q can be eliminated in Equation (92) through the use of the flow equations developed earlier. For example, for the plenum type of air cushion craft,

$$C_Q = \frac{Ch}{S} \cdot D_c \cdot C_L^{1/2} \quad (94)$$

in which case the drag equation can be written as

$$C_D = C_{D_0}' + \dots C_L^2 + 2 \frac{Ch}{S} \cdot D_c \cdot C_L^{1/2} \quad (95)$$

A similar expression can be developed for the nonamphibious or sidehull form of craft, and it can be written as

$$C_D = C_{D_0}' + \dots C_L^2 + \frac{2}{S} \frac{Ch}{S} D_c C_L^{1/2} + F(\text{trim, draft,} \dots) \quad (96)$$

where the hydrodynamic resistance term $F(\text{trim, draft,} \dots)$ depends upon the actual form of the sidehull (Series 62, 64, and so on) and on the particular geometry of the craft.

It can be seen from Equations (95) and (96) that the essential elements such as air gap, aerodynamic shaping, cushion density, skirt drag, and hydrodynamic form are all contained in the drag polar.

The technique just described was used successfully in the design of of the SES-100B.³⁴ Figure 66 illustrates the agreement between theory and model test data of the basic relationships.

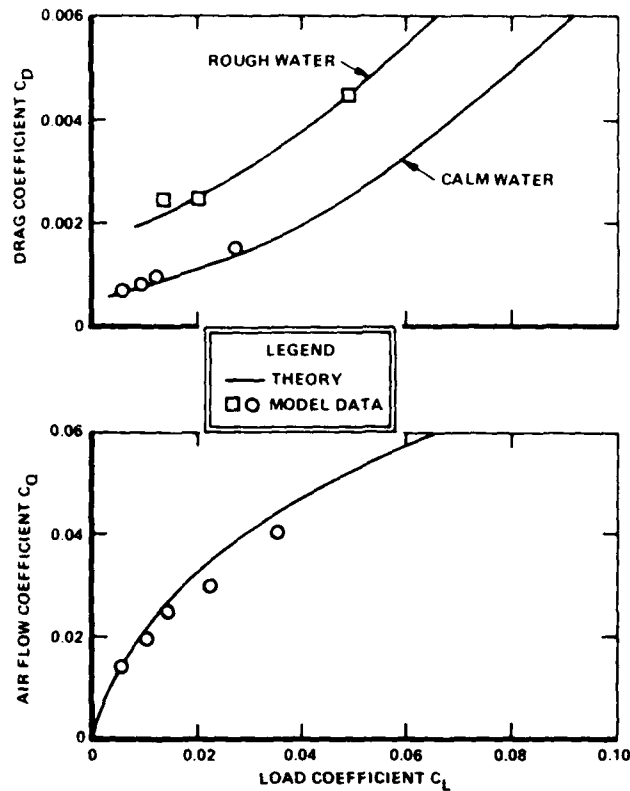


Figure 66 - Drag Polar for SES-100B

Lift-to-Drag Ratio

The previous section summarized the drag components of air cushion craft. If the lift system is now included, the total power to both propel and lift the craft can be studied. The total power, can be summarized as

$$P = P_L \text{ and } P_{WP} + P_M + P_W + P_{SK} + P_{SH} + P_{AERO} \quad (97)$$

where the and/or notation is a reminder to the designer to make sure that there is sufficient power in the lift system to meet any wave pumping requirements. Table 3 summarizes the power in coefficient form for each of the components.

If C_{P_T} designates the total power in coefficient form, then the transport efficiency can be written as

$$\frac{1}{550 \eta} \cdot \frac{WV}{P} = \frac{k^{1/2}}{\frac{Ch}{S} C_{P_T}} \quad (98)$$

Figure 67 shows the typical variation of the effective lift-to-drag ratio (for the case of calm water) with Pressure number k . Several craft performance data have been included to indicate how actual operational craft compare with the basic theory. Typical values of propulsor and fan system efficiencies have been used. The test data for the General Dynamics research craft SKIP-I are taken from Reference 68. The operational data for the SR.N2 are taken from Reference 41.

It can be seen from Figure 67 that the overall efficiency of the aerostatic amphibious air cushion craft is strongly dependent on the air gap, but that competitive performance is available. The optimum cruise speed from Figure 67, which can be derived theoretically, occurs for $0.2 < k < 0.3$, which corresponds to between 50 to 60 knots for low cushion pressure craft ($p_c \approx 50 \text{ lb/ft}^2$) and to between 70 to 80 knots for high cushion pressure craft ($p_c \approx 100 \text{ lb/ft}^2$).

Solving for the conditions of maximum lift-to-drag ratio and the speed at which this occurs involves numerical computational techniques of the drag equations. In certain restricted cases closed solutions can be found

TABLE 3 - AIR CUSHION CRAFT POWER REQUIREMENTS

Component	Power Coefficient		Relevant Figure
Lift	P.J.*	$C_{P_{Lo}} = \frac{F(x)^+}{1+\cos \theta}$	Figure 42
	Plenum	$C_{P_{Lo}} = D_c$	
Wave Pumping	$C_{P_{wp}} = \frac{\pi h w / \lambda}{Ch/S} \cdot F(L/\lambda) \cdot k^{1/2}$		Figure 43
Momentum	P.J.	$C_{P_M} = \frac{2G(x)}{1+\cos \theta} \cdot k \left[1 - C_{L_u} k \right]^{1/2}$	Figure 45
	Plenum	$C_{P_M} = 2D_c k \left[1 - C_{L_u} k \right]^{1/2}$	
Wave Drag Power (at hump)	$\frac{Ch}{S} \cdot C_{P_{wH}} = \sqrt{\frac{\rho g}{2}} C_{D_{wH}} \cdot F_H \cdot (p_c/L)^{1/2} \cdot \frac{L}{B}$		-----
Skirt Power (calm water)	<u>Wetting Component</u> $\frac{Ch}{S} C_{P_{SK_w}} = 0.0058 \left(\frac{h}{c} \right)^{-0.34} \cdot \frac{1 + L/B}{(L/B)^{1/2}} \cdot k^{3/2}$		-----
Skirt Power (rough water)	<u>Wavemaking Component</u> $\frac{Ch}{S} C_{P_{SK_{wm}}} = \left[1.374 \left(\frac{p_c}{L} \right)^{-0.259} - 1 \right] k^{1/2}$ $\frac{Ch}{S} C_{P_{SK_{rough}}} = 0.34 \cdot \frac{1 + L/B}{(L/B)^{1/2}} \left(\frac{2hw}{h_c + h_f} \right)^{5/3} k^{3/2}$		-----
Aero Power	$\frac{Ch}{S} C_{P_{aero}} = C_{D_o} \left(\frac{S_F}{S} \right) k^{3/2}$		-----

*Peripheral jet.

†Only the hover power is given here. The more complete equation showing effect of speed and intake losses is given in the text.

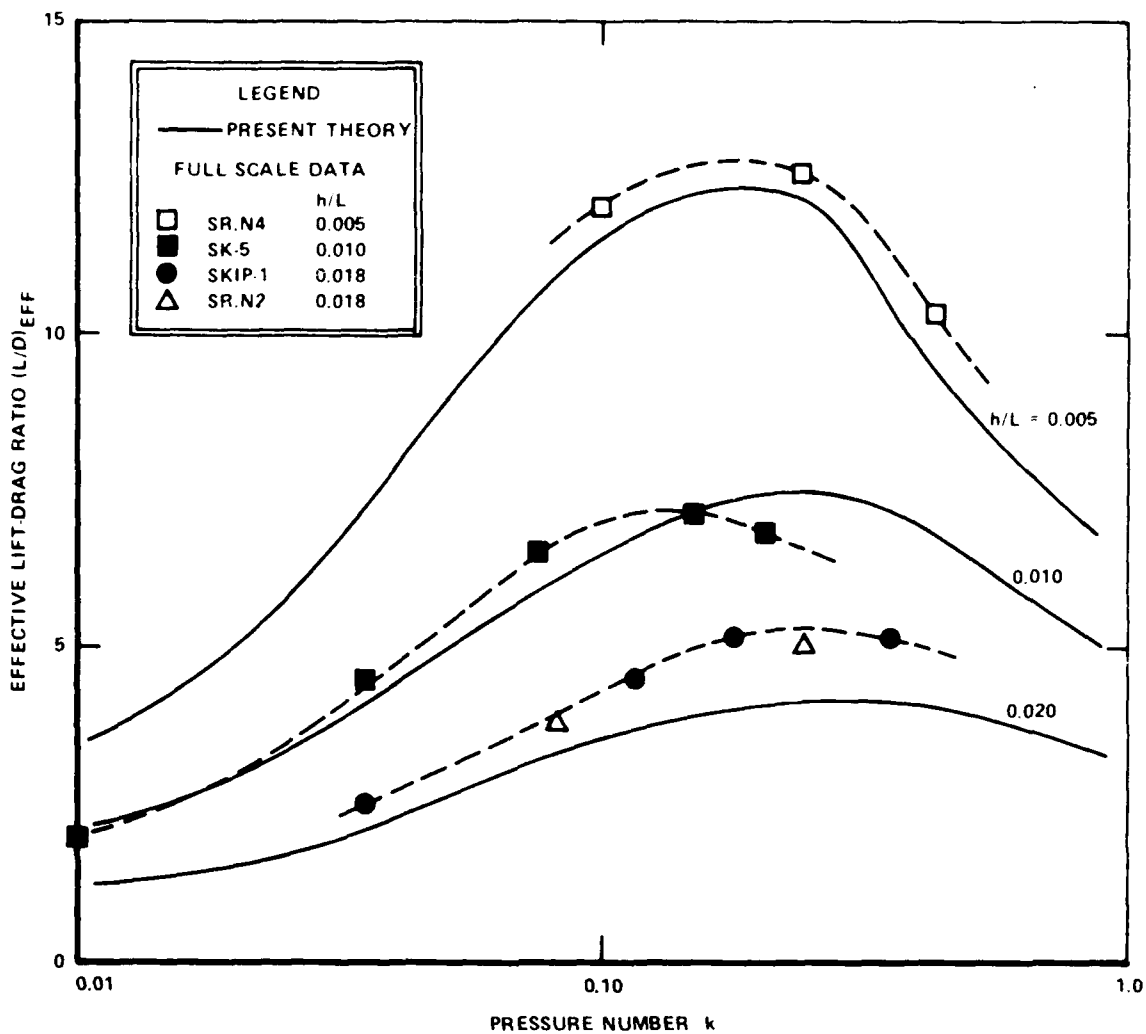


Figure 67 - Typical Effective Lift-to-Drag Ratio

and provide some insight of the significant parameters. For the "upper bound" case of operating in calm water in the trapped air cushion (TAC) mode (i.e., zero air gap) the maximum value of the lift-to-drag ratio is shown to be,

$$[L/D]_{TAC} = \frac{k}{C_{D_o} k + \kappa} \quad (99)$$

and occurs at a speed given by

$$k = \frac{\kappa}{C_{D_o}} = \frac{1.20}{C_{D_o} (L/B)^{1/2}} \cdot \frac{\rho}{\rho_w} \quad (100)$$

Typical values of C_{D_o} and length-to-beam ratio, give values of k in the range quoted. Expressed in terms of dimensional parameters, with all other parameters constant, the speed for the maximum lift-to-drag ratio varies with the square root of the cushion pressure. Figure 68 shows this result with two representative values of aerodynamic profile drag for amphibious air cushion craft together with several other craft. The above calculations apply to the amphibious or fully-skirted craft. Optimum cruise speeds occur at lower values of k for sidehull craft.

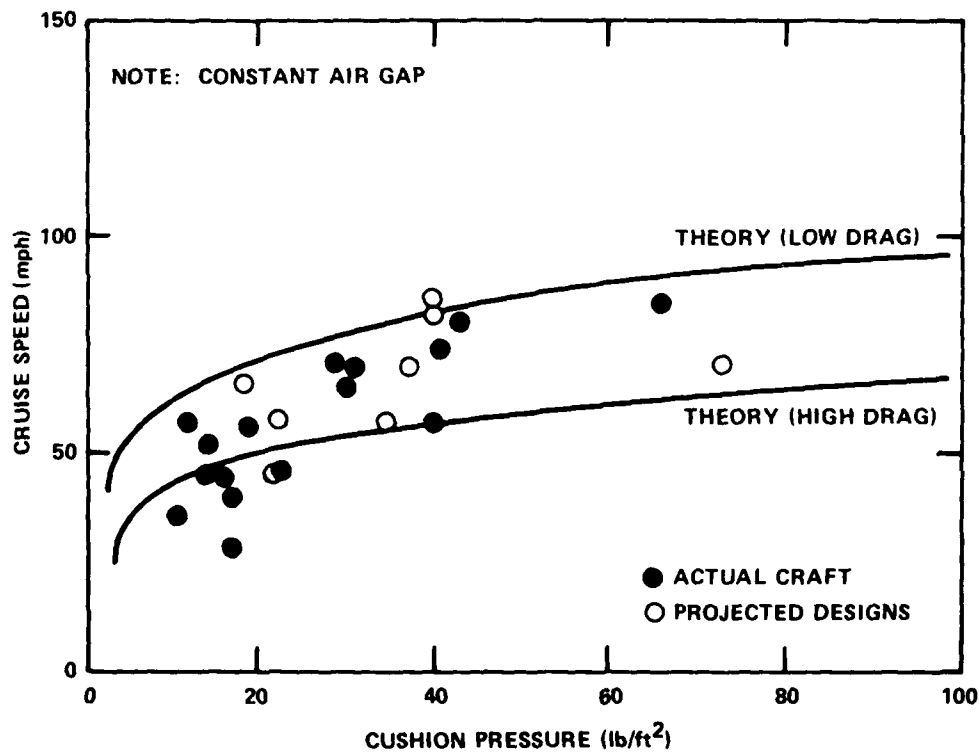


Figure 68 - Cruise Speed of Air Cushion Craft

CHAPTER IV

STABILITY AND RIDE QUALITY

The stability and ride quality characteristics of an air cushion craft have probably received more attention and been the result of more technical literature, published and unpublished, than the performance aspects considered in the previous chapter. Despite this more extensive study, however, it is still the most elusive in terms of understanding. The problems are more complex than simple analysis will allow, due, in part, to the nonlinearity of forces acting on the craft and the constantly changing geometry of its cushion system through the flexing of its skirts while traversing the (random) surface.

Like the aircraft or ship, the air cushion craft operates in six degrees of freedom but, due to its proximity to the surface, is restricted in its pitch and roll attitudes. The low friction characteristic of the cushion results in high yaw and sideslip angles in the case of the amphibious craft or ACV type when attempting maneuvers or operating in high winds.

The complex nature of aerodynamic and hydrodynamic forces acting on the craft occur, in various combinations, due to motion over the waves. The hydrodynamic forces occur in the ACV type through skirt contact, which deflects the skirts and results in a change in the aerodynamic and aerostatic forces in the cushion. This cross-coupling of forces is obviously strongly affected by the type of skirt design. For the sidehull or SES type of craft, additional hydrodynamic forces act on the craft from both hull and appendage motion through the water. The technology of hull forms at high Froude numbers, low cavitation numbers, and operating with asymmetric waterlines due to the cushion depression is still fairly new and is still under development. Despite this added complexity, there is the simplifying effect that the sidehulls in the water provide a positive lateral stability and allow a reasonable theory to be developed. The corresponding stability characteristics of the fully amphibious air cushion craft with its flexible skirt motions is still under development. Since the last summary was issued, some interesting insight is being obtained through both analysis and experiment on the stability characteristics of fully amphibious air cushion craft operating over land.⁷⁰ Some discussion can be found in this useful reference comparing the dynamic characteristics of an air cushion craft operating over land and over water.

This complexity does not mean that craft cannot be designed with known characteristics, however, because in the normal process of design, extensive model testing and computer simulation will give the required design information. This method is still used extensively on new designs to ensure stability and safety of operation. The published technical literature is replete with such important information.

All too frequently, however, the simulation, whether it be analog or digital, contains many constants that must be adjusted to bring the simulation results in line with experiment. Once reasonable agreement has been obtained with model experiment, then the scaling laws are applied to each term in the matrix equations of motion to determine the motion and stability of the full-scale craft. A particular problem that will be discussed in some detail pertains to the problem of predicting full-scale motions and stability characteristics from model experiments. A dominant force in the craft dynamics is the cushion pressure, which appears in the equations of motion in relationship to the absolute pressure in the atmosphere. This complicates the scaling process and the design of model experiments.

Provided the form of the air cushion craft does not change markedly from one design to another, this design method is satisfactory and, to date, good agreement is possible. One such example is the comparison of a simulation⁷⁰ of the acceleration history of an SK-5 during tests over known obstacles.⁷¹ Figure 69 illustrates the comparison, which is considered good in the present state-of-the-art.

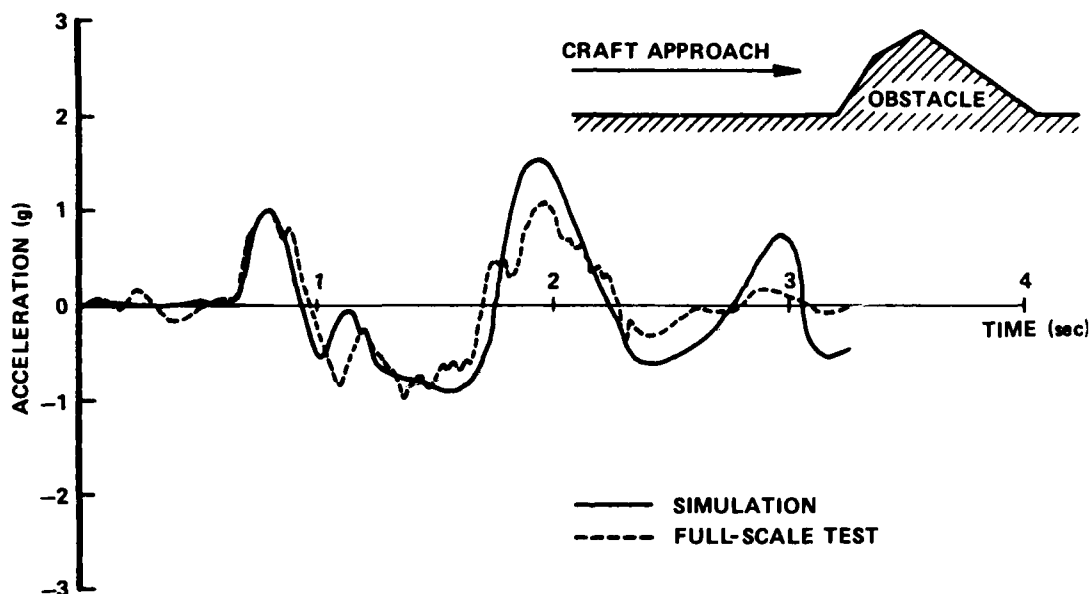


Figure 69 - Typical Simulation Comparison
with Test Data

The difficulty comes, of course, when a radical change in skirt design or craft geometry is to be considered. To date, this requires a prolonged development of model test and simulation to determine the result. It is encouraging to see that work is continuing in this area.⁷²

It would be too cumbersome and of little meaning to summarize the variations in stability characteristics here through such techniques. Instead, attention will be given to a few fundamental characteristics that are peculiar to air cushion craft stability and to those characteristics that are still in need of development. This chapter considers basic static and dynamic stability characteristics; the subject of control is discussed in Chapter V.

Because it is not the purpose of this summary to delve into the intricacies of solving the six-degrees-of-freedom equations of motion for air cushion craft, attention will be restricted to indicating some basic features of importance. The reader is referred to the references for the many papers tackling the general equations of motion.

STATIC STABILITY IN HEAVE

The static stability of the air cushion craft in heave is of basic importance to craft motion and illustrates the interrelationship between the aerodynamic characteristics of the cushion and the mechanical characteristics of the lift machinery. If, for the moment, three-dimensional effects, effects of crossflow in the cushion, and aerodynamic effects are ignored on the main body, then a simple analysis will yield the desired result. To illustrate the key parameters, the heave motion will be discussed first without consideration of the fan pressure-flow characteristics and second with such effects included. The particular scaling problem due to the compressibility of the cushion is then discussed separately.

Consider an air cushion craft heaving over a waveform that may be approximated by

$$h_w = A \cos (Kx - \omega t) \quad (101)$$

where the wave frequency in distance is $K = 2\pi/\lambda$ and in time is $\omega = 2\pi V/\lambda$, with the wavelength λ . In Equation (101), x is the distance along the craft and t is time; there should be no confusion with this notation with the peripheral jet thickness parameters in the previous chapter.

The waveform h_w , as it affects the craft motion, requires some discussion. For long waves, that is, where the wavelength is much greater than the craft length, the craft will tend to follow the surface and the full wave height will be felt (ignoring the coupling effect of the pitch motion). For short waves, however, the craft pitch motion is very small and the heave displacements are high frequency and consequently of small displacement. While the exact motion is complex and is affected by a combination of wave pumping and escape area variations, it is convenient to think of the motion as a simple piston heave motion, where the forcing

function or wave height is an "effective wave height" h_{we} constant along the craft length and modified from the actual wave height, depending on whether the craft is experiencing long or short waves. This effective wave height is defined by

$$h_{we} = \frac{1}{L} \int_0^L A \cos (Kx - \omega t) \quad (102)$$

Upon integration, the effective waveform is

$$h_{we} = A \left| \frac{\sin \frac{\pi L}{\lambda}}{\frac{\pi L}{\lambda}} \right| \cos (\phi - \omega t) \quad (103)$$

The effective wave amplitude is thus seen to be equal to the actual wave amplitude reduced by the function

$$F \left(\frac{L}{\lambda} \right) = \left| \frac{\sin \frac{\pi L}{\lambda}}{\frac{\pi L}{\lambda}} \right| \quad (104)$$

This function occurs frequently in the dynamic analysis of air cushion craft (as well as in wave pumping power as discussed in Chapter III) and is shown in Figure 70. It is suggested that damping and coupling effects

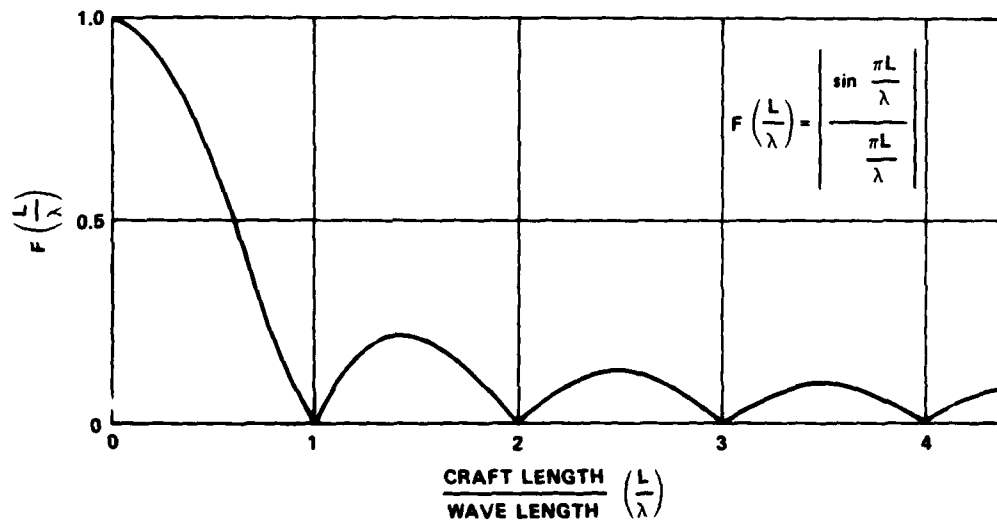


Figure 70 - Effective Wave Amplitude Function

between pitch and heave motion will "round out" the discontinuities at the integer values of L/λ in Figure 70. The effective waveform also incurs a phase shift $\phi = \pi L/\lambda$.

A simple first-order analysis⁷³ will yield, for small heave perturbations (H) about an equilibrium air gap (h), the following equation:

$$\frac{d^2 H}{dt^2} + 2\zeta\omega_n \frac{d}{dt} (H-h_w) + \omega_n^2 (H-h_w) = 0 \quad (105)$$

where ω_n is the natural frequency in heave and ζ is the damping ratio.

The damping is assumed to be the result of the cushion air exhausting beneath the jets in this simplified theory. Now, if a cushion stiffness is defined as

$$K_h = \frac{\partial L}{\partial h} = S \frac{\partial p_c}{\partial h} \quad (106)$$

then, from simple harmonic analysis, the natural frequency in Equation (105) is given by

$$\omega_n = \sqrt{\frac{K_h}{m}} = \sqrt{\frac{\partial L / \partial h \cdot g}{W}} \quad (107)$$

For the case of the peripheral jet, Elsley and Devereux³⁸ show

$$\frac{\partial L}{\partial h} = \frac{Sp_c}{h} \cdot \frac{2\pi}{e^{2\pi}-1} \quad (108)$$

for the general case, and

$$\frac{\partial L}{\partial h} = \frac{2Sp_c}{h} \left[1 - \frac{xe^{-x}}{1-e^{-2x}} \right] \quad (109)$$

for the case of constant cushion power. Elsley and Devereux suggest an average value of

$$\frac{\partial L}{\partial h} = \frac{Sp_c}{h} \quad (110)$$

Returning, however, to the general case, it has been found that data from small models heaving over water⁷⁴ and over hard waves⁷⁵ tend to collapse to a common nondimensional base through use of the normalizing wave amplitude function $F(L/\lambda)$ and the natural frequency given by Equations (107) and (108). Figure 71 shows this comparison of simple theory and small model tests.

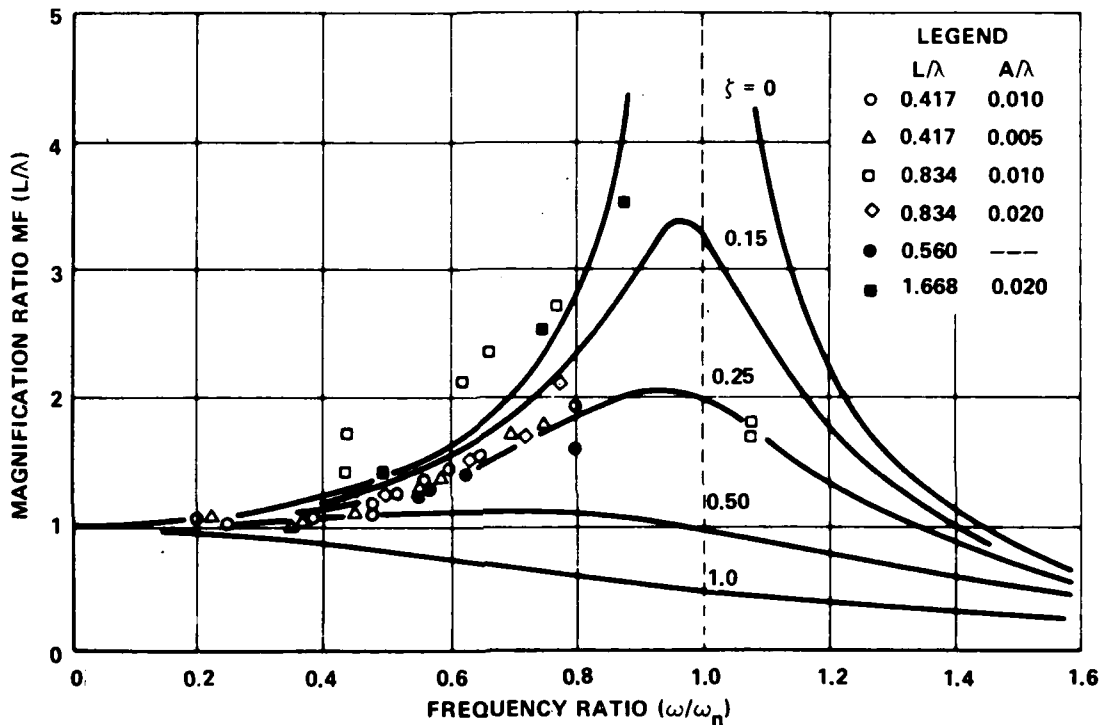


Figure 71 - Normalized Heave Response Over Waves

The simple theory solution to Equation (105) is

$$H(t) = M F(L/\lambda) A \cos (\phi - \omega t) \quad (111)$$

where the magnification ratio is

$$M = \frac{1}{\sqrt{\left[1 - \left(\frac{\omega}{\omega_n}\right)^2\right]^2 + \left[2\zeta \frac{\omega}{\omega_n}\right]^2}} \quad (112)$$

is the factor by which the static height change must be multiplied to give the amplitude of the heave motion in operation over waves.

It is seen from Figure 71 that, allowing for experimental error and oversimplification in the theory, the heave response does normalize by the nondimensional groupings given above. The data tend to cluster around the response curve where the damping ratio ζ given by

$$\zeta = \frac{\frac{\sqrt{gh}}{\frac{Ch}{S} \left(\frac{W}{S}\right)^{1/2}} \cdot \left(\frac{\rho}{2}\right)^{1/2} \cdot \frac{1}{2} \frac{x}{e^{2x-1}}} \quad (113)$$

and has the numerical value of $\zeta = 0.15$.

An illustration of how the damping and the coupling between pitch and heave motion distorts the simple results is shown in Figure 72 which also expresses the magnification ratio in the frequency domain rather than the time domain. Figure 72 shows the heave response amplitude operator defined as,

$$\text{Heave R.A.O.} = \left(\frac{H(t)}{A}\right)^2 \quad (114)$$

The experimental results and mathematical model apply to some early model work on the JEFF(A) amphibious assault landing craft.⁷⁶

However, such simplified treatments can lead to erroneous conclusions on full-scale craft. Later analyses⁷⁷ have taken into account the fan pressure-flow characteristics and cushion compressibility.

EFFECT OF FAN CHARACTERISTICS AND SCALING ON HEAVE RESPONSE

It is known that the fan characteristics affect the heave stability and ride quality of air cushion craft. The exact nature of the effect has

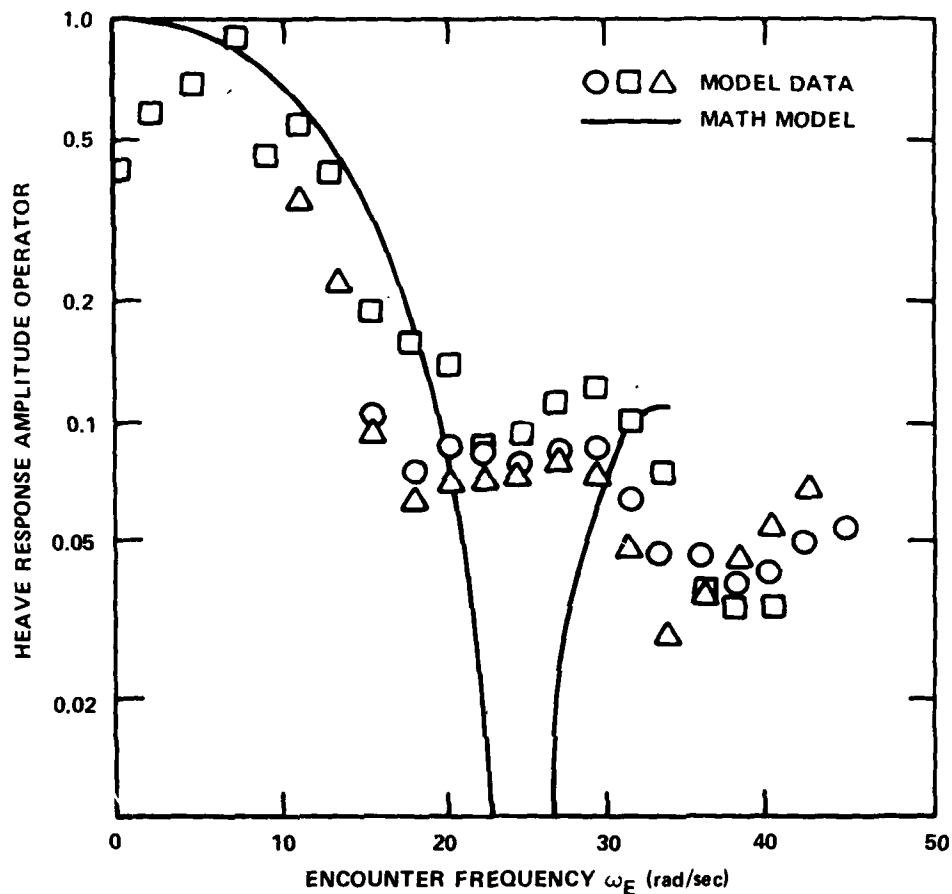


Figure 72 - Heave Response Amplitude Operator

not been well documented and is, in fact, difficult to determine quantitatively in most experiments, especially in the over-water case. Heaving over water in a dynamic motion induces variations in water depression, spray generation, and seal compliance. Some attempts have been made, however, to isolate some of the more obvious parameters for design guidance, and a summary is given here. For simplicity, consider the plenum case, which reflects the majority of today's aerostatic craft, and assume Figure 73 illustrates the essential geometry of the cushion and also the fan and cushion system characteristics.

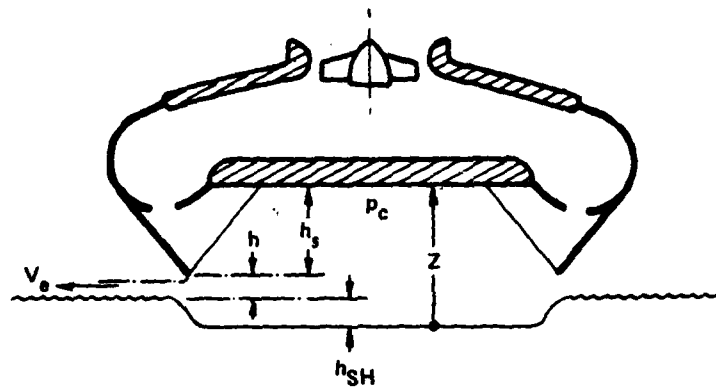
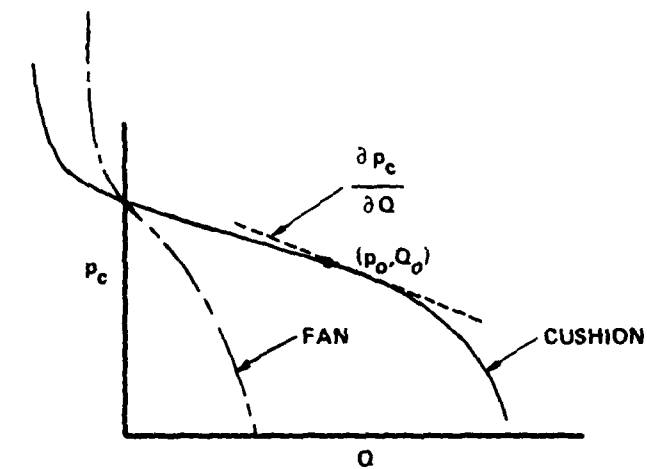


Figure 73 - Plenum Heaving Over Water

It is assumed that the cushion pressure can be written as

$$p_c = p_o + \frac{\partial p_c}{\partial Q} (Q - Q_o) \quad (115)$$

where p_o is the equilibrium value of the cushion pressure (W/S). The rate of change of cushion pressure with flow $\partial p_c / \partial Q$ is normally negative for static stability. It is important to note that the cushion slope $\partial p_c / \partial Q$ is normally less than the individual fan slope in the usual case of multiple fan installations in parallel operation, that is,

$$\frac{\partial p_c}{\partial Q} \approx \frac{\partial p_f}{\partial Q} \quad (116)$$

This is discussed further in Chapter VIII on lift fans where system losses and parallel installations are discussed.

The description of the geometry of the craft hovering over water is a little subjective. The shape of the water surface near the escaping air changes with cushion pressure and frequently induces spray which, if of sufficient magnitude, can invalidate the simple peripheral jet and plenum theories given in Chapter III. Everest and Hogben,⁵³ Kiedrzynski,⁷⁸ Mack and Yen,⁷⁹ and Hirsch,⁸⁰ among others, provided insight into the deformation and the effect of spray.

Breslin⁷⁷ pursued the analysis, however, making certain simplifying assumptions as to seal compliance, free-surface deflection, and cushion flow. In terms of the notation of this report, Breslin showed the following relationships.

The cushion stiffness is written as

$$\frac{\partial L}{\partial Z} = S \frac{\partial p_c}{\partial Z} \quad (117)$$

and the result can be written as

$$\frac{1}{\rho_w g} \cdot \frac{\partial p_c}{\partial Z} = \frac{\frac{CV_e}{\rho_w g} \frac{\partial p_c}{\partial Q}}{1 - \frac{CV_e}{\rho_w g} \frac{\partial p_c}{\partial Q} (1 + \rho_w g K_s)} \quad (118)$$

where K_s is the seal spring compliance. Breslin notes from this simplified analysis that the cushion stiffness is dependent on the dimensionless groupings

$$\frac{CV_e}{\rho_w g} \cdot \frac{\partial p_c}{\partial Q} \text{ and } \rho_w g K_s$$

and, in particular, is independent of the value of the absolute pressure p_A . For simplicity, consider the case of zero seal compliance; then Equation (118) can be written in more easily recognizable form (after some algebraic manipulation):

$$\frac{\partial p_c}{\partial z} = \frac{\frac{Q}{h} \frac{\partial p_c}{\partial Q}}{1 + \frac{Q}{p_c} \frac{\partial p_c}{\partial Q}} \quad (119)$$

whence

$$\omega_n = \sqrt{\frac{g}{h}} \cdot \sqrt{\frac{\frac{Q}{p_c} \frac{\partial p_c}{\partial Q}}{1 + \frac{Q}{p_c} \frac{\partial p_c}{\partial Q}}} \quad (120)$$

which may be compared with the earlier results for air cushion craft heave motion (Equation (107)). In model experiments, the cushion slope differs from the full-scale craft slope by the (scale factor)^{3/2}, that is, the model must have a stiffer fan slope to properly simulate full-scale heave motion.

Unfortunately, there are at least two important corrections to Equation (120) that limit its usefulness in full-scale craft design and hamper interpretation of model test results. These relate to the influence of the absolute pressure and to the compressibility of the cushion. Breslin⁷⁷ considered these effects. The analysis is fairly complex and will not be reproduced here other than to describe the phenomena that Breslin analyzed.

If one considers an air cushion craft to be forced in small vertical heaving motions while proceeding over calm water at constant forward speed, motions will be induced in the water which will determine, in part, the cushion pressure fluctuations. By analysis, Breslin shows that the pressure amplitude is now a direct function of the parameter

$$\frac{p_o}{1/2 \rho V^2} \quad (121)$$

where

$$p_o = p_A + \frac{W}{S} \quad (122)$$

and p_A is the absolute pressure of the air. Then, if a craft is geometrically scaled and tested at the Froude scaled speed over geometrically scaled obstacles, the resulting model motion and acceleration will not necessarily scale by simple Froude scaling relationships. This is because the dynamic response characteristics are affected by the lack of proper pressure scaling that is usually applied; that is, in Equation (122), the atmospheric pressure p_A is not scaled and only the gage pressure values (W/S) in the cushion, fan, and skirt system are scaled. This affects the overall pressure system so that the craft frequency responses are not scalable in accordance with Froude scaling.

A second correction to the simplified analysis result is the compressibility of the air and the relative size of the cushion. With large cushion volumes, the compressibility effects in the cushion can no longer be ignored and the gas laws must be used to determine pressure-flow relationships in the cushion. Both isothermal and adiabatic laws have been used in the literature but, specifically for an adiabatic process, one can write

$$p_c + p_A = \frac{\text{constant}}{\rho^\gamma} \quad (123)$$

where γ is the ratio of specific heat (1.4).

Shenfil⁸¹ analyzed the case of an air cushion craft heaving over a hard ground (no surface deformation) and showed that the characteristic equation in heave was given by

$$\frac{C_c p_c}{Q} s^3 + \frac{\frac{\partial p_c}{\partial Q} - 2 \frac{p_c}{Q}}{2 \frac{\partial p_c}{\partial Q}} s^2 + \frac{gS}{Q} \cdot s + \frac{g}{h} = 0 \quad (124)$$

where p_c and Q are the equilibrium values and (lower case) s is the Laplace transform operator.

The effect of the compressibility appears in the cubic term where a cushion capacitance C_c is defined as

$$C_c = \frac{V_c}{\gamma (p_c + p_A)} \quad (125)$$

which shows the effect of the cushion volume V_c (assumed as the mean value during motion).

For the case $C_c \rightarrow 0$, compressibility effects are ignored. The Shenfil results then reduce to a quadratic form of the heave equation, and the damping and natural frequency is given by

$$\zeta = \frac{S}{Q} \sqrt{gh} \frac{\sqrt{\frac{Q}{p_c} \frac{\partial p_c}{\partial Q}}}{\sqrt{1 + \frac{Q}{p_c} \frac{\partial p_c}{\partial Q}}} \quad (126)$$

$$\omega_n = \sqrt{\frac{g}{h}} \cdot \frac{\sqrt{\frac{Q}{p_c} \frac{\partial p_c}{\partial Q}}}{\sqrt{1 + \frac{Q}{p_c} \frac{\partial p_c}{\partial Q}}} \quad (127)$$

which agrees with Breslin's result for the case of zero seal compliance.

A comparison is made in Table 4 between the third order and second order equation results that show the effect of including or ignoring the compressibility effects when large cushion volumes are involved. The values apply to a typical large air cushion craft of the type currently under construction for the Amphibious Assault Landing Craft (AALC) mission.

Comparison between the two results indicates that, for the full-scale craft, the damping ratios are of opposite sign, indicating that ignoring cushion compressibility would predict a stable craft while including such effects would predict an unstable craft. The natural frequencies, however, are approximately comparable.

On the other hand, in model scale, the damping ratio and natural frequency are approximately comparable. This is a potentially dangerous situation from a designer's viewpoint in that, as the model experiment agrees with the simple theory, it would be assumed that the full-scale craft was well explained. The effect of including cushion compressibility has precluded simple Froude scaling of model test results.

TABLE 4 - EFFECT OF CUSHION COMPRESSIBILITY

Parameter		Full Scale	Model Scale ($\lambda = 7/100$)
Shutoff Pressure		252 lb/ft ²	17.64 lb/ft ²
p_c		100 lb/ft ²	7 lb/ft ²
Q		12,000 ft ³ /sec	15.82 ft ³ /sec
S		3,800 ft ²	18.62 ft ²
h		0.26 ft	0.018 ft
C_c		15.11 ft ⁵ /lb	7.574×10^{-3} ft ⁵ /lb
Ignoring Compressibility	ζ	0.49	0.49
	ω_n	12.2 rad/sec	46.2 rad/sec
Including Compressibility	ζ	-0.13	0.42
	ω_n	10.3	50.8

A further insight into this effect may be seen from the comparison of model test results and simulation results by Lavis et al.⁷⁶ Figure 74, taken from Reference 76 compares model data with the predicted result for the model in the upper set of curves and shows good agreement. Figure 74 also shows the comparison of results when scaled to full scale. The effect is masked to some extent by the different sea spectra considered in each case, but the results tend to confirm the analysis given earlier.

Although the particular issue of the heave response has consumed some space here, it is felt that it has illustrated two important points:

1. Although the nature of the flow phenomena in and around the cushion incurs complicated treatment to describe analytically, prudent use of the different scaling laws, applied to model data allow the designer to proceed.
2. Controlled experiments of both model scale and full scale would go a long way to replacing assumptions with proven fact.

HEAVE STABILITY CRITERIA

For the majority of operational air cushion craft, the pitch and roll stability characteristics can be ascertained by considering the craft cushion as composed of several heave compartments. Hence, heave stability criteria have fundamental application to the craft stability in general.

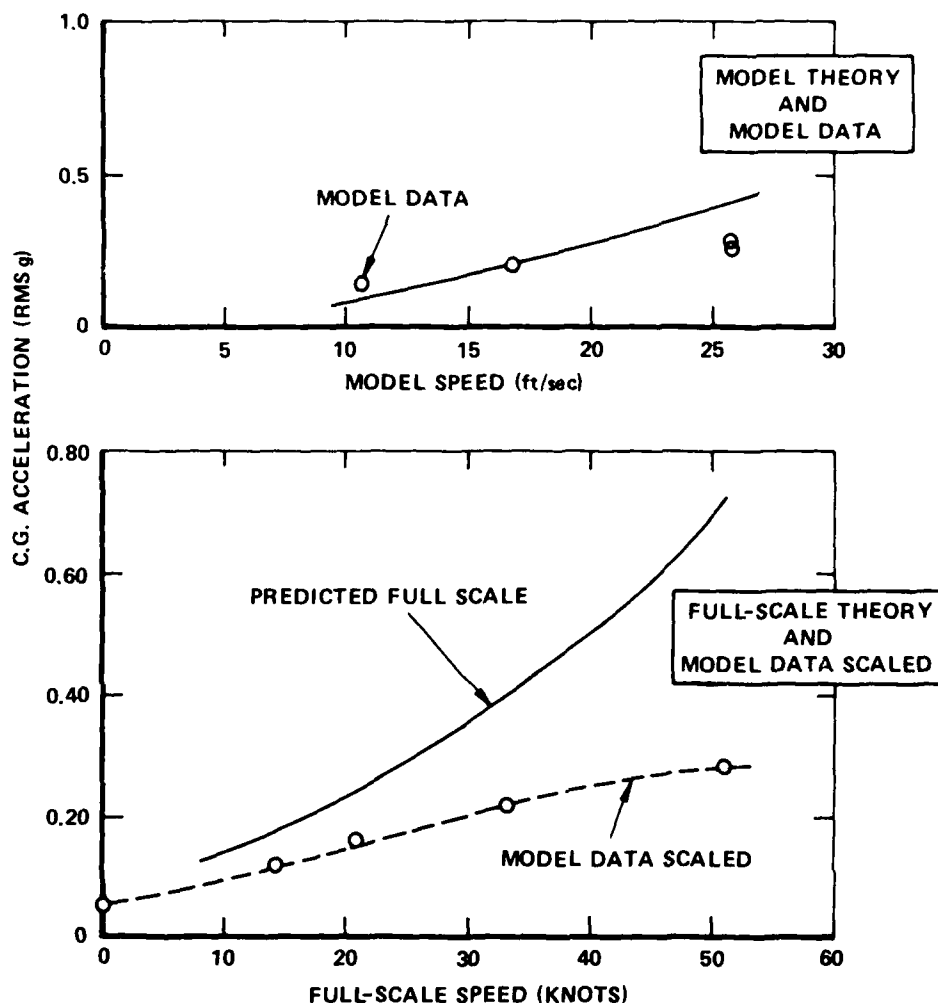


Figure 74 - Effect of Scaling on Model Response

Within the limitations given earlier, the condition for static stability in heave can be obtained from the characteristic equation and can be shown to be, for the general case of $C_c \neq 0$,

$$\frac{Sh}{2p_c C_c} \left[1 - \frac{2p_c/Q}{\partial p_c / \partial Q} \right] > 1 \quad (128)$$

The above equation can be written if the assumption is made that the cushion volume can be assumed to be the product of the cushion area and the skirt height, that is,

$$V_c = Sh_s \quad (129)$$

and then the heave stability criteria can be written as

$$\frac{1}{2} \left(\frac{h}{h_s} \right) \left(1 + \frac{p_A}{p_c} \right) \left[1 - \frac{2p_c/Q}{\partial p_c / \partial Q} \right] > 1 \quad (130)$$

so that, in general,

1. Increasing air gap height (i.e., cushion flow Q) improves dynamic stability in heave,
2. Decreasing skirt height improves dynamic stability in heave,
3. Lower cushion pressures improve heave stability,
4. Higher flows improve heave stability, and
5. Higher cushion (fan) slopes improve heave stability.

These results have all tended to agree with full-scale craft operational experience and, accepting the fact that more detailed analyses are worthwhile, it is felt that the air cushion craft designer can provide the desired heave stability characteristics in his design at the drawing board stage, but that it requires a careful integration of fan, cushion, and craft characteristics.

PITCH AND ROLL STABILITY

The means by which pitch and roll stability are given to air cushion craft depends directly on the skirt design philosophy employed in the craft design. Recognizing that there are many variations on a theme, the currently operational craft employ some form of three basic methods. Some newer designs by BHC and Bell involve combinations of these basic methods. They are:

1. Compartmentation Method

This method consists essentially of compartmentation of the cushion by either downward-directed air jets or inflated flexible skirt keels. This method is employed on all current British Hovercraft Corporation and Bell amphibious craft.

2. Center of Pressure Shift Method

This method, developed by Hovercraft Development Limited (HDL),* employs skirts shaped so as to cause outward movement of cushion area of the downgoing side of the craft. The incurred center of pressure (C.P.) shift, with area change, gives the desired restoring moment. This method can eliminate the need for compartmentation.

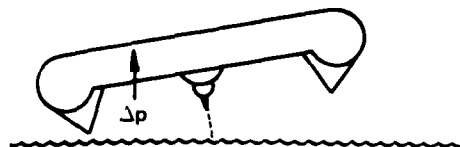
3. "Pressure-Rise" Method

The multicushion designs developed by Bertin et Cie and SEDAM in France obtain pitch and roll stability from the basic stiffness in heave of the individual "jupes" or conical cushions.

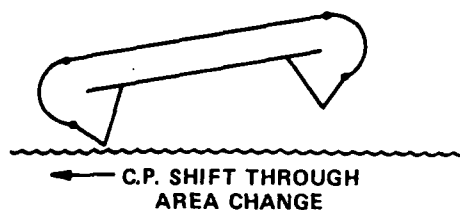
*The original company was established to develop Sir Christopher Cockerell's work and is now a holding company of the basic patents.

Generally speaking, the British Hovercraft Corporation and Bell craft skirts employ a combination of the compartmentation and C.P. shift methods while Aerojet's pericell skirt is a combination of the pressure-rise and C.P. shift methods. Figure 75 illustrates the essential elements of the stabilizing features of each of these basic methods. The specific details and variations of the basic skirt methods are discussed more fully in Chapter VI. Attention will be restricted here to the overall stability characteristics and how they affect the craft as a whole.

COMPARTMENTATION



C.P. SHIFT



PRESSURE RISE

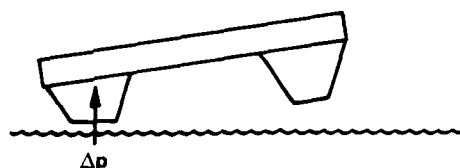


Figure 75 - Basic Methods of Cushion Stability

In the case of the sidehull craft using planing seals (see Chapter VI), additional restoring forces and moments join the hydrodynamic forces acting on the seals for pitch stability and on the sidehulls for roll stability. This particular case is not being treated here for the lack of sufficient data base to provide any "trend" information; accordingly, the remainder of the discussion is restricted to the amphibious form using one of the mechanisms shown in Figure 75.

While admittedly not too rigorous, the following simple derivation of pitch and roll stability captures the essential elements and fits reasonably well with experiment provided the assumptions and constraints are recognized. The upper "compartmentation" diagram in Figure 75 is used as

the model for the derivation. The compartmentation divider of the cushion is shown ideally as a dotted line. In actual craft it has appeared as an inflated bag (also shown in Figure 75) or as an air jet fed by the lift fan system dividing the cushion into pressure "pad" compartments. Nevertheless, assume by whatever means that the divider isolates two pressure pads of values p_{c_1} and p_{c_2} such that, to first order,

$$p_{c_1} = p_c + \frac{K_h B \phi}{2S} \quad (131)$$

and

$$p_{c_2} = p_c - \frac{K_h B \phi}{2S} \quad (132)$$

where K_h = cushion stiffness in heave given by Equation (106)

B = craft cushion beam

ϕ = roll angle

Note: If the analysis were being done in the pitch mode, the corresponding length and angle would be the craft cushion length (L) and pitch angle (α).

The rolling moment is then simply,

$$M_\phi = \frac{B}{2} \cdot L \cdot \frac{B}{4} \left[\left(p_c + \frac{K_h B \phi / 2}{S} \right) - \left(p_c - \frac{K_h B \phi / 2}{S} \right) \right] \quad (133)$$

Substituting the value of the heave stiffness (K_h) from Equation (106) into this equation for the rolling moment gives the reduced form,

$$M_\phi = - \frac{LB}{8} \cdot B p_c \cdot \frac{B \phi}{h} \quad (134)$$

It is important to note that (h) is the air gap beneath the skirt and not the cushion height (h_c).

In air cushion craft work it is usual to express the moments in a nondimensional form where (in this case) the rolling moment M_ϕ would be normalized by the craft weight W ($= p_c LB$) times the craft beam B such that

$$\frac{M_\phi}{WB} = - \frac{B\phi}{8h} \quad (135)$$

and, since this represents a center of pressure (C.P.) shift, then the C.P. shift per degree is given by,

$$\text{C.P. shift per degree, } K_\phi = - \frac{B}{8h} \quad (136)$$

This approximate expression, at best, illustrates some of the basic craft characteristics and, if it is rearranged slightly to show the effect of skirt height (h_s), assumed to be synonymous with cushion height h_c ; then,

$$\frac{h_s}{B} = \frac{h_s/L}{h/L} \cdot \frac{1}{8 K_\phi} \quad (137)$$

which expresses the craft roll stiffness in terms of the overall craft parameters of skirt height (h_s) and beam (B). The values of the roll stiffness (K_ϕ) in terms of C.P. shift per degree vary widely and Trillo⁴⁴ shows typical curves of British and French craft roll stiffness that range from 0.20 to 2.0 depending on the angle of roll and skirt design. Figure 76 shows some of this data. Similar values have been applied in the U.S. designed craft. Values of skirt height (h_s) and daylight air gap (h) from craft discussed heretofore, for example, show that values of skirt height to beam (h_s/B) of between 0.10 to 0.20 give good roll stiffness for today's aerostatic air cushion craft. Here, "good" must be interpreted as reflecting handling qualities with today's skirt designs and should not be regarded as limiting. For example, some of the skirt development pursued during the Arctic Surface Effect Vehicle (SEV) Program⁶³ provided data whereby skirt systems could be provided with h_s/B values greater than 0.20. The current state-of-the-art, however, is more correctly represented by $0.10 < h_s/B < 0.20$ as shown on Figure 77 where the skirt height (h_s) is shown as a function of craft size or weight (W).

The roll stability criterion developed earlier has been superimposed on Figure 77 in the form of "state-of-the-art" boundaries. Plots such as Figure 77 are helpful in determining such basic parameters as terrain or wave clearance of a given craft. It is normally assumed that an air cushion craft can clear waves in normal operation with wave heights approximately 10 to 20 percent lower than cushion depth. With present

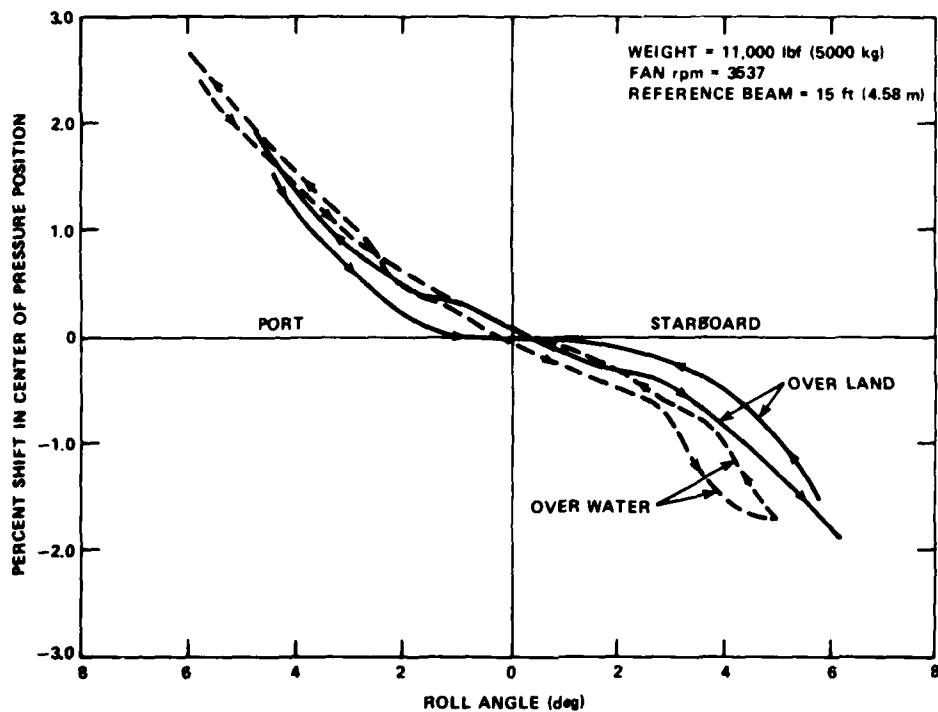


Figure 76a - Static Stability for HD.2 Hovercraft

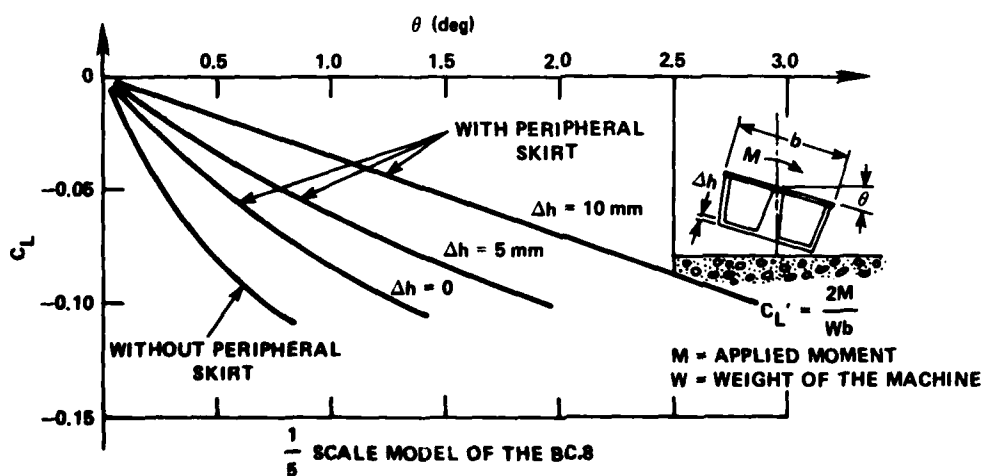


Figure 76b - Static Stability for BC.8 Hovercraft Model

Figure 76 - Typical Roll Stability Curves

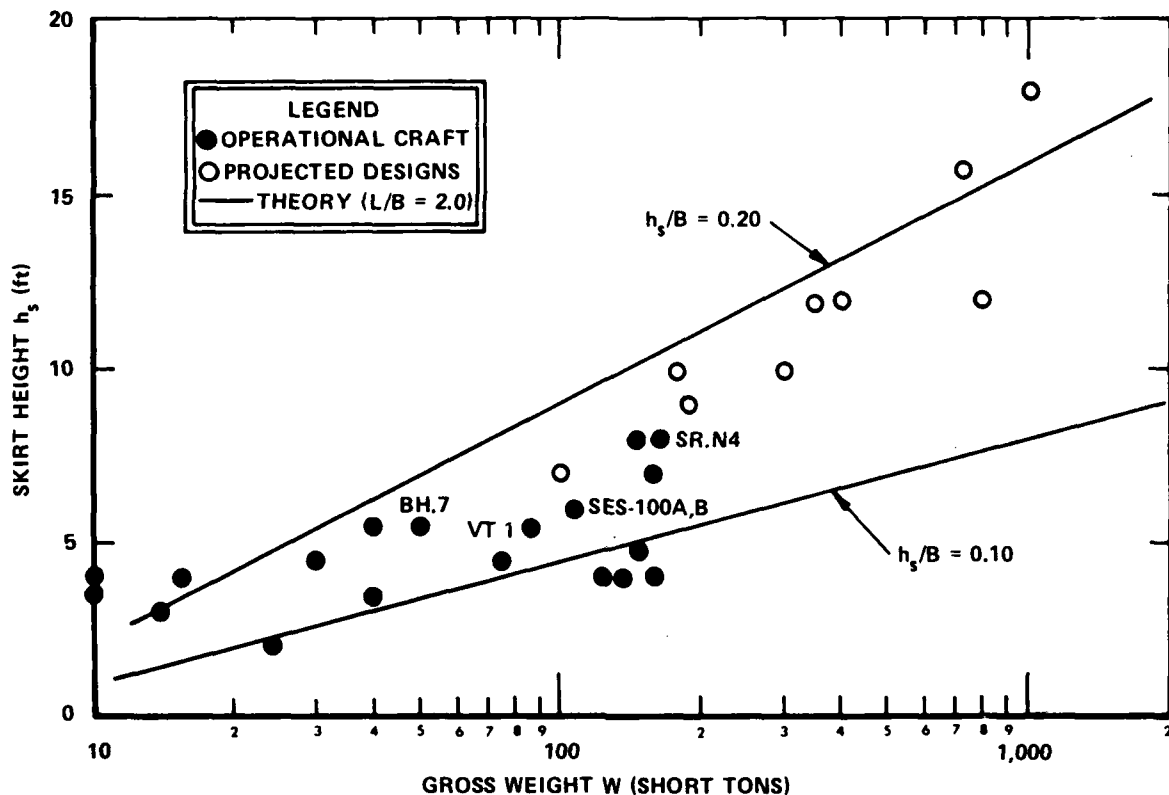


Figure 77 - Skirt Height of Air Cushion Craft

skirt designs, the skirt heights given by Figure 77 have proven, in practice, to give good roll stability and handling qualities. This is a relatively simple treatment for assuring adequate stiffness in roll to prevent capsizing and it is noticed that it is still being used as a guideline in skirt height and beam selection.⁸² Experience has shown, however, that in a practical skirt design, small changes in geometry or pressure ratio across bags and fingers can make significant differences in the pitch and roll characteristics and careful experimentation is required for any particular design.

PLOW-IN

The plow-in is an unstable characteristic that can and has occurred on both amphibious and sidehull forms of air cushion craft. Incidents of pitch instability occurred in such amphibious craft as the SR.N5, SKMR-1, CC-5, and in such sidehull craft as the Aqua-GEM, XR-1, and the SES-100A and SES-100B. Some of these craft have capsized, some plowed-in, and some have experienced a local instability in pitch, that was not necessarily

dangerous. Not all the incidents have occurred for the same reason, but a sufficient number of incidents occurred in the last 15 years of craft development, so that the subject has resulted in significant research to avoid the potentially dangerous plow-in. It is now a fairly well understood phenomena and can be avoided by operational procedures. Over the years, certain design modifications have also been incorporated in skirt design to either eliminate or minimize its effect.

In 1967, Crago⁸³ of British Hovercraft Corporation provided an indepth analysis of plow-in as it related to the SR.N1, SR.N5, and SR.N6. A plow-in occurs when the skirt at the bow of the craft contacts the water because the craft is operating at an excessive nose-down trim. The hydrodynamic drag produced by the skirt contact is usually sufficient to maintain the condition, and the craft gradually decelerates until either corrective action is taken by the operator or the craft comes to rest in the water, or, as frequently happens due to the irregularity of the sea surface, the wave contact is broken. The encounter of plow-in is more dangerous if the design is such that directional control cannot be retained, usually at higher yaw angles and speeds. In which case, during the nose-down maneuver when the skirt at the stern of the craft tends to break away from the water surface, even greater yaw angles tend to develop, and the craft is in danger of going broadside on and eventually capsizing. This can be greatly diminished by hull shaping.

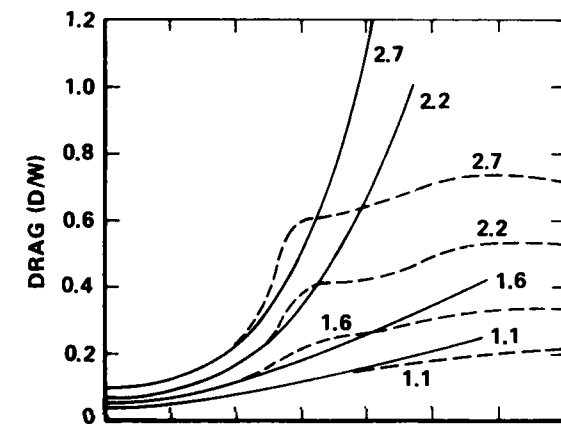
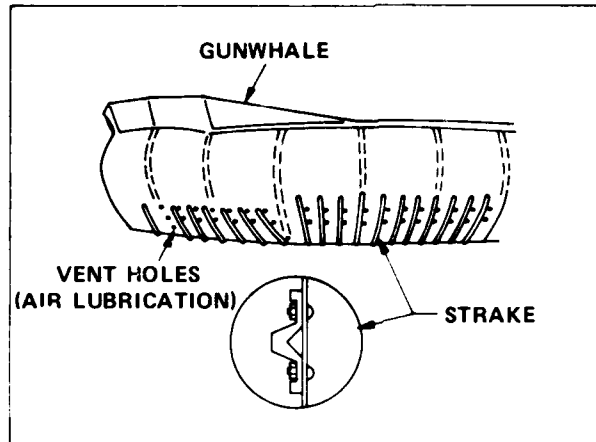
Early solutions to the problem after the rather dramatic plow-in incidents by an SR.N5 in Norway in April 1965 and in San Francisco Bay in May 1965 were to modify the skirt designs. These modifications consisted of adding outside strakes and lubrication or vent holes in the lower region of the skirt (see the upper sketch in Figure 78). The intent here was to stop water from attaching to the skirts and causing the high drag in bow-down maneuvers.

Crago reported⁸³ the results of model tests conducted to show the effect of this lubrication of the skirts. Figure 78 (middle and lower diagrams) includes the drag and moment measurements from these tests that show the significant reduction in both drag and moment and, therefore, less tendency to plow-in as a result of this lubrication. These modifications were made to both the British SR.N5 and those operated by Bell in 1965.

Subsequent skirt designs incorporated fingers and eliminated the need for these lubrication holes and strakes, but speed and yaw angle boundaries as in Figure 79 for the SR.N5 are still imposed on all currently operational air cushion craft.

Additional experience was gained during trials of both the SES-100A and SES-100B relative to plow-in. In the case of the SES-100A, the prevention of this instability required a change in bow seal design. In the case of the SES-100B, it was a local instability termed "pitch click" associated with the particular combination of sidehull hydrodynamic characteristics and seal characteristics at low positive and negative angles of attack.

The original bow seal design on the SES-100A resembled the planing ski type discussed earlier, except that it was fabricated from flexible



NOTES:

1. NUMBERS ON CURVES ARE FROUDE NUMBERS

2. YAW ANGLE = 0 deg

— NO AIR LUBRICATION

- - - WITH AIR LUBRICATION

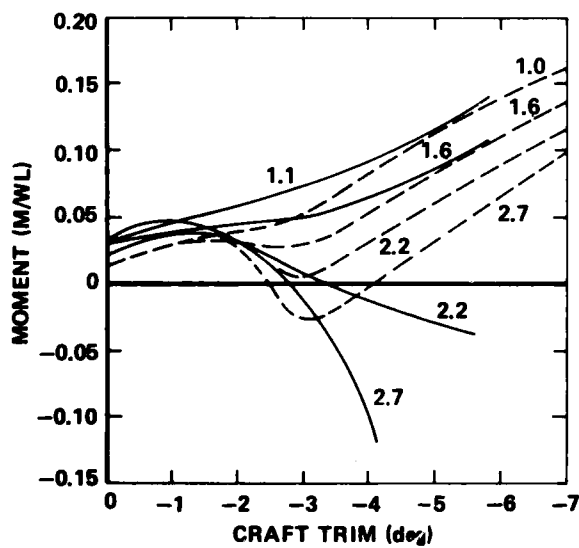


Figure 78 - Early Results on Flow-In Solution

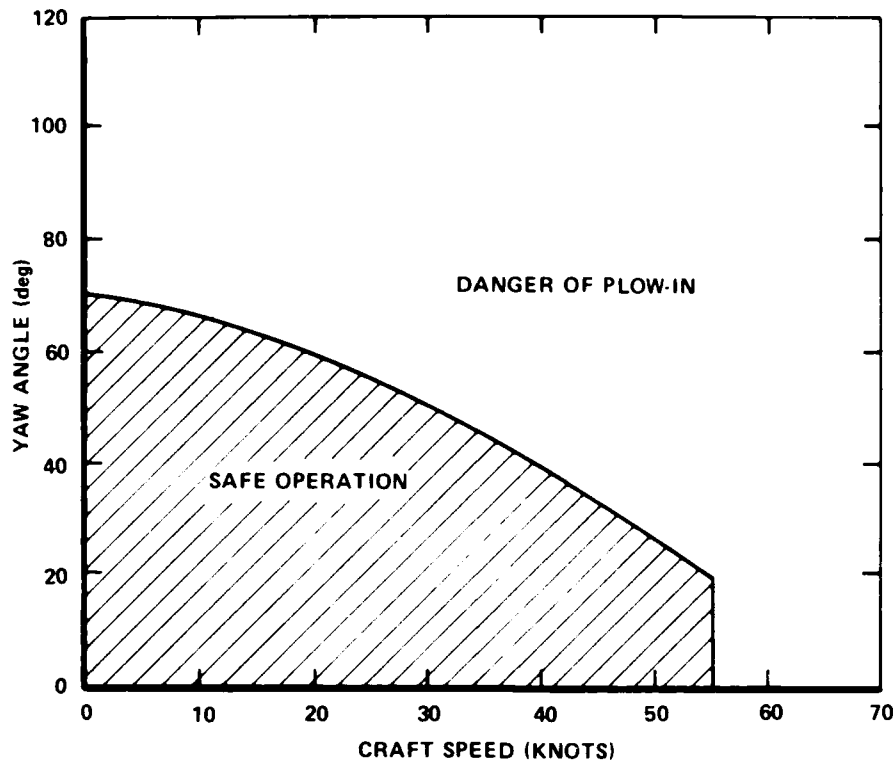


Figure 79 - SR.N5 Speed-Yaw Boundary

material (rubber-coated nylon). There were two contributing causes for the plow-in events as a result of this particular design. The first was due to the large unbroken area that the seal presented to the water surface, such that any wetting rapidly increased due to surface adhesion. The second contributing cause appeared to be due to a drop in cushion pressure in the forward cushion area. This effect was suspected to be caused by momentum exchange between the water and the air incurred by spray generation inside the cushion from the trailing edge of the bow seal. Figure 80 shows both the diagrammatic bow seal and spray generation and the record of the pressure drop during one of the events. It is informative to describe such an event.

The inception of the particular event shown occurred while the craft was traveling at approximately 45 knots in calm water. The craft was trimmed level with only a slight pitch oscillation of 0.10 Hz. Instrumentation showed a slight negative longitudinal pressure gradient (lower pressure in the forward area) of 4 percent. All stability appendages were clear of the water, which was relatively calm. The plow-in occurred after

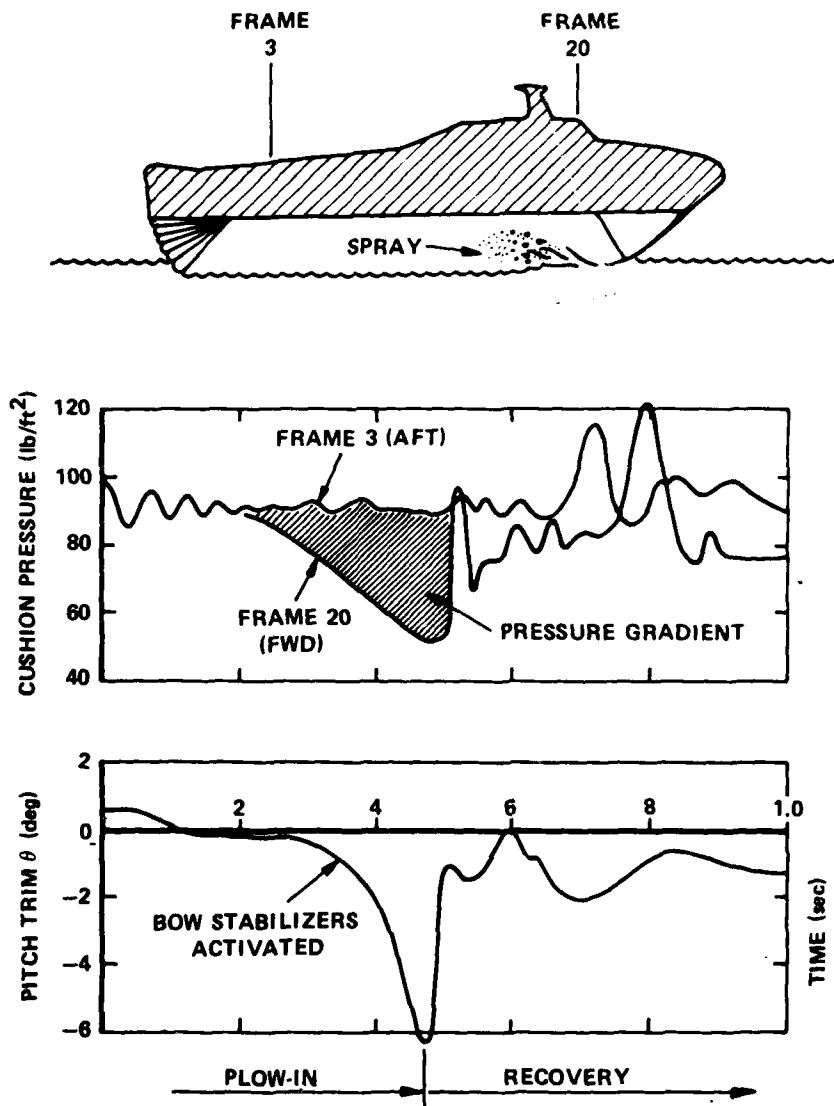


Figure 80 - SES-100A Plow-In with Early Planing Bow Seal

the craft was being throttled back from full-cushion operation to partial-cushion operation in preparation to stop which presented a nose down moment to the craft. The bow and stern seals were being raised gradually to settle into the water. As can be seen from the traces shown in Figure 80, the cushion pressure in the aft area (Frame 3) remained relatively constant throughout the event. The cushion pressure in the forward part

of the cushion (Frame 20) rapidly fell off from the average value of 98 lb/ft² to approximately 50 lb/ft², generating a pressure gradient illustrated by the shaded area in Figure 80. Corrective action was taken by lowering the bow stabilizers (see sketch on Figure 60) after the craft had pitched down 2 deg. The craft stabilized momentarily and then continued to pitch down (plow-in) to -6 deg over a period of 4 to 5 sec. The craft then recovered and the engines were shut down. The cushion flow remained constant until the craft was at the -2 deg level and then increased to 5900 ft³/sec throughout the plow-in.

It is noted from the records that the pressure gradient started well before the pitch-down occurred and overpowered the stabilizers. The craft was not damaged in this or subsequent similar plow-in events.

In analogy with the recorded plow-ins of such craft as the SR.N5, it could be argued that some form of lubrication or other means of breaking up the water contact would have been beneficial. It was not clear, however, that the form of the lower edges with nylon spring supports was not contributing to both adhesion and lower edge flagellation and spray generation. Consequently, a skirt design shown diagrammatically and photographically in Figure 81 was employed in the fall of 1973. This included three essential features to combat plow-in: (a) a low angle (approximately 20 deg) of the middle set of bow skirt members to invoke rapid cushion area increase during nose-down pitch, (b) high tensions in the skirt members again due to the low angle to combat high drag of any water contact, and (c) cones of the Bertin fashion to increase local heave stiffness and combat pitch-down moments. No further incidents of plow-in occurred on the SES-100A because of the modification in seal design.

As part of the continuing development of the stability characteristics of air cushion craft and the surface effect ship (SES) in particular, further modifications have been made to the SES-100A in the period 1975 to 1978. A return has been made to the planing bow seal (see Chapter VI) but of an improved design. The entire bow, forward of the deckhouse, has been replaced with a new section comprising wider sidehulls with built-in dead-rise (replacing the outrigger type stabilizers shown in Figure 60) and a so-called 2-D (two-dimensional) planing bow seal. Although no details pertaining to the stability characteristics of this new combination sidehull and bow seal redesign are available at this time it is reported to be operating satisfactorily in trials. Figure 82 shows the current modified SES-100A under test at the U.S. Navy Test Facility at Patuxent River.

Other modes of stability such as the pitch-yaw mode and pitch-heave mode are amenable to conventional means of stability analysis and are not discussed here. There are several texts published on the stability characteristics in both time domain and frequency domain treatments. While the nonlinearities in the experienced forces limit the validity of linearized treatments, there appear to be few unknowns in the characteristics of air cushion craft.

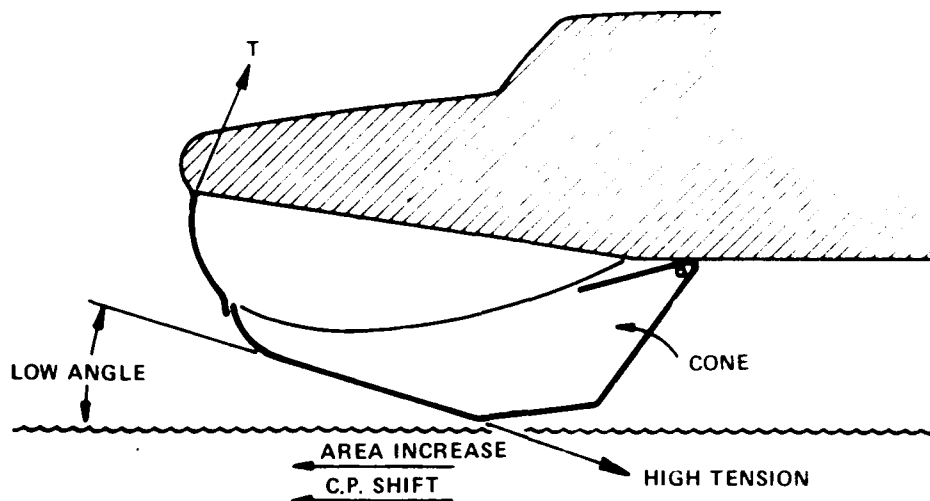


Figure 81 - SES-100A Plow-In Solution

RIDE QUALITY

One of the more elusive subjects in the design of air cushion craft (both amphibious and nonamphibious) is the subject of ride quality. There is the problem of knowing how to design a craft to meet a given ride quality criteria and the problem of determining what form of ride quality



Figure 82 - Modified SES-100A with Planing
Seal and Thick Sidehulls

criteria should be used. There is considerable debate and mountainous literature published seeking better understanding on both these aspects of ride quality. Unfortunately, to add to the woes of the designer, there is no uniform agreement on how to describe the sea conditions in which the craft is to operate. The problem of understanding ride quality is not unique to the air cushion craft and national committees such as those within NASA and DOT diligently work on the general subject of ride quality to place it on a more rational basis for design purposes.^{84,85}

In the case of the air cushion craft the motion in a seaway is influenced strongly by the pressurized air cushion which isolates the main body from the waves such that it is not constrained to follow the irregular surface of the sea. In this sense, the cushion acts much like an automobile suspension as it passes over a rough road. The type of motion varies depending on the magnitude of the roughness of the sea, character (random or regular) of the sea, speed of the vehicle, direction and frequency of encounter with the sea, and other physical and environmental characteristics. Some indication of the degree of severity of motion (magnitude of heave acceleration) was seen in Figure 71. At low encounter frequencies, the craft, which tends to follow the waves, will be resonant at some particular encounter frequency. The craft will finally become supercritical, i.e., motions become less as sea roughness increases, at high frequencies of encounter.

Although there is much work yet to be done on ride quality, sufficient insights now are being gained so that some basic characteristics can be presented.

Some Fundamental Relationships

One of the fundamental issues concerning ride quality is defining it and isolating the key parameters. Clearly, ride quality is concerned with determining the effects on the craft and on its crew and passengers. The craft's subsystems performance may be adversely affected by the vibration levels, amplitudes of motion, and degree of pounding imparted to the equipment. In a similar vein, the crew and passengers are also affected by the motion and other environmental factors. By far, the more complex topic and most difficult to resolve are the onboard personnel requirements for ride quality.

In broad terms, ride quality related to personnel can be divided into two major categories:

1. Motion Sickness - which is normally associated with low frequencies of encounter operation ($\omega_e < 1$ rad/sec), and
2. Working Efficiency - which is concerned with the fatiguing of the personnel. This can occur at all frequencies but is normally associated with the higher frequencies of encounter ($\omega_e > 1$ rad/sec).

There are many expert opinions and sea stories regarding the key parameters that affect motion sickness (kinetosis) and working efficiency. It is known that vertical acceleration and amplitude of motion are instrumental in effecting ride quality. It is also known that lateral or sway and surge accelerations are important as are pitch and roll amplitudes. Environmental factors such as temperature, noise level, smell, and visual reference (or lack of it) can cause a change from an acceptable acceleration level to an unacceptable acceleration level. Further, the age, health, sex, motivation, and workload onboard play important roles in determining acceptable ride quality. For military craft it has been reported that under battle conditions the personnel can tolerate rougher sea conditions than under normal conditions perhaps because, for want of a better phrase the "adrenalin factor" is higher. Some medical researchers claim that for a given set of conditions there is no "learning," yet others will attest to getting their "sea legs" and being able to tolerate rougher seas as the duration of the sea voyage continues.

Despite these many varied and controversial findings it is generally agreed that the vertical acceleration level is the dominant characteristic with the lateral acceleration level being the second most dominant. Because of this, most specifications on ride quality for personnel and equipment are expressed in terms of these particular motion characteristics.^{87,88} Most analysis and experimentation are based on an assessment of the vertical (heave) acceleration of the craft operating in rough seas. Figure 83 is a diagrammatic representation of the problem. It is further

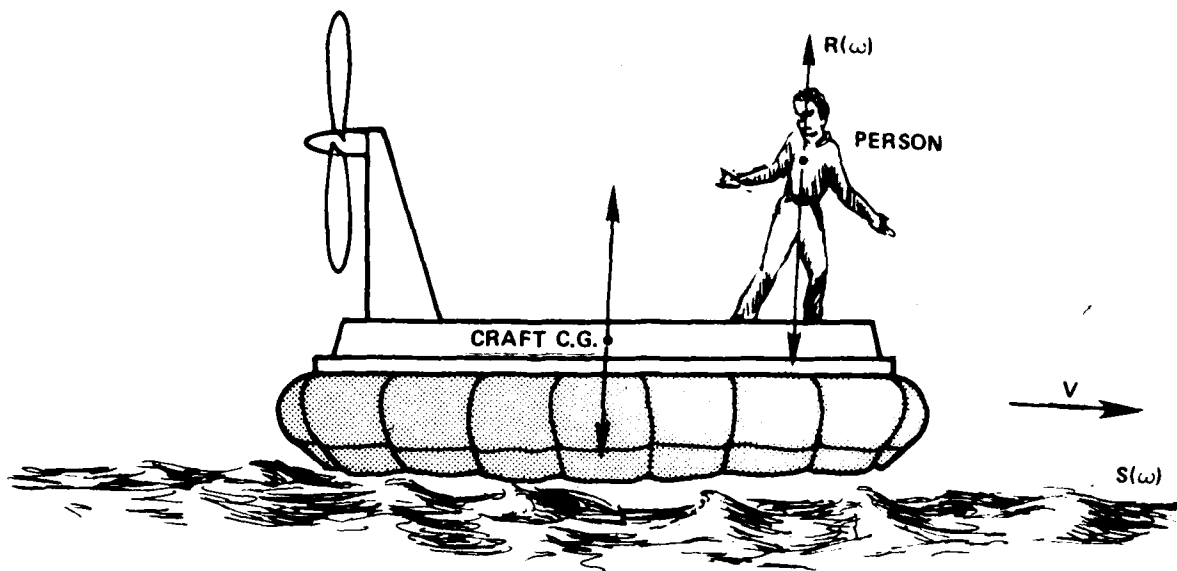


Figure 83 - Motion Response to a Seaway

assumed that the problem can be analyzed under the assumption of a linear system acting under a random forcing function, such that, in the frequency domain, the spectral density of response can be written,

$$R(\omega) = |G(\omega)|^2 \cdot S(\omega) \quad (138)$$

where $R(\omega)$ = response spectral density
 $S(\omega)$ = seaway spectral density
 $G(\omega)$ = transfer function
 ω = wave frequency determined by the wave celerity and wavelength.

This approach provides a direct comparison of craft responses for a given sea condition. If the sea spectrum is known, the motion of different craft can be compared from the same sea conditions.

The encounter frequency of the craft with the waves is given by,

$$\omega_e = \omega - \frac{V \omega^2 \cos \psi}{g} \quad (139)$$

where V is the forward speed of the craft and ψ is the heading with respect to the waves ($\cos \psi = -1$ for head seas).

The transfer function $G(\omega)$, related to the response amplitude operator (RAO), is the heave motion per unit wave amplitude. As Figure 83 indicates, the response $R(\omega)$, being discussed, can be that of a particular part of the craft or of the person on board. The output response $R(\omega)$, therefore, depends on the transfer function $G(\omega)$ which also varies throughout the system from wave input to the person. For example, by the theory of linear superposition, the transfer function can be written

$$G(\omega) = G_1(\omega) \times G_2(\omega) \times \dots \times G_n(\omega) \quad (140)$$

$$\equiv \text{"Cushion to hull"} \times \text{"hull to floor"} \dots \text{"seat to person"}$$

that is, each part of the craft has its own mechanical transfer function that can be determined in the design process. By way of the example, the craft may have a certain response to a wave action which can be attenuated before it reaches the person through, for example, shock absorbing seats. A further complication is that the person can absorb motion by positioning before it gets to critical organs. It is known that one can tolerate better different acceleration levels if one stands and allows the "spring action" in one's legs to absorb the motion than if one is sitting or lying down. Various publications express the criteria as a function of the human characteristics.^{87,88}

Before embarking upon a discussion of Equation (138) some basic observations on the ride quality of air cushion craft in simplistic terms will be given first to provide a reference point for what has remained an elusive analytical problem.

Some Basic Ride Quality Results

The nature of the heave response has received considerable investigation both in private industry and Government because of the incurred problem of ride quality when developing high speed vehicles to operate in rough seas. Much of the criteria^{87,88} was not developed for such craft whose motion characteristics were much different than airplanes, trucks, and displacement ships, for example. The form of measurement of heave response, discussed in the literature, has been determined largely by the type of craft that is being analyzed. Figure 84 illustrates some of the ways used for measuring the response of a particular acceleration trace. The upper trace shows the "peak-to-peak" values of a particular trace. This has been used in the assessment of planing craft that are known to pound from wave crest to wave crest at high speed. It is thought that such a measurement of response would best characterize the motion. However, other techniques used in displacement ship design consider the number of exceedances, i.e., the number of changes in sign of the acceleration; others contend that the number of reversals--a sort of measure

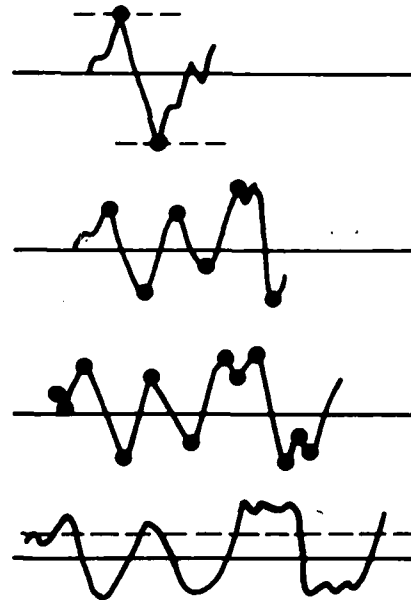
PEAK-TO-PEAK

1/3 HIGHEST
1/10 HIGHEST

NUMBER OF EXCEEDANCES

NUMBER OF REVERSALS

ROOT MEAN SQUARE*



*ANALYZED IN BOTH WIDE BAND AND NARROW BAND.

Figure 84 - Some Current Treatments of Motion

of the "jerkiness" in the acceleration--determines the nature of the motion and its acceptability. The largest body of literature, however, claim that the average level of the acceleration, measured as a root mean square (RMS) value, would be a measure of the energy content and would, thus characterize the motion. A further complication of this averaging technique found in the literature is that the RMS value is sometimes quoted as an average over the broad band (1 octave or more) and sometimes in the narrow band (usually 1/3 octave). These differences have made it difficult to collect data and display it in a common format for comparison and analysis. This particular problem is treated later in this section. However, Figure 85, taken from Reference 89, shows the heave acceleration data in RMSg plotted as a function of sea roughness parameter (h_w/h_s) which is defined as the ratio of the significant wave height (h_w) to the clearance of the main hull above the mean waterline (approximately, h_s).

Herein lies another difficulty in comparing data obtained from full-scale craft and that relates to the measurement of the wave height (h_w).

AIR CUSHION CRAFT	HYDROFOILS
△ SIDEHULL	▲ SURFACE-PIERCING
1. SES-100A	1. BRAS D'OR
2. SES-100B	2. DENISON
○ AMPHIBIOUS	● FULLY-SUBMERGED
3. SR.N1	3. PCH-1 (MOD 1)
4. SR.N4	4. TUCUMCARI
5. SR.N5	5. AGEH
6. SR.N6	6. JETFOIL

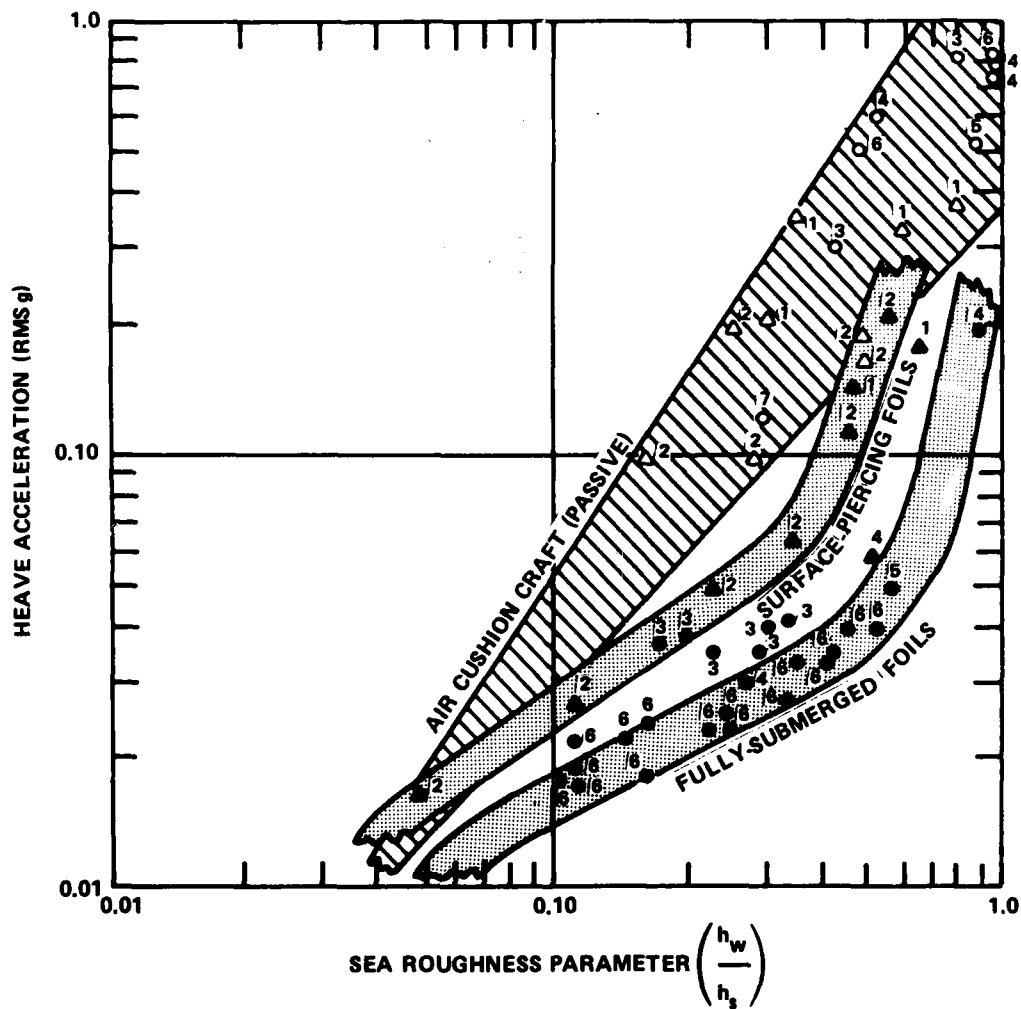


Figure 85 - Ride Quality of Cushions and Foils

It is normally assumed that the wave height quoted is the significant wave height which is not the actual height of the wave at all but the average height of the highest 1/3 waves. This value is used because when the human eye views a seaway it tends to disregard the small waves and perceives an "average" height that is actually very close to the average height of the highest 1/3 waves. Thus, when speaking of a seaway with a given significant wave height, what is really meant is a seaway composed of many different size waves of which the average of the highest 1/3 is the significant wave height. It should not be surprising to find that large discrepancies appear in the literature as to what the acceleration level is, in what sea conditions, and for any given craft under discussion. Appendix D provides some of the most used descriptions and properties of sea conditions. For the purposes of this discussion it is assumed that--on the average!--these represent the motion characteristics of air cushion craft and hydrofoils. The data, shown in Figure 85, are for air cushion craft and, for comparative purposes, both surface-piercing and fully-submerged hydrofoil systems. The air cushion craft data shown are for those employing passive lift fan systems, i.e., no means of adjusting the "spring constant" in the cushion through fan control. Also from Reference 89, Figure 86, on the other hand, shows how, the heave acceleration level has been suppressed or attenuated through the use of active lift fan systems. Some specific details on the nature of the active systems and how the state-of-the-art has progressed since 1975 are provided later in this section (on ride control) and in Chapter VIII on lift fan systems. The particular data shown on the active lift fan system are taken from the early SES-100A trials where the ride control mechanism employed valving to atmosphere of the cushion over pressure. The shaded regions for the passive lift fan system, the air cushion craft, and the fully-submerged foil hydrofoil craft are superimposed from Figure 85 for reference. In gross terms, the ride of air cushion craft using ride control systems is similar to that of surface-piercing hydrofoil craft but not as smooth as in comparable size fully-submerged hydrofoil systems.

As the (average) wave height (h_w) approaches the clearance height (h_s) of the main hull some cresting of the main hull occurs and additional acceleration is incurred through slamming upon waves. Because of this, as expected, a change in character of the acceleration-height relationship is seen in the hydrofoil curves. With the scant data available on air cushion craft no such trend was noticed.

It could be argued that there are insufficient parameters in Figures 85 and 86 to completely characterize the motion. For example, the effect of speed is not evident. Because it is known that as the sea roughness parameter is increased the speed of the air cushion craft is decreased (see Figure 58 showing speed in rough seas), then the frequency of encounter changes with an expected change in the acceleration levels (see Figure 71, for example). Nevertheless, the main comparative points and magnitude of

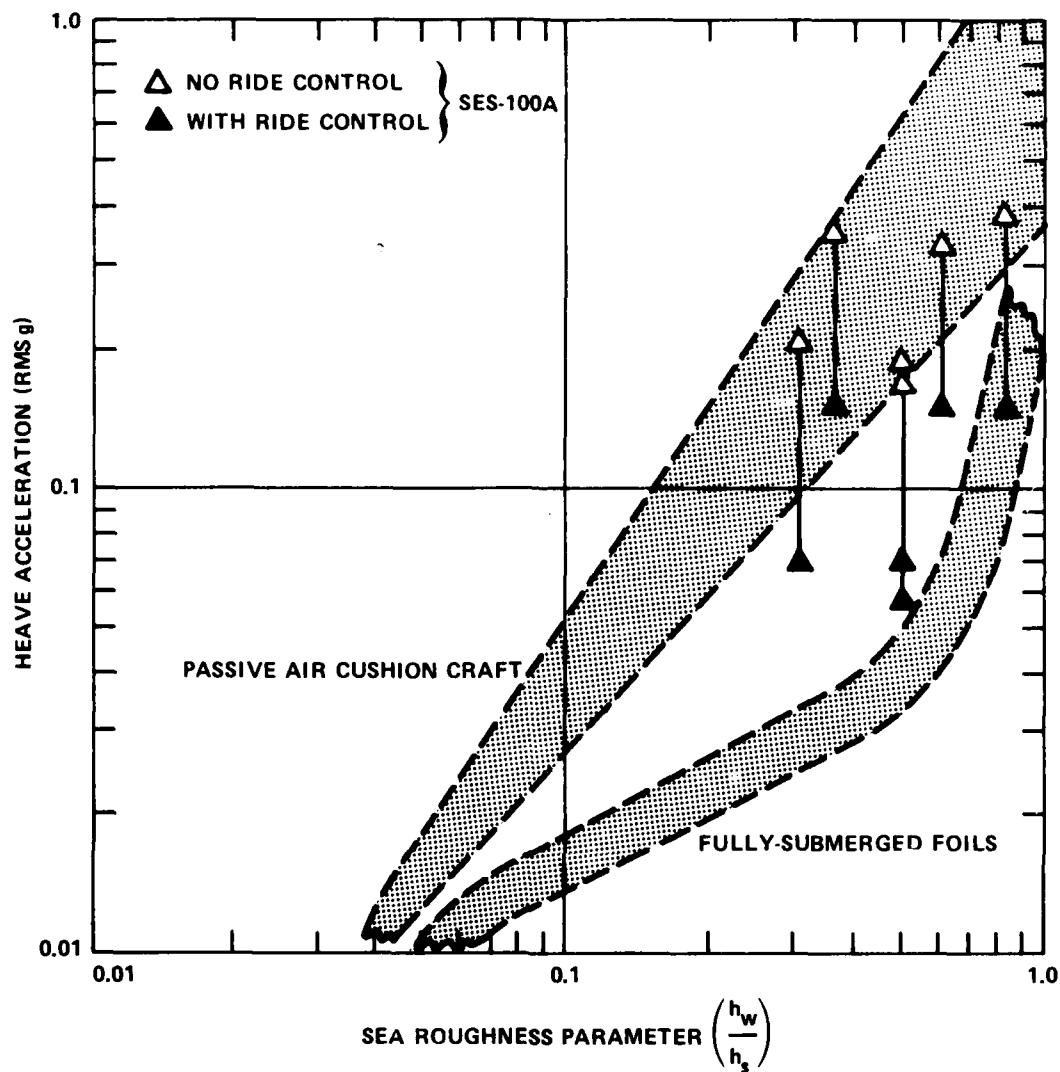


Figure 86 - Air Cushion Craft Ride Quality
with Active Lift System

the acceleration levels under discussion are displayed in Figures 85 and 86. Further discussion must now rely on a more detailed treatment of the seaway and the nature of the particular craft's transfer function.

THE SEA SPECTRA

It has generally been accepted that the occurrence of ocean waves or seas are random in nature, requiring the use of statistics to describe an accumulation of sea characteristics. Characteristics of ocean waves obtained from studies on oceanographic and naval ships indicate that the

occurrence of wave heights approximately approaches a Rayleigh distribution given a large enough sample (greater than 1000 waves). Wave periods, on the other hand, do not generally follow any particular statistical form.

In one specific case⁹⁰ of a freshly generated sea (with no swells superimposed), the distribution of the square of the observed wave periods also approached a Rayleigh distribution. The distinction between the occurrence of wind blown waves as differentiated from swell waves is not noted in most of the available data. The general opinion in this field is that the Rayleigh distribution approximately describes the occurrence of both wind wave and swell wave heights separately or in combination. However, the presence of swell waves may grossly affect the wave period distribution. A trained ocean wave observer describes the sea condition from his visual estimation of a characteristic wave height and period known as the significant wave height and period as already discussed.

No unique relationship has been found between observed wavelengths and periods occurring in a particular area but they are found to be dependent not only on the duration and direction of the wind acting on the sea surface at the time but also on whether the sea is developing, fully developed, or decaying. Figure 87 shows the relationship of observed periods and optically determined wavelengths recorded during the observational voyage of the SS NISEI MARU 1954.⁹¹ Most of the wavelengths lie between the classical trochoidal wavelength $\lambda = gT^2/2\pi$ and $\lambda = gT^2/5\pi$. The observed wavelength for the fully developed sea approximately equals two-thirds of the trochoidal wavelength $\lambda = 2/3 gT^2/2\pi$.

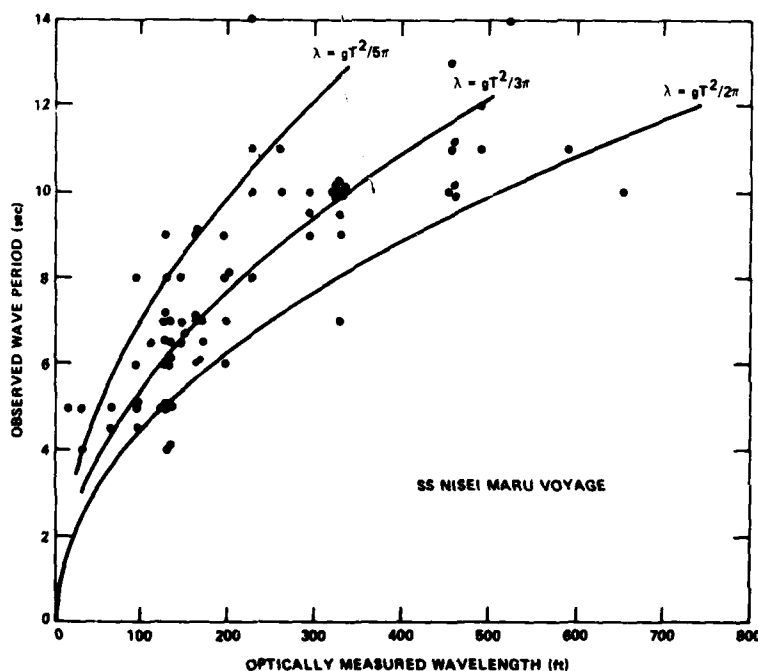


Figure 87 - Wave Period and Wavelength

Because of the random nature of the sea, the wave height spectral density has gained more acceptance in the last few years for describing sea conditions. Unfortunately, spectral data is still sparse in most areas of interest. However, a theoretical wave spectrum, based on the synthesis of the kinetic and potential energy contained in the sea surface, has been devised. The spectrum is assumed to be composed of a large number of small amplitude component sine waves whose energy can be shown to be proportional to the height squared. The energy spectrum is commonly used as it yields useful statistical constants relating to the Rayleigh distribution of wave heights. (See Appendix D).

If the distribution of the actual measured wave heights does not approach the Rayleigh distribution, the statistical characteristics, such as the mean height, must be determined from the actual height distribution. Knowledge of the height squared spectrum alone is not sufficient to describe the occurrence of wave height and yields no information about wave direction, steepness, or shape. The height squared spectrum, along with the height distribution, can be determined from a data record containing wave height as a function of time.

Various theoretical formulations of wave spectra have been devised during the last few years.⁹² The Neumann spectrum has been considered the classic description of the sea, although the Pierson-Moskowitz⁹³ spectrum is the most accepted and is used in most model test tanks in the United States and the United Kingdom. Thus a great deal of model data evaluating the motion characteristics of air cushion craft (as well as other marine vehicles) has been obtained using the Pierson-Moskowitz spectra. This is a single parameter spectra given by,

$$S(\omega) = \frac{\alpha g^2}{\omega^5} \cdot e^{-\beta \left(\frac{\omega_0}{\omega}\right)^4} \quad (141)$$

where $\alpha = 8.10 \times 10^{-3}$
 $\beta = 0.74$
 $\omega_0 = \frac{g}{V_w}$

The wind speed (V_w) is expressed in terms of the significant wave height (h_w) assuming a long fetch by the relation,

$$V_w \text{ (knots)} = \left(\frac{h_w}{0.0182} \right)^{1/2} \quad (142)$$

provided h_w is measured in feet.

Hence, the Pierson-Moskowitz sea condition spectra is dependent only on the wave frequency (ω) and a single variable parameter that can be expressed either in terms of wind speed (V_w) or significant wave height (h_w).

Figure 88 shows this spectra graphically as a function of wave frequency and significant wave height. Appendix D provides tabulated values of the wind speeds, wave heights, wave periods, and wavelengths corresponding to this particular representation of the sea condition.

While the Pierson-Moskowitz spectra is in wide use, especially in tow tanks, it would be remiss not to mention other spectral representation that are in frequent use in various design communities. These other spectra bring in the effects of other properties besides the wind speed. These other factors are meant to represent the effects of waves from surrounding areas, local currents, and land masses. This is accomplished to some degree in the International Ship Structures Conference (ISSC) version of Breitschneider's spectrum. Because the spectrum is defined directly in terms of the statistical properties of wave height and period, it is suitable for use with actual wave data measured in the particular area of interest.

The Breitschneider (two parameter) spectrum is given by:

$$S(\omega) = 0.11 \left(\frac{2\pi}{T_s} \right)^4 \cdot \frac{h_w^2}{\omega^5} \cdot e^{-0.44 \left(\frac{2\pi}{T_s \omega} \right)^4} \quad (143)$$

where T_s is the significant wave period (i.e., average period of the 1/3 highest waves) and h_w is the significant wave height.

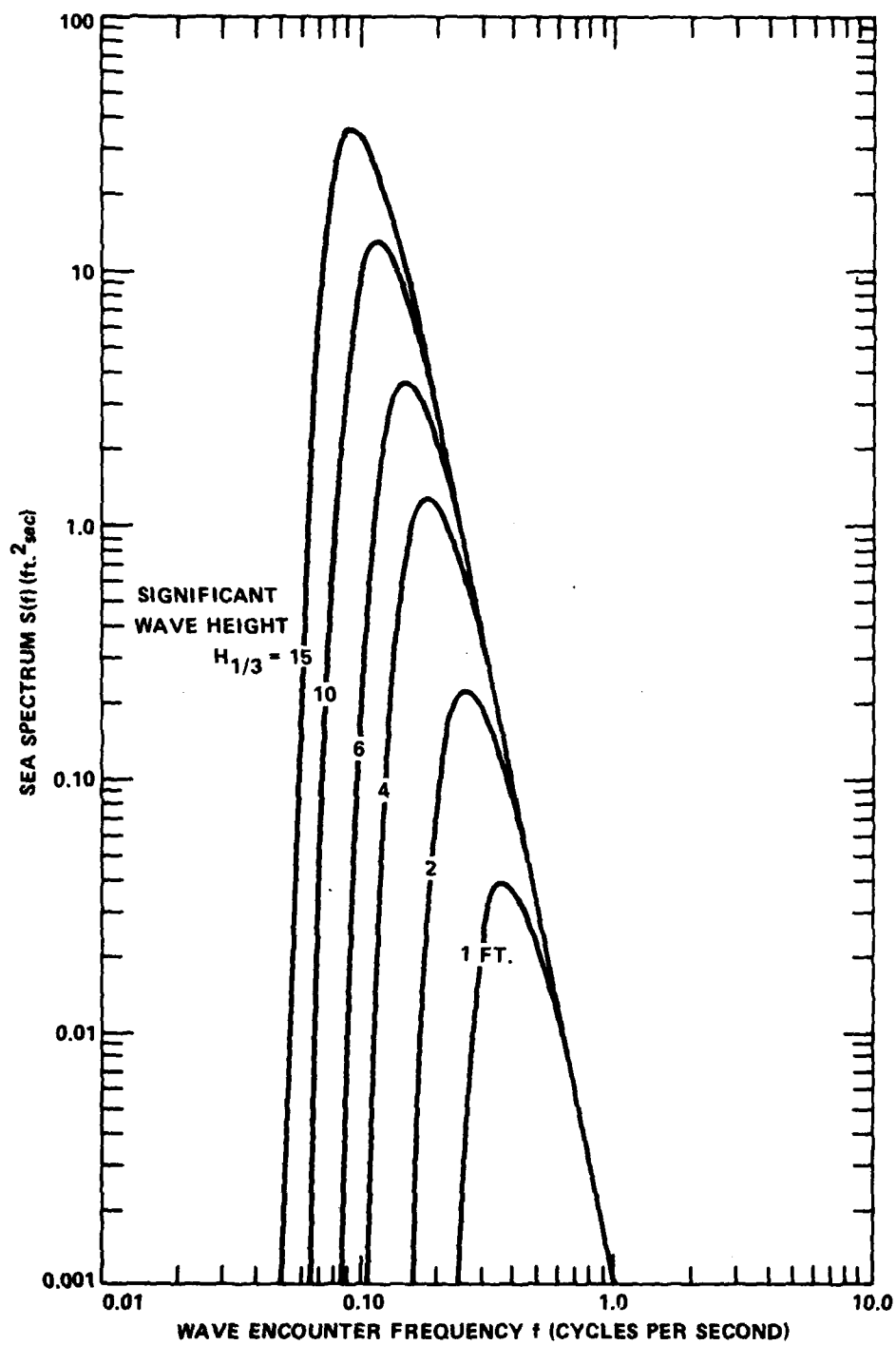


Figure 88 - Pierson-Moskowitz Sea Spectra

The ISSC spectrum can be correlated with the Pierson-Moskowitz spectrum at the same significant wave height and period. Because of this correlation and the commonality with the tow tank testing, the Pierson-Moskowitz spectrum is used in this report.

The Pierson-Moskowitz, wave spectrum has a maximum value at a frequency ω_m that is given by

$$\omega_m \text{ (rad/sec)} = 0.07 \frac{g}{h_w^{1/2}} \quad (144)$$

where $g = 32.2 \text{ ft/sec}^2$ and the significant wave height (h_w) is measured in feet. At this frequency, the maximum value of the spectrum is given by

$$S(\omega_m) = 0.503 h_w^{5/2} \quad (145)$$

The relative significance of the wave height in forcing the motion can be seen from Equations (144) and (145).

TRANSFER FUNCTION

The second term in the craft response Equation (138) is the transfer function which describes the craft response to simple frequency waves of unit height or amplitude. The transfer function is equivalent to the magnification ratio used in linear systems (see, for example, Equations (111) and (112)). If the craft contours or follows the waves exactly, the vertical (heave) acceleration per foot of wave height will be,

$$\frac{\ddot{H}(t)}{h_w} = \omega^2 \quad (146)$$

where $H(t)$ is the amplitude of the heave motion of the craft.

Figure 89 shows some predicted heave acceleration response transfer functions for the fully-submerged hydrofoil Boeing JETFOIL,⁹⁴ the surface-piercing hydrofoil Rodriquez PT-150,⁹⁵ and the U.S. Navy surface effect ship SES-100A.⁶⁷ These are, of course, selected curves to show the general nature of the transfer function, which in today's state-of-the-art is the one term in the response Equation (138) that can be predicted with the greatest confidence. The designer has the most control through design of

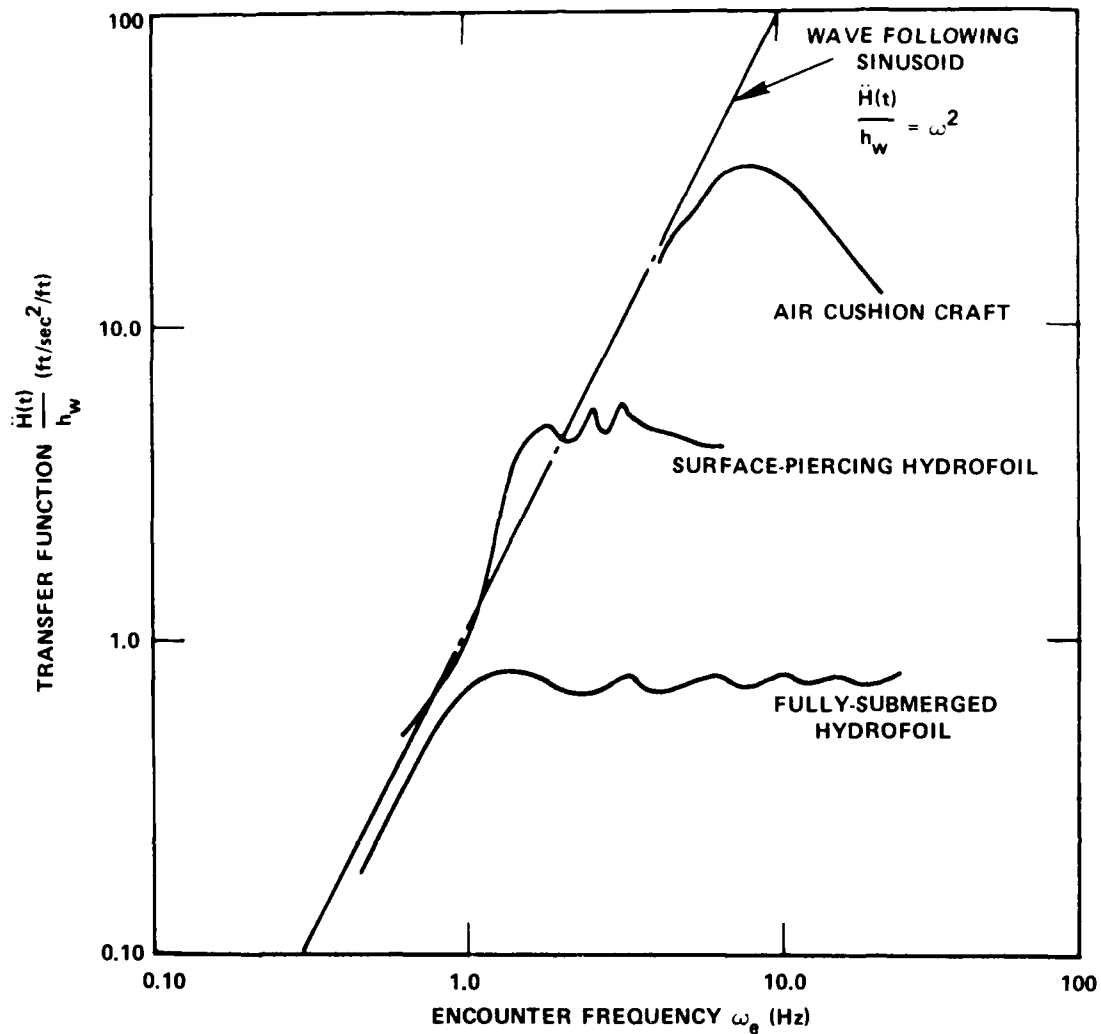


Figure 89 - Transfer Function of Selected Craft

the subsystems. Each of the subsystem's individual spring constant and damping ratios combine to give the desired transfer function from input (sea spectrum) to output (personnel response).

HEAVE RESPONSE AND RIDE QUALITY

The third and final element in the heave response equation is the heave response itself which determines the ride quality of the craft. If the acceleration level is below some specified value then the "ride quality" is deemed acceptable. Earlier discussions of some basic ride

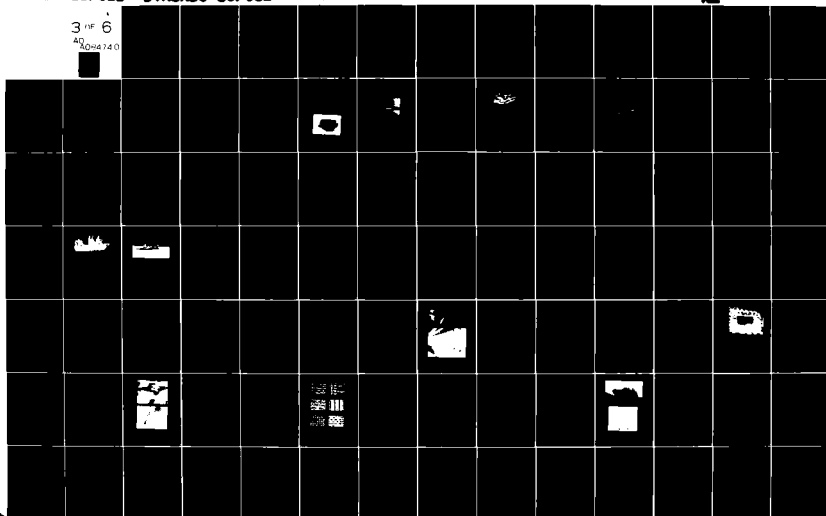
AD-A084 740

DAVID W TAYLOR NAVAL SHIP RESEARCH AND DEVELOPMENT CE--ETC P/6 13/10
AIR CUSHION CRAFT DEVELOPMENT. FIRST REVISION. (U)
JAN 80 P J MANTLE
DTNSRDC-80/012

ML

UNCLASSIFIED

3 OF 6
AD-A084740



quality results indicated the general nature of the motion of air cushion craft, although determination of an "acceptable" ride quality requires a more detailed treatment. The character or nature of the motion is quite different between vehicle types. By way of example, Figure 90 shows two traces of full-scale operational air cushion craft. The upper two traces are for the 212-short ton SR.N4 travelling at 32 knots in 4- to 5-ft seas. These traces show the recorded acceleration levels both at the (C.G.) and at the bow, showing that some pitch motion is superimposed on the heave motion. The lower two traces (for C.G. and bow motion) are for the smaller 50-short ton BH.7 travelling at 35 knots in 2-ft seas. These traces were obtained during the BH.7 demonstration trials sponsored by the U.S./U.K. technical exchange program in August 1973 off Cape Henry, Virginia.⁹⁶ By way of comparison, Figure 91 shows a typical trace of a planing craft, the 80-short ton U.S. Navy Coastal Patrol Interdiction Craft (CPIC) travelling at 38 knots in about 5-ft seas.

The SR.N4 traces shown (Figure 90) are for the original craft prior to its stretching (see Chapter II, Figure 5). It is seen that quite high acceleration levels are achieved. Although no data are presently available, it is believed that the motions of the stretched SR.N4 are reduced below the values shown.

Realization of the rough ride characteristics of air cushion craft prompted the U.S. Navy, in the late 1965 to 1970 period, to initiate development of ride control systems. These ride control systems were primarily heave motion attenuation devices involving valving and active fan systems.

The simplest system, although probably the most wasteful in terms of power, is one of venting. The venting system consists basically of an overboard valve, which dumps the cushion air that would otherwise impart vertical acceleration to the craft due to the piston-like action of the waves. Such a system was designed into the SES-100A to study heave attenuation or ride control as part of the U.S. Navy program. The valve was activated upon a sensing signal from a transducer that sensed the acceleration (or in later tests, pressure changes). A similar venting system was subsequently retrofitted to the SES-100B in 1974, such that comparisons could be made and the necessary data collected for evaluation. Typical data collected during the rough sea trials of the SES-100A off Port Townsend near Seattle in the winter of 1973 are shown in the upper curves of Figure 92. These data show acceleration levels both with and without the ride control system activated.

The predicted values of heave acceleration are also shown. The reduction in acceleration levels was found to be encouraging and incidentally dramatic, whereby an intolerable ride onboard can instantly be converted to a comfortable ride merely by activation of the system. The data shown in the upper curves apply to the case of head seas. The lower set of data in Figure 92 (see Reference 66) shows the effect of heading. This particular set of data is selected for the case of almost pure heave motion, that

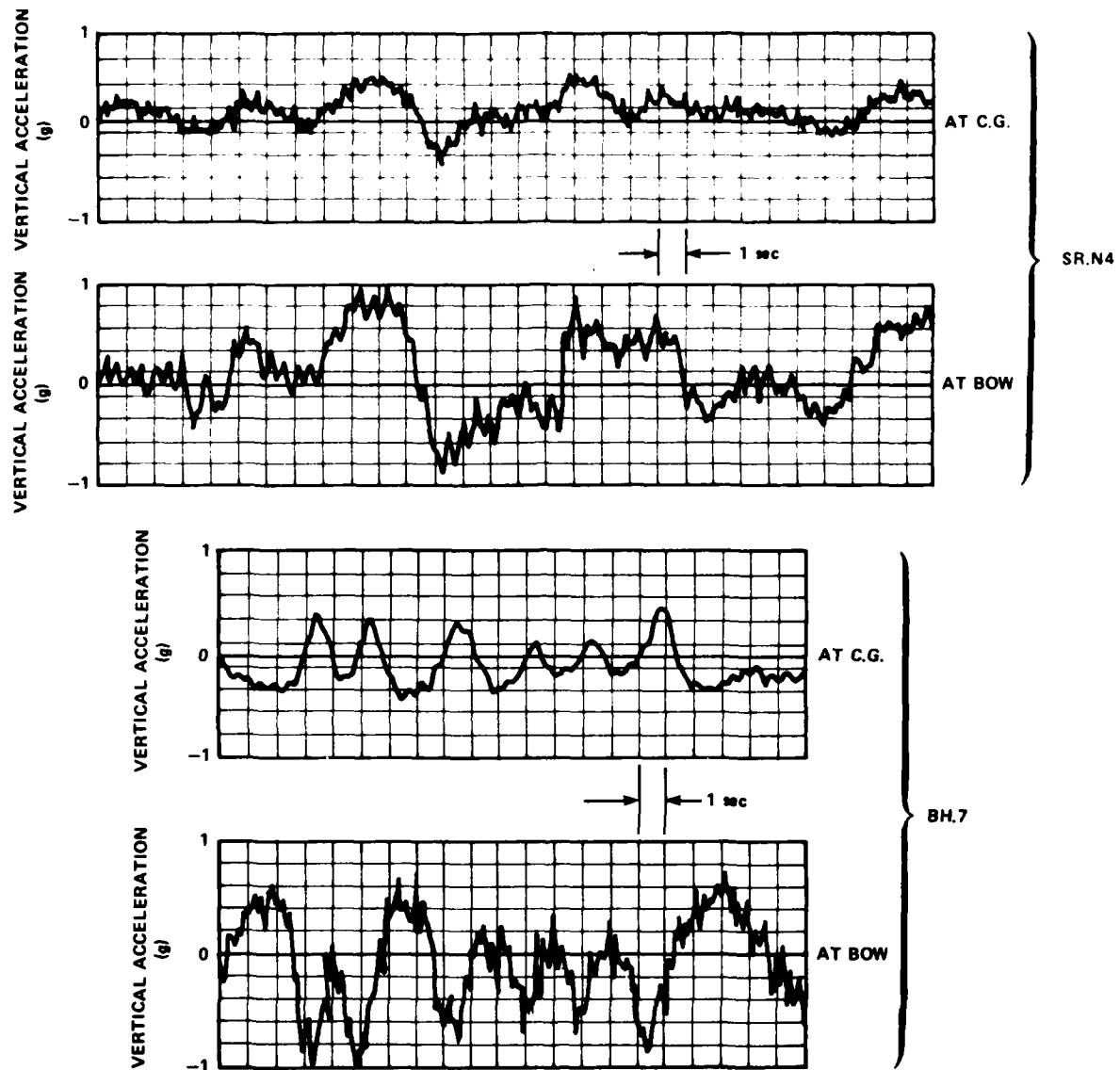


Figure 90 - Typical Traces of Air Cushion Craft

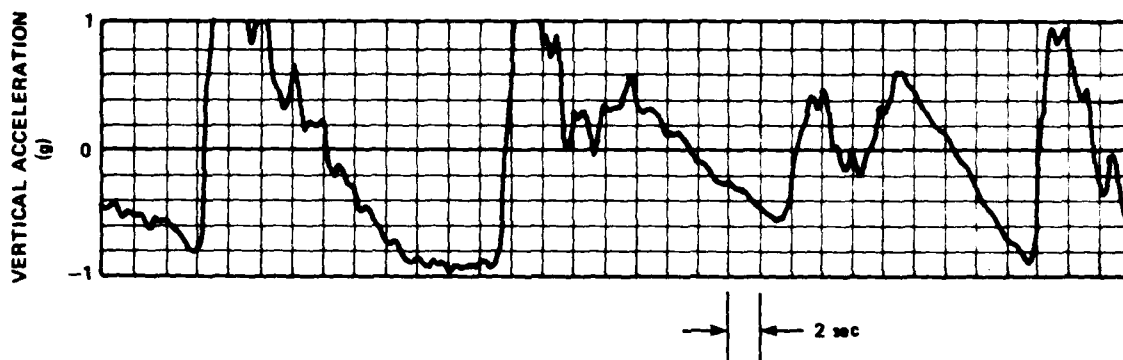


Figure 91 - Typical Trace of Planing Craft

is, where the acceleration in the forward deckhouse is approximately equal to the acceleration at the craft center of gravity. The data are for the craft operating at a gross weight of 200,000 pounds in 2- to 2.5-ft average wave height seas, which might be expected to be a State 2 sea, except that the confused seas in the test area resulted in short wavelengths of approximately 30 ft. The craft speed varied between 28 to 32 knots with the ride control inactive and between 25 to 31 knots with the ride control active. These speed differences were the result of using a venting system because as the cushion air is vented overboard, the craft "tends" to settle in the water, creating more hydrodynamic drag. The word "tends" is put in quotes as it is not always the case, depending upon the interaction of the fan and craft dynamics and wave motion.

The data shown in Figure 92 at various headings show the expected falloff in acceleration as the craft turns away from head seas into beam seas and finally into a following sea condition. Depending on the heading, acceleration reductions of greater than 50 percent are possible with such simple systems. In a similar test run in rough seas (State 3 sea) the craft operated at 41 knots and experienced heave acceleration levels of 0.39 RMSg with the ride control system inactive. This acceleration level would be unacceptable for anything longer than a few minutes. With the ride control system activated, the heave acceleration was significantly reduced to 0.13 RMSg, which could be tolerated for several hours. The vented air in this case caused sufficient settling in the water and increased drag to cause the speed to fall off to 35 knots for the same power setting.

In such a situation, the operator has a choice to increase speed: he can put the power back into the lift system (and reduce drag) either by increasing the lift using engine throttles in the case of nonintegrated systems or by changing the fan pitch setting for integrated systems, or by

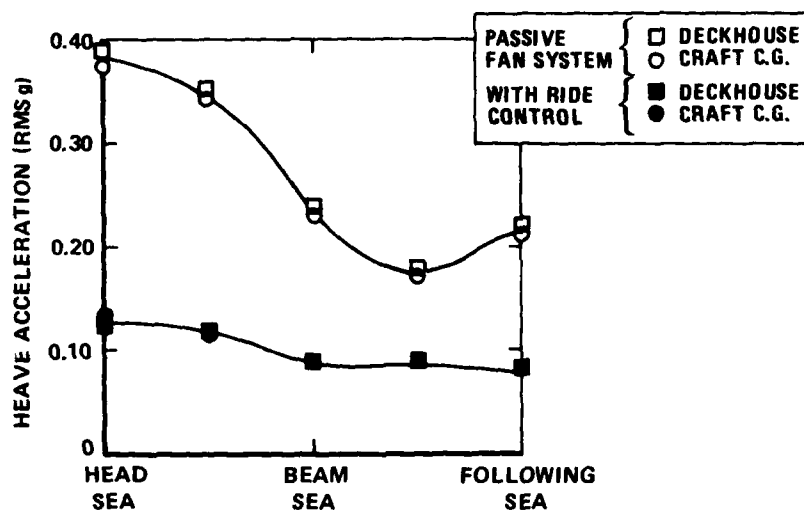
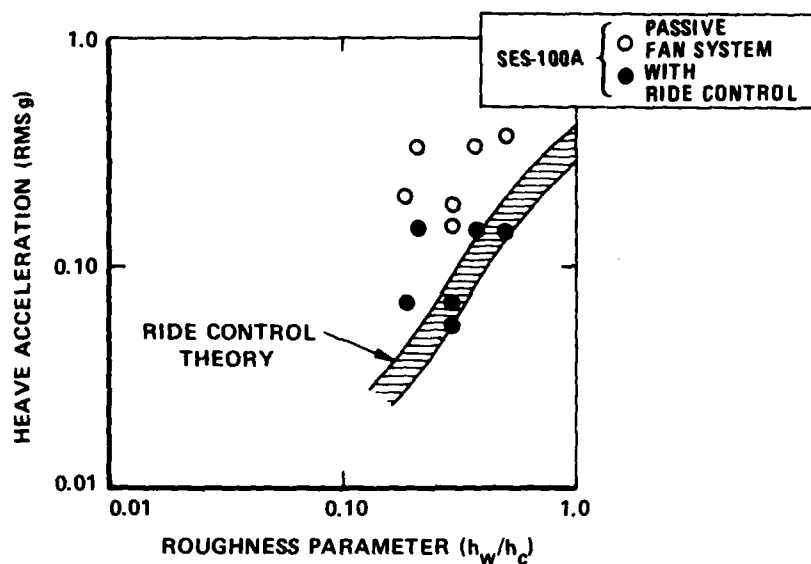


Figure 92 - SES-100A Ride Control System

increasing the propulsion power directly. Which is the least power-consuming is dependent upon the particular design characteristics and relative efficiencies between lift and propulsion systems for the craft.

The simple venting system can be very costly in terms of power for a long duration cruise in rough water, and other systems need to be developed as discussed in Chapter VIII. All these various schemes are designed to improve the ride and, by so doing, change the character or nature of the motion.

Comparing the traces of two vehicle types in Figures 90 and 91 note the strong effect of the ride control systems on air cushion craft (as shown in Figure 92). The nature of the motion can be quite different, making it difficult to assess, on some common basis, the ride quality of the craft.

To provide some guide, several examples of traces such as those shown in Figures 90 and 91 were subjected to analysis and values of peak-to-peak acceleration levels, number of exceedances, RMSg, etc., were determined.* The example results are summarized next.

Example 1. SR.N4 Motion

For the C.G. acceleration trace, shown in Figure 90, the analysis provides the following results:

Peak to peak:

Maximum value	0.73 g
Maximum positive peak	0.58 g
Maximum negative peak	0.43 g
Average of 1/10 highest	0.39 g
Average of 1/3 highest	0.29 g

RMS acceleration 0.12 g

Crest factor:

1. Maximum peak to RMS 4.72
2. 1/2 [Average 1/10 highest/RMS]. 1.59
3. 1/2 [Average 1/3 highest/RMS] 1.16

A similar set of analyses were conducted for the BH.7 trace shown in Figure 90 and the results follow.

Example 2. BH.7 Motion

For the C.G. acceleration level the example trace shown provides the following statistics:

Peak to peak:

Maximum value	0.21 g
Maximum positive peak	0.11 g
Maximum negative peak	0.11 g
Average of 1/10 highest	0.12 g
Average of 1/3 highest	0.08 g

RMS acceleration 0.03 g

Crest factor:

1. Maximum peak to RMS 3.77
2. 1/2 [Average 1/10 highest/RMS]. 1.92
3. 1/2 [Average 1/3 highest/RMS] 1.37

*The author would like to thank J. Luckard of DTNSRDC Code 1170 for providing these results.

In both these examples it is noticed that a wide range in acceleration values exists depending on the definition being used. As an attempt to characterize the "peakiness" of the acceleration a shape factor is defined in the literature. The usual crest factor used is the ratio of the maximum peak acceleration experienced over a given time period to the RMS value for the same time period. The significance of this factor will be established later in the discussion of available ride quality criteria. An intuitive feeling of the author is that a better definition of the crest factor would be to bring in the 1/10 or 1/3 highest values of acceleration as more representative of the character of the motion. These values were computed in the above examples and also will be discussed under the heading of ride quality criteria.

Two other examples provide an indication of the effect of incorporating ride control into an air cushion craft. These two examples pertain to the SES-100B operating at 50 knots in a State 2 sea ($h_w = 1.5$ to 2 ft), both without and with ride control.

Example 3. SES-100B (Without Ride Control)

The statistical analysis of the data tapes during the trials program for the acceleration at the C.G. give the following results:

Peak to peak:

Maximum value	1.82 g
Maximum positive peak	1.55 g
Maximum negative peak	0.86 g
Average of 1/10 highest	1.27 g
Average of 1/3 highest	0.94 g

RMS acceleration 0.33 g

Crest factor:

1. Maximum peak to RMS	4.76
2. 1/2 [Average 1/10 highest/RMS]	1.95
3. 1/2 [Average 1/3 highest/RMS]	1.45

Example 4. SES-100B (With Ride Control)

The ride control system (retrofitted) to the SES-100B is considered a first generation system involving valving to atmosphere and provides some basic insight of the effect of ride control systems. The statistical analysis of the tapes provided the following results for the acceleration at the C.G.:

Peak to peak:

Maximum value	1.04 g
Maximum positive peak	0.62 g
Maximum negative peak	0.57 g
Average of 1/10 highest	0.72 g
Average of 1/3 highest	0.54 g

RMS acceleration 0.16 g

Crest factor:

1. Maximum peak to RMS 3.80
2. $1/2$ [Average $1/10$ highest/RMS] 2.20
3. $1/2$ [Average $1/3$ highest/RMS] 1.65

To continue the discussion of ride quality it is informative to use some of the examples just shown to illustrate the nature of the motion. Although there is not a large amount of data available, what is available indicates that the motion of the amphibious and the nonamphibious forms of aerostatic air cushion craft are very similar. The SES-100B will be used then, as representative of the basic characteristics of air cushion craft.

Figure 93 shows the power spectral density (g^2/ω) of the particular run analyzed in Example 3.

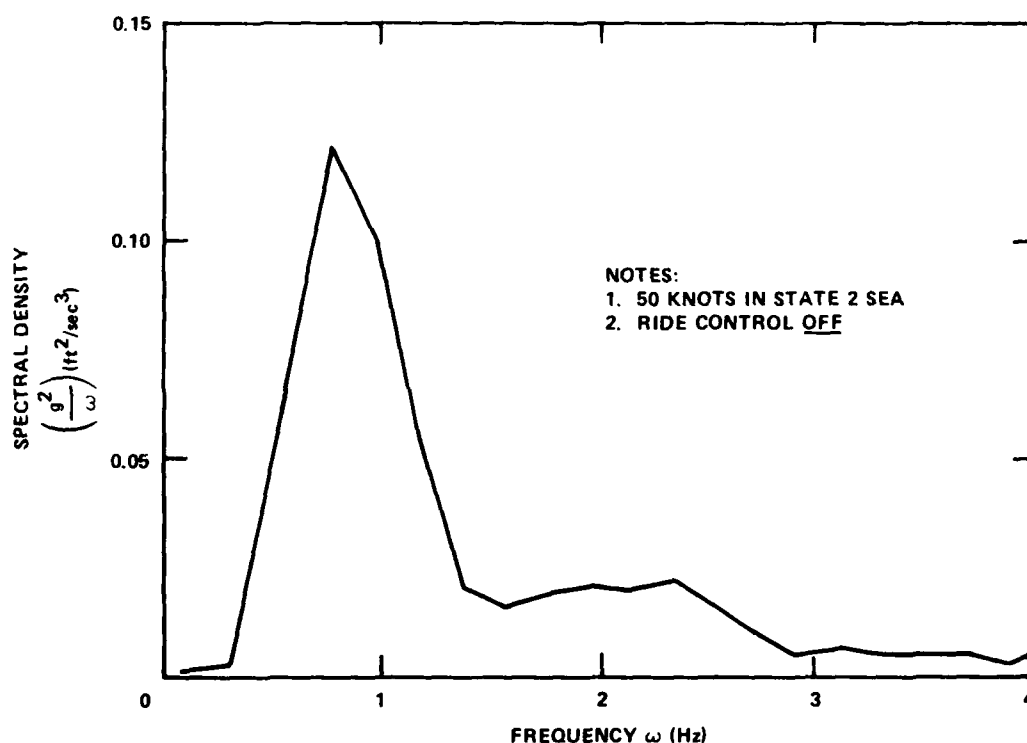


Figure 93 - Power Spectral Density of SES-100B

It is seen that most of the energy in the motion occurs in the frequency range 0.50 to 1.20 Hz. The complete energy (E) content of the response is given by,

$$E = \int_0^{\infty} \frac{g^2}{\omega} \cdot d\omega \quad (147)$$

Because the variance (σ^2), or average of the sum of the squares of the derivations from the mean value measured at equal intervals of time, is equal to the area (E) under the energy spectrum as shown in Figure 93, the root mean square (RMS) value of the acceleration is

$$\sigma = \sqrt{E} = \text{RMS } g \quad (148)$$

The RMS g acceleration, then, is an average time and frequency invariant value for the particular trace being analyzed. It has become common practice, when analyzing vibration occurring over a wide range of frequencies, whether random or discrete, to compute the RMS g over each octave and partial octaves covering the frequencies incurred in the motion. Figure 94 shows the results of computing the acceleration in RMS g over a 1/3 octave, a full octave, and the entire frequency range (i.e., full bandwidth) including the frequency range shown in Figure 93. From Figure 94 can be seen the general shape of the curves and how the value of the acceleration in the band increases in magnitude as the number of octaves increases until it reaches the true mean value for the motion (in this case 0.33 g, as given in Example 3).

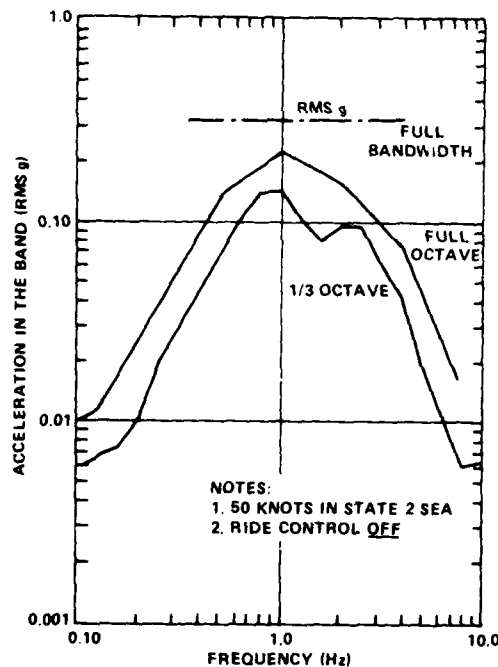


Figure 94 - SES-100B Acceleration (RMS g)
(Ride Control Off)

A similar set of results can be given for the activated ride control system. Figure 95 shows the results for Example 4 of the acceleration in the band in RMSg, i.e., the SES-100B operating at 50 knots in a State 2 sea with the ride control on.

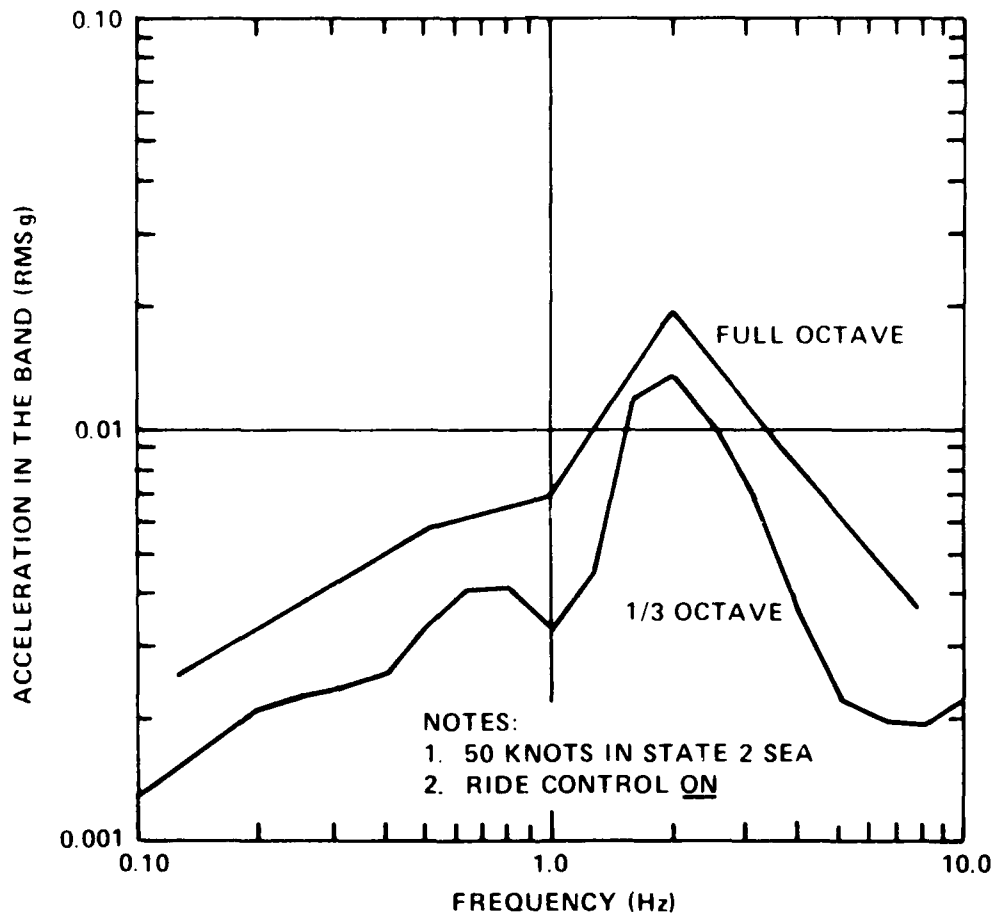


Figure 95 - SES-100B Acceleration (RMS g)
(Ride Control On)

Comparing the two sets of results for the SES-100B (with and without ride control) it will be noticed that in addition to the absolute level of the acceleration being reduced, the distribution of the acceleration with frequency has shifted with amplification occurring around 2 Hz, rather than 1 Hz. To assess the effect of this on ride quality requires a short discussion of the available ride quality criteria.

RIDE QUALITY CRITERIA

The level of acceleration that would be considered acceptable by passengers and crew is, in most cases, subjective in nature. There is the classification of levels by duration, that is, high acceleration can be tolerated for a short period of time, but the level must be much lower for long duration travel. However, the psychological factors must also be included in determining levels of acceptance. One will accept a higher level of acceleration in a personal sport boat than in a commercial means of transportation, for example. The level of acceleration is also affected by whether the person is a passenger in the warm passenger lounge or whether he is a crew member working and trying to read vibrating gages in the engine room.

As stated earlier in this section there are two general areas of interest in ride quality, viz.:

1. Motion sickness (at low frequencies)
2. Working efficiency (at high frequencies)

where the transition from "low" to "high" frequency is in the region 0.60-1.0 Hz.

Significant research of the human tolerance to acceleration levels has been accomplished over the last 40 to 50 years, encompassing travel in aircraft, spacecraft, and trucks, but surprisingly little for marine vehicles. The criteria that is available is based on experimentation that is still under question as to its applicability. Most of the experimentation has been conducted under conditions of single frequency (sinusoidal) oscillation. Very little testing has been accomplished using broad band, random oscillations which, as shown, characterize the motion of air cushion craft. The literature is voluminous on the subject but two particular references^{86,96} will be used here as they capture the essential elements of the two main areas: motion sickness and working efficiency. The criteria taken from these references are shown in Figure 96.

The set of curves shown in the 0.10-1.0 Hz range on Figure 96 are those taken from the O'Hanlon and McCauley work on motion sickness⁹⁶ and the set of curves shown in the 1.0-10.0 Hz range are those taken from the ISO Standard⁸⁶ for fatigue decreased proficiency (FDP) due to vibration. Although these criteria are valuable in being able to assess the ride quality, the limitations of the experiments and analysis used to obtain the criteria are important to consider. A short discussion of the criteria, their limitations, and applicability to air cushion craft use follows.

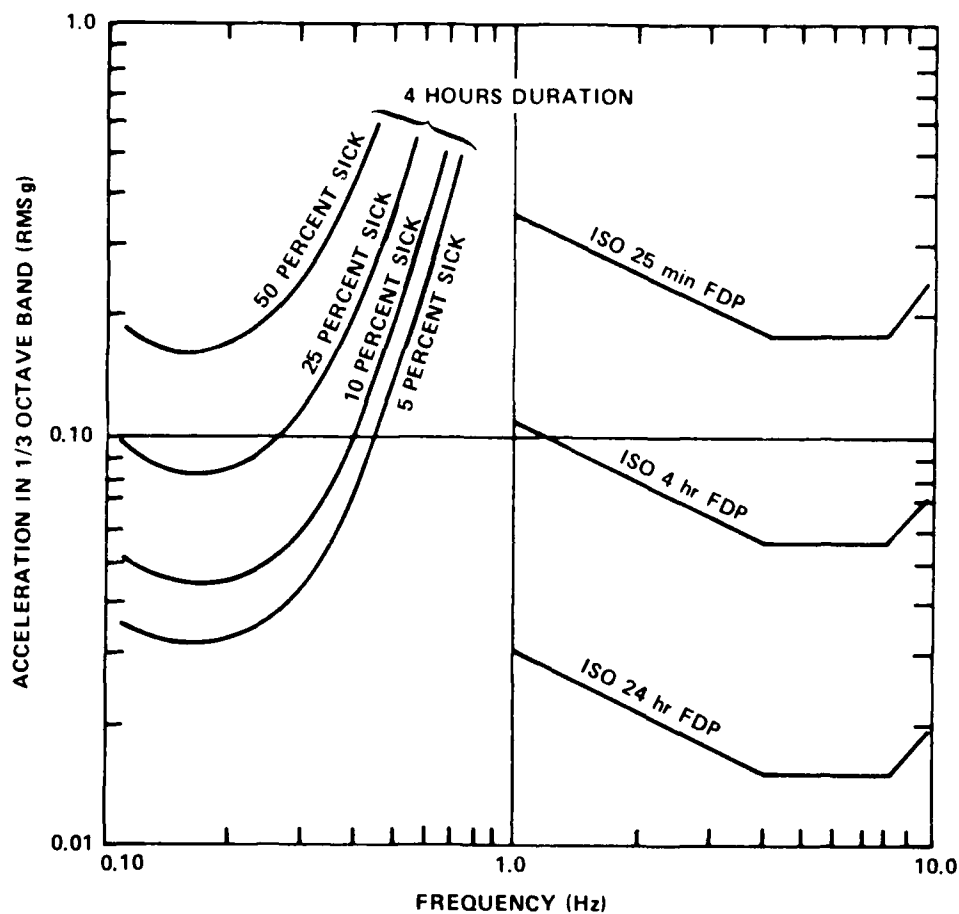


Figure 96 - Ride Quality Criteria

MOTION SICKNESS CRITERIA

The criteria shown in Figure 96 show curves for different percentages of the people getting sick in a continuous 4 hr duration of being subjected to the acceleration level shown. The criterion was obtained by testing untrained, unadapted subjects (college students). The subjects were enclosed in a motion generator "room" that was oscillated in a vertical direction only and the motions were sinusoidal. All subjects were seated on conventional shipboard chairs (i.e., no special padding). Other variables such as complex waveforms, body orientation, visual reference, temperature and smell were not varied. Tests were conducted using the

narrow band frequency only and is not representative of the broad band sea spectrum energy. The criterion used for determining motion sickness was initial vomiting. No assessment was made of the subjects' ability to continue a task or mission after this initial vomiting. No available information has been obtained indicating a difference between "untrained, unadapted subjects" and seasoned naval personnel. The criterion although limited, does, at least, provide a reasonable guide pending more complete testing.

WORKING EFFICIENCY CRITERIA

The curves shown in Figure 96 vary for exposure to the vibration for durations of 15 min, 4 hr and 24 hr. Some thought is being given to changing the 24 hr criterion⁹⁷ but this has not yet been incorporated into the International Standards Organization (ISO) standard. The ISO Standard 2631⁸⁶ states that there are three kinds of vibration (in the frequency range of interest), they are:

1. Whole body vibration
2. Vibration transmitted through the feet (of a person standing) or buttocks (of a person seated)
3. Vibrations applied to particular parts of the body (such as head or limbs).

The ISO Standard applies principally to item 2 but all conclusions are provisional. Also, the criterion is considered (by ISO) to be applicable only in the 1-80 Hz range. The general limits, analyzed by ISO, are for

1. Comfort "Reduced Comfort Boundary"
2. Working efficiency "Fatigue Decreased Proficiency"
3. Safety of health "Exposure Limit"

Of the three limits established by ISO the FDP limit has been adopted for use in the design of advanced marine vehicles. The limits are expressed in terms of vibration frequency, acceleration magnitude, exposure time, and direction of vibration relative to the torso. In selecting the exposure time for Figure 96 this author has chosen the 25 min FDP limit as being representative of very short trips and the 24 hr limit as being representative of continuous exposure to a given vibration limit. The 4 hr FDP limit is considered to be most applicable to U.S. Navy applications as it corresponds to a typical "4 hr watch" for onboard crew members. However, ISO standards were developed for passenger acceptance and the applicability to Navy crews conducting military operations is not clear.

A key cautionary note given in the ISO standard⁸⁶ relates to the manner in which the criterion was obtained and its applicability to other types of motion. The ISO limit curves shown in Figure 96 are envelopes of results obtained by vibrating the subjects at each frequency separately, i.e., the subjects were subjected to simple frequency vibration (sinusoidal) not to a spectrum of frequencies as shown, for example, in Figures 94 and 95. Because of this, ISO cautions the reader:

"..... For the adequate description of vibration, which is markedly nonsinusoidal, random, or broad band, the crest factor (ratio of maximum peak to RMS value) of the time function must be determined or estimated: the limits given in this International Standard should be regarded as very tentative in the case of vibrations having high crest factors (that is, greater than 3 ;)"

Unfortunately, none of the air cushion craft analyzed earlier satisfies this criterion in the absolute sense. A collection of the crest factors for the four example traces examined earlier are given in Table 5. The first

TABLE 5 - CREST FACTORS FOR AIR CUSHION CRAFT

Crest Factor	Air Cushion Craft			
	SR.N4	BH.7	SES-100B (Ride Control Off)	SES-100B (Ride Control On)
Maximum peak to RMS (ISO Standard)	4.72	3.77	4.76	3.80
1/2 [Average 1/10 highest/RMS]	1.59	1.92	1.95	2.20
1/2 [Average 1/3 highest/RMS]	1.16	1.37	1.45	1.65

row in Table 5 is the ISO standard definition of crest factor. The standard indicates that the ISO criterion should not be used because all values are greater than 3. However, such a definition for the crest factor does not distinguish between a type of motion that contains many high maximum peaks (such as those shown in Figure 91 for planing craft) and an isolated peak that might occur in air cushion craft. While not pursued at this point the author suggests that an alternative definition

of crest factor based on either the 1/10 highest waves or the 1/3 highest waves might be more appropriate in defining the character of the motion. These values are shown for comparison in Table 5 taken from the example traces 1 through 4. A further concern is that, as Figures 93, 94, and 95 show, the motion of air cushion craft is quite definitely broadband. The problem comes, then, in understanding the significance of comparing the random motion broadband response with the single frequency criteria. Figure 97 shows such a comparison for the SES-100B traces analyzed earlier.

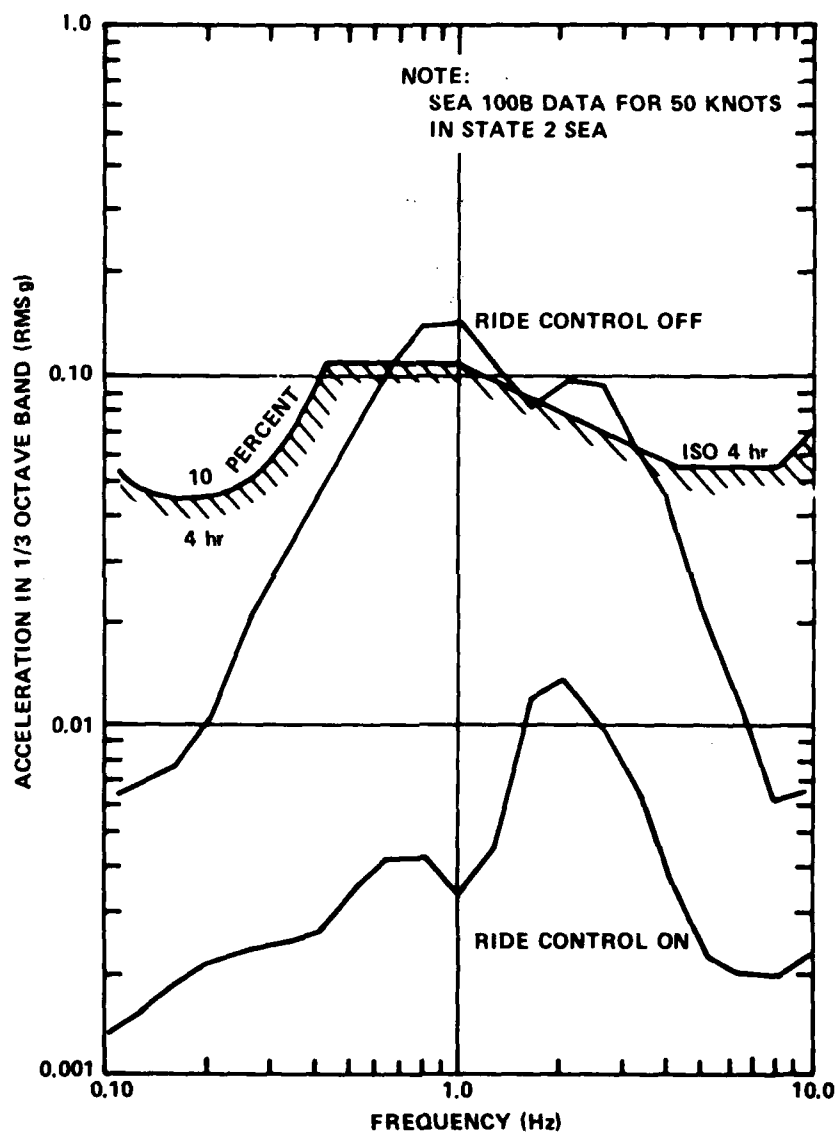


Figure 97 - SES-100B Broadband Response and Narrow Band Criteria

The shaded criteria lines shown are the 4 hr limits taken from Figure 96 with an arbitrary connecting limit line between 0.40 and 1.0 Hz. Based on a straightforward comparison in Figure 97, the SES-100B without ride control would probably experience a fatiguing condition in the 0.60 to 4.0 Hz range but no fatiguing would be noted with the ride control on. It is left as an exercise for the reader to interpret physically for the SES-100B without ride control the difference between several distinct 4 hr tests being vibrated at each of the frequencies between 0.60 and 4.0 Hz and one test for 4 hr where the frequency content varies between 0.60 and 4.0 Hz!

The above discussion on ride quality and ride quality criteria described the state-of-the-art in the subject. Many of the questions raised are being actively pursued in the laboratory but very little "at sea" testing is being accomplished. This definitely needs to be pursued if high speed air cushion craft are to be designed to acceptable ride quality limits in the future.

CHAPTER V

CONTROL

As discussed in Chapter IV on Stability and Ride Quality, the requirements for stability and control for a particular craft frequently become mingled and design decisions are often made according to 'operator handling' needs. As such, it is difficult to give precise criteria of general applicability. There are, however, several basic characteristics and forms of control used on existing air cushion craft which will be discussed.

In many respects the control requirements of the sidehull form of air cushion follow fairly conventional and well documented means of ship control, employing rudders, skegs, and stabilizer fins. The amphibious air cushion craft, on the other hand, is unique and requires new forms of control not found in the textbooks. Accordingly, because of this uniqueness and the desire to keep the size of this report within manageable proportion, this chapter on control will deal, almost exclusively, with the amphibious form of air cushion craft.

Difficult control problems on amphibious air cushion craft have been associated with directional control, specifically, movement in the lateral and yawing sense, but with considerable influence from the roll stiffness and/or method of roll control. The difficulties arise mainly because of the craft's unique necessity to combine relative freedom from the surface over which it operates with the ability to maneuver in a confined space. Amphibious air cushion craft have six degrees of freedom: vertical, longitudinal, and lateral, plus rotation about each of these axes, and although, in ideal conditions, they are designed to operate clear of the water surface, in adverse conditions quite large hydrodynamic forces and moments, especially yawing moments due to excessive asymmetrical skirt contact, can occur. These must be countered almost entirely by aerodynamic means, if the amphibious capability is to be retained.

TYPES OF CONTROL SYSTEMS

A distinction will be made here between "trim" and "control;" although often the same control device is used for both. The distinction is determined by whether the setting is small or large, or whether the control setting is adjusted or variable. For example, adjustment of skirt lifters would provide a roll (or pitch) trim and continuous movement of the skirt lifters would provide roll control. Also, the controls for thrust and lift will not be discussed since they are rather obvious settings of rpm and pitch on the propeller and fan blades.

Primary consideration will be given, therefore, to the difficult control problem of providing directional control to the air cushion craft. An indication of the variety of control methods in use can be seen from the following list:

1. Rear-mounted fins with rudders for yaw control
2. Differential thrust of yaw control
3. Swiveling bow thrusters as on the AALC JEFF(B) for yaw, sideforce, and craft speed control
4. Multiple, swiveling free propellers as on the SR.N4 for sideforce, yaw, and speed control
5. A swiveling ducted propeller mounted near each of the four corners of the craft as on AALC JEFF(A) for yaw, sideforce, and speed control
6. Puff ports for low-speed sideforce and yaw control as on the SR.N5, SK-5, and SR.N6
7. Propulsive thrust from the lift system utilizing multiple rudders in the jets as on the CC-7 for yaw control and reverse thrust buckets for stopping
8. Skirt lift for roll control and to a lesser extent yaw and sideforce control as on the SR.N5 and SR.N6
9. Surface contact devices such as the retractable water rods used on the MITSUI MV-PP05 for turning

Basically, the above specific control method examples can be grouped under the following main methods, viz:

Aerodynamic Control Surfaces

These can be operating either in the free stream or in the slip-stream of the propeller(s) or in cushion bleed air.

Thrust Producing Devices

These may be vectoring of propeller thrust through either angle variation including reverse pitch and rpm change; or cushion bleed systems either from the cushion, plenum, or direct fan blowing.

Lift Vectoring Devices

These devices involve modifying either the cushion pressure distribution and thus indirectly move the center of pressure or move the center of pressure directly through some skirt movement.

Each of these control methods have merit and disadvantages and will be discussed in turn. Much of the material presented here is based on lectures given in the summer and fall of 1975,^{98,99} but expanded to reflect current developments and some novel concepts.

AERODYNAMIC CONTROL SURFACES

Although free stream control surfaces can be used to provide (depending on their position relative to the craft center of gravity) yawing, rolling, and pitching moments as well as lift, drag, and sideforce, their primary use has been to provide a yawing moment and hence directional

control. In this sense they have two main limitations: they are ineffective at low speeds and at high yaw angles. In particular rear mounted fins and rudders can be a positive embarrassment in the tailwind case.

However, mounting the controls in the slipstream of a jet or propeller considerably improves their effectiveness. Again their use is limited in the tailwind case because low thrust is required at high yaw angles. It should be noted that rear mounted control surfaces used for directional control tend to give an adverse rolling moment, by virtue of their height relative to the center of gravity. Also, they are almost noneffective during reverse thrust.

The aerodynamic efficiency of the aerodynamic surfaces at low speed can be improved somewhat by the use of cushion bleed. Cushion bleed, via ducts, on the lower portions of the rudder sides was used on the original SR.N5 and SR.N6 as a convenient modification to improve rudder effectiveness, but it is not regarded as good in principle because of the lift and propulsion power penalty. The, admittedly small, amount of permanent forward thrust can be offset, if necessary, by reverse propeller thrust or by dragging the skirt. Note, however, that the rudder ducts have been eliminated on the later SR.N6 Mk 6 (see Figure 206, Chapter IX) which has twin propellers and can thus achieve a moment by differential pitch.

There are many variations of aerodynamic controls that can be applied to air cushion craft but they have not been pursued vigorously for the intermediate (30-100 mph) speed air cushion craft for the reasons stated. For high speed or aerodynamic air cushion craft (100-300 mph) aerodynamic control surfaces are much more effective. One scheme used to advantage on high speed air cushion craft is the dorsal fin control. Figure 98 shows such a control mounted on the VRC-1 (see Figure 9, Chapter 2). The fin is mounted midship above the craft C.G. and is activated through steering control of the pilot's wheel.



Figure 98 - VRC-1 With Dorsal Fin Control

Such an aerodynamic control provides the necessary sideforce with minimal banking which would be clearly limited for a wing-in-ground effect vehicle such as described here. Figure 99 shows another view of the VRC-1 during its trials at Rogers Dry Lake Bed, Edwards Air Force Base, California in 1964. The fin has been rotated to generate a lift force to starboard for a given radius turn, while the rudders have been operated to rotate the craft into the turn. A single dorsal fin has an advantage over two forward mounted fins in that it has less drag, is not destabilizing and does not obstruct the pilot's view.

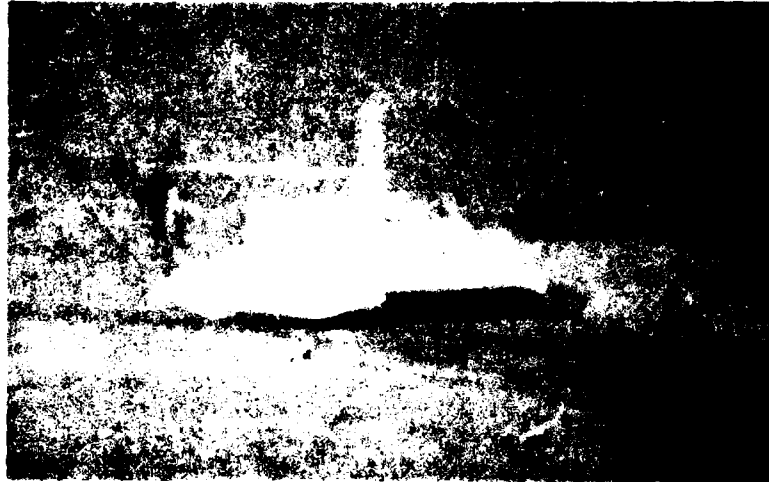


Figure 99 - VRC-1 Initiating Turn to Starboard

THRUST PRODUCING DEVICES

This blanket title includes air propellers, control ports, and jets. Their main advantage, when compared with aerodynamic control surfaces, is that they are relatively independent of wind speed and yaw angle.

The most positive and effective control forces and moments are provided by multi-unit installations of free propeller or ducted air propulsors, suitably distributed over the craft planform area. If the thrust can be vectored by rotating the air propulsor mountings about vertical axes, the control provided is increased, and the propulsors can be arranged, in line, longitudinally.

Typical early examples of the use of propellers for control occurred on the Vickers-Armstrong VA-3 and the British Hovercraft Corporation SR.N3. In the former case the use of twin propellers mounted side by side at the rear of the craft provided a yawing moment by means of differential propeller pitch and thus differential thrust. Figure 100 shows the basic parameters of such an arrangement. Although this a very effective form of control it has the disadvantage that decreasing thrust on one side tends to reduce the craft speed; thus not utilizing all the available power. With this configuration there is no direct means of providing a sideforce relative to the body axis.

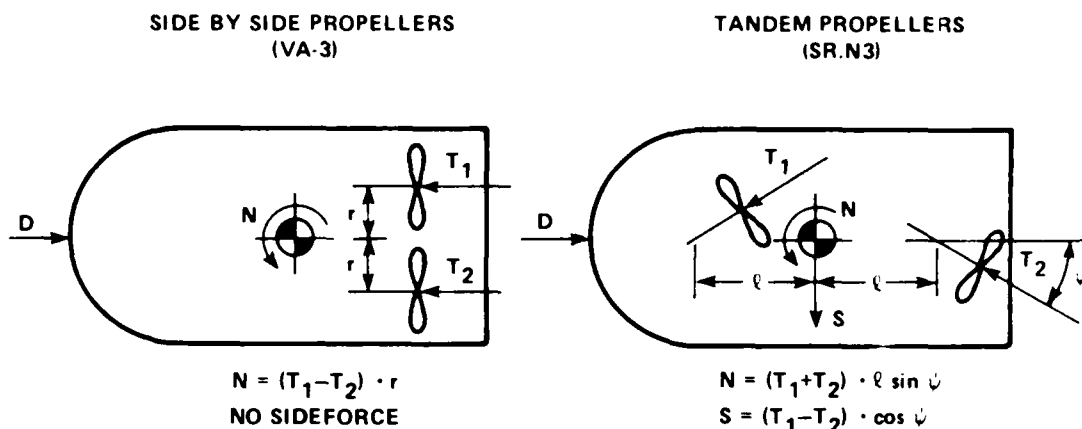


Figure 100 - VA-3 and SR.N3 Thrust Vectoring

In contrast, the SR.N3 with fore and aft swiveling, pylon-mounted propellers can generate sideforce, yawing moment, and rolling moment. In addition, the available moment tends to be higher because the propellers are further from the craft center of gravity and less thrust is lost in producing a yawing moment.

Single swiveling pylon installations have also been considered. In this case it is clear that a single pylon, depending on its position, can produce rolling and yawing moments and a sideforce, e.g., one mounted above the center of gravity would only produce a rolling moment and a sideforce. Similarly a fore- or aft-mounted pylon could produce a yawing moment, but would produce rolling moments, of opposite sense, i.e., a forward-mounted pylon tends to roll the craft into a turn and an aft-mounted pylon tends to roll it out. Whether or not this latter case would have an adverse effect would depend on the craft stiffness in roll and its nominal clearance height because, at low stiffness and clearance, adverse roll might lead to surface contact and thus an adverse hydrodynamic yawing moment. A single unit slightly ahead of C.G. produces desirable roll, sideforce, and yaw.

Swiveling the propulsors to vector the thrust provides a powerful yaw control, and in a multipropulsor arrangement can be used to produce a pure sideforce, the latter depending on the number of propulsors and the angle through which they are permitted to swivel. For example, the SR.N4 with four pylons having a swiveling angle of ± 35 deg can balance the thrust of the front propellers with reverse thrust on the rear ones while producing a pure sideforce. The limiting factor is thus the amount of reverse thrust available.

Figure 101 (provided by courtesy of Blandford Press Ltd)* shows the SR.N4. The inserts show the various control modes available (left to right) through operation of pylons and rudders, and pitch of propellers.

*This figure originally appeared in Reference 4.

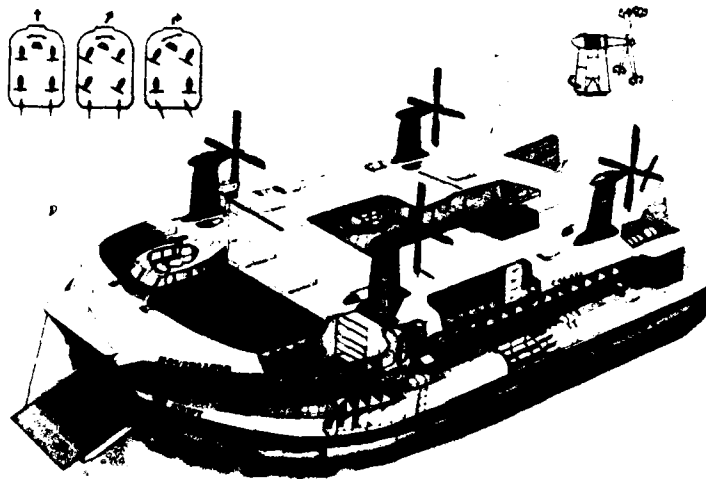


Figure 101 - Control of the SR.N4

In the upper left hand inserts to Figure 101 are shown three combinations of control to effect craft heading. The position of the control wheel and rudder bar is also shown on the inserts. In the upper right hand insert to Figure 101 is shown how propeller pitch is used to control craft speed. Forward movement of the control wheel induces positive pitch to propel the craft forward.

In some cases, swiveling the pylons will not only produce a yawing moment but also a rolling moment as well. Again this depends on the number of propellers and their degree of rotation. The mechanical difficulties discourage large angular movement of the pylons and, therefore, the production of a sideforce by vectoring propeller thrust through 90 deg so far has not been attempted. With this amount of movement, it is possible that the thrust levels used would be limited by the roll stiffness of the craft. Figure 102 shows some of the possible arrangements of propeller configurations that provide various types of control forces and moments.

At this point can be seen the interaction between major subsystems in the design of the craft; in this case, the interaction between the propulsion system and the control system.

As an example of this interaction, consider the propeller installations of the JEFF(A) and JEFF(B) craft. More details on the design of the ducted

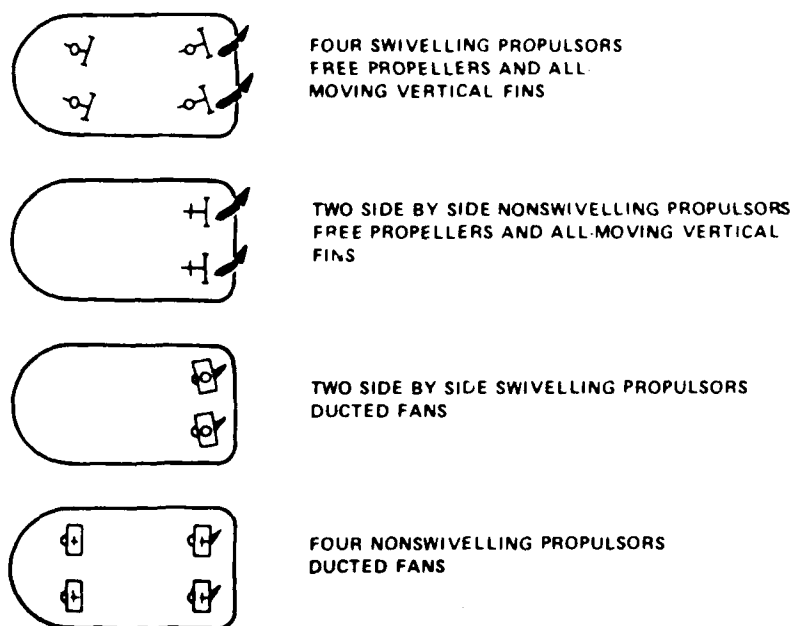


Figure 102 - Free Propeller and Ducted
Fan Configurations

air propulsors are given in Chapter IX. Both craft are required to fit inside the well deck of an LSD and, therefore, had limiting height and width constraints on the design. Figure 103 shows the particular configurations of each craft.

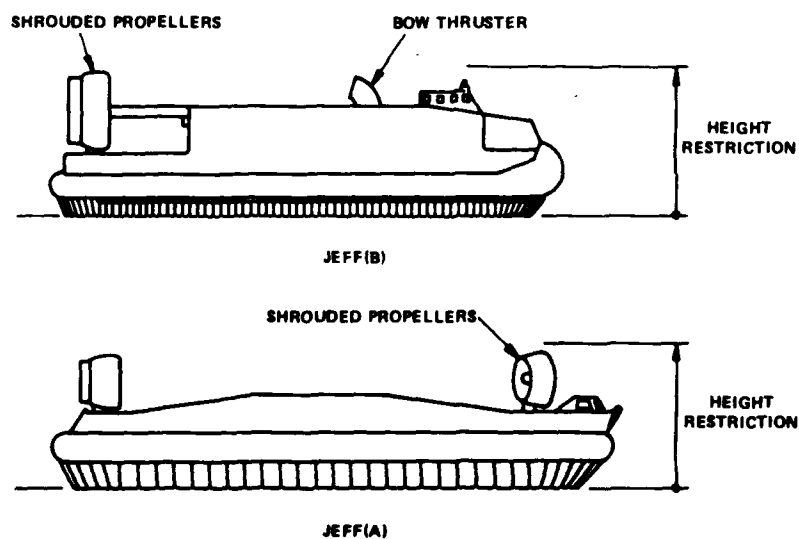


Figure 103 - JEFF Craft Propeller Installations

The JEFF(A) craft uses four swiveling small shrouded propellers of 7.5 ft diameter. These propellers are small to fit the height restriction and suffer a loss in propulsive efficiency as a result of it (see Figure 200, Chapter IX). The JEFF(A) propeller has approximately 10 percent less propulsive efficiency than the JEFF(B) propeller. An advantage of the JEFF(A) installation is that it has a control system independent of the lift system.

The JEFF(B) propeller diameters have been kept large at 11.7 ft, to maximize efficiency, and in this case, are expected to have 55 percent propulsive efficiency (compared to the 45 percent for the high thrust coefficient, JEFF(A) propeller). The two JEFF(B) propellers at the rear of the craft are fixed (nonswiveling) and cannot be used for strong control. An additional system is added for directional control; these are the bow swivel ports that use lift fan air. A sketch of swiveling control ports (not those as used on JEFF(B)) is shown in Figure 104.

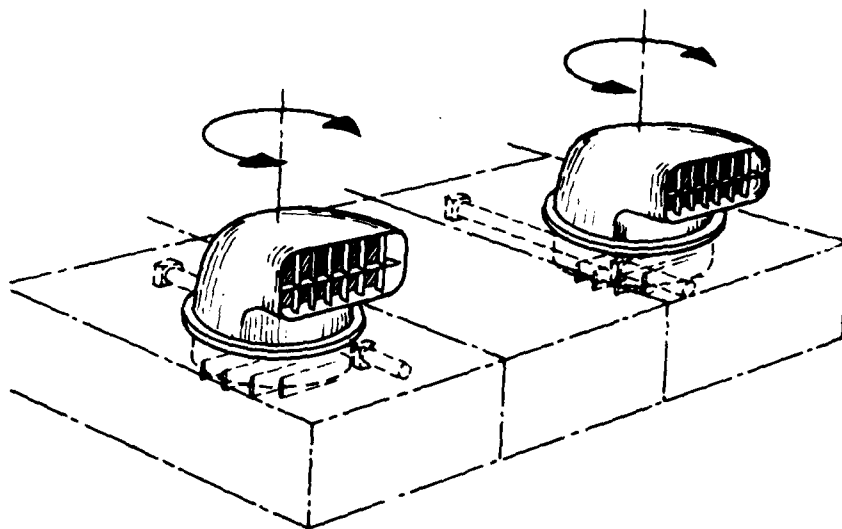


Figure 104 - Swiveling Control Ports

There is no clear advantage or disadvantage between these systems, i.e., whether to integrate or separate the propulsion system from the control system or integrate the control system with the lift system is a matter of design choice to fit the particular needs of the mission or idiosyncrasy of the designer. In the case of the JEFF craft, the mission and performance objectives for each craft were identical and the designs quite different. The ongoing trials program in 1979 should provide some interesting comparative data between these two design approaches.

MULTIPLE PROPELLER CONTROL

The air propeller (free or shrouded) provides the most positive means of control for an air cushion craft and is thus used on more craft than any other scheme. This is despite the high noise level of air propeller propulsion. Swiveling of the propeller pylons and changing thrust settings to achieve the required control, causes fluctuations in the noise level that is annoying to the nearby populace. As discussed in Chapter IX, various improvements are being incorporated into current craft to reduce the noise problem. Nevertheless, swiveling pylons are being used in different multiple arrangements to provide the necessary combination of sideforce and turning moments. Because these installations are mounted high and above the craft C.G., rolling moments are introduced (either out of the turn or into the turn depending on configuration) that must be considered in any maneuvering and control analysis.

Limited information is available on the thrust and sideforces acting on propellers operating at high yaw angles and in multiple installations. Some of this data is provided here for completeness. More data on the thrust and design characteristics of free and shrouded air propellers may be found in Chapter IX. Of particular interest are the propeller characteristics which, when placed in tandem, operates at high angles of yaw and also in reverse. Each of these characteristics will be considered in turn.

Tandem Operation

The desirability of increasing the propeller area to maximize propeller efficiency at cruise speed, coupled with the practical limitations of single installations of large diameter propellers, prompts consideration of tandem installations. Within a given space allotment, such as on the weather deck of an air cushion craft, several propellers, installed in tandem, allow the total propeller disk area to be large. The 190-ton SR.N4 (see Figure 4, Chapter II) is a good illustration of a tandem installation. An alternative method, using contrarotating propellers to increase effective propeller disk area, has not been pursued in US or UK air cushion craft design because of the mechanical complexity and lack of definitive performance information, although this is used in the U.S.S.R. craft, the AIST.

The practical limitations of propeller diameters greatly influence propeller installation selection. The maximum propeller diameter is limited by the beam of the vehicle for safety and handling reasons. Propellers up to 26 ft in diameter have been built, and present technology does foresee propellers larger than 30 ft in diameter in the near future. The new SR.N4, which is the largest air cushion craft in existence today, uses four 21-ft diameter propellers in tandem operation for propulsion.

of air propellers and the effect of the air cushion on the efficiency of the propellers. The effect of the air cushion on the efficiency of the propellers is a function of the air cushion pressure, the air cushion area, and the air cushion velocity. The air cushion pressure is a function of the air cushion area and the air cushion velocity. The air cushion area is a function of the air cushion pressure and the air cushion velocity. The air cushion velocity is a function of the air cushion pressure and the air cushion area. The air cushion pressure is a function of the air cushion area and the air cushion velocity. The air cushion area is a function of the air cushion pressure and the air cushion velocity. The air cushion velocity is a function of the air cushion pressure and the air cushion area.

As pointed out with the tandem operation, the air cushion pressure on the propellers would frequently operate at the edge of the limit of operation, which would lower their efficiency. Some studies have been made of the efficiency of air propellers are shown in Figure 1. The data are taken from Reference 4 based on work by Shank and Hinkle. The references examined tandem operation performance in terms of propeller

efficiency as a function of the thrust coefficient C_T .

For a typical thrust coefficient $C_T = 1.0$, it can be seen from Figure 1b that the overall propeller efficiency of the front propeller in a tandem arrangement might be 66 percent, while the aft propeller would have an overall propeller efficiency of only 51 percent. Some improvement can be made in actual installations by operating the rear propellers at blade angles 5 to 10 deg higher than the forward propellers. Also, canting the forward installations at some small angle can divert their wake from impinging on the rear propellers in certain operating conditions of yaw. In any event, impingement is bound to occur under some conditions because of the wide range of yaw angles in which an air cushion craft is required to operate for maneuverability or operation in crosswinds. Accordingly, it is important in design to determine the effects on propeller performance when an air cushion craft is operated at high yaw angles, whether it be for tandem operation or for single-propeller installations.

Yaw Performance

In maneuvering and in crosswind operation, the propulsors will experience yaw angles of less than 10 deg most of the time, with occasional excursions up to 50 deg. Propellers operating at such yaw angles have lift and drag forces acting on them that can be separated into forces in the propeller thrust and normal directions. Both thrust and normal forces increase with yaw angle. For the free propeller, the normal force is small, however, for the ducted propeller, this normal force is significant because of the aerodynamic forces acting on the duct. To summarize these results, the effective thrust or thrust in the direction of vehicle motion is considered. The normal force subtracts from the effective thrust, and the result is that a free propeller has a much larger effective thrust than a ducted propeller. It should be noted, however, that the large normal forces on a ducted propeller could be useful in maneuvering the vehicle, particularly in turns, or in counteracting crosswind effects. Some typical

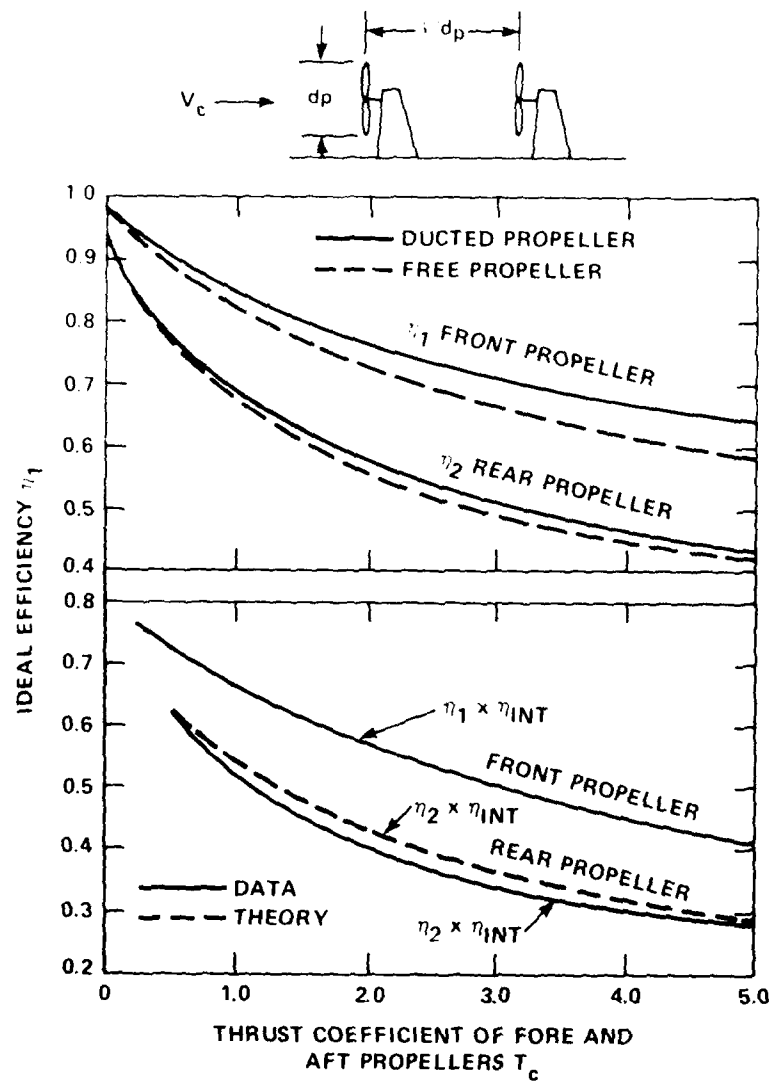


Figure 105 - Efficiency of Tandem Propellers

results of the propeller thrust and sideforce variation with yaw angle are shown in Figure 106 where the effective thrust along the direction of flow and the sideforce normal to the direction of flow are,

$$T_{EFF} = T \cos \alpha + N \sin \alpha \quad (106)$$

$$S = T \sin \alpha + N \cos \alpha \quad (107)$$

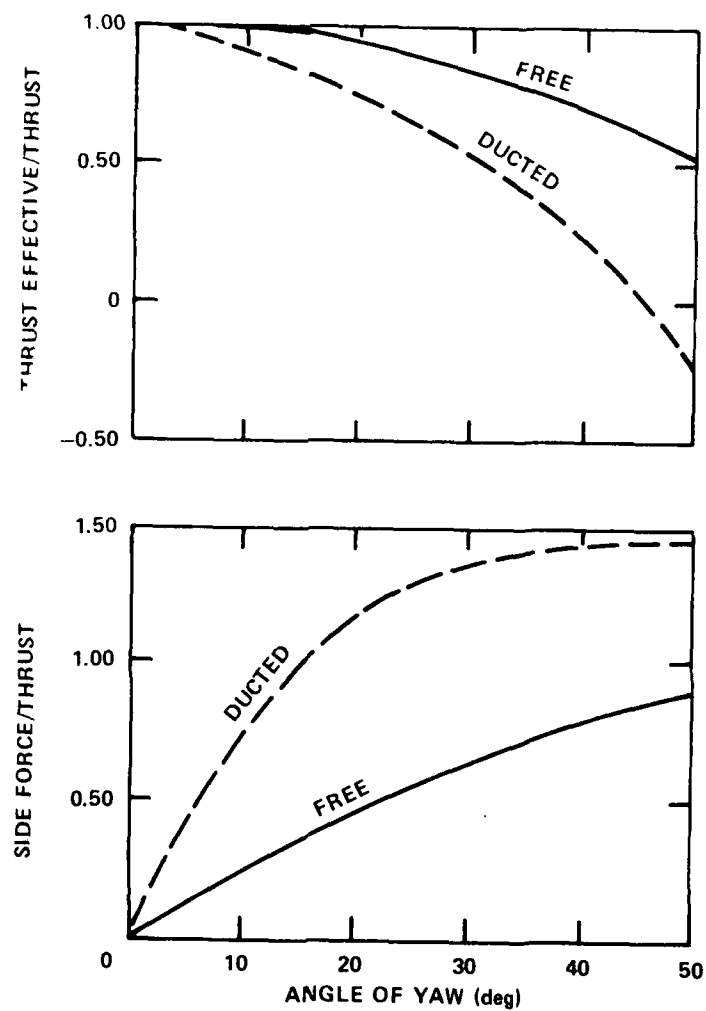


Figure 106 - Typical Propeller Forces in Yaw

where α is the angle of yaw, and T and N are the thrust and normal forces acting on the propeller. These are functions of the propeller parameters that will be discussed in Chapter IX. The data from which Figure 106 was prepared are shown in Figures 107 and 108 for both the free and shrouded propeller.

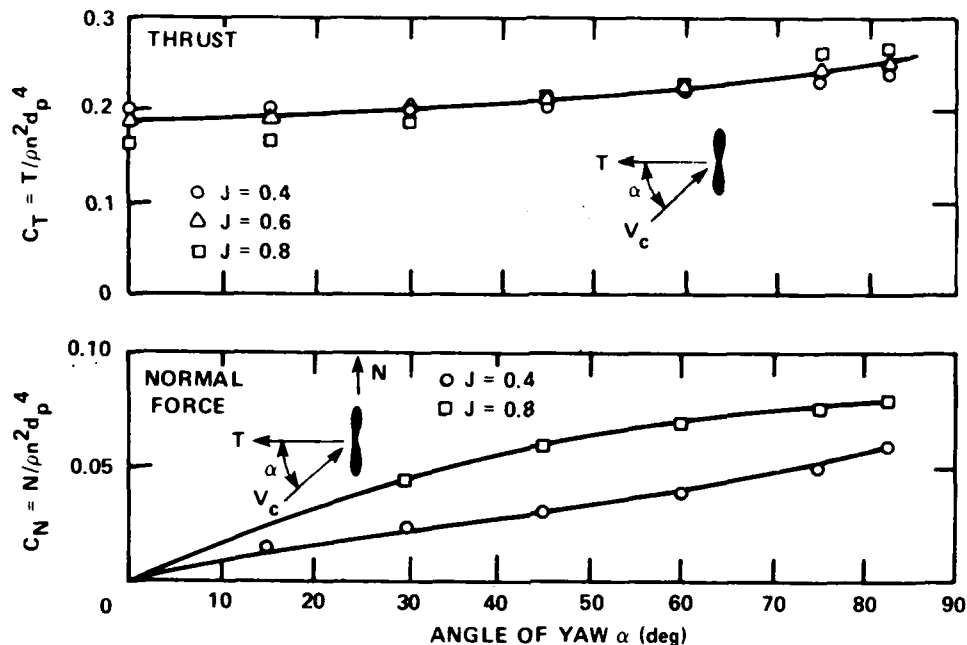


Figure 107 - Thrust and Normal Force on Free Propeller

Reverse Thrust

The low-friction nature of the air cushion requires the air propeller to produce a rapid response and adequate thrust capability in the reverse direction. This is required to minimize stopping distances and also, in some instances, to maintain a hovering capability in wind conditions.

Although no adequate theoretical methods for reverse thrust prediction exist, an empirical method based on the data for free propellers and, to a limited extent, for ducted propellers has been developed. A representative curve for the case $hp/d_p^2 = 15 \text{ hp/ft}^2$ is shown in Figure 109 where d_p is the propeller diameter.

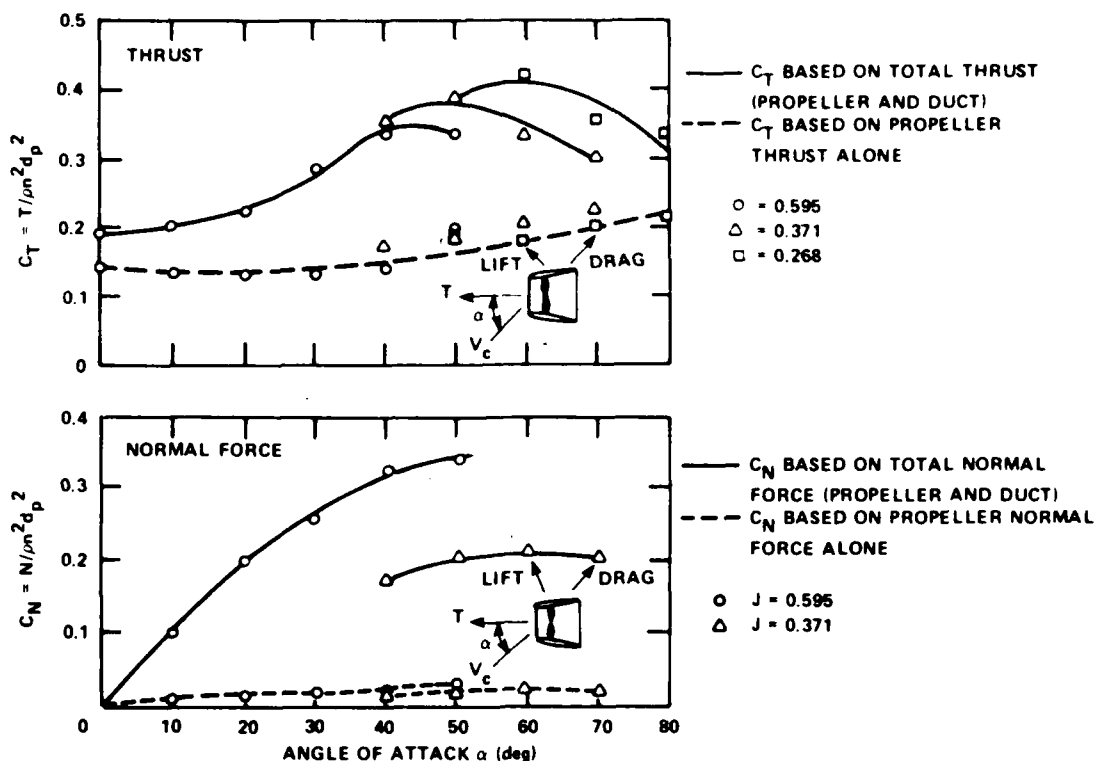


Figure 108 - Thrust and Normal Force on Shrouded Propeller

A free propeller is superior to a ducted propeller when reversed in the conventional manner, that is, when reversed through its flat pitch position. The reverse thrust performance of a ducted propeller can be improved by reversing through its feather position and by including a variable geometry nozzle to avoid flow separation at the shroud trailing edge during reverse flow. When a blade is reversed through flat pitch, its camber is in the wrong direction to enable it to do maximum work on the flow field. By reversing through the feather position (i.e., in the opposite direction) the camber is properly oriented. Improved reverse thrust results even though the blade leading edges and trailing edges are reversed. Unfortunately, the large angular rotation of the blade required to reverse through the feather position is beyond the capability of conventional linear pitch changing mechanisms. Other pitch changing schemes have been demonstrated, however, on high solidity propulsors (Q-fans, see Chapter IX).

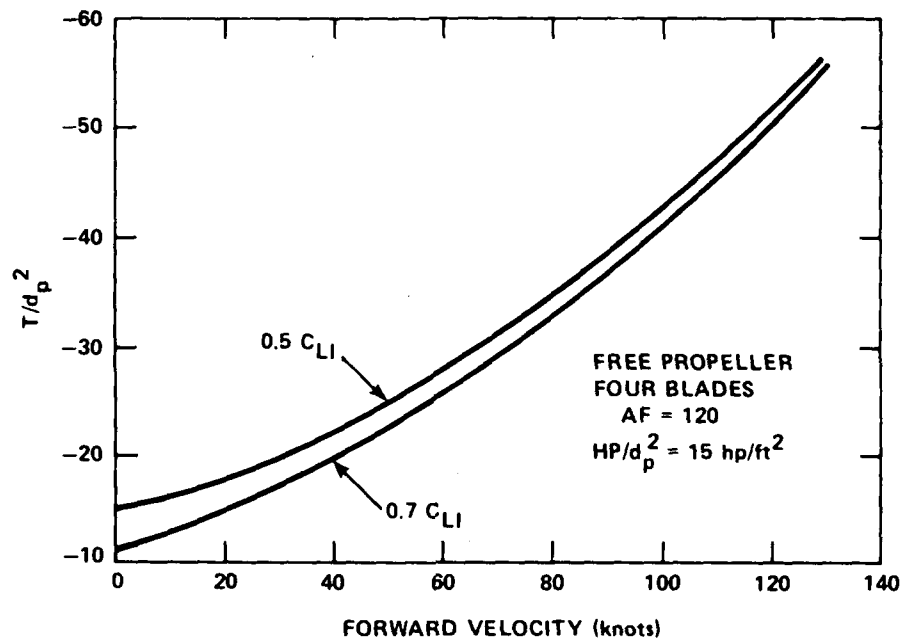


Figure 109 - Reverse Thrust of Free Propeller

PUFF PORTS AND BOW THRUSTERS

A distinction should be made between the various schemes of vectoring thrust from the lift system. Puff ports were the original schemes used on the early SR.N5 and SR.N6 craft. They were placed (roughly) at the four corners of the craft opening directly to the cushion plenum. The arrangements may be seen in the two upper photographs in Figure 13 of Chapter II. The puff ports were used to provide sideforce and could be used independently or in combination to provide both sideways and rotational motion to the craft. The puff port force capability is generally quite low, resulting in a maximum normal acceleration of approximately 0.01 g. As such, they are normally used only for low-speed maneuvering such as docking.

Air-jet thrusters, on the other hand, are high velocity air ejectors where the control is directly coupled with the lift fan system, i.e., upstream of the low air velocity plenum chamber where puff ports are used. The swiveling bow thrusters, discussed earlier, belong to this class of thrust vectoring devices. This type of system is more efficient than puff ports, depending upon the geometry, but less efficient than an air propeller. Various craft have used different versions of these direct lift fan coupled air jet thrusters. The original versions appeared on the CC-4

and CC-5 and now recently on the CC-7.¹ In these applications the air jet thrusters were used for main propulsive thrust with directional control supplied by aerodynamic control vanes placed in the fan air jet exhaust. As discussed in Chapter IX the propulsive efficiency of such schemes rarely exceeds 50 percent. The application of these air-jet thrusters for speed and directional control by the use of swiveling appears on the JEFF(B). Model test data on these schemes showed that these thrusters would be highly successful. Current full-scale testing of the JEFF(B) in Panama City (see Figure 19, Chapter II) is confirming expectations. A more generalized concept of the bow thruster is shown in Figure 110. In this case the bow thruster is a ducted fan producing side thrust in either direction as required and located well ahead of the craft C.G. but not high enough to generate appreciable rolling moments.

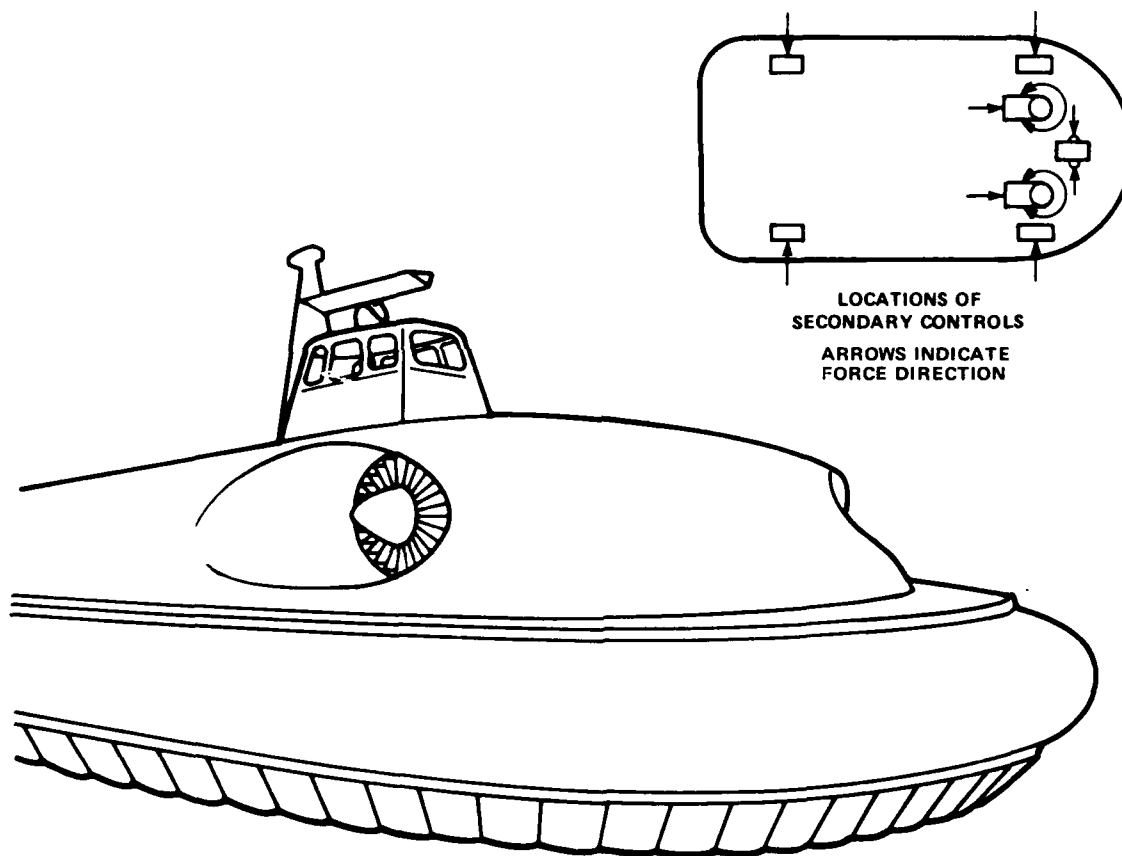


Figure 110 -- Bow Thruster

LIFT VECTORING DEVICES

These devices can be divided into two categories: those which modify the cushion pressure distribution thus changing the C.P. position and hence the lift moment about the C.G., and those which physically move the cushion and hence the C.P. Both these types may be used to provide rolling and/or pitching moments, and hence side and thrust forces, and, should surface contact occur at forward speed, some yawing moment.

Typical examples of the former method are the roll control valves used on the SR.N1 Mk 1 and the skirt lift used on SR.N5 and SR.N6 where cushion air was locally stopped or allowed to escape, respectively.

There are three basic ways of achieving lift vectoring to vary the center of pressure as mentioned. These are cushion feed valves, cushion bleed (i.e., vent) ports, and skirt lift. Note that these methods change either directly or indirectly the C.P. Other methods of lift vectoring are achieved through C.G. shifting. This can be accomplished by moving weights on tracks on the craft as used on the Hovercraft Development Ltd. craft HD.2 or by pumping fuel into ballast tanks as on the SES-100B, JEFF(A), and many of the British Hovercraft Corporation craft. Most C.G. shifting schemes, however, are more in the nature of pitch and roll trim adjustment methods rather than control methods. The discussion that follows is accordingly restricted to C.P. shifting control schemes.

Some possible schemes of cushion feed valves and cushion bleed ports are shown in Figure 111. Cushion feed valves giving differential flows to cushion compartments are effective and can also be used for pitch and heave control. However, with their use, the craft virtually becomes a pure plenum machine. Dumping air from selected cushion compartments via vent ports, as shown in the lower sketch of Figure 111 works well but at the expense of decreasing the nominal air gap. If used at high speed and at high yaw angles such schemes could present a hazard.

Each of the above schemes affect the pressure distribution beneath the craft by differentially altering the pressures in cushion compartments on either side of a flexible divider. An early example of pressure distribution modification was provided by the roll control valves on the SR.N1. With a compartmented cushion and separate fan feeds to different compartments a similar result, again more in the nature of a trim than a control device, can be obtained by differential fan rpm. A jupe skirt system (see Chapter VI) could be used in a similar way by increasing or decreasing the air supply to one side.

The third method employed on operational air cushion craft is one of skirt lift or cushion shifting so as to physically move the C.P. It is important to note that the force produced by skirt lifters is a component of cushion "lift" caused by rolling (or pitching) the craft, not by the reaction to the escaping air, i.e., the force acts towards the part of the craft where the skirt is lifted. Although the use, as a yaw

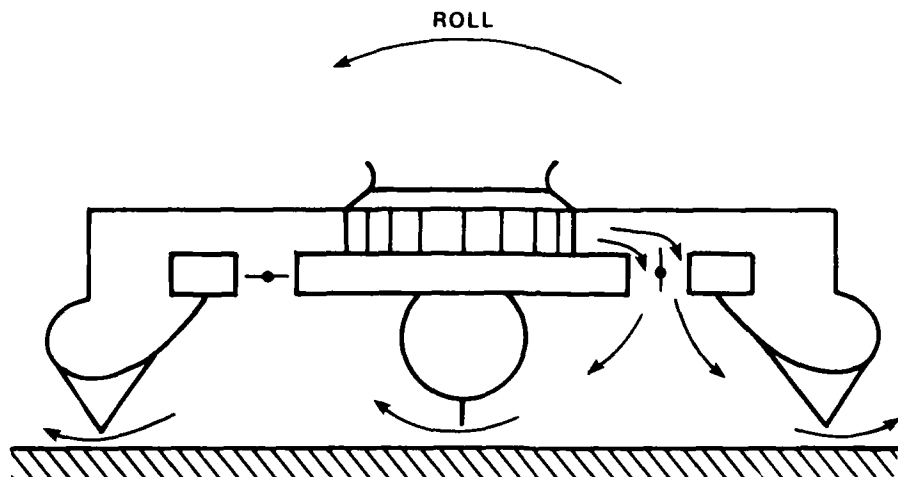


Figure 111a - Cushion Feed Valves

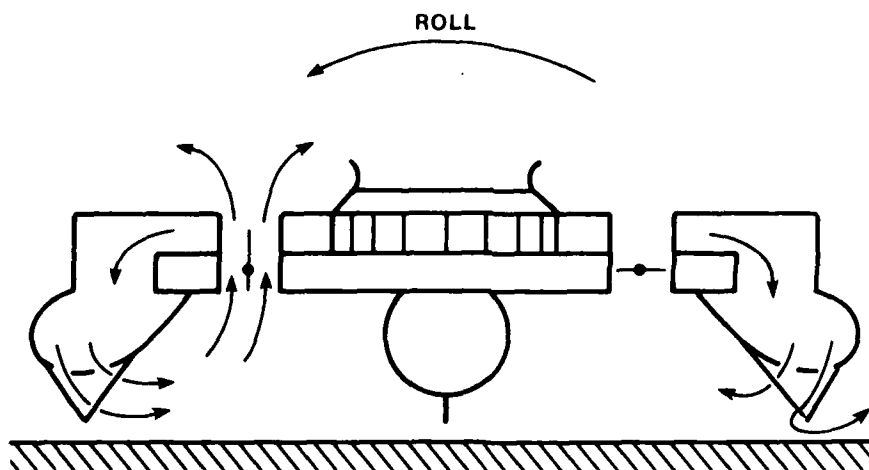


Figure 111b - Cushion Bleed Ports

Figure 111 - Cushion Valves and Ports

control, of asymmetrical skirt contact produced by roll control, is not generally acceptable, because of the associated water resistance, it may be of use in selected circumstances. Figures 112 and 113 show some of the basic schemes used on skirt lift and cushion shifting. Such schemes have

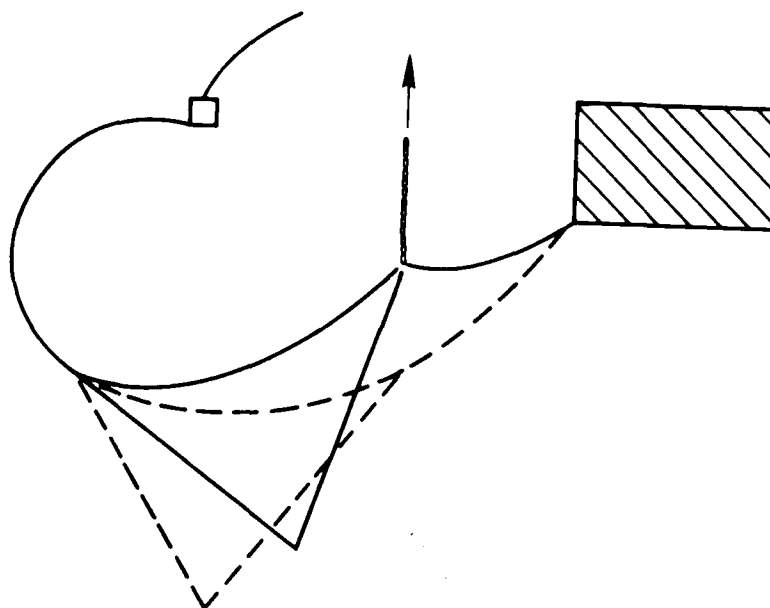


Figure 112 - Skirt Lift

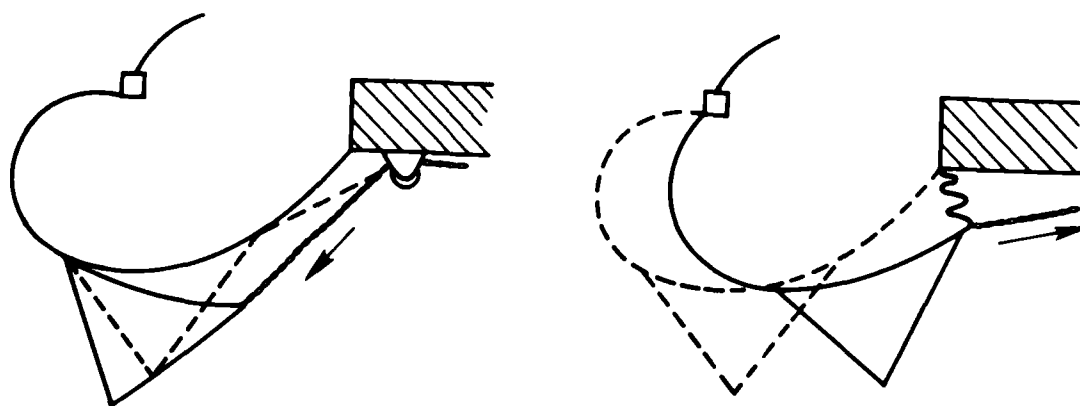


Figure 113 - Cushion Shift

been employed in different mechanical versions on the early SR.N5, SR.N6, and VT 1 as well as on some others. On the HD.2 and VT 1 the skirt hemline was moved horizontally by means of jacks and cables (see Figure 113). This changes the position of the cushion C.P. relative to the craft C.G., thus causing rolling and pitching moments. In practice, it has been found that the movement of the cushion area by changing the angle of the fingers (see Figure 112) or by pulling on the bag incurs engineering difficulties but such a system does not need cushion compartmentation and also does not change the craft nominal air gap. With the general tendency toward lower air gaps this is a pertinent combination. Chapter VI discusses the difference between the "bag-finger" skirt (with its compartmentation) and the "loop-segment" (without compartmentation). Hence, now the integration of cushion C.P. shifters for control with the basic skirt system is seen to be a basic consideration in the design of the craft.

Bodily movement of the skirt as described, at least in principle, can be used as a flying control in addition to being a trimming device to allow for C.G. variation in different craft loading. However, at least for the VT 1 and VT 2, use of the system appears to have been discontinued due to mechanical difficulties and also because the control of the craft was acceptable without it.

AERODYNAMIC AND HYDRODYNAMIC FORCE VARIATIONS

The various control schemes either used or envisaged to be used on air cushion craft have been discussed in the previous sections. Additionally, some of the characteristics of the available control forces and how they vary with the characteristically high sideslip angles of air cushion craft have also been described.

To further complicate the situation, it is found that the aerodynamic and hydrodynamic forces that the control forces must overcome also vary over the same wide range of sideslip angles. Because of this, it has been found that extensive model testing both in tow tanks and in free-flight are required to achieve a complete understanding.

As noted earlier, the stability and control characteristics must be considered together because of the need to analyze handling characteristics. The degree of stability varies considerably with yaw angle and, as an amphibious air cushion craft can generate during maneuvers virtually any sideslip angle, it is necessary to analyze the aerodynamic and hydrodynamic characteristics over the range 0-180 deg. This should be done at various speeds to analyze the important effects of crosswinds and tailwinds.

Solid models (no lift fan system) set up in a wind tunnel are frequently used to check the aerodynamic characteristics of the basic hull. In some cases, a dynamic model, which includes the sink effect of the lift system, is used. If the lift fan system is positioned aft, the sink effect produces a stabilizing moment. By way of example, the aerodynamic yawing moment coefficient for the BH.7 is shown in Figure 114.

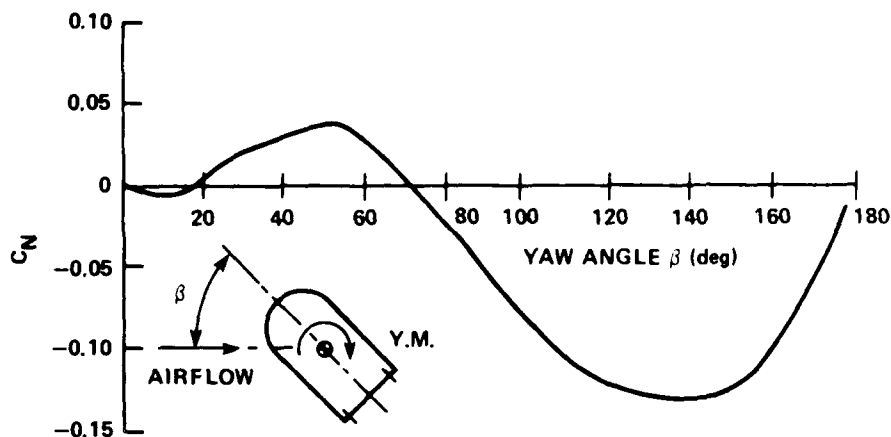


Figure 114 - BH.7 Yawing Moment Coefficient

Much of the information pertaining to the BH.7 and its control problems have been taken from Wheeler.¹⁰² The yawing moment coefficient is defined as,

$$C_N = \frac{\text{Yawing Moment}}{1/2 \rho V^2 \cdot S \cdot B} \quad (151)$$

where S is the overall planform area and B is the craft overall beam. Figure 115 shows the actual yawing moment and the major components contributing to the moment. The conditions for the BH.7 shown in Figure 115 are 40 long tons (gross weight) and calm water.

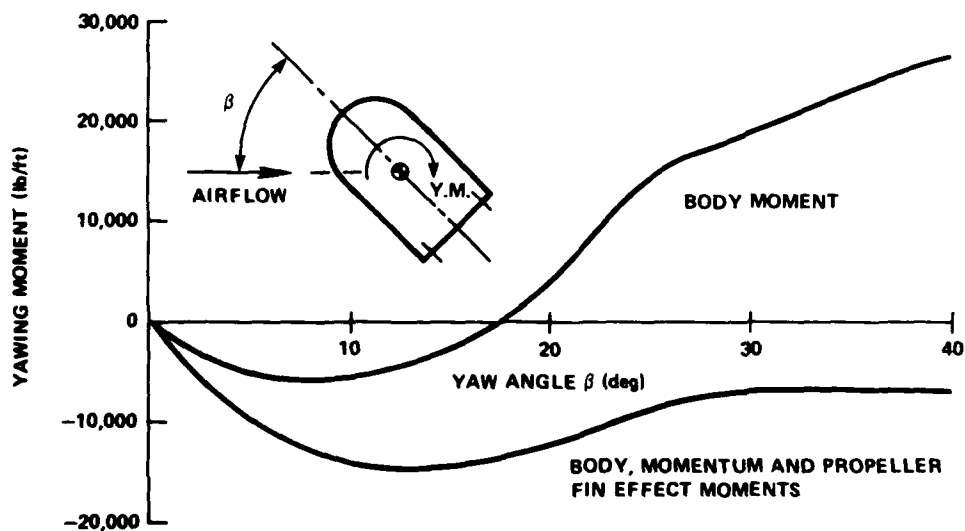


Figure 115 - BH.7 Yawing Moment at 50 Knots

Figure 114 shows the yawing moment (in coefficient form) of the basic hull throughout the full 0-180 deg range showing unstable restoring moments between 18 and 70 deg of yaw. Figure 115 shows the same data for a smaller range of yaw angle but expressed in moment rather than coefficient form. The effects of the propeller fin and the lift fan momentum terms are seen to extend the stable region from 18 deg to beyond 40 deg of yaw.

There are no hard and fast rules governing the degree of stability required, but it is usual to ensure that there is a small amount of positive stability for small angles of yaw, i.e., negative yawing moment coefficient C_N over, for example, the first 20 deg when the intake moment is included. If the directional stability in this range is neutral the demands on the driver for constant corrections via the controls becomes an embarrassment. Conversely if too much "weathercock" stability is provided, the handling characteristics, when on an off-wind heading, may be completely unacceptable. These are some of the reasons for the considerable amount of fin and side area surgery conducted on SR.N5 in its early trial days.

Apart from the aerodynamic forces on the craft, the hydrodynamic forces can also have a considerable effect on the directional stability, and the magnitude of this effect is closely linked to the roll stiffness and the trim. Again, referring to Wheeler¹⁰² and Crewe⁹⁸ some rather interesting hydrodynamic characteristics have been observed peculiar to the traveling air cushion at various yaw angles. From some accurate measurements (using Sea-Fix) of the turning performance of BH.7, the centripetal forces acting in the turn could be estimated. By subtracting the known aerodynamic and thrust components it was then possible to obtain a rough estimate of the hydrodynamic contribution. Prior to these tests it has been assumed that the resultant hydrodynamic force was independent of yaw angle and acted back along the track, i.e., it had been assumed that any component acting normal to the track was small enough to be neglected.

The results obtained indicated that there was, in most cases, a useful component of hydrodynamic sideforce acting normal to the track which reached a peak at between 10 and 20 deg of yaw and increased with inward roll angle. A 1/11 scale model of the BH.7 was tested to confirm these findings and the results are reproduced in Figure 116. The model tests confirmed the findings, indicating a substantial sideforce at low angles of yaw and a rapid fall-off in sideforce beyond 20 deg of yaw. The curves show that the sideforce can be approximately doubled by rolling into the turn although this has the effect of increasing the drag.

The conclusions that can be drawn from these results are that the hydrodynamic sideforce can play a significant part when turning at low yaw angles and can be increased by rolling into the turn. However, in the higher rate turns, which may require yaw angles of up to 60 deg, this component is thought to be of far less importance.

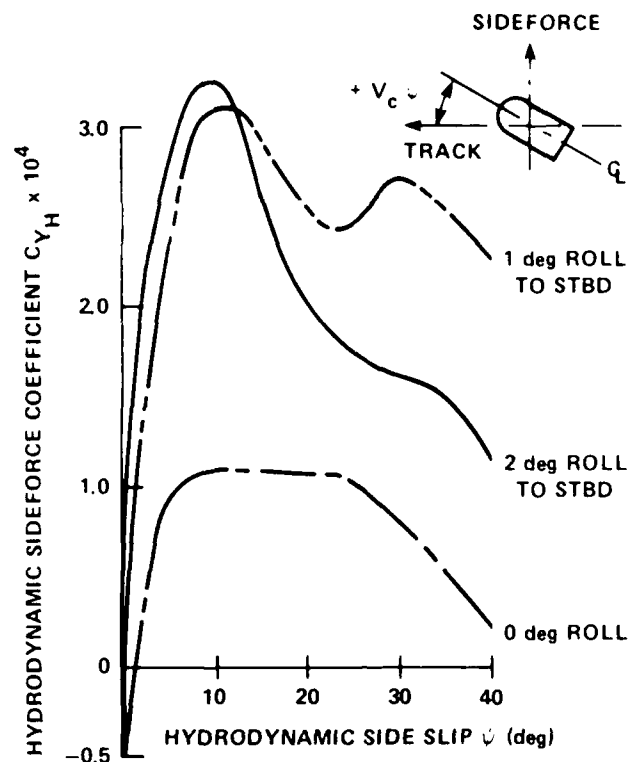


Figure 116 - BH.7 Model Hydrodynamic Sideforce

Insufficient data are available to determine the general applicability of the BH.7 test findings. The single propeller installation and high C.G. gives entirely different control characteristics than would be expected with either the two fixed propeller installations of the JEFF(B) or the four swiveling propeller installations of the JEFF(A). The hydrodynamic characteristics of the cushion, however, should have general applicability.

To this end Everest and Hogben¹⁰³ conducted theoretical and experimental studies on the wavemaking drag of air cushions moving at different Froude numbers and angle of yaw. A detailed summary of their findings will not be presented although it was found that general confirmation of the wave drag theory was obtained. Although some evidence of nonlinear behavior was found at low Froude numbers for heavily laden, yawed craft, Froude numbers in the region of hump speed (F. No. ≈ 0.60), theory predicts a very large rate of change at wave drag with yaw angle; this has been confirmed by experiment. This factor is significant with regard to low speed instability in roll and yaw.

Free wave elevations in the wave pattern have been calculated, including wave profiles under the cushion. In the neighborhood of the craft, some difficulties arise due to transient terms but it is shown that considerations of surface continuity can help to deal with them. These estimates offer a basis for predicting areas of water contact which is particularly useful for the complicated wave pattern produced by a yawed hovercraft. By an analysis of such wave elevations it has been possible to estimate the wave induced sideforce acting on a yawed craft. For the condition of hump speed and 30 deg of yaw, for example, the sideforce was found to be greater than 50 percent of the wave drag!

Figure 117, taken from Reference 103, shows the normalized wave drag in deep water over a range of Froude numbers ($0.40 < \text{F. No.} < 1.4$) and yaw angles from 0 to 90 deg for a "representative" craft the HD.2. The data shown in Figure 117 are based on an effective length (L_e) defined as

$$L_e = \frac{\text{Cushion Area}}{\text{Maximum Beam}} \quad (152)$$

for the particular geometry where the length-to-beam ratio $L_e/B = 1.65$.

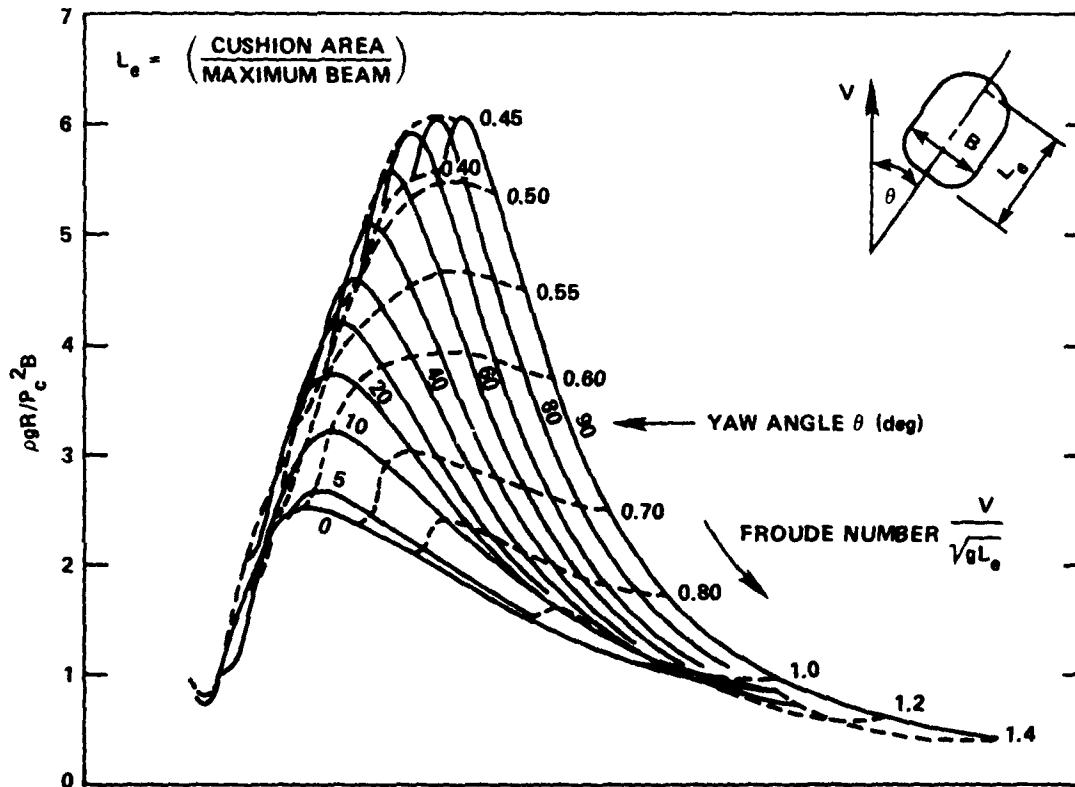


Figure 117 - Variation of Wave Drag with Froude Number and Yaw Angle

Figure 118 compares predicted measured wave drag for a basic rectangular planform of $L/B = 3.2$, at Froude number $V/\sqrt{gB} = 1.51$. The measurements were made in the number 3 tank at National Physical Laboratory, NPL, Feltham, having a cross section 48-ft wide by 25-ft deep. At test speeds this can be regarded hydrodynamically as unrestricted water.

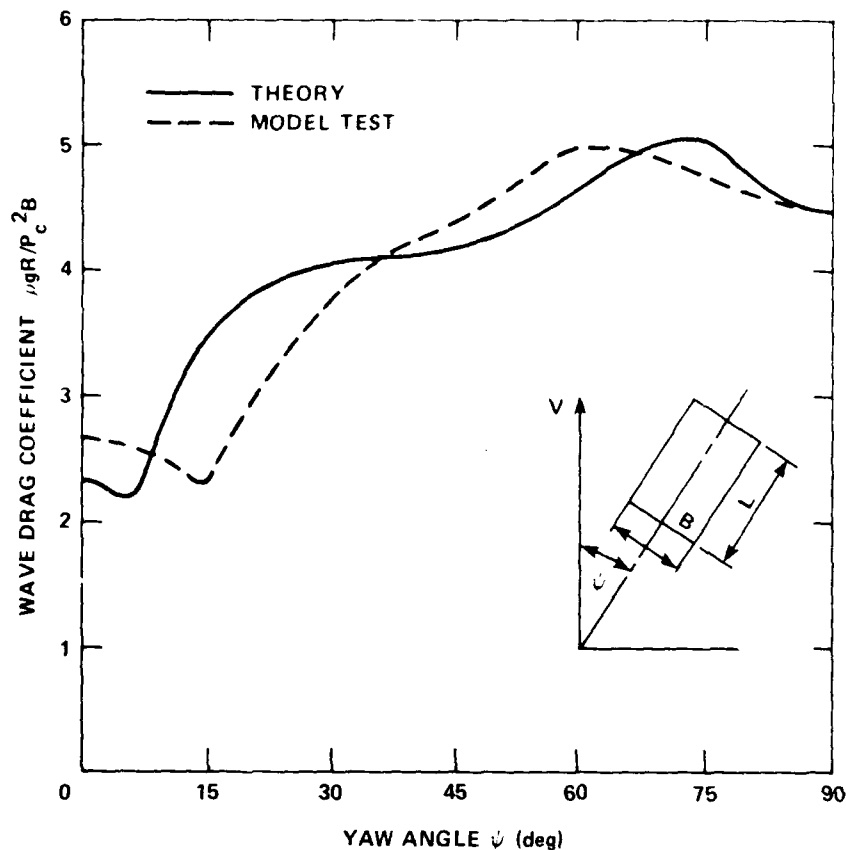


Figure 118 - Wave Drag of Rectangular Air Cushion Craft in Yaw

The rectangular model was free to rise, trim, and roll but was constrained in yaw. It should be noted that the model was unskirted with fixed peripheral jets inclined at 45 deg to the horizontal, and vertical stability jets on the longitudinal and transverse centerlines. However, tests were also made on a skirted, uncompartmented cushion HD.2 model of cushion hemline length 103 in., and area 5320 in.².

The authors¹⁰³ wrote of the Figure 118 results, in effect as follows, "Within the context of wavemaking theory, agreement between theory and experiment was quite good, although difference in "phasing" between the curves tends to exaggerate errors where the rate of change of wave drag is severe. Theory predicts a rapid change of wave drag between 5 and 25 deg of yaw, the experimental results suggest that the rise occurs between 15 and 35 deg of yaw. The predicted doubling of wave drag in relation to the unyawed case is found to occur for yaw angles between 60 and 75 deg. An overestimate of the wave drag at zero yaw was observed in these tests. The same effect was found in earlier tests on this model around hump speed, together with some difficulty in repeating wave pattern drag measurements. At Froude numbers above hump speed, considerably greater precision was achieved. These earlier results imply that the unyawed wave pattern resistance at hump speed may be a little higher than theory predicts, although some experimental error cannot be ruled out entirely. There is a relatively large discrepancy between theory and experiment at yaw angle of about 15 deg, but it may be seen that this is mainly due to a difference in phase between the two curves. Confirmation of the experimental results at this angle was obtained for a range of Froude numbers between 0.46 and 0.67. Correlation was not good in the lower part of the range, but was improving at the higher Froude numbers."

GIMBAL FAN CONTROL

It has often been argued that one of the reasons that the air cushion craft has not made the prophesized large impact on the mass transportation system is due to its lack of precise control. For this reason virtually all development and use (except for recreational purposes) has been in the marine world. The marine development has been on vehicles used for amphibious landings, and in littoral waters, and with projected use in open ocean. The common element in all these uses is the acceptance of lack of precise control (as needed, for example, for an automobile that must stay between painted lines on a roadway).

Various schemes have been tried over the years to provide such precise control. Each of the schemes has had some failing that has rendered it either impracticable or unreliable. One scheme, however, that has been demonstrated with remarkable success on passenger craft of up to 25 ft in length deserves further consideration. This control system called the "gimbal fan concept" by its inventor Dr. Bertelsen^{104,105} combines the lift system, propulsion system, and control system into one integrated system. This is most clearly shown in Figure 119 which is the Bertelsen Aeromobile 14, a small research platform that was first tested in 1969.

The gimbal fan unit is seen at the stern of the craft in Figure 119. The duct is a section of a sphere and is gimbal mounted at its center so that it can be tilted and rotated as required in any direction. The discharge end of the duct faces a filled aperture in the deck, from which air is fed into the cushion. When the fan shaft is vertical, all the discharged air is fed into the cushion. By tilting the gimbal, the operator



Figure 119 - Gimbal Fan Aeromobile 14

allows air from the fan to escape across the deck to provide thrust for propulsion and control. Apart from the propulsion slipstream, there is no loss of lift because the spherical edged duct fits closely into the deck aperture, and rotation of the duct does not increase any air leakage. At the maximum tilt angle of 90 deg for maximum thrust approximately 30 per cent of the fan air is delivered to the cushion. Propulsion and control forces including braking thrust, can be applied throughout 360 deg from the stern by tilting the duct in the required direction.

In early 1978, Bertelsen¹⁰⁴ developed a two unit gimbal fan craft as shown in Figure 120. This highly maneuverable craft is approximately 24 1/2 ft long, and weighs 5,000 lb with eight passengers. Two 150 hp, two-cycle Mercury outboard engines are the total power source. Speed has not been given for the craft but observation of its operation accelerating, stopping, and maneuvering into parking spots in a parking lot leave no doubt as to its speed and controlled maneuverability. Very little work has been done on this type of integrated control system but Bertelsen¹⁰⁴ reports that craft using this scheme could be scaled up to SR.N6 size with no foreseeable problems. Scaling to even larger craft has not been done at this time but no problems are foreseen in applying to at least 200 to 300 tonnes displacement.

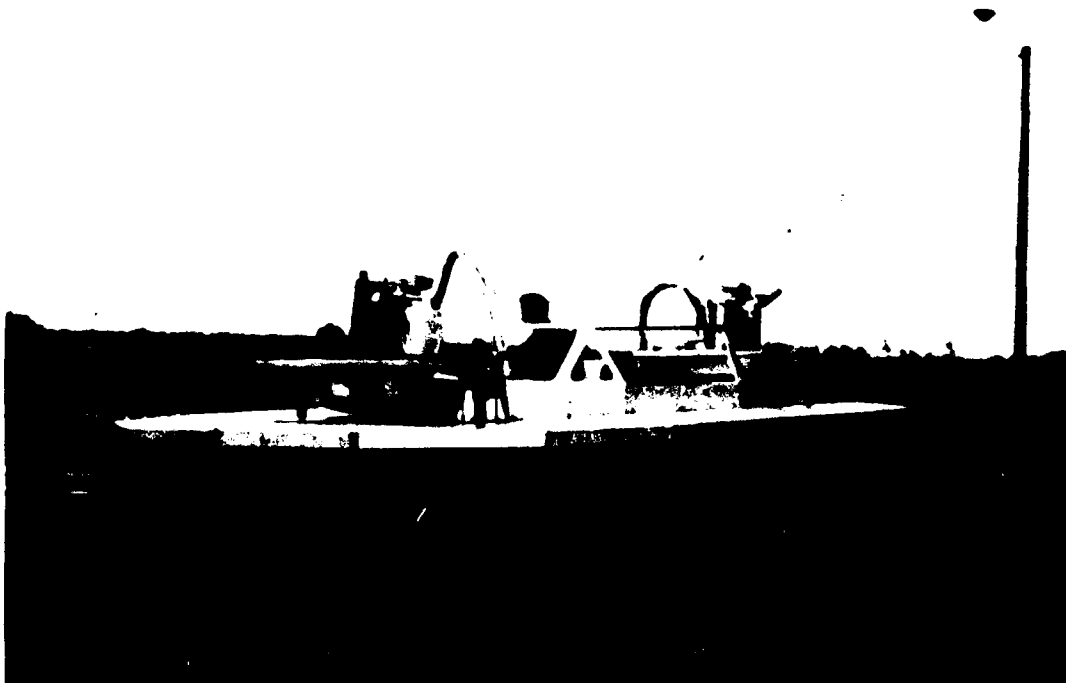


Figure 120 - Gimbal Fan Aeromobile 16

Schemes such as these offer considerable promise to the air cushion craft in opening up uses other than the current limitation to marine use. Off-road transportation may well become practicable with this novel system. A possible complication for larger craft, especially for marine use, is foreseen in the gimbaling of large gas turbines together with their filtering needs.

CHAPTER VI

SEALS AND SKIRT DEVELOPMENT

The seal or skirt system on an air cushion craft started life as a flexible appendage to give obstacle clearance for low power expenditure. Indeed, because of the high power requirements for anything other than small air gaps (see Chapter III for more detailed discussion), the skirt system had to be rapidly developed to avoid an early demise of the air cushion principle.

The skirt system has become not just an appendage but a basic element of prime importance, adding basic stability and, to some degree, control to the craft (as discussed in Chapter V). The skirt determines the craft response characteristics in rough sea conditions, in addition to the basic functions of sealing the cushion flow and providing an obstacle and wave traversing capability.

The terms "seals" and "skirts" do not signify fundamental differences. It has become common practice to refer to skirts when discussing the amphibious form of air cushion craft and seals when referring to the sidehull forms, where seals include planing-type, hinged seals.

Although there are many variants of skirt and seal forms, they can usually be grouped under one of the following headings:

1. Bag-finger
2. Loop-segment
3. Jupe
4. Pericell
5. Hinge seals

In making such a classification, the author has in mind the bow and stern portions of the skirt and not transverse or longitudinal stability keel members or side members. Usually these resemble the bow sections, but certain differences will be discussed. Again, in some craft, the bow seal may belong to one classification while the stern seal belongs to another for reasons of stability, performance, or other design consideration. For clarification and reference, the terminology as used in this report pertaining to the above seal and skirt forms is graphically described in Figure 121. Specific examples of craft using these type forms are illustrated in the following sections on the performance characteristics and the mechanical design aspects of skirts and seals.

PERFORMANCE CHARACTERISTICS

Skirt and seal design adds a new dimension for the designer, embodying principles of flexible membrane analysis and the complex problem of load transfer from the sea through the flexible skirts to the less forgiving hard structure. The design techniques are still under development, but certain basic characteristics are emerging, and some of the "black art" is reducing to rational design methods.

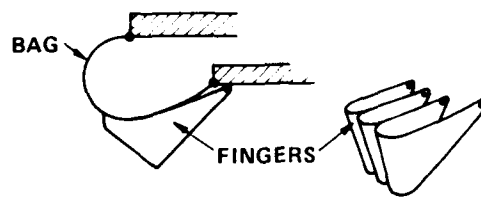


Figure 121a - Bag-Finger Skirt

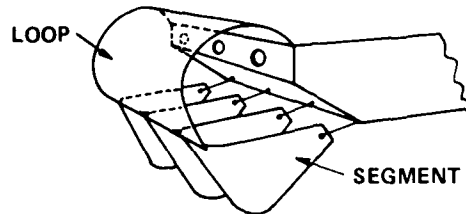


Figure 121b - Loop-Segment Skirt

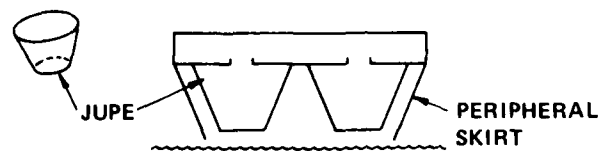


Figure 121c - Jupe Skirt

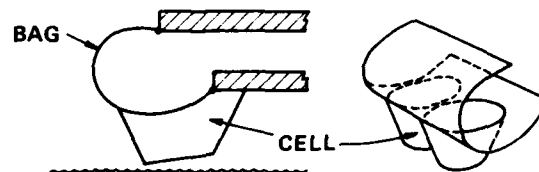


Figure 121d - Pericell Skirts

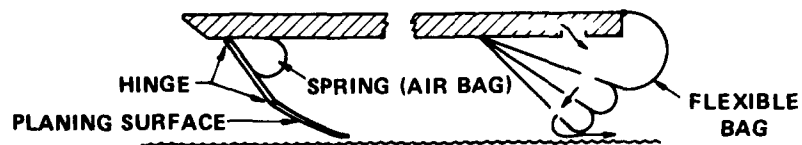


Figure 121e - Hinge Seals

Figure 121 - Basic Skirt Systems

Some of the effects of skirt design on craft performance and stability have been discussed in Chapters III and IV. This chapter will deal with the characteristics of the skirts themselves, considering such items as pressures, loads, and shapes. To aid the discussion each skirt or seal type will be covered separately.

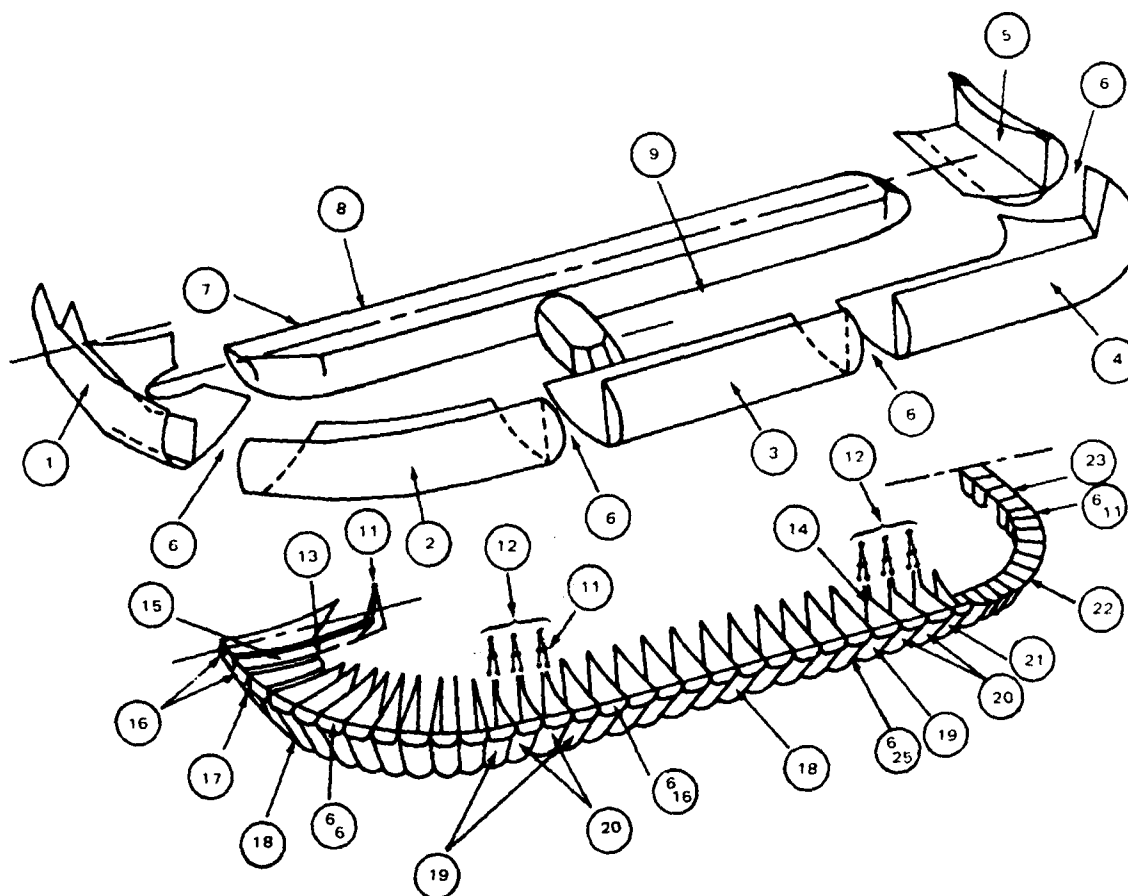
Bag-Finger Skirt

This particular form of skirt design has been pioneered by British Hovercraft Corporation, following the earlier finger development by Vickers and the loop-segment concept developed by HDL. The specific history as it has been applied to the various BHC craft may be found in References 46, 57, and 58. Particular details on the development of this skirt system for the SR.N4 have been amply covered by Wheeler.¹⁰⁶ This form of skirt has also been applied to all Bell craft modeled after the BHC craft such as the SK-5 and SK-6. It has also been applied to the bow seal of the SES-100B and, with slight modifications, to Voyageur and Viking. It is also being used on the Bell JEFF(B), currently undergoing trials. It is seen then that the bag-finger skirt has seen considerable development and most available data on craft are related to this form of skirt.

The most recent U.K. craft to use the bag-finger skirt system is the BH.7 developed for military amphibious operations. Figure 122 shows the BH.7 Mk 2, "typical" skirt system that has been used to date with its variants on many operational craft. The terminology (not always consistent) that has grown up with the development of the skirt system is displayed in Figure 122.

Figure 123 shows the development history since skirts were first used in 1960 on the SR.N1 up to the introduction of the bag-finger skirt on the SR.N5 in 1966. It will be noticed that skirt forms were a form of extended peripheral jet (see Figure 3) until 1963 when the concept of the bag was added to the SR.N2. The peripheral jet extension continued until 1966 when the design evolved into the present bag-finger form.

After 1966, development and improvement on different features of the bag-finger skirt continued through to the present day. The finger, as it was first introduced, was a simple version of the jet, replacing the holding chains (shown as dotted lines in Figure 123) with a simple piece of material. This change is important in that it marked the conversion of a peripheral jet craft into a form of plenum craft (see Figure 3), with the resulting change in performance characteristics. It also separated the main bag from the lower edges that wore away during operation. Now the fingers could be replaced after wear without having to replace or repair the large bag. Due to geometric constraints, the bags required internal diaphragms to hold their shape, which added to their complexity and introduced high localized loads into the bag. In 1967, the skirt design was modified to give a more free supporting shape to the bags (which meant increasing the craft beam), and so the fingers were lengthened to where they became 50 percent of the cushion depth. As might be expected, this



- | | |
|---|--|
| 1. BOW SEGMENT | 13. FINGER BAG ATTACHMENT FLAP WITH STANDARD FINGERS |
| 2. FORWARD CORNER SEGMENT | 14. FINGER BAG ATTACHMENT FLAP WITH SKIRT LIFT FINGERS |
| 3. SIDE SEGMENT | 15. BOW FINGER ATTACHMENT FLAP |
| 4. AFT CORNER SEGMENT | 16. BOW FINGERS |
| 5. REAR SEGMENT | 17. NEW STANDARD BOW FINGER |
| 6. BREAKDOWN JOINTS
(SUBSCRIPT DENOTES FINGERNUMBER) | 18. BASIC FINGER |
| 7. HINGES ON SKIRTS | 19. HANDED SKIRT LIFT FINGERS |
| 8. HINGE RING | 20. STANDARD SKIRT LIFT FINGERS |
| 9. KEEL | 21. NEW STANDARD SKIRT LIFT FINGERS (AFT) |
| 10. STABILITY TRUNK | 22. TAPERED CONE |
| 11. BONIOS | 23. REAR CONE |
| 12. SKIRT LIFTS | |

Figure 122 - BH.7 Mk 2 Bag-Finger Skirt System

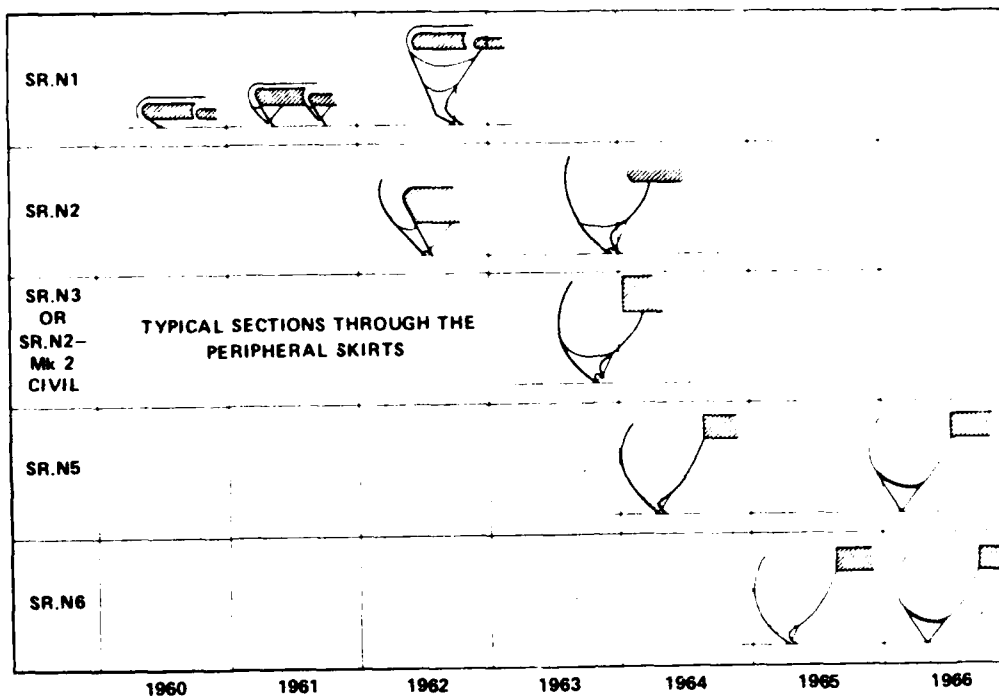


Figure 123 - Development of Bag-Finger Skirt through 1966

decreased the stiffness of the fingers, resulting in lower water resistance* and in a softer ride. More recently, finger depths have been increased further; for example, SES-100B ranges from 58 to 100 percent (at the skirt-sidehull interface) and the BH.7 has 73 percent finger depth. Figure 124 illustrates these refinements to finger length for the BHC series of craft.

This particular improvement brought with it, however, two problems: the increased tendency to plow-in discussed in Chapter IV and the introduction of a new problem known as bounce.

Bounce. Bounce is a very distinct and annoying low frequency limit cycle oscillation that occurs under certain conditions in calm water with the bag-finger skirt, often at low or almost zero craft speed. It becomes a particular problem when the skirt oscillation frequency excites the natural frequency in heave of the craft. Sometimes the bounce can be terminated by changes in lift system power (for example, change in fan rpm) but, at other times, the craft would have to be brought to a stop to

*At this point, the reader may wish to assess the impact on rough water speeds as effected by skirt form as shown on Figure 58 in Chapter III.

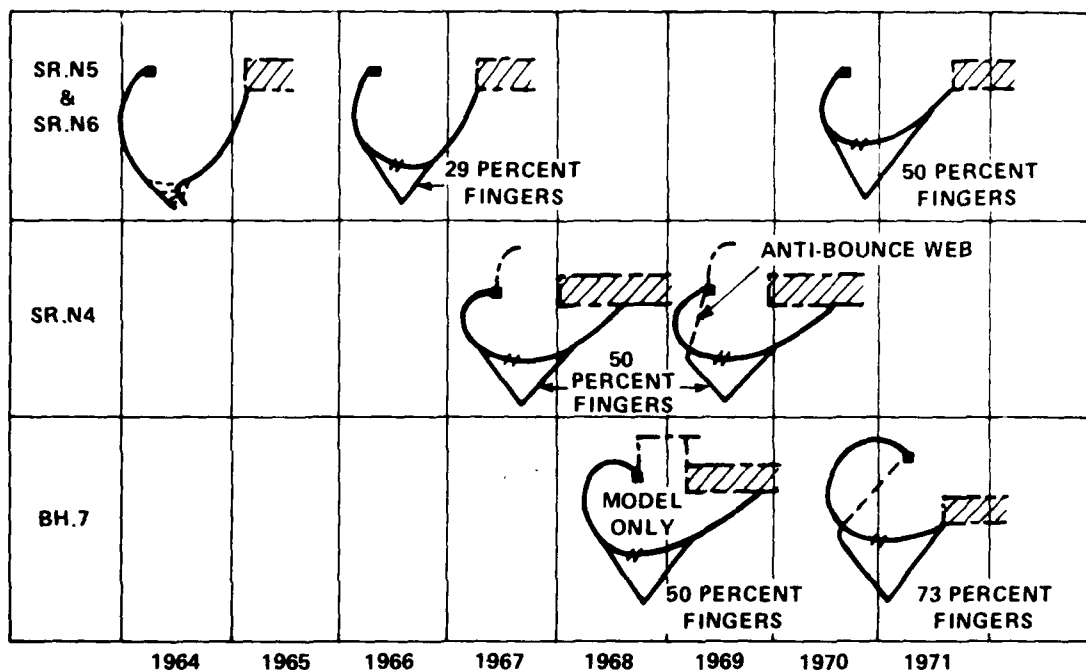


Figure 124 - Developments in Finger Length

eliminate the bounce. Crago⁸³ showed model test results and analysis of this condition of bounce. Figure 125 is a diagrammatic representation of the limit cycle together with the vibration boundaries for the particular skirt form analyzed.

Physically, skirt bounce occurs through the following mechanism: some disturbance causes the fingers to raise, increasing the air gap; this increases the flow rate from the cushion, which is proportional to the square root of the difference between the bag and cushion pressures. This change in pressure incurs a change in the pressure ratio between bag and cushion, which changes the bag shape and, hence, finger depth. This cycle continues and the limits are found to be linear functions of the bag pressures, that is, the boundaries are always straight lines passing through the origin, and thus the bag-to-cushion pressure ratio can be used as a criterion for the possible onset of bounce. It is seen from Figure 125 that pressure ratios just above 1:1, that is, a soft spring system, will be prone to bounce. The solution that was introduced in 1968 on the SR.N6 was a longitudinal diaphragm called the antibounce web. A higher pressure ratio was then introduced into the bag, and higher pressure ratios were employed to avoid the bounce limits. A typical pressure ratio is 1.6:1 to provide

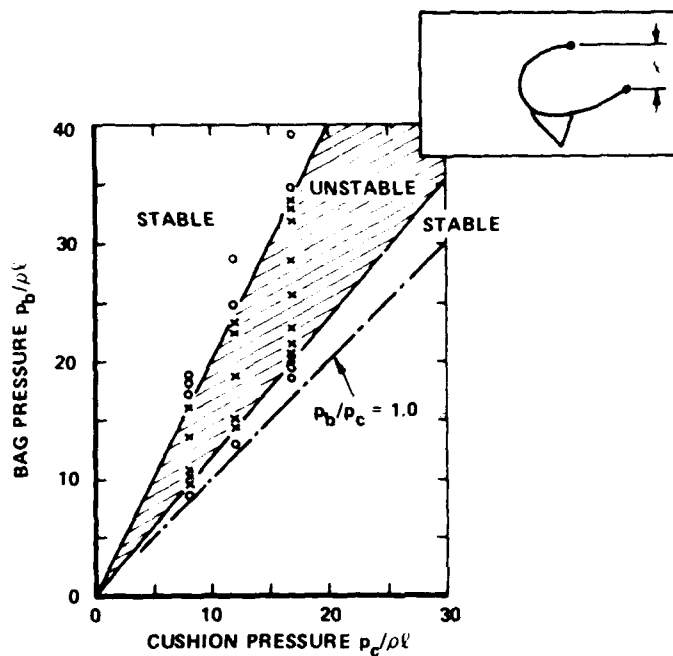
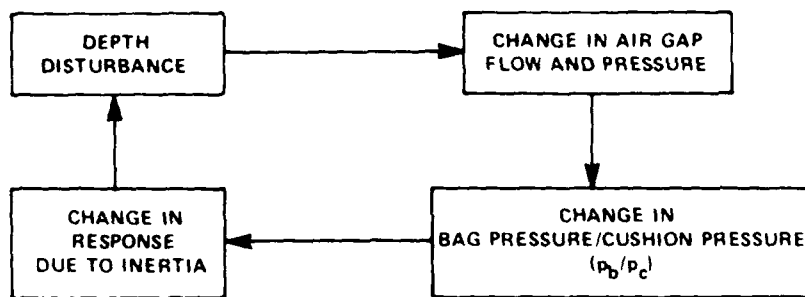


Figure 125 - Skirt Bounce

adequate stiffness and antibounce characteristics, although some designs can be as low as 1.2:1. This need for high pressure ratios increases the demand on the lift fan system (see Chapter VIII) with a corresponding reduction in the lift system efficiency.

The related problem due to the increased depth (50 percent) fingers and the freely supporting bag was an increased tendency to plow-in, and the antiplow web was added in the bow section of the skirt. Both the antiplow web and the antibounce webs are shown in Figure 126 as they were successfully applied to the SR.N4 in 1968. As may be seen from section A-A in Figure 126, the antiplow web provided a compartment within the main bag

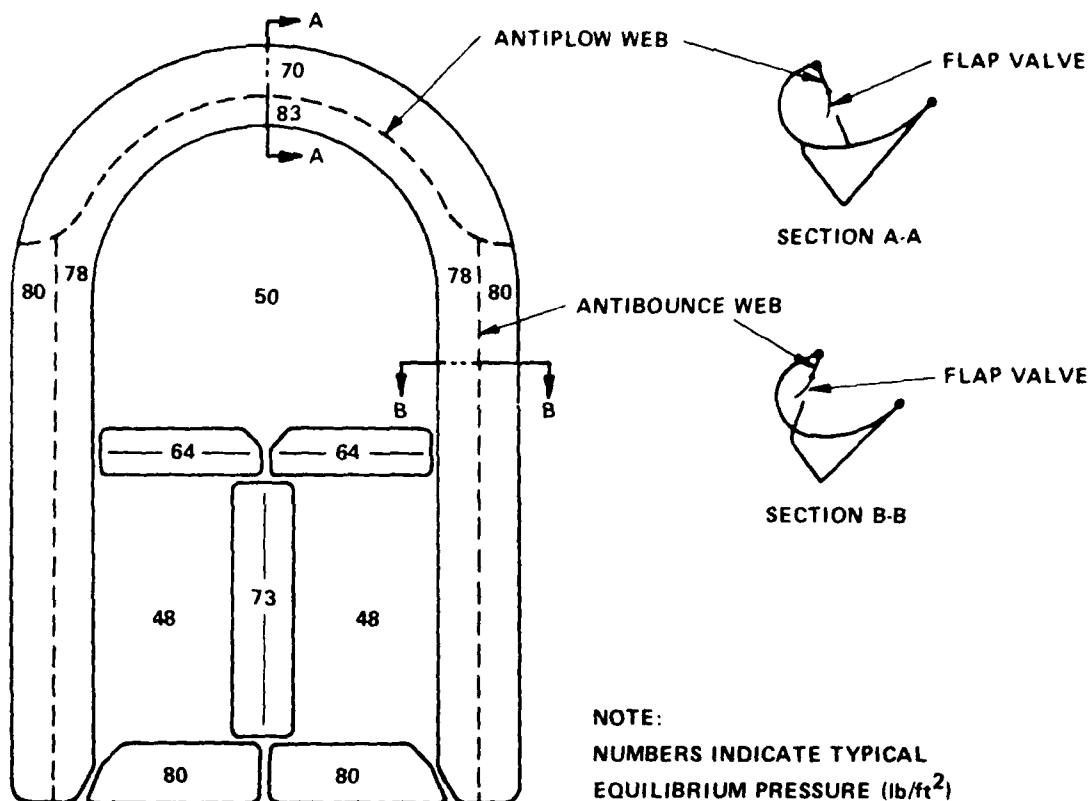


Figure 126 - Antiplow and Antibounce Webs (SR.N4)

that, during plow-in, would remain inflated and provide the necessary additional restoring force at the bow to maintain positive trim. Also shown on Figure 126 are typical pressures as they apply to the SR.N4 at 170 ton gross weight.

Skirt bounce has also been experienced in such craft as the SES-100B, which had a bow seal similar to the BHC bag and finger skirt but with no antiplow web. Its pressure ratio was approximately 1.2:1. Bounce also occurred on the SES-100A with its original planing hinge-type seal but was probably excited by a different physical mechanism discussed later.

Finger Oscillation. In addition to the low frequency oscillation (1 to 3 Hz) or bounce, there are additional high frequency oscillations to which the fingers are subjected. These high frequency oscillations contribute significantly to the high wear rate and failures of fingers on air cushion craft. The first form of high frequency oscillation or vibration is normal to the sides of the fingers and is in the range of 10 to 20 Hz. While the complete description of the oscillation is still under investigation, it appears to be due to variation in tension forces around

the lower edges of the fingers. Figure 127 shows a developed form of a typical finger used on such craft as the SR.N4, BH.7, SES-100A, and SES-100B. The lower edges are scalloped as shown so that, in the installed position, a straight hemline is achieved. If the edge were not scalloped, then, in the installed condition, a much greater equivalent air gap would result from the triangular-shaped gaps between each finger, with the resultant increased power loss.

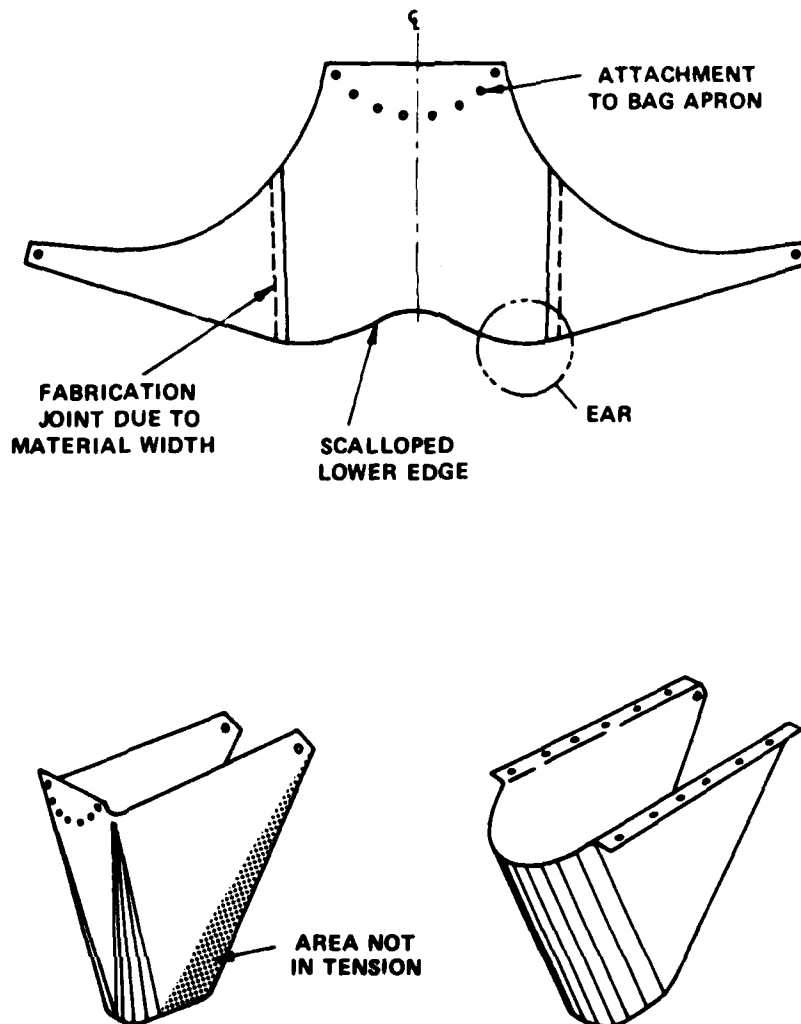


Figure 127 - Typical Finger and Attachment

This scalloping of the developed fingers results in lightly loaded material pieces known as ears. Ears have been observed on the SR.N4²⁶ vibrating at approximately 15 Hz. The vibration transmits up into the side faces of the fingers and induces considerable wear through rubbing. The lower edges themselves, due to the high frequency vibration, suffer material breakdown through delamination and other failure modes that considerably shorten skirt life. Vibration damage occurs as a water spray pattern caused by pressurized cushion air flow mixing with the water as it escapes at high velocity through the air gap.

The finger is subjected to considerable vibration and movement due to such air flow, and it was found that the fingers frequently tore themselves loose. Therefore, in 1968, the simple finger attachment method, shown in the lower left-hand corner of Figure 127 was replaced with the method shown in lower right-hand corner of Figure 127. This reattachment in effect, stabilized the upper edges of the fingers and improved finger life but did not greatly improve the situation relative to the lower edges.

The second form of high frequency oscillation is fundamental if it is required that the finger follow the waves and maintain a constant air gap. It is recognized that such an ideal situation is difficult to achieve, but current practice indicates a fair measure of success as was discussed in Chapter III and was shown in Figure 26 for the SR.N4.

An indication of the forces imparted to the finger by wave following can be seen by considering the accelerations of a particle following a sinusoidal waveform. The acceleration¹⁰⁷ can be shown to be

$$n = 2\pi^2 \frac{h_w}{\lambda^2} \left[V + \sqrt{\frac{g\lambda}{2\pi}} \right]^2 \quad (153)$$

where n = vertical acceleration in units of g (32.2 ft/sec²)

h_w = wave height

λ = wavelength

V = craft forward speed

This result has been plotted in Figure 128 in terms of acceleration in g 's per unit wave height. For the simple case of sinusoidal motion, it can be seen that significant acceleration levels can be experienced. For example, on a skirted craft traveling at 60 knots in 6-ft waves of wavelength 120 ft, the lower finger edges would experience approximately 3 g . If the craft were traveling short wavelength seas, for example, 60-ft wavelengths, this would rise to 15 g . This idealized case does not include the snapback action after the skirt finger has moved up by wave action, from the cushion pressure, where even higher accelerations can occur. Values of 100 g have been measured in the snapback mode.

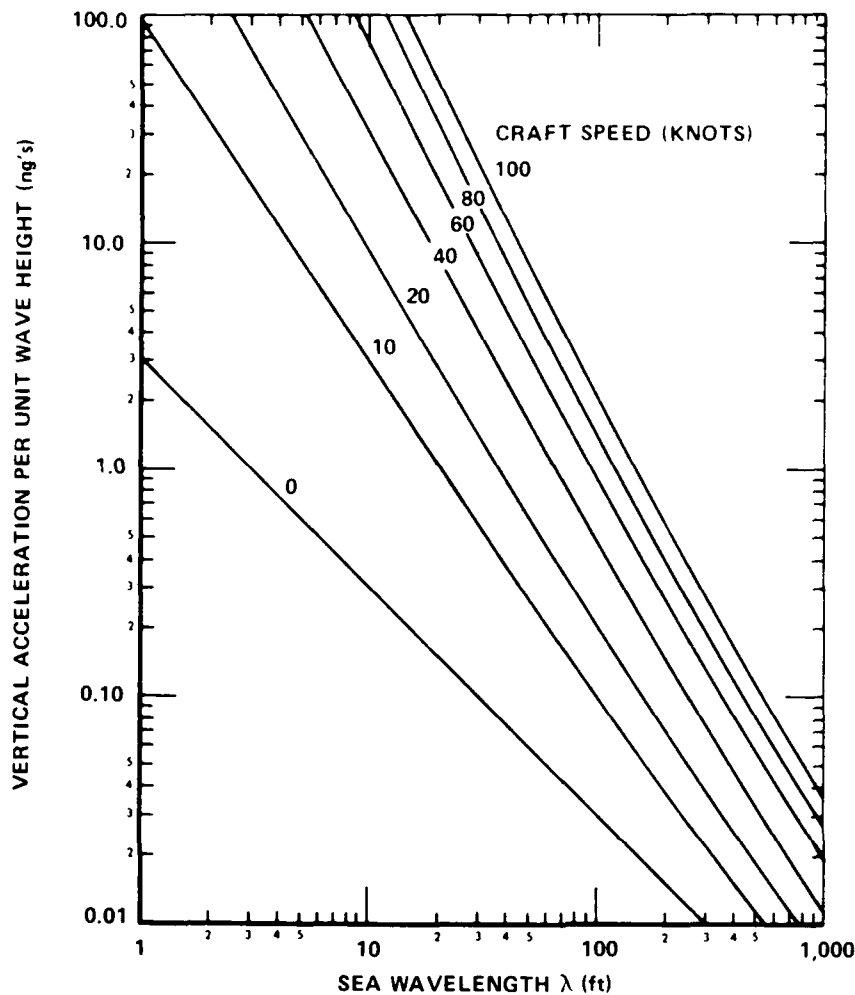


Figure 128 - Wave Following Vertical Acceleration

These accelerations, and those due to wave following, snapback action, and vibration discussed earlier, have a significant effect on the life of skirts. Both material development and skirt geometry changes are under development by air cushion craft manufacturers to combat this problem. Skirt development continued after this period to include a raised hinge line (called the Mark 2 skirt) in 1969 for the SR.N4 among other detail refinements to attachment methods. Two other significant changes include the even deeper fingers (73 percent) for the BH.7 in 1969-1970 and the tapered skirt.

The tapered skirt was introduced to solve two problems. The operators of the craft (SR.N4) on commercial routes across the English Channel tended to operate bow-up (1.5 to 2 deg) to ensure staying away from plow-in boundaries and to give the operator sufficient time to take corrective action in the event of plow-in. The operators also found that the craft rode better in rough sea conditions. Operating bow-up, however, increased the wear on the rear fingers or cones. The tapered skirt, which gave an 8-ft cushion depth at the stern and a 10-ft cushion depth at the bow, would, therefore, allow the nose to stay high but the air gap constant along the hemline, thus reducing wear. For reasons of safety, however, the operators still tend to operate bow-up, since the plow-in boundary is a function of the skirt hemline angle to the water surface. However, there is significant reduction in wave impact in heavy seas due to the increased cushion depth at the bow. Additionally, the tapered skirt gives increased height at the bow without raising the craft C.G. a corresponding amount. Thus, roll stability is less degraded. Additionally, keeping the rear skirt in contact with the water improves the directional stability of the craft.

Other design developments include skirt-lifting features, improved attachment methods (see, for example, Reference 106), and improved fabrication methods such as bonding fingers in a complete piece instead of having to "build up" a finger.

The remaining components in the bag-finger skirt system are the longitudinal and transverse keels used for compartmentation of the cushion. Like the basic concept itself, the method of compartmentation has also developed over the years as indicated in Figure 129.

These compartmentation keels may either have an issuing air jet or be completely enclosed. Both types are in use on air cushion craft, although current preference is to use the enclosed bag type. The pressure in the keel bags is chosen to provide a stable keel to maintain compartmentation, yet it must be flexible enough to minimize drag over water, ice, or other obstacles. These keels contribute appreciably to the total skirt drag discussed in Chapter III. Figure 130 shows some of the types of keel shapes in use on air cushion craft. Figure 130 also shows a typical rear skirt section (as used on the SR.N4), where the finger has been replaced by a closed cone to avoid the scooping of water with an open finger.

The development of the bag and finger geometries, compartmentation, and other skirt properties has resulted in a range of "typical" values. Table 6 summarizes some bag parameters for selected craft and for the same craft Table 7 summarizes the finger parameters.

In the United States, most of the bag-finger skirt development has followed the British experience with an increased emphasis on high density craft, as outlined in Chapter II. The higher densities have incurred higher cushion pressures, which, in turn, have required skirt bags to be subjected to much higher loads. Again, the higher speeds have had an impact on the design of the fingers due to higher drag loads and higher frequencies of oscillations. All these factors have spurred development of improved

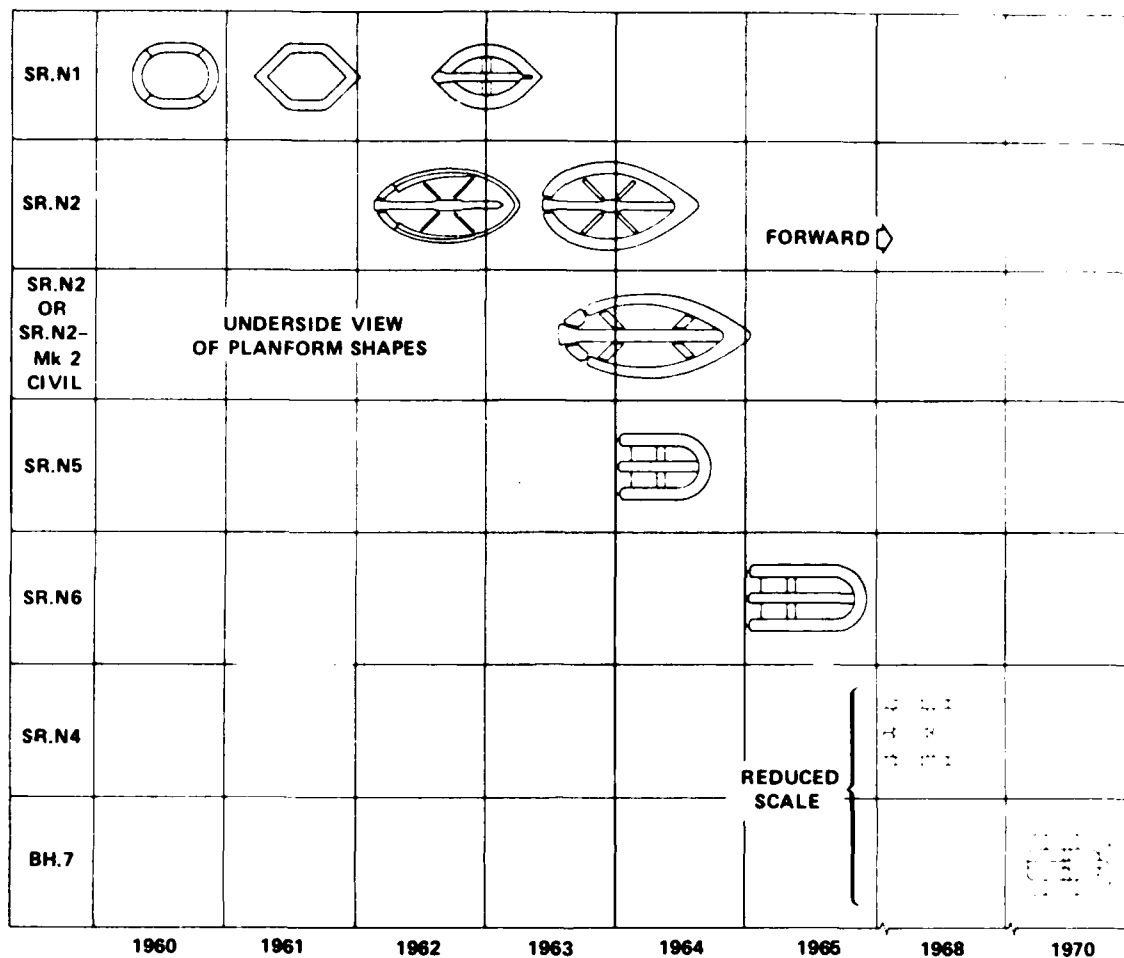


Figure 129 - Compartmentation Development

materials and improved fabrication and attachment methods. Some of the implications of such developments are discussed later in this chapter on material development.

Having described some of the developmental history of the bag-finger skirt concept, some of the basic design parameters are illustrated to indicate the trends in development.

Bag Shape and Size. There is, at present, no adequate theory that can predict the geometry of skirts in their three-dimensional form, taking into account their mass and stiffness, although development is continuing in the United States, England, and France on three-dimensional shape prediction methods. It has been found, however, that simple two-dimensional theories, coupled with experience from previous craft, can be applied successfully to skirt design. This is not to say that, if radical changes in size or speed are contemplated, the simple theories will not break down.

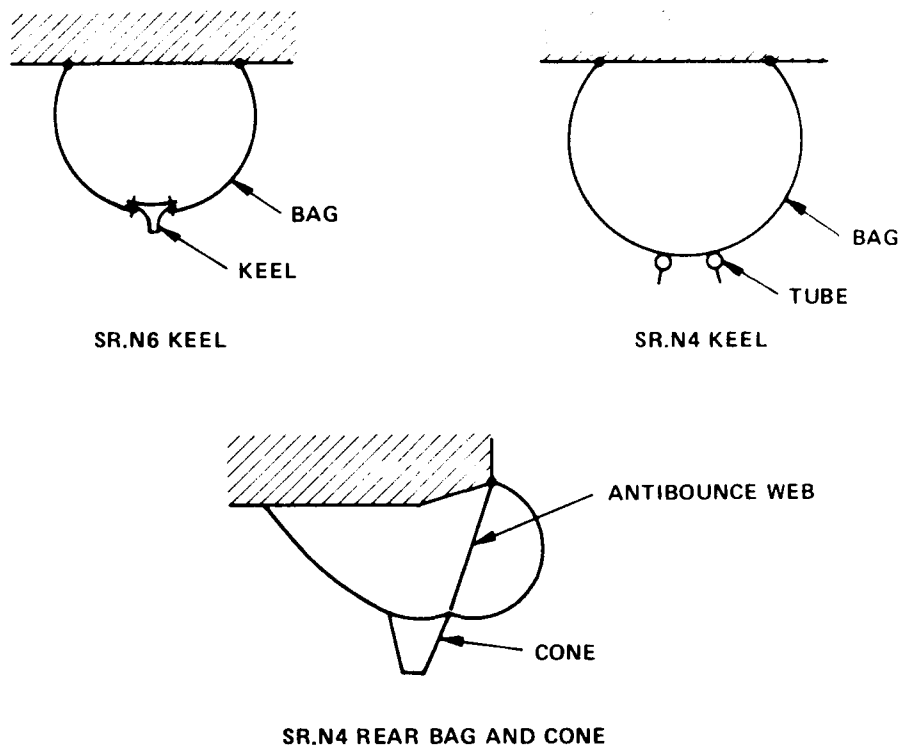


Figure 130 - Keel and Rear Skirt Sections

TABLE 6 - BAG PARAMETERS OF EXISTING CRAFT

Craft	SR.N5	SR.N6 Mk 1	SR.N6 Mk 6	BH.7	SR.N4	HM.2	VI.2
Craft Type	Fully Skirted Divided Cushion	Fully Skirted	Fully Skirted	Fully Skirted	Fully Skirted	Sidehull No Cushion Division	Fully Skirted No Division
Craft Gross Weight (lb)	15,000	22,400	33,000	112,000	413,000	36,000	202,000
Cushion Density $p_c/S^{1/2}$ (lb/ft ²)	1.09	0.95	0.97	1.09	0.62	2.03	0.985
$[L/B]_{\text{cushion}}$	1.64	1.94	2.00	1.96	1.64	2.13	1.85
<u>Bag Pressure (normal)</u> Cushion Pressure (operating)	1.8	1.6	1.57	1.2	1.49	1.1	1.2 Approx.
<u>Skirt Depth at Outer Hinge</u> Bow Cushion Depth	1.21	1.21	1.57	1.68	1.62	2.5 Approx.	1.75 Approx.

TABLE 7 - FINGER PARAMETERS OF EXISTING CRAFT

Craft	SR.N5	SR.N6 Mk 1	SR.N6 Mk 6	BH.7	SR.N4	RM.2	VT.2
Craft Type	Fully Skirted	Fully Skirted	Fully Skirted	Fully Skirted	Fully Skirted	Sidehull No Cushion Division	Fully Skirted No Cushion Division
Finger Depth Cushion Depth	0.3	0.5	(Tapered) 0.40-0.42	0.73	(Tapered) 0.40-0.50	0.7 Approx.	0.75 Approx.
Finger Hitch Finger Depth	0.48	0.42	0.42	0.65	0.69	0.33 Approx.	0.30 Approx.
Finger Base width Finger Depth	1.9	1.65	2.0	1.67	1.85	2.0 Approx.	1.85 Approx.
Finger Tip Angle (deg)	81	71	82	84	82	90 Approx.	90 Approx.
Finger Outer Edge Angle (deg)	51	57	52-46	42	48-42	35 Approx.	45 Approx.
Number of Fingers Around Bow	81	36	37	23	48	22 Approx.	44 Approx.
Number of Fingers Around Rear	44	38	44	30	60	22	44 Approx.

Figure 131 shows a typical two-dimensional section of a bag-finger skirt. Finger attachments and other design requirements will distort the bag shape, but the geometry can be generated from a succession of constant radii arcs such as that shown. Then, from simple structural analysis of cylinders, the "hoop" tension per unit width in the bag material is given by

$$T = p_b R_1 \quad (154)$$

but, because, by this theory there can be no pressure gradient or tension discontinuity within the bag, the tension per unit width is also given by

$$T = (p_b - p_c) R_2 \quad (155)$$

Hence, ignoring all material weights and finger loads, the bag shape can be determined from the geometrical relationship

$$\frac{R_1}{R_2} = \frac{p_b/p_c - 1}{p_b/p_c} \quad (156)$$

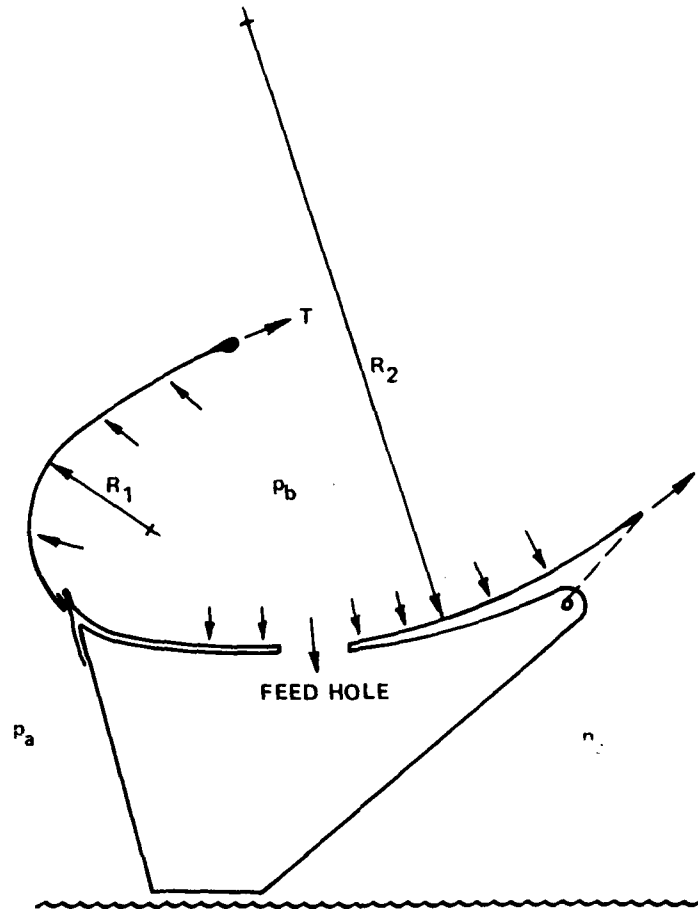


Figure 131 - Two-Dimensional Bag Section

that is, the shape is defined by the bag pressure-to-cushion pressure ratio (p_b/p_c) discussed earlier in connection with bag bounce. It will be noticed that Equation (156) says that the shape is not size-dependent and can thus be used on full scale as well as model scale. The loads in the bag are, however, size dependent. If the cushion pressure increases with the scale factor (λ) (see Figure 24 and Equation (17)) and the bag radius increases by the scale factor, then the load in the bag material increases by λ^2 as shown:

$$T \sim p(\lambda) R(\lambda) \sim p\lambda^2 \quad (157)$$

Similarly, if the thickness of the load-carrying material (predominantly the fabric in current skirt materials) is also scaled as λ^2 , then the stress level in the material remains invariant with size. Both these results have ramifications in the choice of skirt material for strength and weight as discussed later.

Skirt design in the sizes considered for today's air cushion craft based on such simple relationships has been found adequate. More detailed digital computational techniques are actually employed in some cases, and refinements are made to the final lines. These techniques involve finite element grids and, in some cases, flexible membrane analysis. It is normally found that ignoring weight effects and material stiffness has had only slight impact on the geometrical stability determined by the more simple means.

The above geometrical relation applies only in the static case and the situation becomes more complex in the dynamic situation during wave impact. During such action, the bag distorts and significant pressure surges occur, which correspondingly vary the tension (T) in the bag material. Techniques are available for treating such conditions, including the load in the bag during impact and upon reinflation. Another loading condition is the "snatching" of water with the fingers, which transmits high loads into the bag. Although the details of such a method cannot be given in the space available here, it can be said that it is normal practice to design for dynamic pressure surges in the bag up to three times the static inflation pressure for the typical craft sizes, sea states, and bag designs used today. As craft size and speed significantly increase, the bag geometry must take on a different form from that developed thus far, to keep the fabric stresses within the capabilities of current or foreseeable new materials. Some more comments in relation to this and on scaling are given at the end of this chapter after a discussion of material development.

Loop-Segment Skirt

The second major classification of skirt types is that developed by Hovercraft Development Limited. It is similar in many respects to the bag-finger skirt discussed above, except that the bag is replaced by a loop as shown in Figure 121b. This means that the bag pressure becomes the same as the cushion pressure and the geometrical relationships developed earlier do not apply. It is a simpler form of skirt and does not have the interrelationship of finger depth and cushion pressure as discussed for the bag-finger. Instead of the compartmentation keels for stability, it relies on the cushion area change to provide a C.P. shift. These particular features are discussed in Chapter IV on the stability and ride characteristics of air cushion craft.

This form of skirt saw its basic development in 1965 on such research craft as the HD.1 and the HD.2. An advantage is that, as a softer spring, the fingers create a slightly lower rough water drag. Also, because there

is virtually no pressure drop from the loop into the cushion, the lift system efficiency is higher. A disadvantage is that, without the stabilizing feature of the antiplow web indigenous to the bag-finger skirt, it is more susceptible to tucking under and contributing to plow-in. The stability of the skirt is determined by the position of the hinge line, which is placed higher on the craft than an equivalent bag-finger skirt.

The latest application of the HDL skirt system has been on the semi-amphibious craft, the VT 1, and on the amphibious version, the VT 2; both were designed and constructed by Vosper-Thornycroft, a shipbuilder in England. The VT 2, which operated for the first time on 2 September 1975, is actually one of the original three VT 1 craft converted to amphibious operation. Figure 132 illustrates the basic form of the loop-segment skirt and attachments and how it has been applied to the Vosper-Thornycroft craft. The bow and side sections follow the basic form. For the stern sections of the craft, however, (see sketch upper right of Figure 132) to overcome the scooping problem inherent with a rear-facing finger, double segments are used. This is simply a combination of forward-facing and rear-facing segments to form an enclosed member and behaves in similar fashion to the cone in the rear sections of the bag-finger skirt.

An enlargement of the segment, shown in Figure 133, shows how the particular segments in the loop-segment skirt go together.

Jupe Skirt System

The principle of separately fed multiple plenum chambers originated with the late Jean Bertin in 1957 in France, and the development of such skirt systems has been almost exclusively done by Bertin. Specifically, the multiple plenum chambers or jupes have been applied to marine air cushion craft such as the Naviplane series and the Terraplane series of road vehicles. An example of the Terraplane series craft was shown in Figure 12. The first Naviplane craft to enter commercial service was the 27-ton N.300 shown in Figure 14. After initial tests in 1968, commercial service began in 1970 along the Cote d'Azur. All such craft are developed by the Societe D'Etudes et de Developpement Des Aeroglisateurs Marins, Terrestres et Amphibes (SEDAM), a company incorporated in 1965 to develop the Bertin principle of the air cushion craft.

The basic concept, according to Bertin's patents, is that craft stability is achieved by the use of several slightly conical skirt forms. The half-cone angle varies with the design but is usually no greater than 5 to 10 deg. Bertin has given geometrical relationships for the cones. For best performance and stability of shape, the jupe proportions are as follows:

$$0.25 \leq \frac{h_s}{D} \leq 0.80 \quad (158)$$

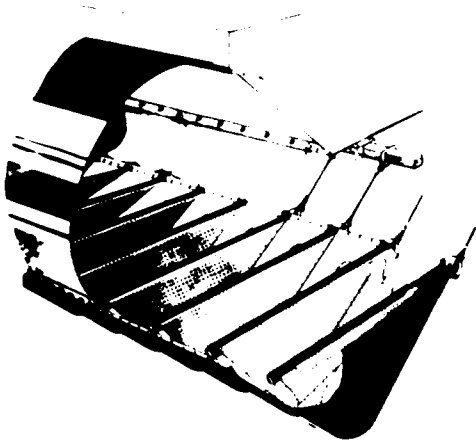


Figure 132a - Side Skirt

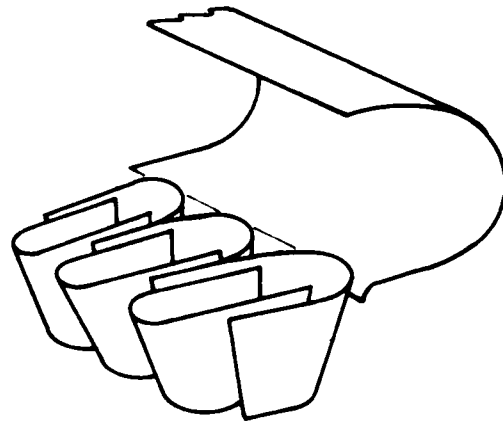


Figure 132b - Rear Skirt



Figure 132 - Schematic and Details of VT 1 Skirt

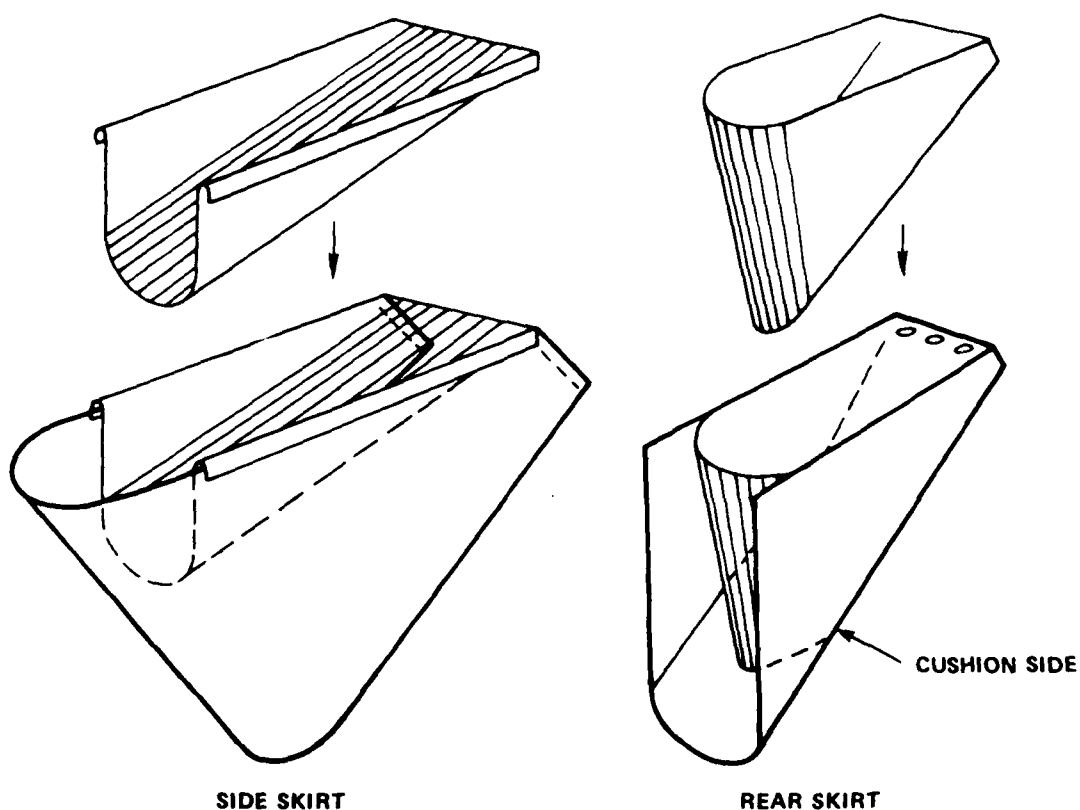


Figure 133 - Segments in VT 1 Loop-Segment Skirt

where D is the major diameter of the jupe. If the jupe is inclined at an angle α , then Bertin shows that the values of the half-cone angle β allowed depend on α . In any event, stable jupes maintain half-cone angles no smaller than 5 deg. Figure 134 (upper sketches) shows some of the basic characteristics of the jupe skirt system. Although it is basically a very simple system, it appears to suffer in its original form by the inefficient

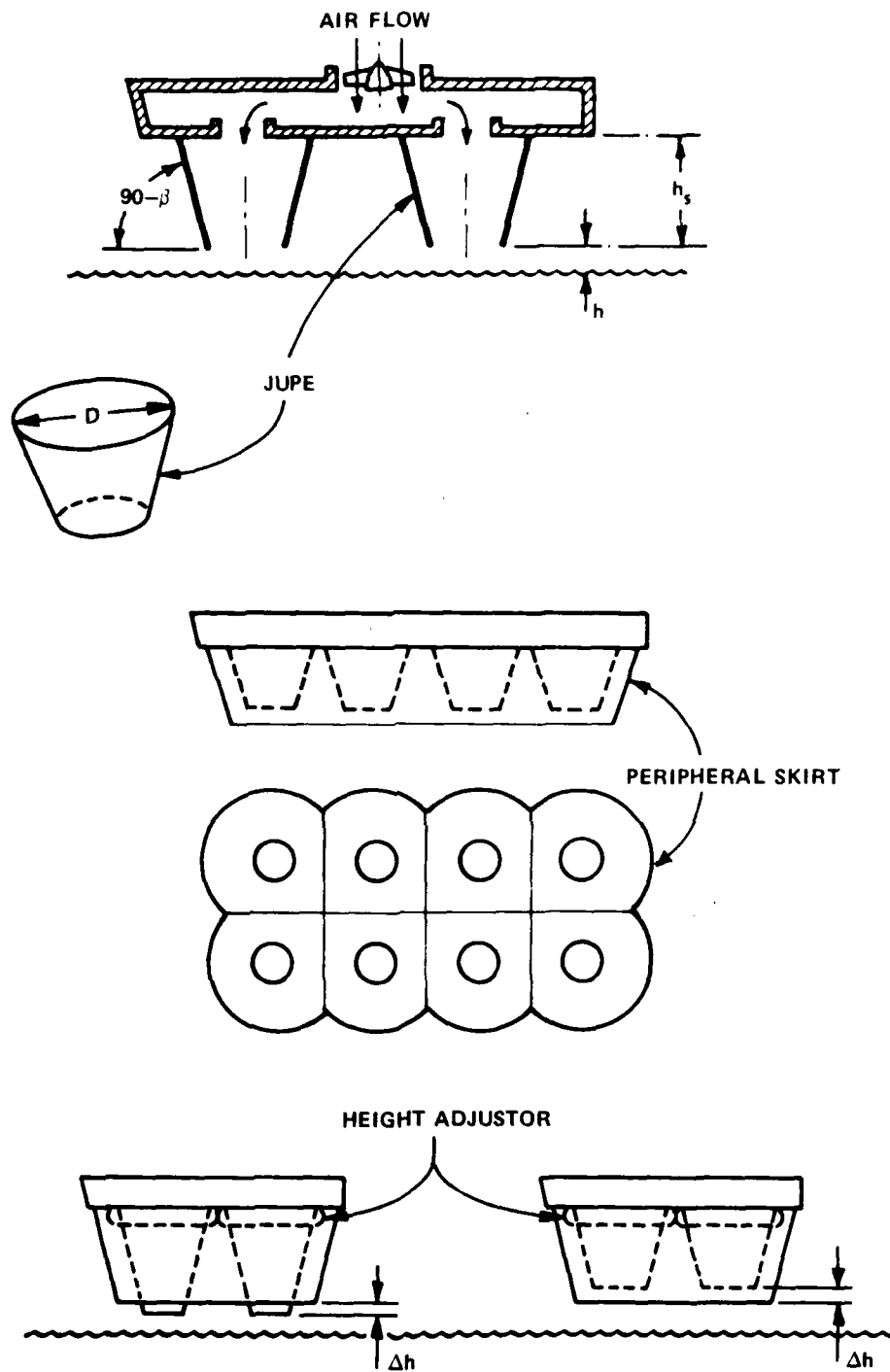


Figure 134 - Some Jupe Skirt Characteristics

use of the available cushion area and through the use of multiple cushions, an increased peripheral hemline length. This increased length increases the flow losses through the system for a given air gap h .

Bertin solved this problem through the use of a wraparound peripheral skirt; shown in Figure 134 (middle sketches). This reduced the air leakage gap to that common to the bag-finger and loop-segment skirts discussed but with the added advantage, due to the low angle of the skirt inclination, of an increased use of available cushion area. It was also found that the relative position between the height of the individual jupes and the peripheral skirt, given by Δh , see Figure 134 (lower sketches), had a marked effect on the heave stiffness of the system. If the jupes were longer than the peripheral skirt, the heave stiffness was high, and if the jupes were shorter than the peripheral skirt, then the heave stiffness was low. Accordingly, Bertin introduced a height adjuster in terms of a pressurized bag that could effectively be used by the operator to control the stiffness of the craft. Thus, Bertin had accomplished for French air cushion craft what Citroen had accomplished for the automobile--a means of adjusting the ride according to the nature of the surface condition being traveled. This change in jupe length to achieve sufficient changes in stiffness is on the order of 0.50 to 1.0 in.

These features have been incorporated in the SEDAM N.300 shown in Figure 14 in Chapter II. For the N.300, the skirts are just over 4.5 ft (55 in.), and the craft is designed to operate in 5-ft seas. The N.500, which is shown in Figure 15 in Chapter II, also has the peripheral skirted jupe system and has a skirt height of approximately 8 ft. On the N.500 there are 24 jupes each of 13 ft 1 in. diameter and although not shown in Figure 134, the jupes are arranged in groups of three such that lift fan air is fed independently to each group. This fan air is regulated by valves activated from the pilot's cabin such that by controlling the air into the jupes the craft can be trimmed according to the operating condition (such as bow up in rough seas). A form of skirt lifting is also employed to reduce the scooping tendency of the jupes and thereby reduce wear. The N.500 (Ingenieur Jean Bertin) entered passenger carrying service on July 5, 1978 and, although it is a little early to pass judgment, it is understood that this particular skirt design is experiencing high wear and reliability problems. The skirt is made of a neoprene coated Terylene fabric material.

Pericell Skirt System

The pericell skirt system described earlier as a combination of the bag-finger and jupe concepts was developed on the U.S. Navy Amphibious Assault Landing Craft (AALC) Program. It is used on the JEFF(A) currently undergoing trials in Panama City, Florida, and it was also used, in part, on the SES-100A to solve the plow-in problem (see Chapter IV, Figure 80) and to give a greater rough water capability. To date, the application to the SES-100A and JEFF(A) are the only full-scale craft use of the pericell.

As stated, it was applied only in part on the SES-100A because of the difficulties of a retrofit design to a sidehull form of craft. The pericell, as shown in Figure 73, was used on the SES-100A in September 1973 prior to the start of rough water trials. The midsections of the SES-100A bow seal were pericells, and the outer sections were the bag-finger form to achieve a better transition into the hard structure sidehulls.*

In the case of the amphibious form, no such transitional problems exist, and the cells run peripherally around the craft attached to the peripheral bag. Figure 135 (upper photograph) shows an underneath photograph of a JEFF(A) model. Like the Bertin system, basic stability is achieved by pressure in the cells during the rolling and pitching of the craft. Air flow to the cushions is provided by the common air feed bag, which also provides additional stiffness during wave encounters. It was found from experiment that, to avoid high drag by the scooping of the afteredges of cells, a canted edge or scallop was required in the bow sections. This is shown in Figure 135 (lower sketches) where typical sections through one form of the skirt is shown. A 15 deg scalloped edge provides adequate reduction in skirt drag while still retaining the required pressure difference for stability. In the stern sections, the cells cannot hold their shape against the water dynamic pressure, and it is necessary to use some form of pressurized closed finger as shown.

These features and geometrical relationships for the pericell skirt system as used on the JEFF(A) are shown in Figure 136.

The pericell skirt will tend to be stiffer than, for example, the bag-finger skirt or the loop-segment skirt concept. A noticeably stiffer ride was experienced on the SES-100A when the skirt system changed from the planing hinge seal to the pericell seal. A change in geometric proportions, however, can give radically different characteristics of skirts. The development for deep skirts conducted for the DARPA Arctic studies²⁸ explored all the concepts discussed thus far, and it would be difficult to summarize the results here. As an indication of the stability characteristics for the pericell skirt, the geometry and roll stiffness of a deep skirt ($h_s/B = 0.30$) are shown in Figure 137. The roll stiffness of approximately 0.85 percent C.P. shift per degree for the deep pericell is within the band of acceptable values discussed in Chapter IV relative to stability and ride quality.

The pericell skirt has not received the development that the bag-finger skirt has received and, thus, hard statements cannot be made relative to its plow-in and bounce characteristics. This development comes as the U.S. Navy JEFF program continues testing at sea.

SES Hinge and Flexible Seals

The skirt systems, discussed thus far, can be applied in one form or another to most forms of air cushion craft. The hinge seal in its present

*As shown in Chapter IV, Figure 82, the SES-100A has now reverted to a bow planing (hinge) seal.

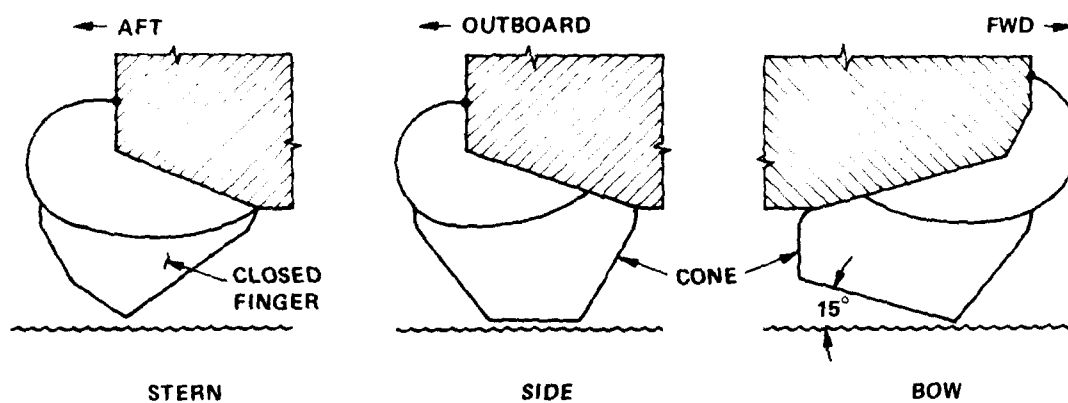


Figure 135 - Pericell Skirt Forms

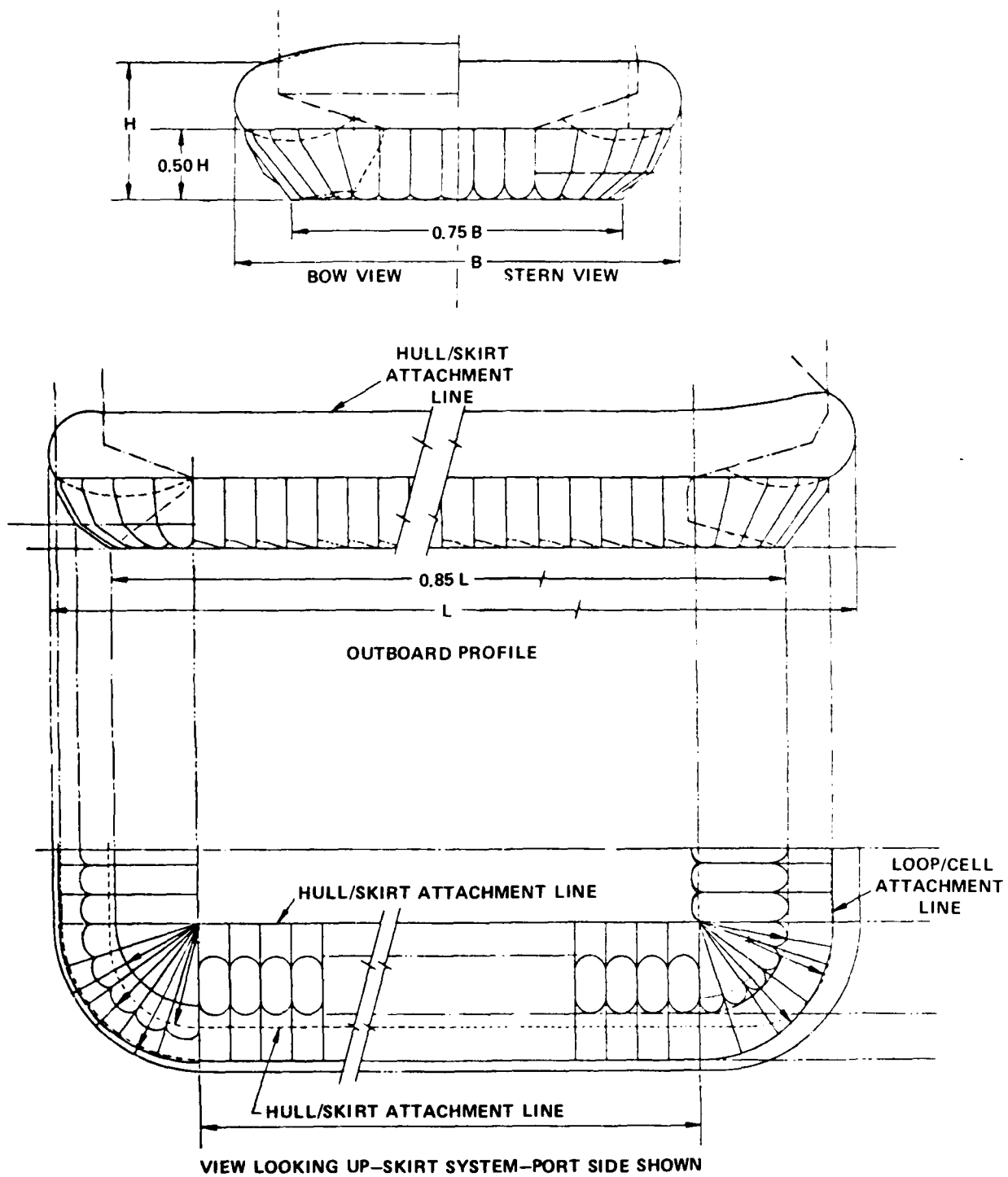


Figure 136 - JEFF(A) Pericell Skirt System

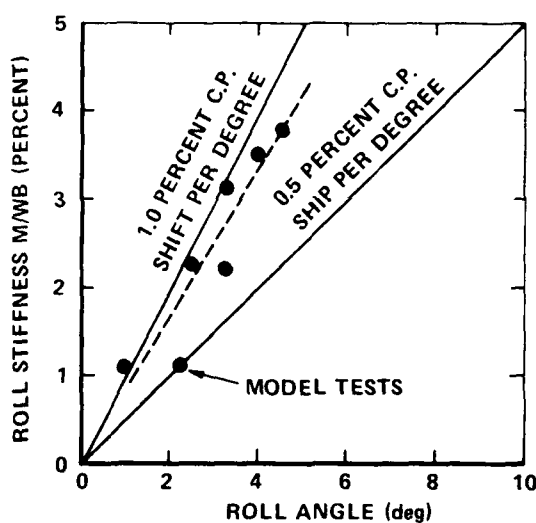
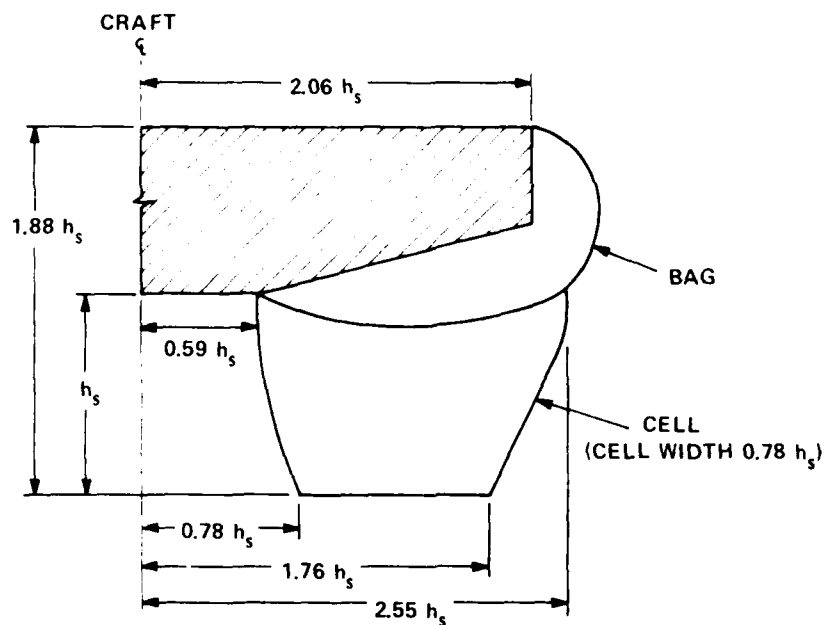


Figure 137 - Deep Pericell Roll Stiffness

form is peculiar to the nonamphibious or sidehull form of craft, and the majority of its development has centered in the U.S. Navy in pursuit of the high speed SES. Hinged seals, one form of which is sketched in Figure 121, have been applied on such craft as Warner's boat in 1929 and on some early craft (1960) in England designed for pleasure boat purposes, but the main development, is proceeding within the U.S. Navy.

In addition to providing aerostatic forces for stability and ride control, the hinged seal offers the possibility of providing significant hydrodynamic forces. The XR-1¹¹ was the first serious attempt to develop this concept whereby the sidehulls could be allowed to remain thin (and, therefore, low resistance) and rely on the seals to provide the necessary stability. The developmental problems of this particular craft in the 1963-65 time frame did not eliminate development of this seal concept, and the seal system was later developed in the segmented form as shown in the XR-3 in Figure 7, Chapter II. It has usually been found that the mass of the nonflexible hinge seal and the spring rate of the hinge could not match the rapidly changing frequencies of operation in random seas. A flexible seal was developed and proved successful on the SES-100B during its trials program in 1972-73. Figure 138 (upper photograph) shows the stern seal of the SES-100B taken at hover. Due to its flexibility, this seal, constructed from the same nylon-coated fabric as the bow seal, followed the waveform even in extreme sea conditions. It was designed to have a multiloop to combine the need for keeping the bag loads within reason and also for minimizing the water contact area as the seal trailed the water. A flexible seal constructed from fabric must contend with the high frequency loads that can lead to seal failures. Figure 138 (lower photograph) shows a typical failure that occurred early in the trials of the SES-100B stern seal and was analyzed as being caused by oscillations due to wave following or induced by unsteady flows arising from its proximity to the propeller. After the initial development period, the flexible stern seal performed satisfactorily.

A planing type hinge bow and stern seal is currently being developed for use on the planned 3000-ton surface effect ship for the U.S. Navy. No details of this seal can be released at this time.

The choice between flexible or nonflexible seals is not clearcut, however, and further development is required, especially as speed and size requirements increase, placing more taxing requirements on the seals. The remaining discussion will be restricted to flexible skirts for use on the amphibious form of air cushion craft pending development of the planing hinge seals for the U.S. Navy SES.

SKIRT MATERIAL

The history of skirt material development has been interesting. The choice of materials is far-reaching and practically every form of material has been considered over the years. These materials ranged from chain mail to glass-reinforced plastics, sheet rubber, and elastomer-coated fabrics. Of these, the elastomer-coated fabrics proved the most successful, received the most development, and are in use today on all the operational craft. The technical literature is well documented with lists of materials tested for air cushion craft skirt use, and they are not reproduced here. It is more instructive to summarize the development, to indicate the current solutions to skirt material selection, and to explain how further development can improve skirt material.

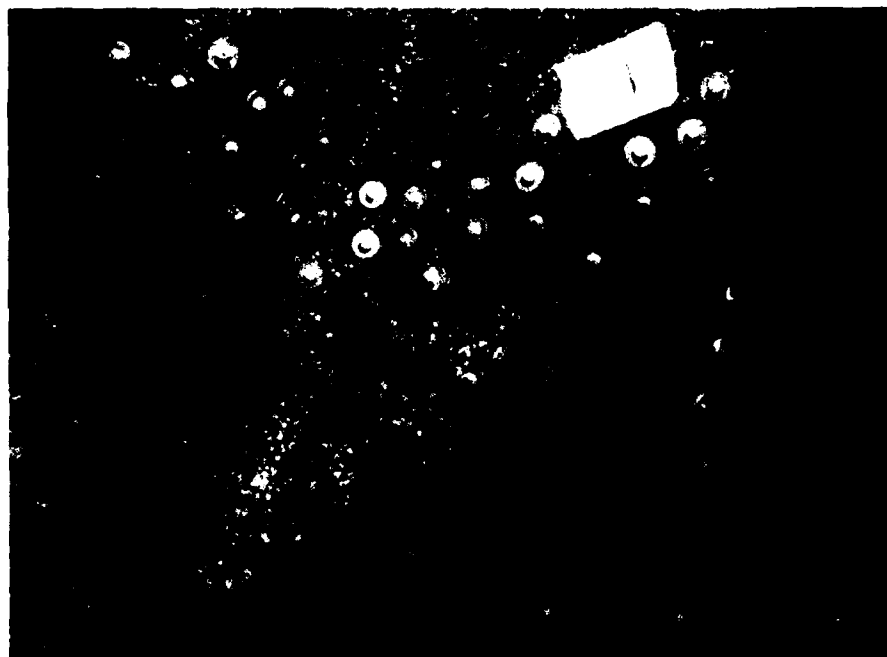
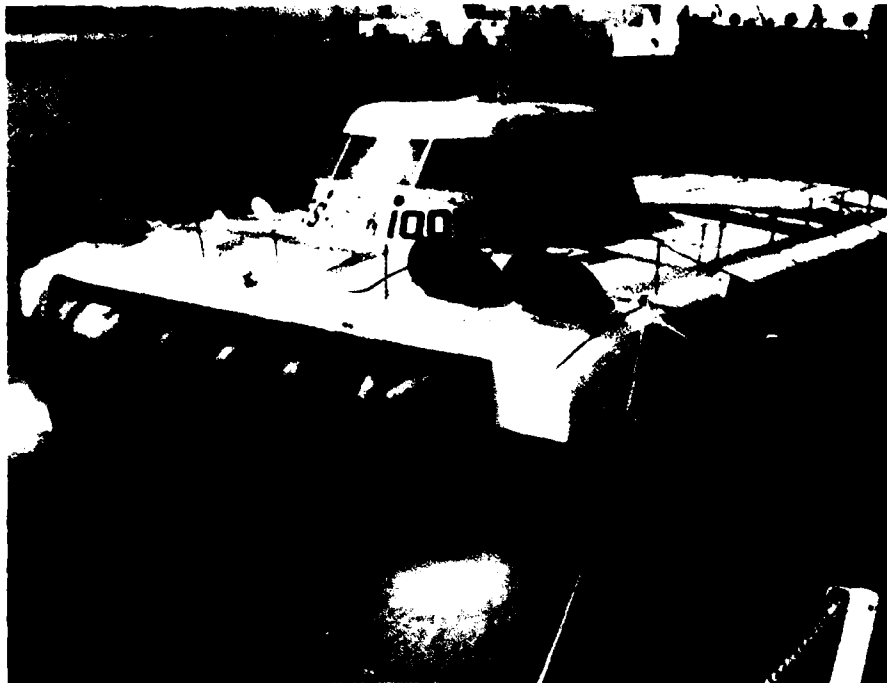


Figure 138 - SES-100B Stern Seal

The complex combination of loads, pressures, and accelerations discussed in previous sections and chapters has complicated the design process and the selection of materials.

When, in 1960, the advent of skirts began to materialize, the air cushion craft designer had to make a selection from manufacturers' materials with unknown characteristics relative to the air cushion craft usage contemplated. Further, he was unaware of what properties to look for in a skirt material. Initial evaluations of materials were based on values of tensile strength, tear strength, peel, and abrasion.

From these initial evaluations, it was generally found that the nylon fabric cloths coated with some form of natural or synthetic rubber produced the best results. It was soon found that selection of the desired material was not obvious and that a wide scatter in material strengths occurred, depending on other factors besides material weight. Figure 139 shows the scatter in data for the tensile and tear strength of nylon-coated fabrics.

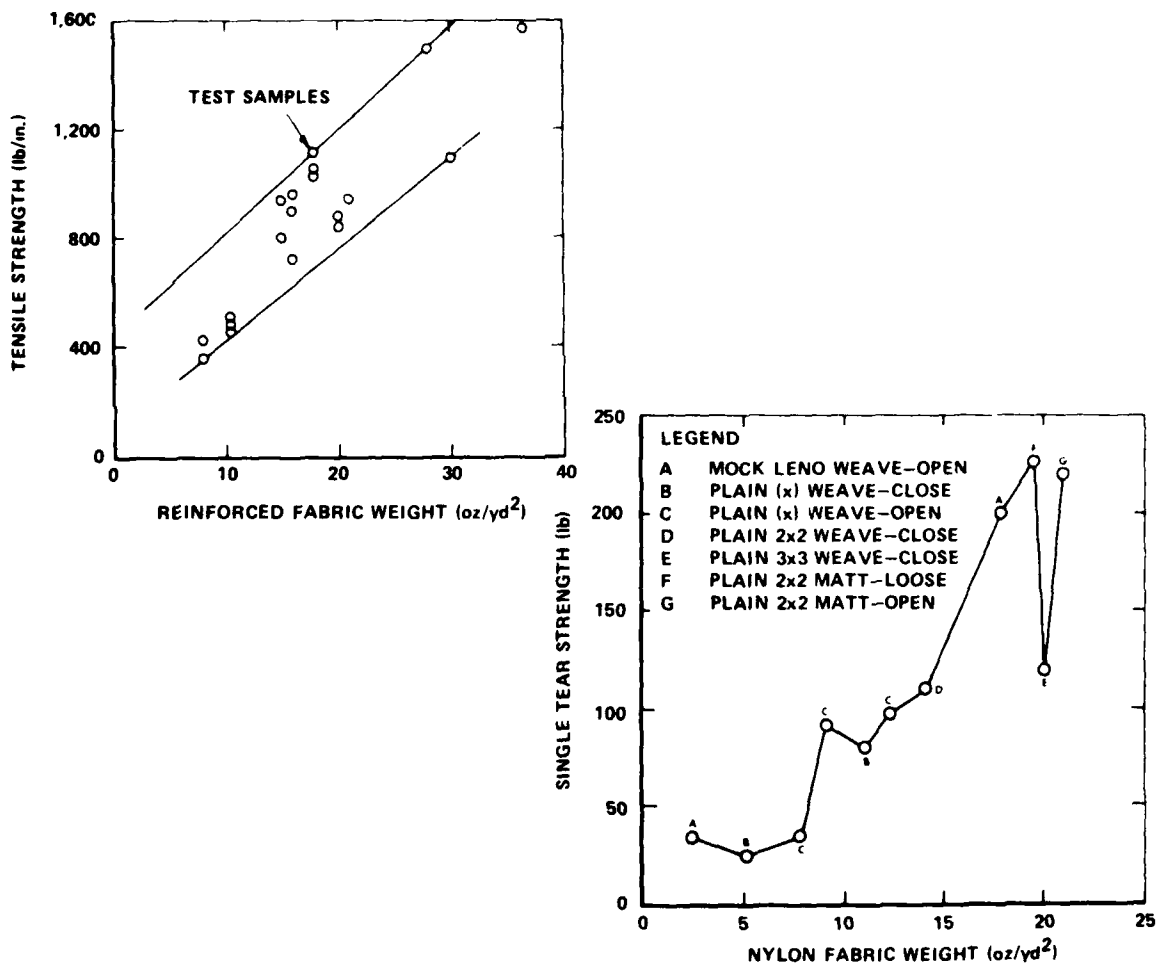


Figure 139 - Tensile and Tear Strength of Skirt Materials

The tensile strength is largely determined by the weight of the (nylon) fabric cloth, which carried the majority of the load. The tear strength, however, is not necessarily determined by the reinforcing cloth weight, as seen in Figure 139, but depends on such factors as the type of weave in the fabric, which may be either open or closed and may take different forms. These forms might be woven one fiber over another (known as a 1-by-1 weave) or in groups of fibers or strands woven over others. An uneven weaving like a 3-by-4 pattern will have different strengths in the warp (load) direction than in the fill or weft (normal to load) direction, for example. The type of ply used is a matter of design selection for the size and type of craft. Further, whether the fiber strands were twisted or not made a large difference in the strength and elongation characteristics. For example, due to the impact loads on the bags in the bag-finger skirt system, the resilience or elongation characteristics of the material influenced the survivability of the material and the ability of the skirt to retain a proper shape for performance and stability. Figure 140 shows six typical examples of open and closed weave fabric patterns.

Whether the weave was open or closed also made a significant difference to the material properties. In the case of open weave, the elastomeric coating actually fused through the weave and became cohesive with the coating on the other side. In the case of the closed weave, the strength depended on the bonding between the fabric cloth and the coating. Due to the high frequency oscillations that the skirt material is subjected to, it follows that the quality of the bond was instrumental in determining whether the coating would delaminate from the basic cloth.

It was soon found that, in the development of skirt materials, delamination was a more significant failure mode than simple abrasion. Because commercial operation by the BHC craft includes frequent sliding to a halt after each trip on a concrete ramp and, in the case of the SR.N4, frequent passes over sand at low tide, it was thought that abrasion would be a significant failure mode. Experience taught that such was not the case. This is not to say that damage by sand abrasion, jagged rocks, and sea shells was not a problem, but that they were not the most dominant mode of skirt failure.

In evaluating materials, the choice between the possible combinations was not clear. For example, the reader might ask himself if the tear strength and delamination properties would be better with an open or a closed weave. In general, the tear strength is limited by the tensile strength of the individual fiber and, thus, present materials have tended to be made of the multiple fiber woven cloth. By way of illustration of the design choice difficulty, Figure 139 shows that, for the same fabric weight (20 oz/yd^2), a 3-by-3 close weave cloth has a lower tear strength than a 2-by-2 open weave cloth. The delamination properties are measured by the peel strength (currently 25 to 60 lb/in.) which, in effect, determines the ability of the coating to adhere to the fabric cloth.

HIGH 'Z' SINGLE YARNS



2 x 2 MATT

MEDIUM 'Z' SINGLE YARNS



4 x 4 MOCK LENO

TREBLED YARNS



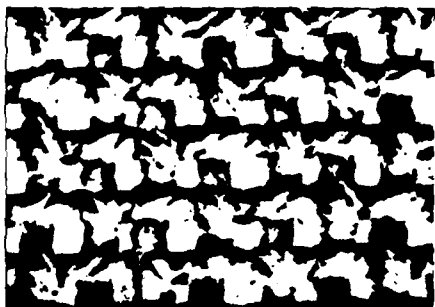
2 x 2 MATT

MEDIUM 'S' SINGLE YARNS



3 x 1 LENO

TREBLED YARNS



PLAIN WEAVE

LOW 'S' SINGLE YARNS



2 x 2 MATT

Figure 140 - Typical Skirt Fabric Weave Patterns

While difficulties persisted throughout the determination of the correct properties, operational experience, backed up by laboratory testing, supported the selection of nylon for the reinforcing fabric to the coated material. This selection applies, of course, to the current size and speeds of air cushion craft; and further research is required to determine its suitability for larger, higher speed craft.

The coatings used to date have also varied among the air cushion craft manufacturers. The British craft use either neoprene or natural rubber coatings. It has been found that the natural rubber coatings, such as the styrene butadiene rubber, have a greater resistance to delamination than does neoprene. Thus, because of the high frequency oscillations to which the fingers are subjected, most fingers are constructed from natural rubber-coated nylon. On the other hand, neoprene is used for the bags because it has excellent nonflammability properties and is more resilient to oil contamination.

In the United States, there was a greater use of the polyvinyl chloride (PVC) coatings because it was found, from laboratory tests at high speeds (in excess of 80 knots), that this coating survived better at these speeds than did the neoprene coating. Consequently, in 1969, the skirts selected for the U.S. Navy craft, the SES-100A and the SES-100B, were of the PVC nitrile-coated nylon fabric. To add further to the difficulties, it was found that, although the PVC nitrile coating performed well in variable temperate climates, it became excessively rigid at low temperatures, causing cracking of the coating with resultant loss of material properties, whereas the neoprene coating retained its resiliency down to Arctic temperatures.

One of the problems in skirt material development has been the inability to accurately predict, by laboratory techniques, the full-scale behavior of skirt material. Development of techniques has proceeded over the years, and it is informative to summarize the main types of failure mode and the laboratory techniques developed to select materials to avoid or minimize the failure.

Skirt Material Failure Modes

Again, the bulk of the experience has been gained on the bag-finger skirts and attention will be addressed to this form. Much of the knowledge gained, however, and the limited data available on other skirt forms suggest a wider application.

While bag failures are potentially more dangerous than finger failures, the mechanisms of failure are more easily understood and controllable. Three bag failures of interest are the SR.N4 incident during trials in 1968, the starboard bow bag (loop) failure on the VT 1 in 1971, and the bow seal failure on the SES-100A in 1972. All failures were found to be due to material defects and manufacture, but all craft gently settled into the water upon failure due to the alleviating and cushioning effect of the

remaining air. The mode of failure, other than material defect, is a fatiguing of the material around an area of stress concentration such as a web attachment or bolted reinforcement area. It has become common practice to design the bags in sections not only to facilitate maintenance but to provide rip stops (not always successful), such that any failure in the bag does not propagate along the entire periphery of the skirt. The history of skirt bags to date has been satisfactory, as bag lives greater than 2000 operational hours in commercial service have been experienced. In the language of the automobile industry, this equates to greater than 100,000 miles before a bag change. Current improvements in both material properties and skirt design are increasing this life even further. There is some indication that this life can be more than doubled in the next 10 years.

The bag failure mode, however, is overshadowed by the short life of the fingers, which today varies from 200 to 600 operational hours, depending upon speed of operation and location on the craft (recall in the earlier discussion of craft operating bow-up for safety reasons causing increased finger wear at the stern). The form of the finger failure, the laboratory methods to simulate the failure, and the solution for its elimination have consumed a large part of the skirt development efforts on both sides of the Atlantic over the last 15 years. Indeed, it was concluded early that it was pointless to attempt to simulate the failure modes in the laboratory and that only full-scale operational craft data would provide the needed design information.

This situation prevailed until about 1967 when it was realized that, if any advancement was to be made in skirt material development, then serious laboratory material exploration would have to begin. Some of the initial experiments were admittedly rather crude and often produced meaningless results. Crago⁸³ describes the ultraviolet radiation tests, the car mud flaps tests, and the tests where wet air was blown between clamped pieces of skirt material producing nothing but obscene noises. In addition to testing for basic properties like tensile strength and tear strength, a means was needed to simulate the main culprit responsible for the short life of fingers, namely delamination.

In the early discussion on the development of the bag-finger skirt form, the existence of different high frequency vibrations in the fingers was noted. These modes of vibration occurred at different locations on the finger: at the lower edges, due to high pressure air blowing over unloaded "ears;" at a point a few inches up on the small radius of the finger, due to flexing of the finger over obstacles or waves; and also on the sides of the fingers on the rubbing surfaces, where again a high frequency vibration occurs.

This experience of high frequency oscillation in the presence of water-laden pressurized air led BHC, in 1967, to develop a device that

held the material specimen in the outlet nozzle of a blower that blew air (wet or dry) over the specimen causing it to flap like a flag. This flagellator, as it became known, proved to be the first means of simulating, in the laboratory, material failures that resembled those experienced on full-scale craft. This device was also used to do comparative tests on candidate skirt materials for selection for craft use. A similar device was used to evaluate the bag material, but in this case the edge of the material was not allowed to flagellate, but, was looped in the form of a bag section. Figure 141 (upper and middle sketches) shows this setup.

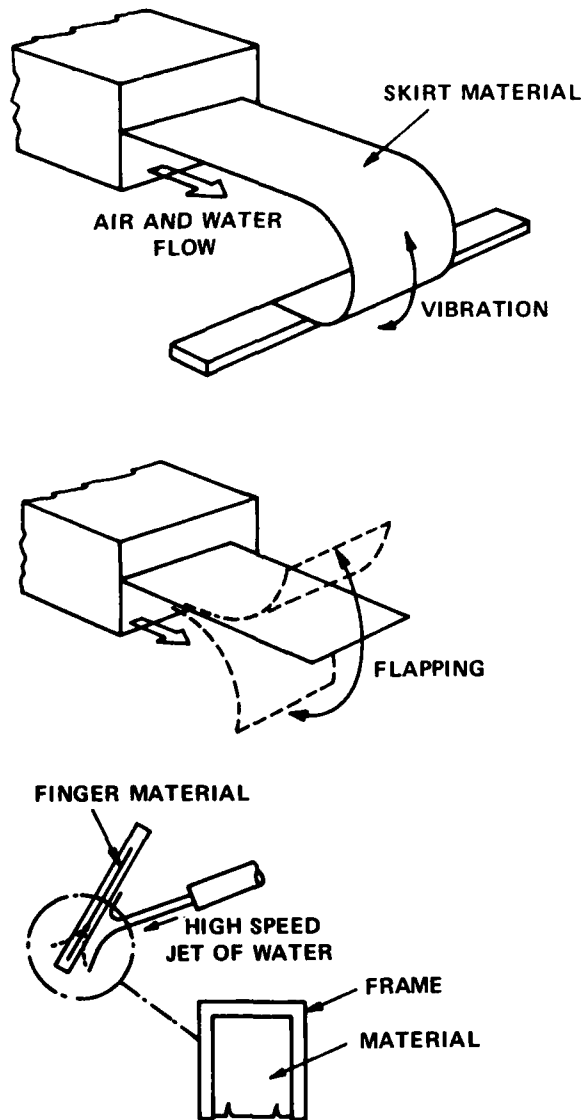


Figure 141 - Skirt Material Testing

While these test methods went a long way to aid in our understanding of skirt failure, it was difficult to correlate life and time on the flagellator to time on an operational craft. Since the introduction of the flagellator, several other methods have been introduced, all attempting to simulate better the operational conditions. One such device employed impinging a jet of water on the skirt material as shown in Figure 141 (lower sketch). The material specimen could be inclined at the finger inclination, and the jet of water could be at craft velocity. What was not simulated was the presence of cushion pressure and the true fixity of the material, but it was another step along the way. This method was introduced in 1968 by Aerojet and was included in the test methods at Bell in 1969. Goodyear later developed a further refinement to the waterjet flagellator in 1970, in which a rotating disk cut off the waterjet flow at high frequency to simulate the intermittent nature of a real environment of a skirt vibrating in and out of the waves. Goodyear also incorporated air pressure behind each finger-shaped specimen to simulate the effect of the air cushion. In 1971, the U.S. Navy Applied Science Laboratory employed rotating wheel test methods for similar reasons. Figure 142 shows a typical delaminated skirt finger (top photograph) from actual operation and a typical specimen (lower photograph) after several hours in a waterjet flagellator. Laboratory tests have also been conducted to investigate skirt material failures during simulated operation over a solid surface.²⁸

The test methods usually demonstrated the types of failures that occurred in fingers. The form of failure was not always obvious and differed from one material to another. A typical form of failure involves a crazing of the surface due to the breakdown of the surface of the coating from the many cycles of oscillation. The finger material may stabilize at this condition for several hours until the crazing develops into cracks that penetrate to the fabric cloth, at which point the bond begins to break down between the coating and the fabric. This mechanism usually occurs at the node point about which the finger is vibrating and then propagates down the finger. The process is accelerated by "wicking," in which water works its way up from the unsupported edge where the fabric is exposed into the area where delamination is occurring. Attempts to eliminate wicking by beading over the free edge of finger material have not been successful, as the increased mass due to beading only serves to increase the destructive forces and thus accelerate the wear.

The high frequency buckling of the finger material and the fatiguing of the coating adhesion led to more sophisticated test techniques in an attempt to isolate the governing mechanism and increase the likelihood of developing an improved material. Fatigue testing to develop "S-N" curves for the material is now being pursued to give further insight into the material failure. Improved tests to determine basic properties such as tear strength and coating adhesion are being pursued to gather the much-needed data. Figure 143 shows the results of some tensile tests on two materials using this technique.¹⁰⁸

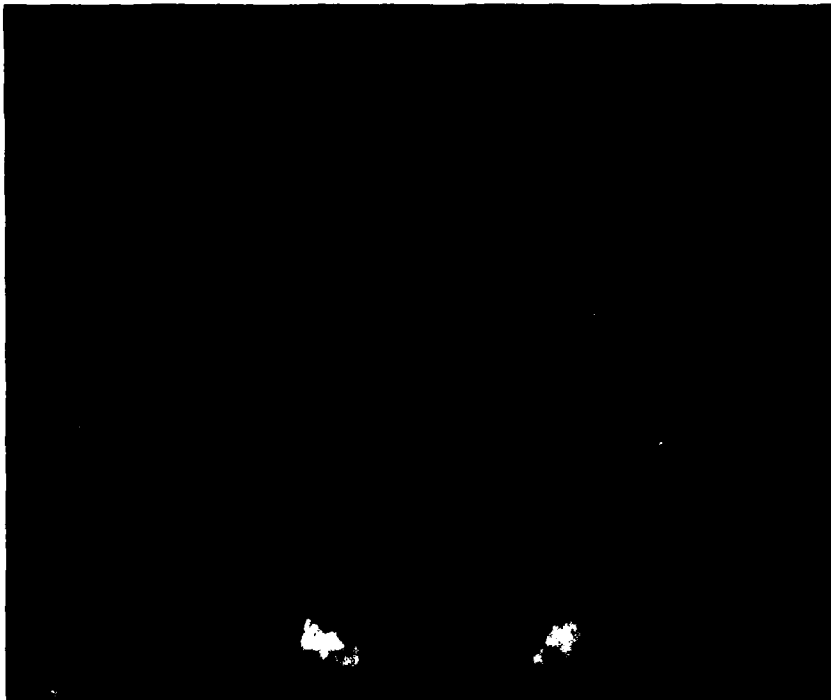
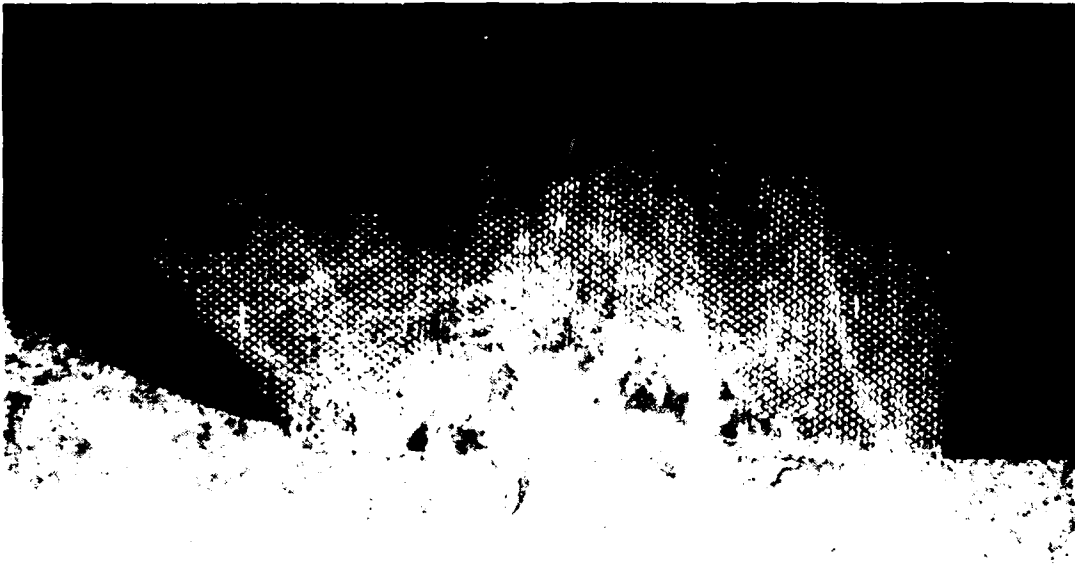


Figure 142 - Delamination and Wear of
Skirt Material

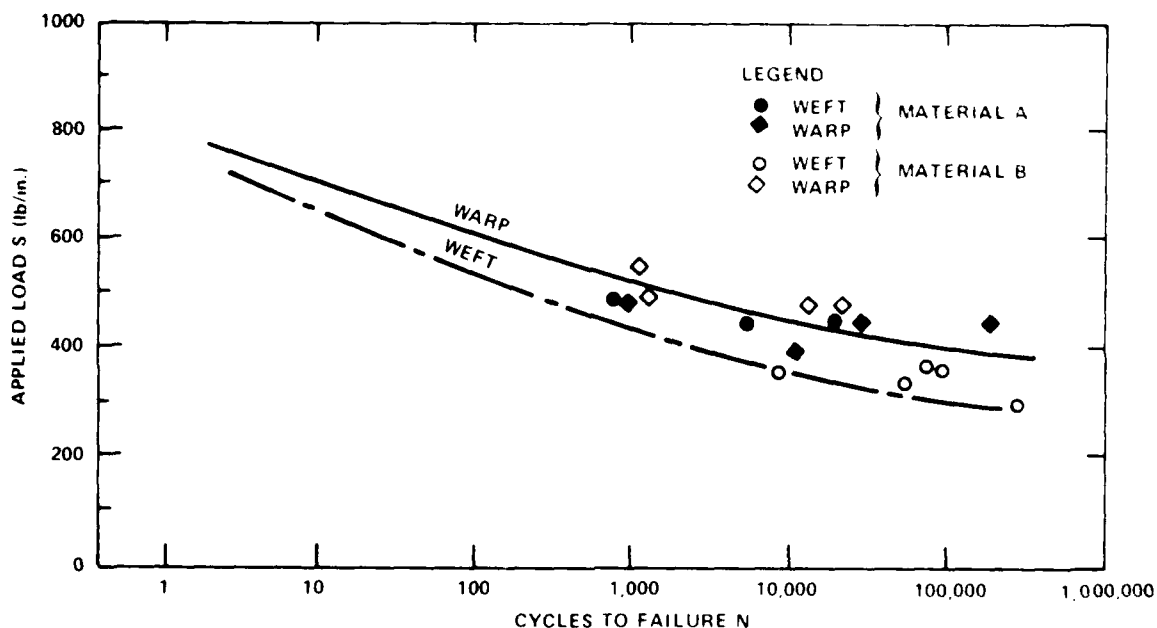


Figure 143 - Tensile Fatigue Tests on Skirt Material

To date, insufficient data is available to make firm design predictions; indeed, widely different viewpoints are held in interpreting the data and its effect on skirt design. This is illustrated best by considering the skirt material weights as used on current air cushion craft and the operational life experienced with such skirts.

Skirt Material Weight and Life

It would be expected that, as the craft size and the cushion pressure increase (for example, see Figure 24, Chapter III), the hoop tensions in the bag or loop would increase. The actual rate of increase depends on several parameters; Equation (157) states that the load in fabric increases by λ^2 where λ is the geometric scale factor but that the rate at which the tensile strength increases with fabric weight (see Figure 139) depends on the types of materials as already discussed. Allowing for some freedom in thickness of material and relative coating weights, the bag weight per unit area should increase only as λ . Figure 144 shows the trend in material weight for skirts of operational air cushion craft. If w is the total specific material weight (fabric and coating) in ounces per square yard, then Figure 144 shows that bag (or loop) weights follow as

$$w_{\text{bag}} = 15 w^{1/3} \text{ oz/yd}^2 \quad (159)$$

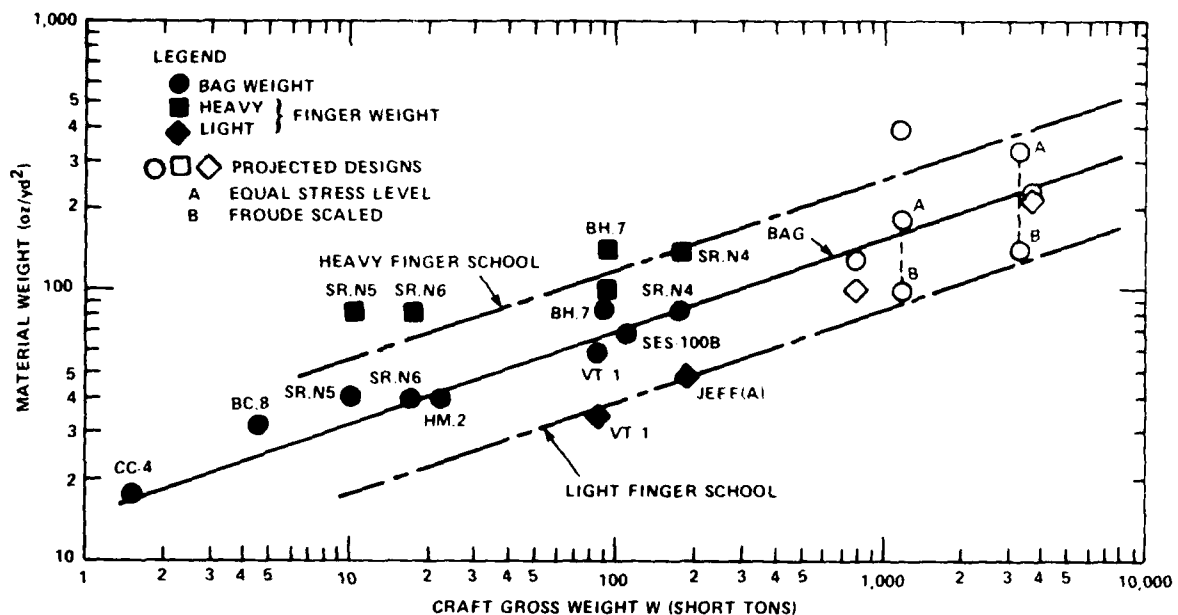


Figure 144 - Skirt Material Specific Weight

It should be pointed out that, although the load is carried by the nylon fabric cloth, most of the weight is in the coating. For example, the SR.N6 used 40-oz/yd² material for the bag, of which only 12 oz/yd² is the nylon fabric. Similarly, the SR.N4 uses 85-oz/yd² material for the bag, of which only the 20-oz/yd² nylon fabric is providing the hoop tension of approximately 850 lb/in.

The choice of material for the fingers, however, is still a matter of development due to the various failure modes discussed and an insufficient data base from which to draw positive conclusions. Working with essentially the same data base, two schools of thought have evolved which, for the purposes of discussion, will be called the "heavy finger school" and the "light finger school."

The heavy finger school believes that the finger should be designed such that the nylon fabric be sufficient to meet the tensile and tear strength requirements and that sufficient coating be applied to combat the wear. It is reasoned that the heavy weight of the coat will actually dampen the oscillations or vibrations of the finger. All of the current BHC craft

fit this category, and it will be noticed that the SR.N4 has a finger weight of 140 oz/yd^2 (with a 30-oz/yd^2 nylon fabric base). In this case, the fingers are actually heavier per unit area than the bag.

The light finger school, on the other hand, believes that, because the forces contributing to the failures are proportional to the mass of the skirt finger for the same accelerations, it would be better to have the finger as light as possible. In the Vosper-Thornycroft VT 1, an example of this school, the finger material is 35 to 43 oz/yd^2 compared to the loop weight of 60 oz/yd^2 .

In Figure 144 trend lines are drawn through craft belonging to each school, and it is noticed that, in terms of weight, the difference is significant.

Since Reference 2 was published, work has continued on skirt design and projections for larger craft³⁰ have been added to Figure 144. While the trend has continued as predicted, there is still a wide scatter in specific material weights depending on the "light" and "heavy" material philosophy. For example, the points labeled 'B' assume that the material would be Froude scaled, while the points labeled 'A' assume that the stress levels (in the load carrying fabric) remain constant as the bag is scaled up. In reality, one would expect that specific weights in between these values might be more appropriate and these points are also shown in Figure 144.

The actual scaling laws for finger material are even less clear, and the trend lines shown in Figure 144 are illustrative only. For example, the scaling of finger material would be expected to depend on the basic weight, which scales as λ but, due to its vibration characteristics, it would be expected that the bending stiffness (EI) should be considered, which scales as λ^4 . If the SR.N4 fingers are scaled by λ^4 , some startling fingers are obtained for large craft. Because most of the available theories today ignore weight, it is not clear what should be used for larger or faster craft.

A numerical example using the various scaling laws and philosophies in vogue might clarify the difficulty in making accurate predictions in material weights at this time pending more reliable large scale test results.

Example on Material Scaling

A particular 170-ton air cushion craft uses skirt material of a specific weight of 50 oz/yd^2 (of which the reinforcement fabric weighs 18 oz/yd^2 and the elastomeric coating weighs 32 oz/yd^2). Both bag and fingers are made of the same material. The craft design speed is 50 knots. It is desired to scale the craft to 3000 tons with a speed capability of 80 knots. What skirt material weight should be used?

Solution 1: Material at Same Stress Level.

The scale factor from the 170-ton craft to the 3000-ton craft is $\lambda = 2.60$ in which case the specific weight would become

$$50 \times (2.60)^2 = 338 \text{ oz/yd}^2$$

Solution 2: Fabric at Same Stress Level, Coating for Wear.

Here it is assumed that the reinforcing fabric takes the entire load and that the coating is used to combat the wear only. If the fabric is to operate at the same stress level and the "wear" coat simply scales linearly then the specific weight becomes:

$$\text{Fabric: } 18 \times (2.60)^2 = 122 \text{ oz/yd}^2$$

$$\text{Coating: } 32 \times (2.60) = 83 \text{ oz/yd}^2$$

$$\text{Total specific material weight } 205 \text{ oz/yd}^2$$

Note: If the speeds of the two craft were the same and the coating (32 oz/yd²) was sufficient to combat 50 knots, it could be argued that the coating would not scale. The Froude scaling here then is arbitrary and is in anticipation that wear at 80 knots is greater than at 50 knots; to be discussed later.

Solution 3: Improved Material.

Assume that a material can be developed that can operate at the higher stress levels such that Froude scaling is sufficient; then the new material specific weight becomes

$$50 \times 2.6 = 130 \text{ oz/yd}^2$$

If the original 50 oz/yd² material had a tensile strength (in the warp direction) of 950 lb/in., which is typical of today's elastomer coated, nylon fabric materials, the new material would have to have a tensile strength of about 2500 lb/in. to be compatible with these conditions. Only a few materials have this capability today and those that do, do not have as good a resiliency. This has unknown ramifications under dynamic loading conditions.

In summary the possible material weights are:

Same stress level	338 oz/yd ²
Fabric only at same stress level	205 oz/yd ²
New material of higher strength	130 oz/yd ²

As can be seen in the above example (for the bag) the range in weights can be quite significant and very little data is available to show in a systematic manner how the proper choice of material should be made. Other considerations are: the stretchability of the material because shape is important in the stability and control of the craft (see Chapters IV and V); the variations in load in the warp and weft directions of the weave; fatigue life especially for the fingers that are subjected to high flagellation loads; and, finally, the effect of the sheer mass of the skirt system in terms of affecting the "sprung-unsprung" mass relationships in the vehicle suspension systems.

Some attempt has been made to compare the results of skirt life of both heavy-fingered and light-fingered craft, based on available full-scale operational data and on flagellator data. Figure 145 shows this comparison, which has been taken from Reference 66. Although Figure 145 indicates trends, certain conditions used in the tests and the full-scale operational craft need to be explained for proper interpretation of the data.

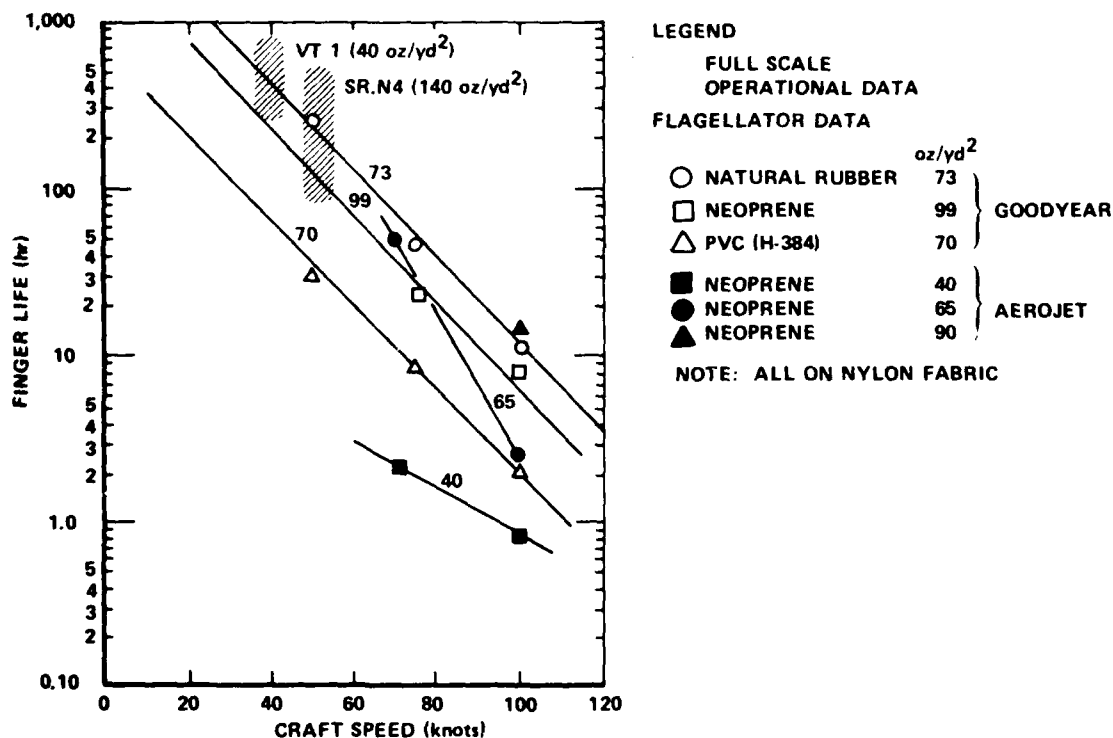


Figure 145 - Skirt Finger Life

For the flagellator data, life is defined as that time (in hours) when the coating has cracked through to the fabric, as discussed earlier. On the other hand, for the full-scale operational craft, life is defined as that time when approximately 18 in. of the finger (originally 5 ft long in the case of the SR.N4) has completely disappeared. The Vosper-Thornycroft data for the VT 1 record a life of 200 to 800 hr for the 40-oz/yd² finger material when operating at 38 to 40 knots over water while data for the Hoverlloyd SR.N4 operations record a life of 100 to 500 hr for the 140-oz/yd² finger material when operating at 50 knots over water and sandy beaches. If it is assumed that the laboratory (flagellator) data predict trends, then Figure 145 would indicate that the light-fingered VT 1 and the heavy-fingered SR.N4 belong to the same class in relation to the speed effect. However, there is no full-scale evidence of the rate of decrease of finger life with speed for two different skirt materials on a common skirt design, and it would be dangerous to draw strong conclusions at this time. The flagellator data shown did show increased life as material weight increased up to a value of approximately 100 oz/yd², after which the life decreased, but again a lack of sufficient data conducted over a range of material parameters precludes a conclusion. One common trend, however, does exist and that is the rapid decrease in finger life as speed is increased. The data show a 10:1 decrease in life for a 2:1 increase in speed. It is hoped that, as material development continues, these data can be enlarged upon and improved.

Figure 146 is another form of expressing skirt finger (segment) life showing the material improvement in life expressed as operating hours per finger change as a function of operating hours.

Although craft speed is not shown explicitly in Figure 146 it is to be noted that the VT 1 is a 35 knot craft compared to the SR.N4 70 knot craft.

Indications are that further improvement in material life is currently being explored. Skirt life today is on the order of 2000 hr for the bag and finger life varying from 400 hr in the bow area to 100 hr in the stern area. The explorations of new materials are worthwhile, because, as reported* concerning Seaspeed (the British Railways SR.N4 that makes regular English Channel crossings) the skirt costs about (£600 to £800) per day to maintain in operating condition.

SKIRT SYSTEM WEIGHT

Because of the considerations previously discussed, it is not possible to give a generalized skirt system weight in a simple and meaningful form. The effect of different material weights and the effect of cushion pressure and skirt depth have strong influences on the total skirt system weight. The choice of skirt form, whether it has stability keels or not, for example, can again make comparisons difficult. Figure 147 has been compiled, however, to show certain trends that have emerged. The BHC craft

*As given in the London "Sunday Times" dated 30 July 1978.

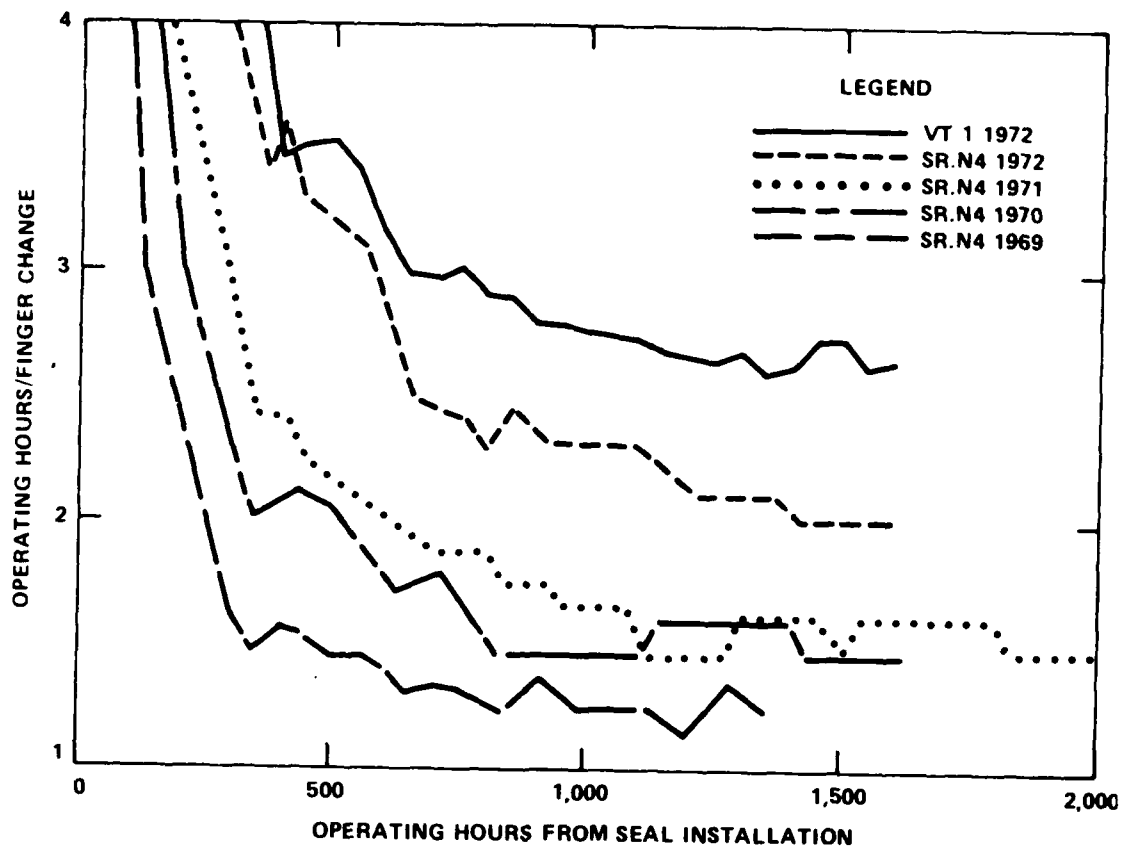


Figure 146 - Finger Life Improvement

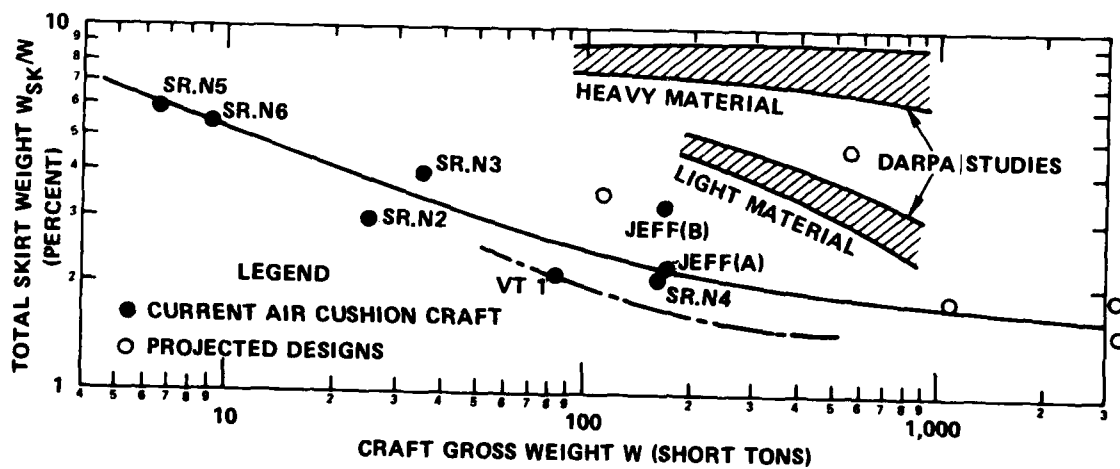


Figure 147 - Skirt System Weight

represent a family of craft where a consistent trend would be expected, which is indeed the case as shown. The VT 1 is not a member of this family because it employs the HDL loop and segment skirt design and, further, uses the lighter material in the fingers. The combination of skirt design differences and material difference has resulted in an approximate 15-percent reduction in skirt system weight. From a simple weight analysis, it can be shown that the skirt weight would be proportional to the cushion pressure times skirt height, all else being equal. It is not surprising, therefore, to see that the projected skirt weights for the high density (100-lb/ft² cushion pressure) U.S. Navy amphibious assault craft (JEFF(A) and JEFF(B)) are higher than the corresponding low density craft of the same displacement; this is despite the fact that the skirt depth at 5 ft is approximately half that of the SR.N4.

The JEFF(A) uses the pericell skirt concept and skirt material of 50 oz/yd² for both bag and cell and has a skirt system weight, including attachment fittings, of 2.2 percent of the gross displacement. The JEFF(B) uses the bag-finger concept and 70-oz/yd² material for the bag and 90-oz/yd² material for the fingers. It has a skirt system weight, including fittings and the stability keels, of 3.3 percent of the gross displacement.

The effect of higher cushion pressures and deeper cushions can be seen from the DARPA studies²⁸ where, for skirt depths compatible with Figure 77 (that is, approaching 20 ft for the 1000 ton displacement craft), skirt weights of 7 to 8 percent appear likely if heavy materials are used and 3 to 5 percent if light materials are used.

Later designs,³⁰ since the DARPA studies,²⁸ would suggest that lower weight skirt systems (less than 2 percent of the gross weight) are more likely as shown by the projected designs on Figure 147, although certainly no conclusive trends can be drawn at this time.

It has been the intent of this chapter to outline some of the more dominant developments that have progressed in skirt design and to provide a point of departure for those who would pursue its development. It has also outlined a background against which the designs currently on the drawing board can be placed as they emerge, and solutions to problems which now appear insurmountable will, in retrospect, look obvious.

As a final comment, mention should be made of recent developments in skirt design intended to suppress spray. Most of this work has been prompted by the need to avoid spray entering the engine systems. More information on this early work is given in Chapter IX on Propulsion (see, for example, Figure 195 for a spray suppressant skirt design).

CHAPTER VII

STRUCTURAL DESIGN

Most of the development to date has been on the intermediate speed (30 to 100 mph) craft where the air cushion craft may definitely be classed as an advanced marine vehicle or high performance ship. The discussion in this chapter is restricted to this particular application. Due to the high speed at sea requirement (high when compared to more conventional ship forms) and the need to maintain low weight, conventional ship structural design techniques do not apply in the case of air cushion craft.

Conventional (monohull) ship structural design has, as its basis, several hundred years of combined data and experience. This background allows the structural design of the hull to be pursued by relatively straightforward design methods. Within limits, one hull form is similar to previous hull forms, and the design is relatively forgiving to under- or over-estimation of the loads. This forgiving background, however, has left a legacy of an incomplete data base on which to design a new form of ship, namely, the air cushion craft, where a knowledge of the loads is essential. Because the kinetic energy of any high performance craft traveling, for example, at 60 to 80 knots, is some 9 to 16 times greater than a conventional craft of the same displacement traveling at 20 knots, then errors in load estimation can be seen to be disastrous. One cannot simply "beef up" the structure arbitrarily and use the conventional ship design methods because this would add weight to the craft. Added weight could be ill-afforded as this robs from the payload that has already suffered due to weight being required for the power to sustain the craft on-cushion and the power to propel the craft at high speed.

The structural weight of air cushion craft is, thus, an important design parameter for economic or payload-carrying considerations. Current craft have structural weight fractions that vary from 25 to 35 percent of the gross weight, with the majority of today's high performance craft being in excess of 30 percent of the gross weight. Referring to Figure 33 in Chapter III, it is seen that this represents approximately 60 percent of the empty weight of the craft.

Figure 148, shown originally in Reference 109, shows the structural weight of several major existing air cushion craft displayed against a backdrop of aircraft, planing boats, and displacement ships (dry cargo and tankers).

Each of these craft operate in a different medium and at different speeds. The highly structurally efficient (low structural weight fraction) tankers and dry cargo ships operate at 15 to 25 knots and are totally supported at the surface with buoyant forces. The aircraft have complex structures comprising fuselages, wings, and appendages and operate at high speeds (100-500 knots) immersed in air but under dynamic loading conditions. The air cushion craft does not have such a complex structure and operates in the intermediate speed range (35-100 knots) at the interface

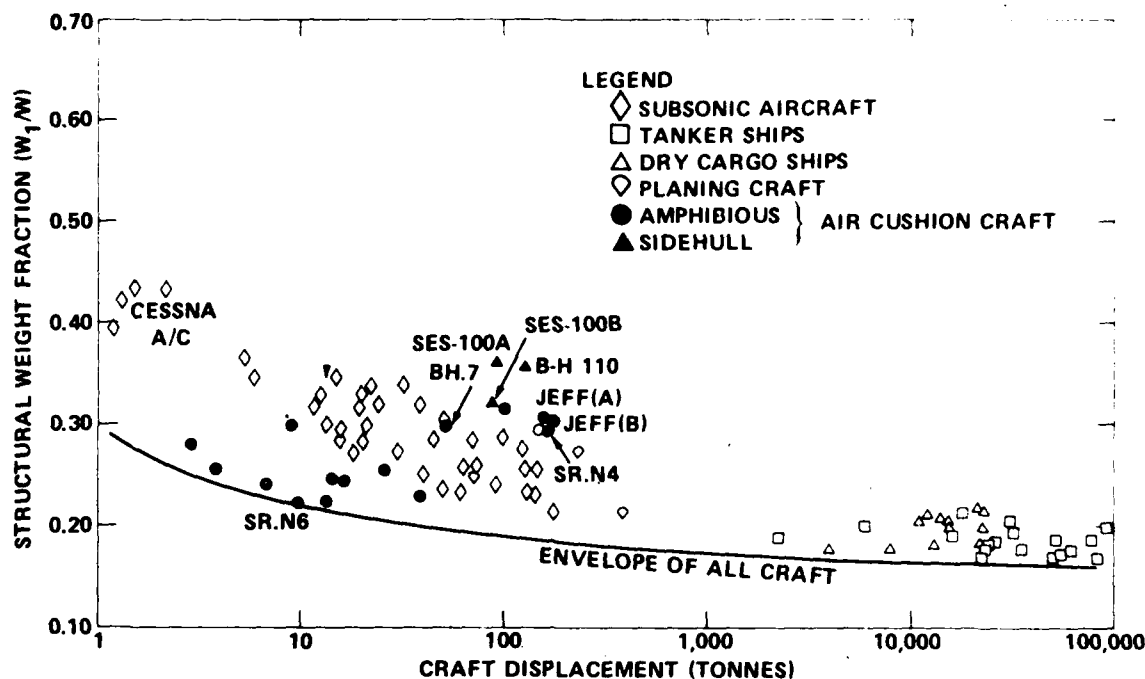


Figure 148 - Structural Weight of Various Craft

of the air and water surface. The envelope of all these craft, as shown in Figure 148, has the equation

$$\frac{W_s}{W} = 0.15 + \frac{0.15}{W^{1/3}} \quad (160)$$

where W is to be measured in metric tons (tonnes).

It should be pointed out that in some earlier references, including Reference 2, inconsistencies appeared in quoting structural weight of air cushion craft. In the U.S. it was usual to quote the structural weight excluding the skirt system, while in the U.K. it is usual to quote the structural weight including the skirt (being considered as a flexible structure). This has led to confusion in comparing weights of various craft and has been corrected in Figure 148* and in subsequent graphs.

*Appendix B summarizes the various weight groups used in this report.

A considerable amount of time and effort has been invested in the structural design of air cushion craft as a result of the high percentage of the gross weight that the structure consumes and the tendency for the craft to reach even higher fractions, as Figure 148 shows.

It is appropriate to point out here that the important element of cost has strongly influenced the history of structural design development. Clearly, one cannot afford the technological luxury of designing the optimum low weight structure even if the loads were known. Such an approach incurs two major elements of cost: the amount of engineering time required to optimize the structure and the amount of fabrication time needed to construct the complex structure that would result from such an optimized design. With the relatively few craft built to date, cost considerations alone have influenced the structural weight fraction toward the high side.

As part of the structural design development and partly influenced by cost, two very distinct design philosophies have evolved. The first philosophy, characterized by the British, has been to design the craft with rather optimistic assumptions relative to the loads, so that relatively light structures evolve. Then, when in service certain breakages occur, the structure is locally strengthened. This has the benefit that the structural weight remains light and, most importantly, very little time is spent in structural redesign. It also has the benefit that, over a period of time, the loads in a seaway as affecting an air cushion craft become known from the breakages. What might be surprising to some is that this is done with craft operating with fare-paying passengers on board. This can be attributed to the Bulldog spirit.

The second distinct design philosophy is one in which the structure is designed with a conservative estimate on loads and is later given sufficient instrumentation to record loads and motions such that the next craft built can be designed with lower structural weight fractions. This philosophy has been followed, by and large, within the U.S. Navy.

Although it is beyond the scope of this report to present any analysis of the cost of air cushion craft in toto or of its structure in particular, however, it is known that heretofore they are expensive craft to build. Whether the craft is designed to military or commercial specifications or whether it follows either of the two structural design philosophies given above, influences strongly (a) the achievable structural weight fraction and (b) the cost of the structure. An indication of the total craft cost can be seen from Figure 149 which shows various air cushion craft costs displayed in conjunction with other craft such as hydrofoils and displacement ships. Each of the influencing factors of design philosophy, viz: commercial versus military specifications and speed, have their effect on the craft cost. The craft cost (which is the "small quantity buy" value of the craft cost without payload) has been expressed in 1978 dollars to help keep track of the effect of inflation. The quantity built obviously effects the cost and the costs quoted represent an average value over a small quantity (for example, 5 to 10 craft as covered by the data base).

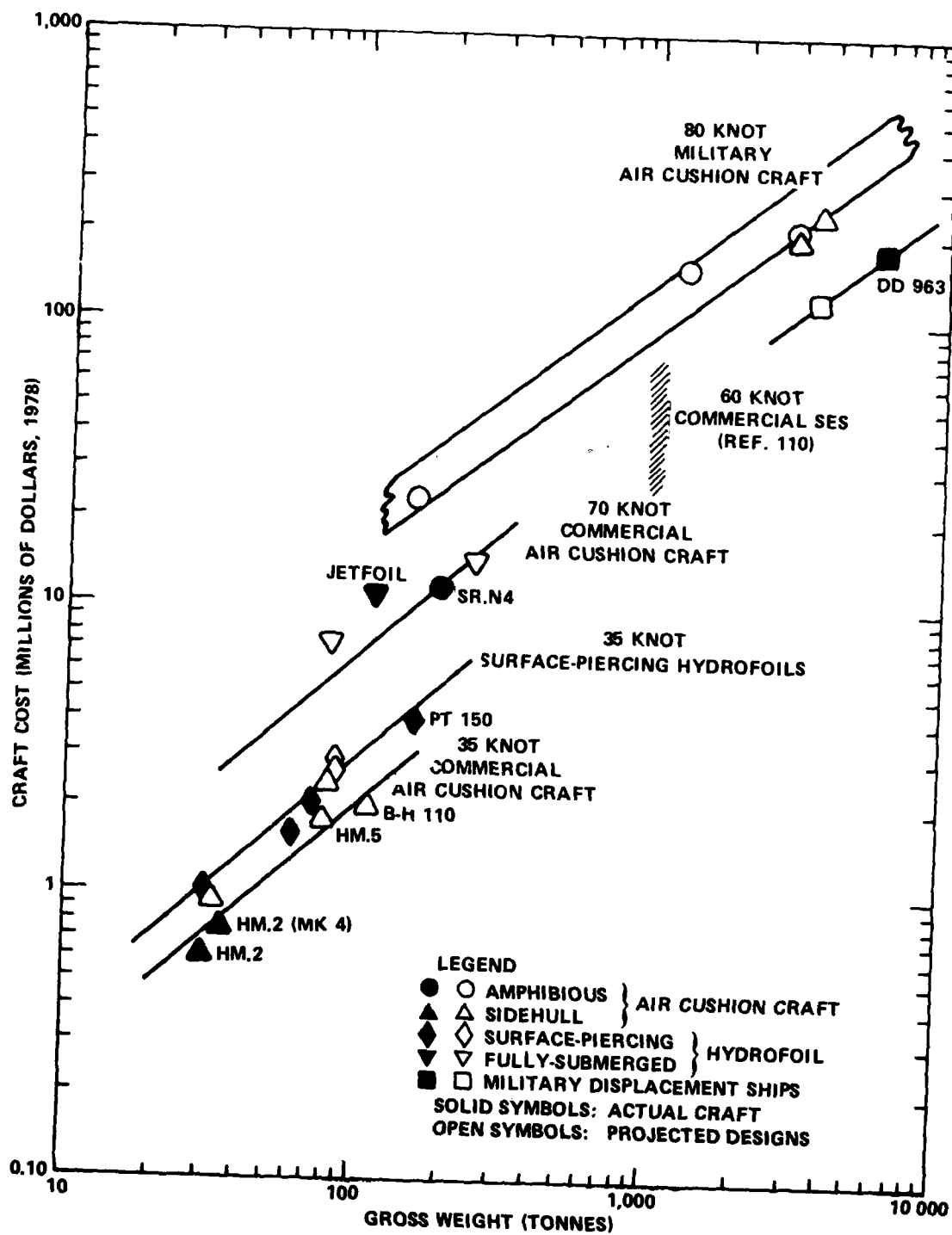


Figure 149 - Air Cushion Craft and Hydrofoil Costs

The one exception would be the surface-piercing hydrofoil of which more craft have been built. For reference purposes, some studies on the cost of commercial surface effect ships have also been included in Figure 149 and these are seen to agree generally with the trends shown here.¹¹⁰

The high cost of the air cushion craft is attributed, in part, to the requirement to be extremely weight conscious in all the subsystems of which the structural system and the propulsion system are the largest. Insufficient data are available in releasable form at this time to ascertain the relative effects of structural weight, speed, and cost of air cushion craft. For example, the weight of the structure, as shown in Figure 148, could be reduced, for example, by another 5 percent of the gross weight from 35 percent to 30 percent. This would incorporate a significant increase in engineering and manufacturing costs employing the same military specifications or could be achieved more simply at no cost by employing commercial specifications. The structure of military air cushion craft to date, for craft in the 100 to 200 tonne displacement and 50-80 knot speed range have been constructed for approximately \$20 to \$25 per pound. Commercial craft, on the other hand, in the same speed range have structural costs in the \$10 per pound range and if the speed is dropped to 35 to 40 knots this cost probably could be almost halved.

Expressing these structural costs in perhaps a more meaningful manner, namely labor costs, today's air cushion craft are constructed for approximately 2 manhours per pound (if mainly of rivetted construction) and about 1 manhour per pound for welded construction. If commercial specifications are followed, construction can be achieved in the 1/3 to 1/2 manhour per pound category. It can be seen from such values that the type of structural design can have strong ramifications in structural costs. Also, there is a greater variation in structural cost than there is in structural weight fraction, which raises questions as to the "return on investment" in expending large amounts of engineering, manufacturing, and quality control manhours on small gains in structural efficiency.

This chapter summarizes the various techniques used and describes several of the representative air cushion craft structure. When making comparisons between craft, however, the above influencing factors of cost, performance, and military or commercial application will be referred to as needed to place the results in perspective. The purpose here is to describe the development to date and to suggest that future development in lower cost structures is a fruitful avenue in lowering the overall cost of air cushion craft. It is left for more detailed papers to explore the important subjects of material properties, detailed fabrication techniques, selection of protective coatings, and quality and weight control procedures, all of which must go on in any particular design program.

DESIGN CRITERIA

The underway loads acting on an air cushion craft are made up of

1. Wave induced loads comprising: shears, bending moments, and torques through operation in various sea conditions at various headings and speeds.

2. Local loads such as deck loading from payload loading, slamming loads (due to wave impact), aerodynamic loading, propulsion and lift system loading, etc.

These loads will vary depending on whether the craft is operating on- or off-cushion (hullborne).

The design criteria used for these loads will depend on whether they are short term loading or long term loading involving considerations of fatigue.

There are also landing and parking loads.

In general two main techniques have been explored pertaining to the understanding of the dynamic loading on air cushion craft and they may be classified under the general headings:

Deterministic Method - This method essentially postulates a set of likely conditions and predicts the loads that will occur such as impacting a given wave, hogging, and sagging in a given sea condition, etc.

Probabilistic Method - This method essentially sets up, in a statistical process, the probability of certain loadings occurring when operating over random waves. The loadings in this case can be expressed in terms of significant values, RMS values, and other statistical descriptions for the loads.

Historically, by far, the bulk of the air cushion craft built to date have been designed using deterministic load conditions and associated design criteria. In recent years, the probabilistic loading methodology has gained popularity in an attempt to gain a more realistic description of air cushion craft loading.⁷⁶ Pending more confirmation data from full-scale operation of craft using the probabilistic technique, the historical precedent of the various deterministic loading design criteria will be briefly outlined here.

Design criteria for loads and pressures acting on air cushion craft hulls began to evolve in the early 1960's as data accumulated on the various craft. The first set of criteria published was included in the British Civil Air Cushion Vehicles Safety Requirements (Provisional) issued in 1962 by the British Air Registration Board (A.R.B.),¹¹¹ the government agency charged with the operational regulations of hovercraft in England. The A.R.B. is now the Civil Aviation Authority (CAA) with the same regulatory authority.

The criteria that evolved at that time were based on data collected on the SR.N1¹¹² before it had skirts fitted and on data collected on sea-plane landings. This combination of data thus took no account of any load alleviation due to the cushioning effect of the air cushion itself or of the bow bags and, thus, treated the craft as a hard structure impacting the waves. Such criteria would be directly applicable to the hullborne or off-cushion mode but requires discussion relative to its applicability to the on-cushion or cushionborne mode of operation. This will be discussed later.

Many craft, operational today, have used these criteria in one form or another; they have subsequently been issued as Reference 113. While the complete criteria, covering such items as towing, mooring, and anchoring loads, will not be discussed here, it is important to consider the overall loading criteria and the wave impact conditions.

It is usually found that the structure for an air cushion craft is designed by a combination of the overall bending moments from wave impact and from the localized wave impact pressures, the latter being dominant for the smaller craft (smaller than SR.N4 size) with increasing consideration to the overall bending loads both hullborne and cushionborne as craft size increases.

From the criteria given in Reference 112, the wave impact load factor is given by

$$n_w = \frac{0.12 K_1 V_v V}{W^{1/3} (1+r_x^2)^{2/3}} \quad (161)$$

where n_w = wave impact load factor (load divided by craft weight)

K_1 = empirical factor

V_v = craft relative vertical velocity

V = craft forward velocity

r_x = distance from craft C.G. to impact point (measured parallel to centerline) divided by the radius of gyration.

The empirical factor K_1 is given in Figure 150. In Equation (161), V_v and V are measured in ft/sec and the weight (W) is in lb. The relative vertical velocity V_v is given by

$$V_v = V_s + \frac{2.26 \pi h_w}{\sqrt{\lambda}} \quad (162)$$

where V_s is the craft rate of sink (usually given as 2 ft/sec if craft motion data are not available) and λ equals wave length in ft. The wave height h_w is assumed to be

$$\left. \begin{array}{l} \lambda \leq 121 \text{ ft} \quad h_w = 0.10 \lambda \\ \lambda > 121 \text{ ft} \quad h_w = 0.10 \sqrt{\lambda} \end{array} \right\} \quad (163)$$

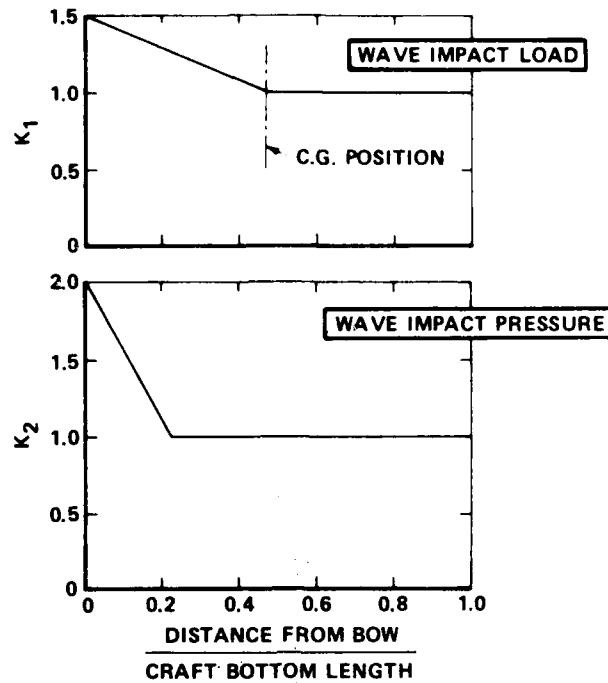


Figure 150 - Load and Pressure Wave Impact Factors

Equation (163) will be recognized as the wavelength assumed in the design of conventional ships in the computation of overall bending moments.

The criteria¹¹³ also give, for the wave impact pressures acting on hard structure craft

$$p = 0.0324 K_2 V_v V \quad (164)$$

where p is the peak impact pressure (measured in lb/in.^2) occurring over a localized area due to wave impact. The factor K_2 is an additional empirical factor and is also shown with the factor K_1 on Figure 150. The dissipation of this peak impact pressure over the bow plating and onto the underbody of the hull has been the subject of much research and development over the years, and the reader is referred to the literature for discussion of the theoretical aspects and results of experimentation on V-wedges and other bow shapes. (For example, Chuang and Milne¹¹⁴ and Jones and Allen.¹¹⁵)

The linear relationship (shown by Equation (164)) between the bow wave impact pressure and the craft velocity was also noticed from the test results taken on the SKMR-1 in 1963, when it was tested in its original hard-bottomed (no skirt) configuration. It will be noticed that, if one substitutes the value of $K_2 = 2$ from Figure 150 (for bow impact conditions) and the values for the relative sinking velocity of the craft from Equation (162), the following relation is obtained (for $1.1 \sqrt{\lambda}$ waves)

$$p \approx V \quad (165)$$

where V is now measured in knots. This observation led to the "1 lb/in.²/knot" rough rule of thumb in determining bow plating pressures, which has been used on all current U.S. craft both for the amphibious form and the nonamphibious form. Figure 151 shows the design plating pressures for the JEFF(A) and JEFF(B), and the SES-100A and SES-100B. The JEFF craft are designed to operate at 50 knots in rough seas and the SES-100 craft were designed to operate at 60 knots in rough seas. The bow impact pressure for these craft is seen to follow the 1 lb/in.²/knot rule of thumb with the appropriate attenuation of pressure as the wave dissipates along the hull bottom analyzed by such methods as discussed above. Analytical and experimental studies, both model and full-scale, are currently being conducted to provide improved load computations and design approaches.

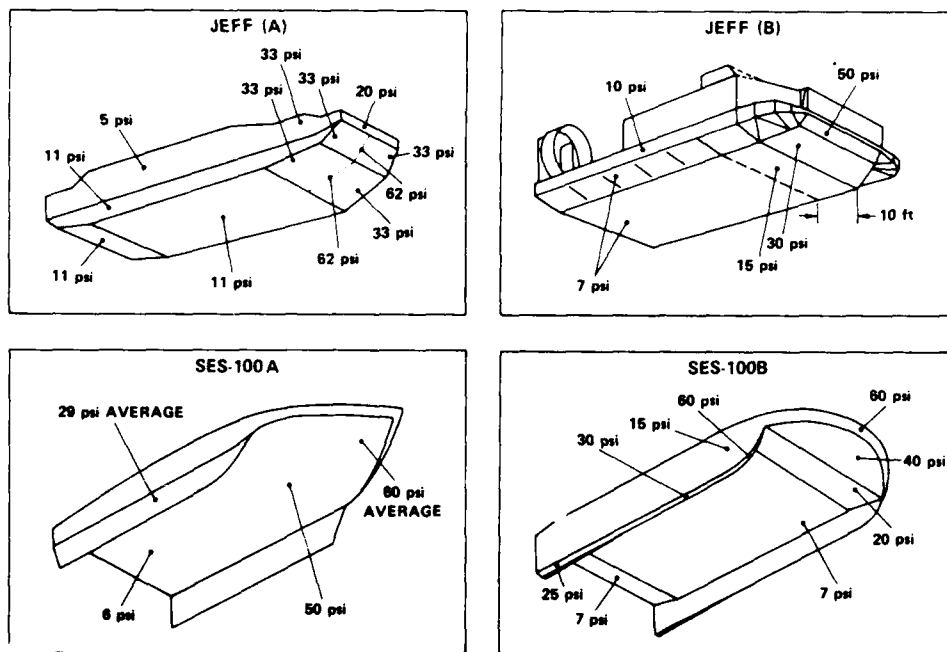


Figure 151 - Hull Impact Design Limit Pressures
(U.S. Craft)

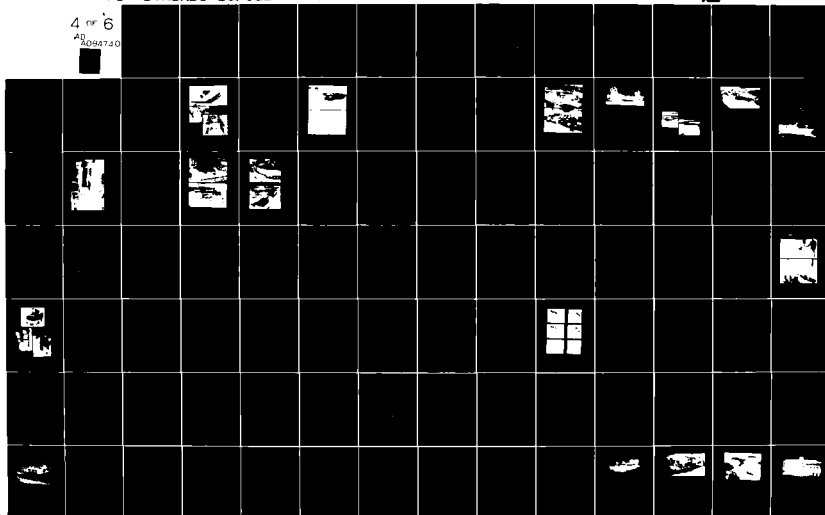
AD-A084 740

DAVID W TAYLOR NAVAL SHIP RESEARCH AND DEVELOPMENT CE--ETC F/G 13/10
AIR CUSHION CRAFT DEVELOPMENT. FIRST REVISION.(U)
JAN 88 P J HANTLE
DTNSRDC-88/012

UNCLASSIFIED

NL

4 of 6
20
0098740



Some recent work by Kaplan and Malakhoff¹¹⁶ provided further insight into the bow plating pressures of air cushion craft when impacting waves. Model tests of a two-dimensional bow, similar to that which is currently envisioned for use on surface effect ships, were conducted and the results of the slam pressure compared to the simple theoretical result,

$$P_{\text{slam}} = \frac{1}{2} \rho [V + v \cot \tau]^2 \quad (166)$$

where ρ = density of water
 V = craft forward velocity
 v = relative vertical velocity of bow
 τ = bow elevation angle measured from the horizontal plane

Figure 152, taken from Reference 116, shows the comparison between the predicted slam pressure given by Equation (166) and that measured from the model test. It is interesting to note that the result shown in Figure 152 is also very nearly a "1 lb/in.²/knot" relationship except that now the velocity is the relative vertical velocity in knots!

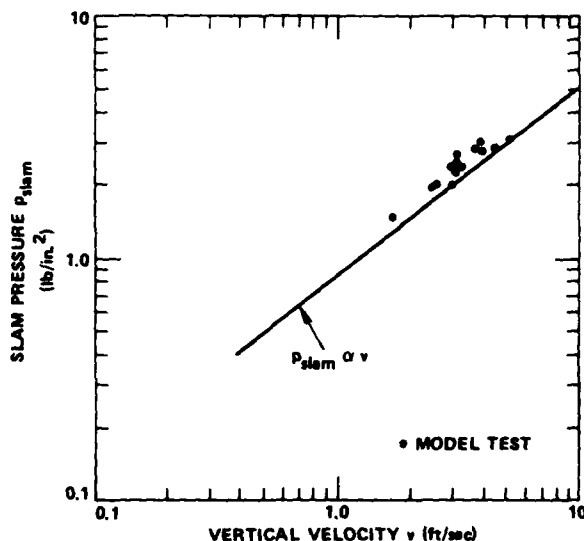


Figure 152 - Slam Pressure on SES Bow

The design case for the bow pressure is suggested by Kaplan and Malakhoff to be some average pressure to more properly reflect the probabilistic nature of the loading in random seas and it is suggested that this average pressure be,

$$p_{avg} = \frac{|Z_{slam}| \tan \tau}{B d} \quad (167)$$

where Z_{slam} = impact force (buoyancy + dynamic)

B = bow span

d = immersion depth of bow

Kaplan and Malakhoff provide a numerical example to illustrate the magnitude of the pressures involved. A 2000-ton surface effect ship impacting waves at 30 knots would generate a slam pressure (p_{slam}) of 150 lb/in.²

The average pressure (p_{avg}), on the other hand, would be reduced to 50 to 60 percent of that value or 75 to 90 lb/in.² That these are very high values compared with other air cushion craft is due primarily to the high pitching of the craft incurring a high relative vertical velocity (v), as will be shown later as pointed out by the authors. Designing to these high pressures without regard to the effect of the dampening effect of the cushion is conservative but regarded as realistic in light of a possible lift system failure in rough sea operation.

A slightly different view is taken for the British Hovercraft Corporation series of craft, to which credit is given for the attenuation effect of the cushion. This attenuation was not always evident, however, as it depended strongly on the skirt design. Prior to the use of the antiplov bags discussed in Chapter IV, pressure impulses in the forward sections of the bag, due to wave impact, were rapidly dissipated around the periphery of the craft inside the bag and gave little attenuation effect. With the antiplov bag, however, (see Figure 126) the pressure built up in the bag and prevented complete bag collapse except in extreme cases.

Accordingly, based on their experience, BHC incorporated a 50-percent reduction in the wave impact pressures due to cushion attenuation. This reduction in pressure manifested itself in lower hull plating pressures and lower plating weights. In the case of the SR.N4 with its 35- to 40-knot rough water speed, the bow plating was originally designed to 22- to 23-lb/in.² impact pressure. Some structural damage to the bow plating of the SR.N4 in 1970 and 1971 in extreme rough water operation, however, tended to indicate that probably the alleviation effect had been overestimated. The bow plating was subsequently strengthened by halving the stringer pitch and now has a strength value far in excess of the original 22- to 23-lb/in.² impact pressure value.

For purposes of illustration, the above discussion has been somewhat simplified to indicate the design trends and load criteria used. The actual detailed stress analysis on the craft incorporated various distributions of pressures and plating areas over which the pressures act. The analysis is also complicated by the inclusion of inertial and damping effects due to craft motion.

As a further illustration into the possible alleviation of hull impact pressures on air cushion craft, one can compare the full-scale operational trials data gained on the SES-100B to the design values shown in Figure 151.

The application of the bag-finger skirt to the SES-100B was the first application of such a skirt design to a high-speed sidehull form of air cushion craft. Because it was designed for the 60-knot condition in rough seas, it was not known whether the small volume of the bag could accommodate the pressure rise expected from wave impact. Accordingly, pressure relief valves were built into the bow to dump overpressure air into the cushion. Rough water trials data¹¹⁷ obtained at 30 to 40 knots in an approximate State 3 sea showed the sidehull bow plating pressure to be approximately 40 lb/in.² What is not known in this case is whether the bow bag attenuated the load, the relief valve effectively reduced the pressure, or none of these occurred and the "1 lb/in.²/knot" unattenuated load occurred. There is also the possibility, of course, that the pressure transducer was not located at the point of peak pressure. The design criteria, it must be remembered, were developed for hull forms similar to that of the SR.N1 and should only fortuitously apply to sidehull craft. The provisional "Green Book" of the Air Registration Board¹¹¹ and the later British Hovercraft Safety Requirements¹¹³ (BHSR) endorse the need for continued development of such criteria.

It is informative to see how the different impact pressure criteria have been applied in several of the more prominent air cushion craft. Figure 153 shows the actual plating pressure used in craft design compared to the rough water speed.

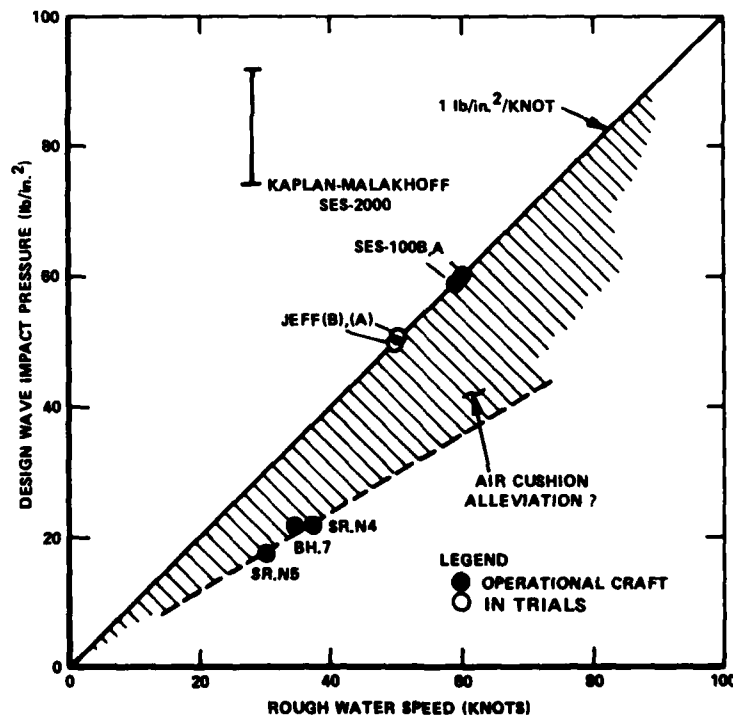


Figure 153 - Bow Impact Pressure Design Criteria

This figure clearly shows the difference in design philosophy between those craft incorporating a factor for the cushioning effect of the skirt system and those that do not. The choice of impact pressure has a considerable effect on the weight of the plating and structural weight of the craft.

Although not elaborated on here, the impact load factors (n_w) as applied to the different craft have also followed different design philosophies. Some craft have followed design criteria similar to those given by Equation (161), and others have again included a cushion alleviation factor. In the majority of the British operational craft today, this alleviation on the load factor has been assumed as 30 percent. In still other cases, for example, completely different methods of determining load criteria have been explored. One method attempts to determine loads by a probabilistic method rather than the straight application of load criteria. As a case in point, for some conceptual design studies done for the Arctic SEV program, it was found by analysis that the probability of impacting ice ridges with the stated skirt height was very low. Accordingly, it was not accounted for in the structural design with a resultant low structural weight. This illustrates the developmental nature of load and pressure criteria as it stands today and the need to exercise caution when interpreting results and trends.

It is to be noted that the above discussion has been directed toward the hard structure load criteria. No specific criteria have been issued by the BHSR¹¹³ relative to skirt design, although it has become common practice to employ a factor of 3 to the static pressure in the bag to obtain the wave impact pressure value. Detailed dynamic analyses and experiments are evolving to provide confidence in such criteria.

In what has gone before it will be noticed that the design criteria have historically been based on loads determined for a representative set of environmental conditions (that is, a certain speed and wave height). This has been dubbed the deterministic approach to design criteria, and all issued specifications on both sides of the Atlantic have been based on this method.

In ship design, considerable research has gone into determining ship response and loads when encountering irregular seas, and methods have evolved for predicting loads depending on the craft motion.^{118,119} Some work is proceeding on applying such probabilistic methods to air cushion craft design and this may, in the future, provide more meaningful design criteria. Insufficient data have been collected on the various craft, relative to wave impacts and other loads inducing phenomena to provide the required statistics on load occurrence. So current craft are still designed using the deterministic design criteria. Some recent calculations done for the JEFF(A) indicate that impact pressures, determined from a probabilistic method, tend to support the values found from the deterministic method discussed above.

In addition to the development of the design (or limit) load criteria, some variations have occurred in the factors of safety applied to the limit loads for use in detail design.

Factors of Safety

It is common practice in air cushion craft design to follow aircraft design methods and terminology. The following definitions apply in air cushion craft design

$$\text{Design Load} = (\text{Factor of Safety}) \times (\text{Limit Load}) \quad (168)$$

where the limit load is the load determined by such methods as discussed in the previous section and shall be the maximum load expected to occur during craft service. The factor of safety (F.S.) is an agreed-upon factor between builder and regulatory board to provide sufficient safety margin over the limit load to provide the design load. The design load is then that load used to design the structure, and there are, for static load analysis, two loads of interest: the yield load and the ultimate load, representing loads to maximum allowable distortion and loads to failure. Typical values of the factors of safety applied in air cushion craft design are given in Table 8.

TABLE 8 - TYPICAL FACTORS OF SAFETY

Load Condition	Factors of Safety	
	Yield	Ultimate
On-Cushion Hullborne Ground Impact	1.0-1.5	1.5-2.0
Emergency	1.0	1.5
Crash	---	1.0
Towing, Hoisting, Jacking	1.5-2.0	2.0-3.0

As can be seen from Table 8 there is quite a variation in the allowable factors of safety. For the British craft, the BHSR¹¹³ used the factors of 1.0 and 1.5, respectively, for the yield and ultimate on-cushion loads, whereas typically the U.S. craft use 1.15 and 1.5, respectively, for the same cases. Two exceptions to this were the SES-100A and SES-100B, which

were the first high-speed sidehull craft designed and built in the world. Because they were the first and there existed no criteria for such craft, the ultimate load factor of safety was raised to 2.0. The Amphibious Assault air cushion craft, however, have used the ultimate load safety factor of 1.5.

The one area where the BHSR criteria are more conservative than the U.S. criteria is in the hoisting and jacking factors (3.0 compared to 2.0), but this has only a small influence on structural weight.

Clearly, there are many other loading cases such as torsional modes, vibratory loads, and structural fatigue among others, but it is left to more detailed papers on structural design to discuss these (for example, see Reference 57). It is the purpose here to indicate trends and overall influence on the structural design and the weight of the structure. Before discussing the different designs, materials, and fabrication techniques, it is good to review the structural weight fraction.

Structural Weight Fraction

The structural weight of air cushion craft, as displayed in Figure 148, has had various predictions made for it that vary from optimistic values approaching that of cargo ships to conservative values that would challenge its economic viability.

In 1968, Stanton-Jones²⁹ cautiously showed the structural weight trends with craft size going both ways, but he expects values approaching 33 percent for large tonnage to appear reasonable. On the other hand, numerous detailed analyses in the U.S. would predict values approaching 25 percent at large tonnage. There are several important factors that enter the discussion to resolve these differences. The apparent paradox is between a low structural weight fraction with conservative design criteria (see previous section) and a high structural weight prediction with more optimistic design criteria. These differences include, in the case of some U.S. craft, use of sophisticated structures and composite materials and also the basic difference due to craft density reflected by the cushion density (p_c/L or $p_c/S^{1/2}$).

There are, of course, well documented and understood methods of structural analysis that can be applied to an air cushion craft structure, once given a set of loads. Each designer usually has, at his disposal, digital computer mathematical models representing every load-carrying member and using such techniques as finite element methods can determine detail loads, size, and weights. In this manner, for a particular design, the structural weight can be determined. Figure 154 shows some examples of such structural element models typically used for designing the structure.

These particular examples have been used quite successfully in designing both hard structure and flexible structure or skirts. The shaded areas on the skirt structural model in Figure 154, for example, indicate where compressive loads would occur which, of course, would wrinkle the fabric. A minor adjustment in geometry removed the wrinkles and the design was

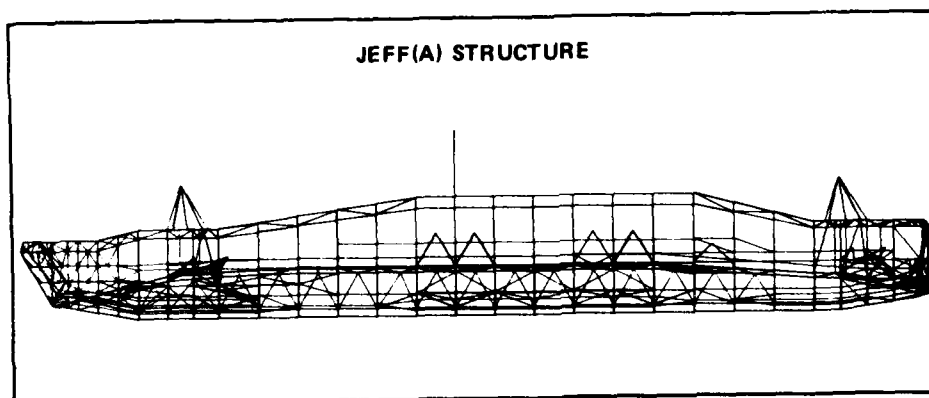
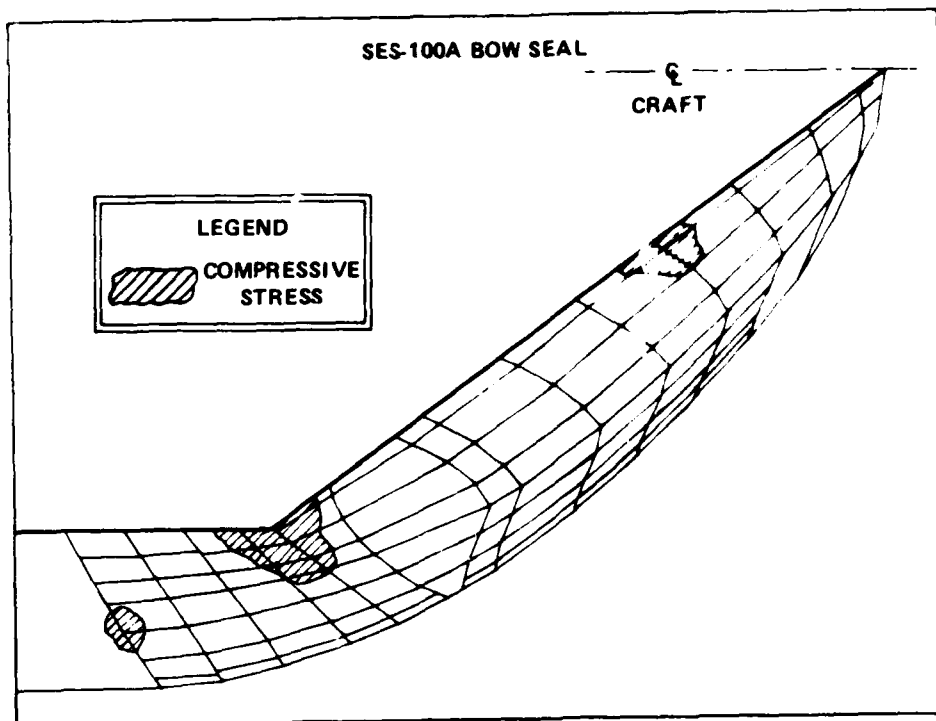
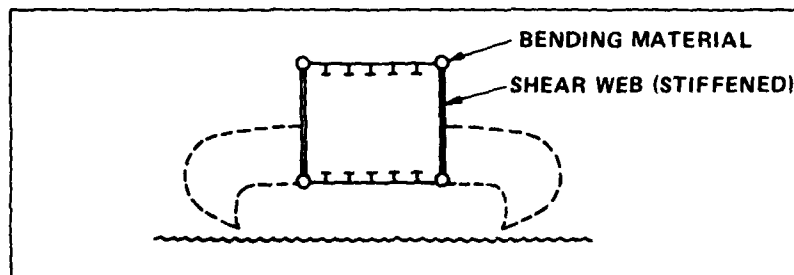


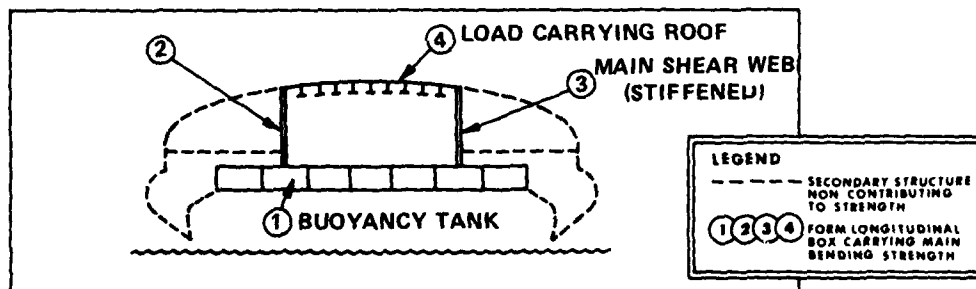
Figure 154 - Typical Structural Models

finalized. Similar adjustments can be made in the hard structure models to remove excessive localized loads, and the structural members can be sized accordingly. Once an acceptable structure has been achieved, weight equations for the type of construction used are applied and the entire structural weight can be determined. However, the use of such techniques in the detailed design process of a given craft is expensive and time consuming. For both preliminary design purposes and for aiding the isolation of key parameters, simpler methods are required.

One such method postulated by the author,¹⁰⁹ considers the air cushion craft structure to be an idealized box acted upon by shears, end loads, and bending moments. Such an idealized box might be as shown in the upper sketch of Figure 155. This idealized structure, although greatly simplified, is representative of closed structures existing on operational craft today. For example, the SR.N4³⁸ main bending strength comes from a longitudinal box formed by the buoyancy tank as its bottom member, two longitudinal deep beam shear webs, and the center portion of the roof. Passenger decks and outer skins are secondary structures. This arrangement is shown for comparison with the idealized structure in the lower sketch of Figure 155.



(a) Idealized Structure



(b) Actual Structure (SR.N4)

Figure 155 - Idealized Structural Model

Similar deep beam construction applies to the SR.N5 and SR.N6 series of craft. The applicability to open structures like the JEFF craft or sidehull craft (see Figures 18 and 19) is not known. What is sought is an expression that would indicate trends with an accuracy somewhere between the statistical relationships given by Figure 148 and a completely detailed structural analysis of the type discussed earlier.

In agreement with the SR.N series of craft, for example, the main bending is taken by two deep beams running fore and aft on either side of the craft centerline. The torsional box is completed in this idealized box by two webs at top and bottom. The dimensions of this idealized structure are L, H, and B, which can be thought of as effective values of the actual length (L), beam (B), and structural depth (H) of an actual craft.

By then imposing on this structure the shears, axial loads, and bending moments due to loads nW , it was found possible¹⁰⁹ to derive the following simplified form of the structural weight fraction

$$\frac{W_1}{W} = \frac{F(t, E, \dots)}{p_c} + \frac{n}{\sigma} G(L/B, H/L, \dots) W^{1/3} \quad (169)$$

In this form, it is seen that the structural weight fraction (W_1/W) comprises two basic elements. The first term reflects the contribution to the weight due to the area of the craft structure, while the second term is determined by the loading conditions and stress levels in the structure.

The first term, determined by $F(t, E, \dots)$, includes the local properties of the panels and stiffeners and reflects the buckling criteria effect on type of construction and minimum gage thickness for structural members.

The second term, governed by the geometric function $G(L/B; H/L, \dots)$, reflects some of the overall sizing or geometric effects on the design; deeper beams with higher H/L are more efficient than narrower beams, within limits. This term also reflects the load factor (n) discussed earlier in connection with the design criteria, and the average stress level (σ) in the structure.

The form of Equation (169) indicates avenues for improved structural weight fraction other than a forcing of low values by making the ship more dense. As has been discussed in the chapters on performance and stability and ride control (Chapters III and IV), increasing craft cushion density ($p_c/S^{1/2}$) can have adverse effects on hydrodynamic resistance, fan power, and stability characteristics. As an indication of possible trends in structural weight, the functional form of Equation (169) was fit to the available craft of low cushion density and found to have the form,

$$\frac{W_1}{W} = \frac{0.25}{W^{1/3}} + \frac{0.04}{[p_c/S^{1/2}]^{1/3}} \cdot W^{1/3} \quad (170)$$

where W is measured in tonnes. This is shown in Figure 156. This curve fit shows some of the basic trends for craft with cushion densities around

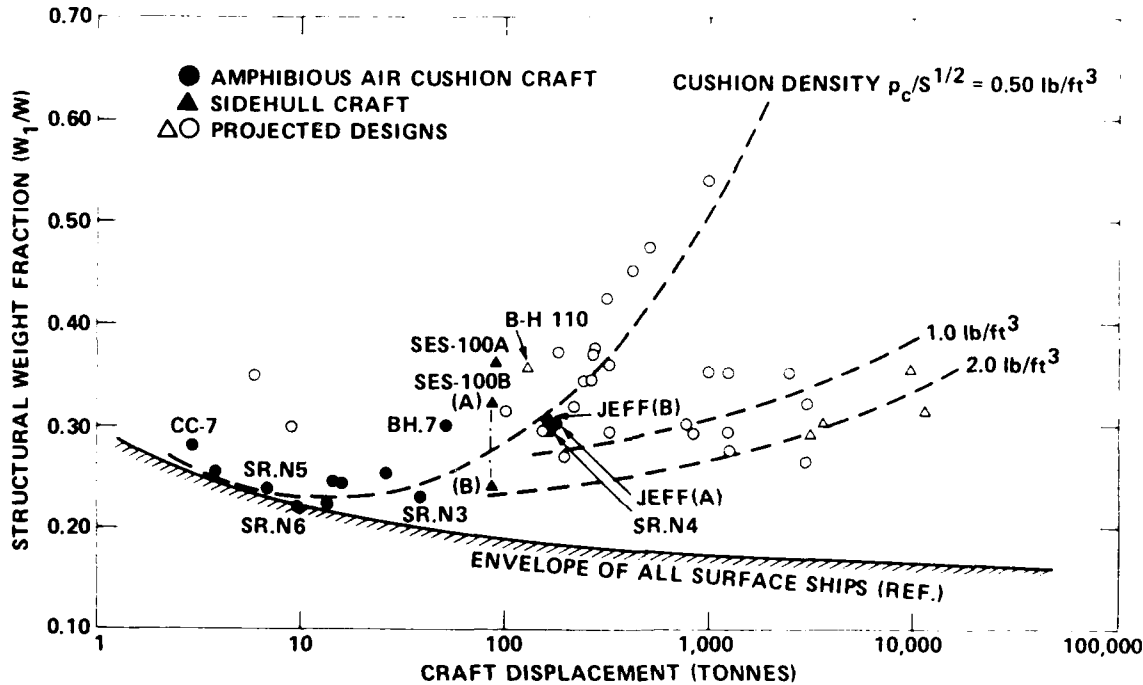


Figure 156 - Structural Weight Fraction

$p_c/S^{1/2} = 0.50 \text{ lb/ft}^3$. The projected designs (taken from some proprietary work) are for craft with cushion densities in the range $0.40\text{--}0.50 \text{ lb/ft}^3$. For higher cushion densities ($p_c/S^{1/2} = 1.0\text{--}2.0 \text{ lb/ft}^3$) the trends do not follow, as closely, the relationship given by Equation (170); many other factors are also influencing the structural weight. These factors include the speed of the craft (as discussed earlier); the number of decks in the craft, which is especially important in the larger displacement designs (5,000–10,000 tonnes); and whether or not the craft is amphibious or sidehull. This latter point is roughly indicated by the SES-100B points

labelled (A) and (B) in Figure 156. The point (A) is for the SES-100B structural weight fraction as built ($W_1/W = 0.33$) and the point (B) is for the SES-100B with the catamaran hull structure below the wet deck removed, i.e., approaching the idealized box of the amphibious air cushion craft. The projected designs, shown in Figure 156 around the high cushion density lines, are taken from Reference 30 and represent air cushion craft designs with design speeds that vary from 50 to 120 knots and with single to multi-deck structures. All designs use high grade, welded aluminum structure with load factors similar to those given in Table 8. Insufficient data are available at this time to isolate the effect of speed, to account for the number of decks, or to adequately remove the scatter. The trends are clear, however, that considerable increases in cushion density are required, coupled with reduced speeds if structural weight fractions below 30-35 percent are to be achieved.

It will be noticed from Figure 156 and Equations (169) and (170) that it is the term including load factors and average stress levels that is contributing to the slow growth in structural weight fraction and that only pushing to higher cushion pressures (that is, making the ship more compact) is causing the weight to decrease. Also, the structural weight fractions of the SES-100A and the SES-100B do not fit the trend line, in that expected gains due to designing to twice the cushion density of the SR.N4 did not significantly change the structural weight fraction. There are several factors contributing to this. Both craft were designed to the more conservative design criteria in terms of wave impact loads and pressures and in terms of applied safety factors. It must also be remembered that all criteria discussed to date and the simplified weight fraction formula apply to the amphibious form of craft. The relative structural efficiency of including sidehulls has not been discussed. The differences in construction have also influenced the difference between the SES-100A at 31 percent and the SES-100B at 33 percent structural weight fraction. These differences, involving choice of materials, craft shape, and fabrication methods, are discussed in the next section.

It is clear that insufficient data are available to draw firm conclusions at this stage of air cushion craft development, and advances in structural design are underway in several programs to improve this situation.

Effort is now being expended in the U.S. Navy, the most active in large ship design, to pursue improved structures for advanced marine vehicles in general. Allen and Aronne¹²⁰ examined structural weight trends of both hydrofoil and air cushion craft and suggested that increasing the structural density (by decreasing the enclosed volume of the working structure) is a major contributor to reducing structural weight. Figure 157 shows this effect by simply plotting the craft density (W/V_s) for a range of structural densities (W_s/V_s). In this presentation, V_s is the enclosed volume of the working or primary structure. Both hydrofoil craft

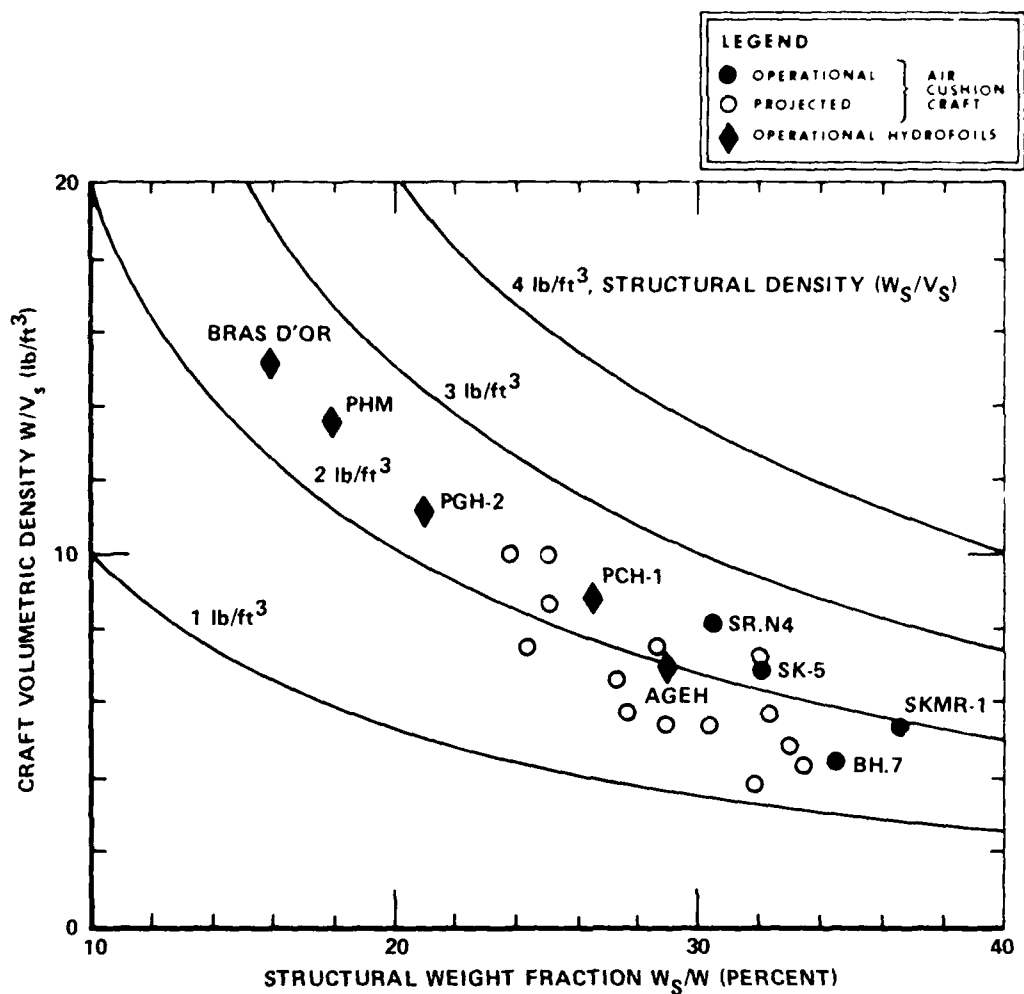


Figure 157 - Effect of Density on Structural Weight

and air cushion craft have been included in Figure 157 to emphasize the strong effect of dense structural volume. These data have been compiled from the paper given by Heller and Clark¹²¹ who have explored the trends in structural weight based on, in their words, reliable documented data. This is important in that, during design stages, usually optimistic values of structural weight are given, and it is not until the construction stage gets underway that the structural weight fraction takes on a reliable value.

In Figure 157, which admittedly includes some projected designs, with the actual hardware craft shown in solid symbols, it is seen that increasing

craft densities from 1.50 to 2.5 lb/ft³ has a significant effect on reducing structural weight fraction, although the cautionary note on the effect of speed and the number of decks should be repeated here.

It appears that there is no major breakthrough on the horizon that will significantly reduce structural weight. It will be the gradual development of a combination of design elements that will bring the structural weight down. Improvement of our knowledge of loads acting on the craft may allow the "n" factor, previously discussed, to be reduced. Use of higher strength-to-weight ratio materials will also improve the situation, as will the use of more efficient structural methods. The average stress level (σ) can be kept high to approximate Oliver Wendell Holmes' "one-hoss shay." Again, the challenge to the air cushion craft designer is to do this without increasing the complexity and cost of the structure. Some recent construction that appears to be accomplishing this will be described in the following sections.

CURRENT CONSTRUCTION

The technical literature is sufficiently complete with the listings of properties of materials used in air cushion craft construction that it would be superfluous to include them here. There are, however, a few comments pertinent to the development of air cushion craft relative to materials. In one respect, it is fortunate that the need to develop high strength, low weight materials that can withstand the severe environmental conditions in marine use is not unique to air cushion craft. Hydrofoils, and to a lesser extent, high speed planing craft have a similar need. This broad base application of structural materials to a common need has enormously aided material development through the increased interest of material suppliers and government agencies. This situation is different to that for skirt materials, where the development has been slow due to the exclusive use by air cushion craft--a small market to material suppliers who are naturally more prone to developing flexible materials for automobile tires. In fact, in the case of skirt materials (see Chapter VI), the history has been one of selecting materials being developed by the material suppliers for automobile use and then testing to see if they have application to air cushion craft operating in a marine environment. In some cases, the results have been rather startling. To illustrate the point, in the search for long life skirt materials, the new core material, the aromatic organic fiber "Kevlar," which appears to have tremendous potential for automobile tire use,¹²² pulverized under fatigue testing for air cushion craft use. Accordingly, the air cushion designer must return to the nylon-based fabric materials to meet his needs.

In returning to the hard structure material, the development of different alloys and tempers of the aluminum and steel materials has provided a broad selection of materials for air cushion craft use. To a lesser extent, but sufficiently broad in selection, are the titanium alloys and glass-reinforced plastics. In the discussion that follows, the main emphasis will be directed toward the current high cushion pressure, high

speed U.S. craft that have been designed to meet common performance specifications. In this way, some of the problems discussed relative to different design criteria can be eliminated. The design philosophy and construction used in some of the British craft will be referred to for illustration. Again, in a discussion such as this, only highlights can be covered, and the reader is referred to the literature for more detailed discussion. Discussions on material and structural methods for the British craft may be found in Reference 39, for example, with a more detailed discussion on the SR.N4 construction in Reference 58. Details of the types of construction for the Bell series of craft may be found in Reference 123.

Because the first air cushion craft was designed and built by a British aircraft and flying boat manufacturer, it is not surprising that similar materials were used in both applications. It was standard practice to employ the high strength, copper-based aluminum alloys and to use protective coatings such as Alclad and sealants for the riveted attachments to protect against the marine environment. It was reasoned that, provided the craft did not spend long periods of time sitting in the water and always settled on land after a mission, corrosion problems would not occur. Using the U.S. terminology, this meant extensive use of the 2000 series and high strength 7000 series (zinc-based) aluminum alloys. When in 1965, the first U.S. equivalent of the SR.N5 was constructed, namely the SK-5, extensive use was made of 2024-T3 in the buoyancy tank, rudders, cowlings, cabin, and other parts of the structure.

For marine application, however, such as envisaged for the U.S. Navy craft, such alloys were found not suitable and attention turned to the nonheat-treatable 5000 series and heat-treatable 6000 series of aluminum alloy. Both alloys are not of such high strength as, for example, the 7000 series but are considerably improved in their performance in a marine environment. Both the 2000 series and the 7000 series were found to be highly susceptible to stress corrosion and of low fatigue strength in a saltwater environment.

Prior to 1969, the U.S. Navy had had considerable experience with the use of aluminum alloys in boat construction and began to draw up guidelines and specifications relative to the use of the different alloys. This experience particularly covered the 5083, 5086, and 5456 designations of the nonheat-treatable alloy and 6061 of the heat-treatable alloy. The three 5000 series alloys were found to be of the highest strength and the lowest corrosion rates when exposed to saltwater application. In some applications, the 6061 alloy was found to be more susceptible to stress-corrosion in the welded condition than the 5083, 5086, or 5456 alloys. Because of this and its low ductility in the welded condition, it was generally used in nonwelded applications and preferably above the waterline. The SKMR-1, constructed in 1963 for BuShips, used 6061-T6 (solution treated, artificially aged) for the primary structure, which used welding along the lower hull surfaces and rivetting at all bulkhead locations. The bow structure for SKMR-1 used the 5083 alloy.

As the corrosion characteristics of the 5000 series improved, the 5086 and 5456 alloys became more prevalent in U.S. Navy craft including hydrofoils and planing craft, and operational experience began to accumulate. The bulk of this experience covered the 5086 in the -H343, -H116, and -H34 tempers. The 5456 alloys proved to have the highest strength of the 5000 series alloys in the welded condition and was used in the primary structure of hydrofoils such as the HS Denison (5456-H321 plate and -H311 extrusions) in 1962, the Fresh I (5456 below the waterline) in 1964, and the AG(EH) (all primary structure 5456). It was also used on planing craft in Vietnam in 1967 where, with the -H321 temper, it was found to develop a form of corrosion called exfoliation that was due to a particular combination of water, dirt, and temperature. The exfoliation took the form of a separation of the basic material and the magnesium alloy. Similar exfoliation was found to occur in the bilges of the hydrofoils that use 5456-H321. The development of a new temper -H116 or -H117, depending on material supplier, cured the problem.

This experience then resulted in the following alloys appearing in U.S. Navy craft and, specifically, in air cushion craft developed for U.S. Navy use:

1. Primary Structure (Welded)
5086-H32, -H34
5456-H117
2. Secondary Structure (Rivetted)
6061-T6

In the above list, only those tempers used for sheet stock (thickness less than 0.1 in.) have been listed. Other temper designations exist for the compatible versions of plate, extrusions, castings, and forgings. It is of interest to note that the Voyageur and Viking craft hulls, not built to U.S. Navy specifications, use 6061-T6 welded primary structure.

In 1969, the U.S. Navy issued instructions¹²⁴ for the maintenance and repair of aluminum hulls using these alloys and tempers. These instructions allowed for construction with either 5086 or 5456 but with the improved tempers, and relegated 6061 to nonwelded structure above the waterline.

In 1969, the SES-100A and SES-100B programs got underway, and two design philosophies were followed. The SES-100A used the more conventional 5086 alloy for the primary structure and relied on hull shaping and considerable use of fiberglass on the weather deck and cabin to keep the structural weight fraction down. The SES-100B, on the other hand, used the higher strength-to-weight ratio alloy 5456-H117 and used a simpler structural design, allowing the heavier structural design concept to be offset by the higher strength material.

Figure 158 shows the structural arrangement of the SES-100A taken at the Tocomo Boat Building Company yard in Washington during construction in 1971. The primary hull structure is an all-welded hull of 5086-H32 aluminum alloy with 5356 filler rod. The plate thickness varies from



Figure 158 - SES-100A Construction

one-half inch at the bow to three-sixteenths inch at the thinnest gages on the aft weatherdeck. As can be seen from the top photograph in Figure 158, considerable shaping and curvature to the structure has been used to minimize aerodynamic and hydrodynamic resistance.* Large portions of the weather deck, as seen in the photograph, are fiberglass panels mechanically attached to the primary structure. The cabin is also mechanically attached and is half-buried in the primary structure, again to reduce aerodynamic drag.

The lower photographs in Figure 158 indicate the form of construction in the high deadrise sidehulls and in the main centerbody. The longitudinal stiffeners are continuous with cutouts at the bulkheads with filler plates. Typical spacing of the stiffeners is 12 in. welded by semiautomatic GMA welding. By controlled fabrication and welding sequencing, very little distortion appeared on the hull.

The overall dimensions of the SES-100A are 81 ft, 11 in. LOA, 41 ft, 11 in. beam, and 17 ft from keel to weatherdeck with a 6-ft deep cushion. The weight of the complete structure at launch on 1 September 1971 was 75,746 lb or 31 percent of the gross displacement.

Because of the design high speed of the SES (80 knots), concern was expressed in 1969 as to the ability of aluminum to withstand cavitation erosion. Studies by the aluminum companies and cavitation erosion tests conducted on high speed rotating water wheels at Chance Vought and at the Naval Applied Science Laboratory showed severe degradation at high speeds. Experience on hydrofoils operating for prolonged periods at high speeds had also shown severe pitting in crevices and on surfaces prone to low pressure from the hydrodynamic flow. The aluminum is particularly prone to cavitation damage, due to the high speed flow constantly washing away the natural protective oxide layer of aluminum and thus accelerating the erosion. Consideration was given to the use of titanium "shoes" to the sidehulls because of titanium's particularly good cavitation erosion resistance, but it was finally decided to apply Tasset, the protective paint coating, to the entire underhull and sidehull. This coating was found to be highly successful. It prevented biofouling and left no evidence of cavitation erosion after the completion of the test programs.

Figure 159 shows the general construction features of the SES-100B during its hull fabrication at Livingston Shipyards in Texas during construction in 1971. The primary hull structure is also an all-welded hull, but of 5456-H117 plate welded with 5556 filler rod. As for the SES-100A, it was a full root penetration weld, continuously welded throughout (except in some localized, specified areas). The plates are staggered, and stringer welding is so arranged that a continuous weld around the area of maximum bending moment did not occur. Maximum use of constant and straight sections was made for ease of fabrication and, as can be seen in the upper right photograph, no double curvature shaping was used. In the forward port and starboard weatherdeck corners can be seen the "orange peel" plate welds used to avoid double curvature.

*Note again that this is the original SES-100A prior to its bow modification to accommodate its new planing seal (see Chapter IV).

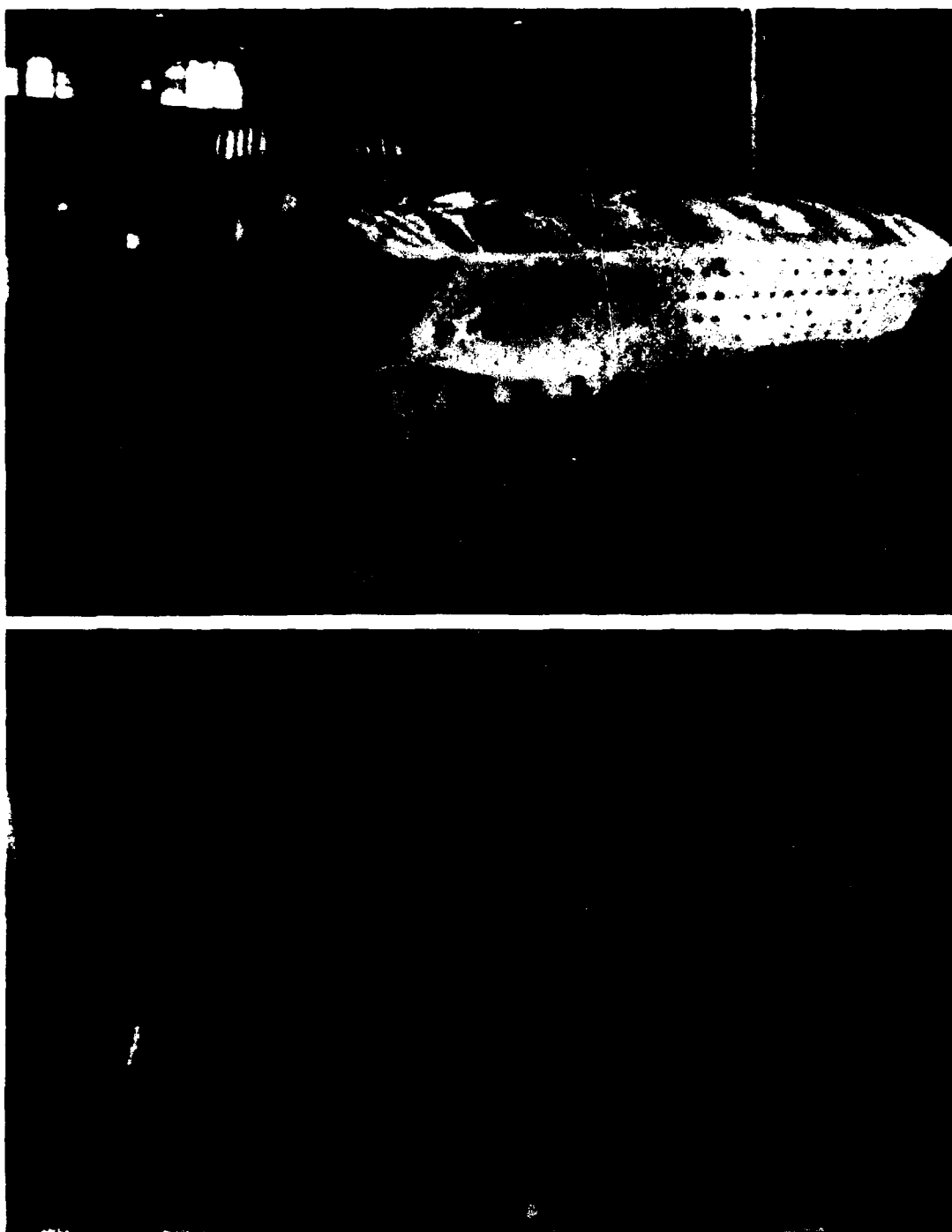


Figure 159 - SES-100B Construction

The SES-100B was GMA spray-welded, except for some fitting areas, with stringers on 12-in. spacings. To provide continuous longitudinal stiffeners without large cutouts at the bulkheads, the caps were allowed to be continuous with the webs stopped at the bulkhead. The "colander" bow effect for bow bag pressure alleviation discussed in the section on design criteria can be seen in the upper photograph of Figure 159.

To avoid direct cavitation erosion on the aluminum hull and also to provide the biofouling action so prevalent in the southern waters of the Louisiana test area, a Glidden paint system was applied. Because this vinyl-based paint system requires four coats of primer, a technique explored on this hull was to have each coat a different color such that any cavitation erosion could be detected by color photography. In the test program completed in 1973, only minor indications of cavitation erosion were found.

Because neither the SES-100A nor SES-100B had significant amounts of operating time at speeds in excess of 75 knots, it cannot be concluded that a more complex form of protection of the aluminum hull would not be required for U.S. Navy ships designed for prolonged cruise at high speeds. The stability appendages (actual form is classified) were fabricated from titanium alloy as were the propeller blades. The propeller housing mechanically attached to the aluminum hull was of 17-4PH steel.

After initial tests during which galvanic corrosion had occurred, the use of a combination of attached zinc anodes to the transom and passive anodes hooked up when dockside provided the desired protection.

The hull of the SES-100B is 77 ft, 8.50 in. long and 35 ft wide and has a height from keel to weather deck of 13 ft including a 6-ft cushion depth. The deckhouse, also constructed from 5456 aluminum alloy, is welded directly to the weather deck. Epoxy-based fiberglass was used for small assemblies such as fan intake ducts and minor parts.

At launch on 22 July 1971 for hover tests, the SES-100B structure weighed 69,300 lb or 33 percent of the gross displacement.

In an effort to achieve lower structural weights than those achieved on the SES program, and hopefully below 30 percent, more sophisticated designs were pursued for the JEFF craft program. Techniques of structural design optimization are fairly well known and are usually the result of optimizing structural modules to be efficient in terms of providing maximum bending moment, shears, or axial loads for minimum weight. The structure can be optimized for single loads or, in the more usual case, for combined loads. Figure 160 illustrates typical results of such structural optimization, where structural indices of bending efficiency and column efficiency of different types of construction and material are compared.

In Figure 160 (upper curves), the beam weight index is given by $w\bar{t}/\sqrt{m}$, where w is the material density, t is the section cross-sectional area per inch width, and m is the applied bending moment per inch width. This weight index is computed for various values of the beam bending structural index

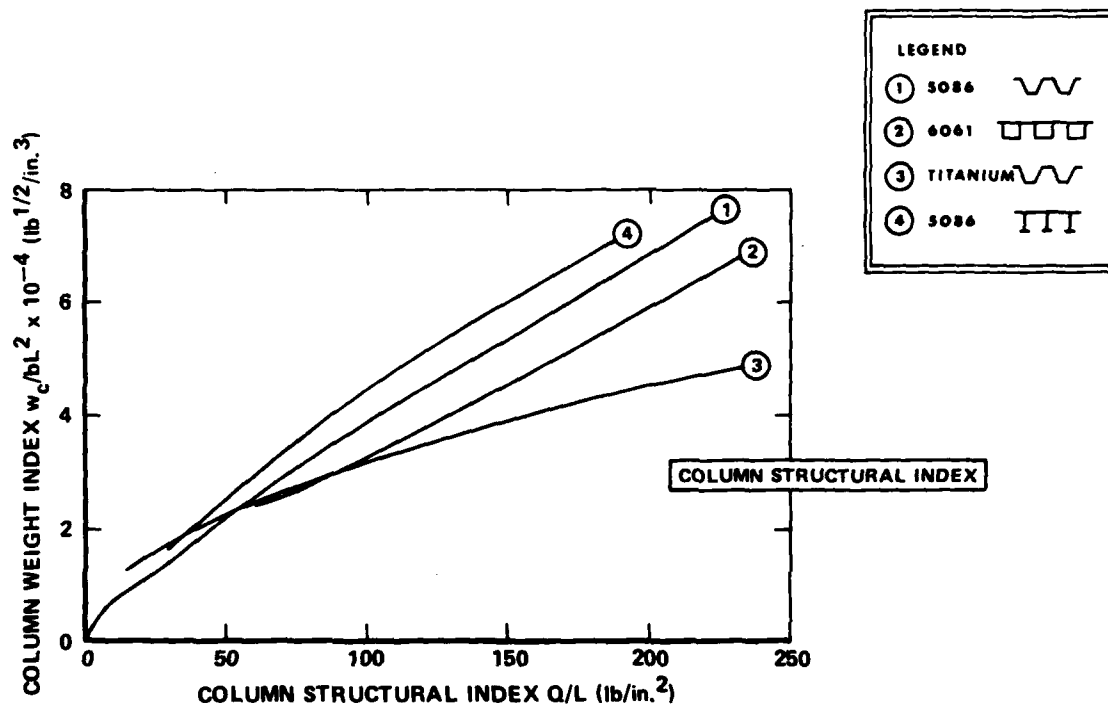
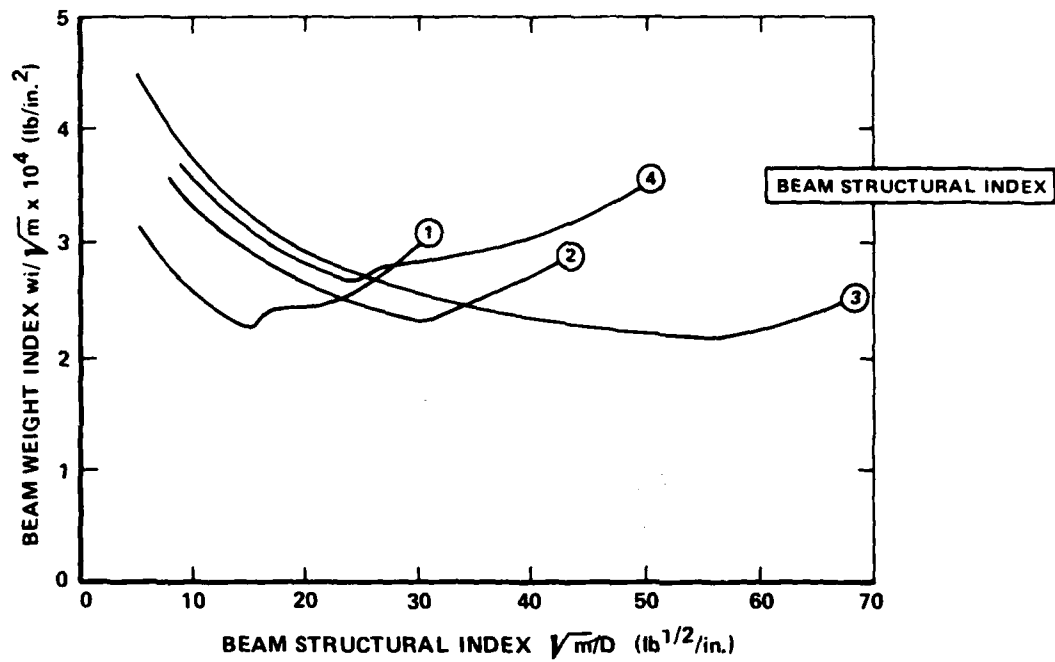


Figure 160 - Typical Structural Index Comparison

$\sqrt{m/D}$, where D is depth of bending material (stiffener or corrugation), and for different materials. From such computations, it can be seen that small variations in the applied bending moment or beam structural index can strongly influence the choice of optimum structure.

For the column efficiency, Figure 160 (lower curves) shows typical variations of the effective column weight index W_c/bL^2 , where W_c is the weight of the column of width b and length L, as a function of the axial load index Q/L, where Q is the axial load per inch width. Again, it is seen for the same selected configurations shown in Figure 160 (upper curves) that choice of configuration to minimize weight must be a careful one. Structural optimization was used for the JEFF craft, including such parametric variations as shown in Figure 160 and, considering the many other structural criteria such as buckling and torsional modes and construction criteria such as material cost and ease of fabrication.

Figure 161 shows the final form of the selected configuration for the JEFF(A). This particular view shows the structure taken at an early stage of construction in 1974 at Todd Shipyards in Seattle, Washington, which reveals the use of the all-welded 5086-H117 corrugated sheet as the main structural element. The top photograph gives a general view showing the corrugated hull bottom plating (0.16 in.) with 3-in. corrugations. The corrugated sheets are fabricated from preformed sheets and semiautomatically welded on approximately 18-in. widths to form the basic sheets. The transverse frames are on 4-ft spacings and are of tubular construction, as seen in the lower photograph.

A view of the finished structure of the JEFF(A) taken at the Aerojet facilities in Tacoma, Washington upon delivery from Todd Shipyards on 9 November 1976 is shown in Figure 162. As shown, the JEFF(A) structure weighed 103,296 lb or 30 percent of the gross weight.

A different optimization result was employed in the JEFF(B) shown in Figure 163. In this case, the "top-hat" stiffened structural form in all-welded 5086-H117 was used for the main structural raft and rivetted 6061-T6 was used for the superstructure. This optimization allowed the best structural design while meeting U.S. Navy requirements not to have welded 6061-T6 in primary structure. The top part of Figure 163 shows a typical transverse section through the structure, showing the several types of structural form used. The outer skins are 0.10-in.-thick welded 5086 sheet with top-hat stiffeners approximately 1.75 in. deep on 8.14-in. centers. The transverse bulkheads are fabricated from 5086 extended tee-stiffened panels 0.125 inch thick. The tee-stiffeners are, again, on 8.14-in. centers with the bulkheads spaced approximately on 4-ft. centers. The main raft structure is welded up to the cargo deck, where extended 6061 panels of a truss sandwich form are mechanically attached. The use of balsa core sandwich can also be seen in Figure 163. The lower part of Figure 163 shows an early stage of construction in the Michoud Assembly Facility, New Orleans, in 1974.



Figure 161 - JEFF(A) Hull Construction



Figure 162 - Finished Structure of JEFF(A)

A view of the finished structure of the JEFF(B) upon roll-out at Michoud on 30 March 1977 is shown on Figure 164. At roll-out the JEFF(B) structure weighed 103,687 lb or 31 percent of the gross weight.

The degree of sophistication of the structure used in the JEFF craft is an indication of the difficulties of achieving low structural weight fractions without resorting to nonstandard marine construction practice. In the size range of craft constructed to date (less than 200 tons displacement), the design calls for extensive use of thin gage material. For the craft discussed, the thinnest sheet is 0.10 in. thick, which incurs problems of quality control if it is to be welded. Aluminum does not permit as much deviation from fabrication specifications as does steel; thus, much closer control is required to ensure adequate welds. This is especially important in the thinner gages (like 0.10 in.) where the danger of burn-through is always present. The strength, fatigue life, corrosion resistance, and ductility of aluminum welds are very dependent upon having clean, sound welds (low porosity), and limitations must be placed on the

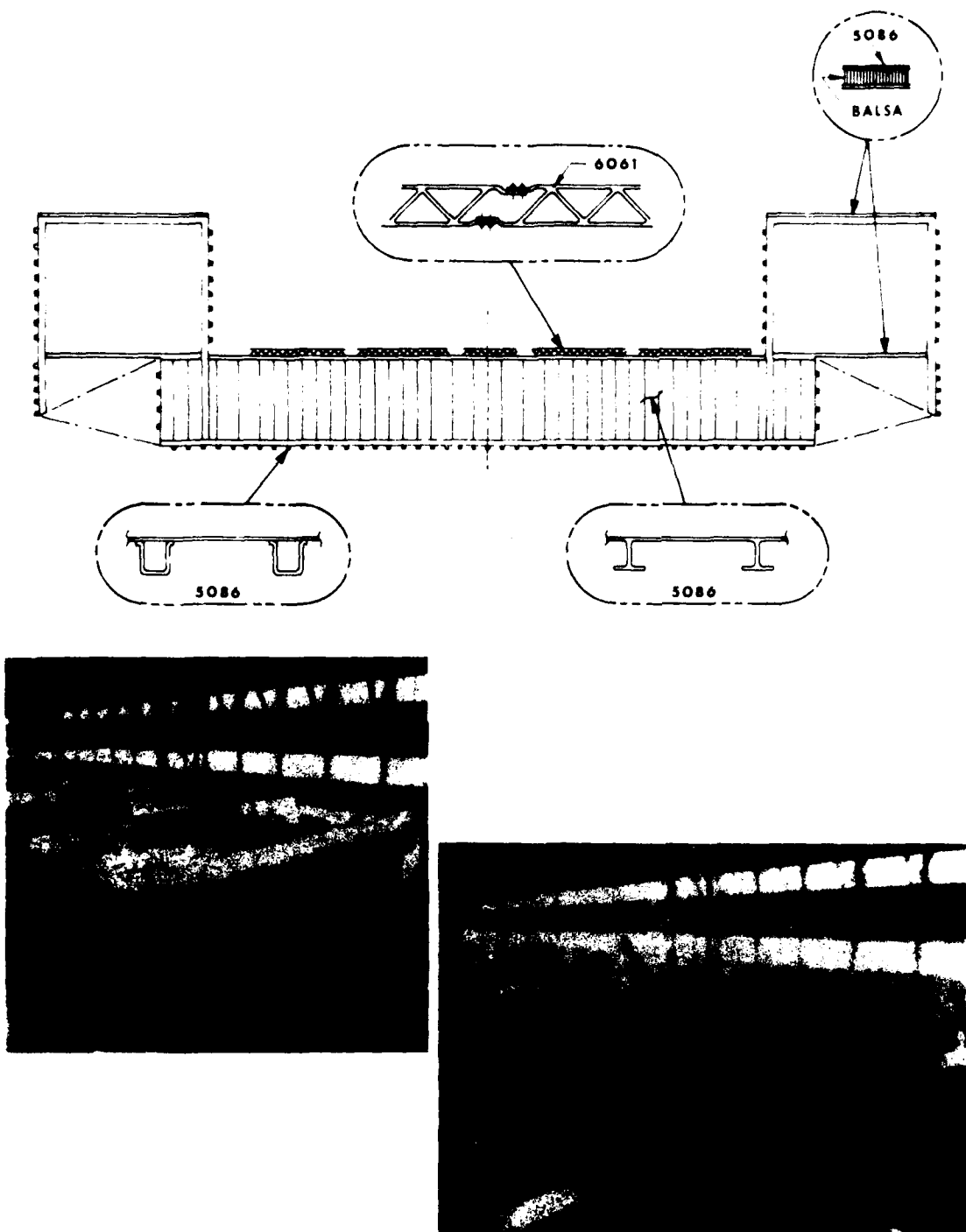


Figure 163 - JEFF(B) Hull Construction

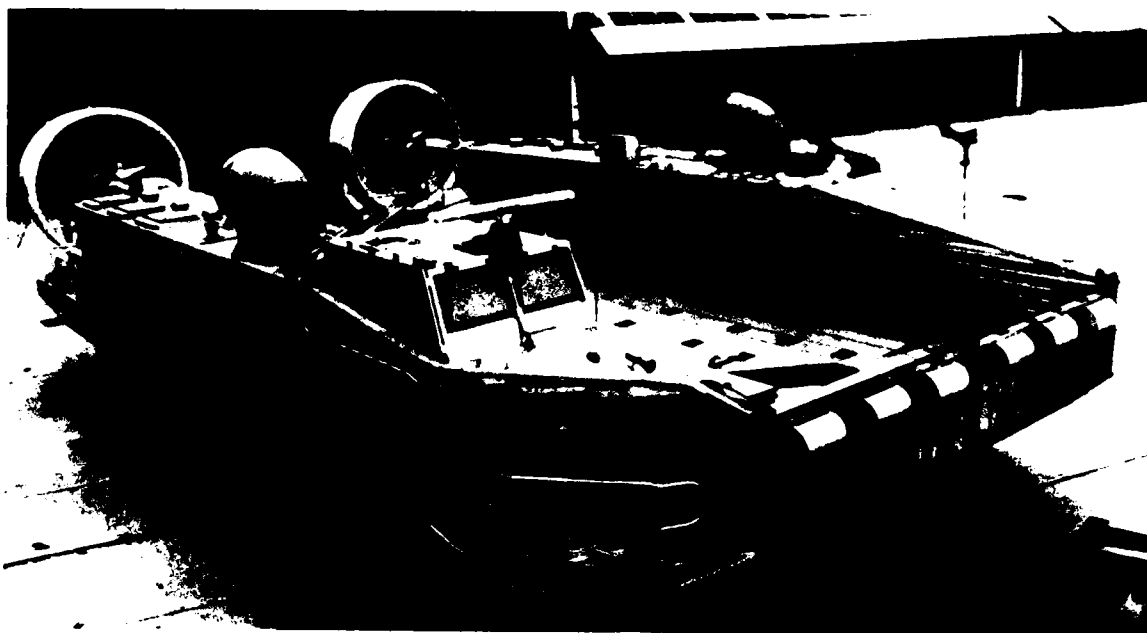


Figure 164 - Finished Structure of JEFF(B)

environmental conditions in the welding area to preclude contamination from other metals, from hydrogen in moisture-laden air, from air by disruptions in the gas shielding process, and from too rapid chilling of the weld by restricting the minimum ambient temperature.

Thus, it can be seen that the requirements for low structural weight coupled with the requirements of watertight integrity through welding have contributed greatly to the complexities and cost of such air cushion craft. As stated earlier, a typical air cushion craft aluminum structure costs, approximately, \$20-\$25 per pound. Many of the problems of welding such structure diminish as the craft size increases into the multithousand-ton range, gage thickness increases, accessibility through larger stringer and frame spacings increases, and quality control becomes easier to maintain.

In any event, however, it has been found necessary on all craft, to date, to run expensive development and training programs, to learn correct fabrication techniques, and to control distortion and strength of the structure. This is an industry-wide problem common to any lightweight aluminum hull construction or planing craft, hydrofoil, and air cushion craft. Most companies involved in such construction are at the start of their learning curve today.

Recognition of the high costs associated with meeting these stringent weight requirements has prompted many groups to investigate lower cost structure at some acceptable (and probable) increase in structural weight.

One particular recent venture, worthy of note in this regard, is the patrol boat built by the newly formed Bell-Halter Company in New Orleans.¹²⁵ This company is a joint venture between Bell Aerospace Co. (builder of the SES-100B and JEFF(B)) and Halter Marine Services, Inc., a major builder of offshore supply vessels. This patrol boat, known as the Bell-Halter (B-H) 110, is shown in Figure 165. This 110 ft long boat which began construction

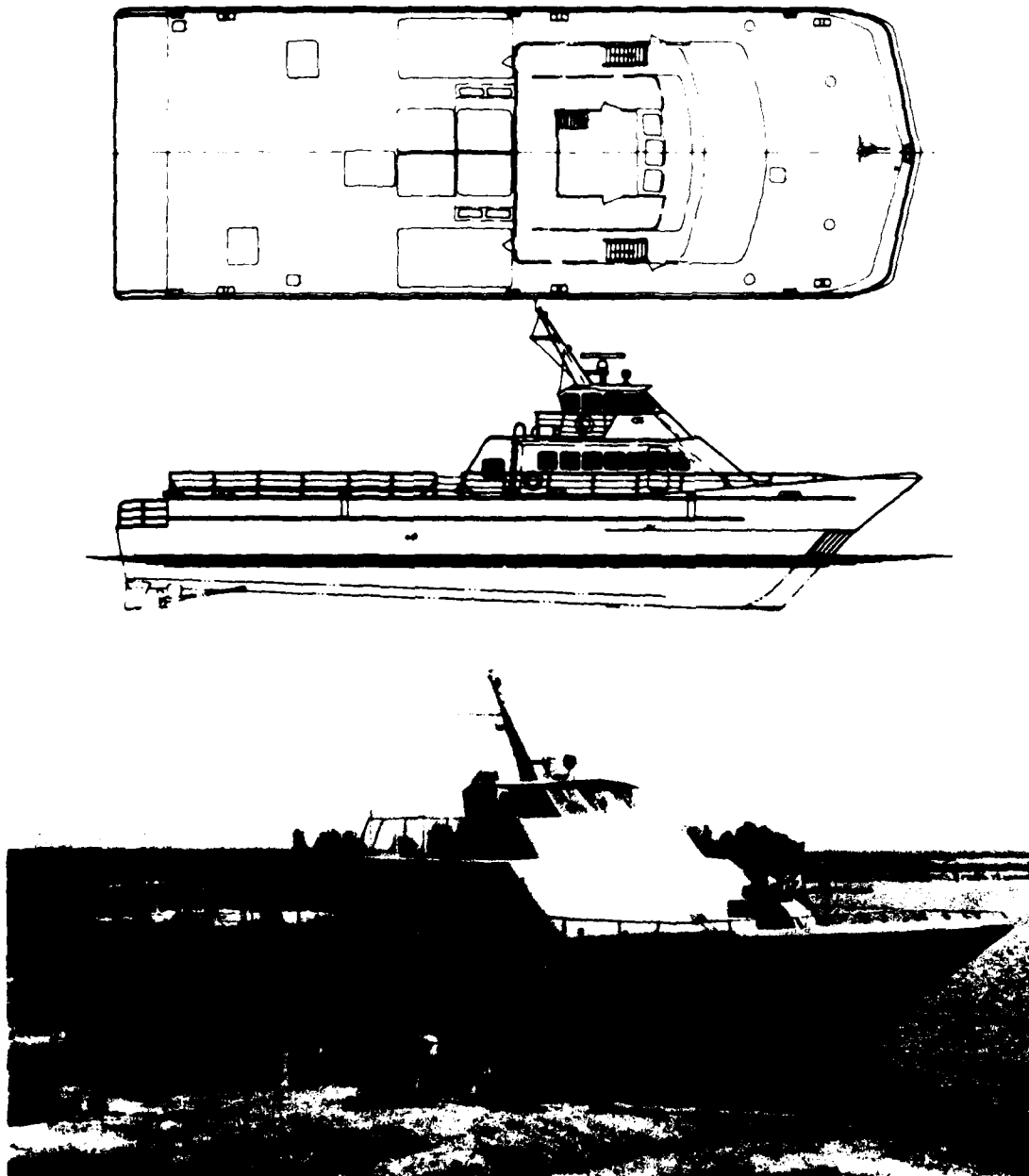


Figure 165 - Bell-Halter 110

in November 1977 and made its first underway run on 20 December 1978 is based on existing and fully proven SES technology (with no new technological improvements). The hull was constructed in accordance with standard marine aluminum boat practice and was capable of being constructed by a typical and conventional displacement boat manufacturing organization. The hull was fabricated using conventional welded 5086 H 111 aluminum construction and the deckhouse and nonstructural bulkheads are of welded 6061 aluminum construction. The B-H 110 is a high performance, air cushion assisted craft with demonstrated speeds of 40 knots in calm water and 33 knots in a State 3 sea using two 16V149TI Detroit Diesel marine engines (rated at 1335 hp each) driving two 42 in. diameter subcavitating fixed-pitch propellers. Lift is provided by two 8V92TI Detroit Diesel marine engines driving two commercially available Sheldon DWDI 490 Class IV 40.2 in. diameter centrifugal fans. The gross weight of the craft is 107 long tons and the structural weight is 36 percent. A unique feature of the B-H 110 is the large off-cushion displacement of the sidehulls as shown in Figure 166.

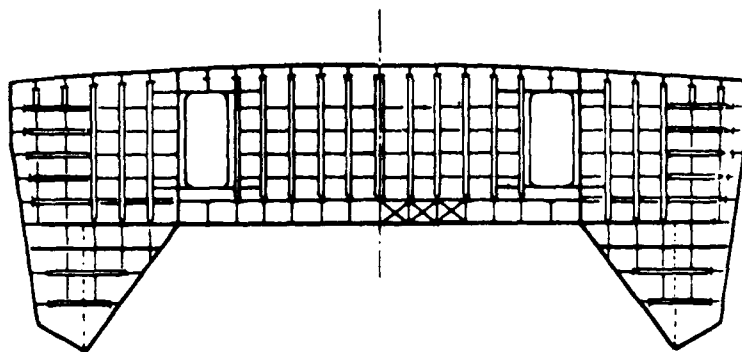


Figure 166 - B-H 110 Midship Section

In the off-cushion mode, the sidehull displacement provides full buoyancy for the craft and the boat will operate with the wet deck above the free water surface. As a result, it is reported¹²⁵ that excellent off-cushion handling and performance are expected. Tow-tank tests have shown that there is almost no additional drag penalty due to the inward sloping of the sidehulls and, consequently, off-cushion speeds of 19 knots in calm sea and 15 knots in a State 3 sea are expected. A photograph of the B-H 110 under construction is shown in Figure 167.

Although detailed costs cannot be revealed at this time it is expected that the cost of hull construction will be accomplished for approximately 25 percent of current air cushion craft hull construction costs. The combination of simple design, common structural elements, and boat construction manufacturing techniques set to commercial standards all serve to bring about significant cost reductions with only a modest increase in structural weight (see Figure 156). This encouraging approach to air cushion craft will be watched with interest as the B-H 110 continues operation.



Figure 167 - B-H 110 Under Construction

By contrast, the British craft have retained extensive use of rivetted aluminum construction with some notable examples of fiberglass construction. The use of rivetted construction was selected for its simplicity and cheapness in the smaller size craft. This philosophy prevailed at British Hovercraft Corporation with its aircraft background and also at Vosper-Thornycroft with its shipbuilding background. Figure 168 (upper photograph) shows the form of construction of the Vosper-Thornycroft VT 1 hull, which is fabricated from thin gage marine corrosion-resistant alloy (BSS-1470 NS6) and is rivetted with NR5 and L58 rivets. To provide watertight integrity, the rivets are sealed with BSS elastic sealant prior to rivetting, and all watertight compartments (26) in the buoyancy raft (shown in the upper photograph of Figure 168) are coated with an epoxy-base paint. The bulkheads are stiffened by Z-stiffeners with various spacings. The closest spacings occur in the bow sections to accommodate the wave impact pressures generated from 6-ft waves at 30 knots. The structure is completed by two main longitudinal vertical stiffened bulkheads that extend the length of the craft, separating the central car bay from the outer machinery and passenger bays. These bulkheads provide the resistance of the craft to overall longitudinal bending and shear. The outer bays of the craft are subdivided by four transverse bulkheads of similar construction linked across the central car bay by beams to provide the overall transverse strength. This form of construction is similar to that discussed earlier in relation to generalized structural weight. It is a simple form of construction and results in a 30-percent structural weight fraction.

The British Hovercraft Corporation BH.7, shown in the lower photograph of Figure 168 is an interesting combination of rivetted aluminum construction in the buoyancy tank raft (just visible behind the scaffolding) and extensive use of fiberglass in the superstructure and bow sections. Like the SR.N4, the main torsional strength is achieved with the buoyancy tank. Bending is resisted through two deep beam longitudinal bulkheads. The fiberglass skins are integrally stiffened with foam-filled top-hat stiffeners clearly visible in the lower photograph of Figure 168. This particular craft was built for the Iranian Navy for logistic missions and coastal defense. The fiberglass structure is particularly robust in the bow sections, using a polyvinylchloride (PVC) foam core to the stiffeners on approximately 27-in. spacing. Considerations of military robustness, other than the minimum weight philosophy discussed earlier, influenced the final configuration choice for the BH.7, contributing to its 30-percent structural weight fraction at a gross weight of 50 tons. This value might be compared with the SR.N4 value of 30-percent structural weight fraction but at a 185-ton gross weight.

While the specific structural details are not immediately available, the general structural form of the stretched SR.N4 (the Super 4 or SR.N4 Mk 3) can be seen from Figure 169. The upper photograph in Figure 169 shows the starboard quarter bow view and the lower photograph shows the

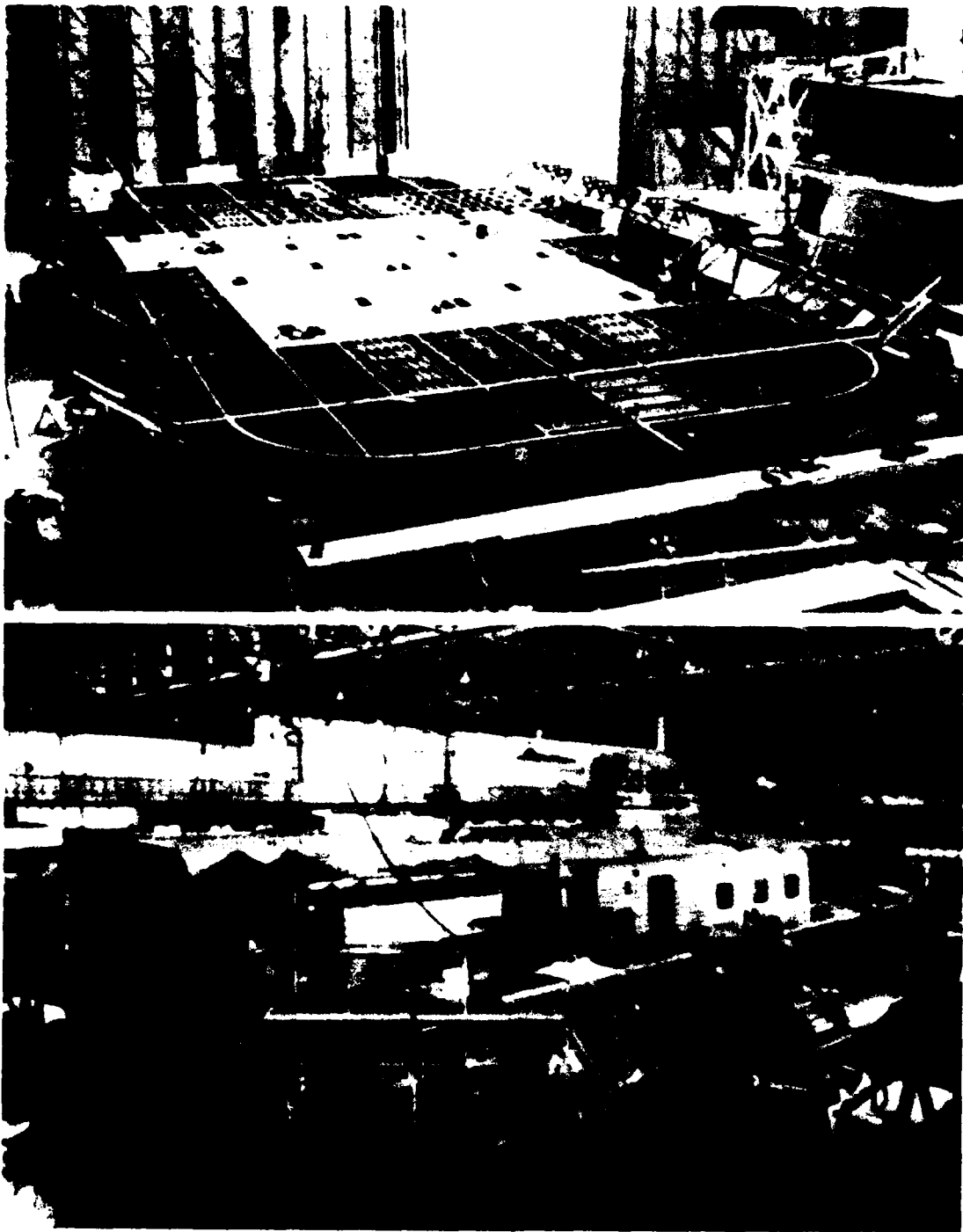


Figure 168 - VT 1 and BH.7 Construction



Figure 169a - Quarter Bow View



Figure 169b - Quarter Stern View

Figure 169 - Construction of Stretched SR.N4

starboard quarter stern view. The rivetted structure use of "top hat" stringers and structural members with lightening holes can all be seen in these views.

Some insight into the contributing factors to such high values of the structural weight fraction can be gained by comparing the weight of plating used in various craft as a function of the design impact pressure and the type of construction. Heller and Clark¹²¹ made such a comparison for the plating weights used in current hydrofoil construction. Figure 170 includes

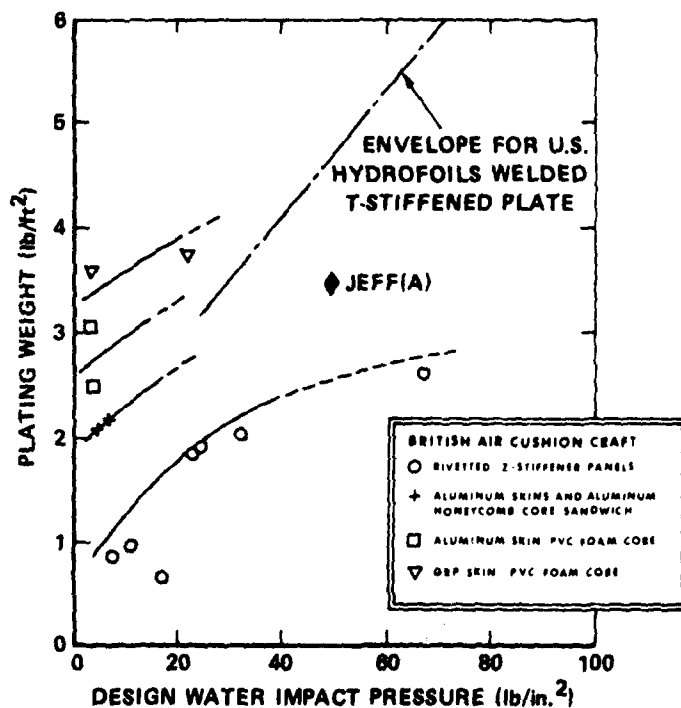


Figure 170 - Plating Weights

the envelope of minimum weight from Reference 121 for aluminum plate stiffened panels for hydrofoil construction. This envelope may be compared to some data for air cushion craft for aluminum plate stiffened panels and other forms of construction. The plating weights are plotted against the wave peak impact pressure used in the design. As previously discussed, these plating pressures have already taken into account the assumed alleviation due to the presence of the air cushion. The weight of the panels includes allowances for joints and attachments and, in the case of the (GRP) panels, includes allowances for the panel edge fittings. The weights are average values. The single data point for the JEFF(A) is for the corrugated plating construction as shown on Figure 161. The high weight for the fiberglass construction is probably contributing to the high structural weight fraction of the BH.7 as shown in Figure 156.

Figure 170 suggests that there is a wide disparity between design methods that is difficult to reconcile in a single plot. For example, the assumption of how the peak pressure alternates over the plating significantly affects the mean value and, further, the assumption of fixity to each panel will again determine the stress level in the panel. The data are given, however, not only as an indication of design trends in air cushion craft as they appear today, but because significant variations are possible in the weight of the plating, depending on the type of construction and the assumed method of loading. In the discussion on the structural weight fraction, it was indicated that the area of structure (plating) was influential in the structural weight and that making the craft more dense (higher p_c/L) would significantly reduce the structural area and volume; thence, the structural weight fraction as shown, for example, in Figure 156. While the cushion density appears to have the overriding influence on reducing structural weight; performance and seakeeping requirements may preclude the continual increase of this parameter, and improved structural weight may have to come from improved design and a better understanding of the loads.

CHAPTER VIII

LIFT FAN SYSTEM

The lift system for an air cushion craft can be considered as comprising an intake, a lift fan and engine, diffuser ducting and controls, and a skirt system. The actual accounting of the weights for the system may place the components in different categories depending on the type of configuration but, in principle, it is as described. The particular weight accounting as used in the U.S. Navy is given in Appendix B.

In particular designs there may be different geometric arrangements, and the lift system may also be integrated with other systems such as propulsion or steering control as discussed in Chapter V, but the basic characteristics remain the same. It could be said that the lift system is the heart of an air cushion craft, and its fan system must provide three basic functions for the craft:

1. To generate sufficient pressure (p_c) to support the craft.
2. To provide sufficient flow (Q) to minimize drag and to satisfy rough water wave pumping.
3. To provide a basic cushion characteristic in terms of cutoff pressure and slope ($\partial p_c / \partial Q$) to satisfy dynamic stability and ride quality requirements.

The lift fan system is a key element in providing the above functions, and it must satisfy the required characteristics with the minimum power for economic reasons and with the minimum space for payload space reasons. The development of fans to provide these functions has continued as an essential part of air cushion craft development since the first craft hovered in 1959. In any design, there are many tradeoff analyses and compromises to be made. These include considerations of other systems, such as main craft structural members occupying the space where the optimum diffuser should go or the cost of highly efficient blade sections beyond the allocated budget, and so on. These must always occur in the design process. However, there are some basic characteristics that have appeared in fan design that can be described as representing today's lift fan system. Some of the more dominant characteristics are described here.

The lift fan is called upon to provide many functions as mentioned. It is important to identify these power consuming functions if a realistic treatment is to be followed and proper comparisons are to be made between systems. Figure 171 provides a typical "tree" of functions that the lift fan or fans must satisfy.

Each branch of this tree has a particular pressure drop (or rise), flow, and efficiency. A network analysis is required either by computer, analysis, or "cut-and-try" to determine the branch conditions to provide a net momentum and energy balance. This "tree" is an important one in that in the literature discussions of total craft power, and the lift fan system

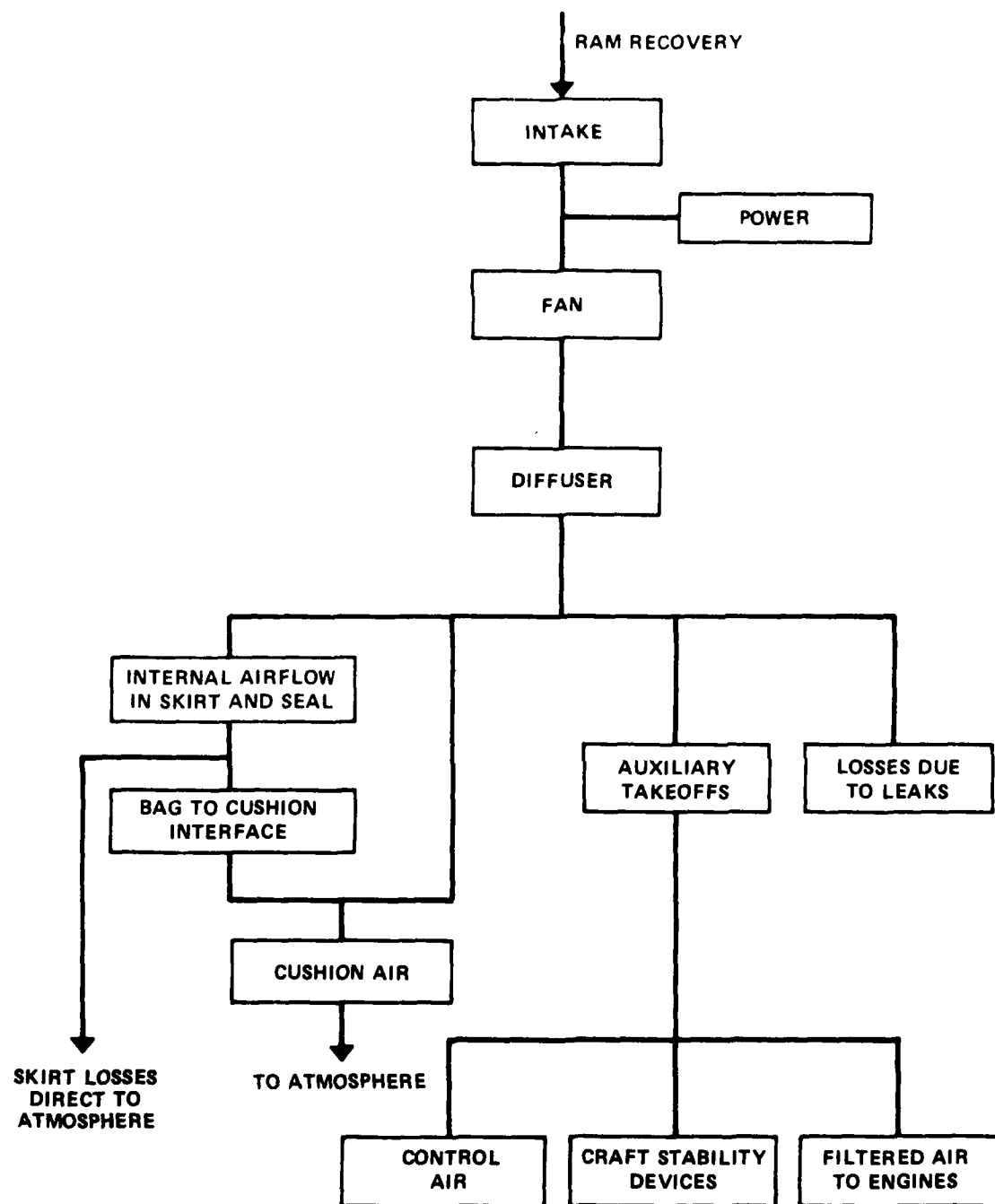


Figure 171 - Typical Lift Fan System

in particular, sometimes overlook some of the functions shown and, accordingly, different values of power and efficiency are quoted among craft.

The first experimental craft, the SR.N1, used an axial flow fan to generate lift, and this fan, with its generous intake and constant diameter duct beneath the fan (see the upper photograph in Figure 4), dominated the configuration. In the intervening years, research and development has continued on other fan types including centrifugal fans, mixed flow fans, and crossflow fans. Figure 172 shows sketches of the various types of fans. These crossflow fans were an attempt to reduce the space allocation for fans to the minimum by laying the fans in rolling-pin fashion along the edges of the craft, directing air immediately into the peripheral ducts, and leaving the main body of the craft free to carry payload. Some of the novel forms of fan systems tried have suffered from lack of development and await either rejuvenation or dust. Other fan systems continue to be developed. The discussion that follows considers, first, the aerodynamic aspects of fan design relative to size and efficiency and, second, the mechanical design aspects of weight, space, and environmental factors of marine use.

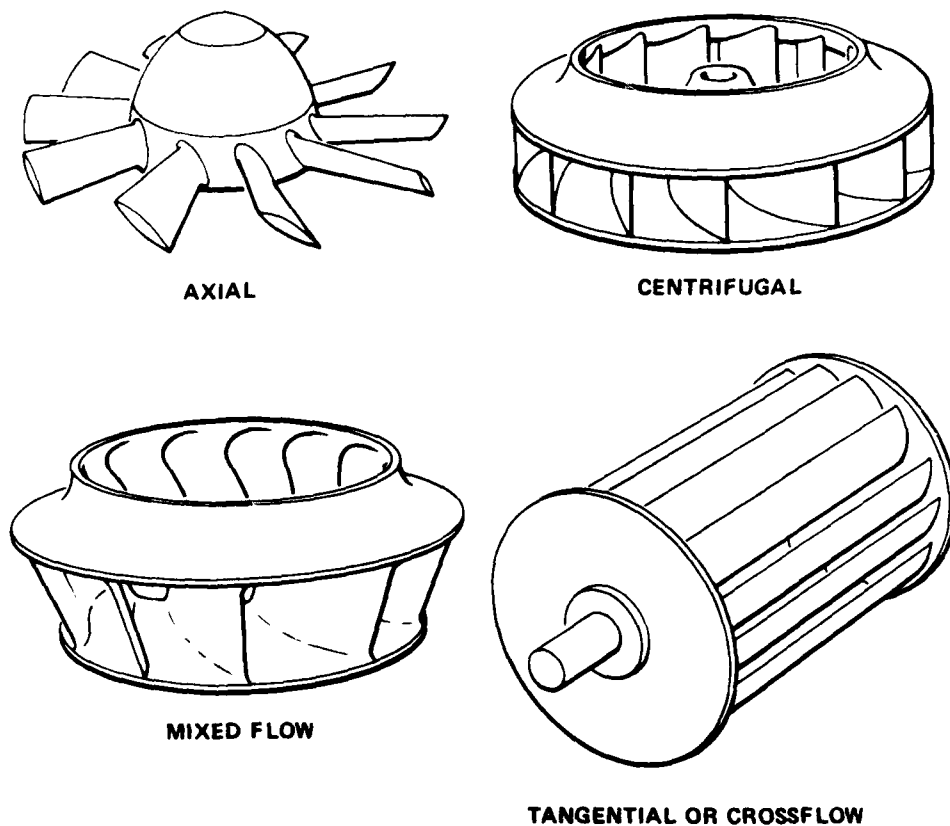


Figure 172 - Types of Lift Fans

AERODYNAMIC DESIGN ASPECTS

Although the lift fan system is obviously a key part of any air cushion craft, it may be somewhat disturbing to note that aerodynamically it is not very efficient. Despite fan efficiencies of 80 to 87 percent, on some current craft the amount of lift power doing useful work in the cushion may be as low as 40 percent; the remaining 60 percent is lost to intake inefficiencies, diffuser losses, and skirt system losses. Some of this wasted power can be attributed to frictional or pressure losses throughout the system and some to wasted flow through skirt attachments and the like. The tolerance or acceptability of such high losses is especially surprising in the light that, compared to some of its competitors in the transportation world, the lift system of an air cushion craft is fundamentally a power-consuming device.

Historically, this may be attributed to the fact that the earlier craft were built with the overriding need to demonstrate the principle with emphasis on simplicity, cheapness, and ruggedness. Also, in the early days, no data existed on fan performance for such uses contemplated for air cushion craft. As an example, all centrifugal fan data published in manufacturers' catalogues assumed the existence of a volute--a deceptively simple device with complex aerodynamic characteristics and strong influences on fan performance. The volute controlled the swirl and flow of the fan air and directed it tangentially in one direction. The early air cushion craft fan, on the other hand, needed to direct the flow radially in all directions to generate even distribution of pressure to the cushion. Not much data was available on such changes in installation, and the aerodynamic principles hidden in the many years of experience and development of the industrial fan performance were not easily isolated for air cushion craft use, with the resultant loss of aerodynamic efficiency.

Lift System Efficiency

As an illustration of the contributors to the pressure (and flow) losses in a typical air cushion craft, consider the pressure distribution through a lift system such as that shown in Figure 173. The sketch shows an installation of a centrifugal fan in, for example, an SR.N5 type installation, but it can be taken as representative of the basic elements in any lift system.

The total pressure rise across the fan (H_f) that must be developed in order to produce the desired static pressure (p_c) in the cushion can be written as

$$H_f = p_c + (p_b - p_c) + K_3 q_3 + K_2 q_2 + K_1 q_1 - \epsilon q_0 \quad (171)$$

Hence, the fan must produce a static pressure equal to the cushion pressure (p_c) plus the increased static pressure in the bag ($p_b - p_c$), which

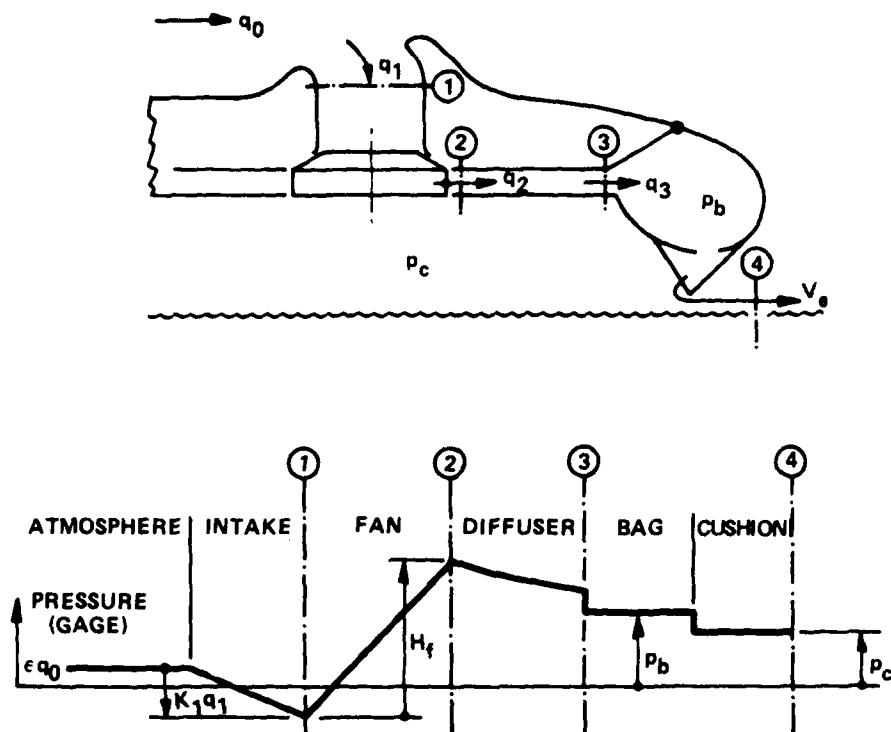


Figure 173 - Typical Pressure Distribution Through Lift System

may be from 10 to 50 percent, depending on the skirt geometry and the anti-bounce or antiplow pressure requirements (see Chapter VI). In addition, the fan must produce sufficient dynamic head to overcome the dump loss ($K_3 q_3$) from the diffuser exit into the bag, where $q_3 = 1/2 \rho U_3^2$ is the dynamic pressure due to the undiffused velocity head. The factor K_3 depends on the geometry but could be as high as 1.0 for a sudden expansion from the hard structure into the peripheral bag (or loop). The remaining dynamic head losses are $K_2 q_2$, which is the pressure loss due to the undiffused velocity head exiting from the fan impeller into the diffuser, and $K_1 q_1$, which is the intake loss into the fan. The $K_1 q_1$ and $K_2 q_2$ losses can be quite large in practical installations where clean fan intake and exits are disturbed by gearbox and shafting protrusions into the intake area and primary structure scantlings in the fan exit area. Some relief to the pressure rise requirements is available from the ram recovery ϵq_0 , where ϵ is the intake ram recovery factor and $q_0 = 1/2 \rho V^2$ is the dynamic head of the oncoming free stream. For the unusual case (except for some early craft) of a forward-facing intake, full recovery ($\epsilon=1.0$) could be expected

but, in such a case, the external aerodynamic drag of the intake usually cancels any such gain. For semiflush intakes, such as on SKMR-1 (see Figure 16), a value of $\epsilon = 0.30$ is more appropriate.

The total fan efficiency is given by

$$\eta_t = \frac{H_f Q}{550 P} \quad (172)$$

where P is the horsepower supplied to the fan, H_f is the total head in lb/ft^2 , and Q is the flow in ft^3/sec . The fan static efficiency is given by

$$\eta_s = \frac{(H_f - q_2) Q}{550 P} \quad (173)$$

Clearly, to provide the best system in terms of maintaining an even distribution of pressure around the craft periphery, it is necessary to minimize the fan exit velocity (q_2), hence, it is important to maximize the static efficiency (η_s) for the system.

To illustrate the distribution of power in the lift system, a typical power breakdown for an early SK-5 air cushion craft is given. The SK-5 in its original form is powered by a single 1000-hp engine (GE 7 LM 100 - PD101). At approximately 43 knots in 3-ft waves, some 430 hp is delivered to the fan system. Due to interference losses, as a result of the particular installation, approximately 392 hp are available at Station 1 (see Figure 173) for use by the fan. The centrifugal fan delivers some 314 hp at the impeller exit at Station 2, representing a fan static efficiency of $\eta_s = 80$ percent. A further 84 hp are consumed in the diffuser and internal ducting (Station 3) and some 60 hp are dissipated through leakage mainly through the skirt hinges. As the cushion air escapes at the hemline of the skirts at Station 4, approximately 170 hp has been consumed. The majority of this power (112 hp) is used in supplying the peripheral jets, the remainder, 58 hp, is used in pressurizing the rear bags. This example has shown that, although a high efficiency fan ($\eta_s = 80$ percent) is used, the efficiency of the entire lift system including fan, ducting, and skirt system is closer to 40 percent.

A cautionary note is in order here, relative to power consumption for the lift system. There are other types of pressure and flow "losses" attributable to the lift system in some air cushion craft as shown in Figure 171. For example, in the case of the SR.N5, a small amount (approximately 5 percent) of the cushion air is blown aft over the rudders to improve rudder control at low speed. Also, in the case of the SR.N4, part of the engine air is filtered through the lift fan air (see Chapter IX)

before entering the engine to avoid salt intake from more conventional filtering systems where air is taken directly from the (salt laden spray) atmosphere. For the SR.N4, approximately 10 percent of the plenum flow is directed into the engine room. Because there was need for improved control for the SR.N5 and improved engine performance for the SR.N4, if the power did not come from the lift system it would have to come from some other power source. Hence, in a total power analysis, because it was more efficient to use the lift system, this power consumption should not be considered losses in the true sense.

As a further example, the breakdown of the pressure and flow losses on the SR.N4 are given in Table 9. The numbers have been rounded and can

TABLE 9 - SR.N4 POWER DISTRIBUTION

Component	Pressure Drop or Loss (Percent) Δp	Flow (Percent) Q	Power (Percent) $\Delta p \times Q$
Intake	12.4	100	12.4
Fan Impeller	15.0	100	15.0
Plenum Chamber or ducts	12.0	86	10.3
Bag/Cushion Interface	20.0	86	17.2
Hinge Leaks	2.0	86	1.7
Engine Air	64.0	14	9.0
Cushion	40.0	86	<u>34.4</u>
			100.0
Note: (a) $\Sigma \Delta p$ is not 100 percent because of parallel paths. (b) ΣQ is not 100 percent because of series paths. (c) Control and stability power takeoff is assumed to be intermittent or negligible.			

be taken as typical of current amphibious air cushion craft with vertical axis fan systems such as the SR.N4. Higher values are achieved in craft such as the JEFF craft because of the horizontal axis for the fans and better diffusion into the cushions. The specific example in Table 9 is the SR.N4 which has a fan total pressure of 125 lb/ft² and approximately 35 percent of the lift power is absorbed by the cushion. The intake, fan impeller, plenum chamber, and bag-to-cushion interface losses vary between 10 and 17 percent or an average of 14 percent.

If lift system efficiency is defined as,

$$\eta_{\text{LIFT}} = \frac{\text{Cushion Pressure}}{\text{Total Fan Pressure}} \times \text{Fan Total Efficiency} \quad (174)$$

then it is seen that a total efficiency value on the order of 35 to 40 percent has rarely been achieved. Ideally, over half the losses due to fan intake, plenum chamber and bag-to-cushion intake; or some 20 to 30 percent of the total lift power might be saved by fan system design changes. However, once a craft is built, restrictions on, for instance, gearing and installations, limit the changes in operating RPM and other improvements. This emphasizes the need to analyze the system performance early in the design process.

Cutting in half the available fan efficiency to give an overall lift system efficiency of 40 percent has prompted research and development into other fan systems and other methods of craft layout to minimize system losses. Some of this research has been in obtaining a better understanding of the basic mechanisms at work in producing high efficiency fans, and other research has been in improving ducting systems and fan system layout in the general arrangement of the craft. The shape of the pressure-flow curve has also received considerable interest as the need has increased to improve rough water craft performance.

Fan Selection and Categorization

The selection of fans for today's air cushion craft has generally followed the rule of seeking the fan with the highest static efficiency and then keeping the craft design operating point (usually the condition for most economic cruise), in terms of pressure and flow, as close to the point of maximum efficiency as possible. Another important factor in fan selection is the craft layout as influenced by payload deck space, mission requirements, number of engines, engine-out capability, and other operational requirements. Figure 174 shows some actual arrangements used by British Hovercraft Corporation (BHC), Hovercraft Development Limited (HDL), and Vosper-Thornycroft.

Different internal ducting arrangements apply to the sidehull air cushion craft and Figure 175 shows the arrangement for the U.S. Navy surface effect ship test vehicle, the XR-1D. The XR-1D is a much-modified test vehicle used for exploring various features of surface effect ship technology. In Figure 175 can be seen the lift fans themselves, the various types of ducting to pressurize the bow and stern seals and the cushion vent valves (shown midships on port and starboard sides) for ride control. While there are several variations on this theme, it is typical of the configurations contemplated for surface effect ship (sidehull air cushion craft) use. Similar comments relative to pressure and flow losses already given apply equally to the type of configuration shown in Figure 175.

To aid fan selection, it is best to express the pressure and flow characteristics in nondimensional form which, from the standard theory of turbomachines, can be written for the pressure coefficient (ψ) as:

DIAGRAM COMPARING FAN, AIR DISTRIBUTION AND CUSHION SYSTEMS OF VARIOUS CRAFT

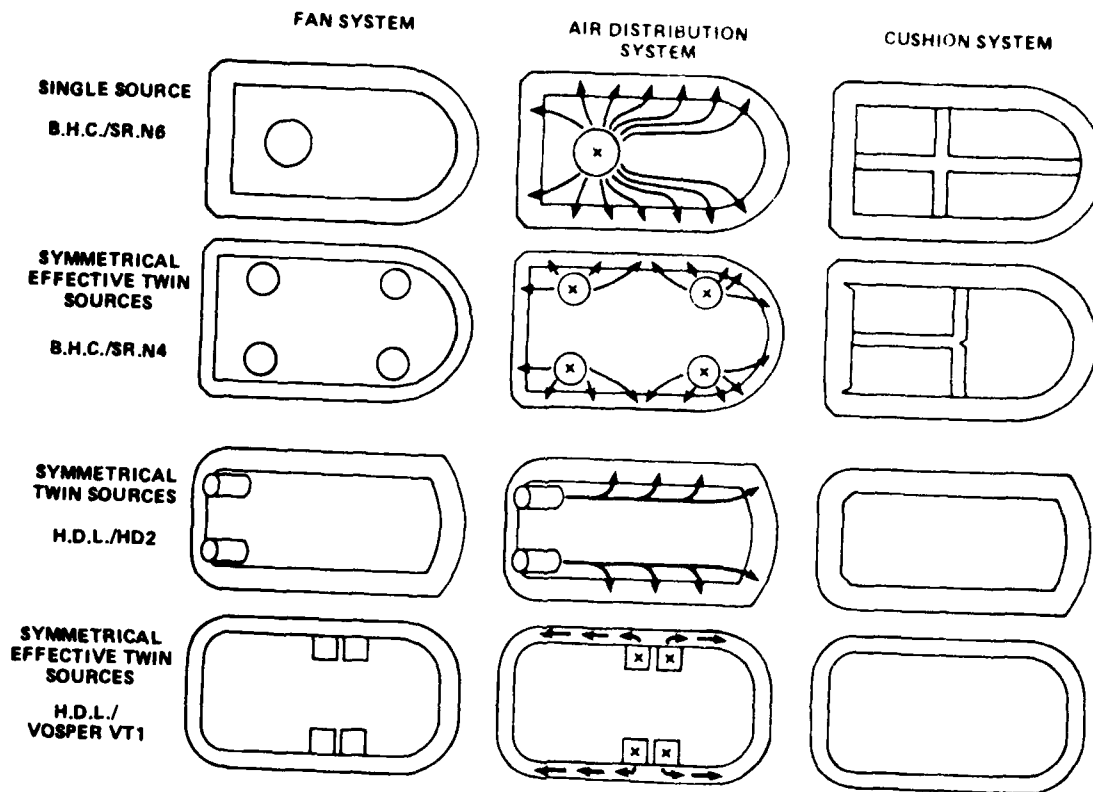


Figure 174 - Some Actual Lift System Arrangements

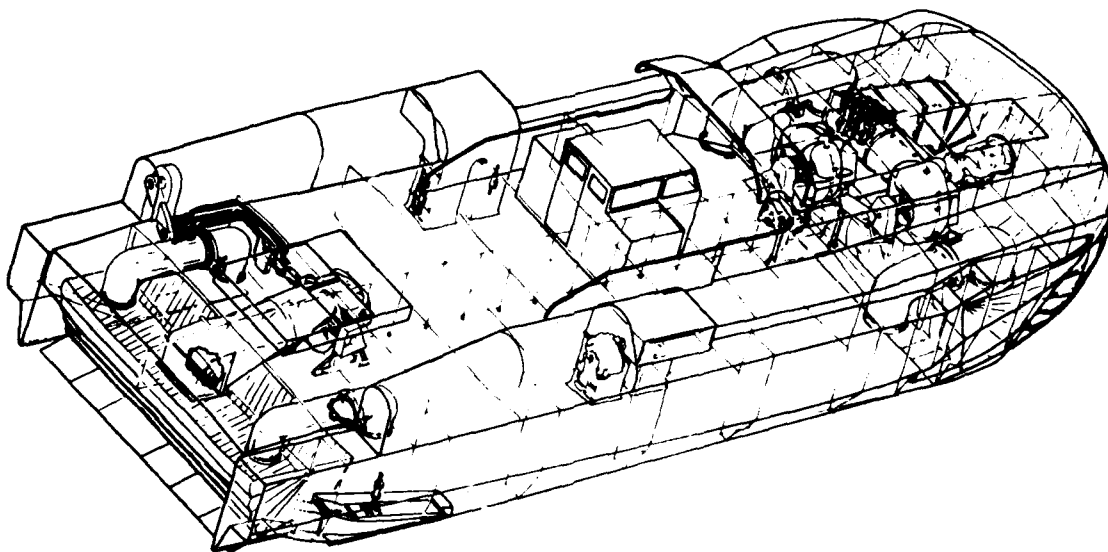


Figure 175 - XR-1D Lift System Arrangement

$$\psi = \frac{P}{\rho n^2 D^2} \quad (175)$$

where p is the pressure rise across the fan,

ρ is the air density in slugs/ft³,

n is the fan rotational speed in rad/sec, and

D is the fan maximum diameter in ft

For the pressure and flow coefficient to be nondimensional, the fan rotational speed is expressed in rad/sec, such that

$$n = \frac{2\pi N}{60} \quad (176)$$

where N is the rotational speed in rpm. The flow coefficient (ϕ) is given as

$$\phi = \frac{Q}{nD^3} \quad (177)$$

where the flow through the fan (Q) is measured in ft³/sec. The performance of a fan can be completely described by these nondimensional pressure and flow coefficients. They apply to the various types of fans, such as axial or centrifugal fans, and they also allow scaling performance within a given type of fan, such as performance at other rotational speeds or diameters from the design point.

In fan design, two other important parameters that may be formed from the basic pressure coefficient (ψ) and flow coefficient (ϕ) are frequently used. These are the specific speed (N_s), defined as

$$N_s = \frac{\phi^{1/2}}{\psi^{3/4}} = \frac{nQ^{1/2}}{(p/\rho)^{3/4}} \quad (178)$$

and the specific diameter (D_s), defined as

$$D_s = \frac{\psi^{1/4}}{\phi^{1/2}} = \frac{D(p/\rho)^{1/4}}{Q^{1/2}} \quad (179)$$

If the pressure rise across the fan is measured in ft of water (H), then the specific speed and specific diameter can be written in the following form:

$$N_s = \frac{nQ^{1/2}}{(gH)^{3/4}} \quad (180)$$

$$D_s = \frac{D(gH)^{1/4}}{Q^{1/2}} \quad (181)$$

As written here, the above coefficients are nondimensional. The significance of this particular form of coefficients is that the specific speed (N_s) and specific diameter (D_s) are the speed and diameter of a fan to deliver unit pressure and unit flow; that is,

$$\psi = \frac{1}{N_s^2 D_s^2} \quad (182)$$

$$\phi = \frac{1}{N_s D_s^3} \quad (183)$$

The reader will frequently find, in the literature and fan handbooks, that dimensionally impure forms occur, and care must be taken in using (for example) catalogue values of these parameters. Fan design has received extensive treatment over several decades of engineering and is well documented in the technical literature on turbomachines, and a summary will not be attempted here. The various intricacies of blade shaping, fan proportions, and the many other facets to control the shape and magnitude of the pressure-flow relationship may be found, for example, in the work of Eck.¹²⁶

Most of the current design methods for air cushion craft have as their basis the work of Osborne¹²⁷ and Shipway¹²⁸ for centrifugal fan systems and Wallis¹²⁹ and Shipway¹³⁰ for axial fan systems.

There are, however, some basic properties that have greatly simplified the fan selection for air cushion craft; some of these are outlined here, and existing fans are examined to indicate the state-of-the-art.

It is fortuitous that optimum designs (maximum total efficiency) of axial, centrifugal, and mixed flow fans can be represented by single curves of specific diameters (D_s) and maximum efficiency (η_t) when plotted against specific speed (N_s). In 1955, Cordier¹³¹ compiled specific speed and

specific diameter data of high efficiency fans and showed that the data exhibited very little scatter over a wide range of specific speeds for axial, centrifugal, and mixed flow fans. This empirical relationship is shown in Figure 176 for both the specific diameter data and fan efficiency data as a function of specific speed.

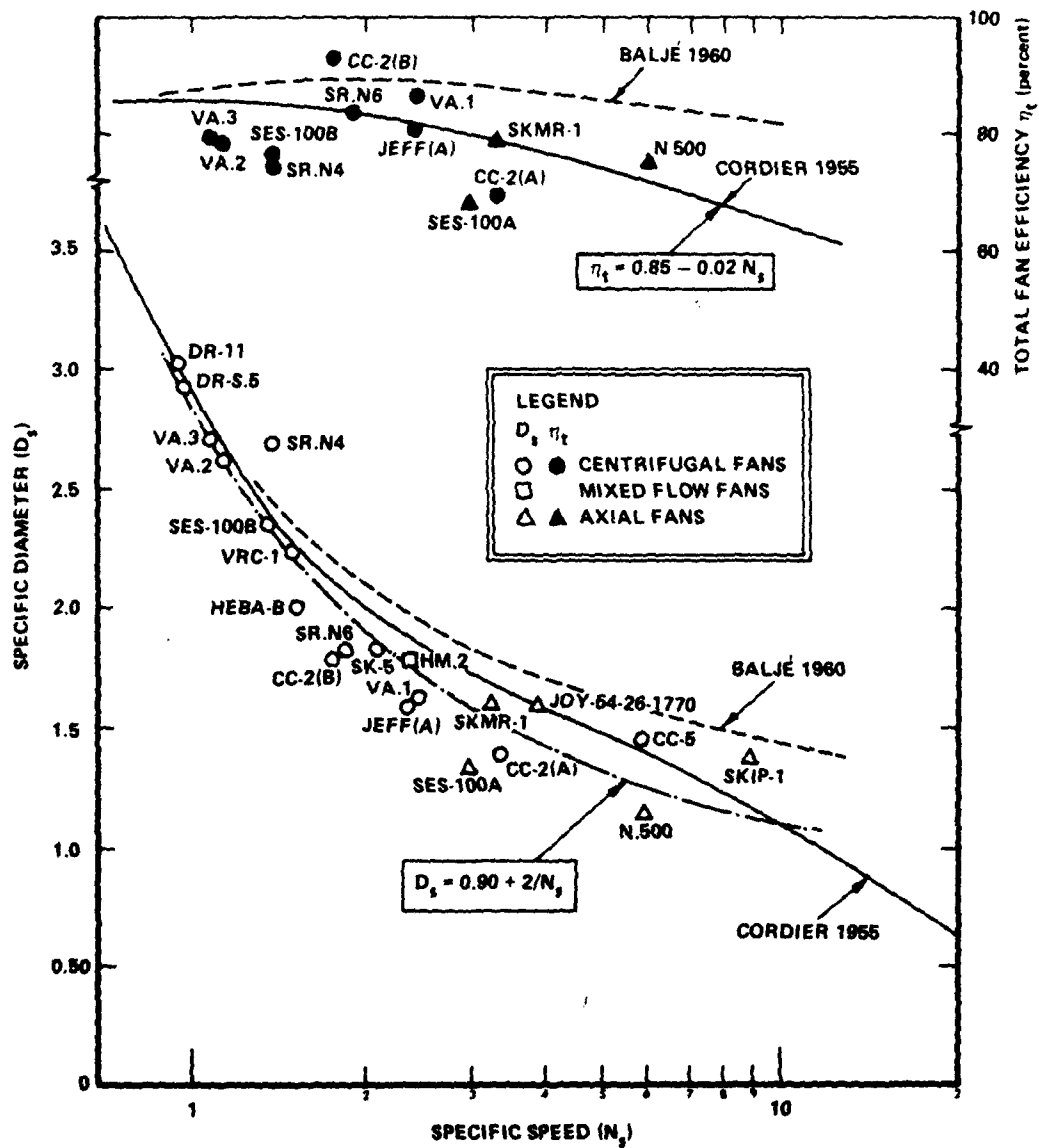


Figure 176 - Generalized Fan Sizing

Included in Figure 176 are the data of several representative air cushion craft fans of both specific diameter and efficiency. The craft data have been taken at the best efficiency point for the fan and not necessarily at the most common operating point. Table 10 summarizes the pertinent details of the fans shown in coefficient form in Figure 176. Note that the value of the SR.N4 full-scale fan given in Table 10 is 85 percent.⁴³ Such a value indicates the effect of scale when compared to the 78 percent peak efficiency of the SR.N4 model fan (designated SR.85 fan) shown in Figure 177. A synthesis of fan design for air cushion craft use is given in Reference 132, where a more detailed analysis of the types of fans and their characteristics may be found. In 1960, Balje^{133,134} derived a theoretical prediction for the same information that Cordier derived empirically. The Balje results are also shown in Figure 176 and give a more optimistic value over the range of interest of specific speeds. The Cordier curve can be considered as representing the results of design compromise in an actual installation.

It is seen from Figure 176 that, with only a few exceptions, air cushion craft fans have been designed to maximize efficiency and can be characterized by the single curves of specific diameter and to a less extent by efficiency, as a function of specific speed.

Although a more complete analysis is available in the Balje and Cordier works, it is noticed that a simple curve fit given by

$$D_s = 0.90 + \frac{2}{N_s} \quad (184)$$

will describe all air cushion craft fans to date and gives a slightly smaller diameter fan than Balje predictions but is more in line with the empirical results of Cordier. Also, for the range of specific speed of interest ($0.70 < N_s < 10$), the empirical results of Cordier for the total fan efficiency can be expressed as

$$\eta_t = 0.85 - 0.02 N_s \quad (185)$$

although, as can be seen from Figure 176, a wide variation in efficiency has occurred for several air cushion craft for reasons that will be discussed. These specific diameter data tend to increase in scatter at the larger values of specific speed ($N_s > 3$). Some of this scatter is

TABLE 10 - AIR CUSHION CRAFT LIFT FANS

Craft	Manufacturer	No. of Fans	Fan Type	Tip Dia. (ft)	No. of Blades	Design Speed (rpm)	Total Press. Rise (psf)	Fan Flow (cfm)	Cushion Pressure (psf)	Fan Total Efficiency ($\eta \times 100$)	Fan hp	N _s	D _s	Rotating Weight (lb)	Remarks
VA. 1	Vickers/Dowty Rotol	2	CF*	4'6"	17	875	26.1	800	18	0.86	55	2.43	1.63	61	Bicycle Spoke Type
VA. 2	Vickers/Dowty Rotol	2	CF	5'6"		870	71	770	20	0.78	128	1.11	2.61	130	Bicycle Spoke Type
VA. 3	Vickers/Dowty Rotol	2	CF	11'0"	19	430	65	2,670	31.7	0.79	400	1.09	2.74	670	Bicycle Spoke Type
MA. 2	Hovermarine	5	CF/NP	2'0"	11	2,900	50/70	180/200	46		30	2.34	1.80	18	Twisted CF approach a NP
HEIF-1	Gen. Dynamics	1	AF	5'3"										63	
SRM-1	Hall/Gen. Dyn.	4	AF	6'6"	10	1,200	60	2,600	47	0.79		3.20	1.61		
VRC-1	Vehicle Research Corporation	2	CF	3'3"	8	1,140	20**	313	17					128	
SRB-100A	Aerofat/sov	3	AF	4'0"	19	2,500	163	2,330	95	0.68		2.94	1.34		Integ. Sys. Verif. Pitch CV
SRB-100B	Hall/Aerospac	8	CF	4'0"		1,700	120	650	100	0.76**	195	1.35	2.351	210	
SR. M6	BMC	1	CF	7'0"	12	800	75	2,650	35	0.85		1.82	1.81		Integ. Sys.
SR. M4	BMC	4	CF	11'6"	12	700	120	4,000	50	0.85		1.38	2.27	1,500	Integ. Sys.
H. 500	Sadon	4	AF	6'1"		900	62	17,000		0.75		5.99	1.15		Prop. Fan
VT. 1	Yonkers-Thornycroft	2	AF	11'10"		1,050					175				Integ. Sys.
JEPF(A)	Aerofat/Aeromith	8	CF	5'0"	12	2,450	170	1,600	96	0.80	785	2.35	1.63	130	
Sormovich	Krasnovo	1	AF	9'0"	12		90	4,000	41						Integ. Sys.

*CF Centrifugal NP Mixed Flow AF Axial Flow

**Static

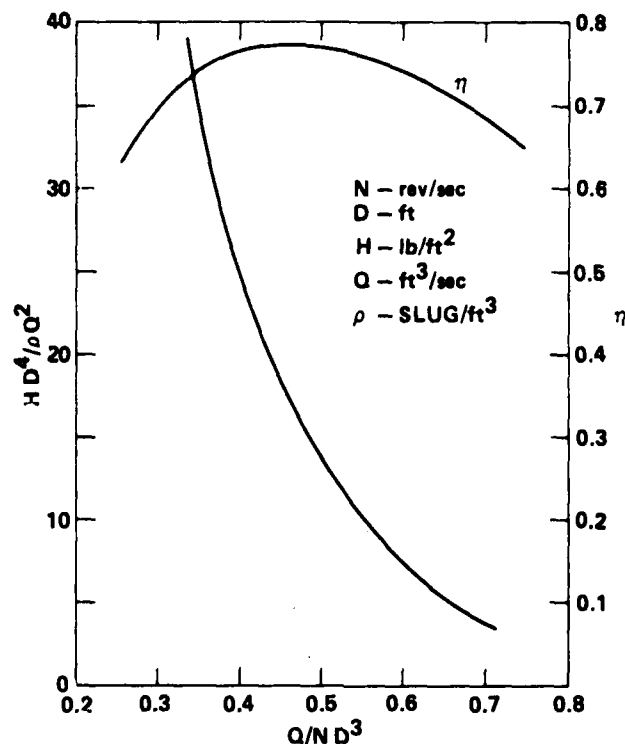


Figure 177 - SR.N4 Model Fan (SR.85) Characteristics

attributed to the effects of some important fan geometric properties that are masked by the simple categorization by major diameter. Some of the scatter is also due to designing the fan in some installations to other than the condition for maximum efficiency. This latter contribution to the scatter is particularly evident in those craft required to operate over a wide range of sea conditions, where it is more desirable to have a flatter pressure-flow characteristic to improve ride quality (see Chapter IV) than to design for maximum efficiency. A particularly interesting and systematic study of how fan efficiency can be improved in a given installation may be found in Reference 135. In this reference, Brotherhood describes the improvements made to the Britten-Norman CC2-001 centrifugal fan to increase its efficiency. In its original form, the fan had a total fan efficiency of 69 percent (static efficiency of 43 percent). The fan was essentially a 24-bladed flat plate bladed fan with splitter plate. This fan is designated CC2(A) in Figure 176. Several modifications were made in a series of some 10 different fan forms that included varying blade depth, shroud radius, inlet and outlet blade angles, flat plate-to-aerofoil blade sections, and inlet-to-exit area ratios. While a complete description may be found in Reference 135, the improved fan, marked CC2(B) in

Figure 176, shows the results of the installed modification. The fan CC2(B) is a 12-bladed aerotail section fan with a well-rounded shroud and smaller blade depth than the CC2(A) fan. The fan operates at a lower specific speed and gives a higher fan efficiency ($\eta_t = 90$ percent; $\eta_s = 61$ percent). Although the original fan used cheapness of construction as a strong influencing factor, the second fan was directly aimed at maximizing efficiency. The difference is the common dilemma of all designers.

In Figure 176, it will be noticed that, in the present notation, the three main types of fans in use are grouped according to the following:

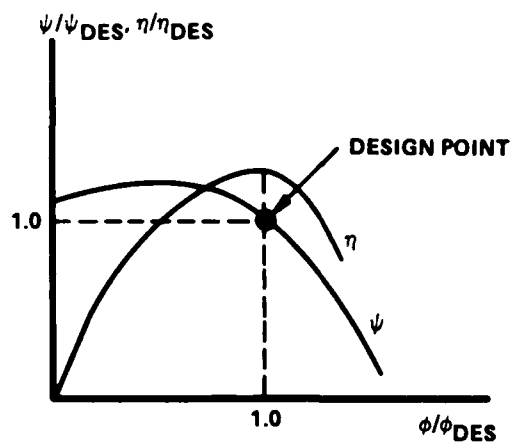
Centrifugal fans	$N_s < 3$
Mixed flow fans	$2 < N_s < 4$
Axial flow fans	$N_s > 3$

The choice of fan to use in a particular design of craft has been influenced by the need to satisfy the three conditions stated at the beginning of the chapter. Some indication of the effect of these considerations may be seen from the following discussion on the pressure-flow characteristics of centrifugal, mixed flow, and axial fans. Particular comments will be given on selected craft installations to indicate the practical solutions that have been applied to date.

Pressure-Flow Characteristics

The typical pressure-flow relationships for centrifugal, mixed flow, and axial fans are as shown in Figure 178. The curves are drawn for ratios of pressure, flow, and efficiency at some selected design point which, in the example, is the maximum efficiency point. Although it is difficult to generalize, there are certain characteristics inherent in each fan type that have influenced their use in air cushion craft. If one considers operation at "off-design" point, for example, to flow variations incurred during seaway operation, then it can be seen from Figure 178 that the flatter characteristic of the centrifugal fan is a decided advantage. Also, the centrifugal fan has a generally monotonic pressure-flow characteristic with no regions of stall near zero flow, which are inherent in high flow axial or mixed flow fans. It is possible to achieve a stall-free axial fan but only in special applications with narrow operating limits.

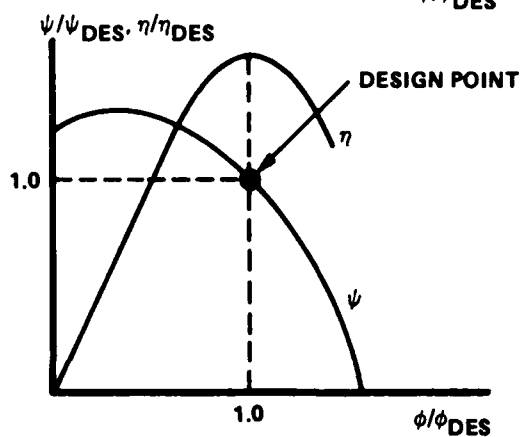
The steep slope and high cutoff pressure of axial fans provide a great deal of heave stability to an air cushion craft not attainable in centrifugal fan installations. The steep slope ($\partial p / \partial Q$ or $\partial \psi / \partial \phi$) of the axial fan, however, generally leads to degraded sea condition ride quality as discussed in Chapter IV. These properties are fairly well understood, and the many years of aircraft propeller technology has made the performance prediction of axial fans very reliable. The centrifugal fan, on



CENTRIFUGAL FAN

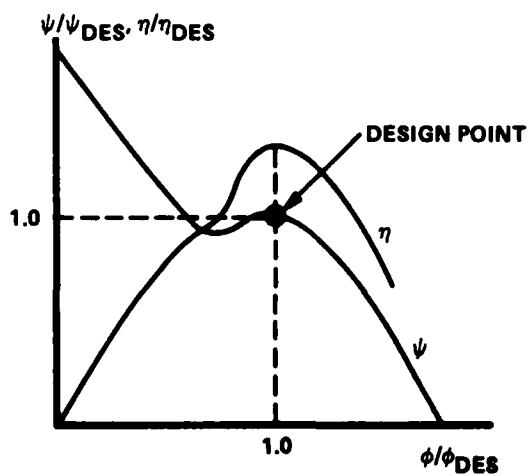
(BACKWARD CURVED)

$$N_s < 3$$



MIXED FLOW FAN

$$2 < N_s < 4$$



AXIAL FAN

$$N_s > 3$$

Figure 178 - Typical Pressure-Flow and Efficiency Curves

the other hand, is less predictable, and performance methods contain several empirical factors that are not always controllable.

The centrifugal fan is a relatively simple device and is rugged in construction. It can withstand being dented by foreign objects, whereas an axial fan can experience more severe vibration problems from such foreign object damage (FOD). Because of these reasons, the centrifugal fan has been used extensively in air cushion craft. Sufficient numbers of axial flow fan craft (see Table 10) have been successively operated, however, that a clear distinction as to which is the best choice is not obvious. The mixed flow fan is not so well developed, and the fan used in the Hovermarine HM.2 is the closest example of such a fan. It avoids the stall characteristic of the axial fan and tends to give a smaller diameter fan than the centrifugal fan for the same pressure and flow delivery. The mixed flow fan has not, however, received the amount of development that the centrifugal or axial fan has, due primarily to the complexity in fabricating twisted blades.

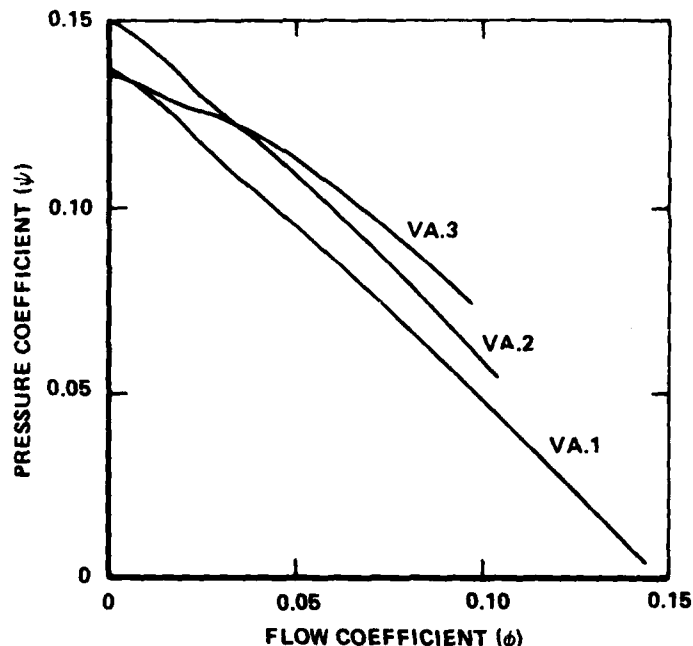
Some notes pertaining to the applications of passive fan systems to air cushion craft are given below.

Passive Fan Systems. A passive fan system is defined as that system where the fan is a simple, rotating, air-moving device and does not include any pitch change mechanism or other means of controlling pressure and flow variations into the cushion. Practically all air cushion craft to date are of this type and, in addition, discussion of pressure-flow characteristics is restricted to quasi-steady state conditions. Except in special operating conditions, it has been found that such an assumption is entirely satisfactory. Usually the weight and inertia of the fan are sufficient to maintain constant speed of rotation such that the designer does not have to contend with variations in a given characteristic $\psi - \phi$ curve due to dynamic conditions, although there is some evidence that dynamics modify the same (see Figure 187 and associated text).

Of the passive fan systems, the centrifugal fan has seen the most application in air cushion craft. The majority of air cushion craft using centrifugal fans have used the fan technology developed at either Dowty-Rotol and Airscrew-Weyroc in England or Buffalo Forge Co. in the United States.

The early Vickers-Armstrong craft, the VA-1, VA-2, and VA-3, used Dowty-Rotol-developed centrifugal fans (see Table 10). To save weight, the development of a bicycle-wheel-type fan, where fan blades were attached to the periphery of a bicycle type spoked wheel, was pursued by Dowty-Rotol in 1959 and resulted in the VA-1 craft. The largest fan of this type was the 11-ft-diameter centrifugal fan built for the VA-3 in 1962. These fans, as can be seen from Figure 176 and Table 10, were efficient, light-weight fans of large diameter. Their tip velocity varied from 206 ft/sec for the VA-1 to 250 ft/sec and 248 ft/sec for the VA-2 and VA-3 fans, respectively, making them also very quiet fans. Unfortunately, Dowty-Rotol no longer manufactures air cushion craft fans (although they are very

active in air cushion craft propellers, see Chapter IX) and ceased their fan work in 1965. Figure 179 summarizes the pertinent details of the Dowty-Rotol fans. Further discussion of the historical development of these fans may be found in Reference 136.



FAN	TIP DIA ft-in.	RPM	HP	DESIGN HEAD lb/ft ²	DESIGN FLOW ft ³ /sec	EYE DIA ft-in.	FLOW AREA ft ²	TIP SPEED ft/sec	INLET BLADE ANGLE deg	OUTLET BLADE ANGLE deg	η_t	W_f lb
VA.1	4-6	875	55	26.1	800	3-1 1/2	5.34	206	44	60	0.86	61
VA.2	5-6	870	128	71	770	3-9	8.5	250	30	69	0.78	130
VA.3	11-0	430	400	65	2670	7-0	31.5	248	30	62	0.79	670

Figure 179 - Dowty-Rotol Fan Data

The majority of air cushion craft use the fan technology developed by Airscrew-Weyroc Ltd. Airscrew-Weyroc developed a series of fans for use in industrial applications for induced draught use and for high air velocity ventilation and air conditioning.¹³⁷ These particular purposes demanded high efficiency and ruggedness of construction and, accordingly, Airscrew-Weyroc developed the so-called HEBA series of fans. The HEBA (high efficiency backward airfoil) fans were developed in two basic forms;

namely, HEBA-A, a narrow-width fan suitable for high pressure and HEBA-B, a wide-width fan suitable for low pressure. The actual pressures are unimportant here as the Aircscrew HEBA fans were industrial fans fabricated from welded mild steel. The HEBA-B fan geometry, however, was found to give the best pressure-flow characteristic for air cushion craft use, and it has been developed in several forms on different craft. Lightweight construction techniques have increased its pressure and load capability.

The HEBA-B fan has been used in such craft as the Britten-Norman CC-1 and CC-2 craft in 1962 (see earlier discussion and Reference 135). It was also used in the continuation of the Cushion Craft series when Britten-Norman became Cushion Craft Ltd. in 1967. Cushion Craft became a subsidiary of British Hovercraft Corporation in 1968. The HEBA-B fan development continued into the CC-4, CC-5, and the current CC-7 craft.

The BHC series of air cushion craft, the SR.N5, SR.N6, SR.N4, and BH.7 craft, all use variants of the HEBA-B fan constructed from rivetted and bonded aluminum construction. Figure 180 shows the SR.N4 11-ft 6-in. diameter fan as it is installed on the Hoverlloyd craft operating across the English Channel. It will be noticed that the internal surface of the fan is coated with heavy nonskid grit material to protect the fan from ingested debris. This illustrates the forgiving nature of the fan in terms of aerodynamic performance and its general ruggedness of construction.

This type of fan has also been incorporated into the SES-100B with a slight modification to the blade profile. From Figure 180, it is seen that the airfoil section used in HEBA-B has a flat undersurface and a typical cambered upper surface. Buffalo Forge Co. has found that a reflex to the upper surface trailing edge provides a more aerodynamically stable characteristic around zero flow.¹³⁸ This was incorporated into the SES-100B fan design. Other craft that have used fans based on the HEBA-B fan series include the JEFF(A) and JEFF(B) craft, Vosper-Thornycroft VT 1, and the Bell series of craft SK-5, Voyageur and Viking. Figure 181 illustrates some of the forms of this fan.

Although the HEBA-B fan has served as a reliable fan with the desired slope to the pressure flow curve around the design point, it has proven difficult to remove the stall condition completely. A typical curve for a craft of the JEFF type is shown in Figure 182 over the complete range of flow coefficients including shutoff condition at zero flow. The actual conditions for any particular design are a complex function of many geometrical parameters involving the fan geometry and the volute geometry. The complete range of the performance maps can be found in the Aircscrew-

Weyroc handbooks.¹³⁷ Some extracted, tabulated values may be found in Reference 132. Each air cushion craft fan designer has usually cross-plotted the HEBA-B curves, and only a typical set of data for one particular geometry is shown in Figure 182. A parameter of importance is the ratio of blade depth to fan diameter (b/D) which, as Csaky¹³² points out, is 0.17 for HEBA-A and 0.23 for HEBA-B fans. Also, the volute volume

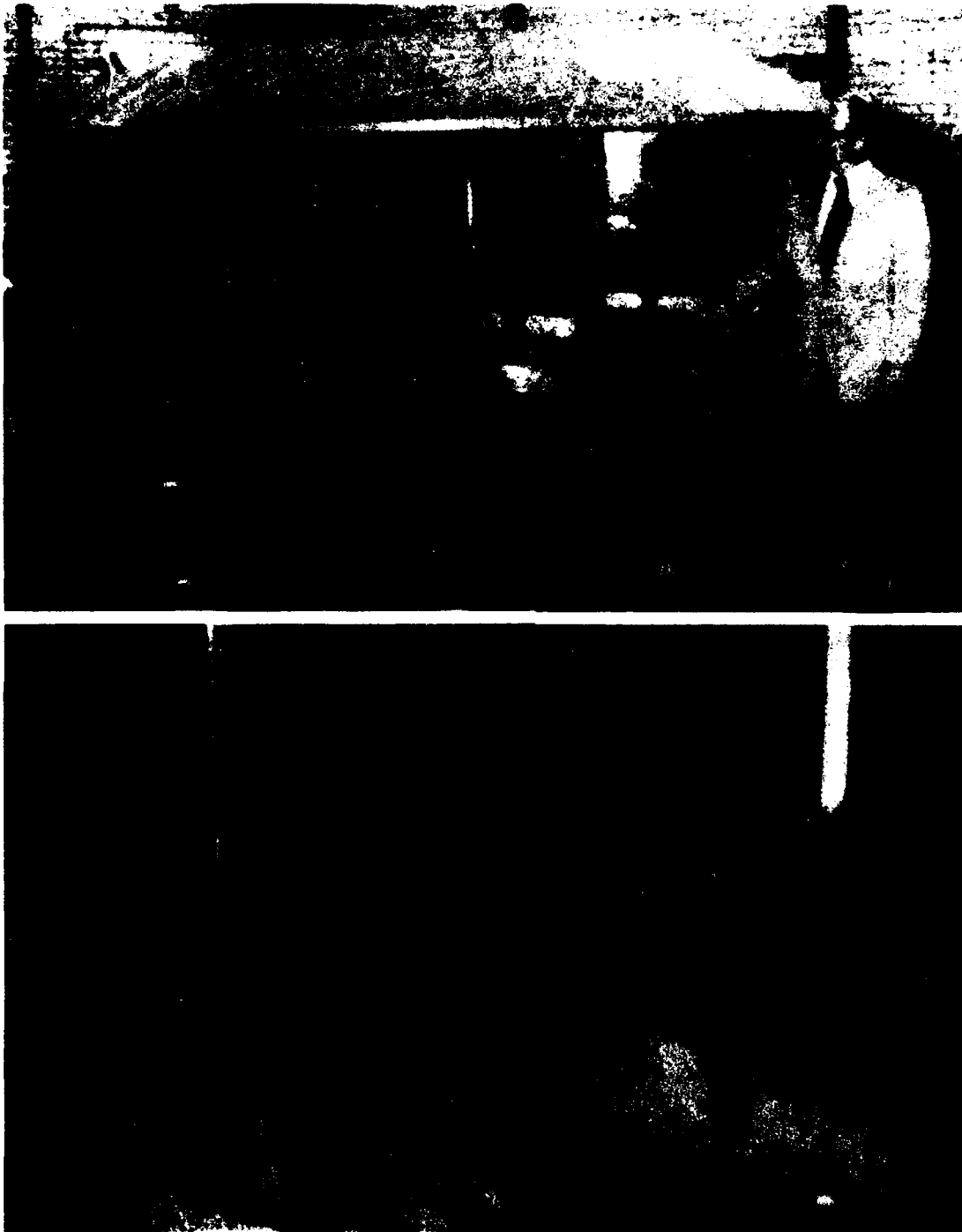
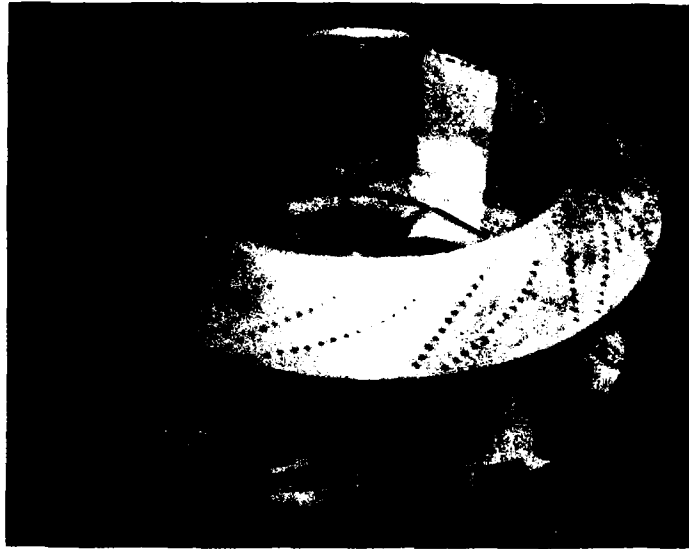


Figure 180 - SR.N4 Fan



SES-100B



VT 1

JEFF(A)



Figure 181 - Some Centrifugal Fans

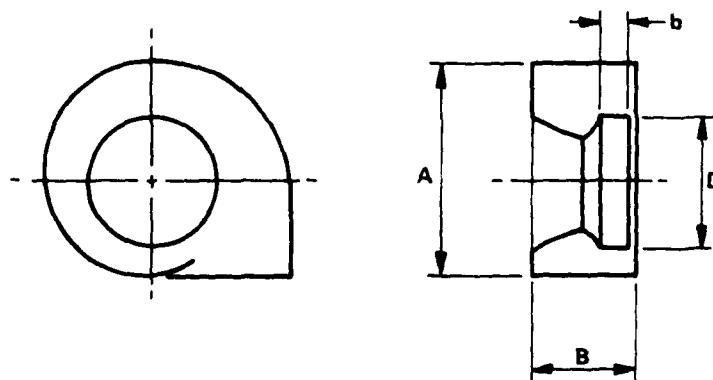
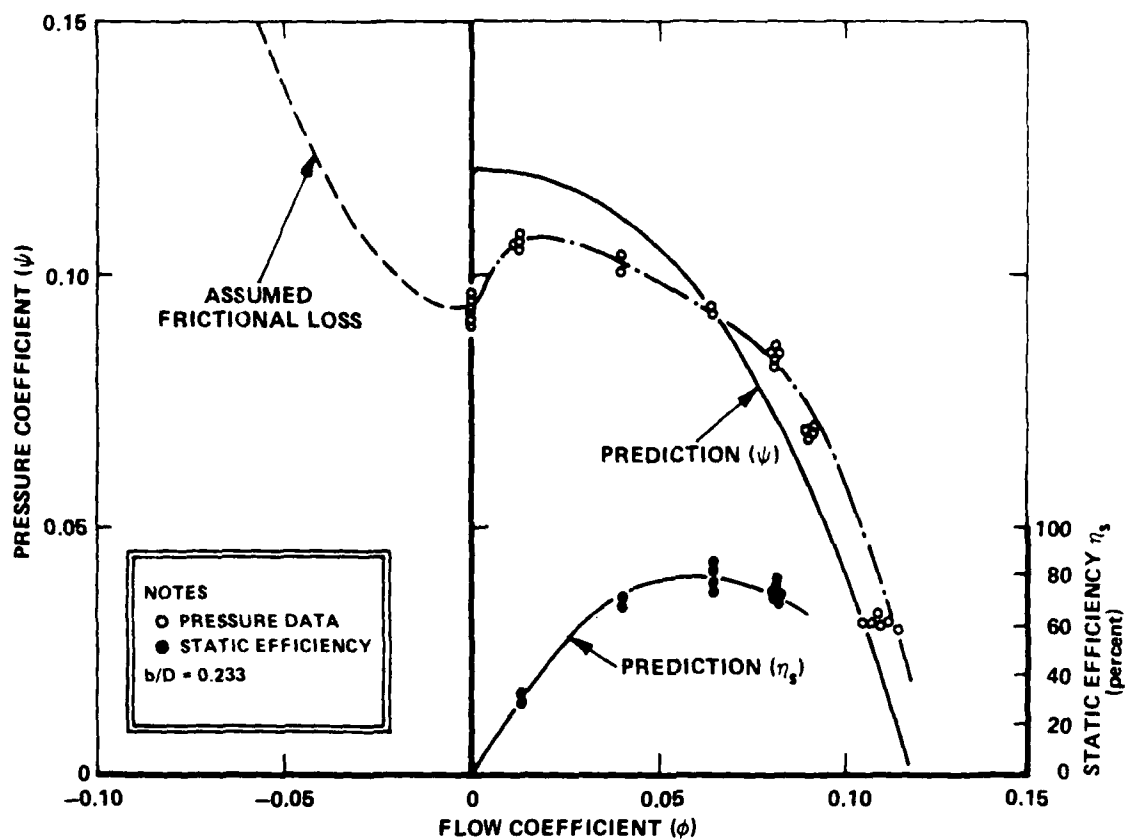


Figure 182 - Typical HEBA-B Fan Performance

parameter U/bD^2 where $U = \pi/4 A^2 B$ is an important parameter in determining fan performance. It is found that increasing U/dD^2 (see Figure 218, Chapter IX) provides a flatter pressure-flow curve but at the expense of a large fan installation. Typically, the volute would have proportions of the volute height (A) approximately 60 to 80 percent larger than the fan diameter (D) and the volute width (B) would be some 80 percent of the fan diameter. While not a general rule, it is frequently found that varying parameters to flatten the curve around the design point will increase the tendency to stall around the zero flow point. For air cushion craft designed to operate in extreme sea conditions where wave pumping can cause large variations in flow and can actually cause reverse flow through the fan, a characteristic curve such as that shown in Figure 182 can occur.

Although not elaborated on here, the stall characteristics near zero or low flow are more pronounced in axial flow fans. In such instances, it is required that the design point on the pressure flow curve be at sufficiently high values of the flow coefficient (ϕ) so that the design flow range about the design point does not include the stall region. Axial flow fans have been employed in such air cushion craft as the SR.N1, SKMR-1, and SKIP-1. French craft have also favored axial flow fans, and the N.300 and N.500 are such examples. In all cases, these have been passive fan systems with no means to rapidly control flow. In the case of the U.S. Navy SES-100A, an active axial fan system was installed to investigate the effect of controlling the fan pressure-flow characteristic.

Active Fan Systems. As discussed above, current air cushion craft have used passive fan systems with emphasis on simplicity and ruggedness. Within these constraints, the design sought always to maximize efficiency influenced by the need to maintain a flat pressure-flow curve over a wide operating range and the avoidance of stall near zero flow conditions. Additionally, the need to ensure sufficient heave stability, which requires a steep slope or large cutoff pressure to design point pressure ratio has also influenced the final outcome of particular designs. As might be expected, the compromises have not always resulted in a high efficiency system or provided the best ride quality fan system. The high accelerations in sea conditions where the wave height approaches the cushion height (see Figures 85 and 86, Chapter IV) prompted research and development into active systems for air cushion craft.

Techniques for controlling the pressure and flow delivery have been investigated over the years for use in turbomachinery, and such devices as mechanical flaps on the blades, jet flaps, discharge guide vanes, and variable camber have all been tried with varying degrees of success. With the SES-100A in 1969, it was decided to incorporate, on an air cushion craft, the ability to control the pressure and flow. Two features were built into the craft: controllable pitch on the axial fan blades and variable inlet guide vanes (VIGV). The VIGV were incorporated to reduce the stall condition at low rpm or flow and to increase the efficiency over a wide range of flow operation. Due to resonance problems when operating

in variable pitch, this feature was "locked-out" in the craft, although the rotor blade angle could be set at different angles. The VIGV provided the active feature to the fan system and worked successfully. In addition to the above features for the fan, wet deck valves were incorporated into the design to provide a path from the cushion to atmosphere for controlled venting in response to wave pumping. The vent valves used for venting or heave attenuation were of a balanced design and could be activated at frequencies as high as 5 Hz, sensed by an accelerometer in the forward part of the ship. The vent valve area was approximately 20 ft^2 or one percent of the cushion area.

Some results obtained during the rough water trials in December 1973 showed dramatic reductions in the accelerations imparted to the craft during operation with the ride control system activated. These results are given in Chapter IV where ride quality is discussed, in Figure 91. Figure 183 shows, for a typical data run, the effect due to valve operation. This particular run was for the SES-100A operating at 29 knots into State 2 head seas. The upper part of Figure 183 illustrates the effective change in the pressure-flow characteristic due to venting; the lower part of Figure 183 is a tracing of the acceleration level (at the cabin location) and the valve position. The cushion pressure is also shown for reference to illustrate the phasing relationships between cushion pressure and acceleration. The venting system effectively reduces the cushion slope $\partial p / \partial Q$ to minimal values and, as can be seen, induces considerable reduction in acceleration levels even if the valves are held open for straight dumping to atmosphere. In another test run at 41 knots with 3 ft average wave height, acceleration levels of 0.39 g (rms) were experienced with the valve closed and the cushion flow approximately $5700 \text{ ft}^3/\text{sec}$. When the valve was held open at 25 percent and the vent flow increased to $4000 \text{ ft}^3/\text{sec}$, the acceleration level fell to 0.19 g rms. The craft speed decreased to 35 knots due to the increased immersion of the sidehulls, and the response frequency was approximately 2.0 Hz. When the valves were activated around the 25-percent setting, the acceleration decreased further to 0.13 g rms, and the ride aboard the craft was considerably improved. A similar venting system was retrofitted to the SES-100B in early 1974 for its continued rough water testing, thus providing an opportunity to compare venting systems with both axial and centrifugal fan systems.

Such techniques are in their early stages of development at this time, and the results as given above and in Chapter IV must be considered preliminary in nature. It is clear, however, that simple venting is very wasteful where significant amounts of power are given up to the atmosphere. There are two other schemes currently being explored, where the control of the flow is vested in the fan itself without venting the cushion overboard. One such scheme involves the use of variable pitch axial fans; this is being pursued by Hamilton-Standard,¹³⁹ a leading supplier in U.S. air cushion craft propellers. Another scheme involves a variable geometry

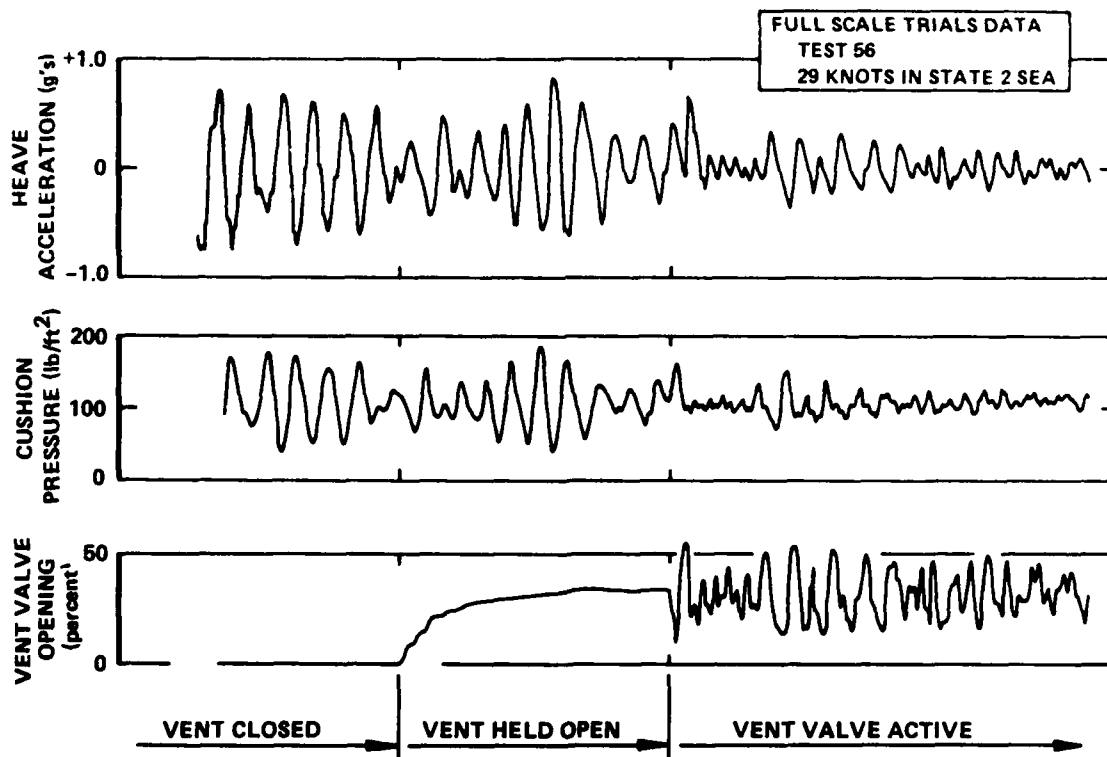
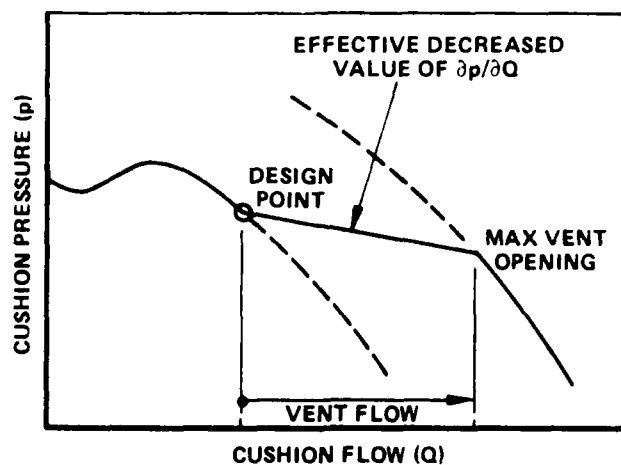


Figure 183 - SES-100A Venting System

feature in a centrifugal fan to control the pressure flow characteristic. This is currently being developed by Aerojet Liquid Rocket Company as part of the U.S. Navy SES Program. Although both these schemes are in their early stages of development and full-scale data are not available, it is considered important enough in a report of this kind to indicate the status of a key developmental item that may make significant improvement to the rough water ride quality of air cushion craft with acceptable power penalties.

A predicted set of pressure-flow characteristics for the Hamilton-Standard controllable pitch axial fan system is given in Figure 184 expressed in the nondimensional coefficient form discussed earlier in this chapter. The curves are shown for a 7-ft-diameter, variable pitch, axial flow, fan operating at 2183 rpm (tip speed 800 ft/sec). Each pressure-flow characteristic curve shown is for a particular pitch setting (blade pitch at $3/4$ radius point) from reverse to forward positions. Envelopes of total fan efficiency are also shown. In the steady state condition, the design point represents a cushion pressure of 250 lb/in.² at 4170 ft³/sec flow, requiring 2400 hp. The dotted line represents a dynamic simulation where the pitch change is modulated to maintain (as near as possible) a constant

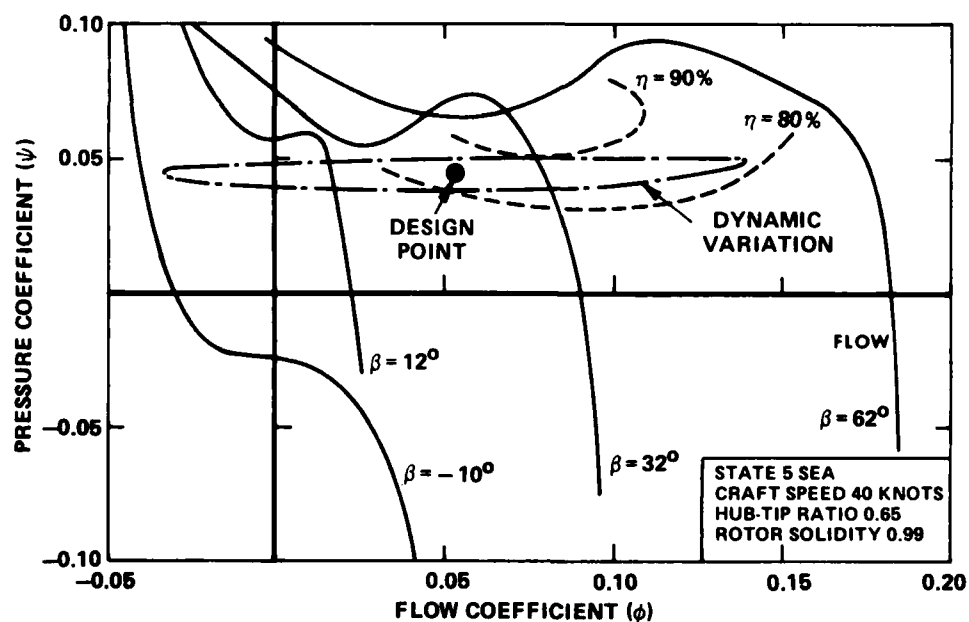


Figure 184 - Hamilton-Standard Active Axial Fan Scheme

cushion pressure. The dotted line would indicate achieving the desired flat pressure-flow characteristic while maintaining a high fan efficiency at the design point and staying away from stall conditions. It also shows operation into the negative flow region. Reference 139 predicts acceleration levels below 0.10 g if such a scheme were installed on a large air cushion craft operating in State 4 to 6 seas. The hysteresis type characteristic shown in Figure 184 collapses to almost a single curve at higher speeds and lower sea conditions.

The second scheme under development by Aerojet Liquid Rocket Company is the variable geometry centrifugal fan where, by means of valving, the flow of the fan is modulated to achieve the desired flat pressure-flow curve. Figure 185 shows the results of model tests in early 1974 illustrating the control of the flow output.

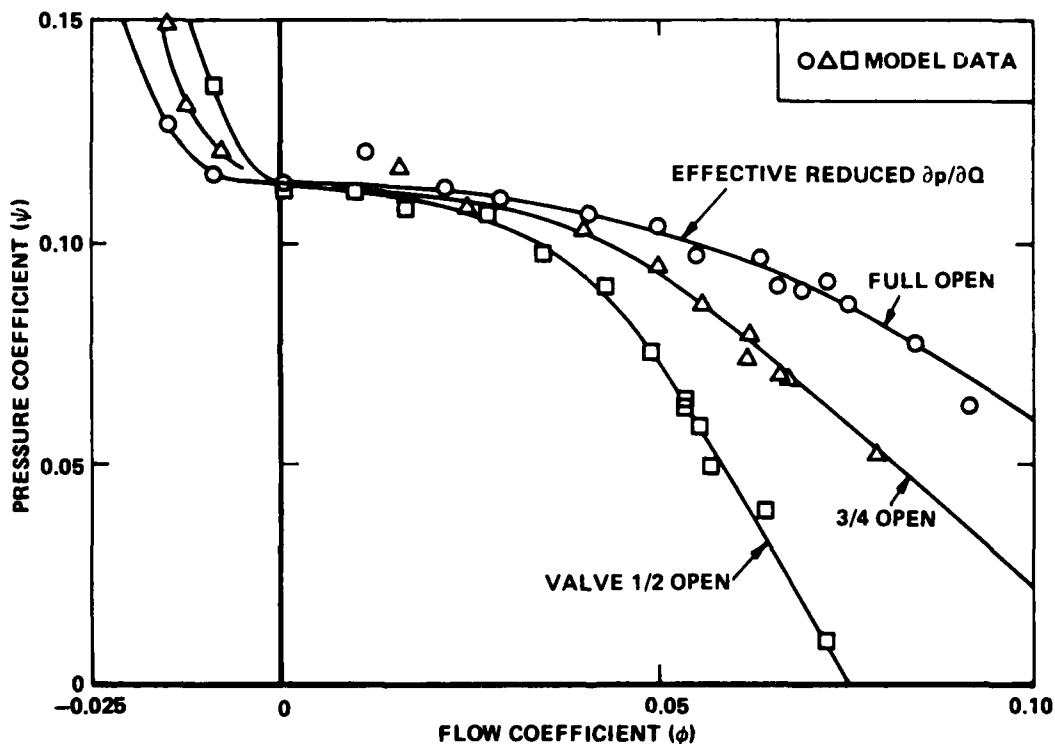


Figure 185 - Aerojet Active Centrifugal Fan Scheme

An isometric view of the full scale fan, based on such model tests, as envisaged for use in the planned 3000-ton Surface Effect Ship is shown in Figure 186. There are six such fans in the 3000-ton displacement SES.¹⁴⁰ These centrifugal fans have 86-in.-diameter rotors encased in 15.25-ft-diameter housings (volute) and incorporate the variable geometry (sleeve) elements shown on the intake to the fan housing in Figure 186. These particular fans incorporate double axial inlet design, airfoil shaped radial blades, constant velocity housings, and a simple circular discharge. The lift system consists of two sets of machinery and ride control

electronics. Each set consists of an LM 2500 gas turbine engine reduction gear, three inline variable geometry ducting fans and ride control vent valves. The forward fan on each side of the ship supplies air to the bow seal, the center fan supplies air to the cushion, and the aft fan supplies air to the stern seal, all of the same design despite varying requirements.

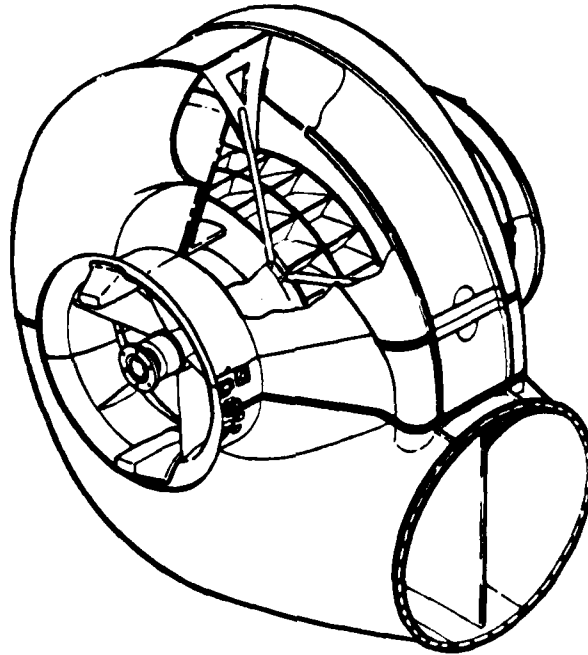


Figure 186 - Variable Geometry Lift Fan

It has been shown in Chapter IV that the shape of the pressure-flow curve has direct influence on the ride quality of the craft. The above two schemes show how this pressure-flow curve can be changed for both axial flow and centrifugal fans. The above discussion, however, has generally been restricted to static conditions. Evidence shows that, under dynamic conditions with variations of pressure and flow in the cushion, hysteresis loops in the fan characteristics will affect the ride quality of the craft and also have fatiguing effects on the machinery. These hysteresis loops have been observed in dynamic tests by DTNSRDC, Aerojet Liquid Rocket Co.,¹⁴¹ and the National Physical Laboratory (NPL)⁴³ in England.

This hysteresis loop behaviour has been attributed to the high frequency motion imparted to the craft during heave over rough seas and the resultant inertia of the air within the fans.

Crewe⁴³ shows some results of a 12-in.-diameter HEBA-B model fan operating under dynamic conditions. These NPL tests were conducted with a time dependent throttle causing fluctuation of the working point.

Figure 187 shows representative oscilloscope traces of variation of total pressure with fluctuating flow, for three model frequencies, 0.5, 2, and 5 Hz. The corresponding full scale frequencies for an SR.N6, for example, would be 0.19, 0.76, and 1.89 Hz, respectively. The traces on the left in Figure 187 are appropriate to the situation when an air bleed is opened to increase the average magnitude of the flow during a cycle. The "bleed shut" oscilloscope traces are shown on the right hand column of Figure 187. A mean line through the 0.5 Hz loops would approximate the steady state pressure-flow curves. It would be seen that each pair of "loops" at a given frequency is orientated along the steady state fan total pressure against flow characteristic curve. However, the dynamic departure in pressure values from the characteristic becomes increasingly large as frequency increases. Thus, during a cycle, rates of change of pressure occur with flow very different from the static values. The reciprocal slope dQ/dP becomes zero twice during a cycle, but over significant lengths of the loop perimeter it has values that are about equal to those of the adjacent static curve. The shape of the loop can become a figure eight, especially at the lower average flow conditions and lower frequencies.

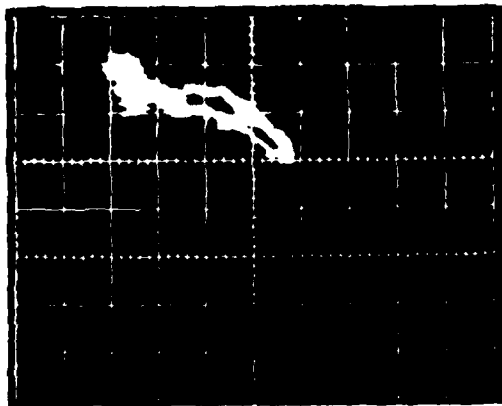
It is considered that only heave motion would cause the type of dynamic effect shown because a large fluctuation in flow is implied. During pitch motion, at least with compartmented cushions, reduction of forward cushion flow is accompanied by an increase in rear cushion flow and this kind of motion, thus, has less effect on total flow. Considering heave motion only, the tendency is for larger relative motions to occur at longer wave lengths and implies low encounter frequencies. For example, assuming a craft speed of 40 knots in a 2-ft-significant wave height sea gives,

$$f_E = 1.32 \text{ Hz for a 30 to 1 wave}$$

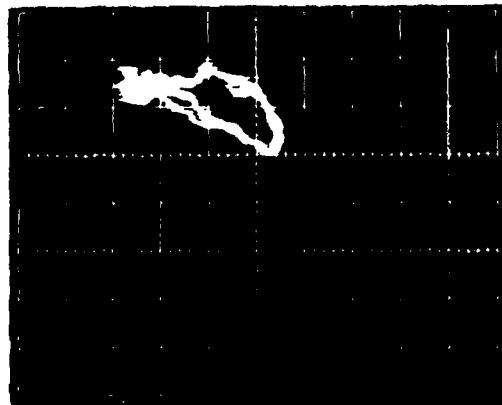
$$f_E = 0.71 \text{ Hz for a 60 to 1 wave}$$

This suggests that the extreme dynamic effects shown for the highest frequency can be ignored and that the central frequency should be taken as an upper limit. Even so, significant variations of fan characteristic slope are seen around the loop and if it were not for the bag suspension characteristic, the system would have a very nonlinear stiffness. It has always been found, however, that, in BHC type air cushion craft, the bag suspension stiffness is the dominant spring term and tends to swamp any fan induced effects.⁴³ The value of the fan efficiency at any point on the loop can be calculated when instantaneous power or torque and rotational speed, are known. Under steady conditions, the efficiency of this type of fan falls by less than 5 percent from optimum as flow is varied by ± 35 percent of design value, so that the loop is considered to represent energy

AIR BLEED OPEN



(a) 0.5 Hz

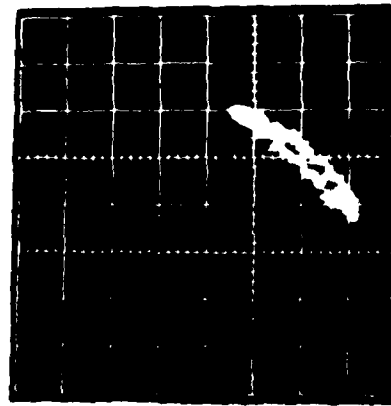


(b) 2 Hz

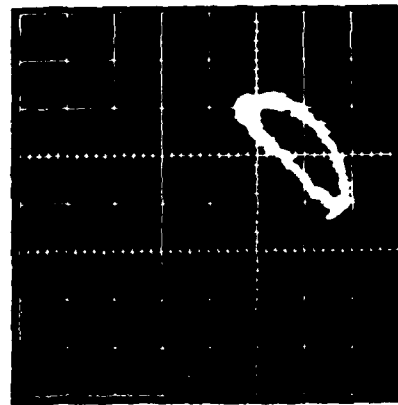


(c) 5 Hz

AIR BLEED SHUT



(d) 0.5 Hz



(e) 2 Hz



(f) 5 Hz

Figure 187 - Fan Pressure-Flow Characteristics Under Dynamic Conditions

storage and release rather than a hysteresis type loss. The basis for this opinion is that if the loops apply to a substantially constant rpm and if a fixed flow is considered, then in the case when the pressure is greater than normal-steady delivery pressure, the external conditions cause deceleration of flow in the fan and vice versa. There is, thus, an energy interchange between the fan and system which in this hypothesis is not reflected in absorbed power because a fixed flow and rpm are being considered.

To sum up, for small frequencies, dynamic oscillatory excursions from a steady fan characteristic do not greatly depart on the average from motion along the characteristic curve, but as the frequency increases the excursion elongates more and more in a direction at "right angles" to the characteristic.

Multifan craft such as the SR.N4 and the JEFF, with several fans operating in parallel and feeding a common plenum, can exhibit another type of flow instability due to dynamic effects, if the fan characteristic has a region of positive slope and the working point is close to the peak in the characteristic. Then it is possible for some fans to work below the peak and others above, for the same pressure requirement. Changes in flow requirement may then drive some fans towards shutoff and the remainder to higher flow. This condition can be guarded against by using fans with completely negative slope. BHC experience with SR.N4 suggests, however,

that this is not a serious problem.⁴³ Clearly dynamic fan behavior, which is influenced by the overall design features of the lift system, can have a considerable effect on craft response. If the system impedance between a fan and cushion are low, as for example in a direct cushion feed situation, then, during wave pumping, considerable amounts of air can flow back through the fan. This was observed recently in tests of a model of an HDL type of system, on the NPL forcing table. The comparatively high impedance provided by BHC lift systems with their internal plenum chambers substantially reduces or eliminates such back flow effects, especially in craft having parallel operating fore and aft fans.

Durkin and Luehr¹⁴¹ conducted similar tests to those at NPL including tests on a variable geometry fan and found the same general conclusions. With the need to reduce the power requirements of air cushion craft in rough water operation, continued development of such schemes will do much to improve craft performance in the future. This will become increasingly important as craft speeds increase, which will likely follow increases in craft size.

MECHANICAL DESIGN ASPECTS

The mechanical design of air cushion craft fans presented no unique problems once the aerodynamic features were decided. Various methods of construction have been used by different manufacturers with no particular advantage being found in any one form of construction. The axial fans were constructed using conventional aircraft propeller construction methods including solid aluminum blades and metal spars with fiberglass blades. The

centrifugal fans have also used a variety of techniques. Fiberglass construction has been used in the VT 1 and HM.2 lift fans. Aluminum construction has been used extensively in the SR.N series of craft and the majority of U.S. craft. The form of construction has varied also; the lift fan blades of the SR.N5 fan, for example, were constructed from light gage sheet redux bonded to light gage ribs, thus leaving no rivet heads or other protuberances in the flow. The fan blades for the SES-100B were extruded aerofoil sections complete with integral webs for strength. The tip speeds associated with centrifugal fans (300 to 500 ft/sec) have placed stress limitations on the fan construction and the attachments of blades to back plate and shrouds have sometimes cracked or failed during overspeed tests. However, conventional design methods have prevented major failures in service of most designs.

Fan Weight

The weight of the lift system (including skirts) varies between 4 and 8 percent of the craft gross weight and the reader is referred to Appendix B for the compilation of the lift system weight. The weight of fans has followed a fairly consistent trend despite the various geometric changes to accomplish the aerodynamic characteristics discussed above. Because the majority of air cushion craft used centrifugal fans, weight data for these fans is available and is given in Figure 188.

Purnell¹⁴² compiled the weight data of the Airscrew-Weyroc HEBA fans, which are constructed from all welded mild steel, from the small diameter fans up to and including their largest fan, No. 60 (5 ft diameter). The data for both HEBA-A (b/D = 0.17) and HEBA-B (b/D = 0.23) show a small effect due to b/D, and the weight data shown follow the trend

$$W_{fan} = 16.72 \left[0.60 + \frac{b}{D} \right] D^{2.42} \quad (186)$$

which would show an approximate 15-percent weight increase for the steel HEBA-B fan over the steel HEBA-A fan. There is some scatter, the weight of the volute, which is often greater than the rotating fan weight, is not included in Equation (186) due to the many possible variations and the fact that it can be integrated with the structure and is, therefore, not completely additive. When one compares the weight of air cushion craft fans given by Equation (186) to the weight of the catalog HEBA fans, it will be noticed that it is almost exactly the ratio of the aluminum-to-steel specific weight. The form of construction that Dowty-Rotol used in the early Vickers-Armstrong craft (VA-1, VA-2, and VA-3) was the bicycle wheel type as discussed, and provided a lightweight fan trend, such that

$$W_{fan} = 1.98 D^{2.42} \quad (187)$$

Insufficient data base has been generated at this time to provide similar weight trends for axial fans, which are more susceptible to hub/tip diameter ratio, number of blades, and material.

Other factors that have influenced fan design for use on air cushion craft are the space requirements, noise alleviation, and environmental protection. The decision to use one fan or multiple fans to meet the pressure and flow requirements is a complex one involving complete craft layout tradeoff studies. It is clear that one large fan will consume a significant amount of payload deck space and that a large number of smaller fans would give more flexibility to the designer and improve "engine out" operation, but would do so with more machinery (and, therefore, more to go wrong). The designs to date have tended to favor the multiple fan installation.

Fan Noise

Noise of fans has not been a significant factor in current operational craft, except perhaps in the SR.N4, where the low frequency noise has defied conventional soundproofing methods and has caused some minor passenger discomfort. The main method of noise reduction has been to keep the tip speeds as low as possible and, for centrifugal fans, it has been found that efficient fans can be designed for tip speeds no more than 500 ft/sec. Axial fans, on the other hand, have to operate at higher specific speeds and higher tip speeds, and it has been found possible to design such fans for tip speeds no greater than 800 ft/sec. This increase in tip speed contributes to the increased noise level of the axial fan, which is approximately 10 dB more than a corresponding centrifugal fan. In any event, fan noise is more than masked by the (gas turbine) engine noise, which, in turn, is usually less than the propeller-generated noise. More discussion on noise is given in Chapter IX, where propellers are discussed. A more complete discussion of noise is given by Trillo.⁴⁴

The environmental protection of fans has also varied somewhat among different designers. In some cases, such as the SKMR-1 and the SR.N4, protection to the blade leading edges from spray and foreign object damage (FOD) is provided by polyurethane coating. In other craft, such as the SES-100B and SES-100A, no such coating is applied. It is a matter of design choice and proximity of fan blades to the outside spray-laden atmosphere. No significant problems have occurred from such environmental factors.

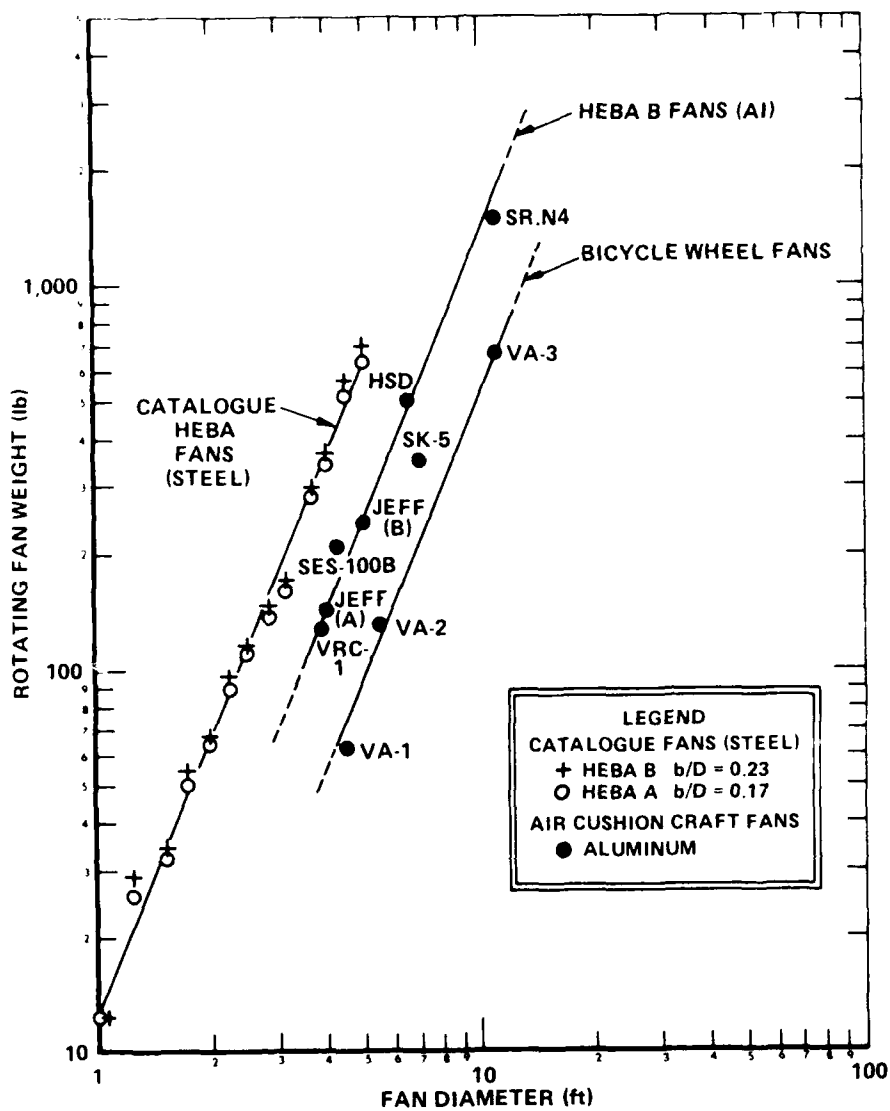


Figure 188 - Centrifugal Rotating Fan Weight

CHAPTER IX PROPULSION

The means of propulsion for air cushion craft developed along several paths over the years with varying degrees of success. These means have included different types of prime mover such as gas turbines, diesels, and, for smaller craft, automobile engines. The types of propulsors included various forms of free and shrouded air propellers, subcavitating and supercavitating water propellers, pod and flush intake waterjets, and propulsion by expelled cushion air. In most cases, however, there have been only one or two craft with the type of propulsion listed except for the gas turbine and air propeller combination. Hence, the data base on a range of propulsion means is somewhat limited.

In the development process, the problems have been somewhat different in each category. For example, in the case of air propellers, the developmental problems have been in converting a well-developed aircraft propeller technology to provide efficient operation at low speed (less than 100 mph) when subjected to varying flow conditions. In the case of water propellers and waterjets, the problem was the opposite, in that the low speed technology was well in hand, but development was needed to explore the characteristics at superhump speeds and in low cavitation number flow.

The propulsion system can be considered as the engine and its intake system, the transmission and the propulsor. Like the lift fan system discussed in Chapter VIII, the designer is concerned with the efficiency of the system, its weight, and its reliability; again, in most designs these requirements are in conflict. The entire machinery system (including lift fan systems) on integrated system air cushion craft typically constitutes 10 to 15 percent of the craft gross weight and is a large contributor to the empty weight of the craft. It is not surprising, therefore, that emphasis has been placed on the use of lightweight, high efficiency components in most designs. The extreme high cost of such components has, however, made economic profit a marginal venture, and this fact has seriously hampered a more rapid acceptance of the air cushion craft in commercial operator inventories. Typical costs of air cushion craft complete propulsion systems (for gas turbine installations) are between \$200 and \$350 per installed horsepower.

While a complete summary of the various technical achievements in propulsion is not possible in the space of this document, some of the more dominant characteristics of engines and propulsors are given to highlight the present state-of-the-art. Transmissions will not be discussed in this report for reasons of space and because the problems of transmitting high power through lightweight, high speed transmission is not unique to air cushion craft. The basic characteristics of transmissions as they apply to air cushion craft may be found elsewhere.³⁸ The problems of power transmission, vibration, lubrication, and weight control must await other discussions.

PROPULSION SYSTEM WEIGHT CONSIDERATIONS

As described above, the choice of the propulsion system for air cushion craft has largely been governed by the need to install lightweight systems due to the airborne nature of the craft and the need to leave as much allocation for payload as possible. Although there is not a large amount of data to clearly define trends, Figure 189 shows how the propulsion system weight fraction (W_2/W) varies with the displacement of the air cushion craft. General groupings are shown on Figure 189 to indicate

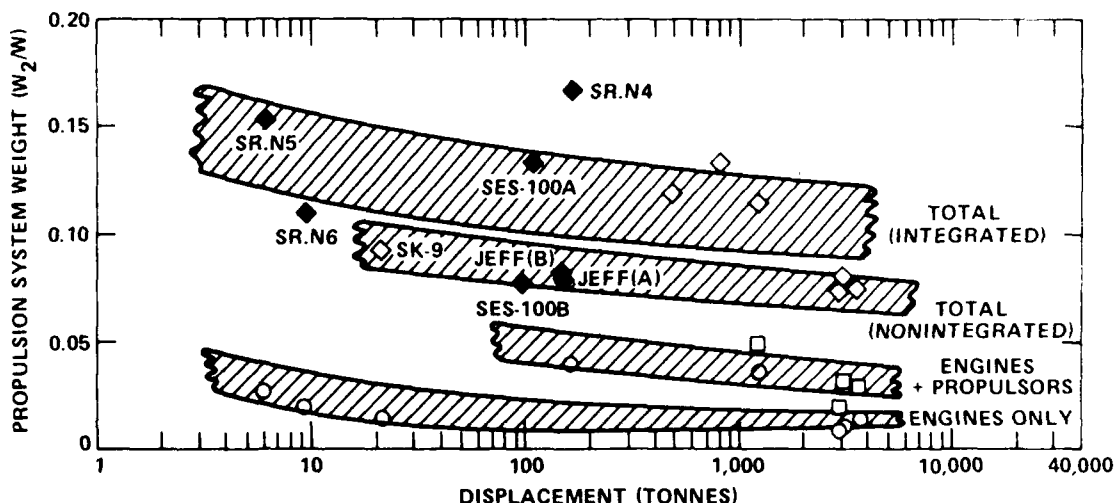


Figure 189 - Air Cushion Craft Propulsion System Weight

the relative contributions each of the major components in the propulsion system make to total system weight. The bands, drawn on Figure 189, are cumulative showing the contribution of the engine system, the propulsors, and the remainder of the propulsion system that is made up of transmission and accessories. The weight accounting is also affected by whether the propulsion system is integrated with the lift system (and thus includes lift engines and any cross-connections) or is a nonintegrated or separate system. With this type of grouping, the differences between air propulsion and water propulsion become submerged within the tolerance band of the available data. The lone point of the SR.N4, on air propelled craft that is showing a higher propulsion system weight than water propelled designs is heavy because of the use of early generation and heavy gas

turbines (Rolls-Royce Marine Proteus) with a specific weight of 1.0 lb/hp and the use of long shafting because of the desire to keep all engines at the rear of the craft to minimize the noise levels near the passengers.

In terms of the specific propulsion system weight, this same data is displayed, along with other craft, in Figure 190. For reference purposes, the specific weight of the marine gas turbine (MGT) engine system is also included in Figure 190. Most of the craft shown (air cushion craft and

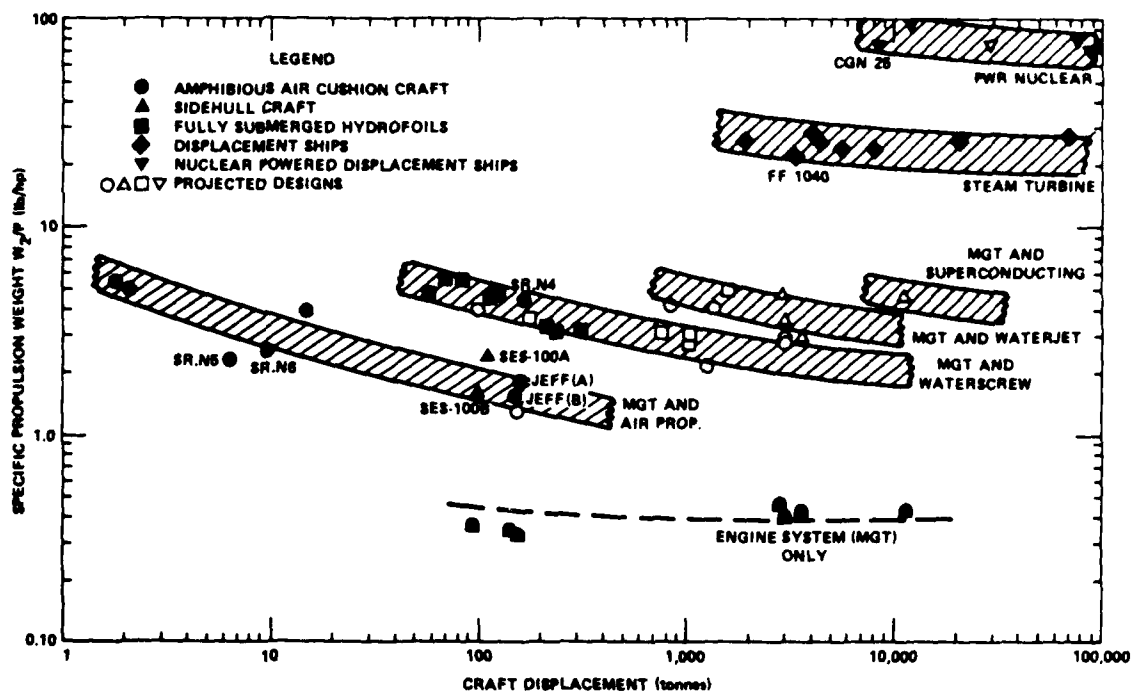


Figure 190 - Specific Propulsion System Weight

hydrofoils) incorporate the marine gas turbine. The two bands of data for displacement ships are for propulsion systems incorporating steam turbines and pressurized water reactor (PWR) nuclear powerplants. These are included for comparative purposes and are certainly not recommended for air cushion craft use!

The need for lighter weight clearly has prompted consideration and use of the gas turbine. The impact of the large use of gas turbines in the aircraft industry has also had a favorable impact in that substantial maintenance capabilities and logistics support exist worldwide. The lightweight feature was the initial attraction to the gas turbine and this outweighed considerations of cost and noise. The high fuel consumption of the gas turbine was found not to be a controlling factor for the mission duration of craft that is measured in hours (as opposed to days for conventional ships). These factors can be seen by consideration of the specific weight of the propulsion system including that of the fuel burnt, as indicated by the following equation:

$$\begin{array}{lcl} \text{System} & \text{Propulsion System} & \\ \text{Specific Weight} = & \text{Specific Weight} + (\text{SFC} \times \text{Time}) & (188) \\ (\text{lb/hp}) & (\text{lb/hp}) & \end{array}$$

where SFC is the specific fuel consumption of the engine system measured in lb/hp·hr, and time (hr) is the cruise duration of the craft.

As seen from Figure 190, the engine system is a large part of the propulsion system for air cushion craft and it is informative to see the impact of the choice of engine system in Equation (188).

The specific weight of engines is given in Figure 191, where mean curves are drawn through data for low speed (100 to 400 rpm) and high speed (1500 to 4000 rpm) diesels, aircraft gas turbines, and marine gas turbines. With some license, the mean curve has been drawn with a slope proportional to the inverse square root of the shaft output power. This variation appears to be influenced by the bearing and torque limiting factors in present state-of-the-art shafting, which vary by the same power relationship.

There is some scatter in the various engine data for several reasons, but Table 11 summarizes the trend lines, which can be used for preliminary design purposes. Because of the scatter, however, it would behoove the designer to carefully check the engine manufacturer's data to ensure that all "optional extras" are included and that marine adaptation, in the case of the gas turbines, has been performed (for example, all magnesium components are replaced by aluminum).

It is not proposed to provide tables of engine data for turbines and diesels including specific fuel consumption and the effect of ambient temperature and operation at off-design points. These data are more

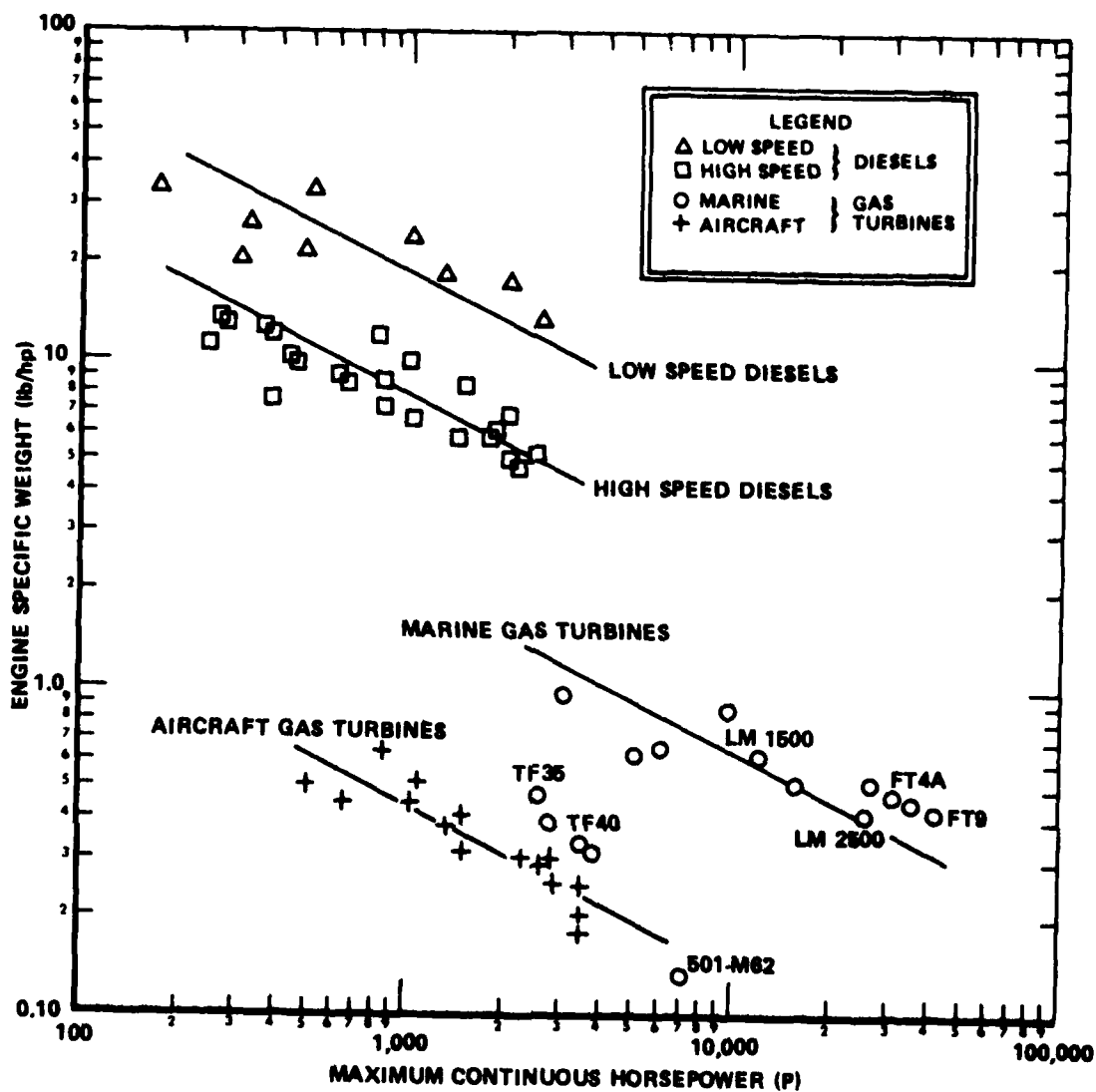


Figure 191 - Specific Weight of Engines

TABLE 11 - ENGINE SPECIFIC WEIGHTS

Engine Type	Engine Specific Weight (lb/hp)
Low Speed Diesel	$580/\sqrt{P}$
High Speed Diesel	$250/\sqrt{P}$
Marine Gas Turbine	$65/\sqrt{P}$
Aircraft Gas Turbine	$14/\sqrt{P}$

readily available in manufacturers' catalogs and designers' files. It can be seen from Figure 191 and Table 11 that gas turbines have a specific engine weight of 0.20 to 1.0 lb/hp in the engine power range of interest, namely, 1,000 to 20,000 hp, depending upon the degree of marinization. High speed diesel engines are almost an order of magnitude heavier at 3 to 10 lb/hp in the same power range.

When considering the specific fuel consumption, however, the situation is reversed in the comparison between gas turbines and diesel engines. The gas turbine has a high specific fuel consumption (SFC) varying from 0.40 to 0.80 lb/hp·hr over the range 1,000 to 20,000 hp with SFC improving with increased power. Over this same power range the diesel engine, due to its high thermal efficiency cycle, has SFC of 0.30 to 0.40 lb/hp·hr. These values are considered typical and actual data for the marine gas turbine is shown in Figure 192. The specific fuel consumption for the diesel engine is given in Figure 193. To illustrate the design choice is the following example based on an SR.N5 type of air cushion craft.

Example Problem

Consider a craft the size of an SR.N5 where approximately 1000 hp is required for propulsion and lift. Design A for such a craft uses a GE LM 100 gas turbine (1100 hp) with a specific engine weight of 0.50 lb/hp and a specific fuel consumption of 0.61 lb/hp·hr. Design B for the same craft uses a CW 12V-142 diesel engine (900 hp) with a specific engine weight of 5.85 lb/hp and a specific fuel consumption of 0.40 lb/hp·hr.

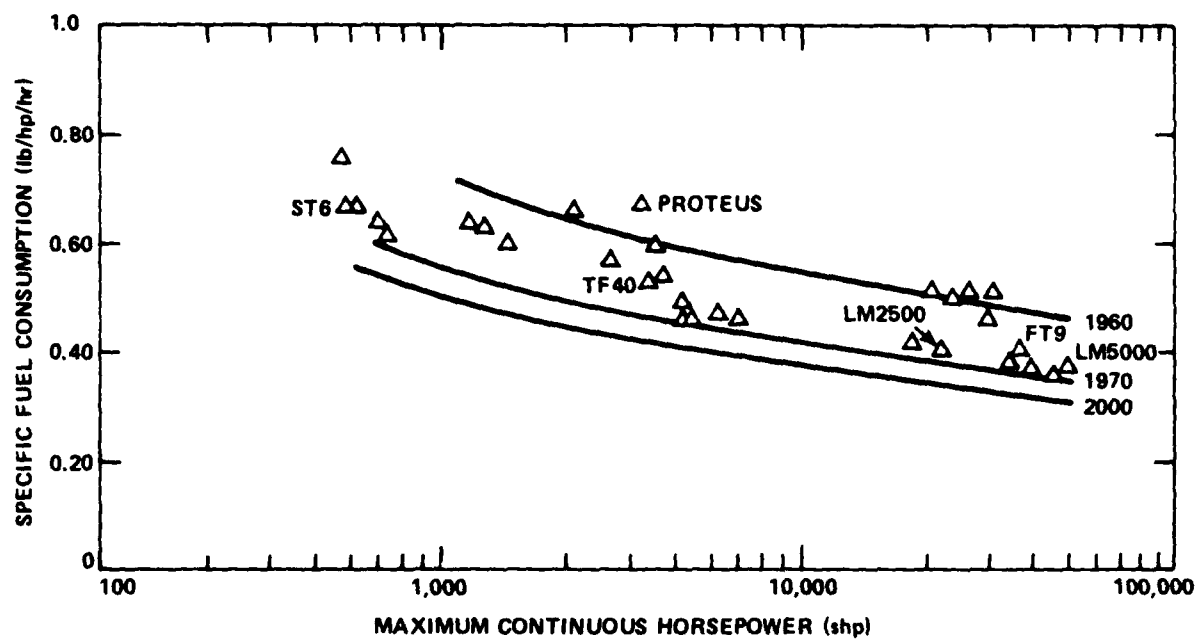


Figure 192 - Specific Fuel Consumption of Marine Gas Turbines

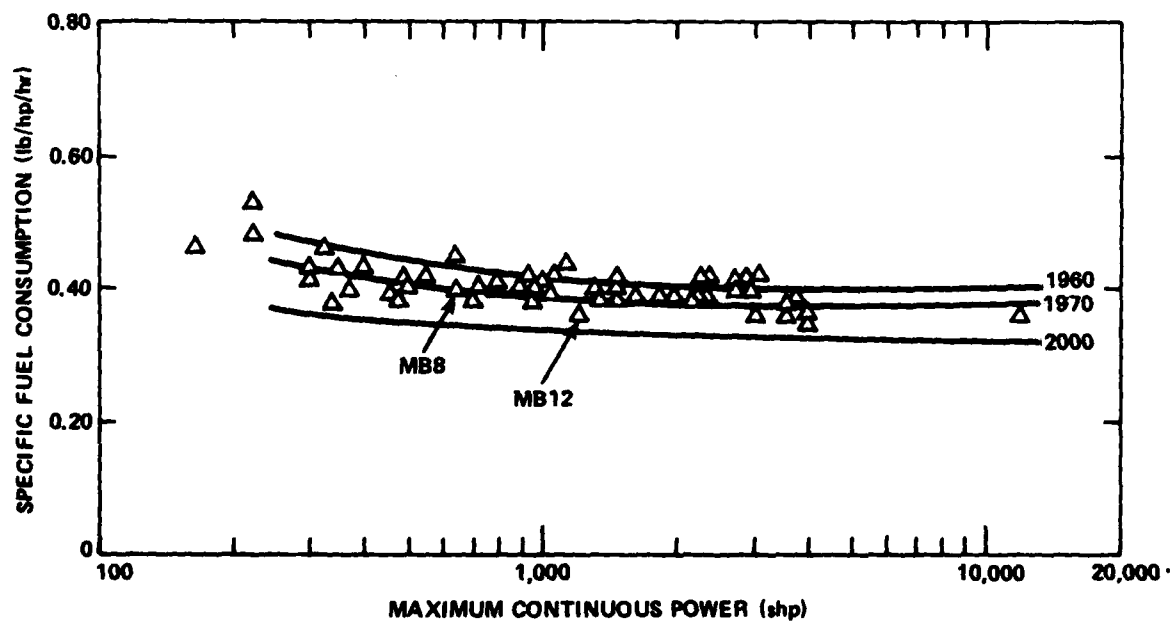


Figure 193 - Specific Fuel Consumption of Diesel Engines

Ignoring differences in installation and transmission, what is the maximum mission duration for which the gas turbine installation is the lighter installation?

Solution

From Equation (188) the weight of the gas turbine powered system is given by:

$$\text{System Weight (lb)} = (0.50 \times 1100) + (0.61 \times 1100) \times \text{Time}$$

Similarly for the diesel powered system:

$$\text{System Weight (lb)} = (5.85 \times 900) + (0.40 \times 900) \times \text{Time}$$

The two systems have the same weight when,

$$550 + 671 t = 5265 + 360 t$$

i.e., when the time (t) = 15.16 hours.

For all mission durations shorter than 15 hours the gas turbine system is the lighter installation.

Such simple analyses illustrate why the majority of air cushion craft use the gas turbine although some notable exceptions such as the HM-2 series and the recent Bell-Halter craft (BH-110) have elected to use the diesel engine on the basis of cost. This cost impact is indicated, for example, by the relative costs of the HM-2 series compared to other air cushion craft (Figure 149, Chapter VII) that are influenced by the choice of powerplant as well as the other cost factors already discussed.

Trillo¹⁴³ gives a more complete economic analysis on these factors.

Marron¹⁴⁴ gives a useful set of parametric equations describing the design performance and off-design performance of the marine gas turbine engine.

With this general introduction to the propulsion system, the various elements of the propulsion system will now be discussed and the state-of-the-art indicated.

The problems that have occurred in air cushion craft use of marine gas turbines may be listed as follows:

- a. Power degradation with increased ambient temperature.
- b. Susceptibility to engine (compressor) stall due to inflow distortions.

- c. High air mass flow requirements.
- d. Susceptibility to FOD.
- e. External noise generation.
- f. Susceptibility to contamination in the fuel and air intake.

Of these, the most severe problem, in that significant costs and delays have occurred in both commercial and military operations, is that of contamination (f), especially that due to the salt from the seawater in the engine intake air. The first five problems, although detrimental to craft operations, have not caused problems as major as those associated with contamination. The following notes pertain to the experienced problems.

Temperature Effect

In the case of (a), the degradation of power with increased temperature is a known characteristic and can be taken into account in any performance analysis. The typical performance loss is approximately 4 percent for every 10°F rise in ambient temperature. For comparison, the diesel engine suffers a 3/4- to 1-percent loss for every 10°F rise.

Air Flow Problems

Problems (b) and (c) are coupled, due to the air flow requirements, and are usually solved by designing large plenum chamber-type inlets to the engines, thereby keeping flow velocities at a minimum and keeping the actual engine inlet away from the external crosswind flows. It has become common practice to design for 10 to 15 ft/sec in the inlet plenum to reduce flow distortion problems and pressure losses. Although this causes large volume requirement gas turbine engine installations, it must be noted that the basic gas turbine engine starts with an advantage in space requirements. The gas turbine occupies a space of between 0.01 to 0.08 ft³/hp over the power range of 100 to 20,000 hp. Thus, on a total system basis, the very compact nature of the gas turbine can accommodate large intakes (and exhausts) to optimize flow and minimize pressure losses.

Foreign Object Damage

The susceptibility to foreign object damage has also been a matter of design and good maintenance procedures. Designing engines to be in engine rooms in common with ship practice as on the SR.N4, the U.S. Navy SES, and AALC craft has minimized this problem. Only isolated incidents of FOD, such as bolts breaking away from a bracket in the engine room and entering the compressor section, have occurred over the many thousands of hours of operation.

Engine Noise

The noise of gas turbine engines is a definite problem that has hampered acceptance of air cushion craft in many residential areas. While

it is recognized that noise analysis involves a complex combination of many factors, among them engine characteristics, method of insulation, and background noise, some typical values have been prepared by different groups.

Hamilton-Standard¹⁴⁵ gives noise values based on available engine data on existing turboshaft engines in the 50- to 3500-hp range. The maximum noise level on the average of the (unmuffled) engines at 100 ft is given as

$$\text{dB(A)} = 72 + 8.2 \log P \quad (189)$$

where P is the power level (in horsepower) of the engine. From the test data, the noisiest engine was 5 dB(A) above the average value given by Equation (189) and the quietest engines were 5 dB(A) below. This equation would predict 96 dB(A) for an average 1000-hp engine at 100 ft, 105 dB(A) for a noisy engine, and 91 dB(A) for a quiet engine. Similarly, for a craft of SR.N4 or SES-100 size, power noise levels on the order of 100 dB(A) would be predicted. Very little systematic evidence of a reliable nature has been collected on noise levels on air cushion craft; data that have been collected are usually very subjective. It is also difficult to distinguish the noise from the propellers, which are noisier than the engines, but this again depends on the installation and method of insulation. It is generally agreed that the craft are very noisy, and ear protection is worn by any personnel assigned to work in the near vicinity. In many respects, the air cushion craft suffers from the same problem as V/STOL aircraft and helicopters, where full power from the engines is experienced during takeoff and landing only a short distance from personnel. This is in contrast to the conventional aircraft that develop the same noise level but do so out on the runway several hundred feet from personnel.

These factors have influenced the design of some air cushion craft that have replaced the gas turbine with the reciprocating automobile engine and the air propeller with fan propulsion. This is discussed later.

Filtration

Inadequate filtration on installed engines in air cushion craft has caused the major headaches in engine reliability. Protecting the engine from the marine environment has been more of a developmental program than initially realized by the air cushion craft designer. Some problems of fuel contamination by seawater have been bothersome but are overshadowed by the contamination by seawater in the intake air.

Although the air cushion craft designer expected the marine gas turbine to be a rugged animal, capable of handling an occasional ingestion of water, the engine manufacturer was requiring this occasional ingestion to be such that the salt concentration in the intake air be no more than 0.01 part per million (ppm) by weight. Much more than this and serious

degradation in engine life would be experienced. In 1959, the spray generated by the SR.N1 approached a maximum value of 3 gallons per hour per square foot of intake (at a craft speed of 10 knots). The salt concentration was as high as 10 ppm!

Since that time, several improvements have been made in the air filtration systems of operational craft to reduce the salt buildup, and it is only now that the engine manufacturer's target is being approached. The problem of salt buildup manifests itself in accelerating the corrosion rate on stressed components such as compressor blades and can rapidly reduce the fatigue life to values like 25 percent of the original value. The problem has occurred on craft installed with what are now considered rugged "workhorse" marine engines such as the Rolls-Royce Nimbus on the SR.N2 (1962), the Gnome on the SR.N3 (1964), the Proteus on the SR.N4 (1969), and the Pratt and Whitney FT12A-6 on the SES-100B (1972). These engines had also seen extensive marine application and had passed the Navy qualification program. The problem has also occurred on engines that have been marine adapted but that have not been subjected to rigid Navy qualification programs such as the Avco-Lycoming TF-35 on the SES-100A. Several compressor failures have occurred due to the salt buildup and, in some cases, have reduced engine life to a matter of minutes.

Although these engines have been used in marine applications in the past, such as in gunboats and hydrofoils, it is the continuous operation in a spray environment of the air cushion craft that causes the problem. The seaplane, with its heavy spray environment during takeoff and landing, did not reveal this problem due to its relatively short exposure times to spray. In addition to the exposure to spray (and salt), it is found that the stress-corrosion has a cumulative effect, causing continual performance degradation. Hence, two essential elements are interwoven in the prevention of engine life degradation: a good filtration system to minimize the salt content and a good engine wash system to prevent buildup.

The early experience gained on the SR.N series of craft proved invaluable in evolving solutions. The initial schemes after the SR.N1 tests involved installation of polypropylene knit-mesh filters at low angles to the flow (15 deg) that were designed to reduce air velocity to 10 ft/sec. Such a scheme for the SR.N2 and the SR.N3 is shown in Figure 194a. Knit-mesh filters with their characteristic low flow velocities (15 to 20 ft/sec) were the main filtration or demister methods used in the SES-100A and SES-100B craft. An indication of the sensitivity of such installations may be gaged by the results of a pinhole that occurred in the structure some 2 ft from the Gnome engine in the SR.N3. This pinhole created a significant leak due to the low pressure in the engine room and, within a matter of minutes, due to salt buildup, reduced the power output by 50 percent!

Another scheme employed on the SR.N5, during operations in 1973 in Aden, employed vortex separators between the knit-mesh filters and the engine intake in an attempt to keep sand ingestion to a minimum. Prior

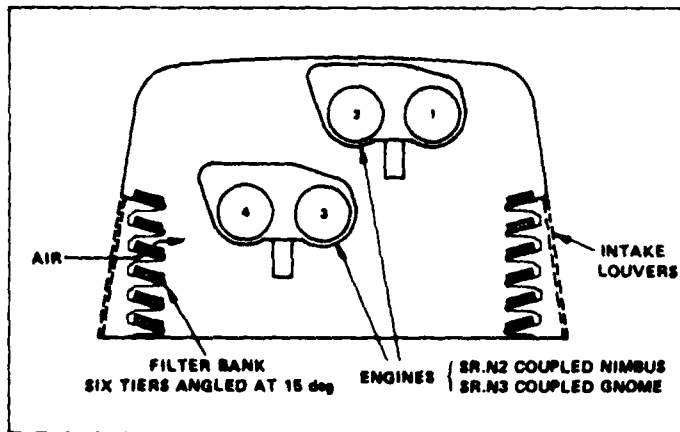


Figure 194a - SR.N2 and SR.N3 Filtration

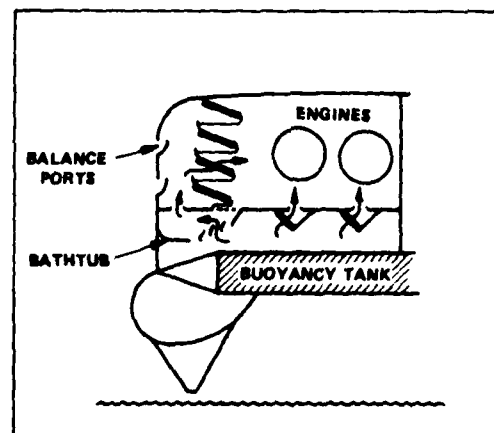
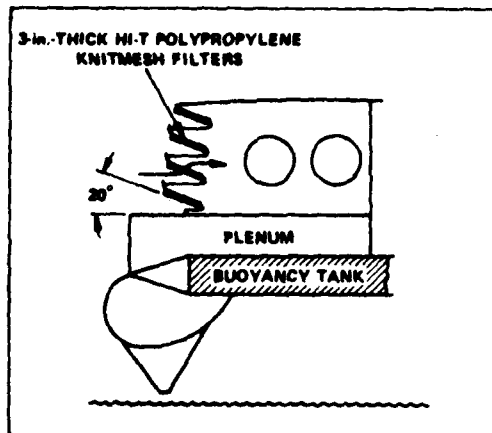


Figure 194b - SR.N4 Initial Installation Figure 194c - SR.N4 1969 Installation

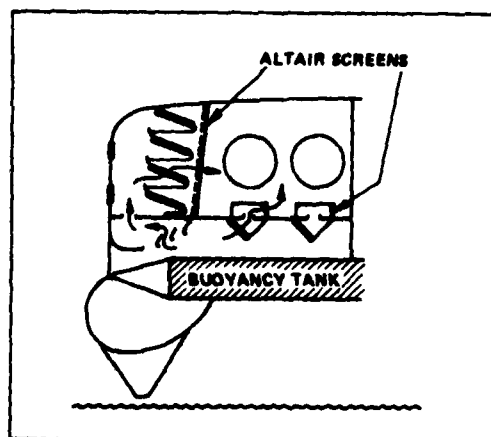


Figure 194d - SR.N4 1974 Installation

Figure 194 - SR.N Engine Air Filtration Schemes

to this modification, the engine life was 6 hr on one engine and 7 hr on another, and the filter efficiency was measured as 94 percent. After introduction of the vortex separators in conjunction with the knit-mesh filters, the filter efficiency was raised to 98 percent, and the engine life increased correspondingly to 1500 hr.

The SR.N4 went through several stages of development before an acceptable filtration system was achieved. Wheeler (Reference 106) discusses the development of the filtration system from its initial form (Figure 194b), where spray-laden air was drawn in directly from atmosphere, through a bank of knit-mesh filters to the form existing in 1969 (Figure 194c), where additional filtration from fan air is used. Since 1969 development has continued and, as of 1974, a double filtration system is used (Figure 194d) where the air coming from the outside and the plenum is first filtered through the polypropylene knit-mesh filters as before, then through finer hair-like material filter pads called Altair. Although this has considerably improved the situation, it is reported that the craft operators (Hoverlloyd and Seaspeed) are still not able to keep salt concentration much below 0.02 to 0.10 ppm and engine life much above 2000 hr.

Engine washing has also been developed. In some cases, simple washing with tap water merely washed the salts from the compressor back onto the turbine blades, which in many respects is a worse problem. This occurred in 1963-64 on the SR.N3 and occurred again in 1972 with simple engine washing of Pratt and Whitney FT12A-6 engines on the SES-100B. The practice now for the U.S. Navy SES is normally to use a demineralized water wash immediately after a run or mission. This procedure was followed with particular rigor on the SES-100A during the rough water trials program in 1973-74 and, provided the engine manufacturer's recommendation of washing after every 45 minutes of engine operation was followed, no further engine compressor failures were experienced.

For the SR.N4 operations in 1974, it was decided that water washing was not adequate in removing salt deposits, and carboblasting was integrated into the preventive maintenance program. This technique, familiar to conventional aircraft maintenance mechanics, consists of introducing crushed walnut shells or soft blast grit into the compressor. This grit is applied at the rate of 1 lb/10 hr of engine operation and is thrown into a hopper that sucks it into the engine compressor. This technique is fairly successful at removing salt deposits and improving engine life, but the grit has a tendency to find its way into the oil system and clog up the jets! But that is what development is all about.

In the light of this experience, other filtration schemes are being developed in connection with air cushion craft, such as the U.S. Navy JEFF craft. These include centrifugal or vortex separators to remove the bulk of the water prior to entering the knit-mesh filters. In some ways, these are similar to the type used on the SR.N5 operations in Aden, although they were used upstream of the knit-mesh filters. Other filtration schemes, such as the Peerless and Farr type filters, are also being explored.

In summary, the engine filtration system would seem to be settling on the following system:

1. Primary debris separator -- in the BHC system as used on the SR.N4 the lift fan is used together with a baffle system to reduce the air pressure fed into the engine room.
2. "Heavy" droplet coalescer -- such as the knit mesh, Peerless or Farr type filters.
3. Particulate filter -- for the finest separation of the salt from the spray, such as the Altair pads.

Because the problem is initiated by the cushion-generated spray, and the trend to high cushion pressures and flows will aggravate this problem, more detailed investigation of spray generation is required. It will be noticed from the above discussion that the spray problem has plagued the sidehull SES designer as much as the fully-skirted air cushion craft designer. The solution may be a simple one, such as that suggested by

Polak¹⁴⁶ where, by notching the hemline of the individual fingers, a cushion-pressure-generated jet pump effect deflects the spray pattern rearward and below the gunwhale level of the craft and, thus, away from the engine intakes. Unfortunately, wear at the skirt hemline rapidly reduces this effect. Only further development, especially on full-scale craft, will provide the necessary information.

Recently,¹⁴⁷ Mackley-Ace have developed a variant of the spray suppressant idea by using an apron-like skirt, hung over the basic skirt to provide a "trap" that turns the spray down and away from the craft before it can be ingested into the engine system. Figure 195 is a sketch of the skirt technique used. Perfection of such techniques, while admittedly in

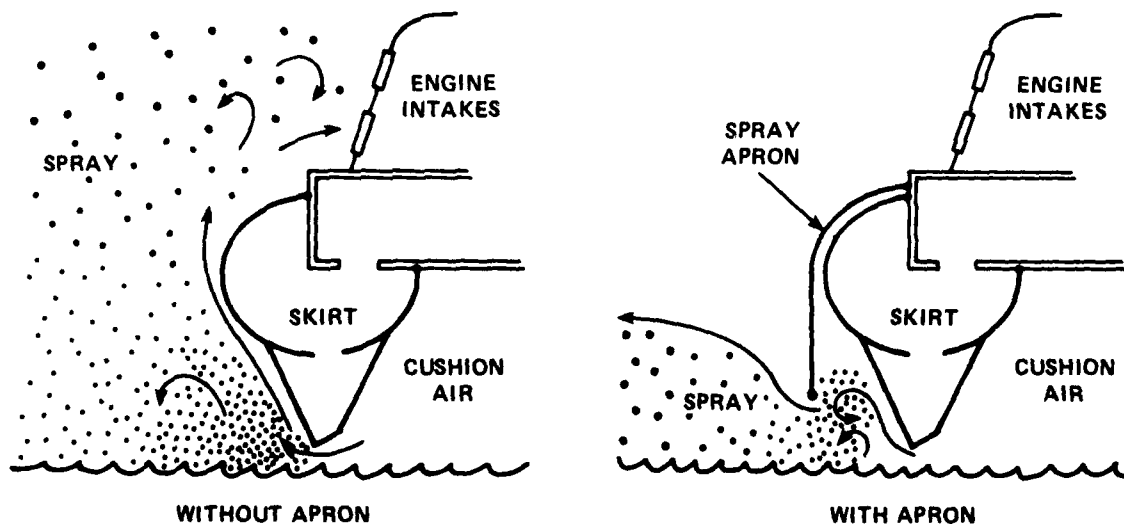


Figure 195 - Spray Suppressant Skirt

in the early development stages now, may well alleviate much of the engine filtration problems discussed above.

The elimination or suppression of spray is also advantageous in increasing the life of other major propulsion elements such as the propellers. This concern is shown, for example, in Figure 196 which shows the spray pattern under certain operating conditions for the JEFF(B).

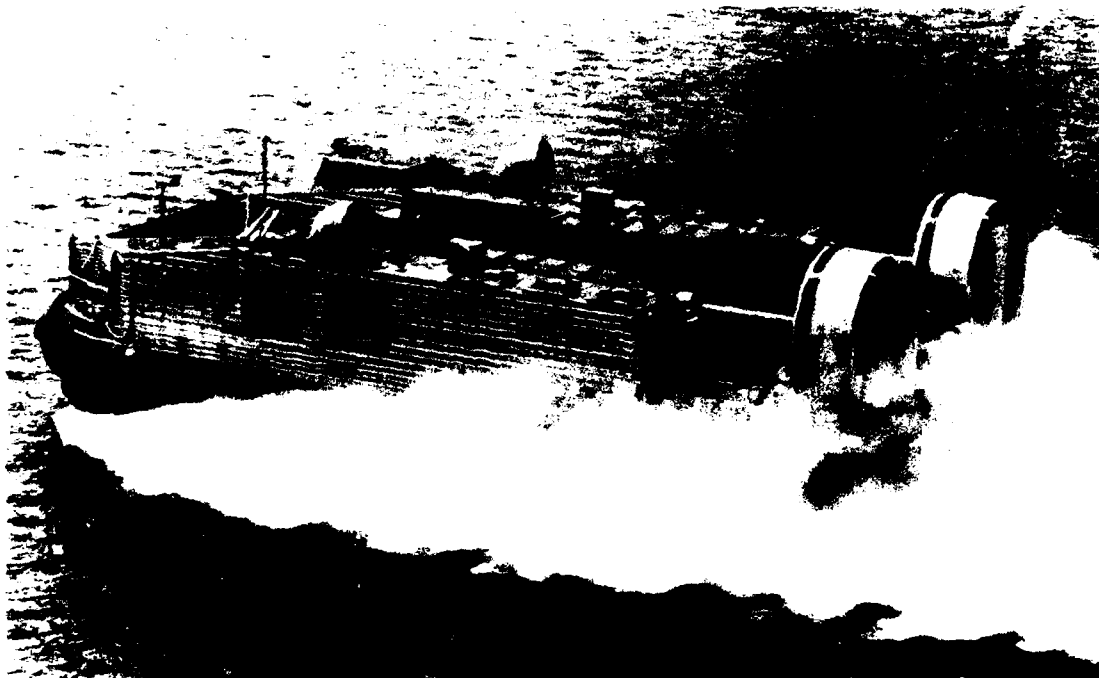


Figure 196 - JEFF(B) Operating in Spray

PROPULSORS

As mentioned at the beginning of this chapter, a variety of propulsor types have been used to propel air cushion craft. These include air propulsion by air propellers (free and shrouded) and by air jets (cushion air and jet engines). Also included is water propulsion by water propellers and by waterjets. The development of each of these types of propulsors as they have been used on various air cushion craft will be discussed.

Air Propulsion

In Chapter III on performance, it was noted that there are two main design points of interest for each of the environmental and weight conditions. The propulsor must produce efficient thrust both to maintain speed, and to accelerate past hump speed. Accordingly, because air propulsion thrust curves are usually monotonic, it is convenient to consider

(a) static thrust and (b) thrust efficiency at speed to categorize air cushion craft air propulsion. A typical set of curves for a high cushion density craft of approximately the 150-ton displacement class is given in Figure 197 showing how, for the air propulsor, hump drag (primary and secondary) sets the requirement for static thrust. The most commonly used means is, of course, the air propeller.

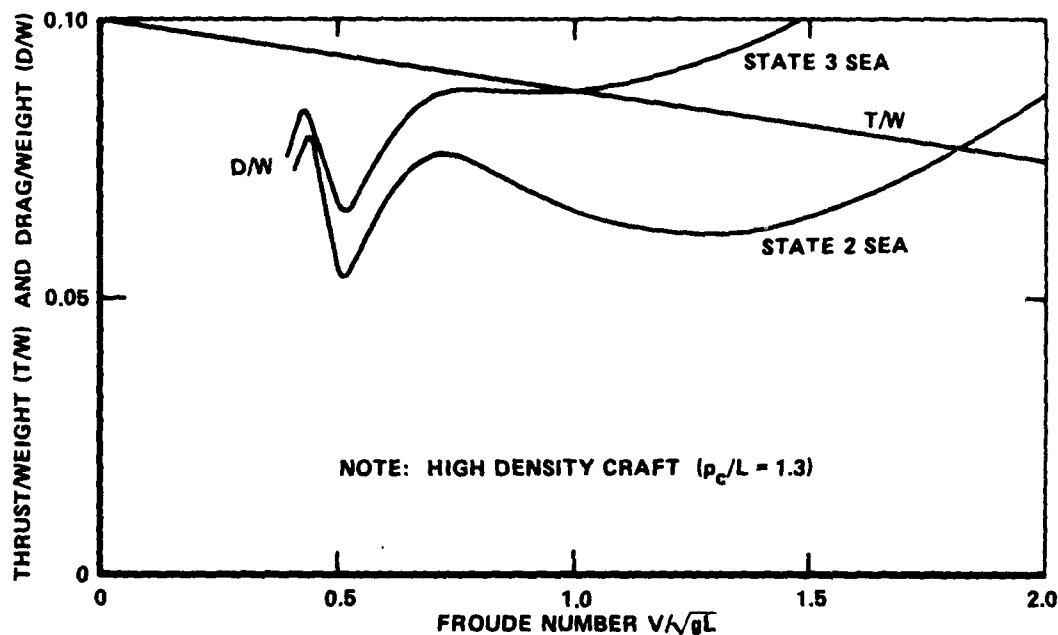


Figure 197 - Typical Thrust and Drag Curves

A more complete treatment of the thrust, to meet certain acceleration requirements to exceed the hump speed, is provided in Appendix C.

Air Propellers. The air cushion craft propeller has had the advantage of a background with a wealth of data available from the aircraft industry. It should not be surprising, therefore, to find that the first propellers for air cushion craft were merely adaptations of existing aircraft propellers. As the craft have developed, this situation has changed somewhat because of the unique requirements for air cushion craft use, and a new form of propeller is emerging. Table 12 is a compilation of several representative air propellers, both free and shrouded, that have been in operation on existing craft. It also includes some propellers about to be installed on craft still in construction and some design study propellers.

The static thrust of these propellers is plotted in parametric form in Figure 198, where a distinction is made between the free or unshrouded propeller (open symbols) and the shrouded or ducted propeller (closed

TABLE 12 - AIR CUSHION CRAFT AIR PROPELLERS

Craft	Manufacturer	No. of Propellers	Propeller Type ^a	Propeller Dia. (ft)	No. of Blades	Design Speed (rpm)	A.P. ^{aa}	C _{L1}	Static Thrust (lb)	Thrust at Speed (lb at knots)	Efficiency, (percent = 10 ³)	hp	Weight (lb)	Material	Remarks	
SEB-1	Hell/Hamilton Standard	2	S	9	3		156	0.465	3,200			450	345	Aluminum		
SE-5	Hell/Hamilton Standard	1	F	9	3		156	0.465	2,900		45	800	340	Aluminum		
Voyager	Hell/Hamilton Standard	2	F	9	3	2,000	156	0.465	3,700			1,200	340	Aluminum		
Viking	Hell/Hamilton Standard	2	F	9	3	1,500	156	0.465	1,600			600	340	Aluminum		
JUPY (A)	Avcojet/Hamilton Standard	4	S	7.5	4	1,780	269	0.984	10,200		45	3,600	820	Aluminum	Michal plate protection	
JUPY (B)	Hell/Hamilton Standard	2	S	11.75	4		183	0.707	17,200		55	5,000	744	Aluminum	Polyurethane Paint	
HP-PP05	Siemens/Hamilton Standard	2	F	8.5	3		109	0.509	940			300	149	Aluminum	Michal Plate	
Arctic 5007	Boeing/Hamilton Standard	4	S	13.5	4		153	0.593	28,800			8,500	830	Steel Spear QCP shell	Design Study	
Arctic 10002	Hamilton Standard		Q	20	9		183	0.700	86,000			3,200		Steel Spear QCP shell	Design Study	
SE-86	ME/Dunwo Metal	1	F	9	4	2,000	115	0.650				800	283	Aluminum		
SE-86 864	ME/Dunwo Metal	2	F	10	4	1,025	145	0.720				1,100	659.5	Aluminum	Spray coated polyurethane Michal plated helical shaft	
SE-86	ME/Dunwo Metal	1	F	9	4										Carbon fibers reinforced forced foam filled QCP microfoils	
SE-86	ME/Dunwo--Stability	4	F	19	4	622	108	0.700	9,000		50-60	1,800		Aluminum	Rubber L.F. Protection	
SE-7	ME/Dunwo--Stability	1	F	21	4	622	117	0.600	12,700			3,000	1,792	Aluminum Spear QCP shell	Michal shaft LP and polyurethane paint	
VT 2	VT/Dunwo Metal	2	S	13.5	7	675			13,700	10,500 at 60 11,200 at 70		4,000	1,244	Foam filled QCP		
H-500	Boeing/Dunwo--Stability	3	F	21	4		127	0.600								

^aQ = Squared propeller; Q = Q fan; F = True propeller
^{aa}SE-2 and Arctic 5007 are Arctic 5007

^aQ = Threaded propeller; Q = Q fan; F = Fan propeller
^{aa}A.P. = Activity factor

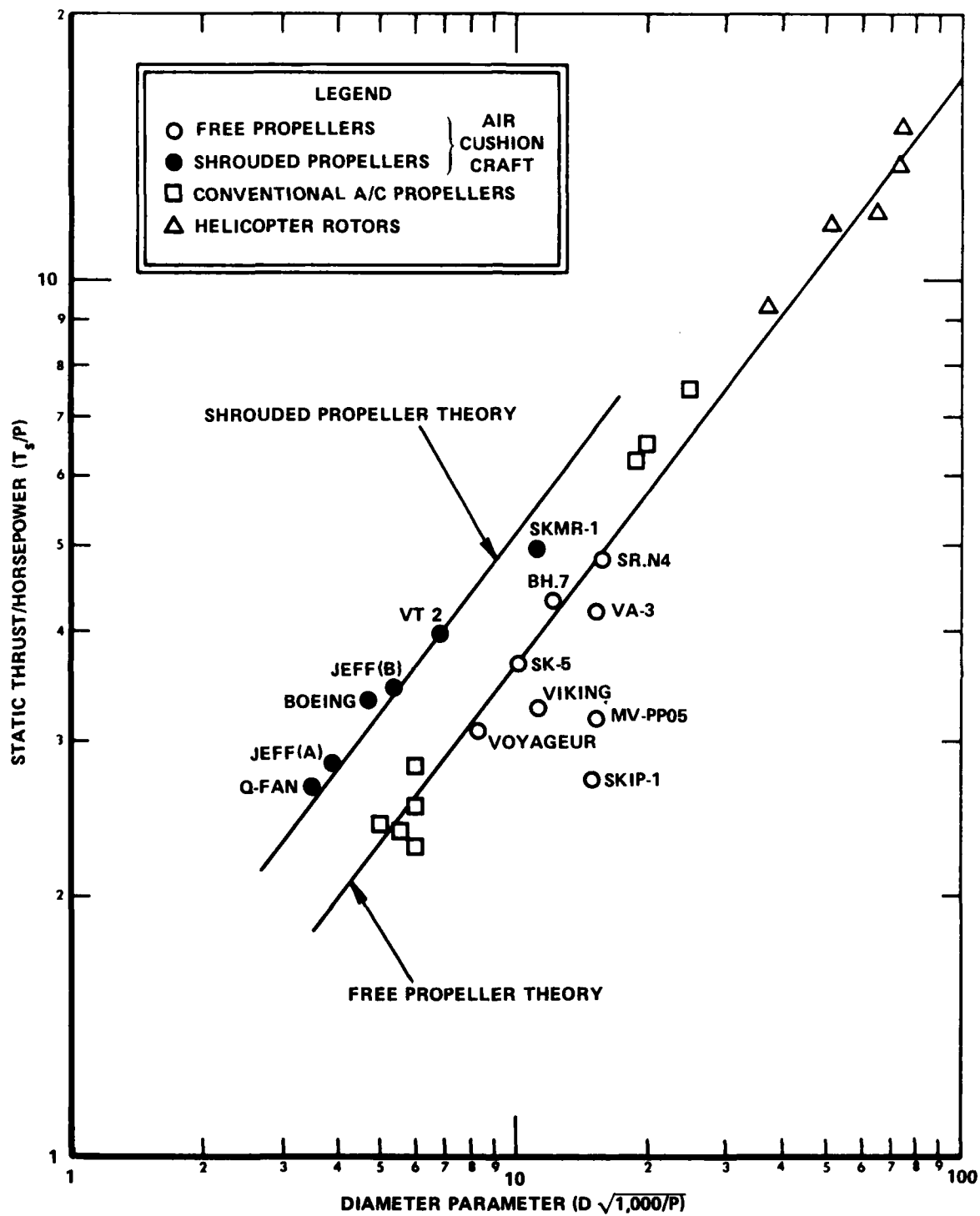


Figure 198 - Static Thrust of Air Propellers

symbols). Included with the free propeller data are some conventional aircraft and helicopter rotor static thrust values to show the family resemblance with the air cushion craft propeller. Even though there is a wide range of propeller activity factor (A.F.) and integrated design lift coefficient (C_{L_i}), there is seen to be a consistent trend except for some isolated off-design propellers. Prior to discussing these propellers and their characteristics, it is necessary to describe the nature of the curves labeled "theory" in Figure 198.

For the free propeller theory, it is known from simple momentum theory¹⁴⁸ that, for an actuator disk of diameter (D) producing a static thrust (T_s), the ideal power (no losses) is given by

$$P_i = \frac{T_s^{3/2}}{\sqrt{2\rho A_p}} \quad (190)$$

where A_p is the propeller area ($\pi D^2/4$) in ft^2 and ρ is the density of air in slugs/ft^3 . In Equation (188), if T_s is measured in lb, the ideal power is in ft-lb/sec .

It is conventional practice to define a "figure of merit" (F.M.) that collects the real fluid effects and is defined as

$$\text{F.M.} = \frac{P_i}{P} \quad (191)$$

where P is the actual power at the propeller shaft. The static thrust per unit power input for the free propeller can then be written, after some rearrangement, as

$$\frac{T_s}{P} = \frac{550^{2/3} (\text{F.M.})^{2/3}}{10} \left(\frac{\pi\rho}{2} \right)^{1/3} \left[D \sqrt{\frac{1000}{P}} \right]^{2/3} \quad (192)$$

where the power (P) is now expressed in hp. Different values of F.M. are given, depending on the number of blades and whether the propeller is dual or single rotation. For the case of single four-bladed propellers, F.M. = 0.75 and the prediction for the static thrust would be

$$\frac{T_s}{P} = 0.86 \left[D \sqrt{\frac{1000}{P}} \right]^{2/3} \quad (193)$$

which is the line labeled "free propeller theory" in Figure 198. It applies to the majority of the air cushion craft propellers and generally applies to conventional aircraft propellers and helicopter rotors. For clarity, conventional aircraft propeller data have been omitted in the diameter parameter range, $7 < D \sqrt{1000/P} < 20$, which is the range for the air cushion craft propellers.

Simple momentum theory also gives the static thrust for the shrouded propeller from the ratio as

$$\frac{(T_s)_{\text{shroud}}}{T_s} = 1.26 \left(\frac{D_s}{D} \right)^{2/3} \quad (194)$$

where D_s is the outside diameter of the shroud. For the typical shroud in use on air cushion craft, the shroud diameter is 15 percent greater than the propeller diameter. Hence, one can construct a shrouded propeller theory including real fluid effects to give

$$\left(\frac{T_s}{P} \right)_{\text{shroud}} = 1.08 \left[D \sqrt{\frac{1000}{P}} \right]^{2/3} \quad (195)$$

which describes the shrouded propeller data shown in Figure 198.

Although most of the propellers shown are of a conventional propeller form with a low number of blades (three or four), two of the shrouded propellers approach the ducted fan geometry. These are the VT 2 ducted propeller with seven blades (see later section on propeller construction) and the Hamilton-Standard Q-fan design study with nine blades for a 1000-ton air cushion craft. It should also be noted that, of the propeller data shown, only the SKMR-1 represents full-scale trial data.

Propulsive Efficiency. The second major design point in the aerodynamic design of the air cushion craft propellers is the high speed condition where, to reduce power requirements, high efficiency is sought. Again, from simple momentum theory, the ideal efficiency can be shown to be a function of the disk loading or thrust coefficient (C_T) defined as

$$C_T = \frac{T}{1/2 \rho V^2 A_p} \quad (196)$$

At equilibrium speed V , it is seen that the thrust coefficient of the propeller(s) must be of sufficient magnitude to equal the drag coefficient through the relation

$$C_T = \frac{S}{nA_p} C_D \quad (197)$$

where n is the number of propellers,

S is the cushion area, and

C_D is the total drag coefficient determined from Chapter III.

The simple momentum theory gives, for the maximum ideal efficiency of the free propeller,

$$\eta = \frac{2}{1 + \sqrt{1 + C_T}} \quad (198)$$

and, for the shrouded propeller,

$$\eta = \frac{4}{3 + \sqrt{1 + 2C_T}} \quad (199)$$

The methods of calculating the real fluid effects with propellers of thickness, camber, and solidity, are well documented. The standard references by Hamilton-Standard on free (unshrouded) propeller¹⁴⁹ and on

shrouded propellers¹⁵⁰ cover a range of design parameters including: activity factors (A.F.) from 100 to 180, three and four blades, and integrated design lift coefficients (C_{L_i}) from 0.30 to 0.70. Other factors

pertinent to propeller design are the hub-to-tip diameter ratio and pitch-to-diameter ratio. The activity factor and integrated design lift coefficients reflect the capability of the propeller to absorb power and are defined by

$$A.F. = \frac{100,000}{16} \int_{r_H/r_p}^{1.0} \frac{c(x)}{D} \cdot x^3 \cdot dx \quad (200)$$

and

$$C_{L_i} = 4 \int_{r_H/r_p}^{1.0} C_L(x) \cdot x^3 \cdot dx \quad (201)$$

In Equations (200) and (201), $c(x)$ is the local blade chord, r_H is the radius of the propeller hub, r_p is the propeller tip radius, and x is the radial distance along the blade divided by the tip radius. The integral expression in Equation (200) is proportional to the power absorbed by the propeller blade for the case of constant lift coefficient and camber; hence, the activity factor is a measure of this power absorption capability. It has an analogy in water propeller work with the solidity and blade area ratio parameters. The constants outside the integrals in Equations (200) and (201) are completely arbitrary constants of proportionality.

If the camber and lift coefficient vary along the blade, then the power absorption is measured by the integrated design lift coefficient given by Equation (201). Hence, the effects of varying blade planform and blade cross section can be determined by varying A.F. and C_{L_1} . Sheets and

Mantle¹⁵¹ compiled the Hamilton-Standard propeller data as a function of the thrust coefficient C_T and showed that the data could be contained within a ± 2.5 -percent bandwidth envelope, with the largest activity factors and integrated design lift coefficient providing the upper values of efficiency. This compilation is shown for the free propellers in Figure 199 and for the shrouded propellers in Figure 200. It can be seen from the two sets of data that the free propeller efficiency is approximately 82 percent of the maximum ideal efficiency predicted by the simple momentum theory (Equation (198)) and that the shrouded propeller efficiency is approximately 85 percent of the maximum ideal efficiency.

Although varying the A.F. and C_{L_1} parameters certainly varies the value of the propeller efficiency, by far the controlling factor is the thrust coefficient C_T which, for a given craft speed, is controlled by the propeller diameter. Superimposed on Figures 199 and 200 are some typical air cushion craft propeller efficiencies. Compared to aircraft, the forward speed of air cushion craft is fairly low at 50 knots (typical), such that the thrust coefficients tend to be high and to the right of most of the Hamilton-Standard aircraft propeller data. This high value of thrust coefficient keeps the maximum attainable efficiencies low. Several distinct approaches have been taken by air cushion craft designers to offset this particular characteristic. The most direct approach is to increase the propeller diameter, and the Hawker-Siddeley Dynamics 19-ft-diameter propellers for the SR.N4 were the first large propellers for such use. Elsley and Devereux³⁸ provide more detailed analyses leading to the selection of the 19-ft-diameter SR.N4 propeller. Propeller curves provided by the propeller manufacturer give the efficiency for the SR.N4 free propeller in Figure 199, showing it to be an extension of aircraft propeller technology using propellers of A.F. = 108 and $C_{L_1} = 0.700$. For the SR.N4 to achieve

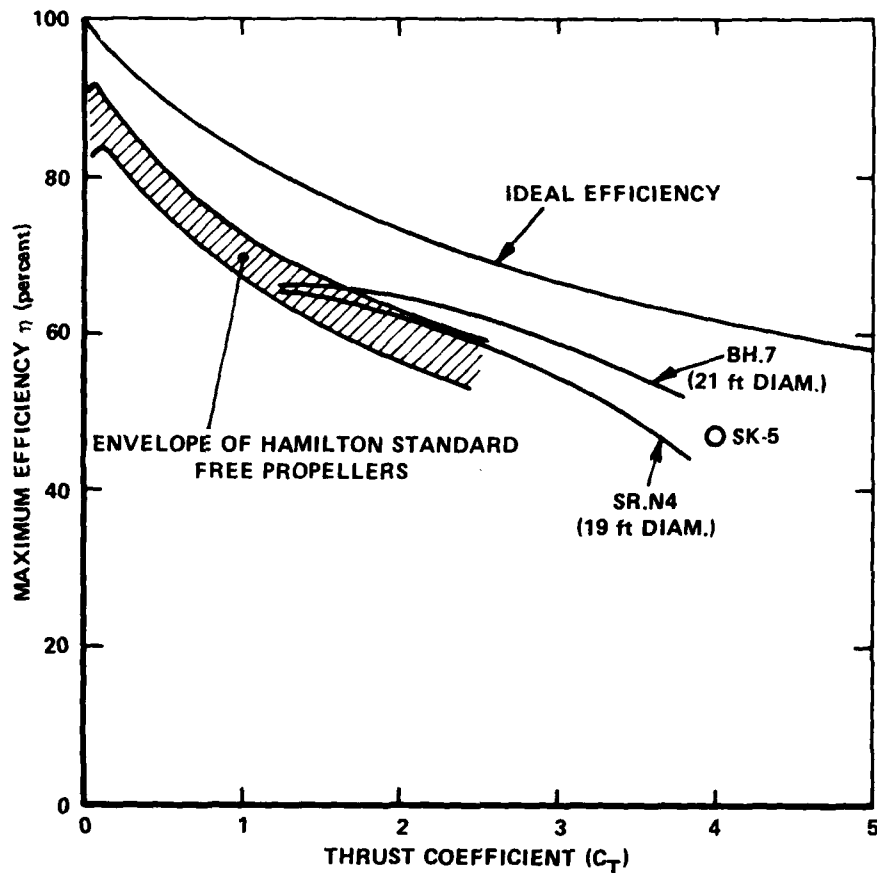


Figure 199 - Free Propeller Thrust Efficiency

propeller efficiencies above 60 percent, craft speeds of 60 knots had to be maintained. At 50 knots, which is the limit placed by the operator on the English Channel crossings to minimize skirt wear, the propeller efficiency would be typically less than 50 percent, similar to the typical efficiencies for an SK-5 craft. The values shown in Figure 199 are for the best pitch setting and rpm and represent an envelope of the maximum efficiencies. The BH.7 propeller, also designed and built by Hawker-Siddeley Dynamics, incorporated two features to improve efficiency: the first was the direct method of increasing the diameter to 21 ft and the second involved increasing the A.F. to 127, making it a broader blade. Approximately 3 to 5 percent more thrust efficiency was achieved for this propeller.

These propellers also represented a new development in blade construction, which is discussed later in this chapter. The 21-ft Hawker-Siddeley Dynamics propeller is also installed on the SEDAM N.500, a 236-ton mixed traffic ferry shown in Figure 15 of Chapter II.

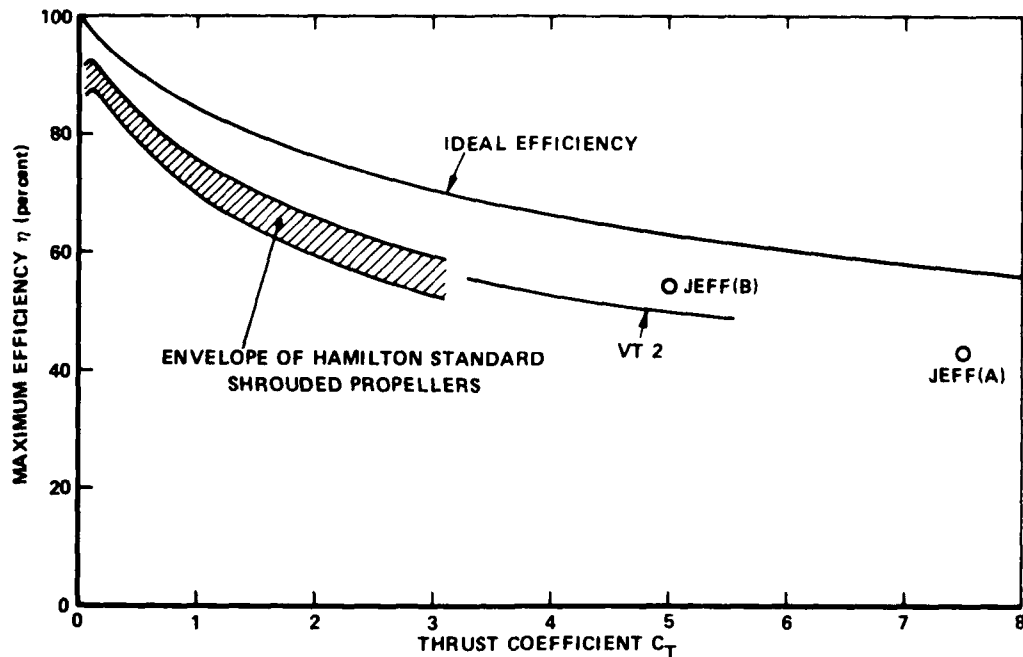


Figure 200 - Shrouded Propeller Thrust Efficiency

As the development of propellers for air cushion craft progressed, several factors started to influence the designs. Constantly increasing the diameter was, of course, not the answer. Large diameter propellers become unwieldy and introduce manufacturing problems and considerable aerodynamic interference. As the diameter increases, so does its mounting point, contributing to a pitch or roll instability. Also, for a given size craft, space is limited and wake interference must be contended with in the case of tandem operation. The high angles of yaw that air cushion craft experience induce high side forces in the propellers that have caused resonance and instabilities in some installations.

The air propeller must also be designed to keep its tip speed within reasonable values, avoiding high noise generation and compressibility losses. Tip speeds are generally kept in the 500- to 900-ft/sec range. Reference 151 gives further details on the design of air propellers to keep tip speeds within such bounds.

The shrouded propeller is one method of combatting most of the previous problems and provides, in addition, a protection to the propeller during any unlikely bumping into objects. Three current craft, the Vosper-Thornycroft VT 2 shown in Figure 201 and the two U.S. Navy AALC craft, use shrouded propellers and their representative thrust efficiencies are included in Figure 200. As in any design, there is a certain amount of compromise. Such is the case for the craft shown, where efficiency was not



Figure 201 - VT 2 with Shrouded Propellers

the controlling factor, and fairly low efficiencies are seen. It will be noted, however, by comparing with Figure 199 that, for the same thrust coefficient (C_T) as the free propeller, the shrouded propellers shown have higher thrust efficiencies.

The JEFF craft were required to fit inside the welldeck of a U.S. Navy LSD. This restricted the propeller diameters that could be used. For the JEFF(B), it was decided to keep the propeller diameter large and to maximize efficiency. This meant developing a configuration shown in the upper part of Figure 103 (Chapter V), where the large propellers rest on the cargo deck. Improved directional control for the craft was then achieved through the use of rotating bow thrusters (using lift fan air). The two shrouded propellers fixed in place are 11.75 ft in diameter. The use of these bow thrusters can be seen in Figures 202 and 203. In Figure 202 the bow thrusters are shown in the cruise condition where they provide additional thrust to the main propellers and also act as directional

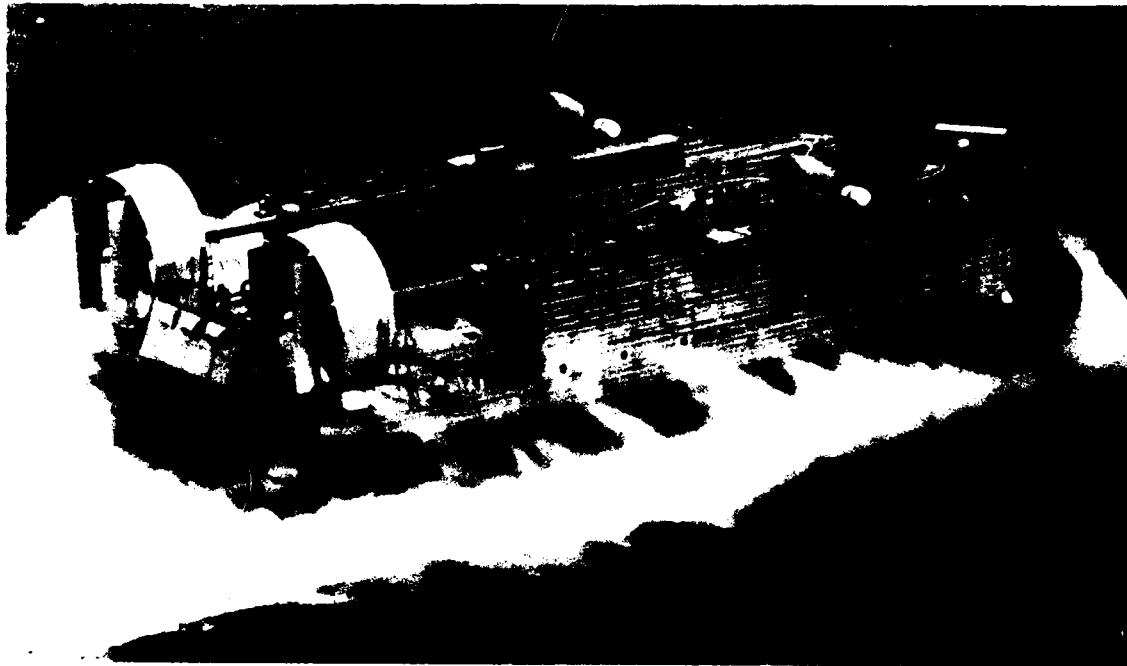


Figure 202 - Bow Thrusters in Cruise Condition

control devices. In Figure 203 the bow thrusters are shown rotated so as to give reverse thrust, as the JEFF(B) comes down the ramp to enter the water, such that the main propellers can operate at a higher power setting and generate sufficient slipstream to give greater directional control with the rudders.

For the JEFF(A) craft, it was decided to sacrifice efficiency and use four smaller identical shrouded propellers for both propulsion and control, as shown in the lower part of Figure 103 (Chapter V). The height restriction limited the shrouded propeller diameter to 7.5 feet. This resulted in a high thrust coefficient and a lower efficiency as seen in Figure 200 but gave a control system independent of the lift system. Having two such different design philosophies is an essential element of the U.S. Navy program of exploring the most promising aspects of such designs.

A similar height restriction has influenced the VT 2, but to a lesser extent; it uses two 13.5-ft-diameter shrouded propellers, thus allowing small thrust coefficients and higher efficiency.

Propeller Construction Development. The form of construction of the propellers has been influenced by several factors. The need to produce high, efficient thrust at air cushion craft speeds is a significant factor as indicated in the earlier discussion. Like the air cushion craft lift



Figure 203 - Bow Thrusters in Reverse Thrust Position

fan system, the efficiency of the propellers has required development to consistently maintain values much above 55 percent. Other factors include the need to develop erosion-free propellers, the need to develop much quieter propellers, and the associated need to develop stronger propellers at the larger diameters.

An illustration of the range of shapes and construction methods developed may be seen in Figure 204, which shows 10 such propellers developed by Dowty-Rotol specifically for air cushion craft use. Most of these propellers have been used on either the SR.N series or the VT 2 craft. The following discussion is arranged by craft for ease of reference, where propellers developed by Dowty-Rotol, Hawker-Siddeley Dynamics, and Hamilton-Standard are used.

The early SR.N5 and SR.N6 craft used conventional aircraft propellers of aluminum construction. The propeller used is a cut-down version of the Viscount aircraft propeller. While these were excellent propellers, they

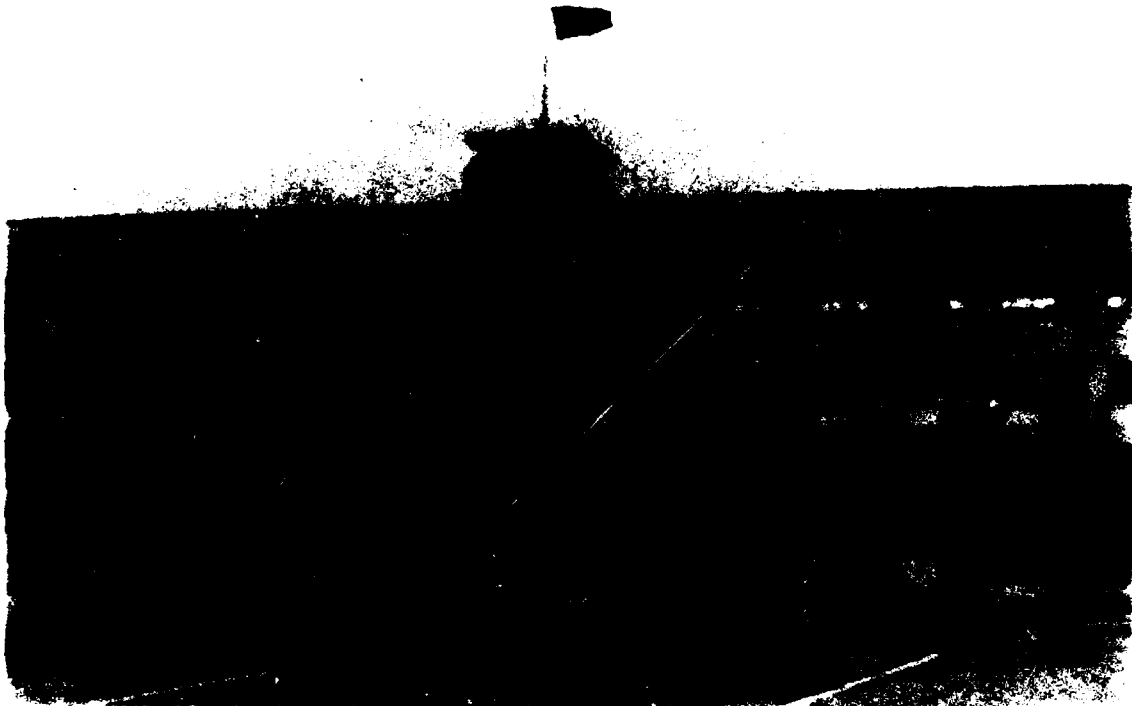


Figure 204 - Dowty-Rotol Air Cushion Craft Propellers

suffered badly from leading edge (L.E.) erosion and impact damage from stones and other objects picked up by the propeller inflow. The continuous operation in salt spray conditions and over sandy approaches to terminals quickly eroded the propellers. Some instances of erosion had also occurred with the SK-5 operations in brackish waters in the swamps of Vietnam but not to the extent of the saltwater operations in southern England. Coating the aluminum propellers completely in polyurethane, sprayed onto a depth of 1 mm, provided good protection for the blade surface but not for the L.E. This coating has enabled a 2000- to 3000-hr propeller life. Dowty-Rotol developed a nickel-plated stainless steel bolt-on guard that has been used successfully for L.E. protections. This guard can be seen on propellers 3, 7, and 8, counting from the left, in Figure 204. Russell¹⁵² reports that the bolt-on guard is easily replaced in the field and the bolt heads reduce the efficiency on the order of 4 percent.

The SR.N5 and SR.N6 were also the first craft to test the nonmetal; developed to produce high strength, quiet propellers. The wide chord propeller (seventh propeller from the left in Figure 204) is one such propeller. It is a foam-filled GRP blade bonded to a steel spar root with a polyurethane coating and equipped with the bolt-on L.E. guard described previously. Tests with over 1000 hr of operation in 1972-73 appear to be

AD-A084 740

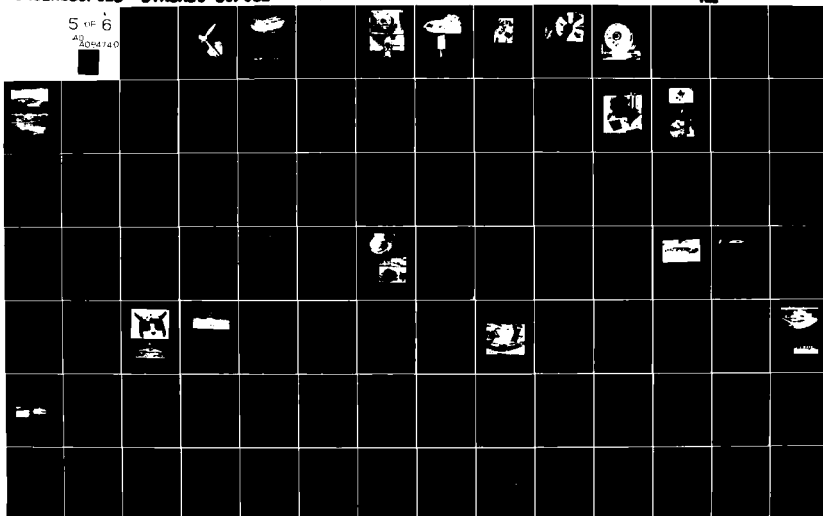
DAVID W TAYLOR NAVAL SHIP RESEARCH AND DEVELOPMENT CE--ETC P/6 13/10
AIR CUSHION CRAFT DEVELOPMENT. FIRST REVISION. (U)
JAN 80 P J HANTLE
DTNSRDC-80/012

ML

UNCLASSIFIED

5 of 6

AD-A084 740



successful. The second form of nonmetal propeller developed on the SR.N6 by Dowty-Rotol is shown in Figure 205. This blade uses a similar foam-filled airfoil section of GRP construction but the spar is also a hollow GRP form, filled with foam and reinforced with carbon fibers. The completed assembly has a polyurethane coating and L.E. bolt-on guard (not shown) used on the earlier SR.N6 propeller. This particular propeller also has had extended testing in commercial service in southern England. The U.S. equivalent of the SR.N5 craft, namely the SK-5, uses solid aluminum propeller blades developed by Hamilton-Standard. These blades have all been coated with polyurethane paint for erosion protection. The identical propellers are used on the Voyageur and Viking craft.

The SR.N6 was also modified in 1973 from its stretched version (SR.N6 Mk 1S) to incorporate a twin propulsor installation V-driven from a single 1000-hp Rolls-Royce Marine Gnome or an optional 1250-hp Lycoming TF 14 marine gas turbine engine. This modification, designated the SR.N6 Mk 6, is shown in Figure 206* and illustrates the two 10-ft-diameter four-bladed Dowty-Rotol propellers. In addition to improving the maneuverability of the craft, these propellers have improved the noise level considerably by operating at the lower speed of 1025 rpm or approximately 500 ft/sec tip speed compared to the 1900 rpm or 900 ft/sec tip speed of the single 9-ft-diameter propeller. Russell¹³⁶ reports that this has reduced the noise level by 10 dB(A). This is a considerable improvement over the annoying 90 dB(A) (approximate) noise level of the single propeller version. The 10-ft-diameter propellers are of solid aluminum construction with sprayed-on polyurethane coating and are of a wide chord form as discussed, with $A.F. = 143$ and $C_{L_1} = 0.72$ compared to the 9-ft-propeller parameters of $A.F. = 115$ and $C_{L_1} = 0.65$. A similar propeller installation to that shown in Figure 206 for the SR.N6 Mk 6 has also been installed on the Bell Canada Viking.

The SR.N4 19-ft-diameter propellers developed by Hawker-Siddeley Dynamics are conventional solid aluminum propellers anodized and protected against corrosion by rubber L.E. sheaths. However, during operations across the English Channel, it was found necessary to constantly repair the sheaths and use spray-on coatings. The noise level of the SR.N4 installation, which is predominantly propeller noise, is approximately 90 dB(A) at 500 ft.

The BH.7 (and N.500) 21-ft-diameter propeller, also developed by Hawker-Siddeley Dynamics, is a departure from the all-metal propeller to meet the needs of high strength. Figure 207 is a sketch showing the construction of this propeller. This propeller blade has an aluminum alloy spar, with a root end similar to the SR.N4 propeller and with a fiberglass blade shell. The shell is made by laminating fiberglass on a mold having the specified shape and airfoil section using a wet layup process. The

*This craft is shown fitted with a tapered skirt that was discussed in Chapter V.

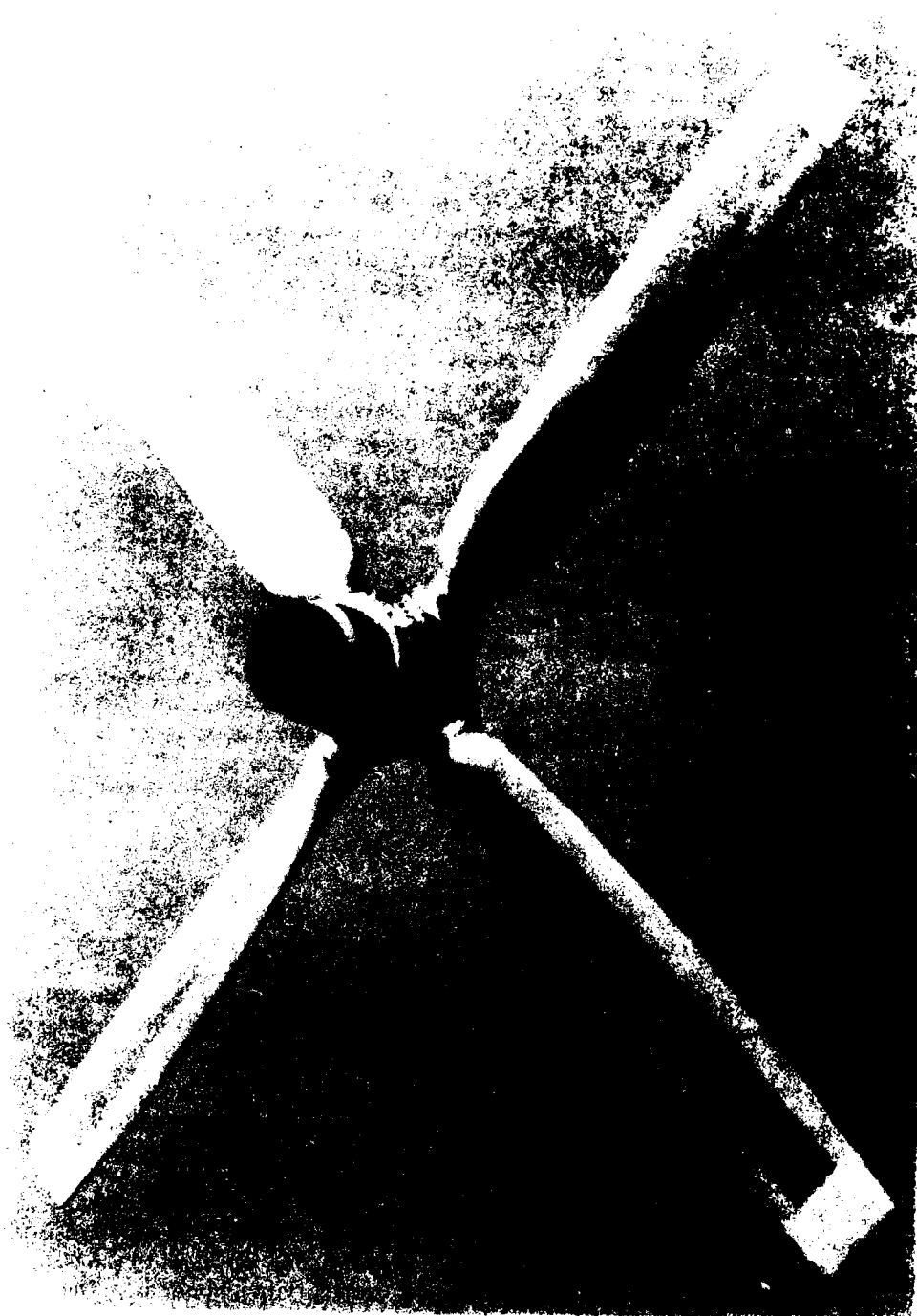


Figure 205 - Carbon Fiber Reinforced Plastic SR.N6 Propeller

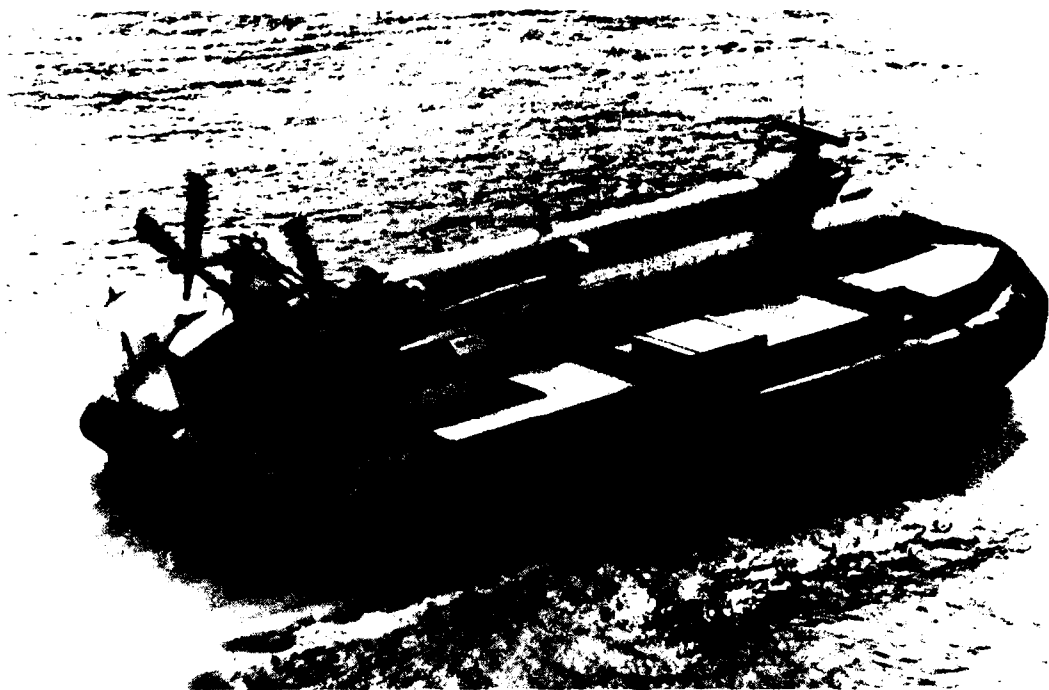


Figure 206 - SR.N6 Mk 6 Twin Propeller Installation

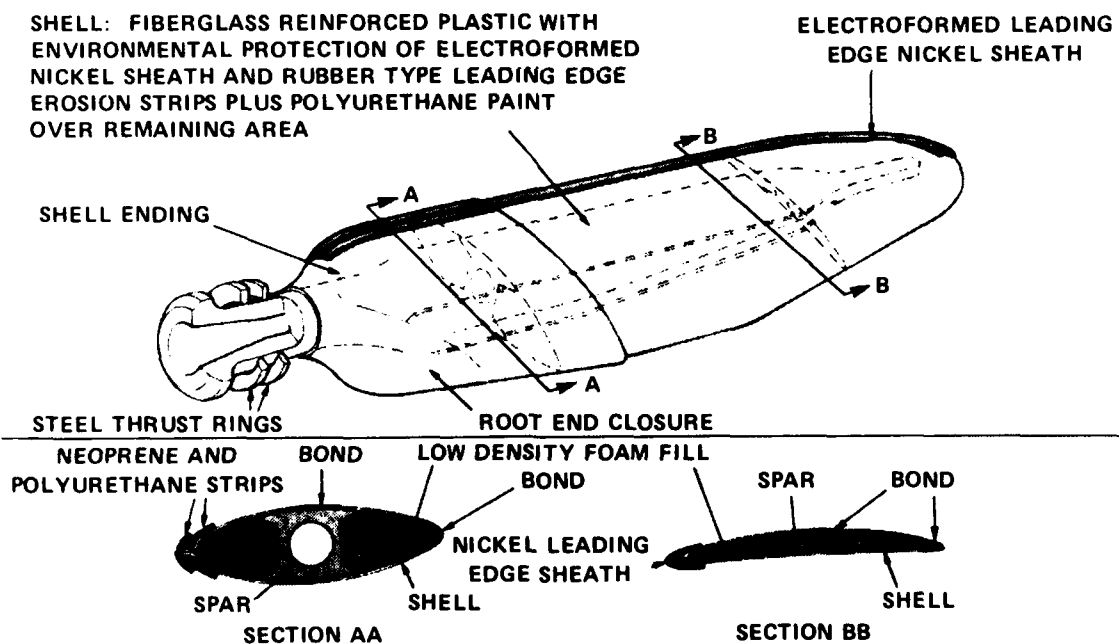


Figure 207 - Hawker-Siddeley Dynamics Composite Blade

shell is then cured in an oven and bonded to the anodic protected spar. Foam is then introduced into the hollow cavities of the blade, and the in-board end of the blade is sealed by fiberglass fairings. The leading edge of the blade is protected by an electroformed nickel sheath and rubber erosion strip. The finished blade is then sprayed with polyurethane paint. This rather elaborate construction method is the result of the very hostile environment, already described in connection with engine life, within which the air cushion craft must operate. This particular propeller has now accumulated more than 1800 hr of successful operation on the BH.7.

Due, in part, to the tip speed of the BH.7 propeller (680 ft/sec), lower than the SR.N4, the noise level of the BH.7 installation is approximately 85 dB(A) at a distance of 500 ft.

Although they have not yet been installed on any air cushion craft, GRP propeller blades for use on V/STOL aircraft have also been developed by Hamilton-Standard. These blades are similar to those already described, except that the blade is bonded to a hollow flattened steel spar and the cavities are filled with a poured-in-place closed cellular isocyanite foam. These GRP blades have been developed since 1960 and have seen over 500,000 blade hours of flight time. A 23-ft-diameter blade is presently being developed for German VC-400 VTOL aircraft and is indicative of the technology that can be applied to air cushion craft.

Turning now to the shrouded propeller installations, it is to be noted that only three craft equipped with shrouded propellers have been operational to date. One craft, the SKMR-1, which has now been decommissioned, used solid aluminum blades coated with nickel plate for protection. The current shrouded propellers (VT 2, JEFF(A) and JEFF(B)) have only had limited operational experience at the time of this writing. Both the JEFF(A) and JEFF(B) propellers were developed by Hamilton-Standard and are of solid aluminum construction. The JEFF(B) uses a polyurethane paint for erosion protection, the JEFF(A) uses a nickel plate coating. Figure 208 shows two of the JEFF(A) shrouds in the packing crates after their fabrication by Rohr Industries in 1974 and also shows the four-bladed propeller in its packing crate from Hamilton-Standard in 1974. The JEFF(A) propeller is actually a C-130 airplane propeller cut down to give it a high power absorption capability ($A.F. = 269$; $C_{L_1} = 0.984$).

The VT 2 shrouded propeller is the result of specific development by Vosper-Thornycroft and Dowty-Rotol to produce a lightweight, quiet propulsor. This craft was launched 2 September 1975 after its conversion from the water propeller driven VT 1 to the shrouded air propeller driven VT 2. Figure 209 shows a wind-tunnel model of the VT 2 in its British Army version, together with a closeup of an actual blade as constructed by Dowty-Rotol. The VT 2 propeller built by Dowty-Rotol is the largest GRP propeller for air cushion craft use so far, with its seven-bladed 13.5-ft-diameter shrouded propeller installation. As can be seen from Figures 204 and 209, it represents a significant departure from the adapter aircraft propellers

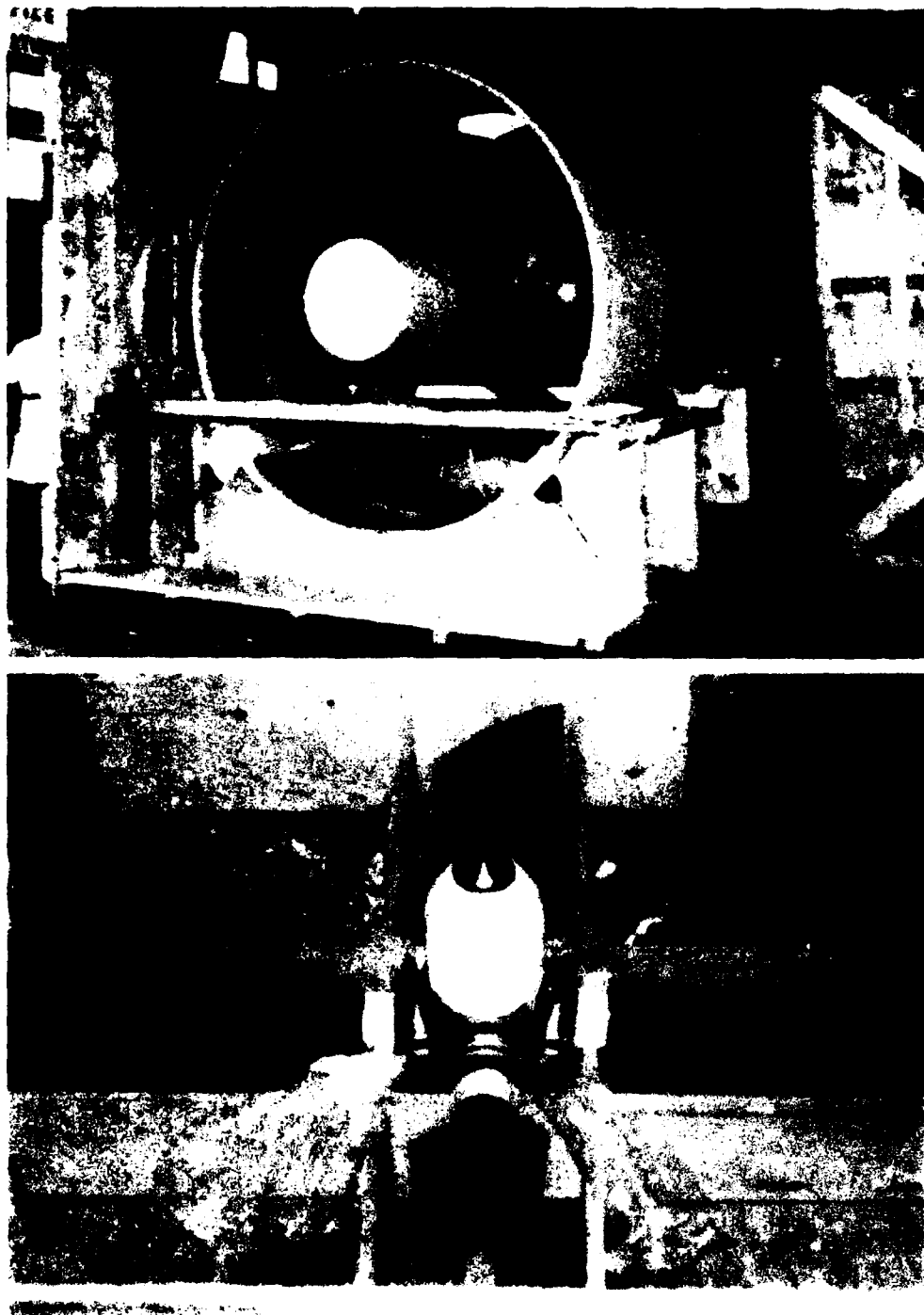


Figure 208 - JEFF(A) Propeller and Shroud



Figure 209 - VT 2 Model and Propeller Blade

used on current craft with its high activity factor of 249. The low rpm has kept the tip speed to 500 ft/sec which, together with the shroud, is expected to keep the noise level well below 80 dB(A) at a 500-ft distance.

Figures 210 and 211 give an indication of the configuration of the hub, blades and shroud installation of the VT 2 propeller.



Figure 210 - VT 2 Propeller

What is an acceptable noise level is a very subjective matter, and it is difficult to find a standard that is agreed to by all. A British standard¹⁵³ classified 70 dB(A) at 500 ft as quiet, 85 dB(A) as moderate, 100 dB(A) as noisy, and 105 dB(A) as very noisy. A U.S. standard¹⁵⁴ permits 1-hr accumulated exposure per day at 105 dB(A) while another standard¹⁵⁵ permits only 99 dB(A) for 1-hr continuous exposure. Despite the difficulty in obtaining firm guidelines, it is clear that the predicted noise levels, such as those for the VT 2 and SR.N6 Mk 6, are encouragingly close to acceptable values and provide the much needed reduction in noise pollution.

The construction of the VT 2 shrouded propeller (or ducted fan) blade is similar to the previously described Dowty-Rotol GRP blades. It is of a monocoque construction of discretely oriented glass fiber laminate bonded

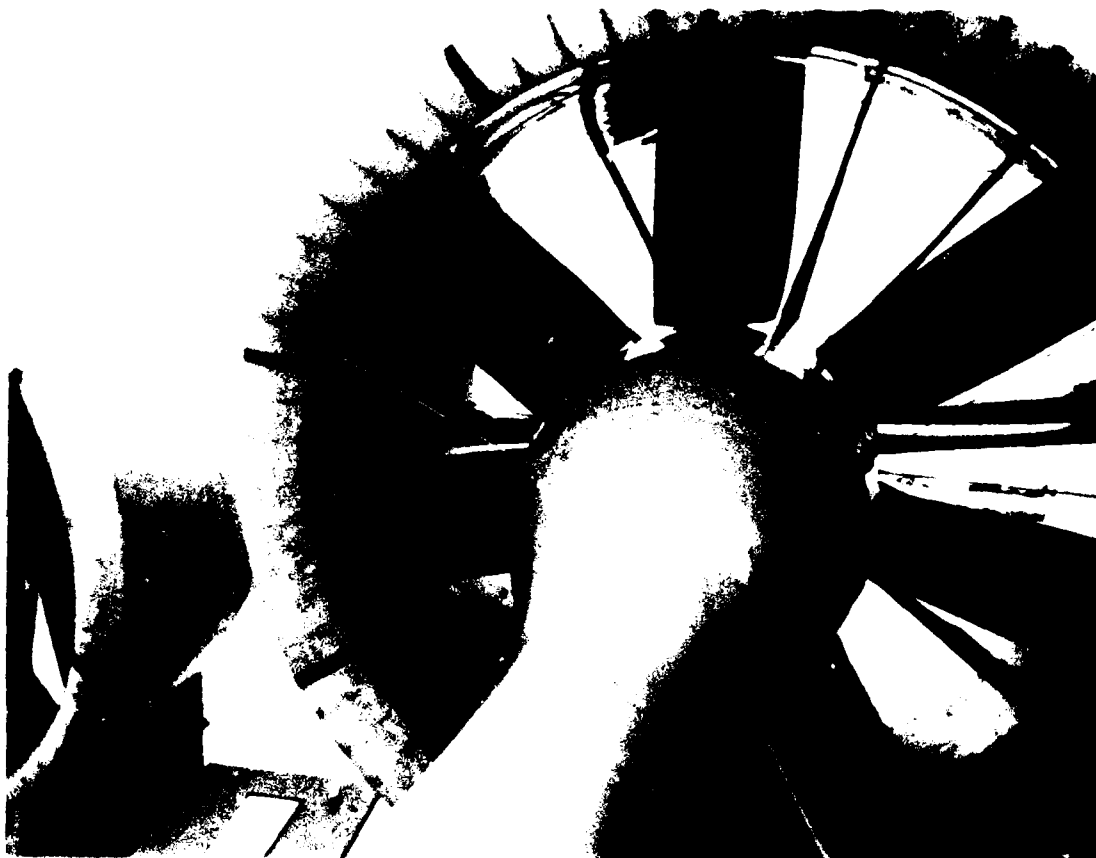


Figure 211 - VT 2 Propeller and Shroud

with epoxy resin. This shell (airfoil section) is then filled with polyurethane foam and bonded to the aluminum root. Protection against water absorption is by an all-over spray coat of 1-mm-thick polyurethane. Erosion protection to the tips and leading edges is provided by replaceable molded polyurethane "shoes." A preliminary weight estimate for the rotating propeller parts is 1244 lb, which is to be compared with 4000 lb for an equivalent solid aluminum version. Such low weights reduce the forces and moments on the pitch change mechanism, thus making a simpler, more reliable design.

The previous discussion covered some of the more recent developments in air propeller type propulsors that have either been demonstrated on actual craft or are in the construction stage. Development is still continuing, both at the drawing board and in the test cells on other forms of propulsion. Rosen and Ketley¹³⁹ discuss some of the needs for air cushion craft propulsion in the specific application of large displacement (500

tons and up) and high speed (approaching 100 knots). In such applications, ducted fans, turbo jets, and other propulsive means, familiar to the aircraft designer, begin to look attractive. Hamilton-Standard work on their trade name Q-fan, a high solidity ducted fan, appears promising for large air cushion craft use. Table 12 showed the application to a large displacement craft. The data are based on extensive testing on full-scale prototypes. Figure 212 shows a 6-ft-diameter, 10-bladed Q-fan on the NASA-Lewis acoustic test stand in 1972, which promises to provide comparable thrust performance to current shrouded propellers but at reduced diameters and lower noise levels. A more detailed description of this type of propulsor is given by Rosen.¹⁵⁶

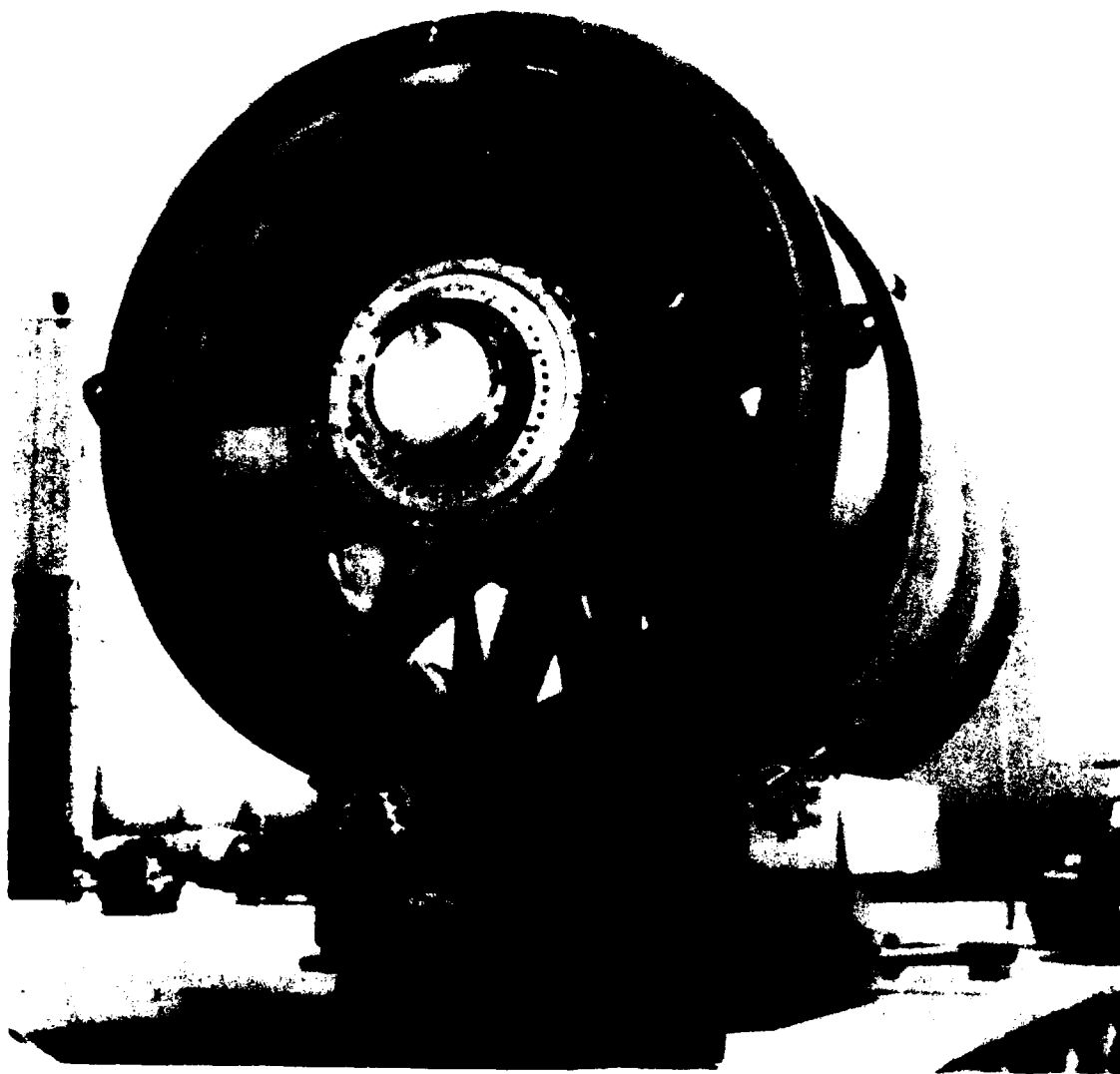


Figure 212 - Hamilton-Standard Q-Fan

Air Propeller Weight. The variety of propeller geometries and materials used in air cushion craft has made weight prediction somewhat difficult because of the small number of propellers available. Figure 213 is a compilation of the weight of various propellers discussed above, plotted as a function of the free propeller diameter. The weight shown for the free propeller data is for the rotating parts only, consisting of blades, hub cylinder, backplate, spinner, and oil. It does not include any transmission, constant speed unit, or feathering pump where applicable. For the shrouded propeller, the weight includes the shroud and stators. Except for the three-bladed SKMR-1 and seven-bladed VT 2, all propellers shown are four-bladed.

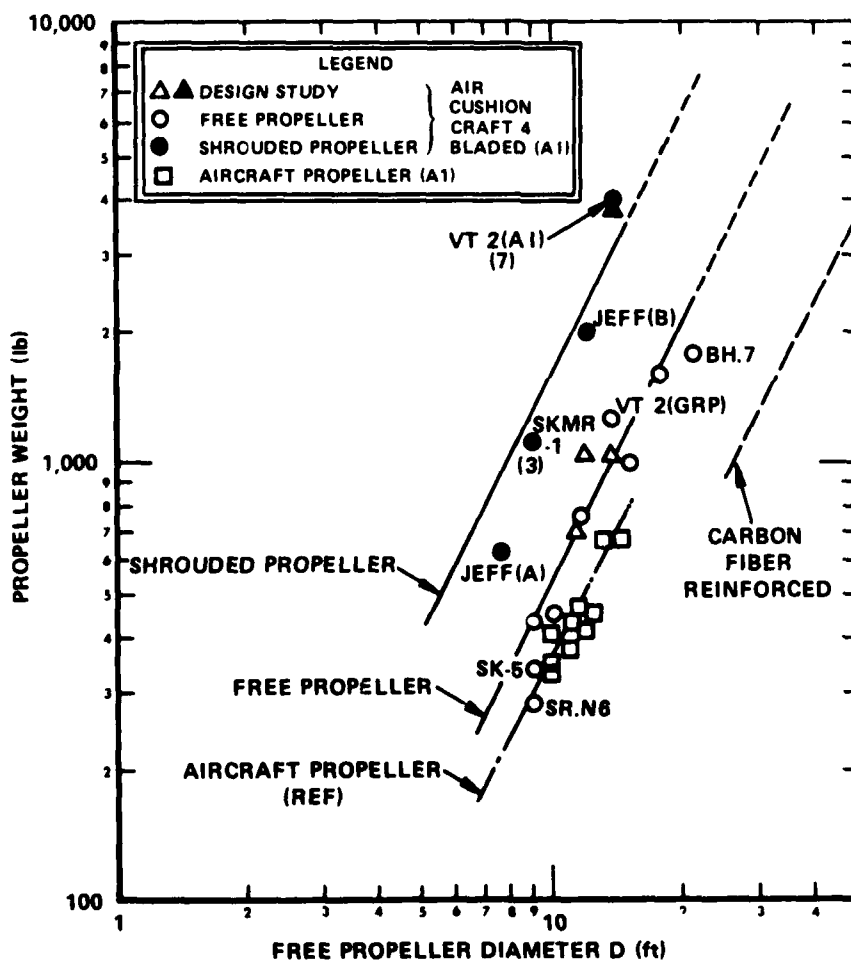


Figure 213 - Free and Shrouded Propeller Weight

The aircraft propellers shown for reference are solid aluminum propellers, as are the majority of the air cushion craft propellers, except where noted. Ketley¹⁵⁷ showed where a carbon fiber reinforced composite blade weight might fall. There is little data to construct meaningful curves through the composite blade data, but it will be noticed that the BH.7 propeller is below the aluminum free propeller line and the VT 2 propeller is above the line, probably due to the number of blades. Although the scatter exists, the weight trends can be approximated by

$$W_{P_F} = 5.40 D^2 \quad (202)$$

where W_{P_F} is the weight of the aluminum free propeller measured in lb for a free propeller diameter D measured in ft. For the shrouded propeller, the trend line is

$$W_{P_F} = 16.0 D^2 \quad (203)$$

which again applies to aluminum construction.

Equations (202) and (203) are empirical relationships only, and the reader is referred to more detailed weight analyses, such as Reference 145, to determine effects of hub/tip diameter ratios, activity factor, and other parameters on propeller weight. Figure 213 represents the propeller weight, after the designer has conducted his various design studies and produced the lightest propeller to efficiently produce thrust for the diameter given.

Air Jet Propulsion. The idea of propelling air cushion craft by air jet is a natural one, considering the availability of the energy source already incorporated into the craft to produce pressurized lift air. The interest in using such a mechanism has been pursued by several groups seeking a means of avoiding the noise, mechanical complexity, and cost of air propeller systems discussed in the previous section.

Various schemes have been tried on different craft since the SR.N1 first propelled itself by air jets ducted from the lift fan duct. Could it be prophetic that the choice of air jet propulsion for the SR.N1 was made on the basis of cost?⁹ Some of the schemes employed on other experimental craft include, in 1963, the Royal Swedish Navy craft, the SAAB 401B,

where plenum air was directed aft through pivotted vanes. In January 1962, Bertin experimented with tilting the individual jupe cushion systems on the BC.4 terraplane. The tilted air cushions provided the necessary forward thrust for speed.

Although the use of lift air deflected rearwards is attractive in terms of quietness and simplicity, it does suffer from low efficiency. The SR.N1 with its admitted poor ducting, had only 18- to 20-percent propulsive efficiency at its top speed of 20 knots.

Latter developments, notably at Cushioncraft Ltd. (then Britten-Norman Ltd.), pursued the concept of integrating fan propulsion with lift fan systems. This manifested itself in late 1964 with the CC-4, a 3570-lb craft built in association with Hovercraft Development Limited (HDL) to explore the concept of quiet propulsion. The CC-4 was powered by a single Rolls-Royce LV-8 automobile engine developing 240 hp at 4200 rpm. This engine drove four 3.5-ft-diameter fans of HEBA-B design (see Chapter VIII). Two-thirds of the flow from the two forward fans provided sufficient flow for lift, and the remaining flow provided sufficient flow for propulsion.

The CC-5, a revision of the CC-4, made its first run at Brading, Isle of Wight, England, on 25 February 1966. This attractive looking craft (Figure 214, top photo) followed the basic concept of the CC-4, except that the fan systems were separated in different volutes to provide air for lift and for propulsion. The four identical fans in the CC-5 are 52 in. in diameter and of HEBA-B design. Of the 240 installed hp, 30 percent is for the lift system and 70 percent is for propulsion. In terms of flow, the aluminum fans provided $850 \text{ ft}^3/\text{sec}$ air flow for lift and $1400 \text{ ft}^3/\text{sec}$ for thrust to propel the 2-ton craft at 40 knots. The CC-5 exhibited good performance and a very low noise level akin to a standard automobile. Unfortunately, it had only a short life due to overturning and being damaged beyond repair in 1967.

In 1968, a larger version of the Cushioncraft series appeared, namely the CC-7 (Figure 214, lower photograph). This craft returned to the integrated lift and propulsion idea developed in the CC-4, but used two aluminum fans, 42 in. in diameter, with a high b/D ratio (see Chapter VIII) of approximately 0.35. The total power for the craft is provided by a United Aircraft (presently United Technologies) free-turbine engine ST6-K-70 with a continuous power rating of 510 hp. This craft has had extensive testing by both the Department of Trade and Industry in England and the British Army in the Northwest Territories, Panama Canal Zone, and Brazil, among other test areas. The maximum speed of the 2.5-ton displacement craft is approximately 40 knots. A stretched version, designated the CC-7(S), increased in length from the CC-7 length of 25 ft 10 in. to 31 ft 3 in. and is presently under construction.

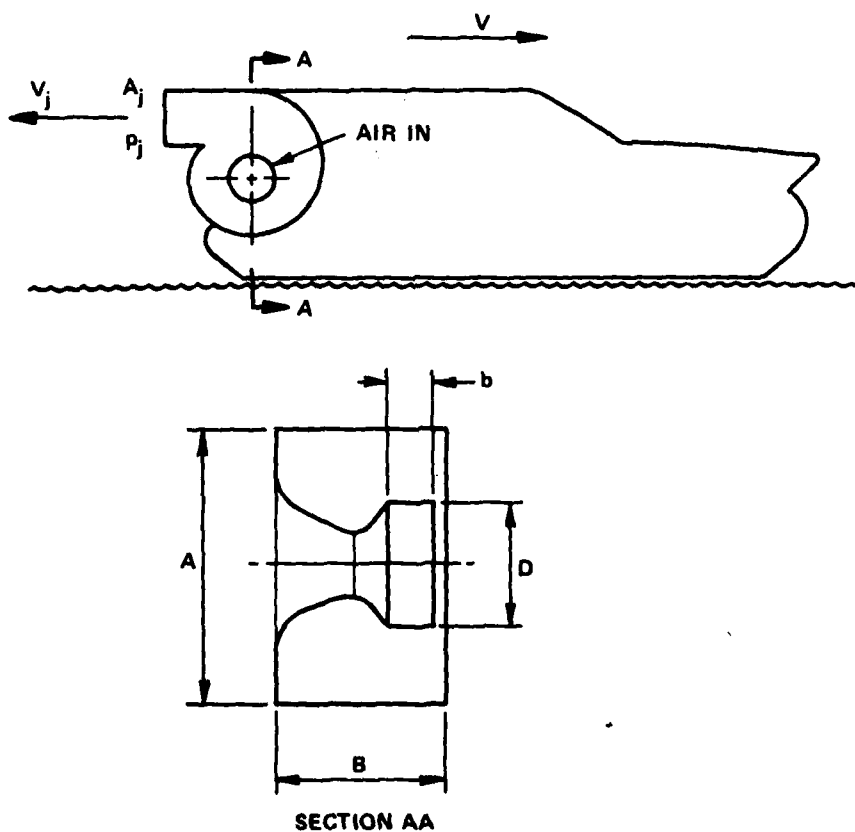


Figure 214 - Air Jet Propelled Air Cushion Craft

When integrated into the design, the fan jet propulsion has many advantages. Control of the craft can be provided by ducting fan flow in the various directions. The CC-5 directs flow from the fans either differentially for control or forward over the cabin roof for braking. This basic idea of using ducted fan air for propulsion and maneuvering control has recently been extended to the rotating bow thruster concept used in the U.S. Navy JEFF(B).

While only scant data exist on full-scale operational craft relative to the performance capability of air jet propeller air cushion, the following is given on the efficiency and size of such installations.

Air Jet Propulsion Efficiency. A diagrammatic representation of the essential elements of a fan air jet propeller air cushion craft is shown in Figure 215.



$$\text{VOLUTE PARAMETER} = U/bD^2 \quad \text{WHERE} \quad U = \pi/4 \, A^2 B$$

Figure 215 - Air Jet Propulsion Elements

Following a simplified approach to capture the main design parameters, consider the thrust from such a device as

$$T = \rho Q (V_j - V) \quad (204)$$

where the flow Q is that required for propulsion. Equation (204) ignores the contribution to thrust by the rise in static pressure at the jet nozzle exit, which is usually zero for the case of rearward-facing jets.

The thrust efficiency is defined as

$$\eta_p = \frac{TV}{550 P} \quad (205)$$

where T is in lb, V in ft-lb/sec, and P is the propulsion horsepower input to the propulsion fan given by

$$P = \frac{P_F Q}{550 \eta_F} \quad (206)$$

where η_F is the fan efficiency discussed in Chapter VIII.

The total pressure rise across the fan can be expressed as the total pressure in the jet less any ram recovery at the fan intake, that is,

$$P_F = P_j - \frac{\epsilon \rho V^2}{2} \quad (207)$$

With these simple relationships, it then becomes possible to express the efficiency of the fan air jet system (excluding transmission losses) as

$$\eta_p = \frac{2\eta_F \left(\frac{V_j}{V} - 1 \right)}{\left(\frac{V_j}{V} \right)^2 - \epsilon} \quad (208)$$

and, for the ideal efficiency with no losses such that $\eta_F = \epsilon = 1$, then

$$\eta_{p1} = \frac{2}{1 + \left(\frac{V_j}{V} \right)} \quad (209)$$

In terms of the thrust coefficient used previously, the expression becomes a little cumbersome, and it is more convenient to note the relationship as

$$C_T = 2 \frac{V_j}{V} \left(\frac{V_j}{V} - 1 \right) \quad (210)$$

The ideal efficiency (η_{pi}) and a typical actual efficiency (η_p) computed for a total fan efficiency of 85 percent and an intake ram recovery of 50 percent are shown as a function of the jet velocity ratio (V_j/V) in Figure 216. Also, to provide comparison with previous curves for air propellers, the general relation between (V_j/V) and thrust coefficient (C_T) is shown in the lower curve in Figure 216. It is seen from Figure 216 that, even with high fan efficiencies, it is difficult to obtain much more than 50-percent propulsive efficiency. For $\epsilon = 0$, the propulsive efficiency is approximately 42 percent and for $\epsilon = 1.0$, that is, full ram recovery, the propulsive efficiency approaches 56 percent for the case of an 85-percent efficient fan.

This maximum efficiency occurs for a jet velocity ratio $V_j/V = 1.75$ or, following the dashed line in Figure 216, at a thrust coefficient $C_T = 2.6$. The free and shrouded air propeller for the same thrust coefficient would have a propulsive efficiency of approximately 60 percent.

For craft speeds of 50 to 60 knots, jet velocities of 150 to 200 ft/sec will thus provide the maximum efficiency. These values correspond roughly with the design values of the CC-5 type craft (175 ft/sec). The advantage of low velocity jet propulsion is the low noise level that is generated. The disadvantage is the space requirement of the fan(s) to produce sufficient thrust.

An indication of the fan requirements can be seen from consideration of the jet velocity given by

$$V_j = \sqrt{\frac{2p_j}{\rho}} \quad (211)$$

which, upon substitution with the fan total pressure and ram recovery expression given by Equation (207), can be rewritten in the form

$$\frac{V_j}{V} = \sqrt{2\psi \left(\frac{nD}{V} \right)^2 + \epsilon} \quad (212)$$

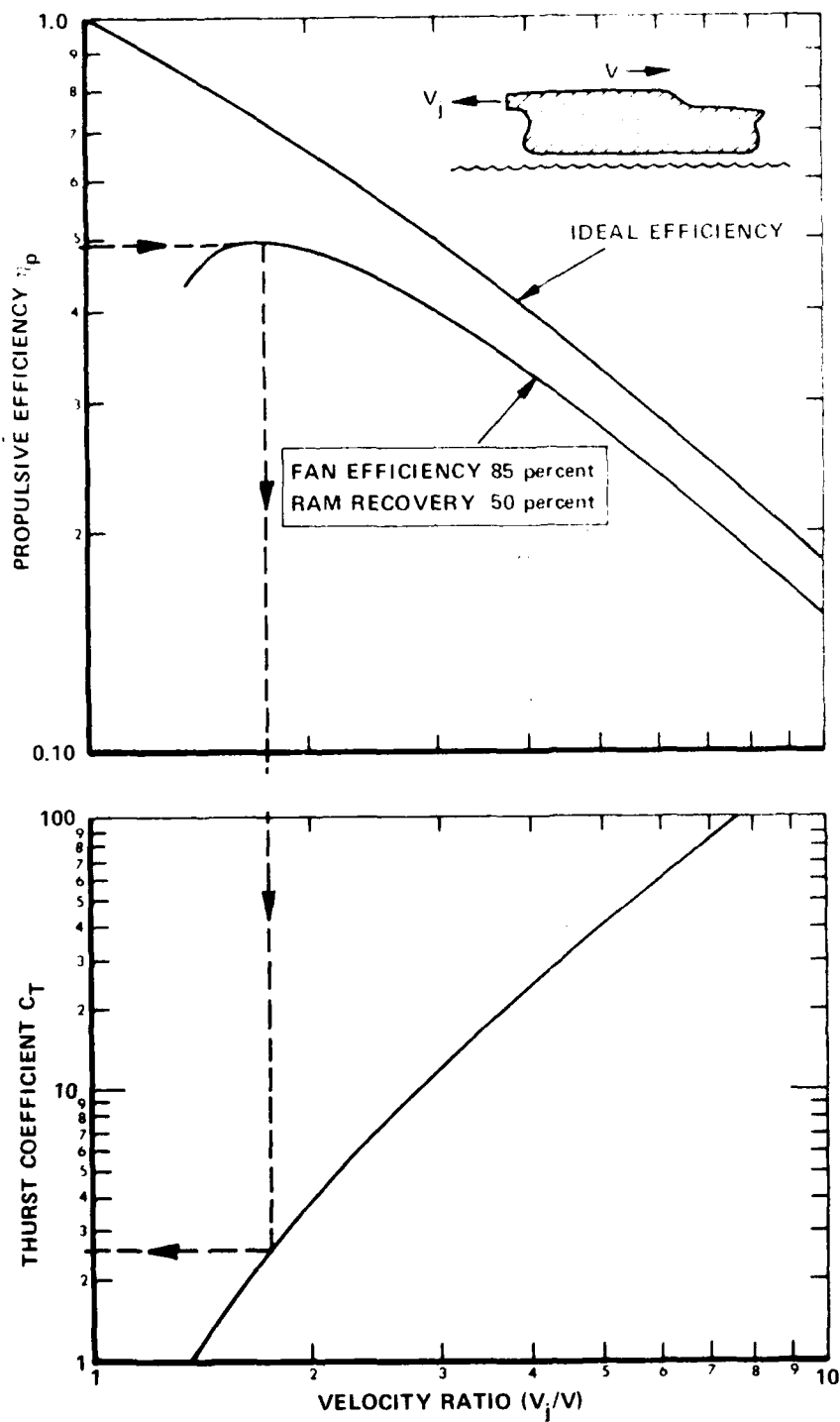


Figure 216 - Fan Air Jet Propulsion Thrust Efficiency

where the fan total pressure (p_F) has been expressed in terms of the pressure coefficient (ψ) defined and discussed in Chapter VIII. The jet velocity ratio is thus seen to be a function of the fan pressure coefficient (ψ), the fan intake ram recovery (ϵ), and an advance ratio $J = V/nD$ that expresses the ratio of craft speed to fan tip speed. Figure 217 gives the relationship between the velocity ratio and the fan parameters for the case of $\epsilon = 0.50$.

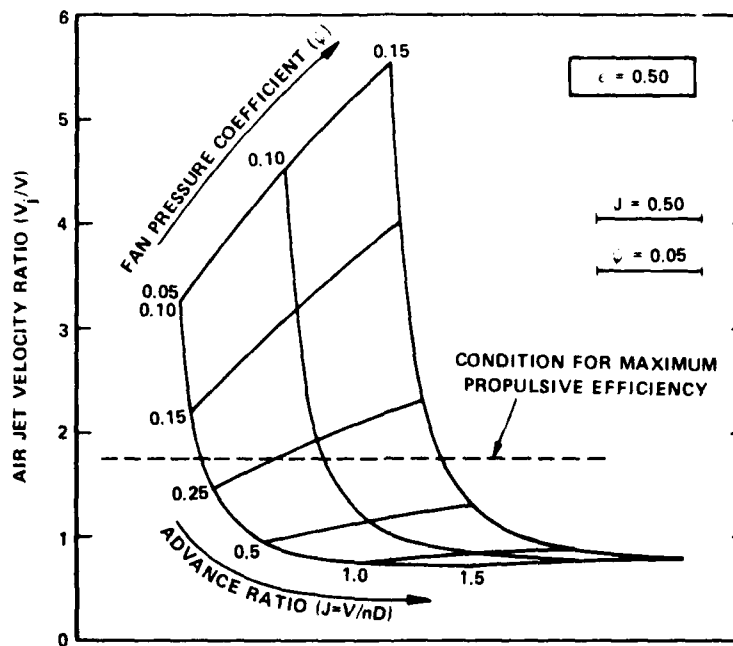


Figure 217 - Jet Velocity Ratio and Fan Parameters

Chapter VIII discussed the various fan concepts used by present air cushion craft and noted that the HEBA-B fan has been used extensively and, in particular, has been used in the CC-4, -5, and -7 series of fan air jet propelled craft. The pressure coefficient (ψ) and total fan efficiency (η_F) can be shown to be functions of the fan geometry such that

$$\psi = \psi \left(\phi; \frac{U}{bD^2} \right) \quad (213)$$

$$\eta_F = \eta_F \left(\phi; \frac{U}{bD^2} \right) \quad (214)$$

where ϕ is the flow coefficient of the fan given by Equation (177) in Chapter VIII and U/bD^2 is the volute volume parameter that will give the size requirements of the jet nozzles to produce the desired thrust. The HEBA-B performance curves¹³⁷ were summarized by Hovercraft Development Ltd.¹⁵⁸ in conjunction with lift and propulsion research on air cushion craft. They are reproduced here in the terminology of this report in Figure 218. The complete performance maps have been incorporated into most

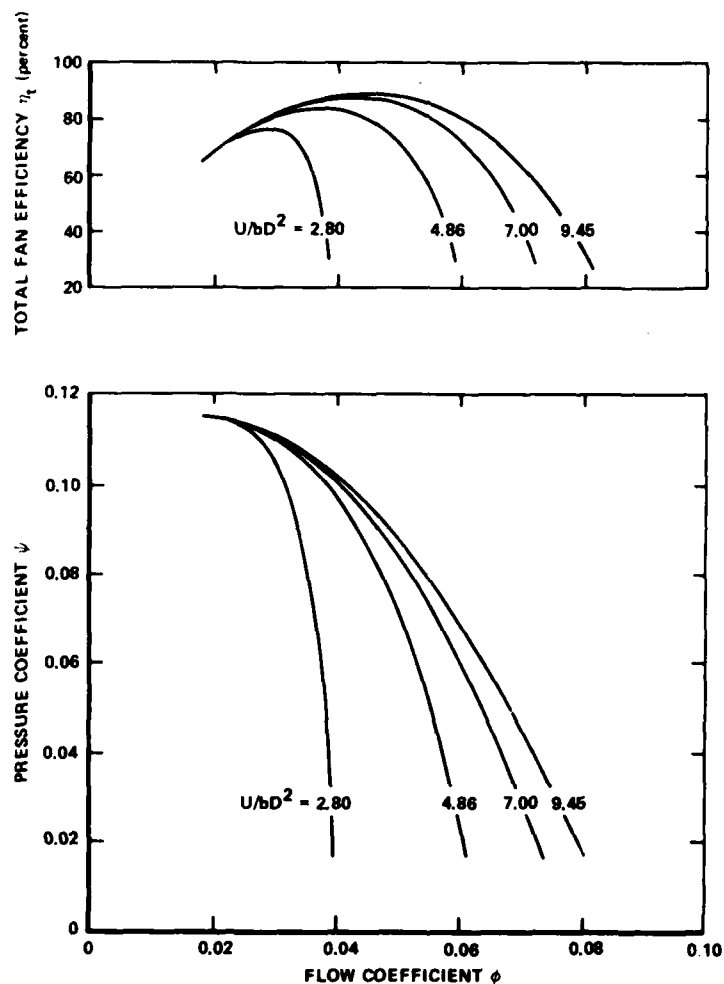


Figure 218 - HEBA-B Fan Performance Characteristics

air cushion craft designers' computer data banks. From the curves, it can be seen that, to achieve high fan efficiency commensurate with the design point ψ , a volute volume parameter of U/bD^2 greater than 2.80 would be desirable, and it has become common practice to select the value $U/bD^2 = 7.0$ in an attempt to compromise slightly on efficiency to gain space. Even at this reduction, the fan volute is approximately 2 times the fan diameter and the width is 0.80 to 1.0 times the fan diameter. On a craft the size of CC-5, the exhaust area is approximately 25 percent of the transom area. This is not unreasonable for a small craft with modest design speeds (30 to 40 knots) and has been used with success in many small air cushion craft of the sport and recreational type.

It is seen that the current state-of-the-art for fan air jet propulsion is that, for 85-percent efficient fans, the propulsive efficiency is approximately 50 percent. Studies²⁹ have shown that, for larger and faster craft, the space requirements become unmanageable. The exact crossover point of when to use fan propulsion and when to use air propeller propulsion must await more developmental craft data.

Water Propulsion

The unique capability of an air cushion craft to hover over practically any surface has resulted in the extensive development of the amphibious form of the craft. This extensive development has, therefore, resulted in the relative abundance of air propeller means of propulsion discussed in the previous section. There are, however, a few craft that have used water propulsion either in the form of waterscrews or waterjets. If the mission allows for a nonamphibious craft such as the sidehull form discussed in Chapter II (see Figure 6), then it becomes a matter of design whether to use air or water propulsion and, further, whether to use waterscrews or waterjets.

A brief synopsis of some of the particular developments relative to waterscrew and waterjet propulsion of air cushion craft is given in the following sections.

Waterscrew Propulsion. Although the waterscrew has had over 200 years of marine application, it has not had a large amount of application to air cushion craft for the previously mentioned reasons. Table 13 summarizes a few selected propellers including two applications other than air cushion craft to provide a data base, namely the AGEH hydrofoil and the planing boat Double Eagle. Some of the data are omitted in Table 13 due to the security classification of the project.

The Hovermarine HM.2, which first entered service in 1967, is a low speed (30 to 35 knots) sidehull form of air cushion craft shown in Figure 61. Each of the two propellers is driven by a Cummins VT8-370M lightweight diesel on a 1:1 ratio vee-drive transmission. The propeller is a conventional wide blade propeller with a blade area ratio (B.A.R.) of 0.95

TABLE 13 - SUBCAVITATING AND SUPERCAVITATING WATERSCREWS

Craft	Propeller Manufacturer or Design	Type*	Dia. (ft)	No. of Propellers	No. of Blades	Design (rpm)	hp per Propeller	Max. Thrust (lb)	Propeller Weight (lb)	Propeller Material	Remarks
HM-2	Gawn-Burrill	Sub P.P.	1.25	2	3	2,600	300	1,800		Steel	
VT 1	Ka-Me-Wa	Super C.P.	2.1	2	3	2,200	1,100			Nickel Alloy Bronze	Outboard rotation.
SES-1008	Hydroautics and Philadelphia Gear	Semi. Super C.P.	3.5	2	6	1,900			2,300	Titanium	Thrust and power data classified. Inboard rotation.
ACEH	Hamilton-Standard	Super P.P.	5.17	2	4		17,500	60,000	775	Titanium	Hydrofoil.
Double Eagle	Hamilton-Standard	Super P.P.	2.67	2	3		3,700	12,500	131	Titanium	Planing boat.
Bell-Halter 110		Super P.P.	3.50	2			1,335			Steel	40-knot SES.

*Sub = Subcavitating Design
 Super = Supercavitating Design
 P.P. = Fixed Pitch
 C.P. = Controllable Pitch
 Semi = Semisubmerged

and a pitch-to-diameter ratio of 1.33. It is mounted beneath the sidehull just ahead of the canted rubber as shown in Figure 219.

The second subcavitating design propeller is that for the Vosper-Thornycroft VT 1 (shown in Figure 13). The VT 1 is a fully skirted, partially amphibious craft fitted with two skegs beneath the hull, lying within and slightly below its cushion, each 10 ft from the longitudinal centerline, to house the inclined shafts driving the two 2.1-ft-diameter waterscrews. These port and starboard waterscrews rotate outboard at the top and are of the Swedish Ka-Me-Wa design that has had extensive service in marine applications since 1937 when Ka-Me-Wa first introduced its particular form of servomotor, single crank, pitch change mechanism.

The next three propellers in Table 13 represent the current state-of-the-art of supercavitating propellers. It is believed that the SES-100B was the first application of semisubmerged, supercavitating controllable-pitch propellers. The SES-100B first got under way on its own power on 4 February 1972. Most of the information on this propeller is classified, but it can be stated that it is a six-bladed, 3.5-ft-diameter propeller. Its blades are of forged titanium mounted on a 17-4PH hub.

The last propeller listed in Table 13 is the fixed pitch, subcavitating propeller that is installed on the Bell-Halter 110 (see Figure 166, Chapter VII). It is a 42 in. (3.5 ft) diameter propeller with a pitch-to-diameter ratio of 1.47 and an expanded area ratio (E.A.R.) of 1.0.

Figure 220 (top photograph) shows the configuration as the SES-100B is being hauled out of the water at the public dock near Lake Pontchartrain during a routine under-hull inspection. The particular blade section used for the SES-100B propeller was developed by Hydronautics, Inc. and constructed by Philadelphia Gear Corporation.

The middle and lower photographs of Figure 220 show two fully-submerged, supercavitating propellers that are also of Hydronautics blade design and were constructed by Hamilton-Standard for use on the Eagle and Double Eagle planing boats (middle photo) and for the AGEH (lower photo).

The subcavitating and supercavitating propellers have very different shapes and performance characteristics, and there is a significant difference in the amount of available data on each on which to base conclusions. Some of the available data on the performance of the propellers are given in the following selections.

Subcavitating Propellers. Probably the most systematic tests conducted on subcavitating waterscrews were done by Troost in 1935 for a range of propeller types from two-bladed through seven-bladed with varying blade area ratios, pitch angle, thrust, and power coefficients. The standard charts derived by Troost to cover these test propellers allow for extraction of the maximum efficiency for several conditions of interest and, in particular, for a given advance ratio $J = V/nD$ or a given thrust

*Note that this classical definition of J differs from the definition discussed in relation to fan air jet propulsion (Equation (212)) by a constant factor 2π .

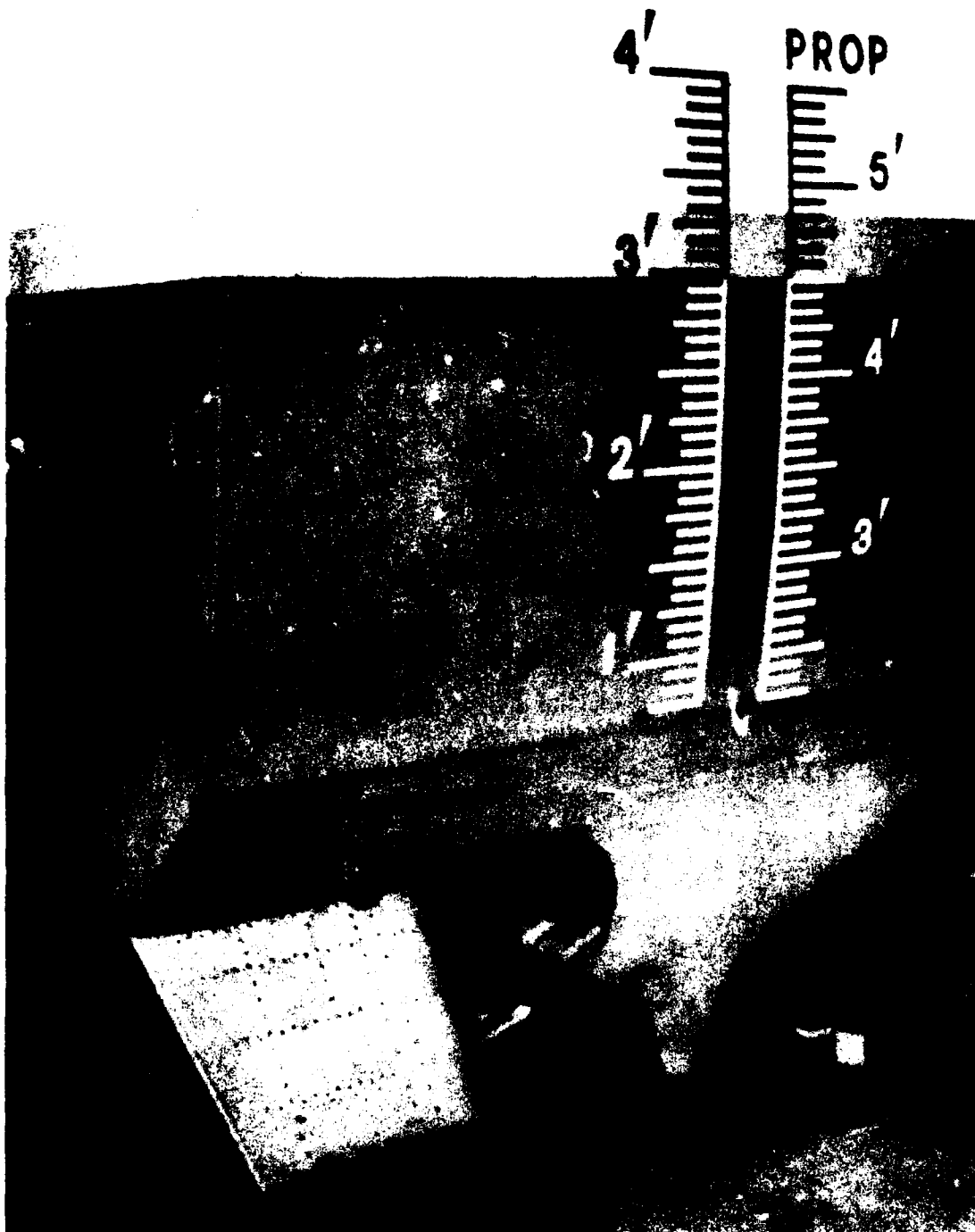


Figure 219 - Hovermarine HM.2 Subcavitating Propeller

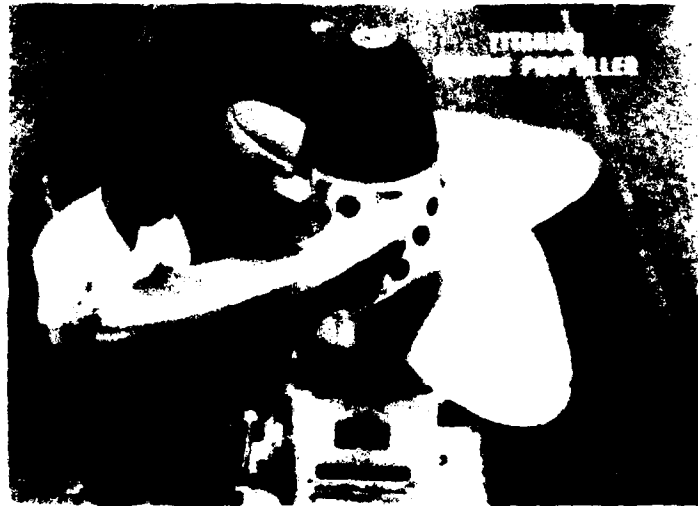


Figure 220 - Some Supercavitating Propellers

coefficient (C_T). Sheets and Mantle¹⁵¹ compiled the Troost data for propulsive efficiency as a function of thrust coefficient. This has been reproduced in Figure 221 showing the band of Troost data and test points of two subcavitating propeller tests at DTMB (now DTNSRDC). The HM.2 propeller efficiency at 70 percent is also shown.

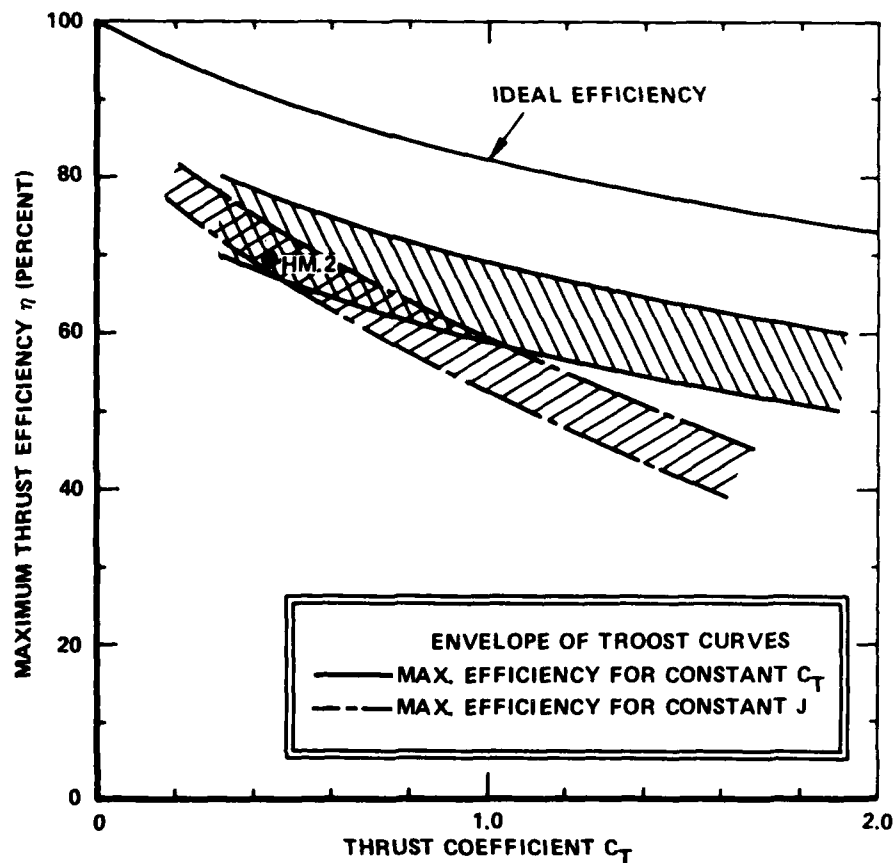


Figure 221 - Subcavitating Waterscrew Efficiency

The ideal efficiency shown is that given by Equation (198), where now the thrust coefficient is based on the density of water. It is conventional practice in ship design to approximate subcavitating propeller efficiency by taking 80 percent of the ideal efficiency given by Equation (198). It can be seen from Figure 221 that this approximates the mean of the Troost curves and the HM.2 air cushion craft data.

Supercavitating Propellers. The supercavitating propeller has had a sporadic history, not all of it well documented. It has been reported that propellers operated in supercavitating flow conditions in the late 19th century on steamships, such as the British steamship Turbinia, in 1894, but not much was done until hydroplanes began seeking faster speed records in the early 1900's.

The development of high (craft) speed propellers proceeded almost hand-in-hand with semisubmerged propellers. It was long recognized that the hydrodynamic resistance of propeller pods was excessive as boat speeds increased, and so hydroplanes developed with shallow draft and surface-piercing propellers operating in the fixed water plane emanating from the transom of the craft. Some early examples of these might be the Faubers hydroplane.¹⁵⁹ The three-bladed propeller for the Hickman Sea Sled¹⁶⁰ had a very sharp L.E. and narrow section comprised of ogival sections, except that the pressure face was flat. Similar sections, but with some reflex in the L.E. and T.E., were developed as the Newton-Rader series of supercavitating propellers in 1960.

In 1948, the hydroplane Slo-Mo won the unlimited class races with a record speed of 183 mph. The propeller used for this race was a two-bladed supercavitating shape where the cross section was a sharp L.E. wedge set at a high fixed pitch. While the hydroplanes were successful in achieving high efficiency, supercavitating propellers, it was usually because of experimentation on many propellers, which then lasted for only one race. Very little of the design of such shapes entered the technical literature, probably due to the keen competition between the designers and builders of the various craft.

The shapes that were being developed experimentally on hydroplanes were being reduced to naval architectural design by Tachmindji and Morgan^{161,162} at DTMB by 1957, based on work by Tulin¹⁶³ in 1955 relative to hydrofoil foil shapes that must contend with the same phenomenon. A summary of the development of the supercavitating foil sections is given by Oakley,¹⁶⁴ and Figure 222 shows some of the more recent and successful supercavitating foil sections that have been applied in supercavitating propellers.

The hydronautics supercavitating section shown in Figure 222, complete with flow field, again evolved through hydrofoil design as described by Johnson and Tulin¹⁶⁵ in 1961 and was subsequently applied to propeller

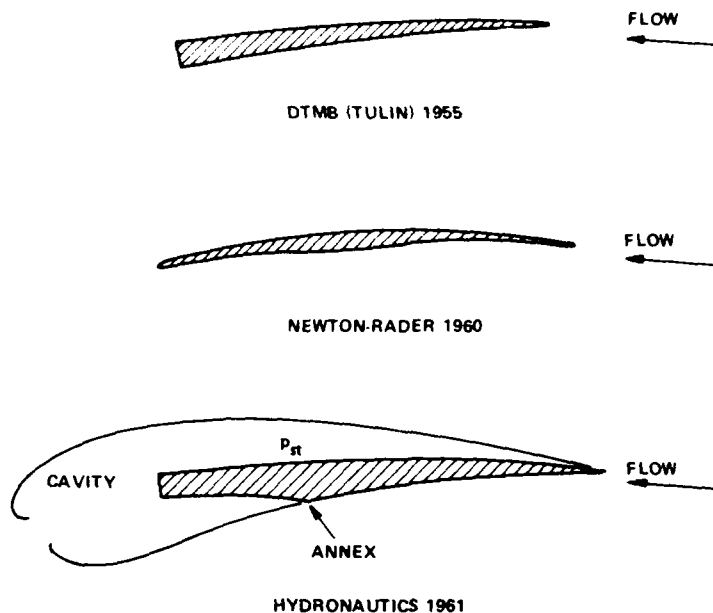


Figure 222 - Supercavitating Foil and Propeller Sections

design. The characteristic "scallop" or annex on the pressure face of the Hydronautics supercavitating propeller section sketched in Figure 222 may be seen on the SES-100B, Double Eagle, and AGEH propellers shown in Figure 220.

Although the subcavitating propeller designer seeks to avoid cavitating flow, the supercavitating propeller designer deliberately designs to operate in such a region. To design a propeller to operate in supercavitating flow with high efficiency and still retain sufficient thrust capability at low speeds in subcavitating flow is a formidable task and one that has not been completely resolved. Figure 223 gives the thrust and drag curves for a craft the size of SES-100B and shows the characteristic loss of thrust of the supercavitating propeller operating at subcavitating flow conditions. Because there is some difficulty at predicting subhump drag characteristics (see Chapter III and Appendix C), a bad prediction of propeller characteristics can reduce the thrust margin at low speed to prevent the craft from ever getting over hump. However, a correctly designed supercavitating propeller should have a sufficiently steep thrust-speed characteristic to avoid the hump thrust margin problem, especially in rough seas.

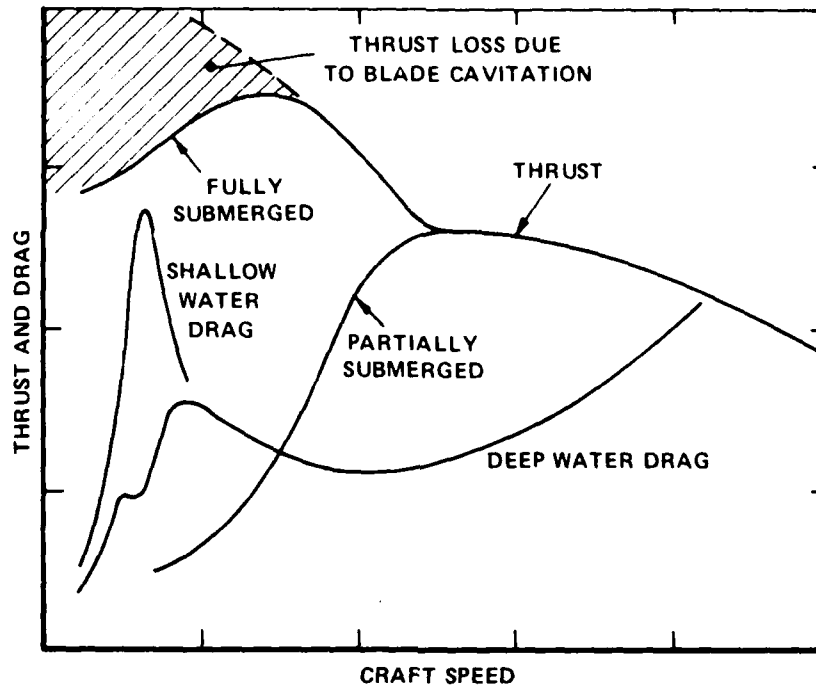


Figure 223 - Typical Supercavitating Propeller Thrust Curve

The change in the thrust curves labelled "fully submerged" and "partially submerged" in Figure 223 is caused on the same propeller (in this case the SES-100B propeller shown in Figure 220) by varying the water inflow conditions. This change is caused by moving a ramp ahead of the propeller and Figure 224, taken from the author's patent,¹⁶⁶ illustrates the essential features. The numbers on the drawings in Figure 224 are the callouts of the component parts described in more detail in the patent.¹⁶⁶

The variable geometry feature was incorporated on the SES-100B during its construction and used to advantage during the trials program by allowing the ship to achieve high speed without the attendant drag penalties of a fully-submerged propeller pod. At low speeds (for example below 25 to 30 knots) the ramp (labelled 10 in Figure 224) is in the up position and water flows up the ramp and allows the propeller disk area (labelled 20 in Figure 224) to be completely submerged and develop the high thrust levels as shown in Figure 223. The pod drag at these speeds is not large. At high speeds, specifically at the maximum speed conditions (80 to 100 knots), the ramp (10) is in the down position and the water flows straight aft virtually eliminating the pod drag and allowing the propeller to

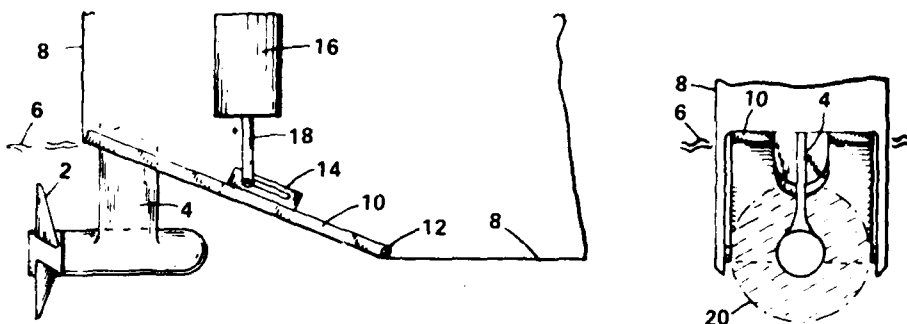


Figure 224a - Fully-Submerged Mode

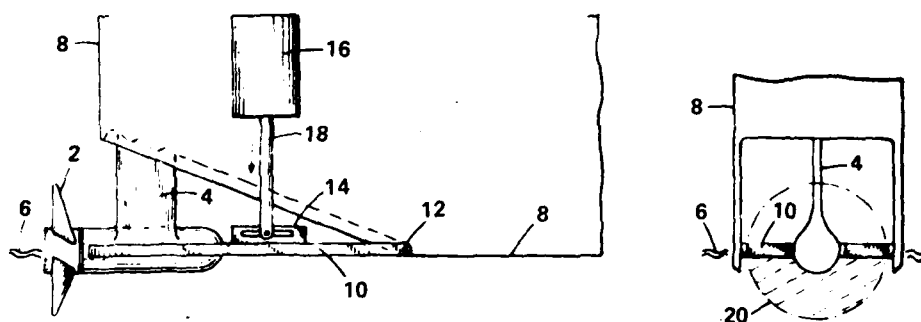


Figure 224b - Partially-Submerged Mode

Figure 224 - Variable-Geometry Marine Propulsor

operate in the partially-submerged mode and generate the thrust curve shown in Figure 223. The outboard starboard ramp on the SES-100B can be seen just ahead of the propeller in Figure 220.

The cavitation number (σ) is a key parameter in the design of super-cavitating flow sections and is defined as

$$\sigma = \frac{p_{st} - p_v}{\frac{\rho V^2}{2}} \quad (215)$$

where p_{st} is the total static pressure on the blade surface,
 p_v is the vapor pressure of water, and
 V is the speed of the oncoming stream of density ρ .

There are other definitions in the literature where other reference pressures are used, but Equation (215) is the most straightforward. In this form, the cavitation number (σ) is analogous to Mach number (M) in air flow in that it is a measure of the compressibility of the water and expresses the ratio of the acoustic velocity (squared) to the local velocity (squared). When the water stream flows over the suction side of the blade, the absolute pressure decreases to a limiting value. This limiting value is the vapor pressure of the water. When this limit is reached, the water vaporizes and vapor "pockets" appear in the flow and, by their subsequent collapse, cause the phenomenon known as cavitation damage. This problem is avoided by designing the propeller section so as to deliberately form a single large cavity within which the blade is enclosed. The supercavitating propeller was designed to ride completely immersed in the cavity, such that the pressure face is producing the lift. Because the backface does not ride in the flow, it now becomes possible to thicken the section to meet the stringent strength requirements as demonstrated with the Hydronautics section. There is always a speed at which any propeller section will experience cavitation on the backface. Venning and

Haberman¹⁶⁷ prepared a chart showing, as a function of J , those conditions under which cavitation will occur and where the best operating condition is for both subcavitating and supercavitating propellers. A band of operating regions was drawn by Venning and Haberman, based on tests at DTMB of a series of propellers. These data, taken from Reference 167, are given in Figure 225.

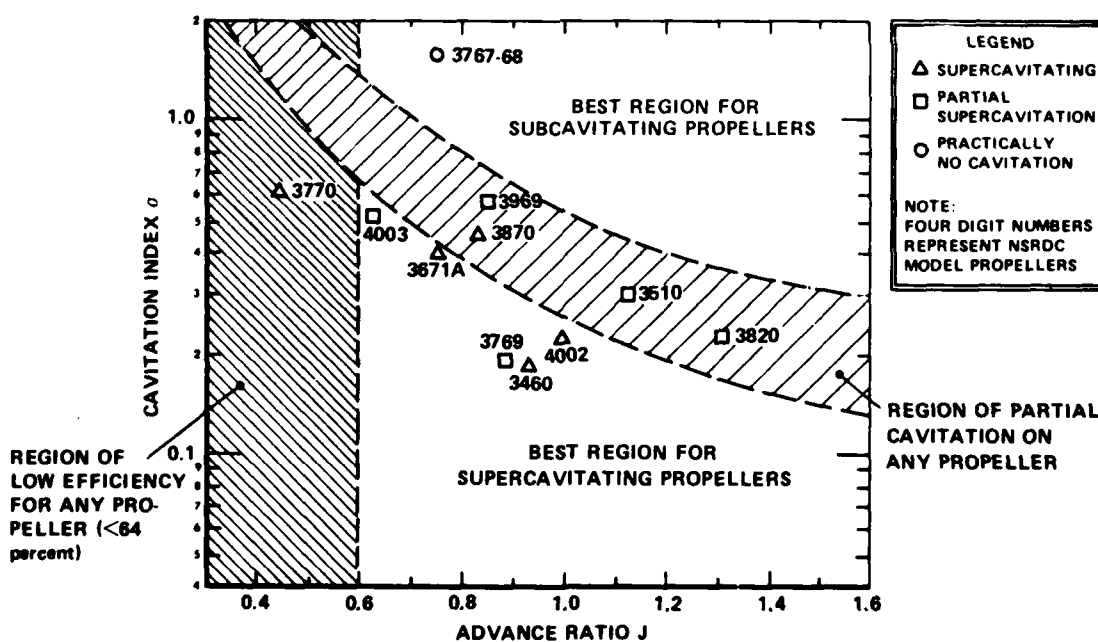


Figure 225 - Operating Regions for Subcavitating and Supercavitating Propellers

The propulsive efficiency of supercavitating waterscrews has been explored by several researchers and some representative data taken from Sheets and Mantle¹⁵¹ are given in Figure 226. The data are by Tachmindji and Morgan¹⁶² in 1958, Venning and Haberman¹⁶⁷ in 1962, van de Voorde and Esveldt,¹⁶⁸ and Taniguchi and Tanibayashi¹⁶⁹ in 1962.

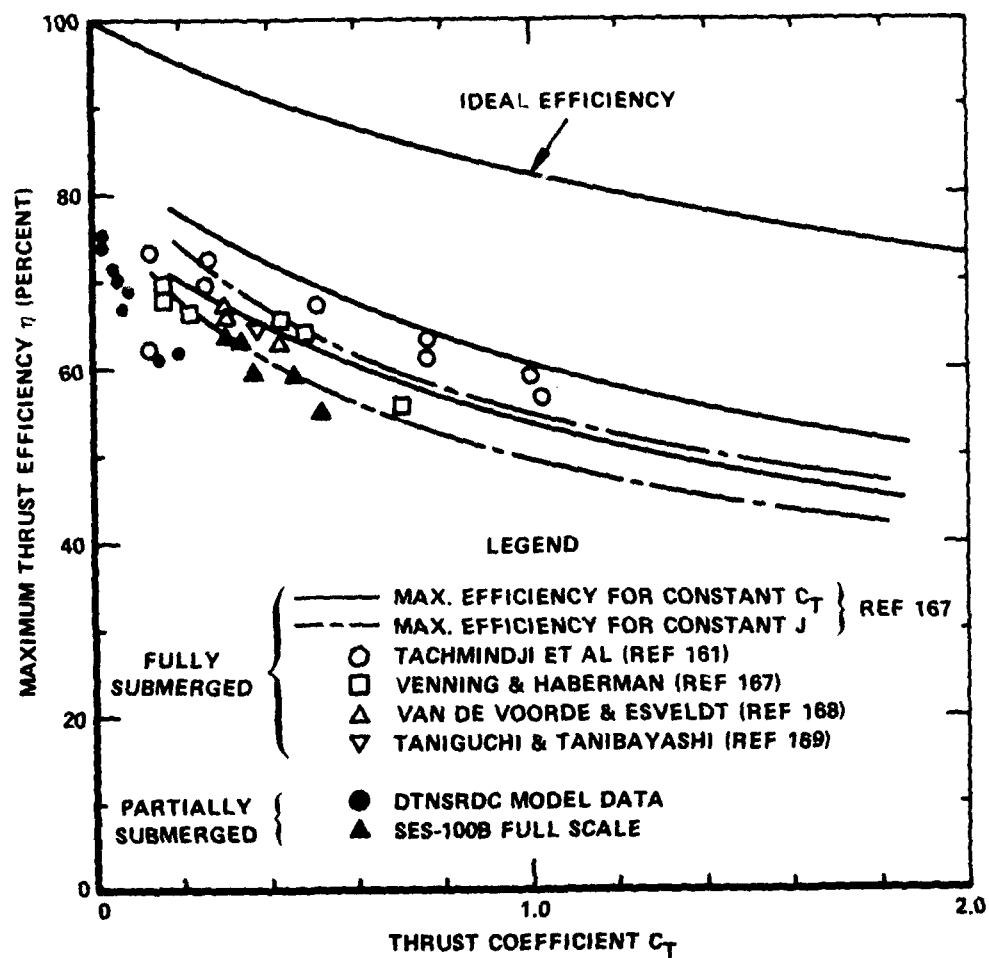


Figure 226 - Supercavitating Waterscrew Efficiency

Following a similar procedure to that used in compiling the sub-cavitating propeller data, Sheets and Mantle¹⁵¹ compiled the efficiency of the supercavitating propeller using the charts of Tachmindji and Morgan and showed that a narrow band around a value of 75 percent of the ideal efficiency given by Equation (198) enveloped the data in the above cited references. These data were all for supercavitating propellers operating in the fully-submerged condition. This compilation and data are given in Figure 226 which show efficiencies from 60 to 70 percent over the thrust coefficient range of $0.02 < C_T < 1.0$. These propellers are two-, three-, and four-bladed with a B.A.R. of 0.20 to 0.50 and with various thickness and camber distributions. The specific details of the propellers may be found in the cited references.

As interest in high speed craft increased in the period of 1960-70, serious consideration of the partially submerged or semisubmerged propeller reestablished itself in many design offices. In the U.S.S.R. in 1961, Yegorov and Sadovnikov¹⁷⁰ examined partially submerged supercavitating propellers for hydrofoil use. In the United States, interest increased mainly in connection with the high speed, sidehull form of air cushion craft. The U.S. Navy began research into such propellers at DTMB in early 1966 and conducted both experimental and analytical studies. Hadler and Hecker¹⁷¹ and Shields¹⁷² provide much of the early work on semi-submerged supercavitating propellers. This work consisted of taking supercavitating propellers, for which DTMB had a large data base, and determining their performance in a partially submerged mode of operation.

It was determined from this work that the efficiency of the partially submerged propeller was comparable to its efficiency in the fully-submerged mode at the same thrust coefficient based on the immersed propeller area. This was an encouraging result when it was realized that the resistance, complexity, and vulnerability of fully-submerged pods were seriously hampering the design of high speed craft (greater than 60 knots).

In light of this, in 1969, it appeared reasonable to pursue a design of a high speed, supercavitating propeller specifically designed for partially submerged operation to propel the SES-100B. It was found, during water tunnel tests at Hydronautics, that, at high speed cruise, a 30-percent immersed area would give the best results. The full-scale efficiency data points for the SES-100B are included on Figure 226.

Although much work remains to be done in refining supercavitating propellers, both fully submerged and semisubmerged, for air cushion craft propulsion, it is encouraging to see that high efficiencies are attainable. A quick design chart designed by the author for determining propeller size to maintain high efficiency and yet operate away from cavitation boundaries is given in Figure 227. It combines the cavitation boundaries of Venning and Haberman (Figure 225) with the efficiency curves for subcavitating and supercavitating propellers given in Figures 221 and 226. An example helps illustrate the use of the design chart.

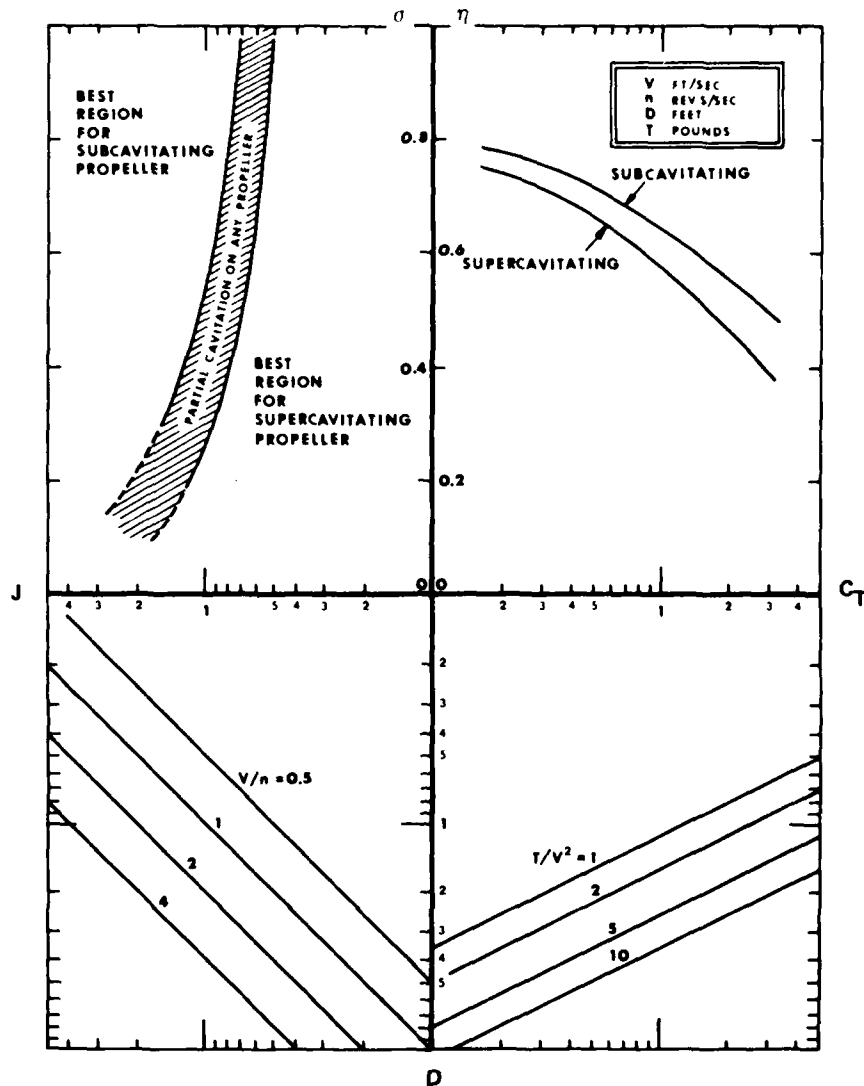


Figure 227 - Preliminary Design Chart for Waterscrews

Example Problem

An air cushion craft using two supercavitating propellers of 66 percent efficiency is to cruise at 60 knots with a drag of 72,000 lb. What are the propeller diameter and RPM to ensure operating in the best region for supercavitating propellers?

Solution

The thrust per propeller (T) = 36,000 lb. Hence, the parameter $\frac{T}{V^2}$ has the value,

$$\frac{T}{V^2} = \frac{36,000}{(60 \times 1.689)^2} = 3.50$$

A line (A) is now drawn vertically down from the supercavitating propeller efficiency curve at the value of $\eta = 66$ percent as shown below on the design chart (Figure 228). The line (A) stops at the intersection of the $\frac{T}{V^2}$ lines at the value $\frac{T}{V^2} = 3.50$. A new line (B) is then drawn horizontally from this point through the vertical axis of diameter (noting on the way that the propeller diameter $D = 3.0$ ft) until it intersects one of the lines of constant $\frac{V}{n}$.

Now at 60 knots the cavitation index σ has the value of 0.20. A third line (C) is then drawn horizontally from this value of σ and ending somewhere to the right of the Venning and Haberman band of cavitation, thus staying in the best region of operation for supercavitating propellers.

A fourth line (D) is now drawn vertically at a convenient intersection point on the constant $\frac{V}{n}$ lines so as to end in the upper left hand quadrant and intersect the $\sigma = 0.20$ line in this best region for supercavitating propellers.

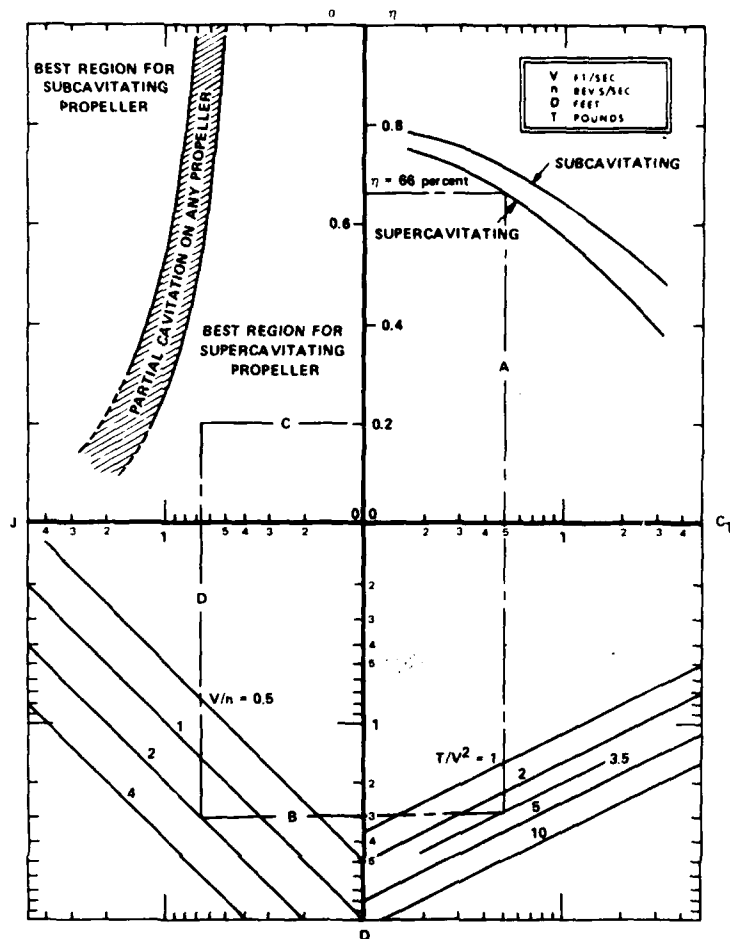


Figure 228 - Preliminary Design Chart Example

Choosing the value of $\frac{V}{n}$ to be 2.0 to meet these conditions completes the solution. Thus, because $V = 60$ knots, then

$$n = \frac{60 \times 1.689}{2} = 50 \text{ ft/sec}$$

and the propeller RPM = $\frac{60 \times 50}{2\pi} = 477$

Hence, the solution is

$$D = 3.0 \text{ ft}$$

$$N = 477 \text{ RPM}$$

and other pertinent parameters from the chart are,

$$J = 0.66$$

$$C_T = 0.50$$

Propeller Weight. Very little data are available on marine propellers applicable to air cushion craft use from which to draw reliable trends. Figure 229 summarizes some selected data to give an indication of propeller weights. Much of the available data on marine propellers apply to three-, four-, or five-bladed bronze or steel blades, very little on three- or four-bladed titanium propellers, and only one data point (SES-100B) to a six-bladed titanium propeller. The data are given, however, for completeness and the hope that more points may be collected as new high speed craft emerge.

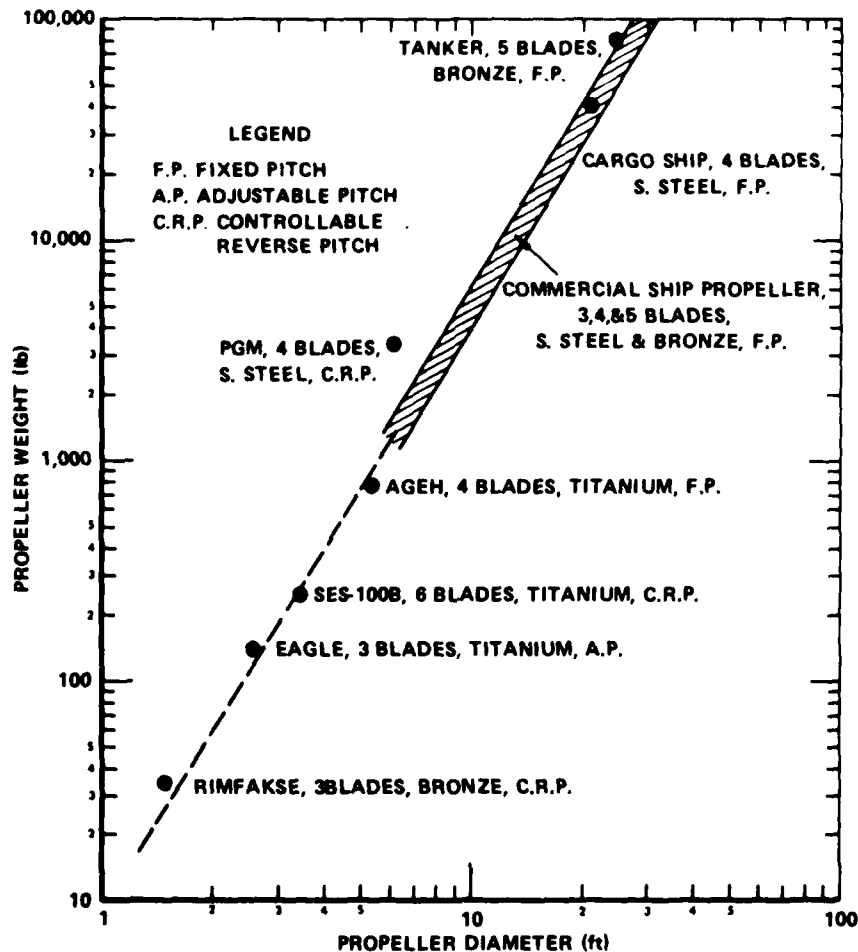


Figure 229 - Subcavitating and Supercavitating Propeller Weight

Waterjet Propulsion. This report has concentrated primarily on the amphibious form of air cushion craft. Consequently, only a brief review will be given of some selected developments associated with waterjet propulsion.

The waterjet is a well-developed device with a fascinating history that dates back several hundred years. Early references¹⁷³ include the design of a waterjet-propelled ship patented by Toogood and Hayes in 1661. In 1786, James Rumsey demonstrated to George Washington and Benjamin Franklin his steam-engine-powered, waterjet-propelled craft, almost a decade before Fulton's steamship! This 80-ft-long craft reached 4 mph on the Potomac River near Alexandria and was designed for passenger service between Alexandria and Washington. It was not a commercial success due, in part, to the low efficiency of the waterjet propulsion system.

The technical literature is replete with such historical examples of the application of the waterjet propulsion system. These include applications to British Navy gunboats (Enterprise, Nautilus, and Waterwitch) in the late 1800's, a fireboat in 1937, and many other similar installations. A brief history may be found in Reference 174. Many of these early uses of waterjet propulsion, however, suffered from poor efficiency that considerably slowed the development of this form of propulsion, and it was not until knowledge of high speed flows became more prevalent that the waterjet became more attractive.

The waterjet has the advantage of adding another dimension to the water propeller, whereby the propulsion designer can control, to some extent, the cavitation operating boundaries and noise levels of the propulsor through the shape of the ducting and the staging of the propellers. As knowledge of the hydrodynamic design increased, so did the efficiency of the waterjet and its use in a variety of craft. Over the last 20 years, there has been an increased application to high speed craft such as planing craft, pleasure craft and, most recently, hydrofoils. It is the application to hydrofoils that has provided the modern treatment and understanding of the hydrodynamics of waterjet propulsion. Although a little outdated, Brandau¹⁷⁵ provides a bibliography of some of the modern treatments on waterjet analysis and applications.

The application to air cushion craft has been somewhat limited. Three craft, the U.S. Navy XR-1B, the SES-100A, and the Vosper-Thornycroft VT 1M (a waterjet-propelled, man-carrying model of the waterscrew-propelled VT 1) represent the only applications to date. The XR-1B is a waterjet-propelled version of the XR-1.¹¹

One of the attractions of waterjet propulsion is the possibility of eliminating the drag associated with the transmission pods of propeller installations. Accordingly, in the original design of the SES-100A, a flush intake was envisaged to achieve low resistance at high speed. In 1969, during the initial design period of the SES-100A, the knowledge of such flush intakes in supercavitating flows was meager, and the design was changed to a pod ram inlet. It was reasoned that the technology of pod inlets was more advanced, based on the vast amount of data accumulated on supersonic aerodynamic pod design and on hydrofoil hydrodynamic pod design. Although this tended to negate some of the advantages, the pod inlet craft did obtain much needed data at the high Froude number flow

The treatment of real fluid effects and the relative effects of using flush and pod inlets has received the attention of many researchers and would be difficult to summarize here due to the many design variables involved. Hatte and Davis,¹⁷⁶ Johnson,¹⁷⁷ and Levy¹⁷⁸ provide adequate treatments of many of the real fluid effects contributing to the losses in a waterjet system.

The waterjet system comprises the pump, nozzle, ducting, and intake. To accommodate the wide operating spectrum from the subhump speeds to the superhump speeds of air cushion craft, it is necessary to have the inlet capable of varying its area: large openings for subhump, and small openings for superhump. The programming of the inlet opening to take proper account of boundary layer growth and cavitation inception has been part of the development for air cushion craft use. To illustrate some of the major effects, consider the thrust generated as

$$T = \rho Q (V_j - V_i) \quad (217)$$

where V_j is the issuing jet velocity from the nozzle and V_i is the stream velocity entering the inlet.

The efficiency of the system can be written as

$$\eta = \frac{(T - D_p) V}{550 P} \quad (218)$$

where now, because of the integrated nature of the propulsor (waterjet) and the ship through the inlet, the drag (D_p) of the inlet external hydrodynamic shape is included.

The pump must provide power (P) sufficient to generate the jet reaction plus the potential energy associated with the nozzle height (h_N) above the mean water level (M.W.L.), plus duct losses, but less any alleviation due to ram recovery in the inlet. The actual method of calculating these contributions differs among the various researchers (see Reference 175), making it difficult to make comparisons among the various installations. For example, Levy¹⁷⁸ assumes frictional losses proportional to jet velocity squared, while Johnson¹⁷⁷ assumes them to be proportional to craft velocity squared. Hatte and Davis¹⁷⁶ make no such assumption and consider the losses individually and give, for the waterjet system efficiency,

conditions. In parallel with the SES-100A program, the U.S. Navy proceeded to develop flush inlet information through both analysis and the modified XR-1B craft. These data have now allowed the SES-100A to be retrofitted with flush inlets and at the time of this writing it is pursuing a test program to explore the performance characteristics of such installations.

Because most of the program data are classified and as the program is also in its infancy, only a few basic elements of waterjet propulsion, as applied to air cushion craft, will be given. The schematics of representative waterjets with both flush and pod inlets are shown in Figure 230.

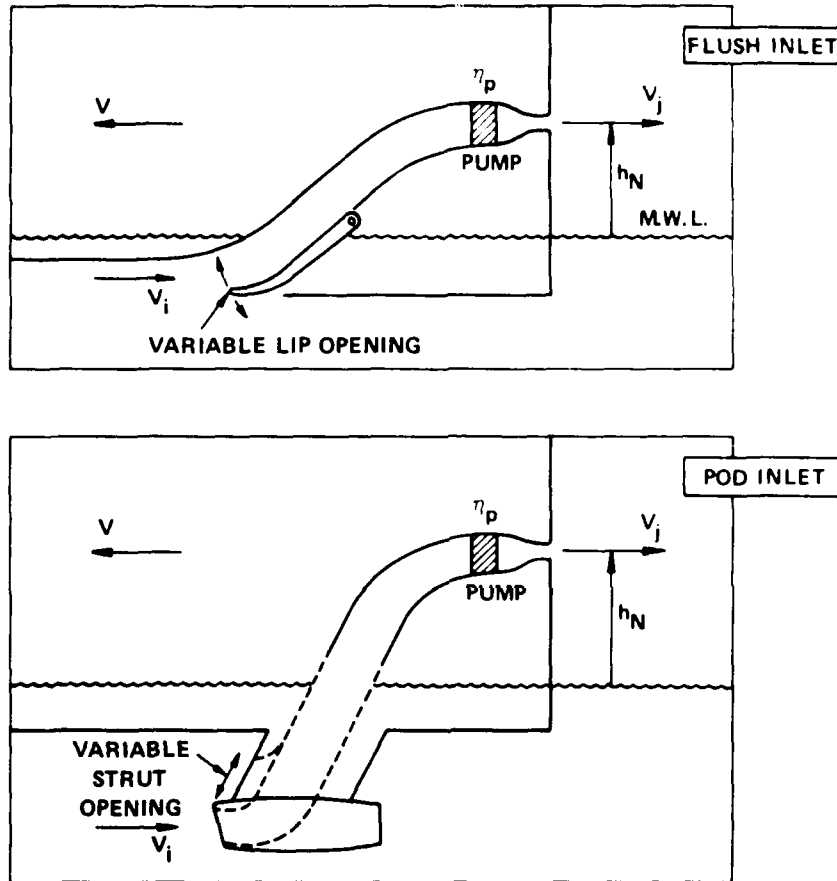


Figure 230 - Waterjet Schematic

The efficiency of a waterjet in ideal flow is the same as that for a shrouded propeller, that is,

$$\eta = \frac{2}{1 + \frac{v_j}{V}} \quad (216)$$

$$\eta = \frac{2 \cdot \frac{p}{2} \left(\frac{V_j}{V} - 1 \right)}{(1+K_2) \left(\frac{V_j}{V} \right)^2 - 1 + \frac{DLF}{\left(\frac{V_j}{V} - 1 \right)^2}} \quad (219)$$

where K_2 is a nozzle loss coefficient and DLF is a duct loss factor that incorporates all of the individual geometric terms of the total duct, the associated fluid mechanic term, and a nondimensional drag term to reflect the variations in the strut and pod parasitic drag. Sheets and Mantle¹⁵¹ take a slightly different approach by basing the friction losses on the exit jet velocity following Levy, but they include an elevation loss term following Johnson, again referred to jet velocity. If the Sheets and Mantle approach is further modified by including the strut-pod drag, as included in Equation (218), then the waterjet system efficiency can be written as

$$\eta = \eta_p \frac{2 \left[\frac{V_j}{V} - IVR \right] - C_{Dp}}{\left(\frac{V_j}{V} \right)^2 - (IVR)^2 + K} \quad (220)$$

where the pod or inlet drag coefficient (C_{Dp}) is defined as

$$C_{Dp} = \frac{D_p}{1/2 \rho V^2 A_p} \quad (221)$$

and where A_p is the area of the inlet opening taken normal to the flow. The inlet velocity ratio (IVR) is given by

$$IVR = \frac{V_i}{V} \quad (222)$$

which describes the ratio of the stream velocity entering the inlet to the craft velocity. This is a critical parameter in inlet design as will be discussed. The loss factor K is given by

$$K = K_L + \frac{2gh_N}{v^2} \quad (223)$$

where K_L is the Darcy-Weisbach friction loss term plus any turning, expansion, and contraction losses in the ducting between inlet and pump. The loss due to raising the water above the M.W.L. by height h_N is included in the K loss factor. It will be noticed that, for the ideal case of $IVR = 1$, $K = 0$, and $\eta_p = 1$, Equation (220) reduces to the simple momentum theory value, Equation (216), if the pod drag is ignored ($C_{Dp} = 0$). This result is given in Figure 231 where, for reference, the thrust coefficient

$$C_T = 2 \frac{v_j}{v} \left(\frac{v_j}{v} - 1 \right) \quad (224)$$

provides a comparative link with the other forms of propulsion considered in this chapter.

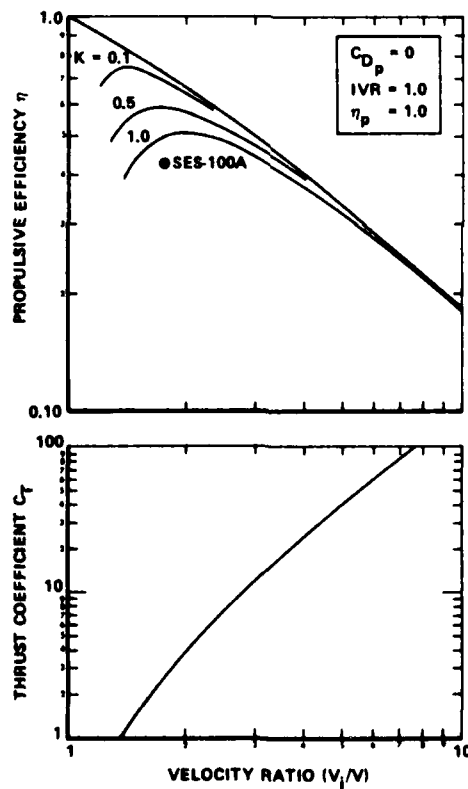


Figure 231 - Waterjet Efficiency

Full-scale test data for the SES-100A* are also given in Figure 231. Efficiencies above 45 percent have been attained, to date, for waterjet-propelled air cushion craft.

For optimum operation of high efficiency without cavitation, it is found that the control of the opening is a sensitive parameter. Figure 232 (upper curves) shows the SES-100A pod inlet cavitation boundaries predicted as a function of IVR for several (3) inlet positions. Cavitation free data are also shown.

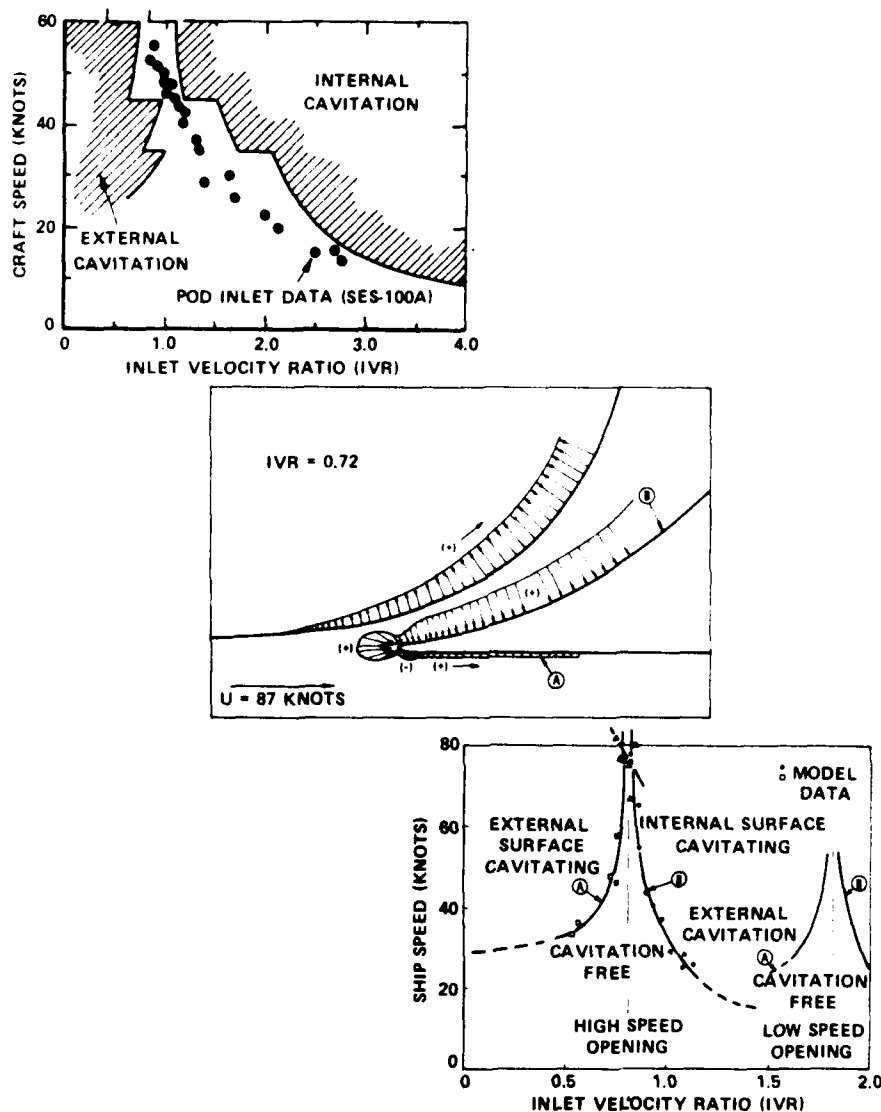


Figure 232 - Waterjet Inlet Cavitation

*Note that these results apply to the SES-100A with its fullysubmerged pod inlet prior to its current modification of a flush inlet.

It was found from tests that, at low IVR, cavitation occurred on the outer surfaces of the pod and strut; for high values of IVR, cavitation occurred on the internal (duct) surfaces of the inlet. To control the opening, the pod area (0.402 ft^2) was augmented by openings in the strut L.E., increasing the opening up to a maximum of 0.802 ft^2 . The area adjustments are by stepped positions incurring the discontinuous boundaries. It is seen that, as craft speed increases, the available inlet area must be controlled to close limits to avoid cavitation. This is a characteristic of all inlets, as may be seen by the cavitation inception curves for a typical flush inlet shown in the middle and lower curves of Figure 232 for both external surfaces (marked A) and internal surfaces (marked B). The ability to predict these cavitation boundaries is not well advanced at this stage of development. Data from the SES-100A with its new flush inlet is not for public distribution at this time.

The pump design has also benefited from the development of both planing boats and hydrofoils. Table 14 summarizes characteristics of some pumps that have been used in the SES-100A and other craft.

The reader is cautioned that the data are from one manufacturer and may not be completely representative of other manufacturers' pumps. The nondimensional performance in terms of specific diameter (D_s) and pump efficiency (η_p) as a function of the specific speed (N_s) of the particular stage is given in Figure 233 for the pumps considered.

The definitions of the parameters D_s and N_s are as used in Chapter VIII with the density of water used instead of air. From the pump data plotted, the specific diameter can be approximated by the equation

$$D_s = 0.012 + \frac{2.5}{N_s} \quad (225)$$

Included in Table 14 are the values of the net positive suction head (NPSH) in ft and the suction specific speed (S_s) defined as

$$S_s = \frac{nQ^{1/2}}{(gH_{sv})^{3/4}} \quad (226)$$

TABLE 14 - WATERJET PUMPS

Craft	Manufacturer	Type	No. of Stages	H (ft)	Q (GPM)	N (rpm)	hp	D (in.)	η_p	NPSH (ft)	S _s	N _s	D _s	Remarks
SES-100A	Aerojet	A	2	260	18,000	2,070	1,460	18.6	0.84	47	292.3	81.27	0.045	Air Cushion Craft
		M		1,250	18,000	4,660	6,540	17.6	0.90	306	160.7	56.7	0.063	
PBM (Foilborne)	Boeing/ALRC	A	2	162	99,500	712	5,000	44.6	0.84	26	340.2	92.61	0.041	Hydrofoil
		M		453	99,500	1,555	13,000	30.5	0.90	196	179.6	94.5	0.036	
PBM (Ballborne)	Boeing/ALRC	M	1	86	31,700	965	800	24.4	0.89	25	291.1	113.4	0.034	Hydrofoil
PBM Test Pump	Boeing/ALRC	M	1	420	16,600	3,600	2,000	12.7	0.90	178	179.6	94.5	0.036	
SES 2000 Design Study	ALRC	A	2	283	130,300	943	11,500	44.6	0.84	45	370.4	94.5	0.041	SES Design Study
		M		750	130,300	2,000	28,500	30.5	0.90			94.5	0.036	
Scout	ALRC	A	1	143	5,340	2,800	250	10.7	0.80	26	340.2	94.5	0.041	
Bridge Erection Barge	ALRC	A	1	19	25,000	950	150	20.0	0.80			311.85	0.021	
KM 521 (2-1/3 ton truck)	ALRC	A	1	16	8,500	1,400	50	11.5	0.69	9	472.5	285.4	0.020	
A = Axial M = Mixed Flow														

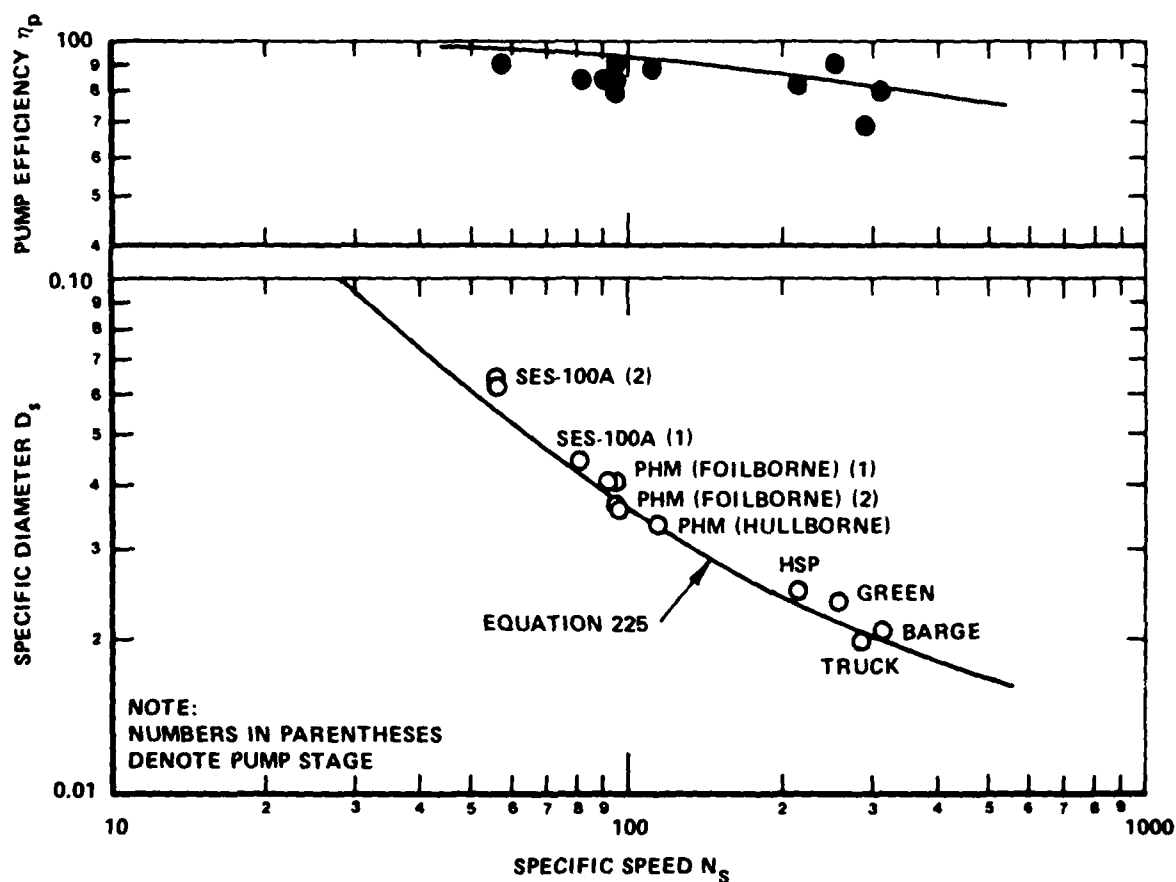


Figure 233 - Nondimensional Waterjet Pump Performance

which is the same as the specific speed (N_s), except that the head, H_{sv} , is the net positive suction head (NPSH) available at the pump inlet rather than the head developed by the pump. The head, H_{sv} (=NPSH), is the net difference between the total inlet head, including any ram recovery, and the vapor pressure of water.

The suction specific speed thus places a limit on the pump operation and characteristically limits the thrust capability at low speed.

The thrust curve for the SES-100A (normalized to comply with security classification) is shown in Figure 234, indicating an area of limited thrust due to pump cavitation. In this respect, it suffers from a limitation similar to that affecting the supercavitating propeller, where care must be taken to ensure sufficient thrust to overcome primary (and secondary) hump drag.

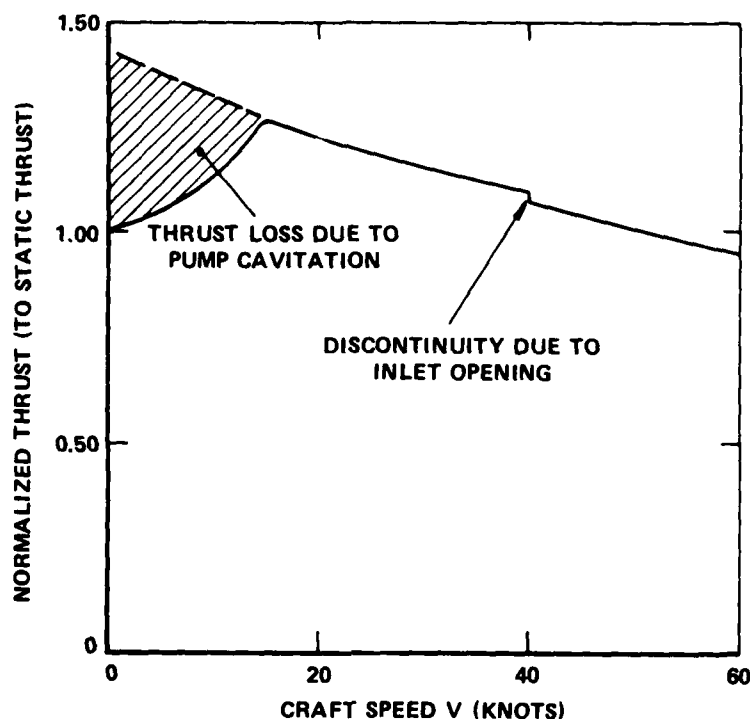


Figure 234 - SES-100A Thrust Curve (Pod Inlet)

The actual value of the suction specific speed and its limit on thrust is variable, depending upon the internal hydrodynamic design of the impeller. The SES-100A was deliberately designed to operate at high suction specific speeds. Figure 235 (upper photograph) shows the SES-100A impeller after approximately 200 hr of test operation, and it shows no signs of cavitation damage. More information is required, gathered during sustained operation representative of commercial and military missions, to determine whether such a design can eliminate the concern of pump cavitation damage.

Although a broad base of waterjet propulsion data from operational air cushion craft does not exist, it can be said that the data that are available are encouraging. Continued development on ongoing U.S. Navy programs will provide the necessary data base on which to base broader predictions. The data available from hydrofoil waterjet pumps, such as the 18,000-hp foilborne unit for the PHM hydrofoil that successfully passed static tests in 1974 and is continuing to show good performance during its trials today, will greatly expand the data base. Figure 235 (lower photograph) shows the foilborne pump during ground tests at full power together with a view of the first-stage rotor during fabrication.



Figure 235 - Waterjet Pumps

CHAPTER X

HIGH AND LOW SPEED DEVELOPMENTS

As described in Chapter II, this summary of air cushion craft development has been divided, albeit somewhat arbitrarily, into three groups: low speed (0 to 30 mph), intermediate speed (30 to 100 mph), and high speed (100 to 300 mph). This chapter will outline some of the activities and the nature of development of those craft designed specifically to operate efficiently at high speed and those designed to operate efficiently at low speed.

HIGH SPEED DEVELOPMENT

Because, in the high speed mode, the ratio of dynamic lift to static (fan-generated) lift is close to unity, that is, $k = 1.0$, the shape of any craft designed for this mode takes on radically different forms from those discussed heretofore.

The shapes of high speed craft become more streamlined and capable of generating aerodynamic lift.

The stage of development of the high speed or aerodynamic form of air cushion craft (see Chapter II, Figures 8 to 10) has not progressed much beyond the state-of-the-art that existed a decade ago when the U.S. Navy concentrated research and development on the intermediate speed form of air cushion craft. There has, however, been some recent interest prompted by the resurgence of the U.S.S.R. developments as shown by the Caspian Sea Monster (Figure 10) and other machines and also by the continued development in Germany with the flight testing of the X-114 (see later). Because of these activities, the U.S. Navy reexamined the high speed aerodynamic air cushion craft and its possible use as a military platform.^{30,31}

A fairly complete summary of the various projects that have evolved in most corners of the world over the last 40 years, until the most recent developments mentioned above, has been given by Belavin.³ A summary of the key features of the state-of-the-art since that time are given here.

In assessing the various developments, it is helpful to categorize the craft into two main groups, viz:

1. Those aerodynamic air cushion craft that are constrained to operate in ground* effect continuously.
2. Those aerodynamic air cushion craft that fly out of ground effect occasionally.

The operative words in the above two categorizations are continuously and occasionally as they have a significant effect on the configuration and the nature of the governing force mechanisms. For example, those craft that operate continuously in surface effect and have to contend with operating close to rough (and random) seas tend to be of low aspect ratio for structural compactness and maneuverability reasons. Their loss of

*It is customary to talk about ground effect even for those craft that operate over water or other media. This report will use the term surface effect when talking about the general form.

aerodynamic efficiency due to low aspect ratio is offset by the gains in aerodynamic lift (and reduction of drag) incurred by operating in surface effect. On the other hand, those craft designed to operate occasionally out of surface effect tend to have higher values of aspect ratio so that, when at altitude, the loss in surface effect lift is offset to some extent by the higher aspect ratio. It is difficult to give a precise definition to "low" and "high" aspect ratio, because this is dependent on many factors. Generally the "low" values might have aspect ratios (AR) of 1 to 2 while "high" values would be greater than 2.

Further, if the craft is to fly continuously out of surface effect then it is no longer an air cushion craft but an airplane! In this case, airplane-like configurations evolve and would have the familiar values of $AR = 6$ or more. Any consideration of the use of the air cushion on such airplanes would then be in the nature of a takeoff and landing device.

The Bell Lake Amphibian LA-4 is such an aircraft.¹ The attention in this summary is restricted to those craft that spend either a considerable amount or all of their time operating in surface effect and their technological development is dominated by this mode of operation.

The various craft that have either been built or are under development fit into either of the two categories described and the ramifications of the design choices can be seen by examining the configurations selected. Common to all high speed aerodynamic air cushion craft has been the need to resolve two technical problems. These problems have plagued the designers developing practical craft that can operate safely over rough water and carry acceptable pay loads. These are:

1. The ability to operate at very low clearances (to gain surface effect advantages) over random waves at high speed without crashing into the waves.
2. The ability to operate in an aerodynamically stable condition in the flow field of varying downwash and the natural surface effect tendency to "pitch up" and become unstable.

An additional problem to (1) and (2) above is that related to the maneuverability of the high speed, aerodynamic air cushion craft. This problem relates to the ability to turn the craft without banking to generate the side force with low clearances to the ground (or waves). This particular problem has already been discussed and solutions described in Chapter V on the control of air cushion craft.

The history of such craft contains, unfortunately, many examples of high speed pitch-up. This problem is also found in hydroplane design where, at high speed, the craft tends to pitch up at a rate that cannot be controlled by the pilot and the craft flips over on its back. Some recent developments in solving both these problems are briefly outlined here, after first describing some of the available basic data.

Some Basic Data

Kaario¹⁷⁹ is attributed with pioneering the aerodynamic form of air cushion craft when, in January 1935, he piloted his towed 8-1/2-ft long (6-1/2-ft wide) craft at 20 ft/sec and generated a lift-to-drag (L/D) ratio

approaching 15. Since that time many configurations and developments have occurred to take advantage of ground effect and evolve a practical machine.

Basically, the intent is to shape the hull or body of the craft with a wing-like geometry such that, for high speed cruise, the lift is generated in whole or in part by the energy of the oncoming stream. The lift may then be treated generally from the change in bound circulation around the body caused by the forward motion and the proximity of the surface. Extensive work both theoretically and experimentally has been conducted on this increased lift due to operating in "ground effect." The stimulus for this work in the main has been the need to understand the characteristics of wings of aircraft as they approach and take off from the ground. A

summary of some of the data appropriate to air cushion craft was prepared²⁸ and summarized here in Figure 236. The data show both the lift coefficient (C_L) and aerodynamic lift-to-drag ratio (L/D) of representative low aspect ratio wings operating close to the surface.

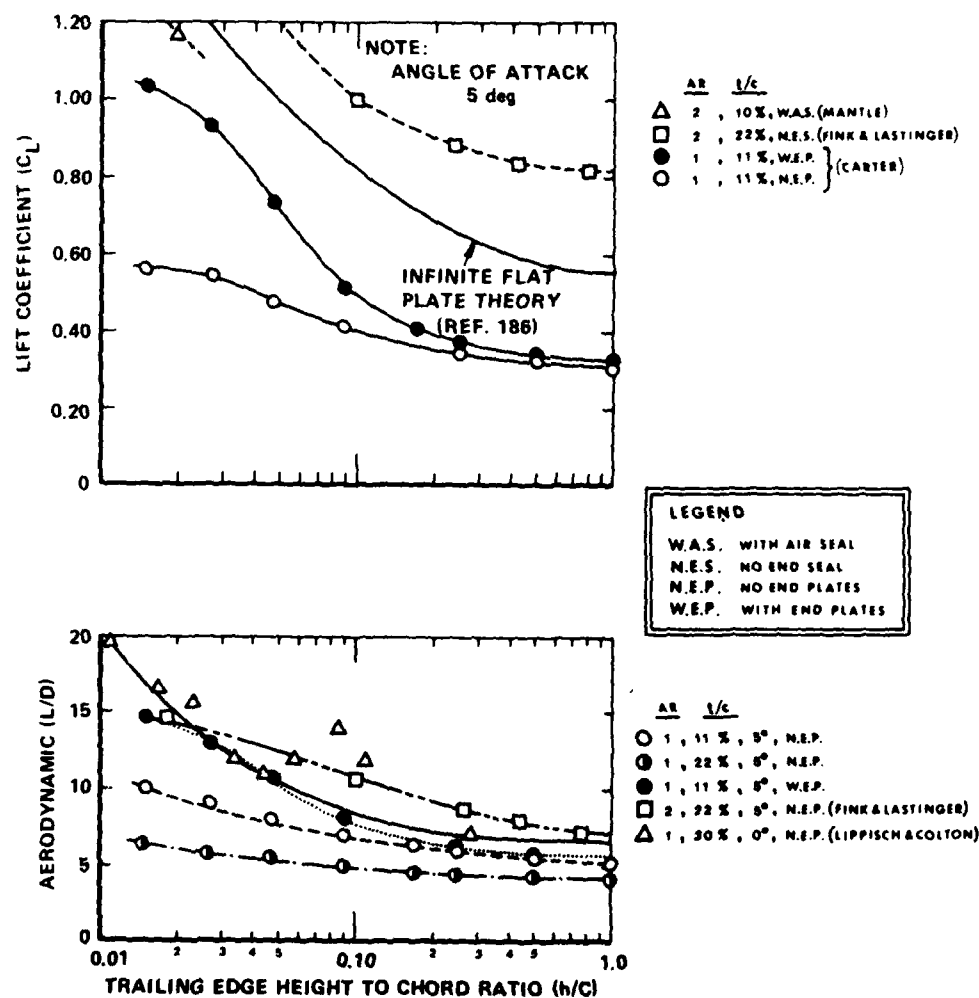


Figure 236 - Aerodynamic Lift and Drag in Surface Effect

The lift coefficient C_L is defined for steady flight as

$$C_L = \frac{W}{1/2 \rho V^2 S} \quad (227)$$

where S is the wing area and, thus, C_L is the inverse of the pressure number (k) used in Chapter III on performance. The data on lift (C_L) and aerodynamic L/D are shown to be a strong function of the height above the surface expressed by the ratio (h/C), where h is the height at the trailing edge (lowest point for positive α) and C is the chord or length of the craft. It is seen that, below heights given by $h/C = 0.20$, surface effect gives substantial improvements in lift. The benefits of surface effect have been known since the pioneering days of aircraft. Betz¹⁸⁰ considered this problem in detail while Wieselsberger¹⁸¹ considered the same problem not only for single wings but for biplanes and, specifically, from the viewpoint of wing resistance based on original work by Prandtl. A more detailed dissertation of the experimentally observed characteristics of wings in motion near the surface may be found in the early work at the Central Aero-Hydrodynamical Institute in Moscow in 1939 by Serebrisky and Biachuev.¹⁸²

More recent experiments of direct application to air cushion craft are those by Fink and Lastinger¹⁸³ in 1961 where wings, with aspect ratios (AR) of 1.0 and 2.0 and of various thicknesses, were tested in wind tunnels to measure lift and drag in ground effect. The Fink and Lastinger data are included in Figure 236. Similar work by Carter¹⁸⁴ is also included in Figure 236. Although the work of Carter is labeled "ground" proximity, it is of particular interest in that the tests were conducted over water. The effect of end plates is also seen in Figure 236 from the Carter experiments.

Theoretical treatments for such wings in surface effect have also received considerable attention in the literature.³ Blenk¹⁸⁵ provides a concise summary of the effects of ground proximity on the lift, lift curve slope, induced drag, pitching moments, and shift of center of pressure (C.P.) on a variety of wing shapes. Blenk summarizes work by Thomas, Ackerman, Bock, Gersten, and Braunss and Lincke, among others. Braunss and Lincke¹⁸⁶ developed the theory shown in Figure 236. More recent experiments may be found in Reference 187, where empirical relationships are given for the lift and drag of ram wings of finite thickness.

In the U.S.S.R. there has been a renewed emphasis in augmenting the lift gained when operating the wing close to the surface, with the added benefits of the propulsion engine efflux. This technique, first used by Kaario in 1935, consists of so positioning the propulsor that the high

velocity jet flows under (and sometimes over) the wing to increase the momentum flux and, thus, augmenting the lift. In the U.S., this has been described as the power-augmented-ram (PAR) wing-in-ground (WIG) effect.¹⁸⁸ The U.S. Navy has been pursuing this particular version of the high speed air cushion craft with the acronym PAR-WIG as part of its evaluation of possible future Navy craft.³¹ Figure 237 shows a model of such a craft

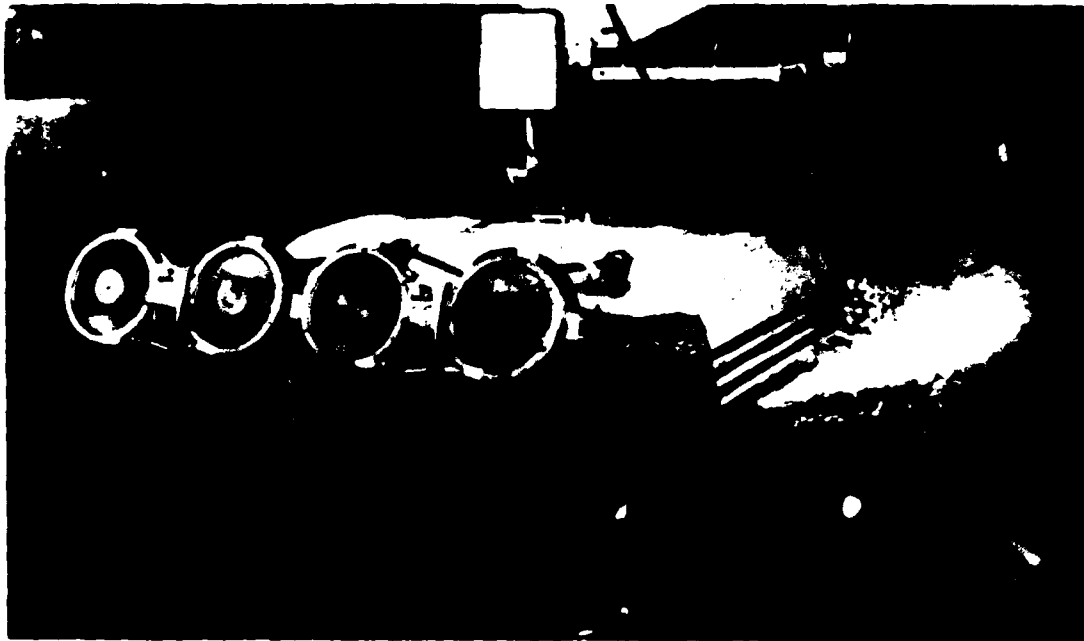


Figure 237 - U.S. Navy PAR-WIG Model in Tow Tank

undergoing tests as part of that evaluation. This particular model has four propulsors mounted forward and angled down to deflect their efflux beneath the wing ($AR=1.0$) to augment its lift. In this photograph the thin end plates (painted with stripes) are clear of the waves but would impact the higher waves in the random (head) seas tested.

Krause et al.¹⁸⁹ provide a concise description of the state-of-the-art of this renewed work into this particular form of air cushion craft. The technology is still in its early stages particularly in regard to obtaining theoretical predictions for the performance and stability at forward speed. Some results for the lift and drag under static conditions are, however, available and summarized here. Figure 238 illustrates the basic elements in the geometry of the PAR-WIG when operating at zero forward speed (static) over a flat ground plane with no oncoming waves. Because of the incorporation of the propulsor efflux and the fact that the results are for static conditions a comparable set of lift and drag values for the unaugmented

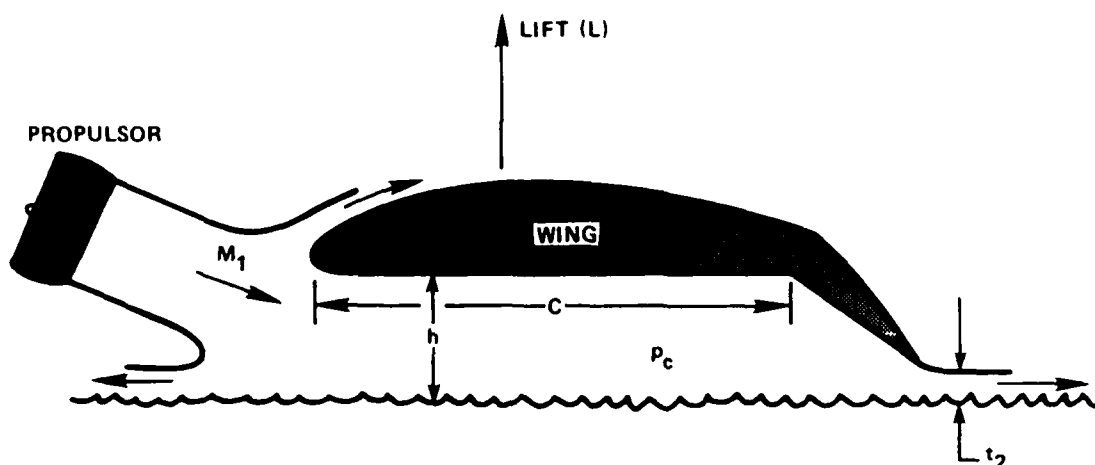


Figure 238 - Geometry of PAR-WIG

case (Figure 236) cannot be easily given. Krause et al.,¹⁸⁹ however, provide an equivalent lift-to-drag polar diagram as shown in Figure 239.

The lift per unit span for the PAR-WIG under static conditions is given by,

$$L = p_c C \quad (228)$$

where C is the chord to the flap (i.e., as shown) of this two-dimensional wing. The momentum of the propulsor(s) at the entrance to the plenum beneath the wing is

$$M_1 = \rho U_1^2 t_1 \quad (229)$$

where U_1 is the velocity of the jet and t_1 is the thickness at the entrance. The results in Figure 239 are expressed in terms of the ratio of this lift to the jet momentum (L/M_1) and to other key geometric parameters such as the thickness (t_2) of the jet efflux emanating beneath the trailing-edge of the flap, the height of the wing (h) measured at the quarter-chord point above the ground plane, and a scaling factor (a) given by

$$a = \frac{9}{4} \frac{h}{\bar{t}(1 + \cos \theta)} \quad (230)$$

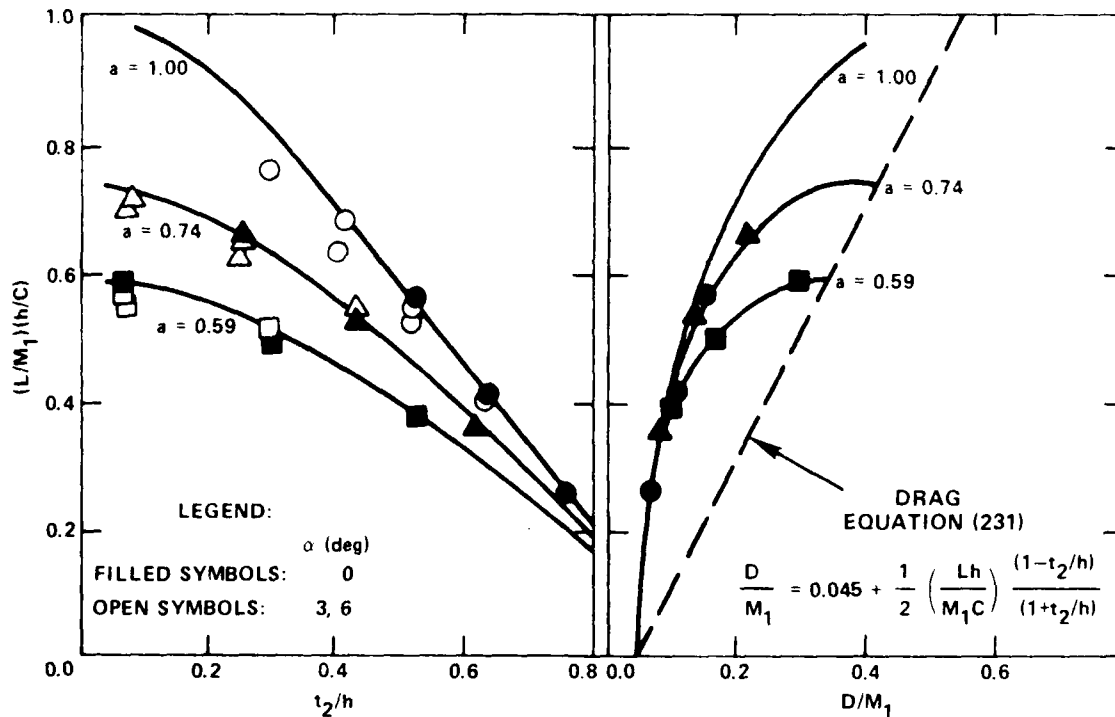


Figure 239 - PAR-WIG Static Lift and Drag

where θ is the inclination of the propulsor and \bar{t} is the average thickness of the jet determined by the nature of the mixing process of the turbulent jet.¹⁸⁹ The experimental results are shown for different values of the angle of attack (α) of the wing to the ground plane. The agreement is quite good (see Figure 239) except for the prediction of the drag which, using the two-dimensional and axisymmetric turbulent jet theory and accounting for leading-edge suction, is given by

$$\frac{D}{M_1} = 0.045 + \frac{1}{2} \frac{L}{M_1} \cdot \frac{h}{C} \cdot \frac{1 - t_2/h}{1 + t_2/h} \quad (231)$$

This relationship¹⁸⁹ is shown by the dotted line in Figure 239 and is seen to overpredict the drag for any given value of lift and geometry. Work is continuing in this area to provide better agreement.

It should be noted that this drag is at zero forward speed. It is computed from the pressure forces acting on the undersurface and from the leading-edge suction. The treatment of drag at forward speeds is not well understood at this time.

In addition to showing this basic data, a summary is included of possible solutions to the two items of concern to the remaining high speed

aerodynamic air cushion craft, whether or not the power augmentation feature is integrated into the design. These are, as enumerated before, (a) the vulnerability of the end plates in rough water and (b) the longitudinal stability of such craft.

Possible End Plate Solutions

At the speeds contemplated for such craft (100-300 mph), the drag and structural loading on any rigidly attached end plates to the wing are unpalatably high and not conducive to practical design. The end plates shown on the model in Figure 237 are very thin for minimizing both aerodynamic and hydrodynamic drag, but clearly, when scaled to full-scale vehicle size, would be structurally unsound, especially in the case of experiencing any slight angle of yaw to the oncoming waves. By way of example, some calculations made for the PAR-WIG designs, shown in Reference 31, illustrate the nature of the problem. These calculations are shown in Figure 240 which also shows the depth of immersion of the end plates in various sea conditions.

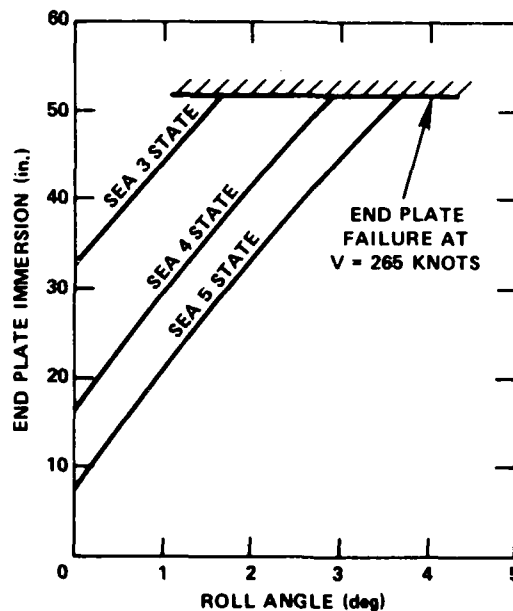


Figure 240 - End Plate Immersion

It is seen from Figure 240 that a roll angle of only 2 to 3 deg will place the end plates in jeopardy of complete structural failure. These calculations were made assuming no distortion of the structure. In reality, end plate deflection would increase the yaw angle of the end plates to the oncoming stream, thus increasing the forces and causing structural failure at even lower immersions and roll angles. Some relief can be surmised if the end plates are shaped to provide hydrodynamic lift and allow the craft to roll back or the end plate to move up independently. Several schemes

have been investigated by different groups to avoid this problem. Figure 241 shows early configurations employing different end plate solutions. In the upper photo, the Kawasaki KAG-3 used large full-length side hulls designed to withstand the hull-pounding directly. This used water propulsion and was not designed for very rough seas. In the lower photo, the Lippisch X-113 used very small floatlike end plates on swept forward wings to minimize the waterlength of the end plates. When the waves became too rough, the X-113 simply flew higher (at the expense of reduced surface effect). Both these craft are no longer operational and further research was needed to solve the end plate problem. One particular scheme is to incorporate a shock-absorber into the end plates. This is done in the Rhein-Flugzeugbau aerofoilcraft RFB-114 (originally called the Lippisch X-114) shown in Figure 242. Rhein-Flugzeugbau (RFB), located in Monchengladbach, Germany, has been involved in the research and development of WIG aircraft since 1968 and recently purchased the Lippisch patents on the concepts demonstrated in the X-112 and X-113 craft (see Figure 9, top photographs). The X-114, shown in Figure 242, has undergone tests in the Baltic Sea although test data in rough water has not been made available. Eighty percent of the time the waves in the Baltic are less than 5 ft, leading to the size of the X-114 which has a wing span of about 23 ft. It accommodates six persons and weighs 2980 lb. When in surface effect, the cruise speed is 81 knots and, when at altitude, the cruise speed is 108 knots. The total installed power (Lycoming 10-360) is 200 hp. The shock-absorber end plates are more like floats, as can be seen from Figure 242, and, judging by the photograph, are of quite short stroke. Although these particular forms of end plates can absorb a certain amount of rough water contact, the main technique would be to climb to a higher altitude when the seas become rough but, of course, this loses the advantage of the surface effect.

Another scheme would be to replace the rigid end plates with some device more resilient or forgiving to wave impact. An air seal was used in the channel flow craft, the Columbia and VRC-1, as described in Figures 8 and 9. The channel flow craft was an attempt to eliminate the need for hard or rigid end plates and to provide the cushion sealing by wing tip, air jets powered by the lift fan system. This feature was also incorporated to provide a hover capability not inherent in the usual WIG concept. Some model data for the Columbia channel flow craft¹²⁰ are shown in Figure 243 for the particular case $h/C = 0.07$, which represents a relatively high cruising altitude (and, therefore, high sea condition capability) for such craft. With the air seals as used on the Columbia and VRC-1, the question of structural impact is thus eliminated at least up to certain clearances until the main hull becomes subject to wave slap. It might be argued that the hard end plate would be a more efficient sealing mechanism than an air seal. One measure of this would be to determine the effective aspect ratio of the sealed wing with air jet edge sealing. If the drag of the craft is written as,

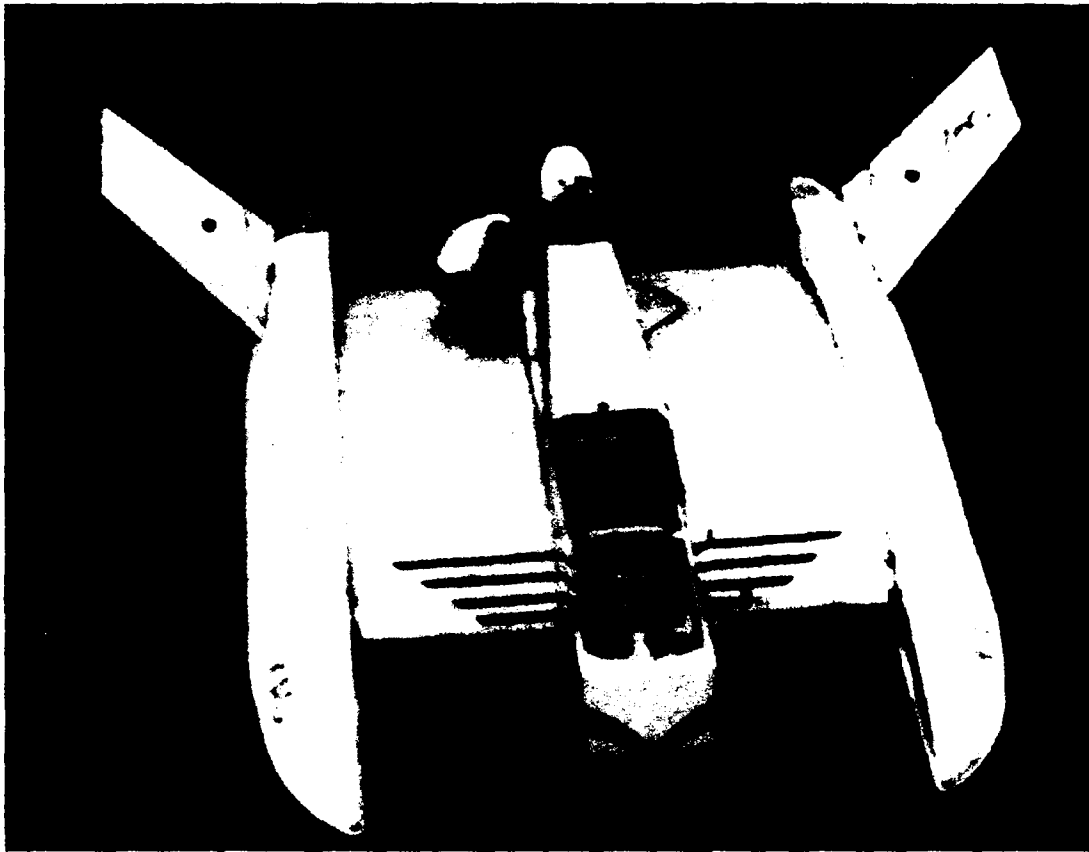


Figure 241 - Kawasaki KAG-3 and Lippisch X-113



Figure 242 - Aerofoilcraft RFB-114

$$C_D = C_{D0} + \frac{C_L^2}{\pi AR_e} \quad (232)$$

where C_{D0} is the aerodynamic profile drag assuming no contact with the waves, then, by comparing Equation (232) with experimental data¹⁹⁰ shown in Figure 243 the effectiveness of the air jet seal can be measured by calculating the effective aspect ratio AR_e and comparing it with the geometric aspect ratio which was 1/2 for the tests. From the data shown, the lift curve slope is 0.12/deg, the zero lift angle is -4.2 deg and the effective aspect ratio is 14, thus yielding an effective sealing factor of 28:1.

The air jet seal was employed on the VRC-1 in 1964 and, therefore, did not have the benefit of the skirt technology that has evolved since that time (see Chapter VI).^{*} It would seem plausible that skirt-like edge seals could be adapted to the high speed aerodynamic air cushion craft to provide further clearances for the main wing and minimize the detrimental hard end plate impacts with waves. Some rudimentary model tests were undertaken by the U.S. Navy in this regard,³¹ but much more work needs to be done to evolve practical solutions. One thought might be to incorporate a variable

^{*}Some skirt-like appendages were added to the air jets but were found to be of short life due to the abrasive action of high speed runs over the desert floor.

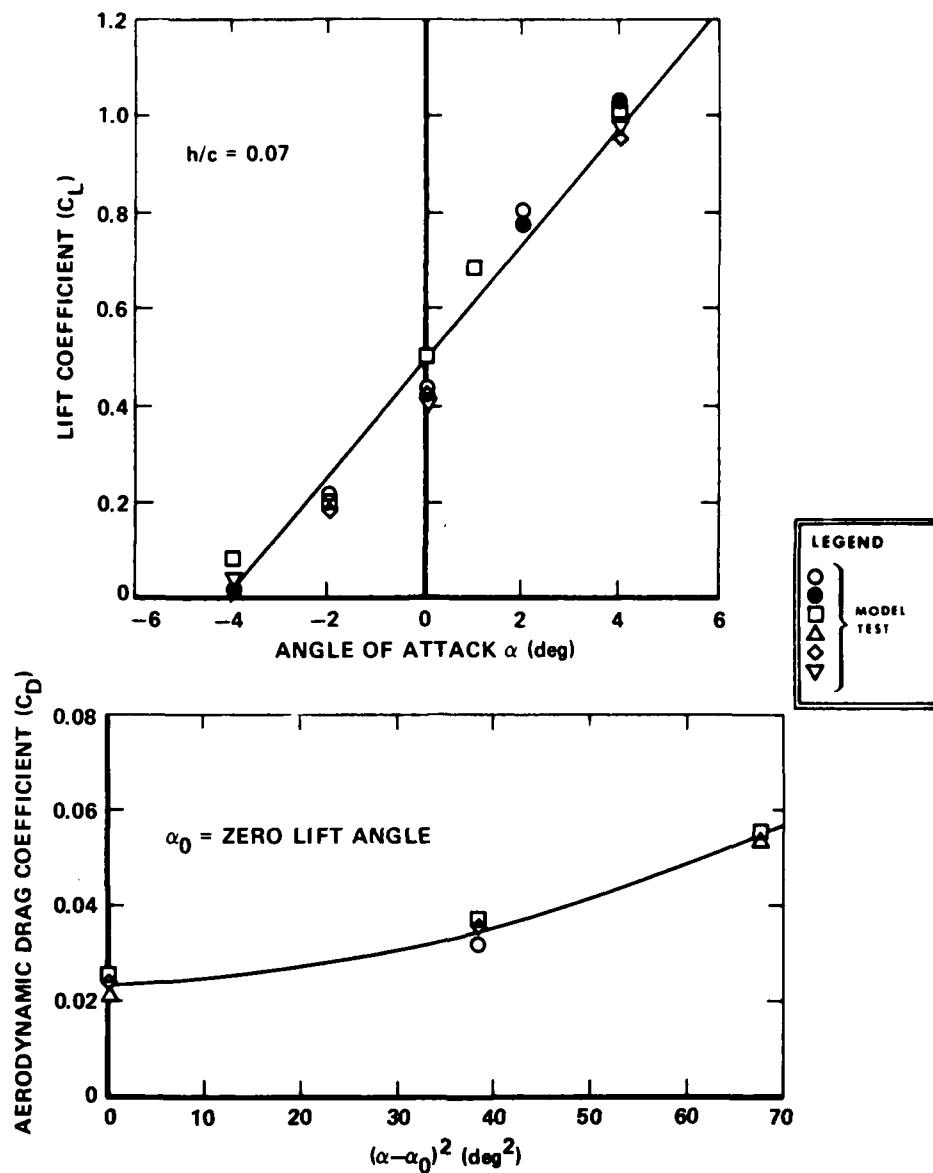


Figure 243 - Channel Flow Craft Lift and Drag

geometry feature such as that shown in Figure 244. Here the edge skirts would be extended for rough water operation to provide high clearance for the main hull, then retracted for calm water operation at lower clearances, thus maintaining the high aerodynamic efficiency offered with such geometries without paying the penalty of having to withstand high structural loads. Possible solutions to problems of these craft are still in the exploratory stages at this time.

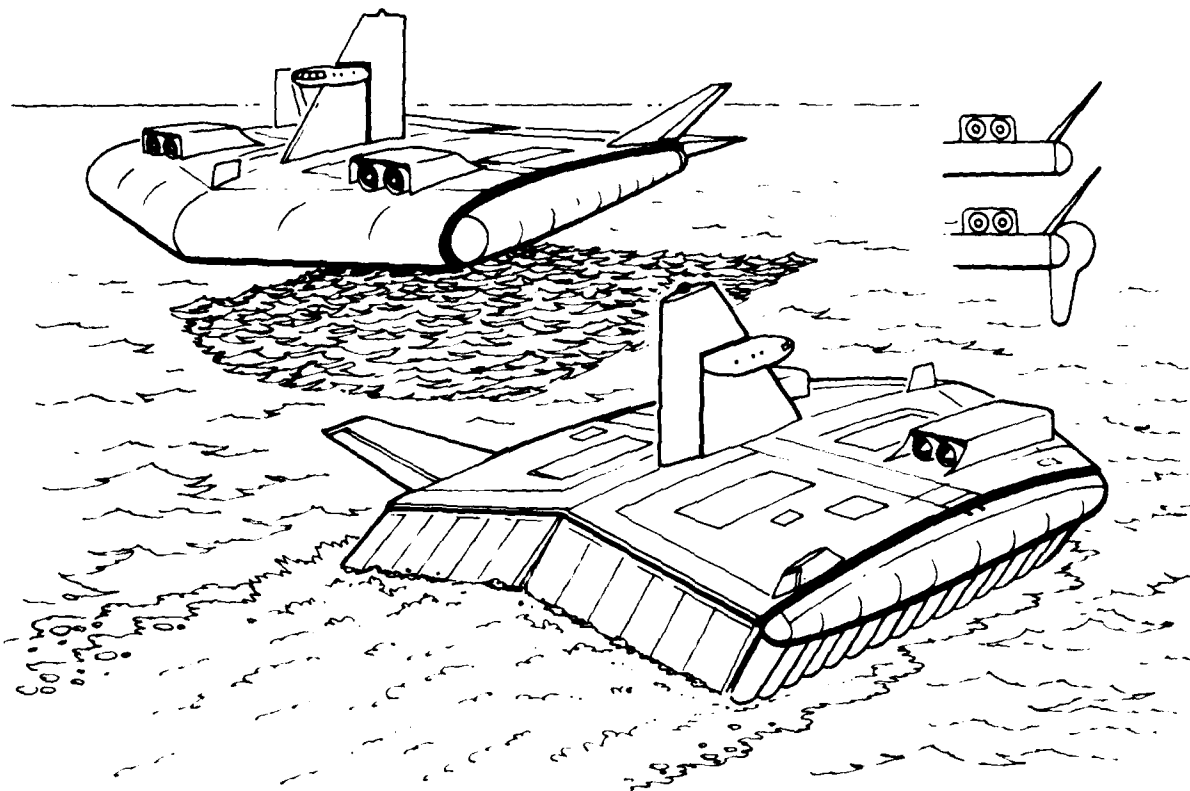


Figure 244 - Variable Geometry Skirted WIG Concept

Stability and Control Considerations

As stated earlier, one of the problems with aerodynamic craft operating in surface effect is the tendency to pitch up. As the height above the surface increases, higher angles of attack are required to maintain the same lift at the same speed. Also, the aerodynamic center in surface effect is at approximately 30 to 33 percent of chord back from the wing leading edge (L.E.) while, when coming out of surface effect, it moves forward to 25 percent of the chord position. Both these characteristics tend to increase the pitching moment and the tendency to pitch up. To combat this characteristic, unusually large (compared to conventional aircraft) horizontal tail stabilizers were needed to provide large variations in pitching moment.

Staufenbiel and Yeh¹⁹¹ provided a recent treatment of the longitudinal stability and control problem down to very low clearances (h), on the order of 4 percent of the span (B). Static and dynamic stability were considered as well as the effect of control inputs. Based on their analysis, there are three main characteristic oscillations, viz.: (a) a rotary oscillation, (b) a vertical oscillation, and (c) a periodic oscillation related to speed stability. Staufenbiel and Yeh¹⁹¹ found that the damping of the rotary oscillation decreased considerably as the surface was approached. It was also found that the vertical (or heave) oscillation is stable at very low clearances ($h/B < 0.5$), becomes unstable for clearances around $h/B = 0.5$, and becomes stable again at higher clearances. It was found that the instability in the vertical oscillation could only be removed by artificial speed stabilization. This could explain, in part, why some of the earlier craft without automatic stabilization systems experienced difficulty. The third mode (speed stability) was found not to be a problem at any altitude. These results, based on theoretical analyses, are a welcome addition to the knowledge on stability of aerodynamic air cushion craft operating at high speed in ground effect.

In practical craft, various schemes have been tried to reduce the tail size and to control this instability or pitch up tendency. The large pitching moment is caused by the need to keep the center of gravity of the craft near the 50 percent chord point for static balance at zero and low speeds and to keep the characteristic position for the center of pressure closer to the 30 percent chord position at high speeds.

For the VRC-1, the use of a blowing jet flap was incorporated to alleviate the size of the horizontal stabilizer necessary to provide the restoring pitching moment. From model tests in 1962¹⁹² it was found that a 5 percent chord T.E. mechanical flap, augmented by blown cushion air, provided the ability to shift the aerodynamic center aft approximately 3 to 4 percent. This is shown in Figure 245 taken from Reference 192 where the results of the wind tunnel tests show how the static stability derivative (C_{M_α}) varies with angle of attack (α), position of center of gravity (x), and jet blowing coefficient (C_μ).

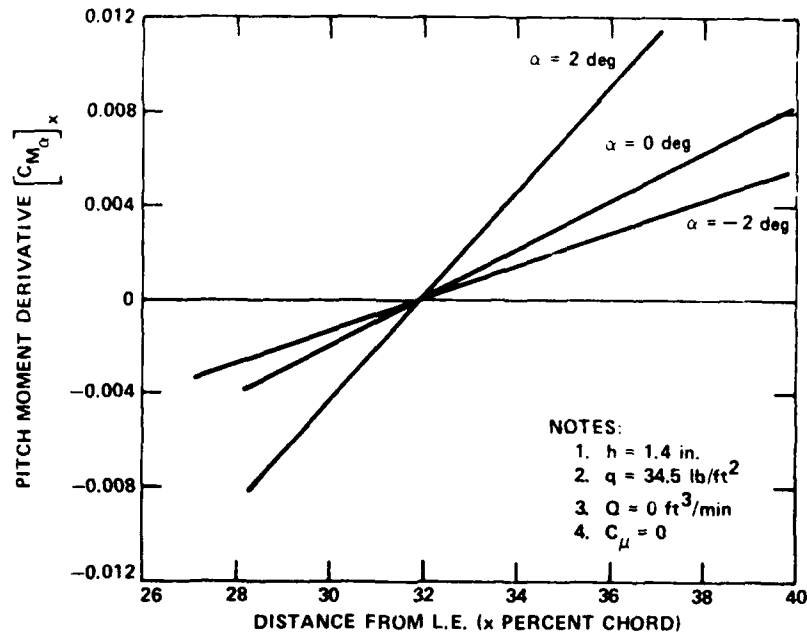


Figure 245a - No Jet Flap Blowing

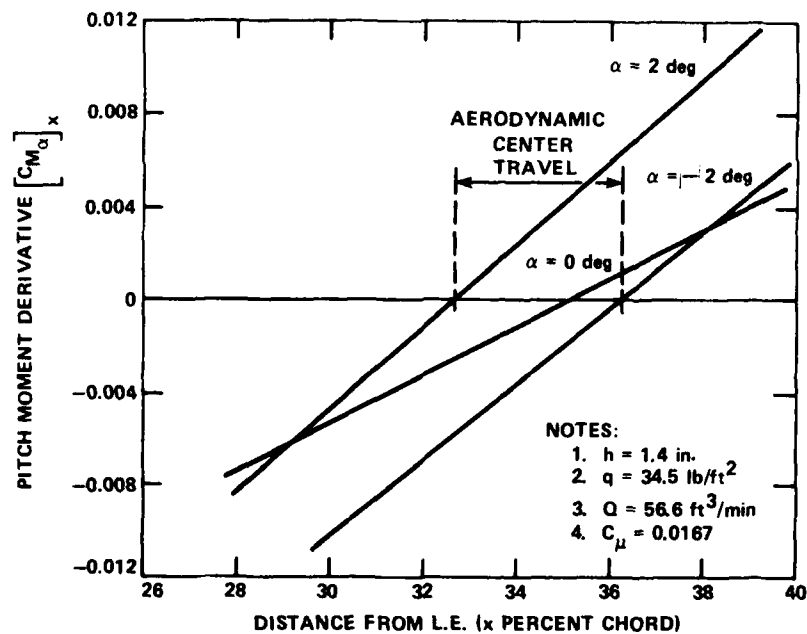


Figure 245b - With Jet Flap Blowing

Figure 245 - Jet Flap Effect on Aerodynamic Center in Ground Effect

The jet blowing coefficient is defined as,

$$C_j = \frac{M V_j}{1/2 \rho V^2 S} \quad (233)$$

where M is the mass of air blown over the flap. For these tests, a value of $C_j = 0.017$, which was equivalent to about 11 percent of the hovering flow cushion air requirement, was needed to provide attached flow on the mechanical T.E. flap and to control the aerodynamic center to the values shown. Figure 246 shows this blown T.E. flap during construction in 1964.



Figure 246 - VRC-1 Jet Flap

CONCLUDING REMARKS ON AERODYNAMIC (HIGH SPEED) AIR CUSHION CRAFT

The author has resisted making conjectures on construction features of future craft on the basis that it would be inappropriate in a state-of-the-art review that deals with proven accomplishments. It is felt, however, that the aerodynamic form of air cushion craft, if properly treated, could provide a very useful and versatile craft in the future and, thus, a slight departure is made from a state-of-the-art review. The air cushion craft has a problem akin to the supersonic aircraft that did not perform very well at subsonic speeds until solutions embodying the principles of variable geometry were invoked. In a similar vein, the aerodynamic air cushion craft, as built for many research craft and as proposed in recent studies, also does not provide a very practical or economical craft at low speeds or at hover. This is felt to be a shortcoming that could be overcome if pursued with technical solutions that are within the state-of-the-art. For example, adding retractable skirts, as practiced on the VRC-1 in 1964, but improved upon with present knowledge on skirt design, could provide a solution. With the skirts down, the craft would function essentially as an aerostatic air cushion craft with a hover and overland capability. As speed was increased and dynamic lift became dominant the skirts could be retracted (at speeds equivalent to $k = 1.0$). Figure 244 illustrated a brief conceptual look at such a design.³¹

Although no specific tests were done on such a configuration, the net effect on hydrodynamic and aerodynamic efficiency throughout the speed range can be postulated by overlaying the test results from several related test data. Figure 247 shows how the variable geometry feature could allow the craft to progress from a waterborne mode, where hydrostatic and hydrodynamic forces dominate, through the aerostatic mode (acting as an intermediate speed air cushion craft), and finally, with bow and stern skirts retracted, to operate at high speed in the aerodynamic mode.

The data shown in Figure 247 originally appeared in 1968²⁷ but are still applicable today. The curve labeled (A) in Figure 247 is for an air cushion hull model tested at General Dynamics²⁷ and represents the attainable efficiency at low speeds of an aerodynamic craft using variable geometry features. Such a craft is represented, for the purposes of identifying the principle, by curve (B) in Figure 247. If the speed were increased into the speed range $0.04 < k < 0.40$, the variable geometry craft (B) would operate in an amphibious mode with a completely peripheral skirt. This is shown by the envelope of the aerostatic air cushion curves shown for different air gaps, $0.009 < h/L < 0.018$. This particular set of data are taken from Figure 67 in Chapter III. As the speed is further increased into the aerodynamic mode, the bow and stern skirts are retracted. This condition would be reflected by the Lippisch and Carter data shown earlier in Figure 236. All curves shown are for a constant height above the surface, except for the aerodynamic mode where height increases with

speed which might be an appropriate safety requirement. What is not shown on Figure 247 is the condition when the end plates or skirts are completely retracted for very high speed over very calm water or during those occasional flights to altitude for military operational tactics purposes. As stated earlier much of these rudimentary tests and postulated developments require substantiation in a controlled development program but the potential appeared sufficiently strong to include them at this writing if, for no other reason, than to stimulate comment!

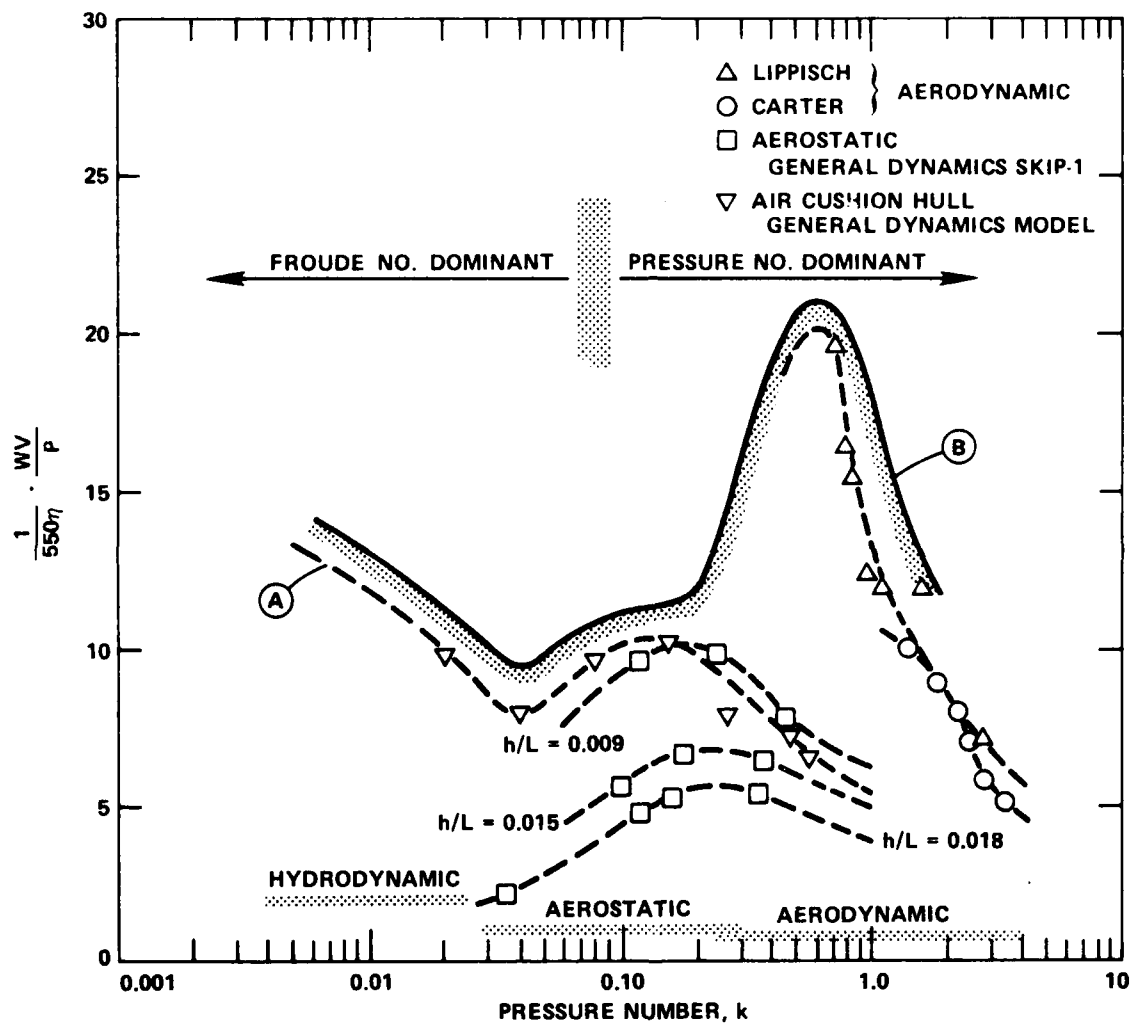


Figure 247 - Efficiency of Variable Geometry Craft

LOW SPEED DEVELOPMENT

When a form of transportation is being considered for incorporation into a transportation system, the economics demands efficiency. This has prompted continued research and development into reducing power requirements, lighter structures to increase payload, and other factors already discussed in the preceding chapters. There is, however, a growing development in the use of the air cushion in craft designed primarily to operate at low speed (and low power). The emphasis in these special craft has been to provide low-cost, utilitarian work horses, with the result that the craft again have taken on a radical change in configuration to that discussed before.

These low speed applications, usually below 5 to 10 mph, allow increased freedom in the design. As an important example, the air gap-to-circumference ratio (h/C) is allowed to be an order of magnitude less than those discussed heretofore. Values of 1/10- to 1/8-in. gaps are not uncommon, which has the result of considerably reducing the lift power requirements. Table 15 summarizes some of the more active examples of the low speed application of the air cushion principle. From the table, it can readily be determined that the lift power requirements are on the order of 2 to 7 hp/ton compared to the 15 to 35 hp/ton of the intermediate speed air cushion craft (see Figure 36, Chapter III).

Figure 248 shows some of the more recent applications. The top photograph shows the ACT-100, a heavy lift transporter designed and constructed (in Edmonton, Alberta, Canada) by Arctic Engineers and Constructors of Texas in 1971. The ACT-100 has been evaluated by the Canadian Ministry of Transport in Tuktoyaktuk, Northwest Territories, Canada, in November 1972 and on the Mackenzie River in the summer of 1973 as a cushion ferry. It has a normal gross weight of 250 tons and a payload capability of 100 tons. The lift power is provided by two 640-hp diesel engines driving two 4.5-ft-diameter centrifugal fans that generate 144 lb/ft^2 cushion pressure in a cushion system enclosed by a skirt system of the HDL design discussed in Chapter V (see Figure 72b). The cushion pressure of 144 lb/ft^2 (1 lb/in.^2) is designed particularly to be low enough in "footprint pressure" to avoid disturbance of the environmentally-sensitive tundra. A maximum acceptable footprint pressure for such a terrain is 1.5 lb/in.^2 .

The lower photographs in Figure 248 illustrate the basic form of the hover trailer, which can evolve into a variety of forms for transporting heavy loads over a variety of surfaces. The particular hover trailer shown is one designed by Mackley-Ace, Ltd., of Southampton, England, for Hover Trailers International, Ltd., based on the first hover-trailer development by Vickers-Armstrong in the early 1960's. A more recent craft produced by Mackley-Ace, Ltd., is the Sea Pearl, a 750-ton towed hover

TABLE 15 - LOW SPEED AIR CUSHION PLATFORMS

Vehicle	Manufacturer	Machinery	W (ton)	Cushion Pressure (lb/ft ²)	Flow Q ft ³ /min	Horsepower P (hp)	Size (L x B)	Speed
BHC Heavy Load Transporter	BHC	4 RR B815V Petrol Engines	155	5.4 psi	13,200	940 hp at 4000 rpm	90 ft x 16 ft 10 in.	
Hover Platform	Mack Ace	Caterpillar Diesel D334A and Volvo TD120A Diesel	178 (95-ton Payload)	128	--	498	84 ft 9 in. x 47 ft 5 in.	12 mph over land 10 knots over water
Hover Platform	Mack Ace	Caterpillar Diesel D334A and Volvo TD120A Diesel	69.95 (30-ton Payload)	124	--	498	49 ft 3 in. x 39 ft 0 in.	12 mph over land 10 knots over water
ACT-100	AEAC	2 Caterpillar D-348 Diesel	250 (100-ton Payload)	144	--	1280	75 ft 3-3/8 in. x 57 ft 0-3/8 in.	6 mph (Dependent on towing vehicle)
Hover Trailer	HoverJak, Ltd.	2 Deutz Diesels	22 (15-ton Payload)	80	10,000	356	40 ft x 18 ft	2 mph (approx.) (Dependent on towing vehicle)

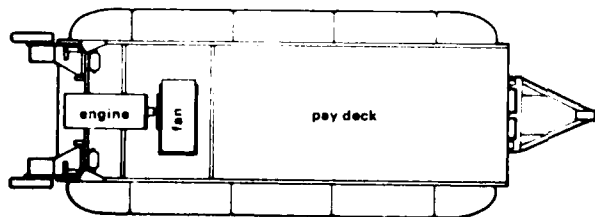
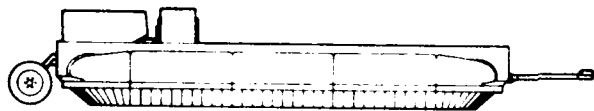
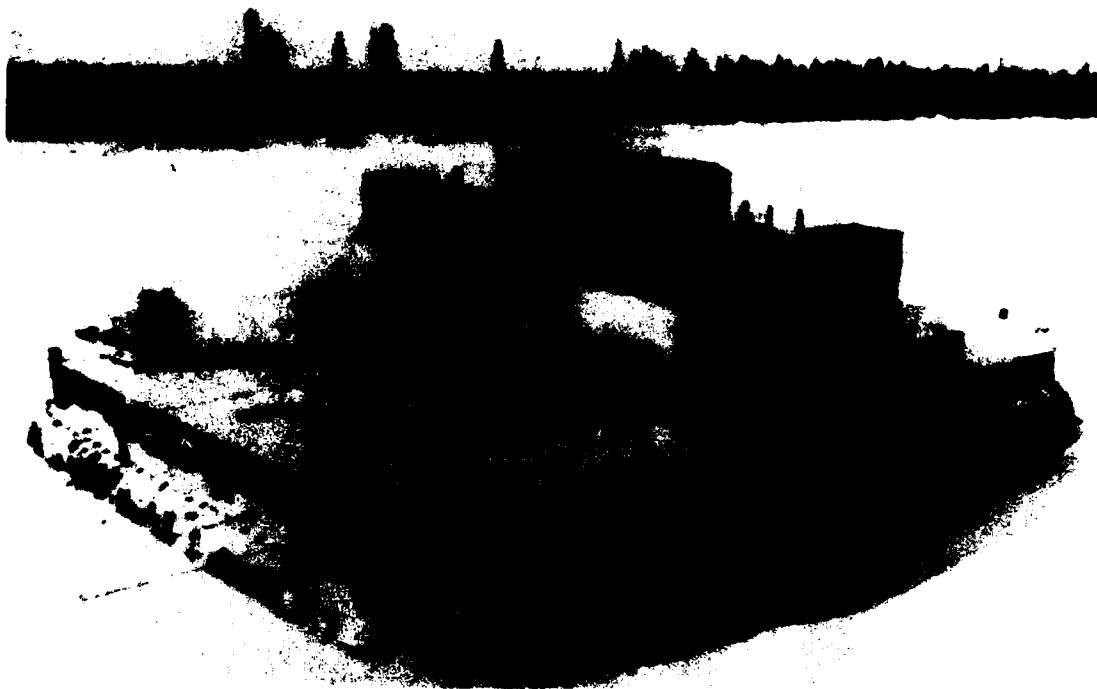


Figure 248 - Some Low Speed Applications of Air Cushion Principle

It was during the trials of the ACT-100 that another possible use of the air cushion was observed--that of icebreaking--by towing the cushion-supported transporter across the frozen rivers so that the waveform generated by the supporting water beneath the craft and traveling with the craft was of sufficient strength to break the ice. The observation showed that the thickness of the ice in inches broken was approximately equal to the cushion pressure, in inches of water.¹⁹³ Since that time the ice-breaking feature of the air cushion has been adapted to conventional displacement ships as shown in Figure 249 shown originally by McCleavy.⁴

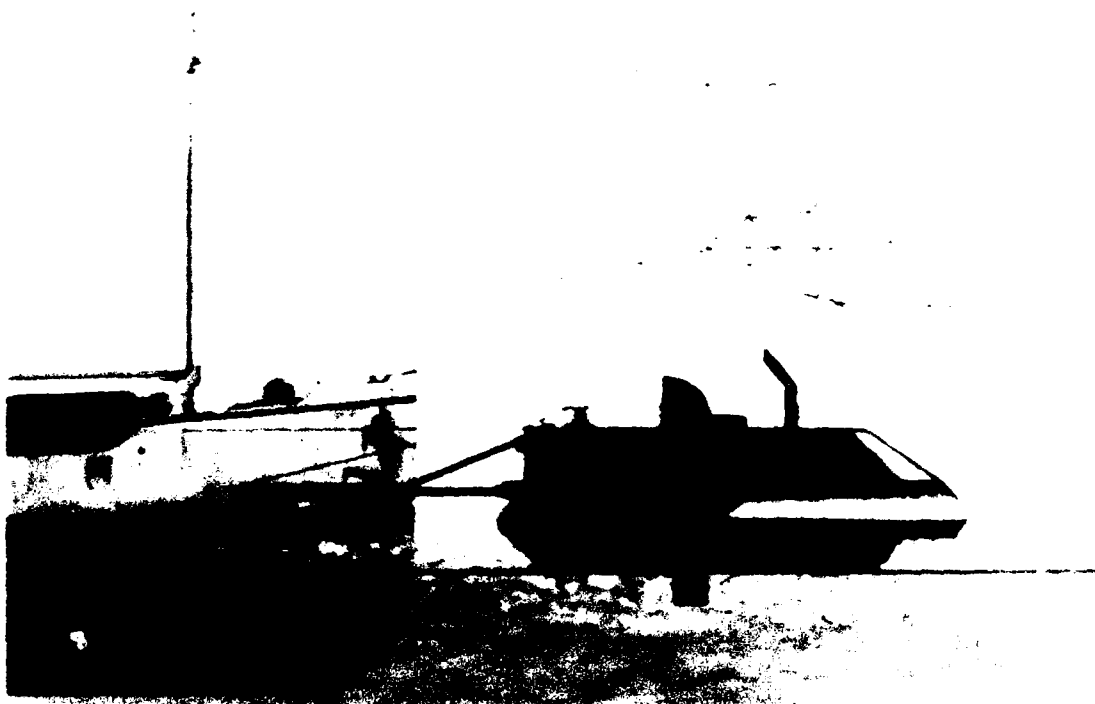


Figure 249 - Air Cushion Icebreaking Attachment

The attachment, shown in Figure 249, operates on the low speed, air cushion icebreaking principle in which the water level within the cushion area is depressed to a lower level than the bottom of the ice layer. The unsupported section of ice reaches a critical length then breaks off. A deflector beneath the cushion then thrusts the broken ice aside before it comes into contact with the conventional ship's bow.

CHAPTER XI

CONCLUSIONS

The present report has summarized several key areas of air cushion craft development. Although the topics have been necessarily selective, it is felt that the essential characteristics have been summarized. Attention has been given to isolating those technical areas where, by concentrating engineering effort, significant improvements to the state-of-the-art can be made.

The air cushion craft has developed to an encouraging degree during its modern development and has provided a capability that is unique in the field of transportation. As in all developments of a new concept, several exploratory applications are tried, not all of them successful, until its true utilization emerges. So far the craft has established itself as an effective, short-haul transport vehicle over water in calm to moderate seas, but it is still expensive to construct and to operate. Considerable development is required to make it a viable long-haul transport over sea routes where rough seas are prevalent. This report has touched briefly on some new applications, specifically the development for operation in the Arctic and over other environmentally sensitive surfaces, and the development for special high speed military missions.

Cost has not been specifically addressed in this review because it deserves a complete and separate treatment covering the many aspects of research and development costs, investment costs, and operating costs that make up the life cycle costs of any particular craft. This omission is probably unfortunate in that the cost considerations are probably the main reasons why, at least in the U.S., there are no operational air cushion craft in the U.S. Navy today and those that are in development are meeting opposition in many quarters due to their high cost despite their potential increase in effectiveness over more conventional ships and aircraft. Some indications of costs have been included in this updated review, however, to add a degree of emphasis and sense of urgency for the air cushion craft designer to seek lower cost versions with the available technology. Some encouraging developments in reducing costs have been noted in the report.

Following the theme established in the first review,² the conclusions are summarized in a list (by chapter heading) to provide an identification of the key problem areas (in addition to that of cost!) that, if resolved, will significantly improve the state-of-the-art and point the way to a better product.

The development of the air cushion craft, both amphibious and non-amphibious, is proceeding rapidly, and answers are being found to many of the questions raised in this report even as it goes to press. It is still of value, however, to "stop the clock" as it were and ask if an answer currently exists or if it will exist in the future, however near. The following specific areas are listed in the first category, even though it

is known that many groups are actively working them to an anticipated acceptable conclusion. With this introduction, some 24 problem areas are summarized under the main subject headings of the report.

PERFORMANCE ASPECTS (CHAPTER III)

Basically, the performance of an air cushion craft can be estimated to a high degree of accuracy, except in the case of rough water where considerable reliance is still made on empirical formulation. Specifically:

1. The rough water drag increment of the amphibious craft is assumed to be equal to the rough water skirt drag increment. The rough water skirt drag is estimated by empirical methods based on a particular skirt geometry, and its application to other skirt forms is unknown.

2. An improved method of presenting rough water performance is required to isolate the key parameters. Weight and geometric properties have not been systematically isolated. Because speed losses exceeding 50 percent are typical for craft operating in waves with height equal to cushion height, a better understanding is required.

3. A surprising lack of data exists on performance in a sea state. No consistent formation of performance exists for operation in head seas, following seas, or seas of different wavelengths. Test programs, to date, all too frequently have not measured sea condition in consort with craft performance, hence correlation and prediction is difficult.

4. For the sidehull air cushion craft, the hydrodynamics of hulls operating in the presence of asymmetric waterlines due to the cushion pressure action has not been adequately explored. This is especially true in the case of supercavitating flow where significant drag increments can be incurred by improper shaping.

Most of the theoretical treatments of rough water drag have assumed that the deduced drag comes from the increased wetted area from wave action. It is now thought that a time-averaged treatment of the longitudinal acceleration during ship motion might lead to more tractable solutions. It is also found that proper scaling of the various terms in the drag equations will provide good predictions of full-scale craft once given the model tests. This still leaves drag prediction, however strongly dependent on model tests. Development of component drag coefficients for a variety of shapes (akin to that available on NACA airfoils and related aerodynamic shapes) would greatly enhance the ability to predict the performance of new high speed sidehull forms in the presence of an air cushion.

STABILITY AND RIDE QUALITY (CHAPTER IV)

Although recognizing that the stability characteristics of craft operating at the interface of two mediums is a complex analytical problem, it is felt that this has not received proper attention in the past. There appears to be nothing in the literature between the oversimplified one degree of freedom analysis and the complex computerized multidegree of freedom treatment of specialized configurations. Since the last review was published there have been several additions to the literature that

provide further insight into the nature of the motion. There is still a need for a consistent treatment on the description of the stability modes and the form of the motion. The conclusions on the two subjects, stability and ride quality, may be summarized as:

1. Isolated specific static stability criteria exist based on operational considerations. Virtually no dynamic stability criteria exist for design purposes.

2. A unified theory, devoid of "folklore constants," is required to describe motion in the different modes such as the pitch-heave mode and roll-yaw modes. These analyses would provide improved insight into the basic characteristics and thus provide improved craft design.

3. Further development of the understanding of the motion of air cushion craft has shown that the wide band frequency nature of the motion indicates that it is inadequate to assess the ride quality of the motion with the existing single band criteria. Much more work in determining the human tolerance limits to wide band frequency motion characteristics of the air cushion craft needs to be done.

4. Improvements in fan design since the last review have made it feasible to keep the lift system power limits to within acceptable values. What is needed now is the design criteria against which to design the fan characteristics to meet the needs of ride quality determined through Conclusion 3.

5. Trade-off information is needed between stability requirements and ride control requirements.

CONTROL (CHAPTER V)

The unique combination of onboard air source, aerodynamic flow field, and hydrodynamic flow field for the air cushion craft allows for a variety of control mechanisms that have not, as yet, been exhausted. The opportunity for improved controls on air cushion craft is great. Specifically one could conclude:

1. Although most craft to date have used conventional means of aerodynamic and hydrodynamic control surfaces, there appears to be potential worth exploring for various forms of integrated lift, propulsion, and control in simple versatile mechanisms.

2. The so-called gimbal-fan concept and possible developments of the concept appear to offer a unique control mechanism applicable to a wide range of craft sizes with added advantages of using less space and exhibiting a lower profile than existing forms of control.

3. Improved displays, including projection of limits, would be beneficial in optimized control of these craft.

SEALS AND SKIRT DEVELOPMENT (CHAPTER VI)

There are two aspects to the design of the suspension system of the air cushion craft. They are the configuration aspects to provide the desired performance and stability to the craft and the durability aspects to improve the acceptance of the craft in an operators' inventory. Specifically, it is concluded that the state-of-the-art can be improved if the following areas are pursued.

1. Performance and stability tests need to be conducted on a systematic, comparative basis of the various skirt forms discussed in Chapter VI. Much of the current design procedure is a cut-and-try procedure in model and full-scale, a procedure that contributes to the high cost of the craft and the promulgation of reinvention by subsequent designers.

2. The durability of skirt materials requires improvement to reduce maintenance costs of current craft and to increase reliability of craft projected for longer range cruise application. For the special case of the nonamphibious sidehull craft, the use of high strength reinforced-plastic materials, designed to configurations that avoid the flagellation mode, appears to offer potential for long-life.

STRUCTURAL DESIGN (CHAPTER VII)

The design of lightweight structures adequate to withstand the rigors of operating in a sea environment is a problem common to all advanced marine vehicles. The problem is expressed in terms of load prediction, lightweight design, and simplified construction as shown by the following list:

1. The speed and payload requirements have precluded the use of structural hull design methods using conventional Navy architecture.

Improved load prediction methods, including the effects of cushion alleviation, are required to yield reliable predictions of loads at all speeds and headings in a seaway. This is especially important as the speeds are increased and the need exists to minimize structural weight to maximize payload capacity.

2. Present craft employ complex combinations of structural arrangements not amenable to production shipyard methods. This fact has contributed significantly to the cost of air cushion craft and hampered their economic viability. Some recent examples of low cost structures should provide valuable cost-performance comparisons.

3. An improved data base on loads and development of structural design philosophy peculiar to air cushion craft, as opposed to the current adaptation of aircraft design philosophy, is required to produce an economic air cushion craft hull form.

4. The lack of a consistent data base especially for loads has made it difficult to produce reliable scaling laws for different forms or larger craft hulls. Hence, prediction of structural weight fraction is largely a matter of conjecture even at this stage of development.

LIFT FAN SYSTEM (CHAPTER VIII)

The aerostatic air cushion craft relies on a lift fan system for its cushion support and, although lift system efficiencies were surprisingly low in the early years, some recent developments in fan design offer some promise. Specifically:

1. Improvements in both rotor and ducting design (including volute) have improved lift system efficiencies. Values of 60 percent would be possible for the overall system, where rotor efficiencies are on the order

of 85 percent. Lower values are expected where there are physical constraints on the fan system. More development of lift fans and the understanding of the controlling parameters is needed before greater efficiencies are likely to be forthcoming. The greater efficiencies must also be obtained without jeopardizing the desired shape of the pressure-flow curves to meet the ride quality requirements.

2. Recent improvements in fan design (rotor and volute) have shown that lift power requirements for ride control purposes can be reduced significantly over that used in the early venting schemes. More development will yield further improvements in fan design and associated power requirements.

PROPULSION (CHAPTER IX)

The propulsion power requirements of the air cushion craft are less than other craft of the same displacement and speed (above about 30 knots) due to its comparative low resistance air cushion. However, the high speed requirements of such craft still require high installed power, with the overall propulsive efficiency between 40 and 60 percent, depending upon the means of propulsion. The operation in the continual spray pattern from the cushion has also incurred low engine life and heavy filtration requirements. The following list represents key areas where improvement would enhance the economic profitability of the craft.

1. Improved methods of spray elimination rather than increased filtration would do much to increase craft component life and operator visibility. Some recent developments in skirt design, tackling the spray problem at its source, offer promise in spray reduction and hence, longer engine life.

2. The (relatively) low air speed of air cushion craft has placed low limits of attainable propulsive efficiency on aerodynamic means of propulsion. Unique methods to improve efficiency, coupled with the need to maintain low noise emission, would greatly increase their acceptability.

3. The high water speed of air cushion craft has incurred high resistance and cavitation problems of water propulsion means, thus effectively reducing net propulsive efficiency and creating different design and operation problems. Improved knowledge on underwater appendage shaping for supercavitating flows would aid reduction of hydrodynamic drag that is a significant problem in present craft.

HIGH AND LOW SPEED DEVELOPMENTS (CHAPTER X)

In the near term, the emphasis of development will continue to evolve around the intermediate speed craft. Exploring the outer limits of the speed spectrum, however, has begun to extend to other applications. Opportunity exists, in the light of the current technology, to make significant advances in the following areas:

1. Reexamining the use of the air cushion in high speed craft, revolves around the need to produce a seakeeping capability not yet existing in aerodynamic forms of air cushion craft.

2. A continued exploration of the application of the simple hovering principle of the basic air cushion is needed to provide heavy lift transportation over surfaces tolerant only to low footprint pressures.

3. The application of the air cushion principle to icebreakerships is an illustration of the use of the principle not immediately apparent upon introduction of the craft. Further uses should be explored to stimulate development and expansion of what is still a very narrow field of application for the principle.

In comparing the above list of problem areas with that prepared in the original review in 1975, there are some encouraging developments in the state-of-the-art. At the same time, it is quickly recognized that in many areas the development proceeds but slowly.

It is encouraging to see developments and improvements emerging that concentrate on producing simpler designs that can enter service and produce the much needed operational data that can be fed back to the design communities for further product improvement.

In compiling this summary, some care has been taken to express the large amount of available data into consistent units for comparative analysis. It is hoped that in this way, a clearer picture is presented for the designer and evaluator alike to make decisions on their products and to aid development of specifications for future air cushion craft.

APPENDIX A

DERIVATION OF RANGE AND PRODUCTIVITY EQUATIONS

If an air cushion craft is cruising under power then its rate of change of weight with time is known from the rate of fuel consumption such that,

$$\frac{dW}{dt} = - \frac{dW_F}{dt} = -sfc P \quad (234)$$

where W = the weight (displacement) of the craft

t = the time

W_F = the weight of fuel consumed

sfc = the specific fuel consumption

P = the total brake horsepower supplying the craft power while cruising at some speed V .

The incremental range dR is determined from the simple relationship

$$dR = Vdt \quad (235)$$

and the range is then given by integration such that

$$R = \int_0^t Vdt = - \int_{W_i}^W \frac{VdW}{sfcP} = - \int_{W_i}^W \frac{WV}{P} \frac{1}{sfc} \frac{dW}{W} \quad (236)$$

where W_i is the initial weight of the craft which may be related to the weight at the end of the cruise W after consuming fuel W_f by,

$$W = W_i - W_F \quad (237)$$

Now, if the craft is operated at trim and power settings such that WV/P and sfc are constant values, then the range integral can be written,

$$R = \frac{WV}{P} \cdot \frac{1}{sfc} \cdot \int_W^{W_i} \frac{dW}{W} \quad (238)$$

which, upon integration, gives the familiar Breguet range equation,

$$R = \frac{WV}{P} \cdot \frac{1}{\text{sfc}} \cdot \ln \left(\frac{W_1}{W} \right) \quad (239)$$

Over long ranges where significant weight changes occur it is unlikely that WV/P will remain constant and the specific fuel consumption (sfc) will also vary as a function of both power and engine speed. In these cases, it is usual to compute the Breguet range over small increments of weight adjusting for the new weights, power settings, and fuel consumption at each increment and summing the results to determine the total range.

The above results are general in that they apply to all power consuming vehicles. In the specific case of the air cushion craft, some discussion of the "transport efficiency" WV/P is in order, but first consider the conventional aircraft.

AIRCRAFT

For aircraft one notes the relationship

$$L = W \quad (240)$$

and

$$\eta P = DV \quad (241)$$

which simply state that, in cruise, lift L equals weight W and the total brake horsepower P times the propulsive efficiency η equals drag D times velocity V . Then, from Equations (240) and (241)

$$\eta \frac{L}{D} = \frac{WV}{P} \quad (242)$$

which may be substituted into the Breguet range equation to give

$$R(\text{nm}) = 325 \cdot \frac{\eta}{\text{sfc}} \cdot \frac{L}{D} \ln \left(\frac{W_1}{W} \right) \quad (243)$$

which has been expressed in consistent units to give the range R in nautical miles as a direct function of the propulsive efficiency η , the specific fuel consumption sfc in lb/HP hr, the nondimensional aerodynamic lift-to-drag ratio L/D and the weight fraction W_1/W .

AIR CUSHION CRAFT

For air cushion craft, however, account must be taken of the power to sustain the craft above the surface such that the power P becomes the sum of the propulsive power P_p and the lift power P_L , i.e.,

$$P = P_p + P_L \quad (244)$$

As for the aircraft (or ship) the propulsive power is written

$$\eta_p P_p = DV \quad (245)$$

but now the additional lift power term

$$\eta_L P_L = p_c Q \quad (246)$$

where p_c is the cushion pressure and Q is the cushion air flow which must be included such that

$$P = \frac{DV}{\eta_p} + \frac{p_c Q}{\eta_L} \quad (247)$$

After some substitution and rearranging, the range integral (Equation (236)) for the air cushion craft can then be written, in the light of Equation (247), as,

$$R = - \int_{W_i}^W \frac{\eta_p}{sfc} \frac{W}{\left[D + \frac{\eta_p}{\eta_L} \left(\frac{p_c Q}{V} \right) \right]} \frac{dW}{W} \quad (248)$$

and if the craft is operated such that,

$$\frac{\eta_p}{sfc} \left[\frac{W}{D + \frac{\eta_p}{\eta_L} \frac{p_c Q}{V}} \right] = \text{constant} \quad (249)$$

then the Breguet range for an air cushion craft can be written,

$$R(\text{nm}) = 325 \frac{\eta_P}{\text{sfc}} \left(\frac{L}{D} \right)_{\text{EFF}} \ln \left(\frac{W_i}{W} \right) \quad (250)$$

where, by definition, the "effective L/D " is given by,

$$\left(\frac{L}{D} \right)_{\text{EFF}} = \frac{W}{D + \frac{\eta_P}{\eta_L} \frac{P_c Q}{V}} \quad (251)$$

which is the familiar aerodynamic lift-to-drag ratio (or hydrodynamic lift-to-drag ratio in the case of ships) modified by the cushion effect

$\left(\frac{\eta_P}{\eta_L} \frac{P_c Q}{V} \right)$ which has the dimensions of drag.

Note that for the air cushion craft, the range Equation (250) can still be written,

$$R(\text{nm}) = 325 \frac{1}{\text{sfc}} \cdot \frac{WV}{P} \cdot \ln \left(\frac{W_i}{W} \right) \quad (252)$$

as for the aircraft or ship but that the total power P is given by Equation (247).

SOME ECONOMIC FACTORS

In economic analyses, it is frequently necessary to evaluate the "productivity" of the craft measured in payload ton-miles and in ton-miles per pound of fuel. While in any specific analysis it is possible to make exact calculations, it is informative to consider an approximation based on an expansion of the natural logarithm in Equation (252). Because the fuel weight fraction W_F/W_i is always less than unity then the natural logarithm term in Equation (252) can be written,

$$\ln \frac{W_i}{W} = \ln \left(1 - \frac{W_F}{W_i} \right)^{-1} = \frac{W_F}{W_i} + \frac{1}{2} \left(\frac{W_F}{W_i} \right)^2 + \dots \quad (253)$$

Dropping the subscript i the range equation can thus be written, to first order,

$$R = 325 \frac{\eta}{\text{sfc}} \left(\frac{L}{D} \right)_{\text{EFF}} \cdot \frac{W_F}{W} \quad (\text{approx.}) \quad (254)$$

For a fuel fraction of 0.10 the approximation underestimates the range by 5 percent and for a 0.30 fuel fraction, the approximation underestimates by 15 percent.

The productivity in payload ton-miles can then be taken as

$$W_P R = 325 \frac{\eta}{\text{sfc}} \left(\frac{L}{D} \right)_{\text{EFF}} \left(\frac{W_F}{W} \right) \cdot W_P \quad (255)$$

and the payload ton-miles per pound of fuel is given (approximately) by,

$$\text{ton-mi/lb (fuel)} = 0.163 \frac{\eta}{\text{sfc}} \left(\frac{L}{D} \right)_{\text{EFF}} \cdot \left(\frac{W_P}{W} \right) \quad (256)$$

where the payload is measured in short tons and the range in nautical miles.

APPENDIX B

AIR CUSHION CRAFT WEIGHT BREAKDOWN

In the main text will be found various charts and equations pertaining to the weights of subsystems and components of air cushion craft. These become important elements in the preliminary design and costing of craft and are informative in establishing the relative emphasis to be placed in the design process. This appendix provides a concise summary of all the subsystems weights, and further, where available, some of the weights of major elements or components that make up the subsystem. In many instances the state-of-the-art has not yet reached the stage where definite trends can be established. These instances are so noted and the available data are given as a base from which, hopefully, trends for the future can be drawn. It is important to understand a subtle difference between the two ways that weight information is presented. Weight information and equations can be presented as:

1. Weight trends as a function of no more than one or two major craft parameters, such as displacement and cushion density; and
2. Weight trends of more detailed parameters at a lower level in the system, subsystem, and component hierarchy.

The first set of information (1) is useful in determining the state-of-the-art at a fairly top level (system and subsystem) so that an appreciation can be obtained in the event that another design of the same family can be rapidly determined. The second set of weight information (2) is useful in the detective process of determining the key driving parameters in a particular system so that departures from the state-of-the-art can be projected and a new family of craft generated. As might be expected, category (2) is much more difficult to obtain, requiring much more data than is usually readily available. In the weight analysis pursued here, the motivation has been to generate (2) with (1) being treated as the minimum information to be presented. In what follows, therefore, it is viewed as a starting set of data in a technology base that is still young.

SUBSYSTEM WEIGHT BREAKDOWN

It is extremely difficult when collecting weight information to be completely consistent in the definition of what constitutes a given subsystem among the many designs by many different design organizations in several countries.

Some effort has been expended in expressing all the weights in this report in the terminology of the U.S. Navy Ship Work Breakdown Structure (SWBS)³³ that was prepared in 1973 to reflect the groupings of displacement ships. The SWBS has been adopted within the U.S. Navy for use on all surface platforms including the air cushion craft. Since the work in this report was prepared, a new version of the SWBS has been issued (dated 1 August 1977) that takes the various elements of the lift system that was grouped in Group 567 and now divides them up among the other groups, viz: skirts (Group 119), lift fans (Group 248), and lift engines (Group 230). This means that the "lift system"--the heart of the air cushion craft--is

not identifiable as an entry in the new SWBS. To maintain the identity of the lift system it is re, it has used the 1973 issue of the SWBS. Since having established this basic accounting system for weights, it is not possible to make departure to other accounting systems that may have been used in the data base. Specific instances of this have already been identified in the main text.

Following the SWBS system,³⁴ the weight of the craft can be accounted for as given in Table 16. Confusion has occurred because the same word are being used in the literature to describe different weight groups of the craft. For purposes of clarification, the definition of each of the light ship weight groups given in Table 16 is summarized in Table 17. Further, the definition of each of the load items is given in Table 18. A review of Tables 16, 17, and 18 should identify where all the items are being accounted for on an air cushion craft. Table 19 has been prepared to provide some continuity between the 1973 issue used in this report and the 1977 issue of the U.S. Navy SWBS³⁴ and to check the accounting on craft using either of the two accounting systems. Further description is provided in each of the individual weight sections that follow where available data and trend curves are provided.

TABLE 16 - AIR CUSHION CRAFT WEIGHT BREAKDOWN

Weight Element	Weight
Light Ship	
Group 100: Structure	xxx
Group 200: Propulsion	xxx
Group 300: Electrical	xxx
Group 400: Command and Surveillance (C&S)	xxx
Group 500: Auxiliary System (including Lift System)	xxx
Group 600: Outfit and Furnishings (O&F)	xxx
Group 700: Armament	xxx
Light Ship Weight	xxxx
Loads	
Crew and provisions	xxx
Stores and Fresh Water	xxx
Disposable Payload (Ordnance, Cargo, ...)	xxx
Fuel	xxx
Total Loads	xxxx
Gross Weight	xxxx

TABLE 17 - LIGHT SHIP WEIGHT GROUPS*

100	STRUCTURE	100	Special Structures
110	Shell and Supporting Structure	110	Structural Details, Forgings and Weldments
111	Shell, Plating	111	Stake and Niche
112	Inner Bottom	112	Sea Heats
113	Shell Appendages	113	Ballistic Plating
114	Stanchions	114	Sonar Dome
115	Longitudinal Framing	115	Sponsons
116	Transverse Framing	116	Hull Structural Connectors
117	Hull Structural Bulkheads	117	De Anque Structural Connectors
118	Longitudinal Structural Bulkheads	118	Special Purpose Connectors and Structures
119	Transverse Structural Bulkheads	119	Master, King Posts and Service Platforms
120	Trunks and Enclosures	120	Masts, Towers and Tetrapods
121	Bulkheads in Torpedo Protection System	121	King Posts and Support Frames
122	Hull Decks	122	Service Platforms
123	Main Deck	123	Foundations
124	Second Deck	124	Hull Structure Foundations
125	Third Deck	125	Propulsion Plant Foundations
126	Hull Platforms and Flats	126	Electric Plant Foundations
127	First Platform	127	Command and Surveillance Foundations
128	Second Platform	128	Auxiliary System Foundations
129	Third Platform	129	Outfit and Furnishings Foundations
130	Deckhouse Structure	130	Armament Foundations
131	Deckhouse Structure to First Level	131	Special Purpose Systems
132	First Deckhouse Level	132	Ballast, Fixed or Fluid and Buoyancy Units
133	Second Deckhouse Level	133	Free Flooding Liquids
134	Hull Repair Parts and Special Tools	134	Hull Repair Parts and Special Tools
200	PROPULSION SYSTEM	200	Transmission and Propulsion Systems
210	Energy Generating System (Nuclear)	210	Propulsion Reduction Gears
211	Nuclear Steam Generator	211	Propulsion Clutches and Couplings
212	Reactors	212	Propulsion Shafting
213	Reactor Coolant System	213	Propulsion Shaft Bearings
214	Reactor Coolant Service System	214	Propellers
215	Reactor Plant Auxiliary Systems	215	Propeller Shafts and Ducts
216	Nuclear Power Control and Instrumentation	216	Water Jet Propellers
217	Radiation Shielding (Primary)	217	Propulsion Support System (Except Fuel and Lube Oil)
218	Radiation Shielding (Secondary)	218	Combustion Air System
219	Energy Generating System (Nonnuclear)	219	Propulsion Control System
220	Propulsion Boilers	220	Main Steam Piping System
221	Gas Generators	221	Condensers and Air Ejectors
222	Main Propulsion Batteries	222	Feed and Condensate System
223	Main Propulsion Fuel Cells	223	Circulating and Cooling Sea Water System
224	Propulsion Units	224	H.P. Steam Drain System
225	Propulsion Steam Turbines	225	Uptakes (Inner Casing)
226	Propulsion Steam Engines	226	Propulsion Support Systems (Fuel and Lube Oil)
227	Propulsion Internal Combustion Engines	227	Fuel Service System
228	Propulsion Gas Turbines	228	Main Propulsion Lube Oil System
229	Electric Propulsion	229	Lube Oil Fill, Transfer and Purification
230	Self-Contained Propulsion Systems	230	Special Purpose Systems
231	Auxiliary Propulsion Devices	231	Propulsion Plant Operating Fluids
232	Transmission and Propulsion Systems	232	Propulsion Plant Repair Parts and Special Tools
233	Propulsion Reduction Gears	233	Propulsion Clutches and Couplings
234	Propulsion Shafting	234	Propulsion Shaft Bearings
235	Propellers	235	Propeller Shafts and Ducts
236	Water Jet Propellers	236	Propulsion Support System (Except Fuel and Lube Oil)
237	Combustion Air System	237	Propulsion Control System
238	Main Steam Piping System	238	Condensers and Air Ejectors
239	Feed and Condensate System	239	Circulating and Cooling Sea Water System
240	H.P. Steam Drain System	240	Uptakes (Inner Casing)
241	Propulsion Support Systems (Fuel and Lube Oil)	241	Fuel Service System
242	Main Propulsion Lube Oil System	242	Lube Oil Fill, Transfer and Purification
243	Special Purpose Systems	243	Propulsion Plant Operating Fluids
244	Propulsion Plant Repair Parts and Special Tools	244	Propulsion Plant Repair Parts and Special Tools
300	ELECTRICAL SYSTEM	300	Lighting Systems
310	Electric Power Generation	310	Lighting Distribution
311	Ship Service Power Generation	311	Lighting Fixtures
312	Emergency Generators	312	Power Generation Support Systems
313	Batteries and Service Facilities	313	SSGT Lube Oil
314	Power Conversion Equipment	314	Diesel Support Systems
315	Power Distribution Systems	315	Turbine Support Systems
316	Ship Service Power Cable	316	Special Purpose Systems
317	Emergency Power Cable System	317	Electric Plant Operating Fluids
318	Casualty Power Cable System	318	Electric Plant Repair Parts and Special Tools
319	Switch Gear and Panels	319	Surveillance Systems (Surface)
320	Surveillance Systems (Surface)	320	Surface Search Radar
321	Surface Search Radar	321	Air Search Radar (2D)
322	Air Search Radar (2D)	322	Air Search Radar (3D)
323	Air Search Radar (3D)	323	Aircraft Control Approach Radar
324	Aircraft Control Approach Radar	324	Identification Systems
325	Identification Systems	325	Space Vehicle Electronic Tracking
326	Space Vehicle Electronic Tracking	326	Surveillance Systems (Underwater)
327	Surveillance Systems (Underwater)	327	Active Sonar
328	Active Sonar	328	Passive Sonar
329	Passive Sonar	329	Active/Passive (Multiple Mode) Sonar
330	Active/Passive (Multiple Mode) Sonar	330	Classification Sonar
331	Classification Sonar	331	Bathythermograph
332	Bathythermograph	332	Countermeasures
333	Countermeasures	333	Active ECM
334	Active ECM	334	Passive ECM
335	Passive ECM	335	Torpedo Decoys
336	Torpedo Decoys	336	Decoys (Other)
337	Decoys (Other)	337	Deгаussing
338	Deгаussing	338	Mine Countermeasures
339	Mine Countermeasures	339	Fire Control Systems
340	Fire Control Systems	340	Gun Fire Control Systems
341	Gun Fire Control Systems	341	Fire Control Systems (Monosensor Data Base)
342	Fire Control Systems (Monosensor Data Base)	342	Fire Control Systems (Sensor Data Base)
343	Fire Control Systems (Sensor Data Base)	343	Fire Control Systems Switchboards
344	Fire Control Systems Switchboards	344	Special Purpose Systems

TABLE 17 - (Continued)

GROUP 500: AUXILIARY SYSTEM (Including Lift System)	
501 Climate Control	555 Fire Extinguishing Systems
502 Compartment Heating System	556 Hydraulic Fluid System
503 Ventilation System	557 Liquid Heaters, Large
504 Machinery Space Ventilation System	558 Special Piping Systems
505 Air Conditioning System	560 Ship Control Systems
506 Refrigeration System	561 Steering and Towing Control Systems
507 Auxiliary Boilers and Other Heat Sources	562 Rudder
508 Sea Water Systems	563 Trim and Heel Roll Stabilization
509 Firemain and Flushing (Sea Water) System	564 Lift Systems
510 Sprinkler System	568 Maneuvering Systems
511 Washdown System	570 Underway Replenishment Systems
512 Auxiliary Sea Water System	571 Replenishment-at-Sea Systems
513 Sumps and Sea Drains	572 Ship Stores and Equipment Handling Systems
514 Firemain Actuated Services	573 Cargo Handling Systems
515 Plumbing Drainage	574 Vertical Replenishment Systems
516 Drainage and Ballasting System	580 Mechanical Handling Systems
530 Fresh Water Systems	581 Anchor Handling and Stowage Systems
531 Distilling Plant	582 Mooring and Towing Systems
532 Cooling Water	583 Boat Handling and Stowage Systems
533 Potable Water	584 Mechanically Operated Door, Gate, etc. Systems
534 Aux. Steam and Drains Within Machinery Box	585 Elevating and Retracting Gear
535 Aux. Steam and Drains Outside Machinery Box	586 Aircraft Recovery Support Systems
536 Auxiliary Fresh Water Cooling	587 Aircraft Launch Support Systems
540 Fuels and Lubricants, Handling and Storage	588 Aircraft Handling, Servicing and Stowage
541 Ship Fuel and Fuel Compensating Systems	589 Miscellaneous Mechanical Handling Systems
542 Aviation and General Purpose Fuels	590 Special Purpose Systems
543 Aviation and General Purpose Lube Oil	591 Scientific and Ocean Engineering Systems
544 Liquid Cargo	592 Swimmer and Diver Support and Protection Systems
545 Tank Heating	593 Environmental Pollution Control Systems
550 Air, Gas, and Miscellaneous Fluid Systems	595 Towing, Launching and Handling for Underwater Systems
551 Compressed Air Systems	596 Handling System for Diver and Submersible Vehicles
552 Compressed Gases	597 Salvage Support Systems
553 Oxygen-Nitrogen System	598 Auxiliary Systems Operating Fluids
554 Low Pressure Blow	599 Auxiliary Systems Repair Parts and Tools
GROUP 600: OUTFIT AND FURNISHINGS	
602 Hull Designating and Marking	640 Living Spaces
603 Draft Marks	641 Officer Berthing and Messing Spaces
604 Locks, Keys, and Tags	642 NCO Berthing and Messing Spaces
605 Rodent and Vermin Proofing	643 Enlisted Personnel Berthing and Messing Spaces
610 Ship Fittings	644 Sanitary Spaces and Fixtures
611 Hull Fittings	645 Leisure and Community Spaces
612 Rails, Stanchions, and Lifelines	650 Service Spaces
613 Rigging and Canvas	651 Commissary Spaces
620 Hull Compartmentation	652 Medical Spaces
621 Nonstructural Bulkheads	653 Dental Spaces
622 Floor Plates and Gratings	654 Utility Spaces
623 Ladders	655 Laundry Spaces
624 Nonstructural Closures	656 Trash Disposal Spaces
625 Airports, Fixed Portlights and Windows	660 Working Spaces
630 Preservatives and Coverings	661 Offices
631 Painting	662 Machinery Control Centers Furnishings
632 Zinc Coating	663 Electronics Control Centers Furnishings
633 Cathodic Protection	664 Damage Control Stations
634 Deck Covering	665 Workshops, Labs, Test Areas (Including Portable Tools)
635 Hull Insulation	670 Storage Spaces
636 Hull Damping	671 Lockers and Special Storage
637 Sheathing	672 Storerooms and Issue Rooms
638 Refrigerated Spaces	673 Cargo Storage
639 Radiation Shielding	690 Special Purpose Systems
	698 Outfit and Furnishings Operating Fluids
	699 Outfit and Furnishings Repair Parts and Special Tools
GROUP 700: ARMAMENT	
702 Armament Installations	740 Depth Charges
703 Weapons Handling and Stowage	741 Depth Charge Launching Device
710 Guns and Ammunition	742 Depth Charge Handling
711 Guns	743 Depth Charge Stowage
712 Ammunition Handling	750 Torpedoes
713 Ammunition Stowage	751 Torpedo Tubes
720 Missiles and Rockets	752 Torpedo Handling
721 Launching Devices (Missiles and Rockets)	753 Torpedo Stowage
722 Missile, Rocket and Guidance Capsule Handling System	760 Small Arms and Pyrotechnics
723 Missile and Rocket Stowage	761 Small Arms and Pyrotechnics Launching Devices
724 Missile Hydraulics	762 Small Arms and Pyrotechnics Handling
725 Missile Gas	763 Small Arms and Pyrotechnics Stowage
726 Missile Compensating	770 Cargo Munitions
727 Missile Launcher Control	772 Cargo Munitions Handling
728 Missile Heating, Cooling, Temperature Control	773 Cargo Munitions Stowage
729 Missile Monitoring, Test and Alignment	780 Aircraft Related Weapons
730 Mines	782 Aircraft Related Weapons Handling
731 Mine Launching Devices	783 Aircraft Related Weapons Stowage
732 Mine Handling	790 Special Purpose Systems
733 Mine Stowage	792 Special Weapons Handling
	793 Special Weapons Stowage
	797 Miscellaneous Ordnance Spaces
	798 Armament Operating Fluids
	799 Armament Repair Parts and Special Tools
*Some weight groups are peculiar to submarines and have thus been omitted causing breaks in the numerical sequence.	

TABLE 18 - LOADS GROUPS

FOO LOADS (FULL LOAD CONDITION)*	
F10 Ships Force, Amphibious Force, Troops and Passengers	
F11 Ships Officers	
F12 Ships Noncommissioned Officers	
F13 Ships Enlisted Men	
F14 Marines	
F15 Troops	
F16 Air Wing Personnel	
F19 Other Personnel	
F20 Mission Related Expendables and Systems	
F21 Ship Ammunition	
F22 Ordnance Delivery Systems Ammunition	
F23 Ordnance Delivery Systems	
F24 Ordnance Repair Parts (Ship Ammunition)	
F25 Ordnance Repair Parts (Ordnance Delivery System Ammunition)	
F26 Ordnance Delivery Systems Support Equipment	
F29 Special Mission Related Systems and Expendables	
F30 Stores	
F31 Provisions and Personnel Stores	
F32 General Stores	
F33 Marine Stores	
F39 Special Stores	
F40 Fuels and Lubricants	
F41 Diesel Fuel	
F42 JP-5	
F43 Gasoline	
F44 Distillate Fuel	
F45 Navy Standard Fuel Oil	
F46 Lubricating Oil	
F49 Special Fuels and Lubricants	
F50 Liquids and Gases (Nonfuel Type)	
F51 Sea Water	
F52 Fresh Water	
F53 Reserve Feed Water	
F54 Hydraulic Fluid	
F55 Sanitary Tank Liquid	
F56 Gas (Nonfuel Type)	
F59 Miscellaneous Liquids (Nonfuel Type)	
F60 Cargo	
F61 Cargo, Ordnance and Ordnance Delivery Systems	
F62 Cargo, Stores	
F63 Cargo, Fuels and Lubricants	
F64 Cargo, Liquids (Nonfuel Type)	
F65 Cargo, Cryogenic and Liquified Gas	
F66 Cargo, Amphibious Assault Systems	
F67 Cargo, Gases	
F69 Cargo, Miscellaneous	
*Other load conditions are designated as follows:	
A00 Minimum Operating Condition,	
B00 Beaching Condition,	
C00 Capacity Load Condition,	
H00 Half Fuel Condition.	

TABLE 19 - CHANGES FROM 1973 SWBS TO 1977 SWBS

<u>Group 100: Structure</u> Add: 119 Lift System Flexible Skirts and Seals Change: 161 Structural Castings etc. ⁽¹⁾
<u>Group 200: Propulsion System</u> Change: 230 Propulsion Units ⁽²⁾ Add: 248 Lift System Fans and Ducting
<u>Group 300: Electrical System</u> No change
<u>Group 400: Command and Surveillance</u> Add: 446 Security Equipment Systems 456 Multiple Mode Radar 463 Multiple Mode Sonar 482 Missile Fire Control Systems 483 Underwater Fire Control Systems 484 Integrated Fire Control Systems 489 Weapon Systems Switchboards 495 Special Purpose Intelligence Systems
<u>Group 500: Auxiliary Systems</u> Add: 549 Special Fuel and Lubricants, Hand'ing and Stowage Change: 565 Trim and Heel (Surface Ships) ⁽³⁾ 567 Strut and Foil Systems ⁽⁴⁾ 583 Boats, Boat Handling and Stowage Systems ⁽⁵⁾
<u>Group 600: Outfit and Furnishings</u> No change
<u>Group 700: Armament</u> No change
<u>Loads (F00)</u> No change
<p>(1) Now includes lift system landing pads.</p> <p>(2) Now includes lift engines.</p> <p>(3) Changed to include fin systems.</p> <p>(4) All air cushion craft related lift system elements removed.</p> <p>(5) Now includes boats.</p>

In the discussion in the main text, other terms are used depending on the subject being discussed that pertain to the weight of the craft. These terms, their interrelationship, and connection with the weight groupings given in this appendix can be easily recognized through the following descriptions: The light ship weight is simply the sum of all seven major subsystem weights,

$$\text{Light Ship Weight} = \sum_{i=100}^{700} (\text{Weight Group})_i \quad (257)$$

Note that, when the craft is built, the weights are actual values. During the project design stage, it is usual to carry a margin in the weight statement for expected weight growths throughout the design and build phases. This would normally be an additional line item in any particular craft's weight statement. It is assumed that the margin has been allocated to each of the seven physical weight groups for the purposes used here.

The empty weight W_E is the light ship weight less any fixed payload items, viz:

$$\text{Empty Weight} = \text{Light Ship} - \text{Fixed Payload} \quad (258)$$

where the fixed payload items are those associated with the disposable payload but are physically connected to the craft. A military craft example might be the guns and shells. The gun, being attached to the craft would be considered fixed payload (armament) but the shells (ordnance) would be considered part of the disposable payload.

The gross weight (or full load displacement as it is sometimes called) is the sum of the empty weight and the useful load, viz:

$$\text{Gross Weight} = \text{Empty Weight} + \text{Useful Load} \quad (259)$$

where now the useful load is given by,

$$\text{Useful Load} = \text{Payload} + \text{Fuel} + (\text{Crew, Stores, ...}) \quad (260)$$

In Equation (260) the payload is comprised of both fixed and disposable payload items. Figure 250 illustrates these various relationships. The

shaded area in Figure 250 is the payload for the craft and, as shown, is made up of fixed payload items that are carried in the light ship weight and disposable payload that is carried in the useful load weight. Comparisons of the "payload" of different craft, therefore, have to recognize this distinction.

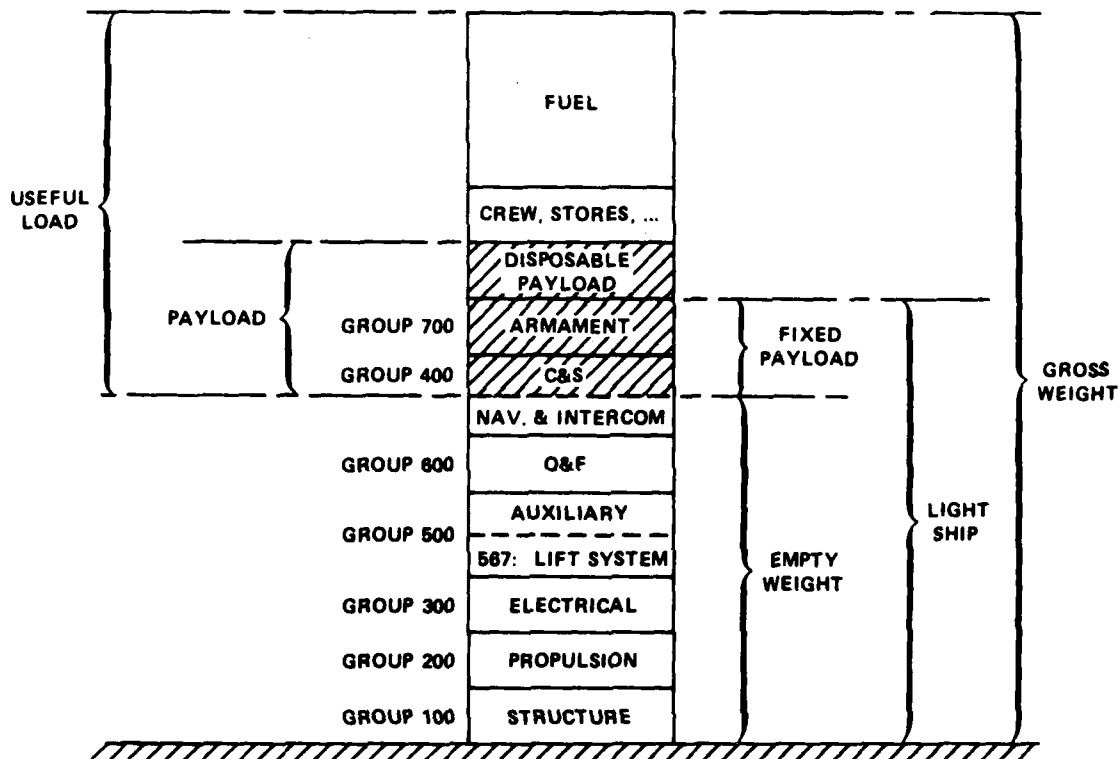


Figure 250 - Identification of Weight Items

SUBSYSTEM WEIGHT DESCRIPTIONS

The definitions of each of the weight groups and the terminology used in describing each of the main weight categories has been given in the first sections of this appendix. The available data on each of the seven weight groups will follow under the respective headings of the SWBS system. Within each of the weight groups other informative weight information is provided wherever available to provide more insight into the composition of the weight element. In this appendix, the data, curves, and equations are provided as a compilation of data for design use. Further discussion may be found in the main text in the pertinent chapters.

Structural Weight (Group 100)

Based on a review of actual craft and projected designs of air cushion craft, the structural weight is seen to follow the trends shown in Figure 251 (also Figure 156, Chapter VII). The data base (admittedly mostly

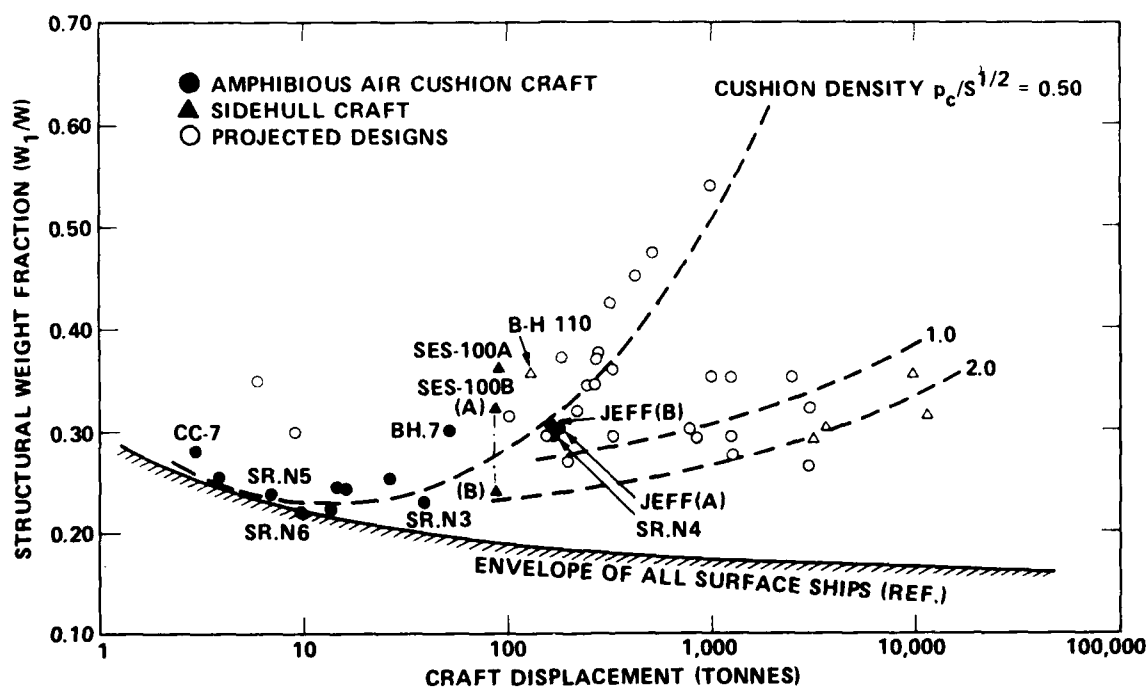


Figure 251 - Structural Weight Fraction

projected designs) has increased in recent years so that trend lines can be established. Following the functional form given in earlier work¹⁰⁹ it is found that the structural weight fraction can be expressed as the sum of two terms containing the full load displacement. The effect of the cushion density (p_c/\sqrt{S}) is quite marked for low values ($p_c/\sqrt{S} < 1.0$) but diminishes for high values ($1.0 < p_c/\sqrt{S} < 2.0$). While not completely collapsible in terms of displacement (W) and cushion density (p_c/\sqrt{S}) the following equations closely approximate the available data

Near $p_c/\sqrt{S} = 0.50$

$$\frac{W_1}{W} = \frac{0.28}{W^{1/3}} + \frac{0.04 W^{1/3}}{\left(\frac{p_c}{\sqrt{S}}\right)^{1/3}} \quad (261)$$

Near $p_c/\sqrt{S} = 1.0$

$$\frac{W_1}{W} = 0.24 + \frac{0.007 W^{1/3}}{\left(\frac{p_c}{\sqrt{S}}\right)^{1/3}} \quad (262)$$

Near $p_c/\sqrt{S} = 2.0$

$$\frac{W_1}{W} = 0.21 + \frac{0.008 W^{1/3}}{\left(\frac{p_c}{\sqrt{S}}\right)^{1/3}} \quad (263)$$

Obviously, much more work needs to be done before a completely acceptable formulation is obtained containing the key parameters. The absence of speed in these equations is disturbing but the current data base does not show any major effects. The above equations fit the available data, especially for the lower values of cushion density and they follow the simple theory expected functional form.

Propulsion System Weight (Group 200)

Considerable variations in propulsion system weights appeared in different craft due to types of powerplants, transmissions and propulsors. It is difficult to draw trend lines on the propulsion system due to the number of driving parameters and the limited data base. This can be seen from the following interrelationship of key parameters to form the propulsion system weight fraction:

$$\frac{W_2}{W} = \left(\frac{W_2}{P} \right) \cdot \left(\frac{P}{WV} \right) \cdot v \quad (264)$$

that is, it is seen to be a product of three key parameters. The first is the specific propulsion system weight (W_2/P) that depends on the type of engine (diesel, marine gas turbine (MGT), etc.), the type of transmission, and finally the type of propulsor (waterjet, waterscrew, air propeller). The second key parameter is the inverse of the transport efficiency (WV/P) already discussed in Chapter III. The third key parameter is the design maximum speed of the craft. It should not be surprising, therefore, to see a wide scatter in the available data as is indicated by Figure 252. For

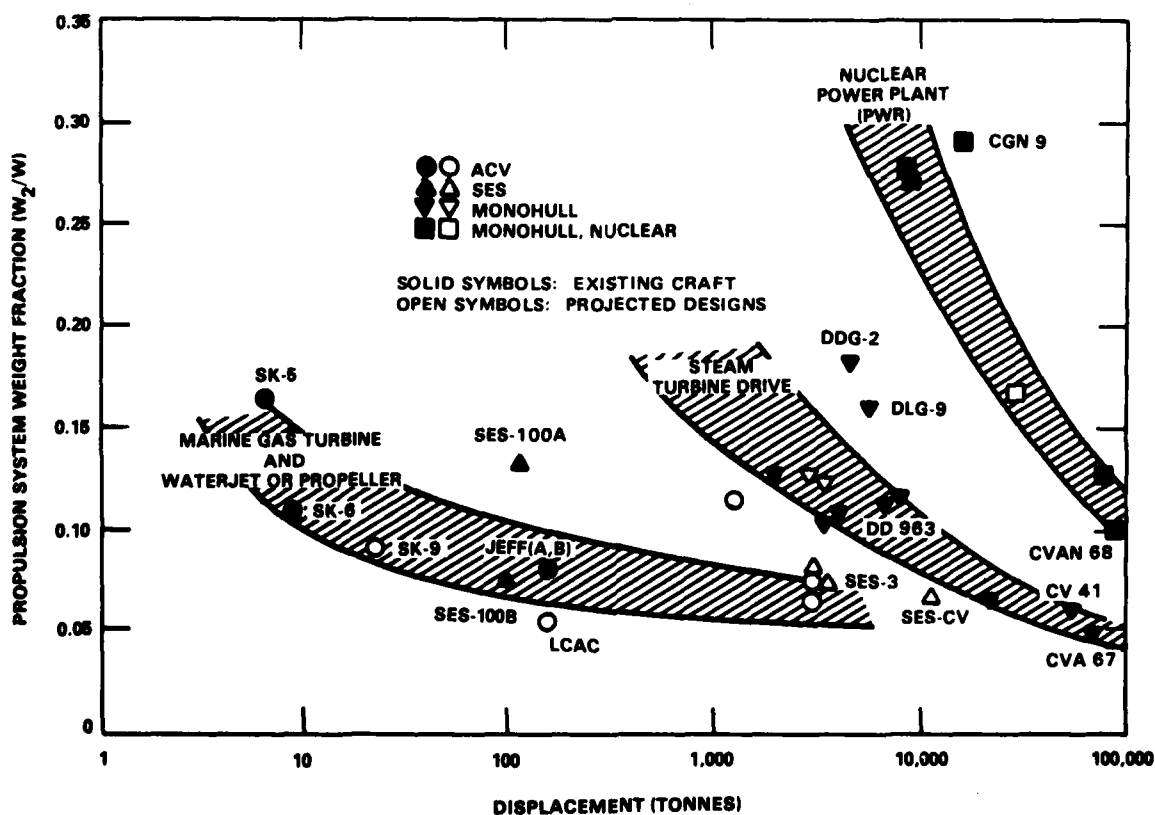


Figure 252 - Propulsion System Weight

information and comparative purposes, the available data on conventional steam turbine and pressurized water reactor (PWR) nuclear powerplant installations on conventional displacement ships is also provided on Figure 252. Note that for the very large displacements (for air cushion craft) the fraction of the craft displacement devoted to the propulsion system is similar to that for displacement ships using steam turbine propulsion.

The data collapses a little better (though not much) when expressed in terms of specific propulsion system weight (W_2/P) as shown in Figure 253 where the same data is plotted against total installed horsepower. This

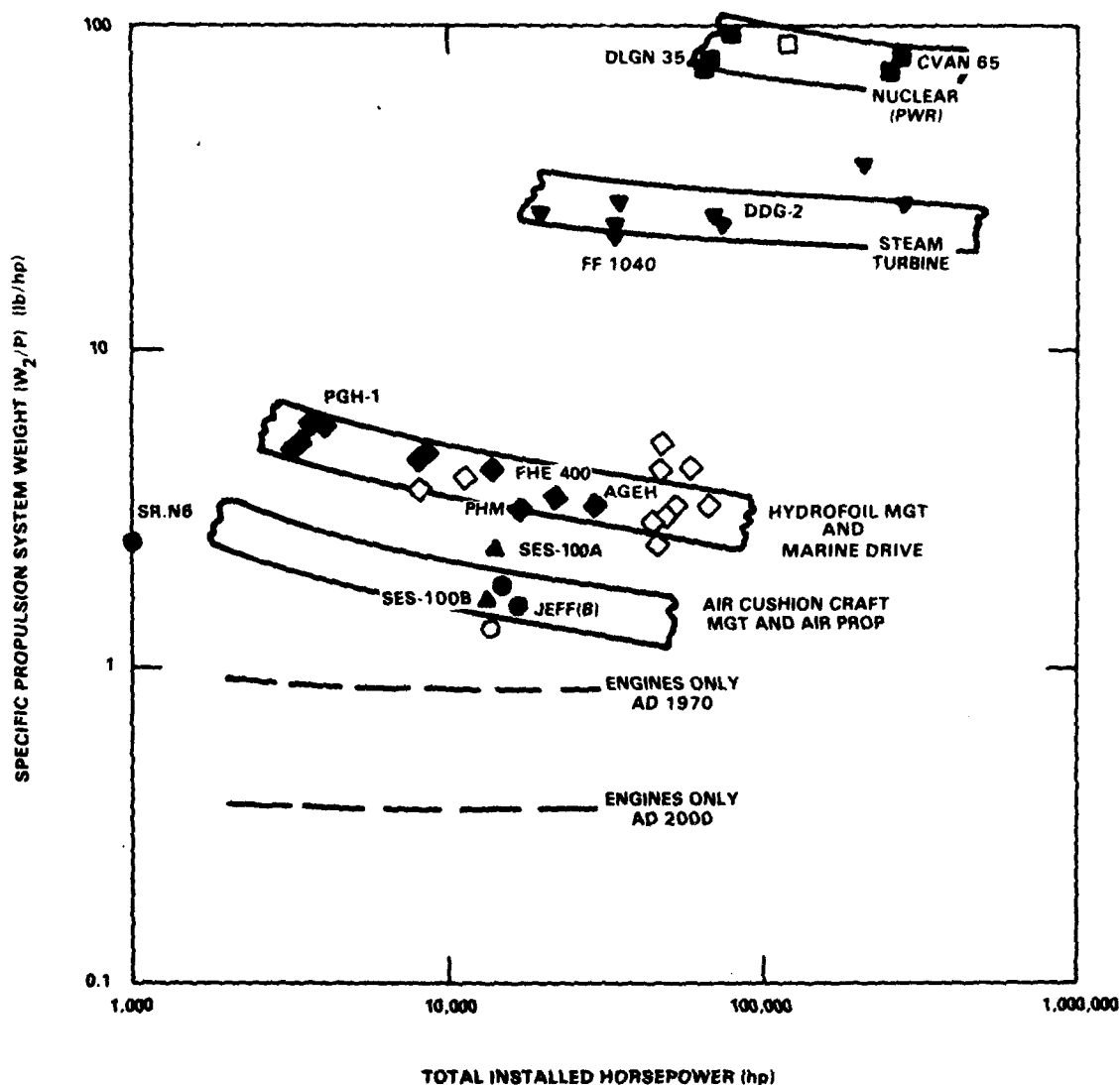


Figure 253 - Specific Propulsion System Weight

form of the data may be compared with the same data plotted as a function of craft displacement in Figure 191, Chapter IX. Attention will be restricted to the air cushion craft data band on Figure 253 where some license has been taken to draw a band labelled "marine gas turbine plus air propeller." The mean line through this band can be approximated by,

$$\frac{W_2}{P} = 1.25 + \frac{74}{\sqrt{P}} \quad (265)$$

where the specific weight is expressed in units of (lb/hp) and the total installed power (P) is in horsepower.

It is important to note the contribution of the various components and the impact of technological improvement. For example, the engine specific weight (see also Figure 191, Chapter IX) is seen to be a large contributor but it is also seen that the "AD 2000 technology" level engine weights are much less than their "1970 technology" level counterparts.

Electrical System Weight (Group 300)

The available data on the electrical system weights is shown on Figure 254. The electrical power requirements and choice of generating

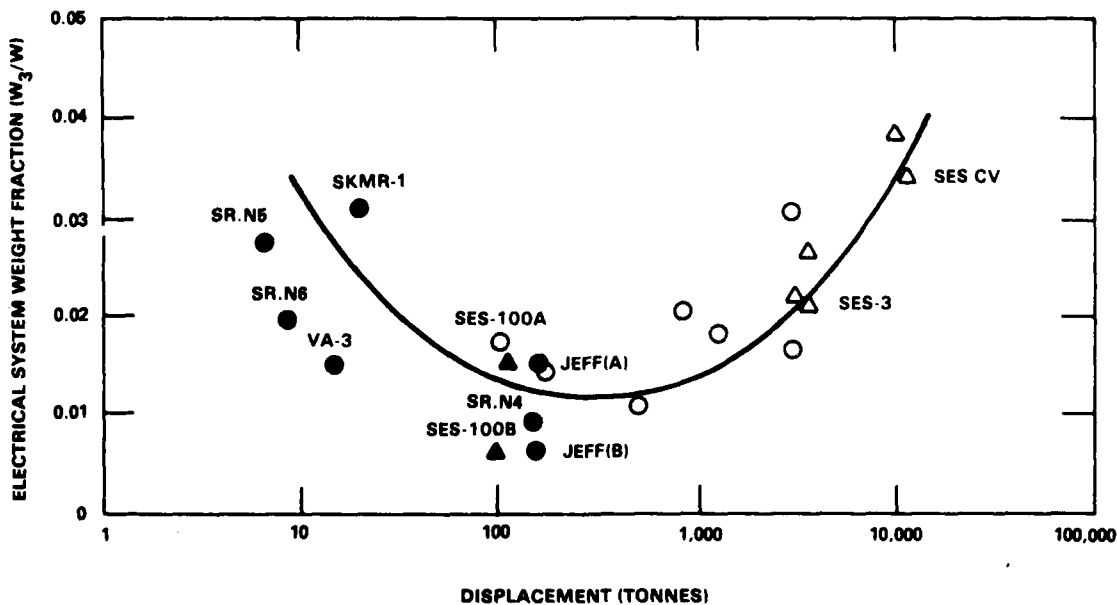


Figure 254 - Electrical System Weight

equipment onboard air cushion craft has not been sufficiently uniform to establish any definite trends. Most of the existing craft use 60 Hz equipment and some of the projected designs will use 400 Hz together with conversion equipment. While these differences in the data base have caused quite a scatter, some overall general trend can be seen which is represented by the equation

$$\frac{W_3}{W} = 0.00034 W^{1/2} + \frac{0.10}{W^{1/2}} \quad (266)$$

where W is measured in tonnes. Attempts to express the data in terms of specific weight (i.e., lb/kW) did not show any reliable trend. Values varied from 25 lb/kW to 80 lb/kW. While no formulation is given because of the scatter, Figure 255, showing the specific weight of the electrical system, is provided for information.

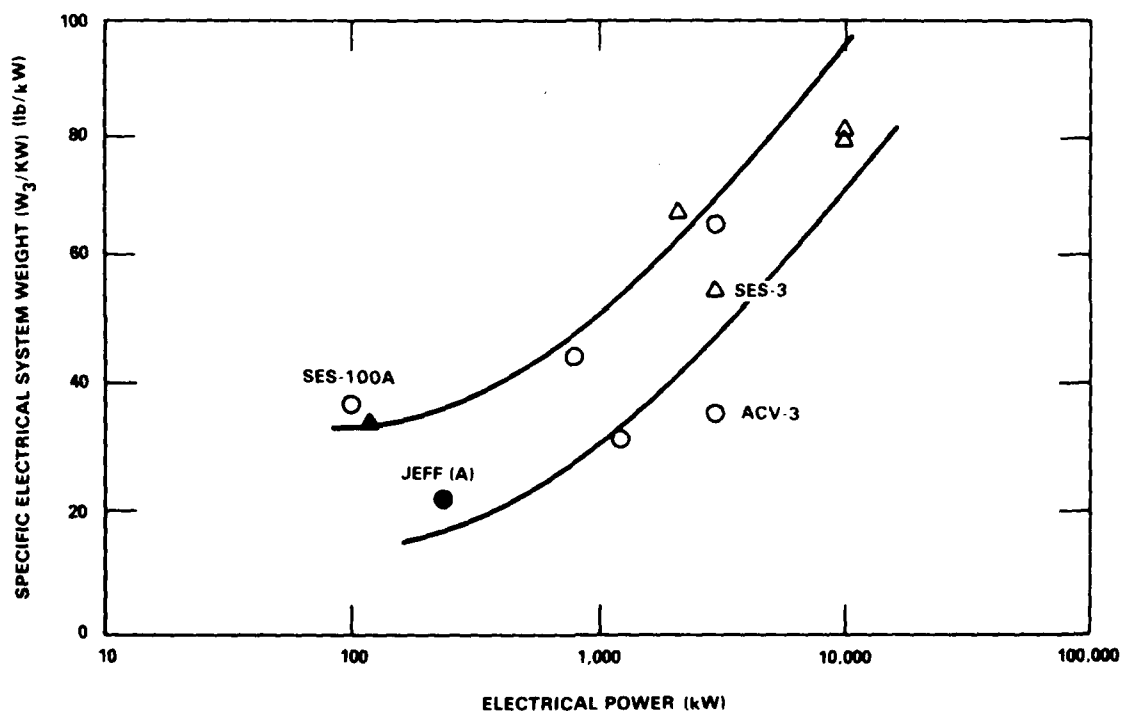


Figure 255 - Specific Electrical System Weight

Command and Surveillance Weight (Group 400)

As can be seen from Table 17, the Command and Surveillance Weight Group is made up of the craft's navigational system, communication system

and, if able to carry weapons, the fire control system. The data base of air cushion craft covers commercial craft, military test craft, and projected designs for fully-operational military craft. Much of the data in the author's files on commercial craft is not in the SWBS format and is difficult to convert. Also, testcraft with limited or specialized equipment onboard is not descriptive of air cushion craft for naval operational use. Accordingly, emphasis here has been given to projected designs destined for naval warfare and, therefore, ships are now being equipped with the associated command and surveillance equipment compatible with the expected combat suite for such craft. Figure 256 shows the various weights for four of the

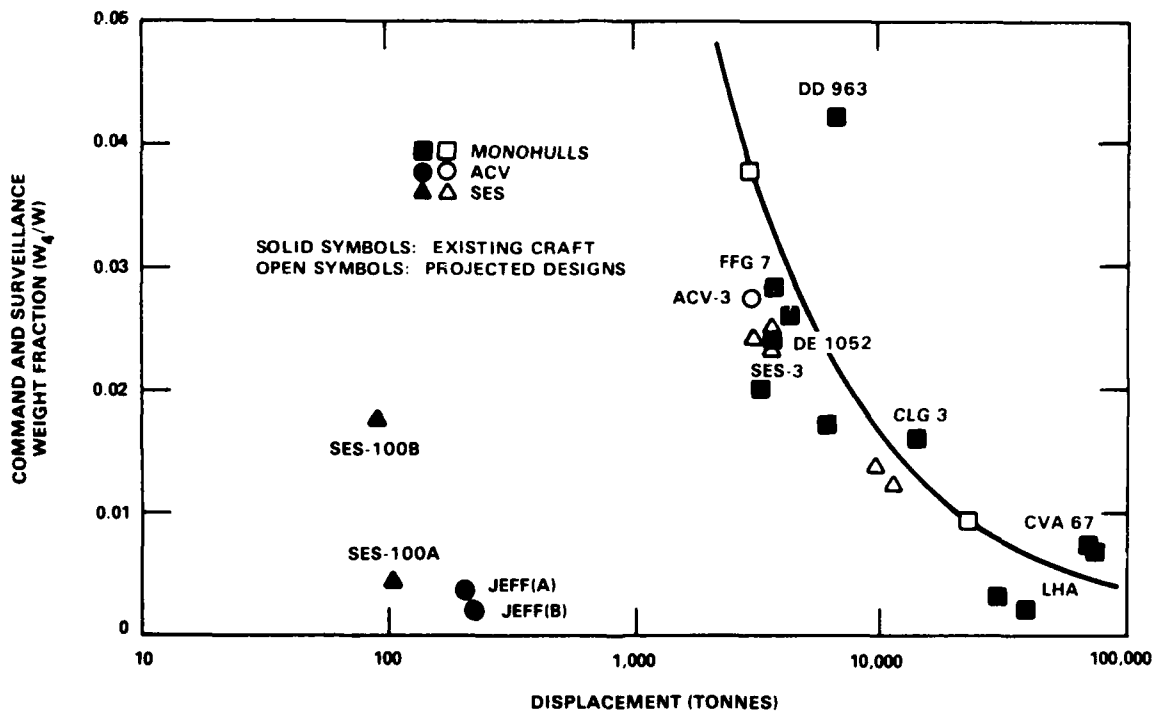


Figure 256 - Command and Surveillance System Weight

small test craft (no weapons) and several projected designs (with weapons). It might be expected that similar command and surveillance equipment would be onboard an air cushion craft as would be onboard a displacement ship of similar size carrying the same military payload. This expectation is confirmed on Figure 256 where data from existing U.S. Navy displacement ships has been included.

The line drawn roughly through the data is given by

$$\frac{W_4}{W} = \frac{15}{W^{3/4}} \quad (267)$$

where W is in tonnes.

Auxiliary Systems Weight (Group 500)

The auxiliary system on an air cushion craft is, as it is on most vehicles, a collection of subsystems, viz: pneumatic, hydraulic, air conditioning, steering, etc. as can be seen from Table 17. It also includes, at least according to the 1973 issue of the U.S. Navy SWBS, the lift system (W_{LS})* comprised of: the lift engines (if separate from the propulsion engines), lift fans, ducting, ride control elements, and the skirt system.

To provide better insight into the auxiliary system makeup, the available data has been separated into the lift system weight (W_{LS}) and the total auxiliary system weight (W_5) less the lift system weight (W_{LS}). Figure 257 shows the weight of the auxiliary system less lift system ($W_5 - W_{LS}$) for both air cushion craft and, for comparative purposes, displacement ships. Although there is considerable scatter, some general trends can be seen.

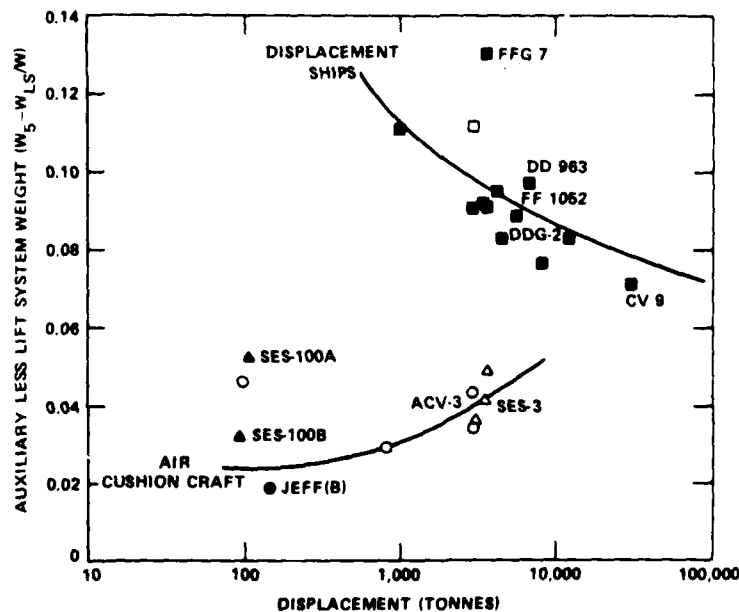


Figure 257 - Auxiliary Less Lift System Weight

*Note: For ease of notation the weight of the lift system will be designated W_{LS} in lieu of W_{567} from the 1973 SWBS.

AD-A084 740

DAVID W TAYLOR NAVAL SHIP RESEARCH AND DEVELOPMENT CE--ETC P/O 13/10
AIR CUSHION CRAFT DEVELOPMENT. FIRST REVISION.(U)
JAN 80 P J MANTLE
DTNRDC-80/012

UNCLASSIFIED

NL

6 IF 6

AS
AD-A084740

END

DATE

FILED

6-80

DTIC

The use of lightweight components in the "airborne" air cushion craft can be seen in Figure 257 for the sizes of air cushion craft built today. It is interesting to note that, as the projected sizes increase to large displacement ship sizes, there is a tendency for the auxiliary system weights to be comparable. From the data the equations for the auxiliary system less lift system weight are as follows:

Displacement Ships

$$\frac{W_5 - W_{LS}}{W} = 0.06 + \frac{0.52}{W^{1/3}} \quad (268)$$

Air Cushion Craft

$$\frac{W_5 - W_{LS}}{W} = 0.0024 W^{1/3} + \frac{0.06}{W^{1/3}} \quad (269)$$

where in both cases the full load displacement (W) is expressed in tonnes.

For the air cushion craft, the lift system weight (W_{567}) can be separated into the weight of the skirt and the remaining components of the lift system (engines, lift fans, controls, and ducting). Figure 258 shows the weight of the total lift system (W_{LS}) as the upper curve and data and the weight of the skirt system (W_{SK}) as the lower curve and data. In all cases, the data is expressed as a fraction of the full load displacement (W). Part of the scatter in the total lift system weight is due to the different functions being performed by the lift system in each of the designs (e.g., ride control) and part is due to the differing power levels. It will be noted that the weight of the sidehull air cushion craft lift system is generally less than the fully-amphibious air cushion craft lift system. Another difference, already discussed in Chapter VI on Seals and Skirt Systems, are the variations in basic skirt design which are manifested in the various weights of the seals and skirts. Recognizing the small data base for each design variation, some general trends can be seen represented by the equations:

Total Lift System

$$\frac{W_{LS}}{W} = 0.044 + \frac{0.08}{W^{1/3}} \quad (270)$$

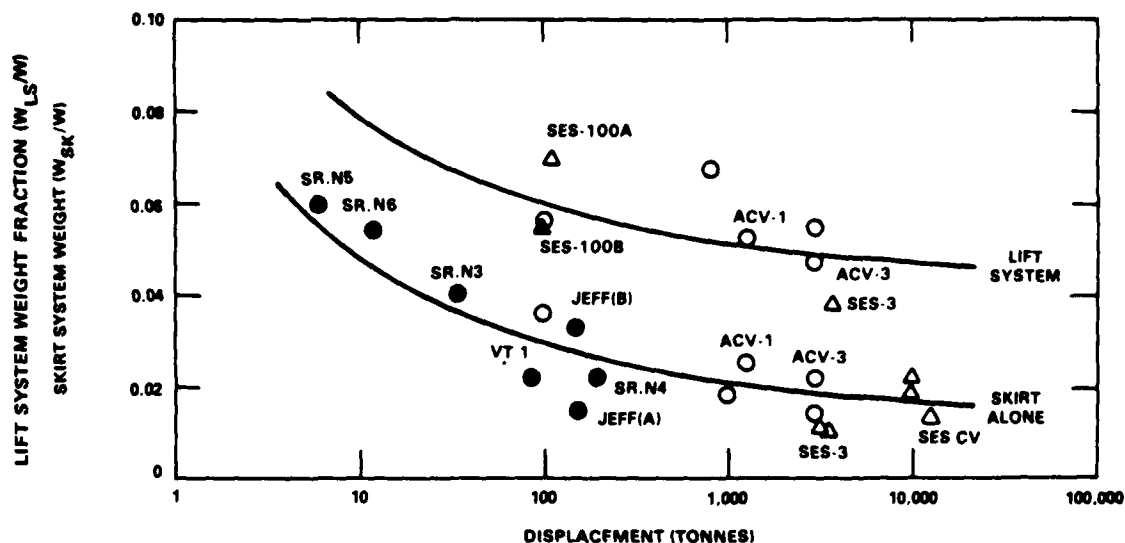


Figure 258 - Lift System and Skirt System Weight

Skirt System

$$\frac{W_{SK}}{W} = 0.014 + \frac{0.08}{W^{1/3}} \quad (271)$$

where the full load displacement (W) is expressed in tonnes. From Equations (270) and (271) can be immediately inferred that the weight of lift engines, lift fans, and ducting can be written as,

$$\frac{W_{LS} - W_{SK}}{W} = 0.03 \quad (272)$$

As a larger data base becomes available (some existing data cannot be released at this time because the data is either proprietary to the manufacturer or classified) a better trend can be determined. The trends shown in Figures 257 and 258 can, however, be used for at least initial design purposes.

Outfit and Furnishings Weight (Group 600)

It is known that the size of the ship's complement or manning has a strong influence on the size of the ship. It is also true that the manning requirements are determined more by the type of functions to be performed

than by the type of ship. Many functions, such as operation of the weapon and sensor systems, navigation, messing functions, and watch stations are not dependent on the type of ship. It should not be surprising, therefore, to find that manning can be expressed almost independently of whether the ship is a displacement vessel, hydrofoil, or air cushion craft. Also, since larger ships are used for more multiple-purpose missions than smaller ships, one might expect the manning requirements to increase as ship size increases. All of these expectations are more or less realized in the data shown in Figure 259 that shows the manning of several displacement ships and air cushion craft. Although not shown, planing craft and hydrofoils

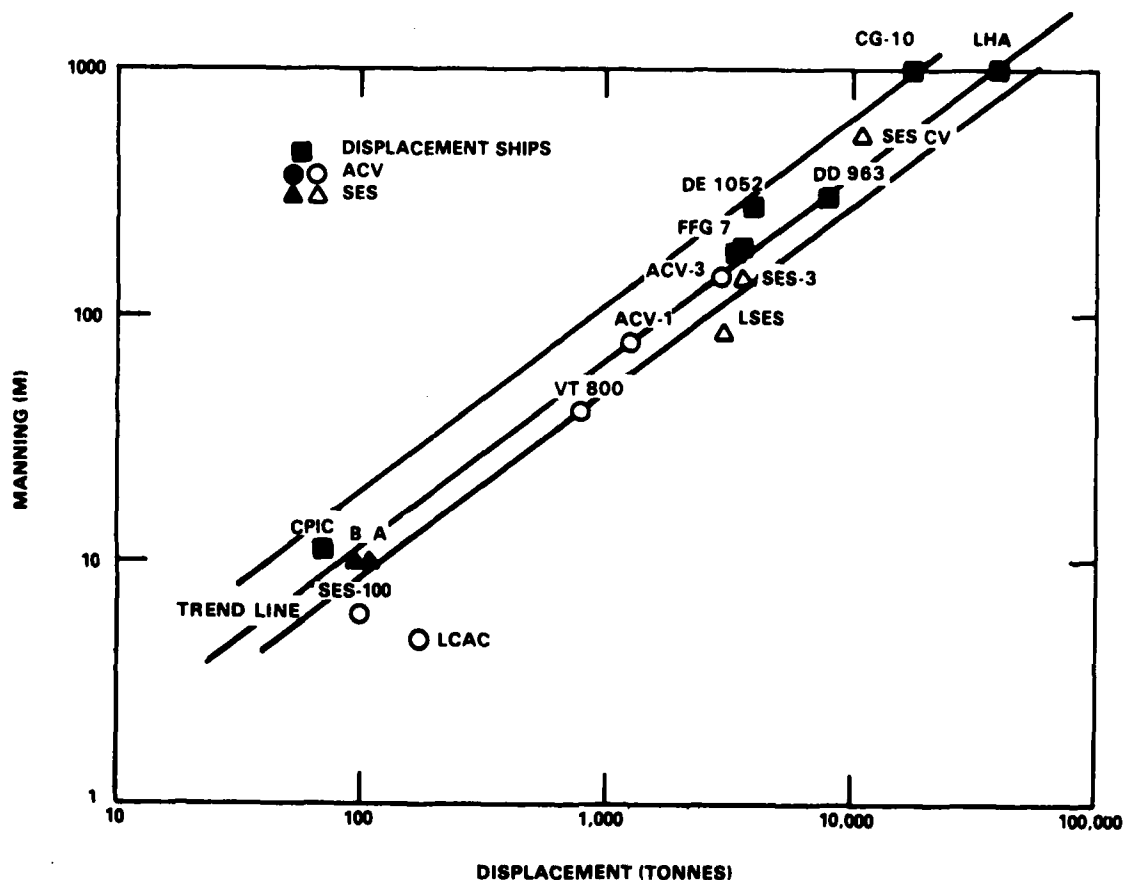


Figure 259 - Manning Aboard Ship

possess a very similar trend. The trend line through the various data is expressed by the equation

$$M = 0.35 W^{3/4} \quad (273)$$

where M is the number of ship's manning and W is the full load displacement in tonnes.

While it is noted that the current data would indicate similar manning for the various types of craft, one cannot help but wonder why the advanced technology that produces the advanced ship forms could not also bring about better use of automatic functions to reduce manning requirements. This would appear to be a fruitful area for development.

Data can be shown for the weight of the outfit and furnishing (O&F) systems either as a function of the manning (M), which is a key driving parameter, or as a function of the craft displacement. From Figure 259 it is seen that there is a direct relationship between manning (M) and displacement (W). Hence, data are shown as a function of the familiar full load displacement as shown in Figure 260.

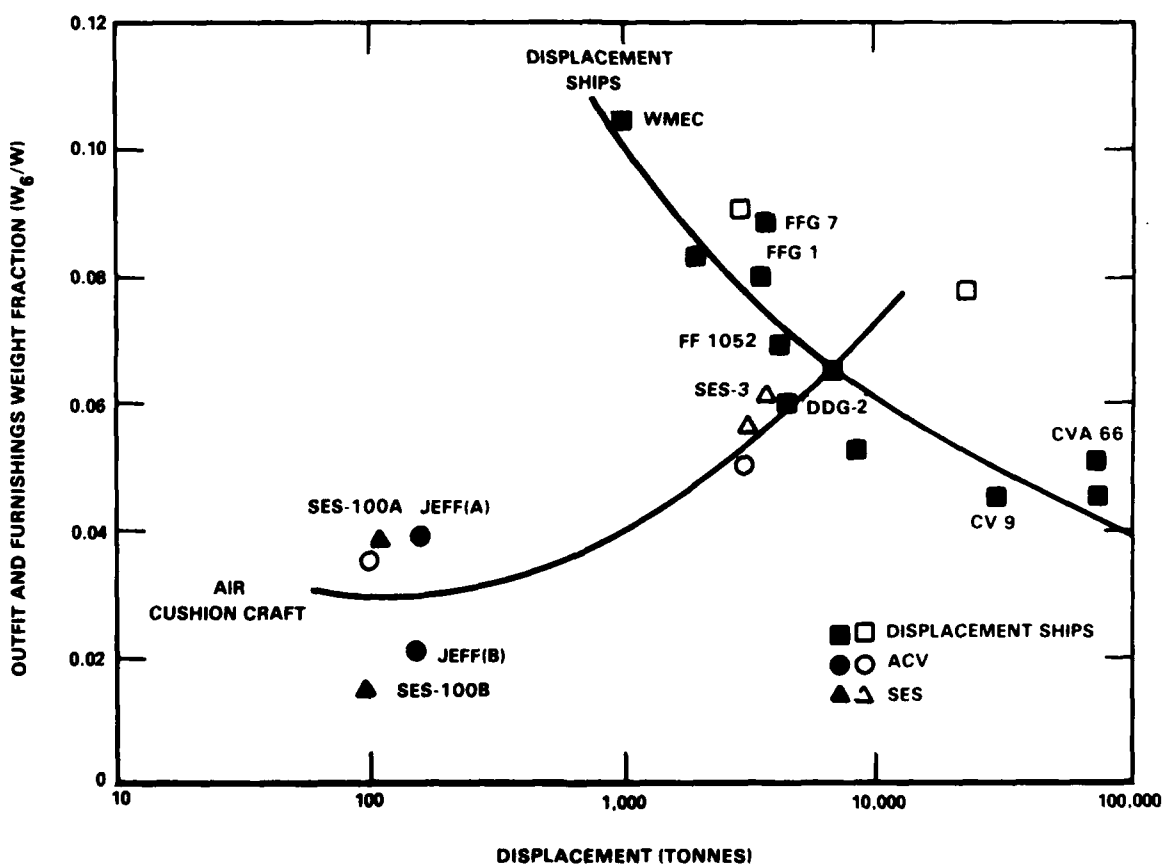


Figure 260 - Outfit and Furnishings System Weight

There is considerable scatter in the data and, while a continuous curve has been drawn through the air cushion craft data curve, care must be exercised in its use. The general trend of displacement ships is also shown and again, while there is scatter in the data, there are a sufficient number of points to demonstrate a general reduction in O and F weight fraction (W_6/W) as displacement (W) increases. All of the displacement ships are designed for long durations at sea with the accompanying increased O and F requirements for the onboard personnel.

The large air cushion craft designs shown (around 3000 to 4000 tonnes) also are designed for many days of operation at sea and again show O and F weight fractions similar to those for displacement ships. The small air cushion craft (around 100 to 200 tonnes), on the other hand, are either testcraft or "less than one day" operation craft with limited need for extensive outfit and furnishings. Thus, it could be that each cluster of craft (small and large) are separate "families" of craft that really lie on separate curves each with the general characteristic of the curve shown for displacement ships.

In the absence of better data, however, the displacement ship and air cushion craft O and F system weights are given by the equations:

Displacement Ships

$$\frac{W_6}{W} = 0.01 + \frac{0.50}{W^{1/4}} \quad (274)$$

Air Cushion Craft (Tentative)

$$\frac{W_6}{W} = 0.003 W^{1/3} + \frac{0.07}{W^{1/3}} \quad (275)$$

where W is the full load displacement in tonnes. The equation for the air cushion craft O and F weight equation is regarded as tentative in the light of the discussion above pertaining to effect of mission duration on the design of the O and F system.

Armament (Group 700)

As Table 17 shows, the armament group is made up of that part of the weapon system that is fixed to the craft, e.g., missile launchers, installed guns, and torpedo tubes. For a given missile system there is usually a choice of launcher system; some lightweight and others integrated with the ships' structure. These choices will cause variations in Group 700 between two different craft carrying the same weapon and sensor suite. It is usual practice to use the lightweight launchers and canisters on weight limited craft and to expect this to show up in the data. However, comparing

the data from both (actual) displacement ships and (projected) air cushion craft it is difficult to express this difference in measurable terms and a single trend line is shown in Figure 261 for both displacement ships and

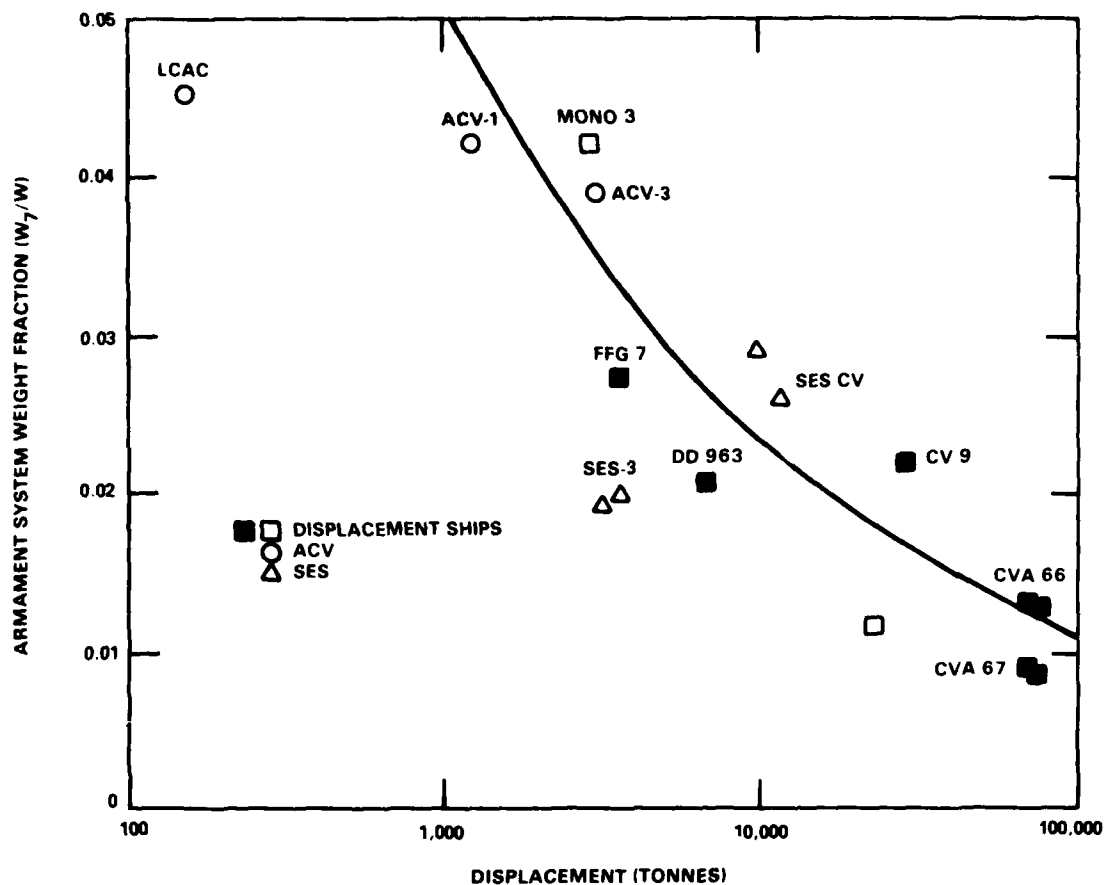


Figure 261 - Armament System Weight

air cushion craft. This trend line is represented by the equation

$$\frac{W_7}{W} = \frac{0.50}{W^{1/3}} \quad (276)$$

where W is measured in tonnes.

Empty Weight (W_E)

The sum of all the above weights is, as seen from Equation 259, the light ship weight. If one then subtracts those items designated as "fixed payload items" then one obtains the Empty Weight. Figure 262 collects

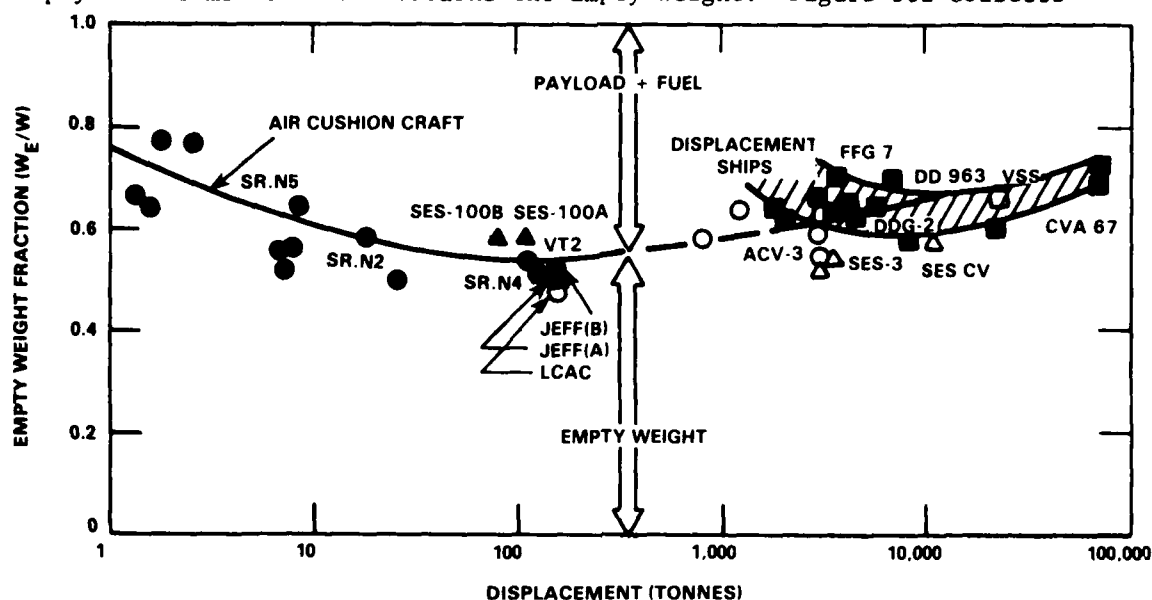


Figure 262 - Empty Weight Fraction

this aggregate result for a wide range in sizes of air cushion craft. Superimposed on Figure 262 for reference purposes is the equivalent set of data for empty weight of displacement ships.

While one could construct the algebraic sum of the equations for the seven weight groups to derive the empty weight equation, it was thought of more value to provide a "curve fit" of the available weight data for the empty weight of air cushion craft as shown by the single curve on Figure 262. This is represented by the equation,

$$\frac{W_E}{W} = 0.25 W^{0.10} + \frac{0.50}{W^{0.25}} \quad (277)$$

where W is measured in tonnes. From Equation (277) and Figure 262 it can be seen that empty weight fractions of approximately 50 to 60 percent are typical. Accordingly, the amount left for the payload (fixed and disposable) and fuel is correspondingly 50 to 40 percent of the craft displacement.

It will be noticed that, in all the weight groups discussed in this appendix, there are gaps in the data base. However, the equations given with the displayed data serve as a basis for further improvement as more data become available.

APPENDIX C
HUMP THRUST MARGIN

The question of hump thrust margin is a key issue in the design of air cushion craft in that it can result in a vehicle that has either excessive thrust (with incurred power and cost increases) or a vehicle that wallows at below hump speeds and, therefore, is incapable of continuing with its mission.

There has been no consistency in the air cushion (or hydrofoil) field in setting thrust margins. Each design used different margins depending on the particular requirements of the design or availability of powerplants.

To understand a little more fully the various design interactions that can occur in determination of the hump thrust margin, consider the basic equation for accelerated motion of the craft,

$$T - D = \frac{W}{g} \cdot \frac{dV}{dt} \quad (278)$$

where T = total thrust of the propulsor(s)

D = total craft drag

W = displacement

g = gravitational constant

$\frac{dV}{dt}$ = acceleration of the craft at any instant

Due to the characteristics of the propulsor and of the craft itself, the thrust (T) and drag (D) vary in quite a different manner as speed changes. Equation (278) can be written in two forms, viz:

$$\frac{T-D}{W} = \frac{1}{g} \frac{dV}{dt} \quad (279)$$

and

$$\frac{D}{W} \left(\frac{T}{D} - 1 \right) = \frac{1}{g} \frac{dV}{dt} \quad (280)$$

The definition of "thrust margin" varies among the technical community. Some refer to the thrust margin being the difference between the thrust and the drag expressed as a fraction of the craft's weight, i.e., the acceleration of the craft expressed in "g's" as given by Equation (279). Other groups simply use the ratio of thrust to drag as occurring in Equation (280). Both forms are used depending on the application and presentation; however, in this analysis, concentration will be given to determining the acceleration.

BACKGROUND

To illustrate how the accelerating force (T-D) varies with speed and craft characteristics, Figure 263 shows the thrust and drag curves for the

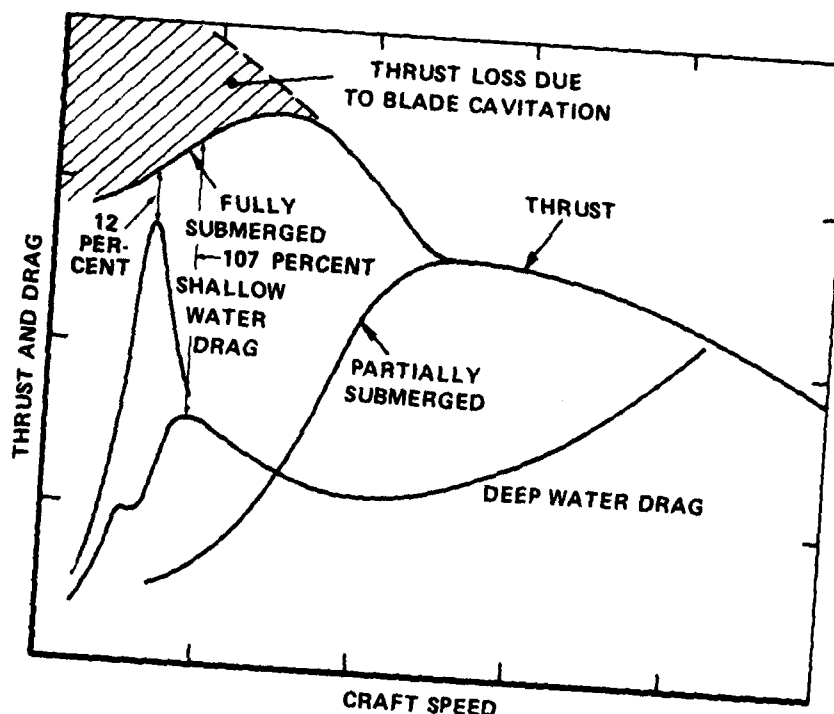


Figure 263 - Typical Supercavitating Propeller Thrust Curve

SES-100B which is a supercavitating water propeller driven SES. Figure 264 shows the thrust and drag curves for the JEFF(A) which is an air propeller driven ACV. It can be seen, from Figures 263 and 264, that the accelerating force varies radically both between SES and ACV, between shallow and deep water operating conditions, and further between forms of propulsion.

It has become common practice to characterize the thrust and drag curves, and further to ensure adequate thrust capability, by establishing, for any given design, a "hump thrust margin" of a certain acceleration level. For example,

$$\left| \frac{T-D}{W} \right|_{\text{hump}} = 0.025 \quad (281)$$

or from Equation (279):

$$\left| \frac{dv}{dt} \right|_{\text{hump}} = 0.025 \text{ g} \quad (282)$$

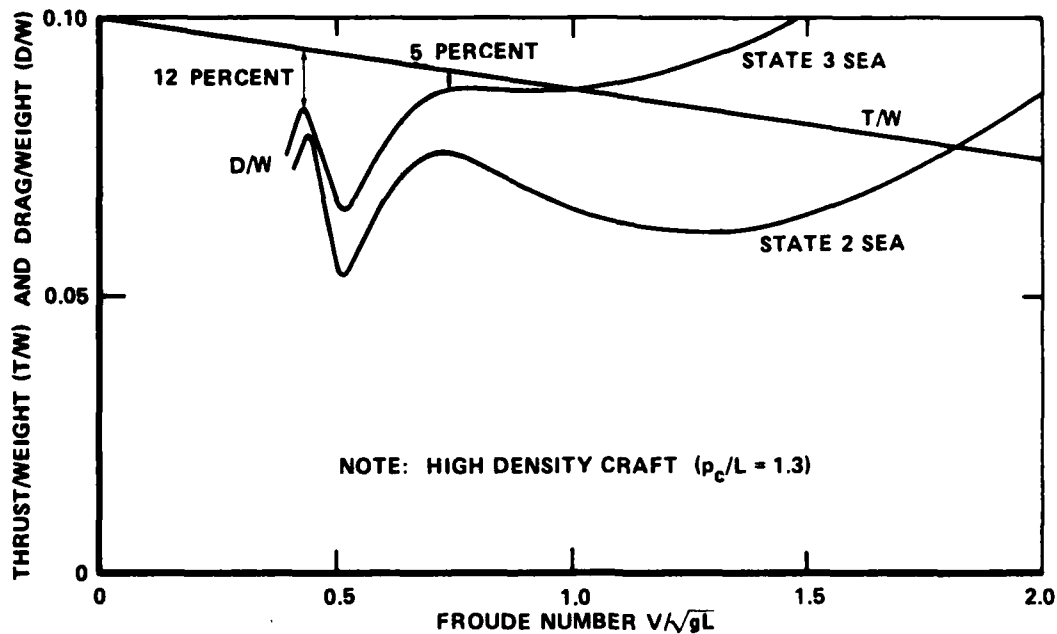


Figure 264 - Typical Thrust and Drag Curves

which states that at the (primary) hump speed (that speed where the wave drag is a maximum) the instantaneous value of acceleration is 0.025 g. Other numerical values can, of course, be substituted for any particular design.

It can be seen from Figures 263 and 264 that radically different values occur in the various designs. In the case of the SES-100B it can be seen that a substantial margin ($T-D = 107$ percent D) exists at the primary hump in deep water but a critical margin is at the shallow water condition where the same thrust margin is now reduced to 12 percent excess thrust. In the case of the JEFF craft (Figure 264), an excess thrust of 5 percent over the drag at the primary hump speed determined the thrust requirements. A higher thrust margin exists at the secondary hump speed.

By way of comparison, similar situations exist in determining the thrust margins for hydrofoils. Figure 265 shows the thrust and drag curves for the TUCUMCARI hydrofoil. Here, the margin is to be computed as the thrust divided by the hullborne drag as the hydrofoil goes through a transition from the hullborne mode to the foilborne mode. As shown in Figure 265, the consideration of thrust margin becomes more complex. Due to the drag of the struts and their hydrodynamic interference with the hull, an 11.6 percent excess thrust exists over the drag curve at "takeoff speed" but due to the cavitation limits on the waterjet pump, only a 6 percent thrust excess exists at a slightly slower speed. In the case of the

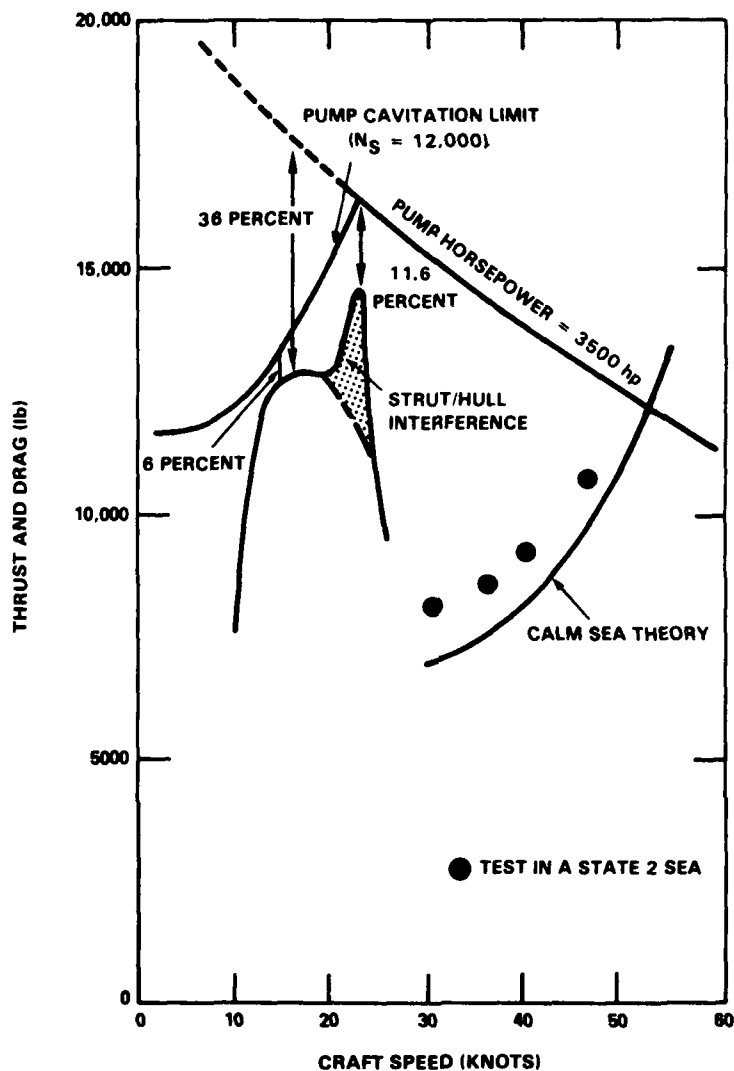


Figure 265 - TUCUMCARI Thrust and Drag

HIGHPOINT (PCH-1), in its original form, a significant thrust margin (105 percent of the drag) was integrated into the design, as shown in Figure 266, because it was a deliberate program decision that the craft be able to takeoff with one engine inoperative. With only one propulsion engine operational, the excess thrust at takeoff speed falls to 3 to 5 percent over the drag at that speed.

With this background, several air cushion craft (both ACV and SES) were analyzed to seek the relationship between the hump thrust margin and the performance of the craft. Both actual operational craft and design studies done in the U.K. and the U.S. were included in the analysis. Figure 267 shows the thrust and drag curves for a 200 tonne displacement ACV done for

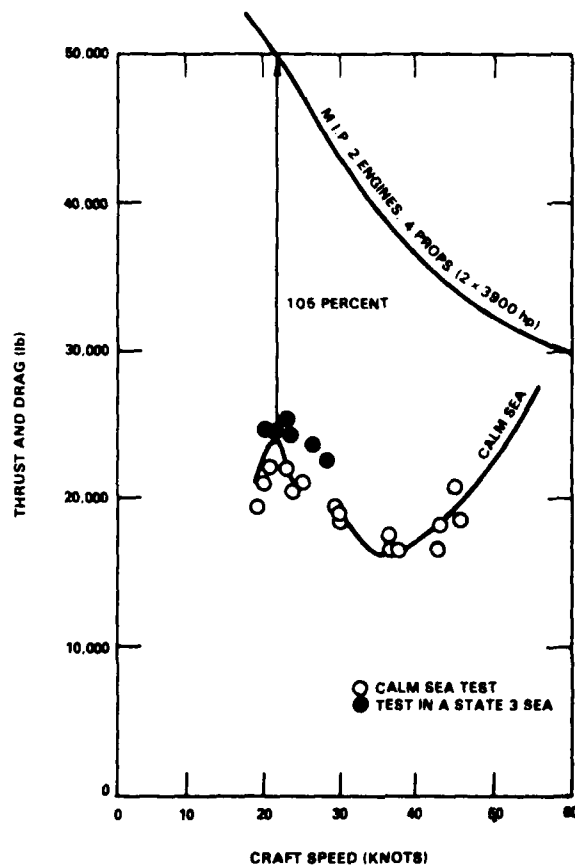


Figure 266 - PCH-1 (MOD 0) Thrust and Drag

the Advanced Naval Vehicles Concepts Evaluation³⁰ project. A similar set of curves for the 1264 tonne ACV design is shown in Figure 268. Both craft use air propulsion similar to that used on the JEFF craft. For comparative purposes, two 3000 tonne ACV designs are shown in Figures 269 and 270. An ACV using water screw propulsion is shown in Figure 269 and a similar 3000 tonne ACV but using air propellers for propulsion is shown in Figure 270. This latter design done for the Advanced Naval Vehicles Concepts

Evaluation³⁰ project by Vosper-Thornycroft in England shows the typical 25 percent excess thrust margin over the calm water drag at the (primary) hump speed. It will be noticed that in rough seas, intermittent power ratings are needed to "get over hump."

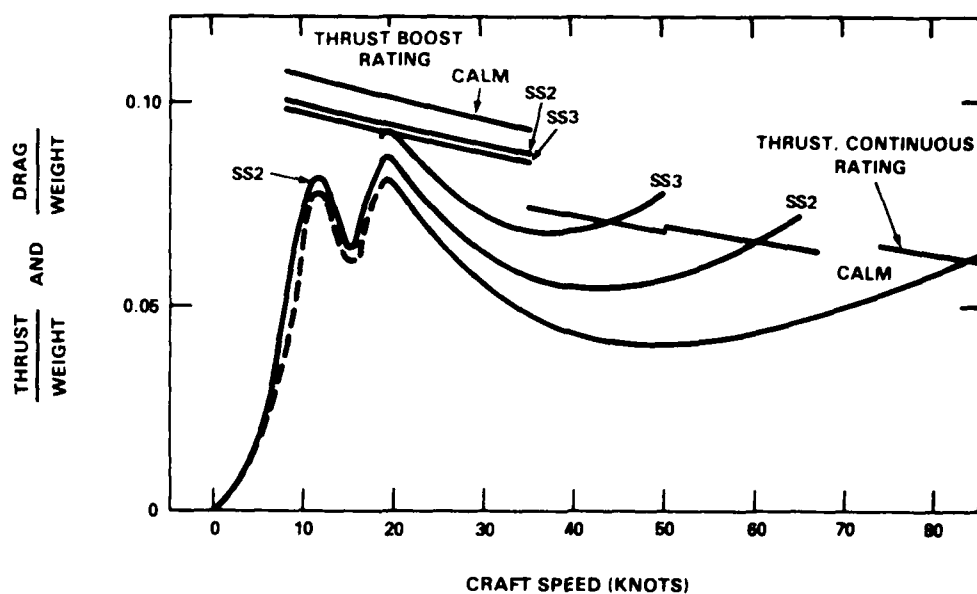


Figure 267 - 200 Tonne ACV Thrust and Drag

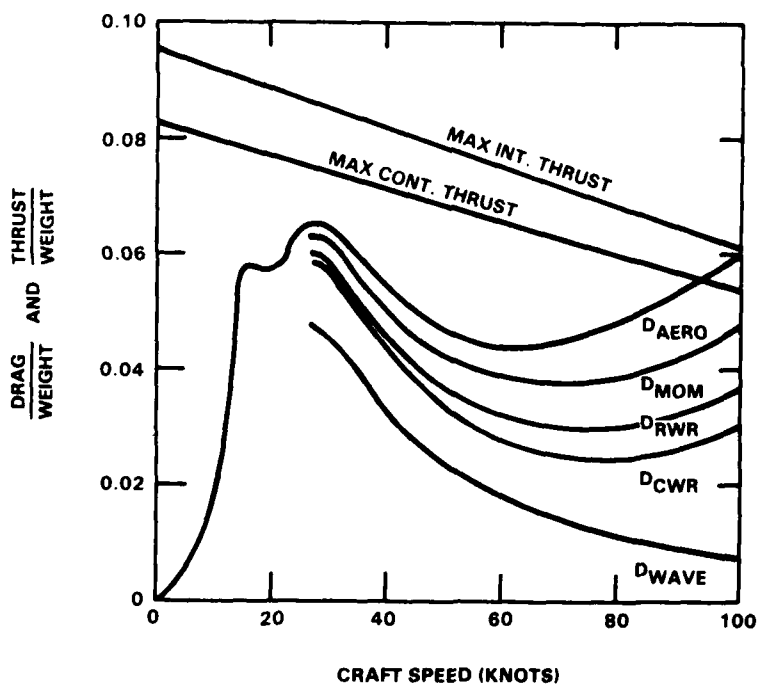


Figure 268 - 1264 Tonne ACV Thrust and Drag

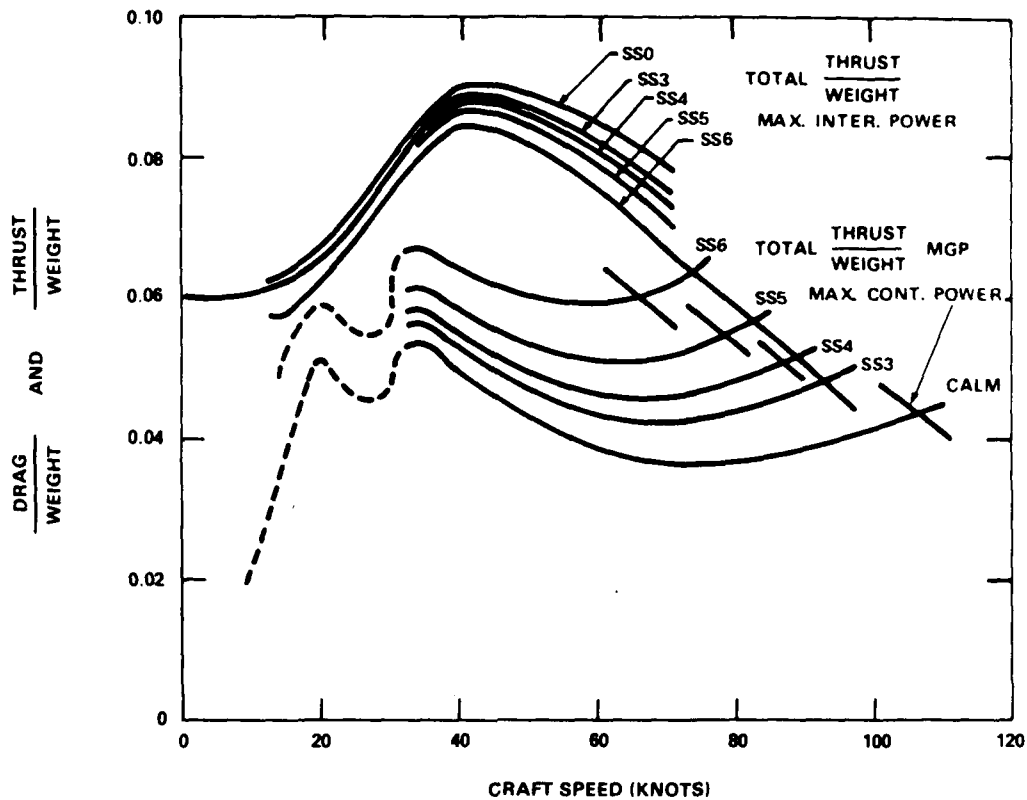


Figure 269 - 3000 Tonne ACV Thrust and Drag (Water Propelled)

ACCELERATION TIME

It is suggested that there are two performance criteria associated with hump thrust margin, they are:

- (a) *There shall be sufficient thrust margin over calm water drag to account for such items as uncertainties in drag prediction, variations in drag due to the "as-built" configuration and rough water drag increments.*
- (b) *The thrust margin shall be sufficient throughout the entire speed range from 0 to hump speed to achieve a given total time to speed suitable for the operation envisaged for the craft.*

Clearly, criterion (a) is a "go/no-go" criterion that must be met and represents a minimum value for the thrust margin. Criterion (b) is associated with the handling performance of the craft. Too much excess thrust gives a rapid acceleration craft while too little results in a sluggish craft that takes a long time to get over hump.

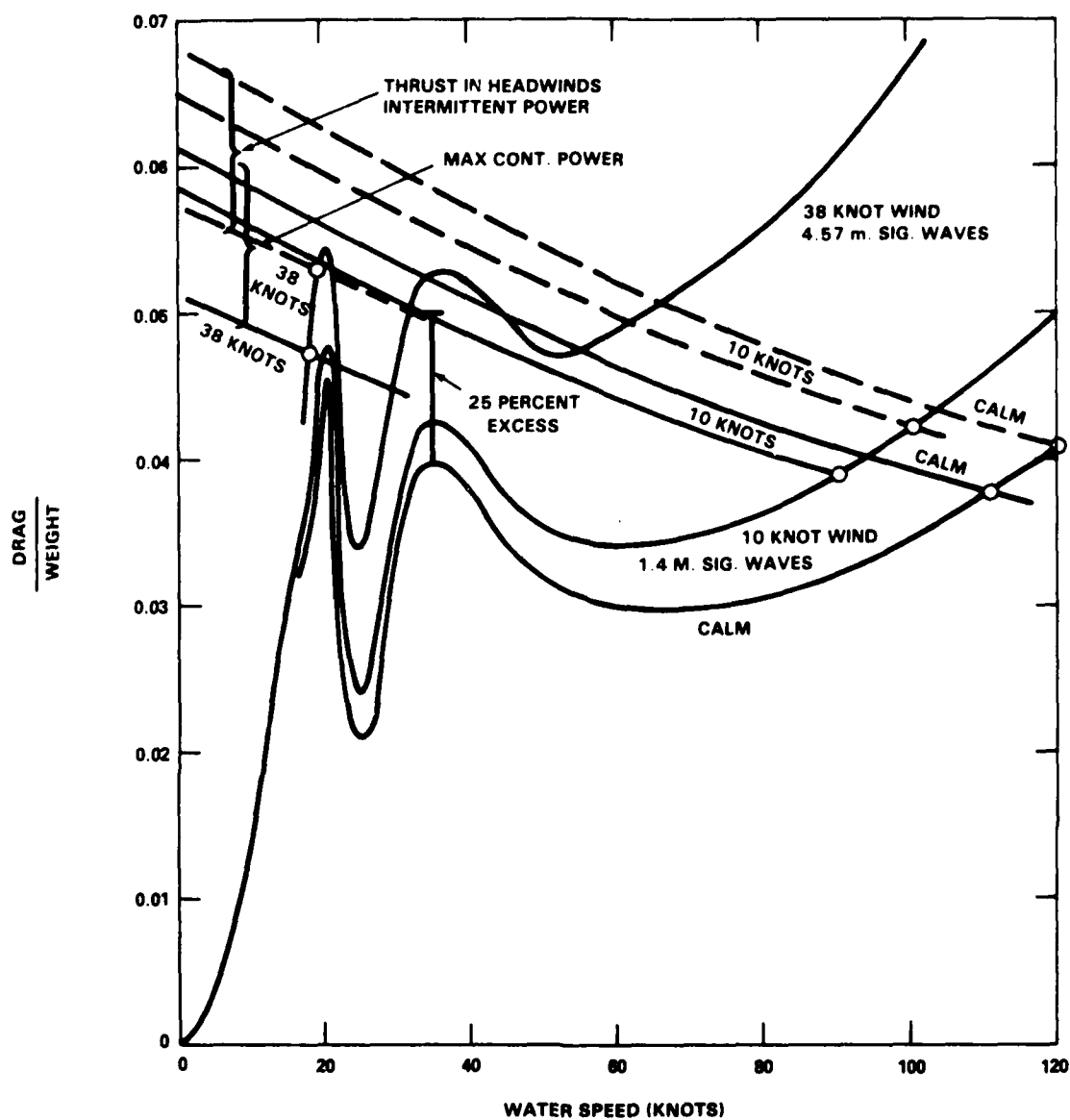


Figure 270 - 3000 Tonne ACV Thrust and Drag (Air Propelled)

To provide an appreciation of the time (t_H) taken to achieve hump speed (V_H), Equation (278) can be transposed and expressed in integral form, as follows:

$$t_H = \frac{1}{g} \int_0^{V_H} \frac{dV}{\frac{T-D}{W}} \quad (283)$$

This can be normalized to give a nondimensional time (τ) as

$$\tau = \frac{g^t_H}{V_H} = \int_0^1 \frac{Wdv}{T-D} \quad (284)$$

where the speed ratio $v = V/V_H$. The functional form in the integrand is not amenable to simple analysis and a series of graphical integrations was performed to determine the time. In all cases, maximum intermittent power was used up to hump speed, after which the engine was throttled back to maximum continuous power for superhump speeds. Only the time to reach hump speed is considered here.

The results of the analysis are shown in Figure 271 where the time to reach hump speed, expressed nondimensionally to minimize scale effects, is shown as a function of the hump thrust margin and the size of the craft.

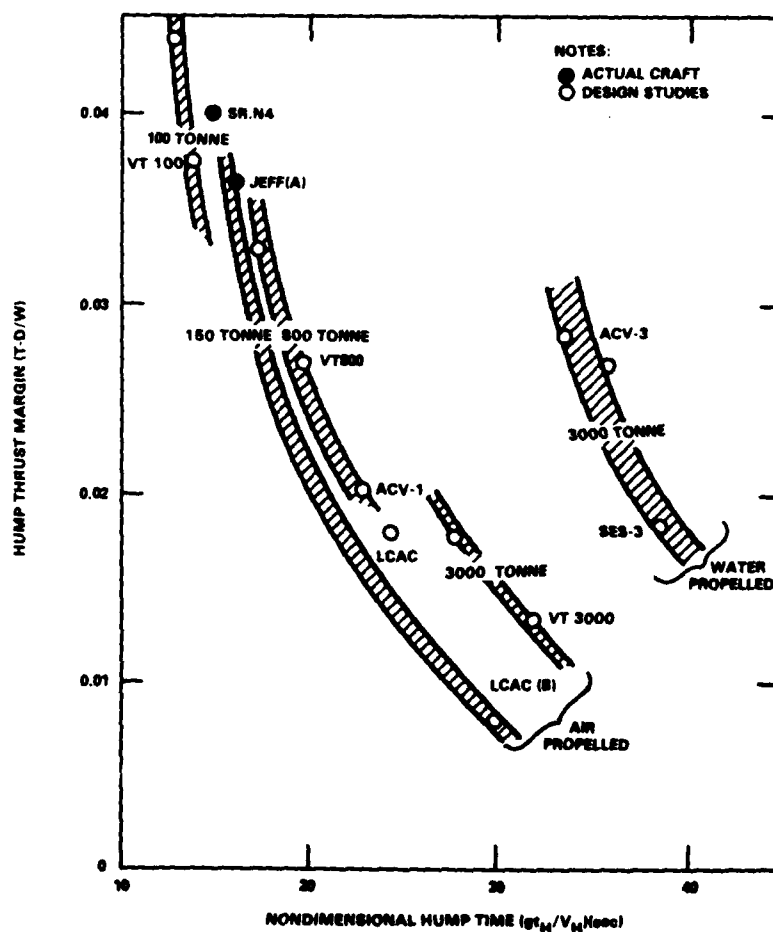


Figure 271 - Thrust Margin and Hump Time

The shaded bands cover the available data for thrust levels on a 59° F day and an 80° F day. The SR.N4 and JEFF craft are shown in Figure 271 for reference. There are very distinct trends as shown. It will be seen that considerable reduction in the thrust margin at hump makes only a slight change in acceleration time suggesting that a power savings could be realized without any major change in performance. For example, from Figure 271, for a 150 tonne displacement, air propelled ACV with a hump thrust margin of $T-D/W = 0.04$, the time to get to hump speed was 15 seconds (expressed in nondimensional time); while reducing the margin to $T-D/W = 0.02$, i.e., half the thrust level, the time to get to hump speed was 20 seconds. Is this extra 5 seconds worth the power difference?

Obviously, the thrust level cannot be reduced to where it violates criteria (a)--i.e., the craft does not get over the hump and so some indication of the level of uncertainty is needed to determine the minimum amount of thrust margin needed. This will be referred to later, but first Figure 272 has been prepared to see if there are any design rules that can be established between hump thrust margin and the time to accelerate to hump speed.

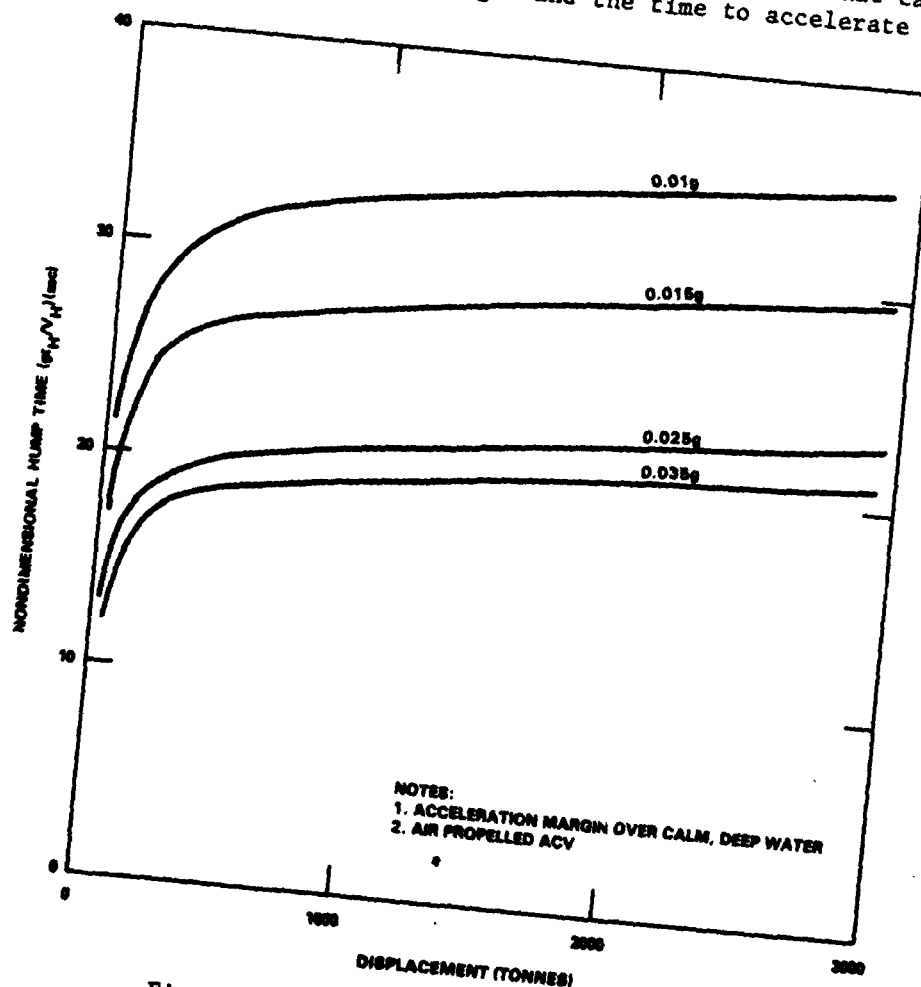


Figure 272 - Hump Time and Displacement

This is a cross-plot of Figure 271 for four selected hump thrust margins, expressed in terms of acceleration in "g's." From this cross-plot it is seen that, above about 200 tonnes displacement, the acceleration time becomes approximately constant. The values of acceleration times for a representative set of hump margins are given in Table 20. The actual time in real seconds will change from the nondimensional times as a result of the change in hump speed (V_H) as displacement changes. Table 20 can be used as a guide in determining the required acceleration margin (and thus thrust level) at hump speed to achieve a given acceleration time at least for those craft with a displacement greater than about 200 tonnes. The accuracy of this approximation improves as displacement increases.

TABLE 20 - ACCELERATION AND TIME
TO HUMP SPEED

Hump Acceleration Margin (g's)	Nondimensional Hump Time $\tau = \frac{gt_H}{V_H}$ (sec)
0.010	32
0.015	28
0.025	22
0.035	20

Returning to the necessary criterion (a) that the thrust shall at least be sufficient to overcome the uncertainties in the drag prediction, rough water effects, and other drag considerations it is unfortunate that no consistent trend is seen in the available data. Figure 273 shows, for a set of ACV and SES designs, the predicted increase in hump drag in rough water over that predicted in calm water. In an attempt to minimize the scale effect, the significant wave height of the sea has been divided by the cube root of the displacement to give a normalized sea roughness parameter. The available "data" are from projected designs with displacements ranging from 100 to 3600 tonnes, vary with skirt designs and cushion pressures, and represent both U.K. and U.S. designs.

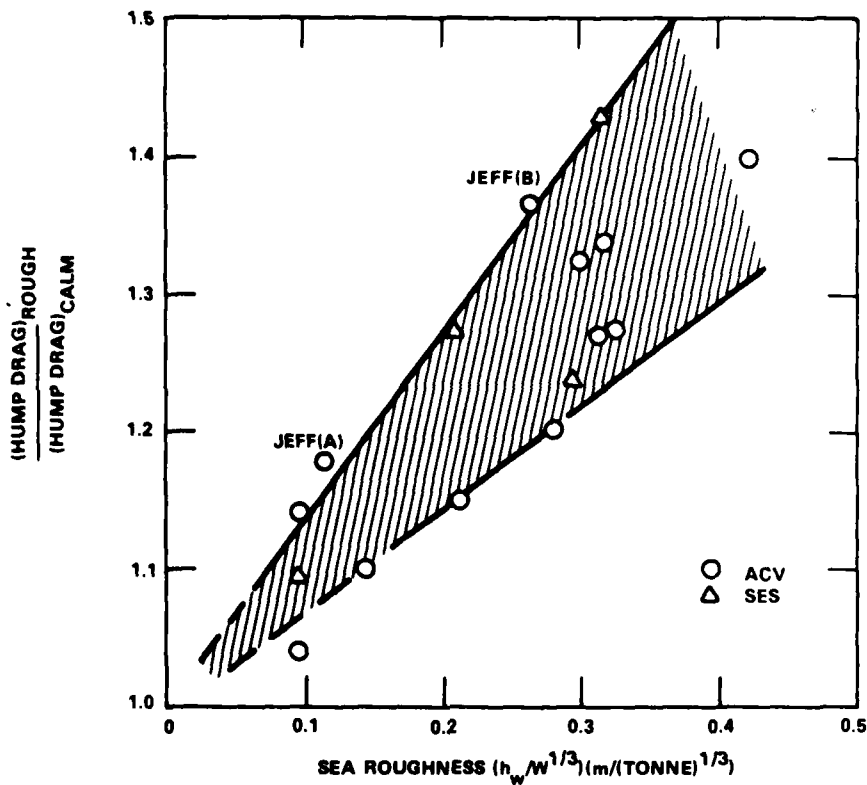


Figure 273 - Hump Drag in Rough Water

A significant point in Figure 273 is that those craft that have received the most extensive analysis and model test in the recent past namely the JEFF craft and the LSES or 3KSES are in the uppermost parts of the band and those projected designs in the future are in the lower part of the band. This is probably reflected in the degree of optimism that frequently occurs early in any program. Thus, it would seem conservative or at least realistic to assume that the upper line in Figure 273 represents a more likely representation of the rough water drag.

The equation to this line is given by

$$\left[\frac{D_{\text{rough}}}{D_{\text{calm}}} \right]_{\text{HUMP}} = 1 + K \frac{h_w}{W^{1/3}} \quad (285)$$

where D_{rough} = the hump drag in rough water
 D_{calm} = the hump drag in calm water
 h_w = the significant wave height (measured in meters)
 W = the full load displacement (measured in tonnes)

The constant K varies within the band but for the upper (realistic) line $K = 1.40$.

Now, by definition, the hump thrust margin is given by

$$\left[\frac{T - D_{\text{calm}}}{W} \right]_{\text{HUMP}} = n(g) \quad (286)$$

where $n(g)$ is the instantaneous acceleration at the hump speed measured in units of gravitational acceleration ($g = 32.2 \text{ ft/sec}^2$). Clearly, the amount of hump thrust margin required must depend on how rough a sea the excess thrust must contend with. If it is taken that the desired thrust (T) shall be equal to the rough water drag (D_{rough}) in some limiting sea state, then

$$[T]_{h_w\text{-limit}} = D_{\text{rough}} \quad (287)$$

Then, combining Equations (285), (286), and (287) gives the unique relationship

$$\left[\frac{D_{\text{calm}}}{W} \right]_{\text{HUMP}} \cdot K \cdot \left[\frac{h_w}{W^{1/3}} \right]_{\text{LIMIT}} = n(g) \quad (288)$$

Equation (288) is thus the required hump thrust margin criterion expressed now in terms of known quantities that can be varied at the designer's option.

The above criterion gives the minimum value for the thrust. The other criterion would pertain to the maximum value of thrust which would now be set by the time required, i.e., is the designer (or operator) looking for

a rapidly accelerating craft or is he content with a "reasonable" acceleration at much less power and cost? A reasonable approximation to the acceleration times given in Table 20 is obtained from

$$\frac{T-D_{\text{calm}}}{W} = 0.05 - 0.0014 \left[\frac{gt_H}{V_H} \right] \quad (289)$$

Equation (289) only applies (as may be seen from Figure 272) for displacements greater than 200 tonnes.

Example

An amphibious air cushion craft has a full load displacement of $W = 340,000$ lb. The drag in calm water at hump speed is $D_{\text{calm}} = 21,500$ lb. Operationally, it is acceptable, if the craft is limited to a State 3 sea condition, i.e., a State 3 sea speed can be limited to hump speed V_H which for this craft example shall be given as $V_H = 21$ knots. What is the hump thrust margin expressed as an acceleration in g's and how long will it take to get to hump speed in calm water?

Solution

The limiting state of sea parameter is given by

$$\frac{h_w}{W^{1/3}} = \frac{1.4}{\left(\frac{340,000}{2204} \right)^{1/3}} = 0.26$$

Then, from Equation (288), the instantaneous acceleration at hump speed is given by

$$\left(\frac{21,500}{340,000} \right) (1.4) (0.26) = n(g) = 0.022 \text{ g}$$

The nondimensional time to hump speed is obtained from Figure 272 (the equation cannot be used because $W < 200$ tonnes) and is seen to be, for $n = 0.022 \text{ g}$,

$$\tau = \frac{gt_H}{V_H} = 20 \text{ sec}$$

Then, in real time,

$$t_H = \frac{20(21 \times 1.689)}{32.2} = 22 \text{ sec}$$

In summary,

$$\text{Hump margin} = 0.022 \text{ g}$$

$$\text{Time to hump speed} = 22 \text{ sec}$$

The above example illustrates how the hump margin and time to attain hump speed can be calculated. Table 21 summarizes the two criteria for rapid use. So in any particular design, the amount of excess thrust would be set between the minimum and the maximum values given in Table 21. With this particular method, the rather arbitrary choice of acceleration level at the hump speed has been replaced by the calculation of the acceleration level based on design parameters within the control of the designer. Once fairly accurate rough water drag prediction methods become available (see Chapter III) the drag factor K can be refined.

TABLE 21 - COMPUTATION OF HUMP THRUST MARGIN

Criterion	Description	Equation
Minimum Value (Go/no-go)	There is sufficient thrust margin over calm water drag to account for uncertainties in drag prediction, variations in drag due to "as-built" configuration and rough water drag increments.	$n(g) = K \left(\frac{D_{\text{calm}}}{W} \right) \left(\frac{h_w}{W^{1/3}} \right)$ $K = 1.40$
Maximum Value (Amount of acceleration capability)	The thrust margin shall be sufficient throughout the entire speed range from zero to hump speed to achieve a given total time suitable for the operation envisaged for the craft.	<ol style="list-style-type: none"> $n(g) = 0.05 - 0.0014 \tau$ $\tau = \frac{gt_H}{v_H}, \text{ sec}$ $W > 200 \text{ tonnes}$ See Figure 272 for $W \leq 200 \text{ tonnes}$

APPENDIX D SOME SEAKEEPING FORMULAE

In analyzing the seakeeping characteristics of air cushion craft it is necessary to understand the basic formulae used in analyzing both the nature of the sea surface and the response of the craft to that sea. Many treatments may be found in the literature each using their own notation and form of analysis. Unfortunately, the same words are used in many cases to describe different characteristics of the sea and craft response and in yet other cases different descriptions are given for the same phenomena. This has contributed to some confusion in comparing the seakeeping characteristics of different craft where the points of reference are frequently not provided with the reports. Several writers such as Michel¹⁹⁴ and Hutchison and Bringloe¹⁹⁵ have attempted to clarify much of the confusion and these works have been used as a basis here to document the various pertinent formulae used in the analysis of the seakeeping characteristics of air cushion craft.

Chapter IV provides the analysis and results of the air cushion craft seakeeping. This Appendix summarizes the more important assumptions, formulae, and tabular values used in such analyses.

REGULAR WAVE SEAS

Before providing the characteristics of irregular waves or random seas, it is helpful to keep in mind the basic characteristics of regular seas, i.e., those simple wave forms described as single frequency, sinusoidal seas given as,

$$h_w(t) = A \cos (\kappa x - \omega t) \quad (290)$$

where A = the maximum value, single amplitude

ω = circular or wave frequency

t = time

x = distance

κ = wave number

For such regular waves, used in most simple analyses, the following characteristics are familiar, viz:

$$\text{Wave Height, } h_w \text{ (ft)} = 2A \text{ (double amplitude)} \quad (291)$$

$$\text{Wave Period, sec} = T \quad (292)$$

$$\text{Wave Length, } \lambda \text{ (ft)} = \frac{gT^2}{2\pi} = \frac{2\pi C^2}{g} = \frac{2\pi g}{\omega^2} \quad (293)$$

$$\text{Wave or Circular Frequency, } \omega \text{ (rad/sec)} = \frac{2\pi}{T} = \frac{Tg}{\lambda} \quad (294)$$

$$\text{Cyclic Frequency, } f \text{ (Hz)} = \frac{1}{T} = \frac{\omega}{2\pi} \quad (295)$$

$$\text{Wave Number, } \kappa = \frac{2\pi}{\lambda} = \frac{\omega^2}{g} \quad (296)$$

$$\text{Wave Celerity, } C \text{ (ft/sec)} = \sqrt{\frac{g}{\kappa}} = \frac{\lambda}{T} = \frac{gT}{2\pi} = \frac{g}{\omega} \quad (297)$$

$$\text{Wave Energy, } E \left(\frac{\text{ft-lb}}{\text{ft}^2} \right) = \frac{\rho g}{\lambda} \int h_w(x) dx \quad (298)$$

$$= \frac{\rho g}{8} \cdot h_w^2 \quad (299)$$

This last result, relating the energy of the wave to the square of the wave height, is the key connecting link to the description of irregular seas and gives rise to the treatment of irregular seas by the "energy spectrum" as will be described.

IRREGULAR OR RANDOM SEAS

The description of random seas is not simple and is still being pursued by mathematicians, oceanographers, and others. In most of the treatments used thus far and, in particular, those used in this report, random seas are considered to be two-dimensional and created by a broad-scoped continuously blowing wind. The wave crests are continuous in a breadth direction and all waves move in the same direction. In actual seas, of course, the fetch or the distance over which the wind has been blowing is of varying length and the seas become confused due to the effects of wind strength and duration, the presence of storm centers, proximity of land masses, and other effects that cause the sea to take on definite three-dimensional characteristics. Nevertheless, treating the seas as two-dimensional but of a random nature is assumed to be fairly representative of real seas.

Regular seas, as shown earlier, can be easily characterized by their amplitude and frequency. This cannot be done for random seas as can be shown by Figure 274 which, for illustrative purposes, assumes the sea to be made up with the combination of four regular seas of given amplitudes and frequencies.

From this simple illustrative example, it is seen that there is no way that the observer once shown the combined random sea at the bottom of Figure 274, could identify the "amplitude" and "frequency" of the sea or

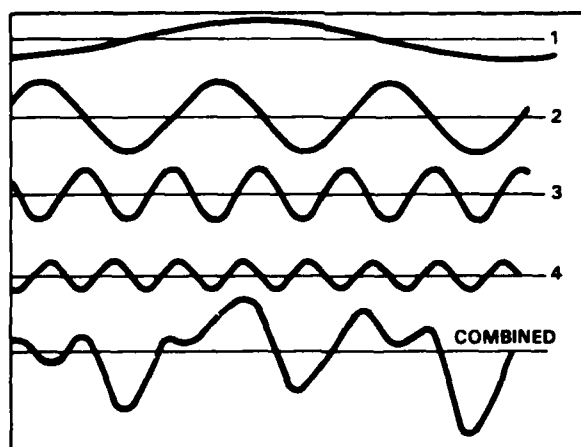


Figure 274 - Wave Pattern Combining Four Regular Waves

relate it back to the four (in this example) regular seas. So an irregular sea, unlike a regular sea, cannot be characterized by its pattern or shape.

The characterization of an irregular sea comes from the simple assumption that its total energy is equal to the sum of the energies of all the small, regular waves assumed to make up the sea. From what has gone before, the energy of a simple sinusoidal wave is $\rho g h_w^2 / 8$ for each square foot of the sea surface where h_w is the maximum wave height (trough to crest) of the wave form. Then the total energy in each square foot of surface of the random sea is given by,

$$E = \frac{\rho g}{8} (h_1^2 + h_2^2 + h_3^2 + \dots) \quad (300)$$

where h_1, h_2 , etc. are the wave heights of all the simple, single frequency wave forms that make up the random sea as illustrated by the example in Figure 274. If each of the single frequency waves are of different frequencies ($\omega_1, \omega_2, \omega_3, \dots$ etc.), then this energy can be thought of as being distributed over these frequencies in an "energy spectrum." This energy spectrum is such that it resembles a plot like that shown diagrammatically in Figure 275.

In order for the area under the curve in Figure 275 to be the total energy of the sea, then, by necessity, the ordinate must have the units of "energy-seconds." This ordinate is an abstract term, i.e., has no physical

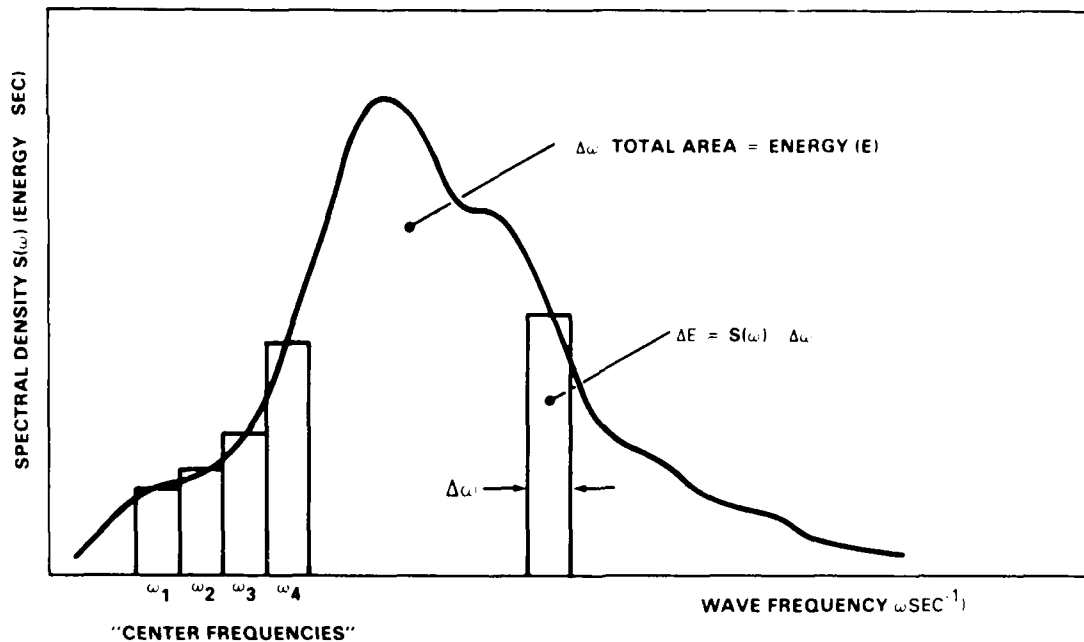


Figure 275 - Energy Spectrum of Random Sea

meaning, that is called the spectral density of the seaway, $S(\omega)$.^{*} This is the term shown in Chapter IV, Equation (138) in the treatment of the craft response to a random seaway. Now, since the energy (E) is proportional to the wave height squared, it is usual to drop the awkward units of "energy-seconds" for the spectral density $S(\omega)$ and substitute (ft²/sec) so that the energy (E) or area under the energy spectrum curve can be expressed in units of square feet, i.e.,

$$E \text{ (ft}^2\text{)} = \sum_0^{\infty} S(\omega) \cdot \Delta\omega \quad (301)$$

where $S(\omega)$ = seaway spectral density (ft²-sec)
 ω = wave frequency (sec⁻¹)

^{*}In some reports this is referred to as "power spectral density" because, in certain physical instances, the square of the function is related to power. For example, if p is the pressure in a plane acoustic wave, then p^2 is proportional to the instantaneous intensity (power per unit area) and $\int p^2 dt$ is proportional to the energy transmitted!

The energy Equation (301) is written here as a sum rather than an integral to emphasize that the sea spectrum is made up of a finite set of frequencies (ω) and the spectrum is more correctly thought of as a histogram, with the spectral density $S(\omega)$ plotted at the center frequencies ($\omega_1, \omega_2, \dots$) as shown in Figure 275. This point will be returned to later in the discussion of "bandwidth" and narrow band versus wide band response.

The shape of the energy spectrum "curve" (treating it as a continuum) depends on the location in the world's oceans being studied but it is found that it generally follows a Rayleigh distribution. From such a realization, it can be easily determined what the probability is that a given wave height would occur in the seaway. In any given seaway record where, by spectral analysis methods, the various wave heights can be retrieved for each of the frequencies one can compute the average of all the squared values of the wave heights $(\bar{H})^2$. This can be written,

$$\bar{H}^2 = \frac{1}{N} \sum_{i=1}^N h_i^2 \quad (302)$$

From knowledge of the properties of Rayleigh distributions the probability $P(h_i)$ that any given wave height would occur is given as,

$$P(h_i) = \frac{2 h_i}{\bar{H}^2} \cdot e^{-h_i^2/\bar{H}^2} \quad (303)$$

Using such relations, one can now compute such descriptive characteristics as "average wave height," or "average height of the one-third highest wave," and so forth.

Before listing these properties, it is well to caution the reader as Michel¹⁹⁴ has done that the numerical values multiplying each of the wave heights will vary according to the assumptions made on the units of the energy and also whether the spectrum is an "amplitude spectrum," "amplitude half-spectrum," "height spectrum," or some other choice. As stated earlier, because the energy is normally measured in ft-lb/ft^2 of ocean area, then the units of the ordinate $S(\omega)$ become cumbersome energy-sec. To simplify this, and in recognition of the fact that the energy (E) is proportional to the wave height or amplitude squared, the energy is "measured" in units of ft^2 . While purists of dimensional analysis will recoil at this corruption, the use of this in spectral analysis has become wide spread. It would only add confusion to reconvert the constants which would be academic because, the analysis is using an abstract form $S(\omega)$ anyway.

The energy (E) is now considered to be the area under the curve measured in ft^2 . The energy (E) is also closely represented by the average value over the entire sea, i.e.,

$$E \approx \frac{\rho g}{8} \bar{H}^2 \quad (304)$$

but the constants are submerged in common practice as discussed. The variance (σ^2) is thus taken to be the area under the energy spectrum curve or one-half the area under the amplitude spectrum curve, i.e.,

$$\bar{H}^2 = E = \int_0^{\infty} S(\omega) d\omega = \frac{1}{2} \int_0^{\infty} 2 S(\omega) d\omega \quad (305)$$

From knowledge of Rayleigh distributions and the probabilities of certain wave heights occurring, it becomes possible to determine the various wave heights of interest. These are summarized in Table 22.

TABLE 22 - RANDOM SEA WAVE HEIGHTS
(Double Amplitude)

Root mean square amplitude, RMS	\bar{H}
Average amplitude	$2.50 \bar{H}$
Average of highest 1/3 amplitudes (significant)	$4.00 \bar{H}$
Average of highest 1/10 amplitudes	$5.10 \bar{H}$
Highest expected amplitude in 100 successive amplitudes	$6.06 \bar{H}$
Highest expected amplitude in 1000 successive amplitudes	$7.44 \bar{H}$
Highest expected amplitude in N successive amplitudes	$\sqrt{2 \ln N} \bar{H}$

These statistical values are useful properties in discussing the characteristics of a random sea. It should also be pointed out that the relationships in Table 22 are true for any random variable characterized by a Rayleigh distribution. Accordingly, the relationships are true for the response $R(\omega)$ as well as for the forcing function $S(\omega)$.

Other properties of the Pierson-Moskowitz sea such as period and wavelength, among others, can be calculated using similar spectrum formulae as shown for the wave height. Early descriptions of the sea included charts known as the Beaufort scale and others. Pierson and Moskowitz, using the

wind speed (V_w) as the anchor point, correlated their spectrum with the Beaufort scale. Table 23 shows such a correlation for a fully arisen sea. As mentioned earlier in the main text, the Pierson-Moskowitz sea spectrum is used extensively in model tank testing. Comparisons with other spectra and sea charts will show differences in the values of wave heights and periods but not to any significant degree.

NARROW BAND AND WIDE BAND TREATMENTS

In analyzing the response $R(\omega)$ to the random sea characterized by the energy spectrum $S(\omega)$, it is usual to analyze the response using bandwidths of frequency in various multiples of octaves and partial octaves. Figure 94 in Chapter IV showed the RMS accelerations when computed over 1/3 octave, one octave, and the full bandwidth (true RMS value) of the response record of the SES-100B. That the response should be "different," according to the method of computation, highlights the need to understand the relationship of the criterion and upon what it is based, and the method of computation. The following notes are provided to help interpretation of response records analyzed over different bandwidths. Since 1/3 octave (through analogy with acoustic analyses) and full octave analyses are most commonly used, these two bandwidths are used to illustrate the characterization although it is clear that this could be applied to any bandwidth selected.

Figure 276 is an illustrative example of a response spectral density, $R(\omega) = g^2/\omega$, for a hypothetical craft. From what has gone before, the RMS g in the band is proportional to the square root of the energy (E)* so that, for the response amplitude,

$$\sigma = \int_{\omega_i}^{\omega_{i+1}} R(\omega) d\omega = \int_{\omega_i}^{\omega_{i+1}} \frac{g^2}{\omega} d\omega \quad (306)$$

This may be compared to the value of the RMS g over the full bandwidth given by the equation

$$\sigma = \int_0^{\infty} \frac{g^2}{\omega} d\omega \quad (307)$$

Unfortunately, the same terminology of "RMS g acceleration" is used interchangeably in the literature to apply both to the true RMS value over the entire bandwidth as well as to the RMS value computed over the smaller intervals. This sometimes causes confusion in interpretation of data.

*Note that the energy(E) here is used to represent the energy under the response spectrum to yield the RMS acceleration (σ) as opposed to the earlier use of energy (E) to represent the energy of the sea spectrum to yield the RMS of wave heights (H).

TABLE 23 - PIERSON-MOSKOWITZ WIND AND SEA SCALE

Sea State (a)	Sea-General		Wind (c)				Sea (c,d)							
	Description (b)	(Beaufort) Wind Force	Description	Range (knots)	Wind Velocity (knots)	Average Wave Height (ft.)	Significant Wave Height (ft.)	Average 1/10 Highest Wave Height (ft.)	Significant Range of Periods (sec.)	Period of Max Energy of Spectrum, T _m (sec.)	Average Period, T (sec.)	Average Wave Length, L (ft.)	Minimum Fetch (m)	Minimum Duration (hr)
0	Sea like a mirror.	0	Calm	Less than 1	0	0	0	0	-	-	-	-	-	-
1	Ripples with the appearance of scales are formed, but without foam crests.	1	Light Airs	1-3	2.0	0.05	0.07	0.09	0.30-0.94	0.75	0.53	0.98	5	18 min.
2	Small wavelets, still short but more pronounced; crests have a glassy appearance, but do not break.	2	Light Breeze	4-6	5.0	0.29	0.46	0.59	0.74-2.34	1.88	1.34	6.10	8	39 min.
3	Large wavelets, crests begin to break. Foam of glassy appearance. Perhaps scattered white horses.	3	Gentle Breeze	7-10	8.5	0.84	1.34	1.70	1.26-3.98	3.20	2.27	17.62	9.8	1.7
4	Small waves, becoming larger; fairly frequent white horses.	4	Moderate Breeze	11-16	10.0	1.16	1.86	2.36	1.49-4.68	3.76	2.67	24.39	10	2.4
5	Moderate waves, taking a more pronounced long form; many white horses are formed. (Chance of some spray.)	5	Fresh Breeze	17-21	12.0	1.67	2.67	3.40	1.78-5.61	4.51	3.20	35.11	18	3.8
6	Large waves begin to form; the white foam crests are more extensive everywhere. (Probably some spray.)	6	Strong Breeze	22-27	13.5	2.12	3.38	4.30	2.01-6.32	5.08	3.60	44.44	24	4.8
7	Sea heaps up and white foam from breaking waves begins to be blown in streaks along the direction of the wind. (Spindrift begins to be seen.)	7	Moderate Gale	28-35	14.0	2.28	3.64	4.62	2.08-6.35	5.26	3.74	47.80	28	5.2
8	Moderately high waves of greater length; edges of crests break into spindrift. The foam is blown in well marked streaks along the direction of the wind. Spray affects visibility.	8	Fresh Gale	34-40	16.0	2.97	4.75	6.04	2.38-7.48	6.02	4.27	62.43	40	6.6
9	High waves. Dense streaks of foam along the direction of the wind. Sea begins to roll. Visibility affected.	9	Strong Gale	41-47	18.0	3.76	6.01	7.64	2.68-8.42	6.77	4.81	79.01	55	8.3
10	Very high waves with long overhanging crests. The resulting foam is in great patches and is blown in dense white streaks along the direction of the wind. On the whole the surface of the sea takes a white appearance. The rolling of the sea becomes heavy and shock-like. Visibility is affected.	10	Whole Gale (f)	48-55	19.0	4.19	6.70	8.51	2.62-8.89	7.14	5.07	88.03	65	9.2
11	Exceptionally high waves (small and medium-sized ships might for a long time be lost to view behind the waves). The sea is completely covered with long white patches of foam lying along the direction of the wind. Everywhere the edges of the wave crests are blown into froth. Visibility affected.	11	Storm (f)	56-63	20.0	4.65	7.42	9.43	2.97-9.36	7.52	5.34	97.54	75	10
12	Air filled with foam and spray. Sea completely white with driving spray; visibility very seriously affected.	12	Hurricane (f)	64-71	22.0	5.62	8.98	11.42	3.27-10.29	8.27	5.87	118.02	100	12
					24.0	6.69	10.69	13.59	3.57-11.23	9.02	6.41	140.46	130	14
					26.0	7.85	12.55	15.94	3.86-12.16	9.78	6.94	164.84	160	17
					28.0	9.11	14.55	18.49	4.16-13.10	10.53	7.48	191.18	230	20
					30.0	10.46	16.70	21.23	4.46-14.03	11.28	8.01	219.47	280	23
					32.0	11.90	19.00	24.15	4.76-14.97	12.03	8.54	249.70	340	27
					34.0	13.43	21.45	27.27	5.05-15.91	12.78	9.08	281.89	420	30
					36.0	15.06	24.05	30.57	5.35-16.84	13.54	9.61	316.03	500	34
					38.0	16.78	26.80	34.06	5.65-17.78	14.29	10.15	352.12	600	38
					40.0	18.59	29.69	37.74	5.94-18.71	15.04	10.68	390.16	710	42
					42.0	20.49	32.74	41.61	6.24-19.65	15.79	11.21	430.16	830	47
					44.0	22.49	35.93	45.68	6.54-20.58	16.54	11.75	472.10	960	52
					46.0	24.58	39.27	49.91	6.84-21.52	17.30	12.28	515.99	1110	57
					48.0	26.77	42.76	54.34	7.13-22.45	18.05	12.82	561.84	1250	63
					50.0	29.04	46.40	58.97	7.43-23.39	18.80	13.35	609.63	1420	69
					52.0	31.41	50.18	63.78	7.73-24.33	19.55	13.88	659.38	1610	75
					54.0	33.88	54.12	68.78	8.03-25.26	20.30	14.42	711.07	1800	81
					56.0	36.43	58.20	73.97	8.32-26.20	21.06	14.95	764.72	2100	88
					58.0	41.13	65.70	83.50	8.64-27.13	21.77	15.49	863.90	2500	101
					64-71	>64	(b)	(b)	10-(35)	(26)	(18)	-	-	-

(a) Encyclopedia of Nautical Knowledge, W.A. McIlwain and A.W. Lewis, Cornell Maritime Press, Cambridge, Maryland, 1953, p. 483.

(b) Manual of Seamanship, Volume II, Admiralty, London, H. M. Stationery Office, 1952, pp. 717-718.

(c) Practical Methods for Observing and Forecasting Ocean Waves, Pierson, Neuman, James, N.Y. Univ., College of Engineering, 1953.

(d) Revised for Pierson-Moskowitz Spectrum.

(e) A heavy box around this value means that the values tabulated are at the center of the Beaufort range.

(f) For hurricane winds (and often whole gale and storm winds) required durations and fetches are rarely attained. Seas are therefore not fully arisen.

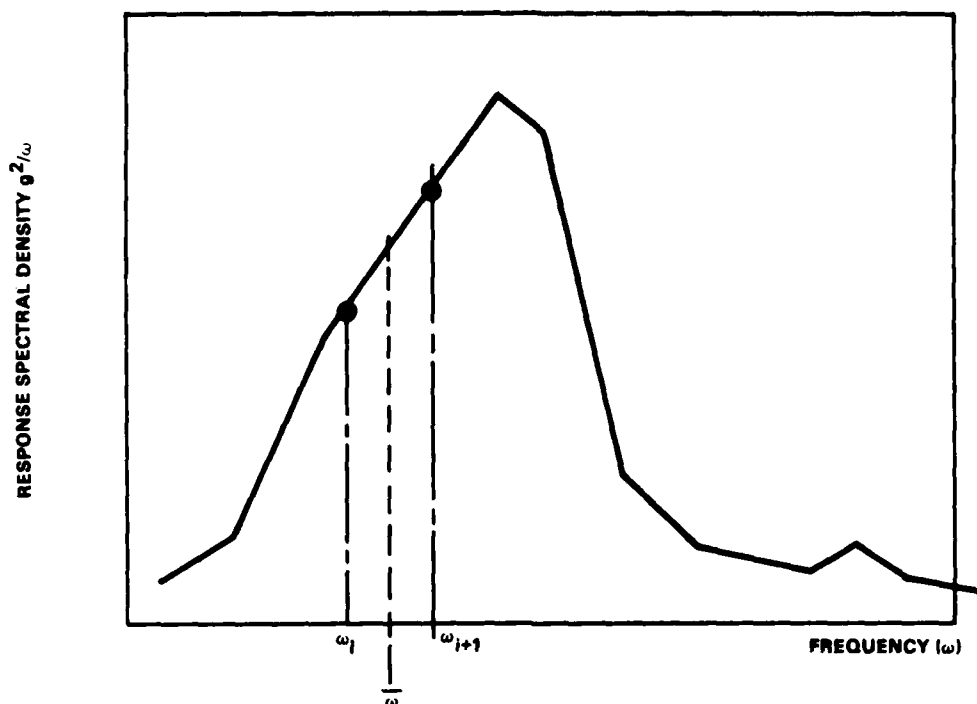


Figure 276 - Spectral Density for Hypothetical Craft

The relationship between successive frequencies ω_i and ω_{i+1} is simply,

$$\omega_{i+1} = \alpha \omega_i \quad (308)$$

and the center frequency $\bar{\omega}$ is given by

$$\bar{\omega} = \sqrt{\omega_i \cdot \omega_{i+1}} \quad (309)$$

The constant α determines how the full bandwidth is divided up into octaves and the values are as given in Table 24. Numerically, it is seen that the 1/3 octave or the 10 equal log intervals are very close. Also, through common usage in the air cushion craft community, the "counting" of the frequencies start at $\omega = 0.01$ Hz so that some consistency can be maintained in comparing different craft responses. The energy level at such a low frequency is very small and thus should not distort any such comparisons.

TABLE 24 - FREQUENCY INTERVAL FACTORS

Bandwidth Interval	Factor	Comment
1 Octave	$\alpha = 2$	
1/3 Octave	$\alpha = 3\sqrt{2} = 1.25992$	Common use
10 Equal Log Intervals	$\alpha = 10^{1/10} = 1.25895$	Used by ISO

Given these relationships, one can see why the "RMS g in the band" values depend on the choice of bandwidth interval (see, for example, Figures 94 and 95 in Chapter IV) as shown by the following. If E_1 designates the energy when integrated over 1 octave, then

$$E_1 = \int_{\omega_1}^{2\omega_1} \frac{g^2}{\omega} \cdot d\omega \quad (310)$$

which, if constructed from 1/3 octave intervals, would be given by

$$E_1 = \underbrace{\int_{\omega_1}^{1.26\omega_1} \frac{g^2}{\omega} \cdot d\omega}_{E_{1/3}} + \underbrace{\int_{1.26\omega_1}^{1.59\omega_1} \frac{g^2}{\omega} \cdot d\omega}_{E_{1/3}} + \underbrace{\int_{1.59\omega_1}^{2\omega_1} \frac{g^2}{\omega} \cdot d\omega}_{E_{1/3}} \quad (311)$$

where $E_{1/3}$ represents the energy computed over 1/3 octave with the frequency limits determined from the values given in Table 24.

It is reasoned that the narrow band, and specifically 1/3 octave, is more in keeping with the physiological response of the human body and thus is a better measure of tolerance to acceleration levels. Also, as stated earlier, all the available criteria have been determined on the basis of single frequency testing and thus broadband frequency response compared to single frequency criteria raises many questions. Some of the basic formulae used have been summarized here and will serve as computational tools pending the arrival of more systematic testing and analysis of human response and tolerance levels to broadband, random sea motion.

REFERENCES

1. Janes' Surface Skimmers: Hovercraft and Hydrofoils, Roy McLeavy, Ed., McGraw-Hill Book Company (1976-77).
2. Mantle, P.J., "A Technical Summary of Air Cushion Craft Development," DTNSRDC Report 4727 (Oct 1975).
3. Belavin, N.I., "Surface Effect Vehicles," Sudostroyeni Press, Leningrad (1968). See also U.S. Army Foreign Science and Technology Center Translation FSTC-HT-23-437-69 (Oct 1969).
4. McLeavy, R., "Hovercraft and Hydrofoils," Blandford Press, Poole (1976).
5. Benya, Y.Y. et al., "Basic Theories of Air Cushion Vehicles," U.S. Army Foreign Science and Technology Center Translation FSTC-HT-23-496-71 (Oct 1971).
6. Hayward, L., "The History of Air Cushion Vehicles," Kalerghi-McLeavy Publications, London (1963).
7. Cockerell, C., "Improvements in or Relating to Vehicles for Traveling Over Land and/or Water," British Patent 854,211 (1955).
8. Cockerell, C., "Some Remarks on the English Channel Crossing of the Hovercraft on July 25, 1959," Symposium on Ground Effect Phenomena at Princeton, Paper 14 (21-23 Oct 1959).
9. Stanton-Jones, R., "The Development of the Saunders-Roe Hovercraft SR.N1," Symposium on Ground Effect Phenomena at Princeton, Paper 13 (21-23 Oct 1959).
10. Chaplin, H.R., "Ground Effect Machine Research and Development in the United States," Third Symposium on Naval Hydrodynamics, The Hague (20 Sep 1960). See also DTMB Report 1463 (Dec 1960).
11. Ford, A.G., "Captured Air Bubble Over-Water Vehicle Concept," Naval Engineers Journal, pp. 223-230 (Apr 1964).
12. Lippsich, A.M., "Dynamic Air Cushion Vehicles," Air Cushion Vehicle Supplement to Flight International (25 Jun 1964).
13. Rethorst, S., "VRC Surface Effect Ship Columbia," Proceedings of National Meeting on Hydrofoils and Air Cushion Vehicles, Institute of Aerospace Sciences/U.S. Navy, Washington, D.C. (17-18 Sep 1962).
14. Wade, R.G., "Air Cushion Vehicle Development in Canada," American Institute of Aeronautics and Astronautics/Society of Naval Architects and Marine Engineers Advanced Marine Vehicles Conference, Paper 74-320 (25-27 Feb 1974).
15. Bingham, A.E., "VT.2-100 Ton Amphibious Hovercraft," Second International Conference on Hovering Craft, Hydrofoils and Advanced Transit Systems, Amsterdam, Holland (17-20 May 1976).

16. Bertin, J., "French Marine Air Cushion Vehicles," The Aeronautical Journal of the Royal Aeronautical Society, Vol. 74, No. 717, pp. 726-735 (Sep 1970).

17. Daley, R.E. and J.U. Kordenbrock, "U.S. Navy Tests of SKMR-1 in an Operational Environment," American Institute of Aeronautics and Astronautics/U.S. Navy Second Marine Systems and Antisubmarine Warfare Conference, Paper 66-729 (8-10 Aug 1966).

18. Rethorst, S. and T. Potter, "Maritime Administration Surface Effect Ship," Society of Automotive Engineers/American Society of Naval Engineers National Aeronautical Meeting, Paper 697D (8-11 Apr 1963).

19. "Surface Effect Ships for Ocean Commerce (SESOC)," Final Report on a Study of the Technological Problems, SESOC Advisory Committee, published by U.S. Government Printing Office, Washington, D.C. (Feb 1966).

20. Schuler, J.L., "The Amphibious Assault Landing Craft Program," Naval Engineers Journal, Vol. 85, No. 2 (Apr 1973).

21. Brown, M.W., "JEFF Craft-Navy Landing Craft for Tomorrow," American Institute of Aeronautics and Astronautics/Society of Naval Architects and Marine Engineers Advanced Marine Vehicles Conference, Paper 74-319 (25-27 Feb 1974).

22. Postle, R.S., "A Landing Craft JEFF(B) Project Progress Report," American Institute of Aeronautics and Astronautics/Society of Naval Architects and Marine Engineers Advanced Marine Vehicles Conference, Paper 78-731 (17-19 Apr 1978).

23. "Standard Method of Estimating Comparative Direct Operating Costs of Turbine Powered Transport Airplanes," (Revised version) published by Air Transportation Association (Oct 1967).

24. Mantle, P.J., "Interface Craft for Future Transportation," 1966 National Transportation Symposium, American Society of Mechanical Engineers Publication, pp. 332-341 (May 1966).

25. Chaplin, J.B., "The Air Cushion Vehicle Evaluation and Potential," Naval Engineers Journal, pp. 421-442 (Jun 1966).

26. Crewe, P.R., Skirt Design, Lecture Series 33 Aerodynamics of Air Cushion Vehicles, von Karman Institute for Fluid Dynamics (22-26 Feb 1971).

27. Mantle, P.J., "Some Design Aspects of Air Cushion Craft," Annals of the New York Academy of Sciences, Vol. 154, Article 2, pp. 924-952 (Nov 22, 1968). (Paper also presented at the International Congress of Subsonic Aeronautics, New York, N.Y. (3-6 Apr 1967)).

28. "Arctic Surface Effect Vehicle Program Vol. I: Program Overview and History of Related Developments" (NSRDC Report 4594), "Vol. II: Technology Summary and Design Development" (NSRDC Report 4595) (Aug 1975).

29. Stanton-Jones, R., "The Future Development of Hovercraft" (The 1968 Lord Semphill Paper), International Hovercraft Conference of the Institute of Production Engineers (4-5 Apr 1968).

30. Meeks, T.L. and P.J. Mantle, "The Advanced Naval Vehicle Concepts Evaluation," American Institute of Aeronautics and Astronautics/Society of Naval Architects and Marine Engineers Advanced Marine Vehicles Conference, Paper 76-846 (20 Sep 1976).
31. Mantle, P.J., "Advanced Concepts For Sea Control," Society of Engineers Aerospace Meeting, Paper 770-966 (14-17 Nov 1977).
32. von Karman, Th. and T.G. Gabrielli, "What Price Speed?" Mechanical Engineering, pp. 775-781 (Oct 1950).
33. "Ship Work Breakdown Structure (SWBS)," by the Naval Ship Systems Command, NAVSHIPS 0900-039-9010 (Mar 1973).
34. Mantle, P.J., "Development of the USN Surface Effect Ship, SES-100B," American Society of Naval Engineers Day 1973 Paper, Naval Engineers Journal, Vol. 85, No. 5, pp. 65-77 (Oct 1973).
35. Walker, N.K., "Some Notes on the Lift and Drag of Ground Effect Machines," Proceedings of the Hydrofoils and Air Cushion Vehicles, International Aerospace Sciences/U.S. Navy (Sep 1962).
36. Cockerell, C.S., "Ripplecraft," Report 1/55 (25 Oct 1955). See also Air Cushion Vehicle Supplement to Flight International (28 Feb 1963).
37. von Glahn, V.H., "Exploratory Study of Ground Proximity Effects on Thrust of Annular and Circular Nozzles," National Advisory Committee for Aeronautics TN 3982 (Apr 1957).
38. Elsley, G.H. and A.J. Devereux, "Hovercraft Design and Construction," published by Cornell Maritime Press, Inc. (1968).
39. Payne, P.R., "Curved Jet Flows," United States Army Material Laboratory Technical Report 65-20 (May 1965).
40. Elsley, G.H., "Two-Dimensional Hovercraft Lift," Report A/A/53, Saunders-Roe Ltd. (Nov 1958).
41. Stanton-Jones, R., "Some Design Problems of Hovercraft," Institute of Aerospace Sciences Paper 61-45 (1961). Also Saunders-Roe Publication S.P. 404 (Jan 1961).
42. Carmichael, B.H. and M.P. Southcote, "Air Cushion Feasibility Investigation, Performance and Stability Experiments. Configuration and System Evaluation Studies," Ford Aeronutronic Co., Publication U-1066 (Nov 1960).
43. Crewe, P.R., Lecture on "Air Cushion Vehicle Fan System," MIT Professional Summer Course (9 Jul 1975).
44. Trillo, R.L., "Marine Hovercraft Technology," Leonard Hill Publishers, London (1971).
45. Beardsley, M.W., "Wave Pumping and Its Effects on the Design and Operation of Air-Cushion Ships," U.S. Navy Marine Engineering Laboratory, MEL Tech Memo 48/67 (Mar 1967).

46. Crewe, P.R., "The BHC Contribution to Hovercraft Development," Hovercraft Conference, Adelaide, Australia (15 Nov 1968). See also Hovering Craft and Hydrofoil, Volume 8, No. 6 (Mar 1969).
47. Havelock, T.H., "The Effect of Shallow Water on Wave Resistance," Proceedings Royal Society, Series A, Vol. 100, No. A706 (1922).
48. Lamb, H., "Hydrodynamics," published by Dover Publications, Sixth Edition (1932) (First Edition 1879).
49. Crewe, P.R. and W.J. Eggington, "The Hovercraft--A New Concept in Maritime Transport," RINA Lecture (19 Nov 1959). See also Transactions Royal Institute of Naval Architects (1960).
50. Newman, J.N. and F.A.P. Poole, "The Wave Resistance of a Moving Pressure Distribution in a Canal," DTMB Report 1619 (Mar 1962).
51. Barratt, M.J., "The Wave Drag of a Hovercraft," Journal of Fluid Mechanics, Vol. 22, Part 1, pp. 39-47 (1965).
52. Doctors, L.J., "The Wave Resistance of An Air Cushion Vehicle," University of Michigan (Dec 1970).
53. Everest, J.T. and N. Hogben, "Research on Hovercraft Over Calm Water," Transactions Royal Institute of Naval Architects, Vol. 109, pp. 311-326 (1967).
54. Wilson, R.A. et al., "Powering Prediction for Surface Effect Ships Based on Model Results," American Institute of Aeronautics and Astronautics Society of Naval Architects and Marine Engineers Advanced Marine Vehicles Conference, Paper 78-744 (17-19 Apr 1978).
55. Doctors, L.J., "Wave Resistance of an Air Cushion Vehicle in Accelerated Motion," Naval Architecture and Marine Engineering Report 099 (Dec 1970).
56. Ford, A.G. et al., "High Length-to-Beam Ratio Surface Effect Ship," American Institute of Aeronautics and Astronautics/Society of Naval Architects and Marine Engineers Advanced Marine Vehicles Conference, Paper 78-745, San Diego, California (17-19 Apr 1978).
57. Wheeler, R.L., "The Amphibious Hovercraft," presented at Diamond Jubilee International Meeting, Society of Naval Architects and Marine Engineers, Paper 23, New York, N.Y. (18-21 Jun 1968).
58. "Parametric Design Analysis and Concept Exploration," Artic Surface Effect Vehicle Program, Bell Aerospace, Final Report 7416-950001, Vol. 1 (Feb 1973).
59. "VA-3 Air Cushion Vehicle Test Program," Republic Aviation Corporation, Report RAC 2612 (Oct 1974).
60. Chaplin, H.R., Jr., "The New Trend in Ground Effect Machines," Astronautics and Aeronautics, pp. 46-51 (Oct 1965).
61. Chaplin, J.B., "Amphibious Surface Effect Vehicle Technology--Past, Present and Future," American Institute of Aeronautics and Astronautics/Society of Naval Architects and Marine Engineers Advanced Marine Vehicles Conference, Paper 74-318, San Diego, California (25-27 Feb 1974).

62. "Skirt System Problems, SR.N4," British Hovercraft Corporation Report (Mar 1973).
63. "Skirt System Study," Arctic Surface Effect Vehicle Program, Aerojet Surface Effect Ship Division, Final Report AGC-T-394, Vol. III (Oct 1973).
64. "500 Ton Arctic SEV Configuration Study," Boeing Company Model Test Program, Final Report D180-18139-3, Vol. 3 (Aug 1974).
65. Locke, F.W.S., Jr., "An Empirical Study of Low Aspect Ratio Lifting Surfaces with Particular Reference to Planing Craft," Journal of Aeronautical Sciences, pp. 184-188 (Mar 1949).
66. Mantle, P.J., "Large High Speed Surface Effect Ship Technology," First International Hovering Craft, Hydrofoil and Advanced Transit Systems Exhibition and Conference, Brighton, England (13-16 May 1974).
67. Hoerner, S.F., "Fluid Dynamic Drag," published by author (1958).
68. DeLaura, E.D., "Some Performance and Dynamic Stability Characteristics of the SKIP-I Air Cushion Vehicle," General Dynamics Corp., Electric Boat Division Report P413-66-159 (Dec 1966).
69. Moran, D.D., "Air Cushion Vehicle Overland Dynamics," American Institute of Aeronautics and Astronautics/Society of Naval Architects and Marine Engineers Advanced Marine Vehicles Conference, Paper 78-732, San Diego, California (17-19 Apr 1978).
70. Arctic Surface Effect Vehicle Program Final Technical Report, Boeing Company Report D180-15356-1 (Apr 1973).
71. "Arctic Surface Effect Vehicle Program, Ten Ton SEV Obstacle Crossing Data Related to Cushion System Dynamics," NSRDC Report 27-229, Dept Code 27 (Aug 1972).
72. Carrier, R. et al., "The Effect of Skirt Configuration on the Seakeeping of Air Cushion Vehicles," American Institute of Aeronautics and Astronautics/Society of Naval Architects and Marine Engineers Advanced Marine Vehicles Meeting, Paper 76-864 (20 Sep 1976).
73. Mantle, P.J., "On the Dynamic Heave Motion of Single Peripheral Jet GEMS Over an Undulating Surface," Vehicle Research Corporation, Paper 9 (May 1962).
74. Uyeda, S.T., "Study of Loads and Motions of Two Types of Ground Effect Machines," General Dynamics Convair, Report ZH-150 (1961).
75. Tinajero, A.A. and J.N. Fresh, "Aerodynamic Response of a Seven Foot Ground Effect Machine Flying Over Uneven Surfaces," DTMB Report 1436 (1960).
76. Lavis, D.R. et al., "On the Prediction of Acceleration Response of Air Cushion Vehicles to Random Seaways and the Distortion Effects of the Cushion Inherent in Scale Models," American Institute of Aeronautics and Astronautics/Society of Naval Architects and Marine Engineers/U.S. Navy Advanced Marine Vehicles Meeting, AIAA Paper 72-598, Maryland (17-19 Jul 1972).

77. Breslin, J., "The Dependence of Surface Effect Ship Heave Response on Model Scaling Parameters as Deduced from a Simplified Linear Analysis," Surface Effect Vehicle Summer Study Report for Institute of Defense Analyses (Oct 1968).
78. Kiedrzyński, A., "Cushion Mechanics in Hovering Flight Over Water," Lecture Series 33, von Karman Institute for Fluid Dynamics (22-26 Feb 1971).
79. Mack, L.R. and B. Yen, "Theoretical and Experimental Research on Annular Jets Over Land and Water," Symposium on Ground Effect Phenomena, Princeton University, Paper 21 (21-23 Oct 1959).
80. Hirsch, A.E., "The Hovering Performance of a Two-Dimensional Ground Effect Machine Over Water," DTMB Report 1426 (Oct 1960).
81. Shenfil, L., "Heave Motion and Its Effect on the Design of an Air Cushion Vehicle," Aerojet Surface Effect Ship Division Report AGC-T-518 (Apr 1974).
82. Plackett, M.J. and R.B. Wade, "Design Aspects of Seal Systems for Air Cushion Vehicles," American Institute of Aeronautics and Astronautics/Society of Naval Architects and Marine Engineers Advanced Marine Vehicles Conference, AIAA Paper 78-755, San Diego, California (17-19 Apr 1978).
83. Crago, W.A., "Problems Associated with the Use of Skirts on Hovercraft," paper presented to Automobile Division, Institution of Mechanical Engineers (12 Dec 1967). See also Proceedings, Institute of Mechanical Engineers, Vol. 182, Part 2A (1967-68).
84. Kuhlthau, A.R. and A.M. Wichansky (Editors), "Workshop on Ride Quality," National Aeronautics and Space Administration Report CP-2013 (Jul 1977).
85. "Proceedings of the 1975 Ride Quality Symposium," Department of Transportation, DOT-TSC-OST-75-40 (Sep 1975).
86. "Guide for Evaluation of Human Exposure to Whole-Body Vibration," International Standard Organization (ISO) Document ISO/DIS 2631 (1972).
87. "Exposure Criteria for Whole Body Vibration," MIL-STD-1472A (15 May 1970).
88. Mantle, P.J., "Cushions and Foils," Society of Naval Architects and Marine Engineers Spring Meeting Papers, SNAME Paper 2 (2-5 Jun 1976).
89. "Ocean Wave Spectra," Proceedings of Conference sponsored by U.S. Naval Oceanographic Office (1-4 May 1961).
90. Korvin-Kroukowsky, B.U., "Theory of Seakeeping," Society of Naval Architects and Marine Engineers (1961).
91. Hoffman, D., "Analysis of Measured and Calculated Spectra," International Symposium on the Dynamics of Marine Vehicles and Structures in Waves, Paper 2, University College, London (Apr 1974).
92. Pierson, W.J. and L. Moskowitz, "A Proposed Spectral Form for Fully Developed Seas Based on the Similarity Theory of S.A. Kitaigorodskii," Journal of Geophysical Research, Vol. 69, No. 24, pp. 5181-5190 (1964).

93. Gornstein, R.J., "JETFOIL Ride Specifications," Boeing Document D320-10050-3 (1974).
94. von Schertel, H., "Design and Operating Problems of Commercial Hydrofoils," Supramar A.G., Switzerland (1962).
95. Magnuson, A.H., "Seakeeping Trials of the BH.7 Hovercraft," DTNSRDC Report SPD-574-01 (Aug 1975).
96. O'Hanlon, J.F. and M.E. McCauley, "Motion Sickness Incidence as a Function of the Frequency and Acceleration of Vertical Sinusoidal Motion," Human Factors Research, Inc., Technical Report 1733-1 (Sep 1973).
97. Allen, G.R., "Ride Quality and International Standard ISO 2631," 1975 Ride Quality Symposium, Paper 21, National Aeronautics and Space Administration TMX-3295 (Nov 1975).
98. Crewe, P.R., Lecture on "Air Cushion Vehicle Control System," MIT Professional Summer Course (9 Jul 1975).
99. Mantle, P.J., Lecture on "Air Cushion Vehicle Control," NAVSEC U.S. Navy Seminar (Oct 1975).
100. Shank, S.R., Jr., "Performance Prediction of Tandem Air Propeller Arrangements for Large Surface Effect Vehicles," NSRDC Report 27-664 (Dec 1973).
101. Trebble, W.J.G., "Investigation of the Mutual Interference of Propellers Mounted in Tandem," Royal Aircraft Establishment Technical Report 68282 (AD857118) (Dec 1968).
102. Wheeler, R.L., "Control of a Single Propeller Hovercraft with Particular Reference to BH.7," Canadian Aeronautics and Space Journal, Vol. 17, No. 5 (May 1971).
103. Everest, J.T. and N. Hogben, "A Theoretical and Experimental Study of the Wavemaking of Hovercraft of Arbitrary Planform and Angle of Yaw," Royal Institute of Naval Architects (1969).
104. Bertelsen, W.R., "The Gimbal Fan Air Cushion Vehicle," American Institute of Aeronautics and Astronautics/Society of Naval Architects and Marine Engineers Advanced Marine Vehicles Conference, AIAA Paper 78-734 (17-19 Apr 1978).
105. Bertelsen, W.R., "The Air Cushion Vehicle in a Mass Transit System," Ninth Canadian Symposium on Air Cushion Technology (CASI) (21 Oct 1975).
106. Wheeler, R.L., "The Development Phase of the Mountbatten Class (SR.N4) Hovercraft," American Institute of Aeronautics and Astronautics Second Advanced Marine Vehicles and Propulsion Meeting, AIAA Paper 69-410 (21-23 May 1969).
107. Hogben, N., "Hovering Craft Over Water," Advanced Hydrosience, No. 4, Academic Press, New York (1967).
108. Crewe, P.R., Lecture on "Air Cushion Vehicle Skirt Systems," MIT Professional Summer Course (9 Jul 1975).

109. Mantle, P.J. and D.R. Lavis, "Domain of the Air Cushion Craft," Society of Automotive Engineers Air Transportation Meeting, SAE Paper 680273, New York, N.Y. (29 Apr-2 May 1968).
110. Eggington, W. and N. Kobitz, "The Domain of the Surface Effect Ship," Society of Naval Architects and Marine Engineers Annual Meeting, Paper 11 (Nov 1975).
111. British Civil Air Cushion Vehicle Safety Requirements (Provisional) published by Air Registration Board, England (1962).
112. Crewe, P.R. et al., "Analysis of Acceleration and Pressure measurements on the SR.N1," Hydrodynamics Note PRC/DGG/MFKi/3823, Saunders-Roe Ltd. (now British Hovercraft Corporation) (Nov 1960).
113. British Hovercraft Safety Requirements, published by Civil Aviation Authority (Apr 1972).
114. Chuang, S.L. and D.T. Milne, "Drop Tests of Cones to Investigate the Three-Dimensional Effects of Slamming," NSRDC Report 3543 (Apr 1971).
115. Jones, R. and R.G. Allen, "A Semi-Empirical Computerized Method for Predicting Three-Dimensional Hull Water Impact Pressure Distributions and Forces on High Performance Hulls," NSRDC Report 4005 (1973).
116. Kaplan, P. and A. Malakhoff, "Hard Structure Slamming of SES Craft in Waves," American Institute of Aeronautics and Astronautics/Society of Naval Architects and Marine Engineers Advanced Marine Vehicles Conference, AIAA Paper 78-746 (17-19 Apr 1978).
117. Forrest, C.L., "Test and Evaluation of the SES-100B," American Institute of Aeronautics and Astronautics/Society of Naval Architects and Marine Engineers Advanced Marine Vehicles Conference, Paper 74-317 (25-27 Feb 1974).
118. Tick, L.J., "Certain Probabilities Associated with Bow Submergence and Ship Slamming at Sea," Journal of Ship Research, Vol. 2, No. 1 (Jan 1958).
119. Ochi, M.K. and L.E. Motter, "Prediction of Extreme Values of Impact Pressure Associated With Ship Slamming," Journal of Ship Research, Vol. 13, No. 2 (Jun 1969).
120. Allen, R.G. and E. Aronne, "Challenges For Structures Research," Proceedings of the Second Ship Structures Workshop, Structures for High Performance Ships, Vol. I, NSRDC (13-14 Feb 1973).
121. Heller, S.R. and D.J. Clark, "The Outlook For Lighter Structures in High Performance Marine Vehicles," American Institute of Aeronautics and Astronautics/Society of Naval Architects and Marine Engineers Advanced Marine Vehicles Conference, AIAA Paper 74-330 (25-27 Feb 1974).
122. "Tire Cord Makers Race for the Radial Market," Business Week (22 Sep 1973).

123. Chaplin, J.B. and F.C. Anderson, "An Overview of the Design of Air Cushion Vehicle/Surface Effect Ship Structures," Proceedings of the Second Ship Structures Workshop, Structures for High Performance Ships, Vol. III, NSRDC (13-14 Feb 1973).
124. "Maintenance, Repair and Operational Care of Aluminum Craft and Boat Hulls," NAVSHIPNOTE 4700 (May 1969).
125. Kelly, J.J., "The Advanced Patrol Boat, Its Technology and Applications," Bell-Halter, New Orleans publication (Aug 1978).
126. Eck, B., "Ventilatoren," Springer-Verlag, Berlin, Germany (1962).
127. Osborne, W.C., "Fans," Pergamon Press, London, England (1966).
128. Shipway, J.C., "Estimation of Head-Flow Curves for Centrifugal Fans," National Physical Laboratory Report, Hovercraft Report 5 (Oct 1968).
129. Wallis, R.A., "Axial Flow Fans," Newnes Academic Press, London England (1961).
130. Shipway, J.C., "Aerodynamic Design of Axial Lift Fans," National Physical Laboratory Report, Hovercraft Report 4 (Jul 1968).
131. Cordier, O., "Ähnlichkeitsbedingungen Für Strömungsmaschinen," VDI Berichte, Vol. 3, pp. 85-88 (1955).
132. Csaky, T.G., "A Synthesis of Fan Design for Air Cushion Vehicles, Phase I," NSRDC Report 3599 (Oct 1972). See also "Some Aspects of Optimum Design of Lift Fans," paper presented to Sixth Canadian Symposium on Air Cushion Technology, Paper 76/9, London, Ontario (12-14 Jun 1972).
133. Baljé, O.E., "A Study on Design Criteria and Matching of Turbo-machines, Part A--Similarity Relations and Design Criteria of Turbines," American Society of Mechanical Engineers Paper 60-WA-230 (1960).
134. Baljé, O.E., "A Study on Design Criteria and Matching of Turbo-machines, Part B--Compressor and Pump Performance and Matching of Turbo-components," American Society of Mechanical Engineers Paper 60-WA-231 (1960).
135. Brotherhood, P., "Development of Improved Fans for the Britten-Norman CC2-001 Cushioncraft," Royal Aeronautical Establishment Technical Report 66271 (Aug 1966).
136. Russell, J.G., "Research and Development Work Associated with Lift and Propulsion of ACVs," First International Hovering Craft, Hydrofoil and Advanced Transit Systems Exhibition and Conference, Brighton, England (13-16 May 1974).
137. "Performance Curves for Airscrew Standard HEBA-A and -B Fan Ranges," Airscrew-Weyroc Ltd., Weybridge, Surrey, England, not dated.
138. Fan Engineering (5th Edition), published by Buffalo Forge Co., Buffalo, New York (1966).

139. Rosen, G. and G.R. Ketley, "Powering Systems for Advanced Surface Vehicles," First International Hovering Craft, Hydrofoil and Advanced Transit Systems Exhibition and Conference, Brighton, England (13-16 May 1974).

140. McGhee, G.D., "3K SES Design Development and Construction," Hovering Craft and Hydrofoil, Vol. 17, No. 3 (Dec 1977).

141. Durkin, J.M. and L.H. Luehr, "Dynamic Response of Lift Fans Subject to Varying Back Pressure," American Institute of Aeronautics and Astronautics/Society of Naval Architects and Marine Engineers Advanced Marine Vehicles Conference, AIAA Paper 78-756, San Diego, California (17-19 Apr 1978).

142. Purnell, J.G., "Evaluation of Potential Fan Concepts and the Lift Fan Requirements for Large SEC," NSRDC Report 27-182 (Aug 1972).

143. Trillo, R.L., "What Price Hovercraft?" Flight International ACV Supplement (Aug-Sep 1963).

144. Marron, H.D., "A Parametric Analysis of the Marine Gas Turbine Engine," NSRDC Report 3910 (Apr 1973).

145. Barry, F.W. and H.E. Deabler, "Powering Systems Study for a Range of Arctic Surface Effect Vehicle Sizes and Performance Requirements," Hamilton-Standard Division, United Aircraft Corporation Report (Mar 1973).

146. Polak, P., "Airflow Phenomena at Hoverskirt Edges," First International Hovering Craft, Hydrofoil and Advanced Transit Systems Exhibition and Conference, Brighton, England (13-16 May 1974).

147. Turner, D.G.W., "Amphibious Hover Platforms," Mackace Ltd Hovering Craft and Hydrofoil (May 1974).

148. Wood, K.D., "Technical Aerodynamics," published by McGraw-Hill Book Co., Inc. (1947).

149. "Generalized Method of Propeller Performance Estimation," Hamilton-Standard Handbook PDB 6101, not dated.

150. "Generalized Method of Shrouded Propeller Performance Estimation," Hamilton-Standard Handbook PDB 6220, not dated.

151. Sheets, H.E. and P.J. Mantle, "Air Cushion Craft Propulsion," American Institute of Aeronautics and Astronautics/U.S. Navy Second Marine Systems and ASW Conference, AIAA Paper 66-731 (8-10 Aug 1966). See also "Air Cushion Craft Propulsion," Journal of Aircraft, Vol. 4, No. 3, pp. 237-244 (May-Jun 1967).

152. Russell, J.B., "Hovercraft Propellers," paper presented to United Kingdom Hovercraft Society (31 Oct 1973).

153. "Noise--Final Report of the Committee on the Problem of Noise," Her Majesty's Stationery Office Command 2056 (1963).

155. "CHABA: Hazardous Exposure to Intermittent and Steady-State Noise," Journal of the Acoustical Society of America, Vol. 39, pp. 451-464 (1966).
156. Rosen G., "Prop-Fan--A High Thrust Low Noise Propulsor," National Air Transportation Meeting, Society of Automotive Engineers Paper 710470, Atlanta, Georgia (10-13 May 1971).
157. Ketley, G.R., "Propellers for Hovercraft," Hawker-Siddeley Dynamics (Jul 1969).
158. Wheatley, J.N., Hovercraft Development, Ltd., Technical Memo 67/2 (1967).
159. Fauber, W.H., "Hydroplane Boat," U.S. Patent 1,121,006, Filed 25 November 1912, Issued 15 December 1914.
160. Hickman, A., "Tests of Partially Submerged Propellers of the Sea-Sled Type," U.S. Navy Experimental Model Basin Report R-132 (Apr 1919).
161. Tachmindji, A.L. et al., "The Design and Performance of Supercavitating Propellers," DTMB Report C-807 (Feb 1957).
162. Tachmindji, A.L. and W.B. Morgan, "The Design and Estimated Performance of a Series of Supercavitating Propellers," Proceedings of the Second Symposium on Naval Hydrodynamics (Aug 1958).
163. Tulin, M.P. and M.P. Burkart, "Linearized Theory for Flows about Lifting Foils and Zero Cavitation Number," DTMB Report C-638 (Feb 1955).
164. Oakley, O., "Hydrofoils: A State of the Art Summary," Aerospace Engineering, pp. 10-20 (Dec 1962).
165. Johnson, V.E. and M.P. Tulin, "The Hydrodynamic Characteristics of High-Speed Hydrofoils," presented at Institute of Aeronautical Sciences 29th Annual Meeting, IAS Paper 61-41, New York (23-25 Jan 1961).
166. Mantle, P.J., "Variable Geometry Marine Propulsor," U.S. Patent 3,830,190, Issued 20 August 1974.
167. Venning, E. and W.L. Haberman, "Supercavitating Propeller Performance," Transactions of the Society of Naval Architects and Marine Engineers, Vol. 70 (1962).
168. van de Voorde, C.B. and J. Esveltdt, "Tunnel Tests on Supercavitating Propellers," Proceedings of the Fourth Office of Naval Research Symposium on Naval Hydrodynamics, ACR-73, Vol. I (Aug 1962).
169. Taniguchi, K. and H. Tanibayashi, "Cavitation Tests on a Series of Supercavitating Propellers," Proceedings of the IAHR Symposium on Cavitation and Hydrodynamic Mach, Tohoku University, Sendai, Japan (1962).
170. Yegorov, I.T. and Y.M. Sandovnikov, "Effect of Instability of Hydrodynamic Characteristics of a Propeller Cutting the Water Surface," Sudostroy Press, No. 1 (1961).

171. Hadler, J.B. and R. Hecker, "Performance of Partially Submerged Propellers," paper presented at Seventh Office of Naval Research Symposium on Naval Hydrodynamics, Rome, Italy (Aug 1968).
172. Shields, C.E., "Open Water Performance Characteristics of Several Semi-Submerged Supercavitating Propellers," DTMB Report 193-H-01 (Dec 1966).
173. Taggart, R., "Early Development in Marine Propulsion," Journal of the American Society of Naval Engineers, Vol. 70 (1958).
174. Engel, W.N. et al., "The Use of Axial Flow Pumps for Marine Propulsion," presented at Automotive Engineering Congress, Society of Automotive Engineers Paper 442A (8-12 Jan 1962).
175. Brandau, J., "Aspects of Performance Evaluation of Waterjet Propulsion System and a Critical Review of the State of the Art," presented at American Institute of Aeronautics and Astronautics/Society of Naval Architects and Marine Engineers Advance Marine Vehicle Meeting, AIAA Paper 67-360 (22-24 May 1967).
176. Hatte, R. and H.J. Davis, "Selection of Hydrofoil Waterjet Propulsion Systems," presented at American Institute of Aeronautics and Astronautics/U.S. Navy Second Marine Systems and ASW Conference, AIAA Paper 66-732 (8-10 Aug 1966).
177. Johnson, V.E., Jr., "Waterjet Propulsion for High Speed Hydrofoil Craft," Journal of Aircraft, Vol. 3, No. 2 (Mar-Apr 1966).
178. Levy, J., "The Design of Waterjet Propulsion Systems for Hydrofoil Craft," Marine Technology, Vol. 2, No. 1 (Jan 1965).
179. Kaario, T.J., "Process for Eliminating Friction between a Surface Vehicle and the Surface," Finish Patent 18630 (Jan 1935).
180. Betz, A., "Lift and Drag of a Wing Near a Horizontal Surface," Zeitschrift für Flugtechnik und Motorluftschiffart (1912).
181. Wieselsberger, C., "Wing Resistance Near the Ground," Zeitschrift für Flugtechnik und Motorluftschiffart, No. 10 (1921). See also National Advisory Committee for Aeronautics TM 77 (1922).
182. Serebrisky, Y.M. and S.A. Biachuev, "Wind Tunnel Investigation of the Horizontal Motion of a Wing Near the Ground," Central Aero-Hydrodynamical Institute, Moscow, Report 437 (1939). See also National Advisory Committee for Aeronautics TM 1095 (Sep 1946).
183. Fink, M.P. and J.L. Lastinger, "Aerodynamic Characteristics of Low Aspect Ratio Wings in Close Proximity to the Ground," National Aeronautics and Space Administration TND-926 (Jul 1961).
184. Carter, A.W., "Effect of Ground Proximity on the Aerodynamic Characteristics of Aspect Ratio 1 Airfoils With and Without End Plates," National Aeronautics and Space Administration TND-970 (Oct 1961).

185. Blenk, H., "Recent German Contributions to Aerodynamics," First Reynolds-Prandtl Lecture delivered to Royal Aeronautical Society, 16 April 1962, and published in Journal Royal Aeronautical Society, Vol. 66, pp. 617-630 (Oct 1962).

186. Braunss, G. and W. Lincke, "Die Auftriebsverteilung einer Ebenen Platte in Bodennahe," Zeitschrift für Flugwissenschaften, No. 10 (1962).

187. Gallington, R.W., "Vortex Shedding from the Ram Wing Vehicle," First International Hovering Craft, Hydrofoil and Advanced Transit Systems Exhibition and Conference, Brighton, England (13-16 May 1974).

188. Gallington, R.W., "Theory of Power Augmented Ram Lift at Zero Forward Speed," DTNSRDC Report ASER 365 (Feb 1976).

189. Krause, F.H. et al., "The Current Level of Power-Augmented-Ram Wing Technology," American Institute of Aeronautics and Astronautics/ Society of Naval Architects and Marine Engineers Advanced Marine Vehicles Conference Paper 78-752 (17-19 Apr 1978).

190. Mantle, P.J., "Thrust and Drag Estimate for the Channel Flow GEM," Vehicle Research Corporation, Wt 36 (Sep 1962).

191. Staufenbiel, R. and B-T. Yeh, "Stability and Control of Ground Effect Aircraft in Longitudinal Motion," Zeitschrift für Flugwissenschaften, Vol. 24, No. 1, pp. 3-9 and Vol. 24, No. 2, pp. 65-70 (1976). See also Translation DTNSRDC Report 77-0048 (Jun 1977).

192. Norstrud, H., "Wind Tunnel Tests on Jet Flaps in Ground Effect," Vehicle Research Corporation, WP 50 (Nov 1962).

193. Fowler, H.S., "Some Air Cushion Technology Research in Canada," International Hovering Craft, Hydrofoil and Advanced Transit Systems Conference, Brighton, England (13-16 May 1974).

194. Michel, W.H., "Sea Spectra Simplified," Marine Technology (Jan 1968).

195. Hutchison, B.L. and J.T. Bringloe, "Application of Seakeeping Analysis," Marine Technology, Vol. 15, No. 4 (Oct 1978).